

R-08-61

Thermal properties Laxemar

Site descriptive modelling SDM-Site Laxemar

Jan Sundberg, John Wrafter, Geo Innova AB

Pär-Erik Back, Lars Rosén, SWECO AB

December 2008

Svensk Kärnbränslehantering AB

Swedish Nuclear Fuel
and Waste Management Co

Box 250, SE-101 24 Stockholm
Phone +46 8 459 84 00



ISSN 1402-3091

SKB Rapport R-08-61

Thermal properties Laxemar

Site descriptive modelling SDM-Site Laxemar

Jan Sundberg, John Wrafter, Geo Innova AB

Pär-Erik Back, Lars Rosén, SWECO AB

December 2008

This report concerns a study which was conducted for SKB. The conclusions and viewpoints presented in the report are those of the authors and do not necessarily coincide with those of the client.

A pdf version of this document can be downloaded from www.skb.se.

Preface

This report presents the SDM-Site Laxemar thermal site descriptive model applicable to the Laxemar local model volume.

In addition to the authors, the following persons have participated in the project:

- Fredrik Mossmark (thermal properties from field measurements),
- Märta Ländell (temperature, heat capacity and temperature dependence),
- Anders Sundberg (stochastic thermal simulation),
- Nils Kellgren (stochastic geologic simulation),
- Tommy Norberg (transformation and statistical analysis of stochastic geologic simulations).

The report has been much improved by comments and suggestions from the appointed reviewers: Johan Andersson (JA Streamflow AB), Lars O Ericsson (Chalmers University of Technology, Göteborg), John Hudson (Rock Engineering Consultants, UK and member of expert review group – SIERG), Harald Hökmark (Clay Technology AB), and Raymond Munier (SKB). Anders Winberg (Conterra AB) and Rolf Christiansson (SKB) have also contributed with comments.

Summary

This report presents the thermal site descriptive model for the Laxemar area, version SDM-site. The thermal modelling is based on the methodology outlined in Figure A. The methodology is applied separately for each rock domain. Starting at the upper part of Figure A the simulation scale (1) is defined as one of the first steps in the methodology. This scale determines how lithological data (2) should be prepared and if a change of support (5) (change of scale) is required for the thermal data (4). The lithological data obtained from boreholes and mapping of the rock surface are, if necessary, reclassified into thermal rock classes (TRCs) (3) in order to keep the complexity of the subsequent simulations at a reasonable level.

The lithological data are used to construct models of the transition between different TRCs, thus describing the spatial statistical structure of each TRC (7). The result is a set of transition probability models that are used in the simulation of TRCs (8). The intermediate result of this first stochastic simulation is a number of realisations of the geology, each one equally probable. Based on the thermal data, a spatial statistical thermal model is constructed for each TRC (9). It consists of a statistical distribution and a variogram for each TRC. These are used in the stochastic simulation of thermal conductivity (10) and the result is a number of equally probable realisations of thermal conductivity for the TRC.

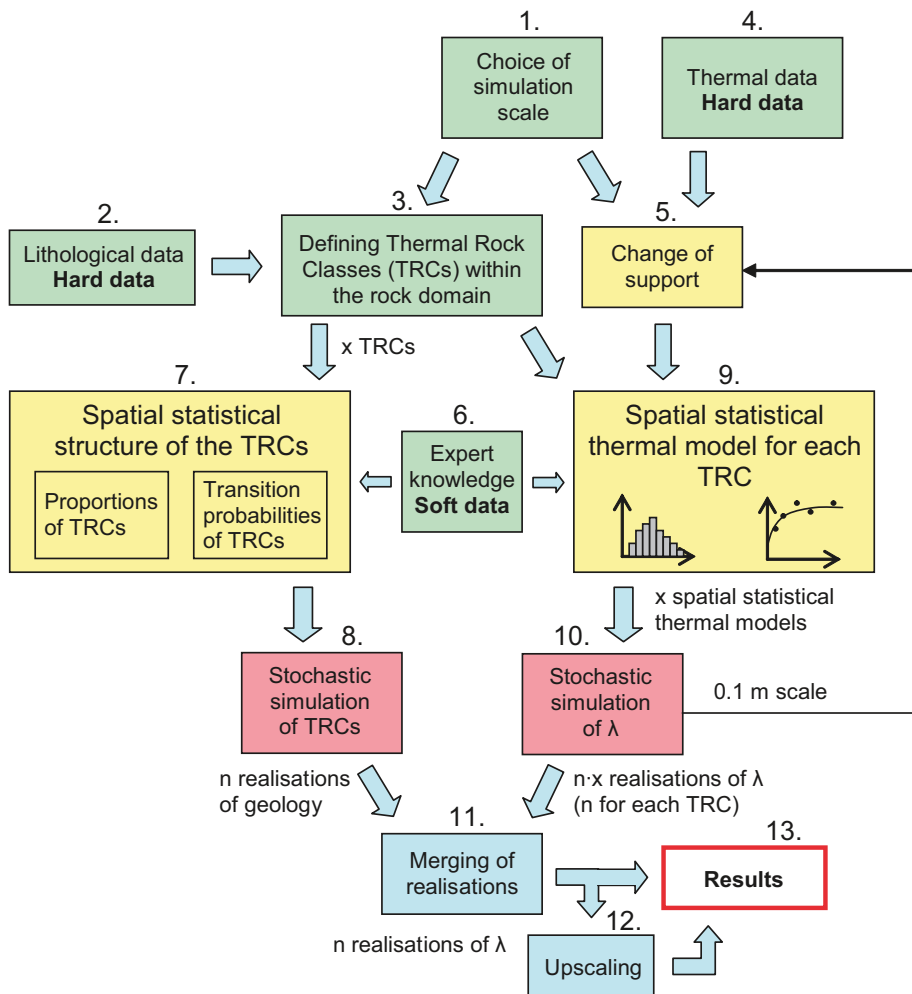


Figure A. Schematic description of the approach for thermal conductivity modelling of a rock domain (λ represents thermal conductivity).

In the next step, the realisations of TRCs (lithology) and thermal conductivity are merged (11), i.e. each realisation of geology is filled with simulated thermal conductivity values. The result is a set of realisations of thermal conductivity that considers both the difference in thermal properties between different TRCs, and the variability within each TRC. If the result is desired at a scale different from the simulation scale, i.e. the canister scale, upscaling of the realisations can be performed (12). The result (13) is a set of equally probable realisations of thermal properties.

The presented methodology was applied to rock domains RSMA01, RSMD01, and RSMM01. The main results are sets of realisations of thermal properties that can be used for further processing, most importantly for statistical analysis and numerical temperature simulations for the design of repository layout (distances between deposition holes). The main conclusions of the thermal modelling are:

- The choice of scale has a significant influence on the distribution of thermal conductivity values. The variance decreases and the lower tail percentiles increase as the scale of observation increases from 2 m to 5 m. Best estimates of the 0.1 percentile of thermal conductivity are:
 - Domain RSMA01: 2.09 W/(m·K) for the 2 m scale and 2.16 W/(m·K) for the 5 m scale.
 - Domain RSMM01: 2.06 W/(m·K) for the 2 m scale and 2.11 W/(m·K) for the 5 m scale.
 - Domain RSMD01: 2.38 W/(m·K) for the 2 m scale and 2.41 W/(m·K) for the 5 m scale.
- It is mainly the low-conductive Ävrö quartz monzodiorite that determines the lower tails of the thermal conductivity distributions for domains RSMA01 and RSMM01.
- Confidence in the lower tails of the thermal conductivity distributions for the modelled rock domains is generally high, although slightly higher for rock domains RSMA01 and RSMM01 than for rock domain RSMD01. The uncertainties that do exist are primarily associated with uncertainties in the spatial statistical thermal models (distribution models and spatial correlation models) for the certain TRCs.
- The aspect of the model with the highest confidence is the overall distribution (the main body of the distribution, tails excluded) of thermal conductivities for domain RSMD01, because of its higher degree of homogeneity in geology and thermal properties. The aspect of the model with the lowest confidence is the overall distribution of thermal conductivities for domains RSMA01 and RSMM01, which is related to the higher degree of geological heterogeneity present. However, the lower percentiles of thermal conductivity for all domains are not very sensitive to the uncertainties linked to geological heterogeneity.
- The factor of anisotropy of thermal conductivity of the rock mass resulting from foliation may be as high as approximately 1.15. Thermal conductivity parallel to the foliation plane is higher than conductivity perpendicular to the foliation. The spatial variability of this anisotropy is not known.
- There is good mutual consistency between the understanding of geology and the thermal properties description.
- The thermal conductivity of altered rock is approximately 5–15% higher than fresh rock. The impact of alteration has been incorporated into the thermal modelling and is therefore reflected in the domain results.
- The mean heat capacity at the 2 m scale for the modelled rock domains varies between 2.16 and 2.23 MJ/(m³·K).
- The temperature variation with depth is rather well established. The mean *in situ* temperatures at –400 m, –500 m and –600 m elevation are estimated at 13.3°C, 14.8°C, and 16.3°C, respectively.
- The mean thermal expansion coefficient for the dominant granitoid rock types varies between $6.9 \cdot 10^{-6}$ and $7.4 \cdot 10^{-6}$ m/(m·K).

Contents

1	Introduction	11
1.1	Background	11
	1.1.1 Overview	11
	1.1.2 Thermal properties	11
1.2	Scope and objectives	13
1.3	Setting	14
1.4	This report	14
	1.4.1 Structure of this report	14
	1.4.2 Terminology	14
2	Previous thermal model versions and input from geology	17
2.1	Previous model versions	17
2.2	Geological model overview and input from thermal modelling	17
3	Overview and assessment of investigation data	21
3.1	Databases	21
3.2	Determination of thermal transport properties	24
3.3	Thermal conductivity and diffusivity from laboratory measurements	25
	3.3.1 Method	25
	3.3.2 Results	25
3.4	Thermal conductivity and diffusivity from field measurements	32
	3.4.1 Method	32
	3.4.2 Results	33
3.5	Thermal conductivity from mineral composition	34
	3.5.1 Method	34
	3.5.2 Results	36
	3.5.3 Influence of alteration on thermal conductivity	37
	3.5.4 Comparison with laboratory measurements	40
3.6	Relationship between thermal conductivity and density	42
	3.6.1 Introduction	42
	3.6.2 Results	42
3.7	The use of borehole density logging in thermal modelling	44
	3.7.1 Introduction	44
	3.7.2 Quality control of density logs	44
	3.7.3 Subdivision of Ävrö granite in boreholes on the basis of density logs	45
	3.7.4 Thermal conductivity from density	48
3.8	Evaluation of anisotropy of thermal conductivity due to foliation	52
	3.8.1 Introduction	52
	3.8.2 Analysis	53
	3.8.3 Results	53
	3.8.4 Summing up	56
3.9	Heat capacity	57
3.10	Thermal conductivity vs heat capacity	60
3.11	Temperature dependence in thermal properties	61
3.12	Pressure dependence on thermal conductivity	66
3.13	Coefficient of thermal expansion	66
3.14	<i>In situ</i> temperature	67
	3.14.1 Method	67
	3.14.2 Results	68
3.15	Geological data	69

4	Strategy for thermal modelling	73
4.1	Conceptual model	73
4.2	Modelling approach	74
4.2.1	Introduction	74
4.2.2	Outline of the methodology	74
4.2.3	Important adaptations of the modelling approach to Laxemar	76
4.3	Feedback from other disciplines	77
4.4	Modelling assumptions	78
5	Geostatistical analyses and stochastic simulations	79
5.1	General	79
5.2	Conceptual descriptions of the rock domains	79
5.2.1	Introduction	79
5.3	Geological input	81
5.3.1	Thermal Rock Classes (TRC) – Definition, properties and proportions	81
5.3.2	Orientation and geometry of subordinate rock types	83
5.3.3	Characterisation of domains and division into thermal subdomains	86
5.3.4	Lithological data preparation	90
5.4	Spatial statistical structure of the TRCs (lithology)	91
5.4.1	Establishment of lithological models	91
5.5	Stochastic simulation of TRCs (lithology)	95
5.5.1	Introduction	95
5.5.2	Example results	95
5.5.3	Analysis and verification of results	97
5.5.4	Modelling of size distribution of TRCs	100
5.5.5	Uncertainties in estimates of TRC proportions	101
5.6	Spatial statistical models of thermal conductivity	106
5.6.1	Approach	106
5.6.2	Statistical distribution models – 0.1 m scale	107
5.6.3	Variogram models – 0.1 m scale	120
5.7	Stochastic simulation of thermal conductivity	134
5.7.1	Procedure	134
5.7.2	Spatial statistical thermal models – 2 m scale	134
5.7.3	Upscaling and results of simulation of thermal conductivity	134
5.8	Evaluation of models of thermal conductivity and simulation results	145
5.9	Statistical models of heat capacity	148
5.10	Conditional stochastic simulation of thermal conductivity	148
5.10.1	Introduction	148
5.10.2	Model for simulated volume	149
5.10.3	Evaluation of simulation results	150
6	Thermal domain model	155
6.1	Domain modelling results	155
6.2	Thermal conductivity	155
6.2.1	Rock domain RSMA01	155
6.2.2	Rock domain RSMM01	159
6.2.3	Rock domain RSMD01	164
6.3	Heat capacity	166
6.4	Evaluation of domain modelling results	170
6.4.1	Rock domain RSMA01	170
6.4.2	Rock domain RSMM01	171
6.4.3	Rock domain RSMD01	173
6.4.4	Anisotropy due to subordinate rock bodies	174
6.4.5	Impact of rock type (TRC) proportions on lower tail percentiles	174

6.5	Summary of domain thermal properties	174
6.5.1	Introduction	174
6.5.2	Thermal conductivity	175
6.5.3	Thermal anisotropy	178
6.5.4	Heat capacity	178
6.5.5	Temperature dependence in thermal properties	178
6.5.6	Thermal expansion coefficient	178
6.5.7	<i>In situ</i> temperature	178
7	Evaluation of uncertainties	179
7.1	Data uncertainty	179
7.1.1	Thermal conductivity and heat capacity	179
7.1.2	Thermal expansion coefficient	179
7.1.3	Temperature	179
7.1.4	Boremap data	179
7.2	Model uncertainty	180
7.2.1	Major model uncertainties	180
7.2.2	The simulation scale	180
7.2.3	The simulation volume	180
7.2.4	The spatial statistical structure of TRCs (lithology)	181
7.2.5	The spatial statistical thermal models	182
7.2.6	The simulation technique	183
7.3	Summary of uncertainties	183
8	Conclusions	185
	References	187
Appendix A	Thermal conductivity from density logs – histograms	193
Appendix B	Thermal conductivity from density logs – borehole profiles	199
Appendix C	Histograms of thermal conductivity	205
Appendix D	Variogram models	207
Appendix E	Variogram model reproduction	211
Appendix F	Histograms of thermal conductivity – simulations for each TRC	215
Appendix G	Visualisations of TRC thermal realisations	223
Appendix H	Visualisations of domain thermal realisations	231
Appendix I	Verification of stochastic simulations of TRCs	247
Appendix J	Histograms of TRC length distributions in realisations	255
Appendix K	Histograms of TRC length distributions in boreholes	265
Appendix L	Spatial analysis for 4 m and 8 m data.	271
Appendix M	TRC proportions and confidence intervals	275
Appendix N	Conditional stochastic simulation of thermal conductivity	279
Appendix O	Conditional stochastic simulation of geology	285
Appendix P	WellCad borehole plots	293

1 Introduction

1.1 Background

1.1.1 Overview

The Swedish Nuclear Fuel and Waste Management Company (SKB) is undertaking site characterisation at two different locations, the Forsmark and Simpevarp/Laxemar areas, with the objective of siting a geological repository for spent nuclear fuel. A site descriptive model (SDM) is a synthesis of geology, rock mechanics, thermal properties, hydrogeology, hydrogeochemistry and a surface system description.

The heat generated by the spent nuclear fuel will increase the temperature of all components of the KBS-3 repository: barriers, tunnels, seals and the host rock itself. To ensure the long-term sealing capacity and the mechanical function of the bentonite buffer surrounding each individual canister, a maximum bentonite temperature is prescribed in the design premises. This important requirement, which relates to the safety assessment, implies that the canisters cannot be deposited arbitrarily close to each other. Unnecessarily large distances between the canisters, on the other hand, will mean inefficient and costly use of the repository rock volume. In order to determine the minimum canister spacing required to meet the temperature criterion for all canister positions, including those in the least conductive parts of the different rock domains where near-field temperatures will be particularly high, it is necessary to establish an adequate description, of the site's rock thermal properties and their spatial variation at the relevant canister scale. In addition to being needed for the design, or layout, issue, the thermal site model will be important for predicting the thermo-mechanical evolution of the repository host rock at different scales.

The methodology employed for thermal modelling has been fundamentally revised compared with previous model versions, and has been documented in a separate strategy report /Back and Sundberg 2007/. The modelling involves stochastic simulation based on both the spatial statistical structure of rock types and the spatial distribution of thermal conductivities. By merging the realisations of the lithological and thermal simulations, a distribution of thermal properties is produced that takes into account the spatial variability both within and between different rock types. The realisations of thermal properties can be used for subsequent numerical temperature simulations for the thermal design of a repository, i.e. for determining the minimum canister and tunnel spacings required to meet the buffer temperature criterion and to perform any layout optimisations. The strategy for such thermal dimensioning is described in /Hökmark et al. 2009/.

The complete site investigation (CSI) work comprises two stages/versions, Laxemar 2.1 and SDM-Site Laxemar, concluding with a final multi-disciplinary site descriptive model (SDM) of Laxemar. An important component of this modelling is to address and continuously try to resolve uncertainties of importance for repository engineering and safety assessment. The most comprehensive thermal modelling efforts within the CSI are performed as part of model version SDM-Site Laxemar. The results of this concluding thermal modelling of Laxemar are compiled in this report. The findings from the thermal analyses are summarised in the final multi-disciplinary SDM-Site Laxemar report /SKB 2009/, cf. Figure 1-1 for overview of associated reporting structure.

1.1.2 Thermal properties

The temperature field around a canister is of primary concern for the design of a repository. The current design criterion is specified as the maximum temperature (currently 100°C) allowed in the bentonite buffer outside the canisters /SKB 2006a/. To fulfil the temperature requirement, a low rock thermal conductivity leads to larger distances between canisters than in the case of a high thermal conductivity. This is because low conductivity rock will give rise to higher bentonite temperatures.

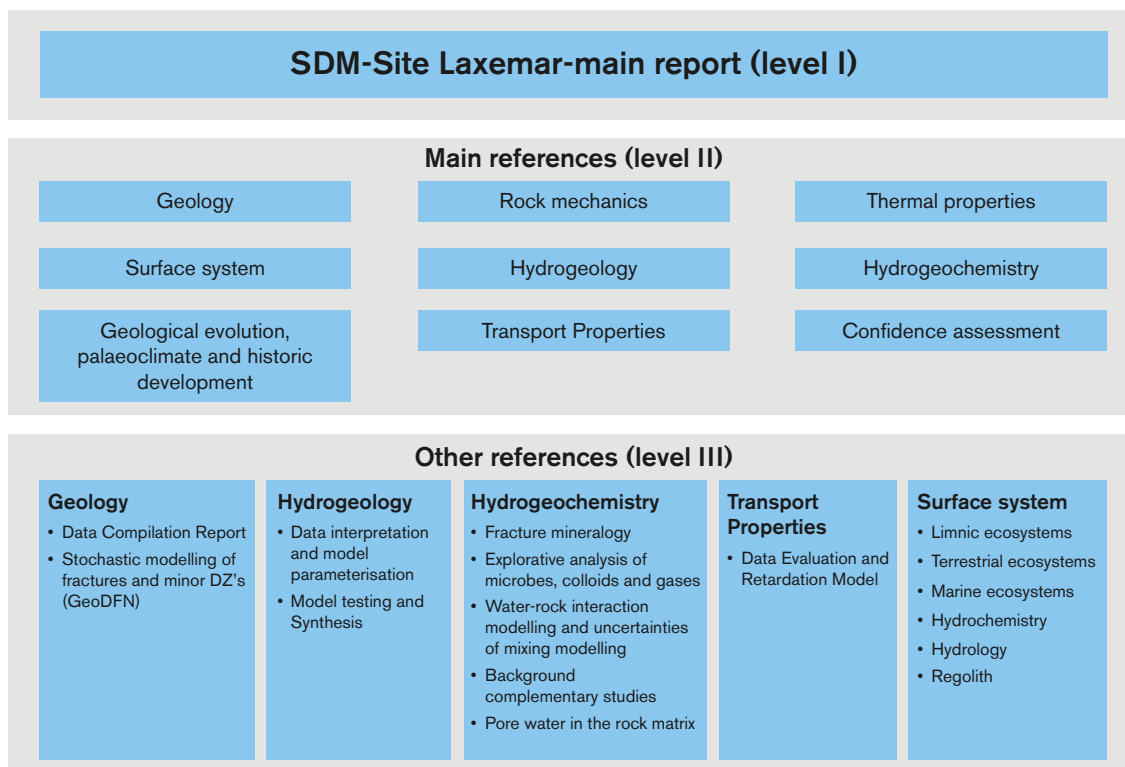


Figure 1-1. Overview of reporting structure in model version SDM-Site Laxemar.

The sensitivity in canister temperature to changes in the thermal properties is highest for the area closest to the canister. It is therefore of special interest to analyse if there is a spatial variation in the thermal properties in the rock mass at the canister scale that will influence the canister temperature. The accuracy of the description of thermal properties needs to be high since even small changes in the thermal properties influence the maximum bentonite temperature and consequently the canister distance, see /Hökmark et al. 2009/.

In order to analyse the scale at which variations of thermal conductivity is significant for the temperature on the canister, a preliminary numerical study based on rock thermal conductivity distribution has been made /Sundberg et al. 2005b/. They found that the spatial variability started to have an influence on the canister temperature at a scale as small as 1 m and that the influence increased approximately linearly up to at least 10 m. Consequently, the maximum canister temperature is influenced by thermal conductivities for a range of scales. The characteristic scale would be in the order of 5 m, which is logical considering the dimensions of the canister and the dominating role of the contribution of the local canister to its own temperature. The result of the thermal modelling is therefore upscaled to 5 m.

The main result of the thermal modelling in this report is a set of realisations of thermal properties for the rock domains. Each cell in the realisation contains information about thermal conductivity, heat capacity and the lithology. These realisations can be used for further processing in design, most importantly for numerical temperature simulations for design of repository layout (e.g. distances between deposition holes). The methodology implies that all relevant scales of the thermal conductivity are considered. Also the anisotropy in the geology is taken into account.

The term “thermal properties” involves thermal conductivity, thermal diffusivity, heat capacity, *in situ* fluid temperature and the coefficient of heat expansion.

Thermal conductivity λ [W/(m·K)] is defined as a materials ability to transport thermal energy. Thermal conductivity is the most important transport property. Thermal diffusivity κ [m²/s] is a

measure of a materials ability to level out temperature differences. Heat capacity C [$\text{J}/(\text{m}^3\cdot\text{K})$] is defined as a materials capacity to store heat. These properties are related to each other as follows:

$$\kappa = \lambda/C$$

Due to the relation, it is only necessary to discuss two of these three properties. In this report the interest is concentrated on thermal conductivity and heat capacity. The temperature dependence for these properties is also of interest due to the temperature increase in a repository. Anisotropy in thermal conductivity influences the temperature field in a repository and is therefore also of interest to determine.

The *in situ* fluid temperature is of primary interest in order to determine the temperature at repository depth, the starting temperature for the heat increase in a repository. The coefficient of heat expansion describes the expansion of rock versus the increase in temperature. However, there has been no focus on this property in the current report.

A table summarising the thermal properties and parameters that should be predicted/described by the thermal model is provided in /Back and Sundberg 2007/, including the acceptable uncertainty for the various parameters.

1.2 Scope and objectives

The rationale for establishing thermal site models is primarily to be able to forecast the thermal evolution for different design solutions in order to meet design criteria. The main objective of the thermal modelling SDM-site for Laxemar is to provide an adequate spatial statistical description of the rock mass thermal conductivity and its uncertainties for the needs of repository design and safety assessment.

This report synthesizes the thermal investigations at the Laxemar site. The report reviews the thermal data available and describes the statistical evaluation of this data. The data employed originate from the Laxemar 2.3 data freeze. The temperature at repository depth is determined directly from data. Stochastic modelling produces a set of 3D realisations which describe the spatial distribution of thermal properties. Together, the realisations of thermal properties and the results of the statistical analysis of these realisations constitute the thermal model. From the different stochastic realisations, the low percentiles of thermal conductivity are determined, and the scale dependence of thermal conductivity is evaluated. These are two parameters of importance for repository design. The lower tail of the thermal conductivity distribution at a scale relevant to the temperature development of the canister is of central importance to the decision of canister spacing and must therefore be properly described. In forthcoming work, the realisations of thermal property distribution will be used as input to numerical temperature modelling of a repository /Hökmark et al. 2009/.

The rock mass at Laxemar has been divided up into several subvolumes or “rock domains” on the basis of their geology. The rock domain model forms the geometric framework for modelling of thermal properties /Wahlgren et al. 2008/. The methodology employed for thermal modelling has been fundamentally revised compared to previous model versions, and has been documented in a separate strategy report /Back and Sundberg 2007/. This revised modelling strategy involves stochastic simulation based on both the spatial statistical structure of lithologies and the spatial distribution of thermal conductivities. By merging the realisations of the lithological and thermal simulations, a statistical distribution of thermal properties is produced that takes into account the spatial variability within and between different rock types.

The thermal properties of three rock domains, RSMA01, RSMM0101 and RSMD01, are modelled. Results are presented for different scales. Anisotropy of thermal conductivity of the rock mass resulting from foliation is evaluated from analysis of measurements in different directions. The impact of alteration on thermal properties is investigated. The remaining uncertainties in understanding the thermal properties are outlined.

1.3 Setting

The rock volume for which thermal properties have been investigated in this modelling stage is defined by the local model volume for SDM-Site Laxemar as defined in /Wahlgren et al. 2008/. The thermal model applies in particular to the southern and south-western parts of the Laxemar local model volume to which the investigations were focused during the complete site investigation.

The bedrock at Laxemar is dominated by well-preserved intrusive rocks, with only a faint to weak foliation. The bedrock was formed 1.80 Ga ago during an intense period of igneous activity at the waning stages of the Svecokarelian orogeny. The dominant rock types at Laxemar are the porphyritic Ävrö granite and Ävrö quartz monzodiorite, and the equigranular quartz monzodiorite. For illustration of the surface geology, see Figure 1-2. Apart from younger dolerite intrusions (not shown in Figure 1-2), the remaining rock types at Laxemar were formed more or less synchronously.

Three rock domains dominate within the local model volume: RSMA01, RSMD01 and RSMM01. RSMA01 is dominated by Ävrö granodiorite, RSMD01 by quartz monzodiorite and RSMM01 by Ävrö quartz monzodiorite. Diorite-gabbro bodies are an important component of domain RSMM01 /Wahlgren et al. 2008/.

1.4 This report

1.4.1 Structure of this report

The thermal modelling work presented in this report relies heavily on the methodology described in the strategy report for thermal modelling during site investigations, version 2.0 /Back and Sundberg 2007/. This represents a major departure from the modelling approach employed in model version 1.2 and model stage 2.1. Integration of geological information critical to thermal modelling was performed through close cooperation with the geology team.

Chapter 2 presents an overview of the previous thermal modelling work, and briefly describes the geological model, which forms the geometrical framework for the thermal modelling. Chapter 3 summarises the primary thermal and geophysical logging data that where available for the final model stage. Preliminary statistical analyses of these data are also covered in Chapter 3. Chapter 4 begins with a presentation of the conceptual model and is followed by a brief description of the strategy employed for the thermal modelling.

The first part of Chapter 5 describes aspects of the geology and the geological model that are relevant to thermal modelling. This is followed by the spatial statistical models and simulation of both geology (lithology) and thermal conductivity. Chapter 6 presents and evaluates the results of the thermal modelling at rock domain level. Chapter 7 summarises these results in a concise form. Chapter 8 describes the uncertainties inherent in the thermal model. Chapter 9 summarises the conclusions of the thermal modelling work.

The report contains a number of appendices that are linked to various modelling steps in Chapter 5.

1.4.2 Terminology

Definitions of terms important in the thermal modelling work and used in this report are defined below.

Rock type. Each rock type identified in the mapping of bedrock and drill cores has been assigned a name by SKB. Each rock name has an associated name code. Subsequently in the description of the thermal properties, rock types will generally be identified and described by their rock code, as well as by their name. Table 1-1 lists the name codes for the rock types referred to in this report. Porphyritic Ävrö granite (which includes both Ävrö granodiorite and Ävrö quartz monzodiorite) and the equigranular quartz monzodiorite are considered to be dominant rock types at Laxemar. The remainder are defined as subordinate rock types.

Rock unit. A rock unit is defined primarily on the basis of the composition, grain size and inferred relative age of the dominant rock type. The term rock unit has been used in the bedrock mapping work at the surface (2D) and in connection with the single-hole interpretation work (essentially 1D) /Wahlgren et al. 2008/.

Rock domain. A rock domain refers to a rock volume having rock units that show similar composition, grain size, degree of homogeneity, and degree and style of ductile deformation /Munier et al. 2003/. Rock domains are used in 3D geometric modelling work.

Deformation zone. A deformation zone refers to an essentially 2D structure, along which there is a concentration of ductile and/or brittle deformation /Munier et al. 2003/. A complete list of deformation zones identified in single-hole interpretations are given in /Wahlgren et al. 2008/.

Thermal rock class (TRC). A thermal rock class comprises one or more rock types having similar thermal properties. Geological properties such as composition and mode of occurrence may also be considered when classifying thermal rock classes.

Thermal subdomain. A part of a rock domain defined by borehole sections that are judged to be lithologically homogeneous, or can be shown to be homogenous in a statistical sense with regards to lithology. Thermal subdomains are defined primarily for the purpose of modelling thermal properties but are not necessarily limited to this usage. A thermal subdomain has no defined spatial boundaries; only its proportion of the rock domain is defined. The proportion may be based on borehole lengths and/or geological expertise.

Anisotropy. Two types of geological phenomena are believed to result in anisotropy of thermal conductivity. These are (1) anisotropy due to foliation/lineation, and (2) anisotropy due to the preferred orientation of subordinate rock bodies.

Local model volume. The local model volume for SDM-Site Laxemar includes the rock volume identified as potentially suitable for hosting a final repository. The investigations in Laxemar during the complete site investigation focus particularly on the southern and south-western parts of the local model volume. The local model area has been extended southwards compared to version 2.1 to incorporate a greater volume of the quartz monzodiorite.

A glossary of geostatistical terms used in the report is provided in /Back and Sundberg 2007/.

2 Previous thermal model versions and input from geology

2.1 Previous model versions

Thermal modelling of the Laxemar subarea has been performed in different stages and versions. Model version Laxemar 1.2 is reported in /Sundberg et al. 2006, SKB 2006b/ and model stage Laxemar 2.1 in /Wrafter et al. 2006, SKB 2006d/. Data from the Laxemar subarea were rather limited in version 1.2, so that the modelling work relied heavily on data from the adjacent Simpevarp subarea, as well as from Äspö. Thermal properties were reported for five rock domains, three of which could be considered to be volumetrically important; RSMA01, RSMD01 and RSMM01. Results indicated that the mean thermal conductivities for the three major domains vary from 2.58 to 2.82 W/(m·K). Standard deviations for the 0.8 m scale were expected to range from 0.17 to 0.29 W/(m·K) with lower 2.5 percentiles estimated at between 2.3 and 2.4 W/(m·K) /Sundberg et al. 2006/.

In model stage 2.1, new data, together with limited modelling efforts, indicated rather similar mean thermal conductivities for domains RSMA01, RSMD01 and RSMM01 /Wrafter et al. 2006/. More importantly, however, the standard deviations were considerably higher than in stage 1.2, ranging from 0.28 to 0.36. Precise lower tail percentiles of thermal conductivity were not estimated in stage 2.1.

It is important to point out that previous model versions were based on the 1.2 version of the geological model, which during the current SDM-Site Laxemar modelling underwent significant modification. This is particularly relevant for domains RSMA01 and RSMM01.

Associated with the thermal models of version 1.2 and stage 2.1 were several uncertainties, the most important of which were the method for upscaling of thermal conductivity from cm-scale to canister scale, the quality of rock type models, and the representativeness of the boreholes for the domains. Uncertainties were particularly large for domain RSMM01 because of its large heterogeneity in both lithology and thermal properties.

2.2 Geological model overview and input from thermal modelling

The local model volume includes the rock volume identified as potentially suitable for hosting a final repository. The rock mass for which thermal modelling has been carried out during SDM-Site is contained within the local model volume. The 3D rock domain model presented for SDM-Site Laxemar (see Figure 2-1) forms the basis for the following discussion concerning the thermal properties of the rock mass within the local volume at Laxemar /Wahlgren et al. 2008/. A rock domain refers to a rock volume having rock units that show similar composition, grain size, degree of homogeneity, and degree and style of ductile deformation /Munier et al. 2003/. Since thermal properties are intimately related to lithological properties, the rock domain model provides an appropriate framework for modelling thermal properties.

The thermal properties of the three major rock domains in the Laxemar local model volume are evaluated within this report. These are:

- RSMA01-domain: dominated by Ävrö granite,
- RSMD01-domain: dominated by quartz monzodiorite,
- RSMM01-domain: characterised by a high frequency of minor bodies to small enclaves of diorite/gabbro in particularly Ävrö quartz monzodiorite.

As regards domain RSMA01, only its central, southern and western parts, north of domain RSMM01 are included in the thermal modelling. Two additional rock domains present in Laxemar but not modelled here are:

- **RSMB01**-domain: characterised by a mixture of Ävrö granite and fine-grained dioritoid. Identified at depth only, this domain was excluded from thermal modelling because it is volumetrically very subordinate.
- **RSMB06**-domain: dominated by fine-grained dioritoid. Defined at the surface only, this domain has not been modelled in 3-D in the rock domain model /Wahlgren et al. 2008/.

The rock domain model presented for SDM-Site Laxemar has been modified compared to the older 1.2 version. The main modification is related to the subdivision of Ävrö granite into two varieties, namely Ävrö granodiorite and Ävrö quartz monzodiorite.

The Ävrö granite is the dominant rock type in the RSMA01 domain, constituting over 80% of the volume. The Ävrö granodiorite variety dominates. Subordinate rock types comprise fine-grained granite (511058), fine-grained diorite-gabbro (505102), granite (501058), fine-grained dioritoid (501030) and quartz monzodiorite (501036).

The RSMD01 domain is strongly dominated by equigranular, medium-grained quartz monzodiorite. In contrast to Ävrö granite, it is considered to be compositionally homogeneous. Fine-grained granite (511058), fine-grained diorite-gabbro (505102) and pegmatite (501061) are the most important subordinate rock types. Dolerite is present as isolated occurrences.

The RSMM01 domain is also dominated by Ävrö granite, but in this case by the Ävrö quartz monzodiorite type. It is also characterised by a much higher proportion of diorite-gabbro than the other rock domains though variably distributed both at the surface and in domain sections in boreholes. The subordinate rock types are similar to the other domains. For a more detailed description of the rock type compositions in the different domains, see /Wahlgren et al. 2008/.

Fine-grained diorite-gabbro (505102) commonly occurs as minor composite intrusions (dyke-like bodies) together with fine-grained granite /Wahlgren et al. 2006c/. Fine-grained granite makes up between 5 and 50% of the total /Wahlgren 2008/. When encountered in the boreholes, however, these bodies have been mapped simply as fine-grained diorite-gabbro.

Numerous deformation zones have been modelled deterministically in the geological model /Wahlgren et al. 2008/. In the thermal modelling work, focus is placed on characterising the properties of the intact rock outside these deformation zones, since deposition holes for canisters in a future repository will be positioned some distance from these zones.

Based on the borehole length, approximately 15–30% of the bedrock between the identified deformation zones in Laxemar is affected by alteration /Wahlgren et al. 2008/. The degree of alteration is in general classified as faint to weak. Oxidation (red staining) is generally the most abundant type of alteration in rock domains RSMA01 and RSMM01 whereas in domain RSMD01, a high degree of saussuritisation and epidotisation is present in addition to oxidation. Whereas the saussuritisation is thought to be a product of late magmatic processes, the oxidation is related to fractures and hydrothermal alteration, Much of this oxidation is associated with fracture fillings related to the intrusion of the 1.45 Ga old Götemar granite (and probably also Uthammar granite) /Drake et al. 2007/. However, this does not mean that all red-staining is of the same genesis. Since alteration has resulted in a different, more variable mineral composition, the thermal properties are likely to have been affected.

Laxemar is bounded both to the east and west by prominent ductile shear zones. Although not devoid of shear zones, the bedrock at Laxemar is dominated by well-preserved intrusive rocks. However, a faint to weak foliation, which is not uniformly distributed over the area, is commonly present. Much of this ductile fabric is inferred to have developed at a late stage in the magmatic evolution. All rock types are affected by the foliation, in particular the dyke-like bodies of fine-grained granite and fine-grained diorite-gabbro.

An east-west oriented and near horizontal antiformal structure is indicated by the foliation data /Wahlgren et al. 2008/. The subordinate rock types display a similar change in orientation as the foliation. The foliation has given rise to a weak anisotropy of the magnetic susceptibility (AMS). Furthermore, the foliation and orientation are discordant to the boundaries between the dominant rock types.

Input from geology to the thermal modelling includes:

- A lithological domain classification of each borehole used for geometric modelling of rock domains within the Laxemar area /Wahlgren et al. 2008/.
- Lithological data (rock type and alteration) from the Boremap mapping for c. 20 cored boreholes.
- Deformation zones, both deterministically modelled and minor deformation zones, extracted from the single-hole interpretations /Wahlgren et al. 2008/.
- The orientation, size and shape of subordinate rock types based on both hard data from borehole mapping, in addition to expert judgements by the geological team.

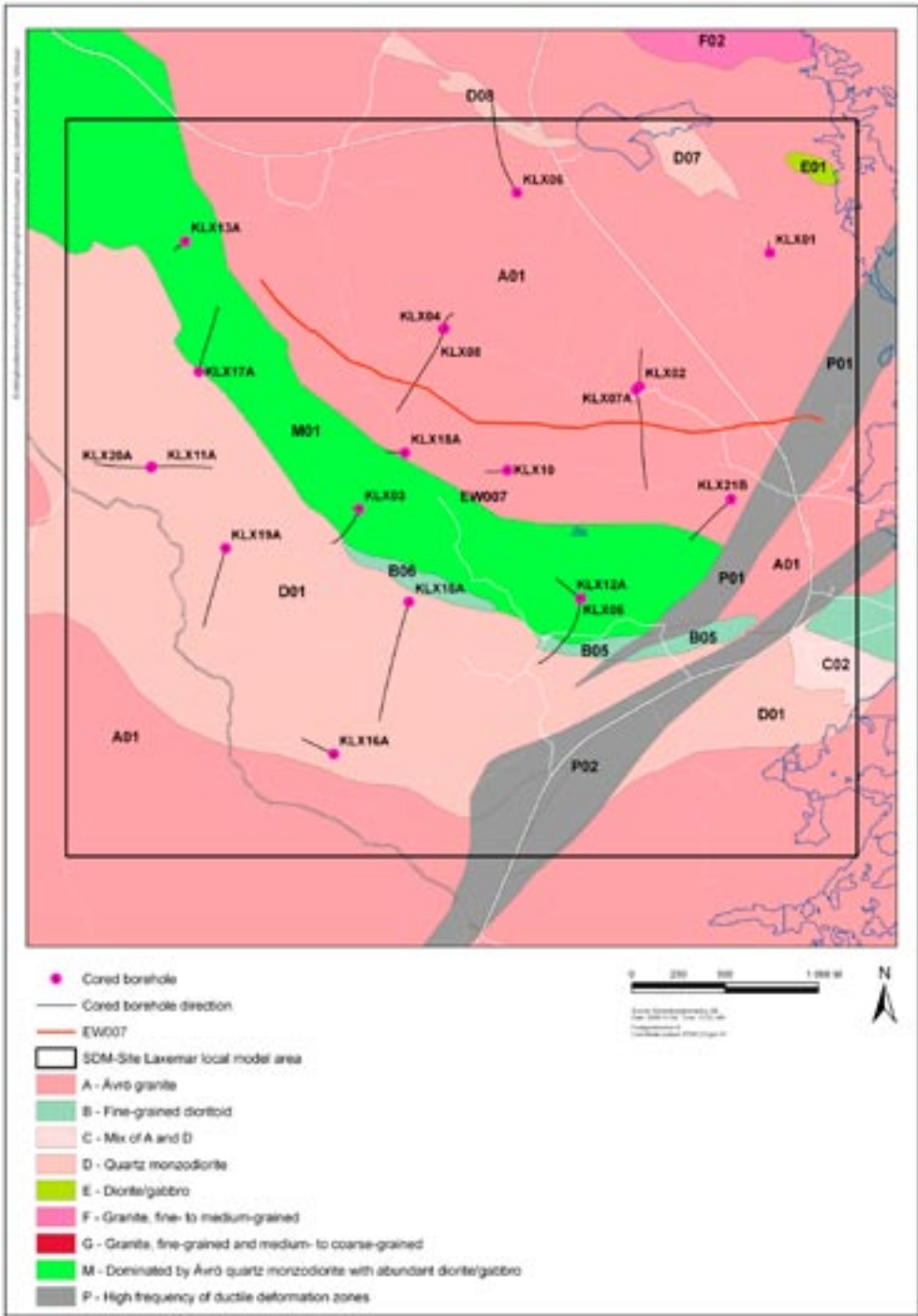


Figure 2-1. Two dimensional representation at ground surface of the 3D local scale SDM-Site Laxemar rock domain model. Boreholes referred to in this report are indicated.

3 Overview and assessment of investigation data

3.1 Databases

The Laxemar thermal model version Site has used quality-assured primary data available prior to the data freeze 2.3, dated 31 August, 2007. The data used in modelling includes all data available in previous model stages in addition to new data acquired between data freezes 2.1 and 2.2 and between 2.2 and 2.3. An overview of all the available data used in the thermal modelling work conducted for model version Site is compiled in Table 3-1. The main additions to the database relevant to thermal modelling after data freeze 2.1 are:

- Laboratory measurement of thermal properties and density for most rock types. Of the 96 samples tested, 20 were of altered rock.
- Field measurement of thermal properties on rock outcrops at 26 locations, mainly in Ävrö granite.
- Modal analysis data from 64 samples of both fresh and altered rock.
- Boremap mapping of 13 cored boreholes.
- Geophysical borehole logging data (density and temperature) from 13 cored boreholes.

The primary data are described and evaluated in more detail in the subsequent sections of this chapter. The thermal data, as well as relevant geological and hydrogeological information, are visualised in WellCad plots for each borehole in Appendix P.

Table 3-1. Available data relevant to rock thermal properties and their treatment in Laxemar thermal modelling, version Site. Report numbers in italics show data available at data freeze 2.1.

Data specification	Reference to data report		Usage in Laxemar model version Site (Rock type and no. of samples, where relevant)
Data normally from core-drilled boreholes			
<i>Fluid temperature and density logging</i>	<i>Results</i>	<i>Interpretation</i>	Temperature logging: Description of natural temperature variations with depth. Temperature gradients.
KLX02	<i>P-03-111</i>	<i>P-04-214</i>	
KLX03	<i>P-04-280</i>	<i>P-05-34</i>	
KLX04	<i>P-04-306</i>	<i>P-05-34</i>	Density logging:
KLX05	<i>P-05-144</i>	<i>P-05-189</i>	Estimation of thermal conductivity from density based on relationship between these two parameters.
KLX07A	P-05-228	P-05-259	
KLX08	P-05-270	P-06-65	
KLX10	P-06-20	P-06-162	
KLX11A	P-06-197	P-06-157	Modelling of spatial correlation in thermal conductivity.
KLX12A	P-06-198	P-06-253	
KLX13A	P-06-307	P-06-317	
KLX15A	P-07-152	P-07-114	Subdivision of Ävrö granite
KLX16A	P-07-56	P-07-97	
KLX17A	P-06-315	P-07-25	
KLX18A	P-06-290	P-06-292	
KLX19A	P-06-314	P-07-21	
KLX20A	P-06-290	P-06-292	
KLX21B	P-07-15	P-07-75	

Data specification	Reference to data report	Usage in Laxemar model version Site (Rock type and no. of samples, where relevant)
<i>Temperature data from Posiva flow-logging</i>		Description of natural temperature variations with depth. For comparison with fluid temperature loggings.
KLX05	P-05-160	
KLX08	P-05-267	
KLX18A	P-06-184	
<i>Boremap mapping</i>		Major and subordinate rock type distribution. Data used for identification of rock types at drill core locations where different measurements have been performed. Data used as input to stochastic simulation of lithologies.
KLX02	P-04-231	
KLX03	P-04-275	
KLX04	P-04-239	
KLX05	P-05-185	
KLX07A	P-05-263	
KLX08	P-06-42	
KLX10	P-06-51	
KLX11A	P-06-237	
KLX12A	P-06-242	
KLX13A	P-06-255	
KLX15A	P-07-157	
KLX16A	P-07-211	
KLX17A	P-07-158	
KLX18A	P-06-238	
KLX19A	P-07-210	
KLX20A	P-06-241	
KLX21B	P-07-218	
<i>Laboratory test of density</i>		Data used for investigation of relationship between density and thermal conductivity.
KAV01	P-04-58	
KAV04A	P-04-271	
KSH01A	P-04-56	Ävrö quartz monzodiorite (501046): 33 samples
KSH02	P-04-57	Ävrö granodiorite (501056): 60 samples
KA2599G01	R-02-27	Quartz monzodiorite (501036): 63 samples
KLX02	P-04-259	Fine-grained dioritoid (501030): 28 samples
KLX03	P-05-94, P-07-61	Diorite-gabbro (501033): 22 samples
KLX04	P-04-268	Fine-grained granite (511058): 4 samples
KLX05	P-05-127, P-07-61	Granite (501058): 3 samples
KLX06	P-05-130	Fine-grained diorite-gabbro (505102): 4 samples
KLX07A	P-05-207, P-07-61	
KLX08	P-06-30	
KLX10	P-06-35, P-07-61	
KLX11A	P-06-268, P-07-61	
KLX12A	P-06-71	
KLX13A	P-06-274	
KLX16A	P-07-141	

Data specification	Reference to data report	Usage in Laxemar model version Site (Rock type and no. of samples, where relevant)
<i>Laboratory test of thermal properties</i>		Estimation of thermal conductivity, thermal diffusivity and specific heat capacity.
KAV01	P-04-55	
KAV04A	P-04-270	Ävrö quartz monzodiorite (501046): 33 samples
KSH01A	P-04-53	Ävrö granodiorite (501056): 60 samples
KSH02	P-04-54	Quartz monzodiorite (501036): 63 samples
KA2599G01	R-02-27	Fine-grained dioritoid (501030): 28 samples
KLX02	<i>P-04-258</i>	Diorite-gabbro (501033): 22 samples
KLX03	<i>P-05-93, P-07-62</i>	Fine-grained granite (511058): 4 samples
KLX04	<i>P-04-267</i>	Granite (501058): 3 samples
KLX05	<i>P-05-126, P-07-62</i>	Fine-grained diorite-gabbro (505102): 4 samples
KLX06	<i>P-05-129</i>	
KLX07A	P-05-208, P-07-62	
KLX08	P-06-31	
KLX10	P-06-36, P-07-62	
KLX11A	P-06-269, P-07-62	
KLX12A	P-06-72	
KLX13A	P-06-275	
KLX16A	P-07-144	
Surface	<i>P-05-169</i>	
<i>Modal analysis</i>		Estimation of thermal conductivity from mineralogical composition of the bedrock. Impact of alteration on mineralogy and thermal conductivity.
KAV01	<i>P-04-55</i>	
KAV04A	<i>P-04-270</i>	
KSH01A	<i>P-04-53</i>	Ävrö quartz monzodiorite (501046): 68 samples
KSH02	<i>P-04-54</i>	Ävrö granodiorite (501056): 96 samples
KLX01	<i>Sicada database</i>	Quartz monzodiorite (501036): 41 samples
KLX02	<i>P-04-258</i>	Fine-grained dioritoid (501030): 33 samples
KLX03	<i>Sicada database, field note 676, P-06-07</i>	Diorite-gabbro (501033): 20 samples
KLX04	<i>P-04-267, P-06-07</i>	Fine-grained granite (511058): 10 samples
KLX05	P-07-62	Granite (501058): 6 samples
KLX06	P-06-07	Fine-grained diorite-gabbro (505102): 12 samples
KLX07A	P-06-07, P-07-62	Dolerite (501027): 1 sample
KLX08	P-06-07, P-06-279	
KLX10	P-06-07, P-06-279, P-07-62	
KLX11A	P-06-279, P-07-62	
KLX12A	P-06-279	
KLX15A	P-07-191	
KLX16A	P-07-191	
KLX18A	P-06-279	
KLX19A	P-07-191	
KLX20A	P-06-279	
Surface	P-04-102, P-05-180	

Data specification	Reference to data report	Usage in Laxemar model version Site (Rock type and no. of samples, where relevant)
<i>Laboratory test of thermal expansion</i>		Estimation of the thermal expansion coefficient.
KAV01	P-04-61	Ävrö quartz monzodiorite (501046): 12 samples
KAV04A	P-04-272	Ävrö granodiorite (501056): 37 samples
KSH01A	P-04-59	Quartz monzodiorite (501036): 11 samples
KSH02	P-04-60	Fine-grained dioritoid (501030): 17 samples
KLX02	P-04-260	Diorite-gabbro (501033): 6 samples
KLX03	P-05-95	
KLX04	P-04-269	
KLX05	P-07-63	
KLX07A	P-07-63	
KLX10	P-07-63	
KLX12A	P-07-63	
<i>Field measurements of thermal properties</i>		Field measurements represent a larger scale compared to laboratory measurements, and are used for comparative purposes. Analysis of anisotropy in thermal conductivity.
Surface	P-07-77	Ävrö quartz monzodiorite (501046) and Ävrö granodiorite (501056): 24 samples Quartz monzodiorite (501036): 1 sample Diorite-gabbro (501033): 1 sample

3.2 Determination of thermal transport properties

Thermal conductivity, and in some cases thermal diffusivity, have been determined using the following methods:

- Laboratory measurements using the Transient Plane Source (TPS) method.
- Calculations from mineralogical composition (modal analyses).
- Field measurements.
- Modelling from density logging.

The main purpose of these data is to produce probability distribution models of thermal conductivity for rock types or rock classes (one or more rock types). These models will be used in the subsequent stochastic simulations.

3.3 Thermal conductivity and diffusivity from laboratory measurements

3.3.1 Method

Laboratory measurements of thermal conductivity and thermal diffusivity on rock samples have been performed using the TPS (Transient Plane Source) method at room temperature (c. 20°C). In this method a thin disc (heat generating/temperature measuring) is placed between two pieces of a sample, see description in /Sundberg 2003a/. The 136 measurements available in stage 2.1 /Wrafter et al. 2006/ are supplemented by 96 new measurements, including samples from boreholes KLX05, KLX07A, KLX08, KLX10, KLX11A, KLX12A, KLX13A and KLX16A /Adl-Zarrabi 2006abcdef, 2007ab/. The majority of samples selected for measurement are from rock that is either unaltered or mapped as having faint alteration. About 20 samples are of rock having a degree of alteration higher than faint (weak or medium). These altered samples are mainly of Ävrö granite (501044) and quartz monzodiorite (501036).

3.3.2 Results

Summary statistics of thermal conductivity and thermal diffusivity for each rock type are presented in Table 3-2 and Table 3-3, respectively. The statistics are based on data from the Simpevarp and Laxemar subareas. Data from Äspö Hard Rock Laboratory (Äspö) have been largely excluded from the analysis. An exception is two samples of fine-grained granite (511058) from Äspö, included to supplement the two samples from KLX10 in Laxemar. Data for fine-grained dioritoid are based largely on samples from Simpevarp boreholes, this rock type being much less common in Laxemar. The main improvements of the database compared with the previous model version concern rock types quartz monzodiorite, diorite-gabbro and fine-grained diorite-gabbro.

Ten samples from drill core mapped as quartz monzodiorite (501036) have been excluded after consideration of their densities and appearance. These samples are from boreholes in Simpevarp (KSH01A) and Ävrö (KAV04A) and are deemed not to be representative of quartz monzodiorite in Laxemar. Their high densities (2,840–2,910 kg/m³) suggest that they may belong to the diorite-gabbro group of rocks instead.

Table 3-2. Measured thermal conductivity (W/(m·K)) of samples using the TPS method. Samples are from the Laxemar subarea (KLX boreholes and the surface), the Simpevarp subarea (KAV and KSH boreholes) and Äspö (borehole KA2599G01).

Rock name	Name code	Sample location	Mean	St. dev	Max	Min	Number of samples	Comments (new data since model stage 2.1)
Fine-grained dioritoid	501030	Boreholes KSH01A, KSH02, KLX10	2.79	0.16	3.16	2.51	28	2 new samples
Quartz monzo-diorite	501036	Boreholes KSH01A, KLX03, KLX05, KLX11A, KLX12A, KLX16A and surface.	2.74	0.17	3.30	2.42	63	34 new samples
Ävrö granite	501044	Boreholes KAV01, KAV04A, KLX02, KLX03, KLX04, KLX05, KLX06, KLX07A, KLX08, KLX10, KLX12A, KLX13A	2.88	0.43	3.76	2.01	93	34 new samples
Fine-grained granite	511058	Borehole KA2599G01, KLX10	3.69	0.08	3.76	3.58	4	2 new samples
Granite	501058	Borehole KLX05	3.01		3.11	2.89	3	No new samples
Diorite-gabbro	501033	Borehole KLX05, KLX08, KLX10, KLX12A, KLX13A	2.64	0.46	3.65	2.06	22	11 new samples
Fine-grained diorite-gabbro	505102	Borehole KLX06, KLX11A	2.49	0.24	2.73	2.25	4	All new samples

Table 3-3. Measured thermal diffusivity (mm²/s) of samples using the TPS method. Samples are from the Laxemar subarea (KLX boreholes and the surface), the Simpevarp subarea (KAV and KSH boreholes) and Äspö (borehole KA2599G01).

Rock name	Name code	Sample location	Mean	St. dev	Number of samples	Comments (new data since model stage 2.1)
Fine-grained dioritoid	501030	Boreholes KSH01A, KSH02, KLX10	1.26	0.07	28	2 new samples
Quartz monzodiorite	501036	Boreholes KSH01A, KLX03, KLX05, KLX11A, KLX12A, KLX16A and surface	1.23	0.08	63	34 new samples
Ävrö granite	501044	Boreholes KAV01, KAV04A, KLX02, KLX03, KLX04, KLX05, KLX06, KLX07A, KLX08, KLX10, KLX12A, KLX13A	1.31	0.22	93	34 new samples
Fine-grained granite	511058	Borehole KA2599G01, KLX10	1.81	0.04	4	2 new samples
Granite	501058	Borehole KLX05	1.40	0.12	3	No new samples
Diorite-gabbro	501033	Borehole KLX05, KLX08, KLX10, KLX12A, KLX13A	1.13	0.16	22	11 new samples
Fine-grained diorite-gabbro	505102	Borehole KLX06, KLX11A	1.09	0.16	4	All new samples

Ävrö granite has been previously recognised as bimodal with respect to thermal conductivity /Wrafter et al. 2006/. An investigation of the mineral composition indicates a broadly bimodal quartz content, which has resulted in the subdivision of Ävrö granite into two distinct rock types: Ävrö quartz monzodiorite (501046) and Ävrö granodiorite (501056) /Wahlgren et al. 2008/ (Figure 3-7). The former is quartz poor (commonly < 15%) while the latter is quartz rich (usually > 20%). In the absence of modal analysis, a density of 2,710 kg/m³ has been identified as a suitable threshold value for distinguishing between the two rock types /Wahlgren et al. 2008/. The thermal conductivity and diffusivity statistics for each type are summarised in Table 3-4 and Table 3-5, and a histogram of thermal conductivity values for both types is presented in Figure 3-1. The thermal conductivities of Ävrö quartz monzodiorite and Ävrö granodiorite are clearly differentiated from each other; the distributions show little or no overlap.

Diorite-gabbro (501033) samples have yielded a wide range of thermal conductivity values, from 2.06 W/(m·K) to 3.65 W/(m·K), suggesting that more than one statistical population may be represented (Figure 3-2).

Table 3-4. Measured thermal conductivity (W/(m·K)) of Ävrö quartz monzodiorite (501046) and Ävrö granodiorite (501056) based on samples using the TPS method.

Rock name	Name code	Sample location	Mean	St. dev	Max	Min	Number of samples	Mean density
Ävrö quartz monzodiorite	501046	Boreholes KLX03, KLX04, KLX05, KLX07A, KLX10, KLX12A, KLX13A	2.36	0.20	2.71	2.01	33	2756
Ävrö granodiorite	501056	Boreholes KAV01, KAV04A, KLX02, KLX04, KLX06, KLX07A, KLX08, KLX10, KLX12A, KLX13A	3.17	0.17	3.76	2.81	60	2677

Table 3-5. Measured thermal diffusivity (mm²/s) of Ävrö quartz monzodiorite (501046) and Ävrö granodiorite (501056) based on samples using the TPS method.

Rock name	Name code	Sample location	Mean	St. dev	Max	Min	Number of samples
Ävrö quartz monzodiorite	501046	Boreholes KLX03, KLX04, KLX05, KLX07A, KLX10, KLX12A, KLX13A	1.07	0.13	1.38	0.86	33
Ävrö granodiorite	501056	Boreholes KAV01, KAV04A, KLX02, KLX04, KLX06, KLX07A, KLX08, KLX10, KLX12A, KLX13A	1.45	0.11	1.71	1.16	60

Thermal conductivity: Ävrö quartz monzodiorite (501046); Ävrö granodiorite (501056)

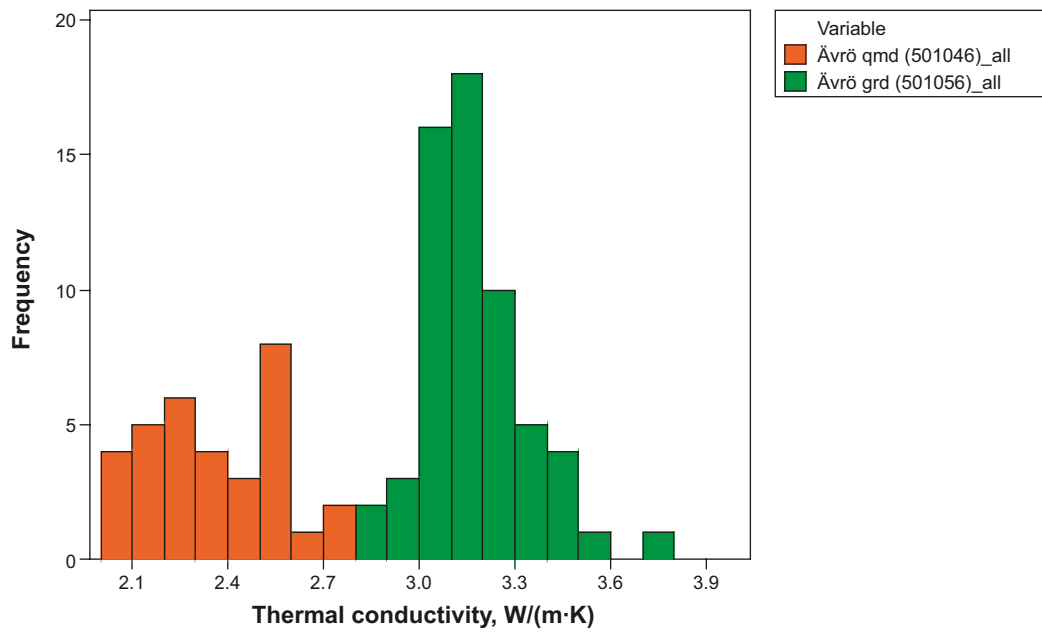


Figure 3-1. Distribution of thermal conductivity values for different varieties of Ävrö granite measured using the TPS method.

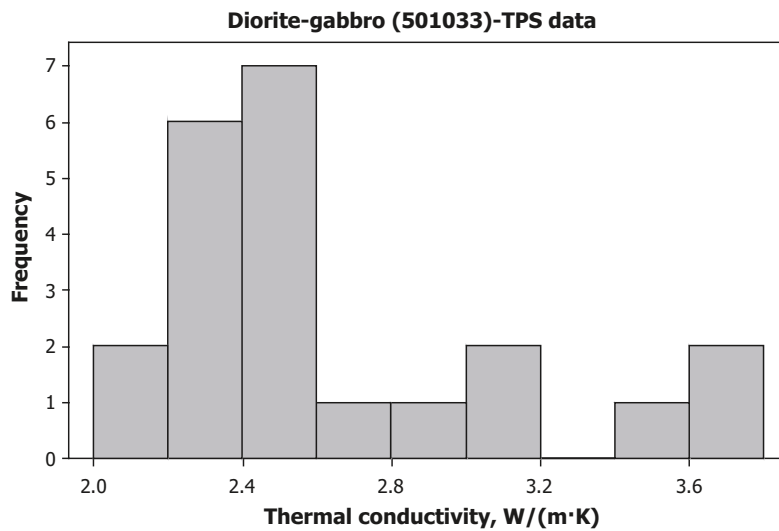


Figure 3-2. Distribution of thermal conductivity values for diorite-gabbro (501033) measured using the TPS method.

The results of all thermal conductivity measurements are plotted against elevation in Figure 3-3 and Figure 3-4. For most rock types, there is no obvious depth dependence in thermal conductivity. Diorite-gabbro does show higher and more variable values above 500 m than below 500 m, although this may be due to the rather low number of samples.

Good spatial coverage has been achieved by the sampling programme for Ävrö granodiorite, Ävrö quartz monzodiorite and Quartz monzodiorite. Samples have been taken from drill cores in several boreholes representing vertical depths varying from 100 m to 750 m. In the case of Quartz monzodiorite, 10 samples were taken at the surface. Many of the samples in boreholes KLX02, KLX03 and KLX04 were taken in groups of approximately 3–5 samples located close to each other. Declustering techniques were applied to evaluate possible bias caused by such a sampling procedure (see Section 5.6.2). A comparison of data from different boreholes (Table 3-6) and different depths (Figure 3-4) indicates little large-scale spatial variation in thermal conductivity for Ävrö granodiorite. The differences between the borehole means are not statistically significant at the 95% confidence level. Too few samples of Ävrö quartz monzodiorite have been taken to calculate meaningful statistics. The data from borehole KLX03 and KLX05 indicate, however, that there may be differences between Ävrö quartz monzodiorite in different parts of the local model volume (Table 3-7). The statistics for thermal conductivity of Quartz monzodiorite for three boreholes as well as the surface are given in Table 3-8. The observed differences in the means are generally not statistically significant at the 95% confidence level. An exception is the surface samples whose mean differs significantly from the means of KLX05 and KLX16A. However, when altered samples are removed from the borehole data the differences are no longer statistically significant.

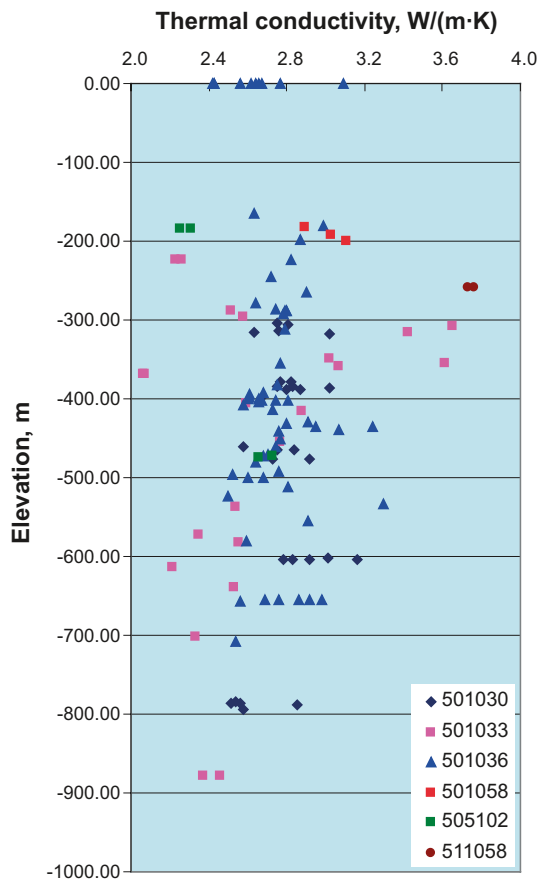


Figure 3-3. Thermal conductivity versus elevation for different rock types. Thermal conductivity measured using the TPS method. For rock type names see Table 1-1.

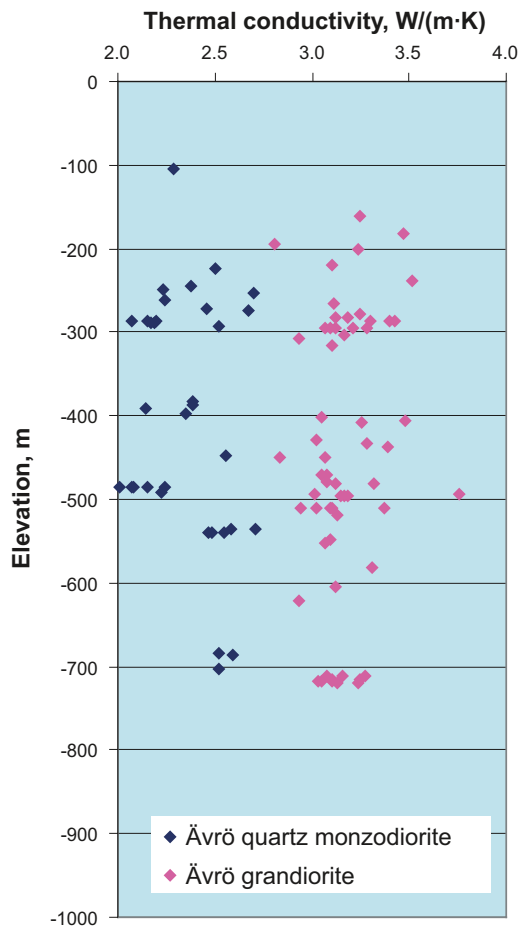


Figure 3-4. Thermal conductivity versus elevation for Ävrö granodiorite and Ävrö quartz monzodiorite. Thermal conductivity measured using the TPS method. Samples from Laxemar boreholes, as well as boreholes KAV01 and KAV04 at Ävrö.

Table 3-6. Measured thermal conductivity of Ävrö granodiorite (501056) using the TPS method. Comparison of samples from boreholes KLX02, KLX04, KLX06, KLX07A, KLX08 and KLX10.

Borehole	KLX02	KLX04	KLX06	KLX07A	KLX08	KLX10
Mean	3.13	3.23	3.32	3.17	3.06	3.20
St. dev.	0.09	0.12	0.17	0.17	0.03	0.15
Number of samples	14	10	5	8	4	6

Table 3-7. Measured thermal conductivity of Ävrö quartz monzodiorite (501046) using the TPS method. Comparison of samples from boreholes KLX03 and KLX05.

Borehole	KLX03	KLX05
Mean	2.18	2.44
St. dev.	0.13	0.15
Number of samples	13*	5

* sampled at 5 borehole locations

Table 3-8. Measured thermal conductivity of Quartz monzodiorite (501036) using the TPS method. Comparison of samples from boreholes KLX05, KLX11, KLX16 and the surface.

Borehole	KLX05	KLX11	KLX16	surface
Mean	2.84	2.71	2.82	2.63
St. dev.	0.22	0.13	0.13	0.20
Number of samples	10	24	6	10

Data for subordinate rock types, fine-grained granite (511058), granite (501058) and fine-grained diorite-gabbro (505102) are rather sparse, which means that the quoted mean and standard deviations are rather uncertain estimates of the population statistics. Given the wide range of thermal conductivities displayed by diorite-gabbro (Figure 3-3), the data set (22 values) may suffer from lack of representativeness.

The degree of alteration has been classified in the Boremap mapping as faint, weak, medium or strong, and is dominated by both oxidation and saussuritisation (Section 2.2). The available data, summarised in Table 3-9, indicates that the thermal conductivity of rock showing a weak or medium degree of alteration is generally higher than that of fresh rock. For Ävrö granodiorite, altered samples indicate a 4% higher thermal conductivity, whereas for Quartz monzodiorite a 15% difference is noted. These calculations are based on rather few data and are, therefore, somewhat uncertain. Little or no difference in thermal conductivity was noted between samples from drill core mapped as faintly altered and samples from core mapped as fresh, although it must be stated that this is based on only a few faintly altered samples. If this is the case, then a possible explanation may be found in the fact that even samples mapped as “fresh” have undergone some degree of alteration, a feature observed in thin section analysis /Drake and Tullborg 2006ab/.

Table 3-9. Comparison of thermal conductivity (W/(m·K)) for fresh and altered rock for rock types Ävrö quartz monzodiorite (501046), Ävrö granodiorite (501056) and quartz monzodiorite (501036) based on TPS measurements.

Rock name	Alteration	Mean	St. dev	Max	Min	Number of samples	Mean density, kg/m ³	Comment on altered samples
Ävrö quartz monzodiorite	Fresh ¹	2.34	0.20	2.71	2.01	31	2,758	Too few altered samples for meaningful comparison.
Ävrö quartz monzodiorite	Altered ²	2.56		2.59	2.52	2	2,723	
Ävrö granodiorite	Fresh ¹	3.15	0.16	3.76	2.81	51	2,678	4% higher thermal conductivity
Ävrö granodiorite	Altered ²	3.27	0.15	3.48	3.05	9	2,675	
Quartz monzodiorite	Fresh ¹	2.71	0.13	3.09	2.42	58	2,788	15% higher thermal conductivity
Quartz monzodiorite	Altered ²	3.11	0.15	3.30	2.95	5	2,787	

¹ Fresh also includes samples of drill core mapped as having faint alteration.

² The altered groups include samples from drill core mapped as having weak or medium alteration.

3.4 Thermal conductivity and diffusivity from field measurements

3.4.1 Method

Field measurements of thermal conductivity and thermal diffusivity on rock outcrops have been performed in the Laxemar subarea /Mossmark and Sundberg 2007/. The primary objective of the investigations is to measure thermal conductivity of rock at a larger scale compared to laboratory measurements. The method used is the multiprobe method described in /Sundberg 1988, Sundberg 2003a, Mossmark and Sundberg 2007/. The principle of the field measurements tests is as follows. A heater probe is placed in a centrally positioned borehole, see Figure 3-5. In two shorter parallel boreholes, located at a short distance from the heater, probes for monitoring temperature during a measurement were installed. As a contact medium between the probes and the rock, bentonite clay was used. Evaluation of the time – temperature relationship is made by single and multiprobe theory. If possible, the probes were oriented according to the results of measurements of magnetic susceptibility (AMS) /Mattsson et al. 2004/ in order to enable further evaluation of anisotropy.

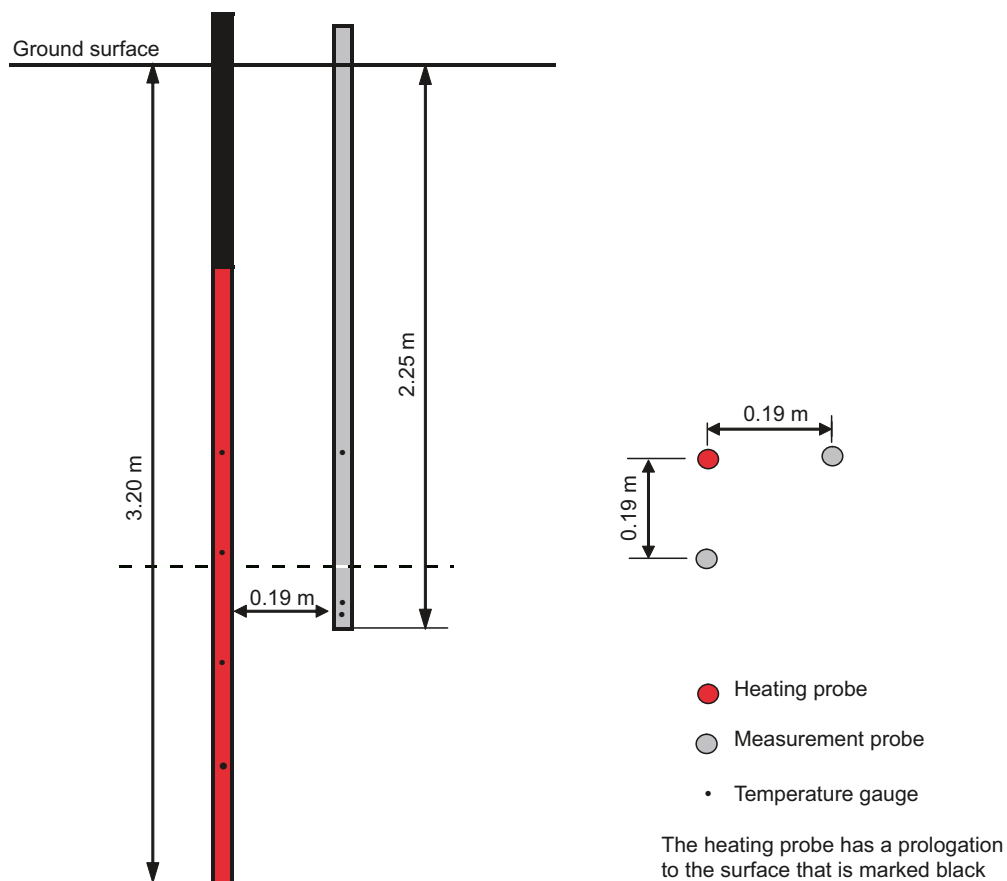


Figure 3-5. Side view of setup of measurement probes after installation for measurement. The extension rod for the heating probe is marked with black colour (the distances are approximate). The second measurement borehole is hidden behind the borehole containing the heating probe /Mossmark and Sundberg 2007/.

3.4.2 Results

The results from the measurements of thermal conductivity are presented in Figure 3-6. The two evaluation methods (single probe and multiprobe) in combination resulted in a total of eight different results for thermal conductivity for each location. A geometric mean has been calculated for the four results from each method in order to establish a large scale value. This has been followed by the calculation of mean of the two methods. The complete set of results from the evaluation of the measurements is presented in /Mossmark and Sundberg 2007/.

As mentioned earlier the Ävrö granite has been subdivided into two varieties, Ävrö quartz monzodiorite and Ävrö granodiorite and the density of 2,710 kg/m³ has been identified as a suitable threshold for distinguishing between the two varieties. The mean thermal conductivity and density for each group is presented in Table 3-10. The higher density group had a mean thermal conductivity of 2.36 (W/(m·K)) while the lower density group had a conductivity of 2.97 (W/(m·K)). The measurement scale of the field measurements can be approximated to 0.2–0.3 m which is substantially larger than for laboratory measurements, which is about 0.05 m.

Table 3-10. Mean density and thermal conductivity of Ävrö quartz monzodiorite and Ävrö granodiorite based on the density division of the Ävrö granite.

Division by density	Number of measurements n	Mean density kg/m ³	Mean thermal conductivity (W/(m·K))	Standard deviation (W/(m·K))
>2,710 kg/m ³ Ävrö quartz monzodiorite	16	2,732	2.31	0.09
<2,710 kg/m ³ Ävrö granodiorite	6	2,672	2.97	0.20

The data set on which the statistics for Ävrö quartz monzodiorite are based exclude sample number 1488 which is interpreted as an outlier. In this respect the summary statistics differ slightly from those given in /Mossmark and Sundberg 2007/. In /Mossmark and Sundberg 2007/ sample 1488 was included whereas sample 1496 was excluded.

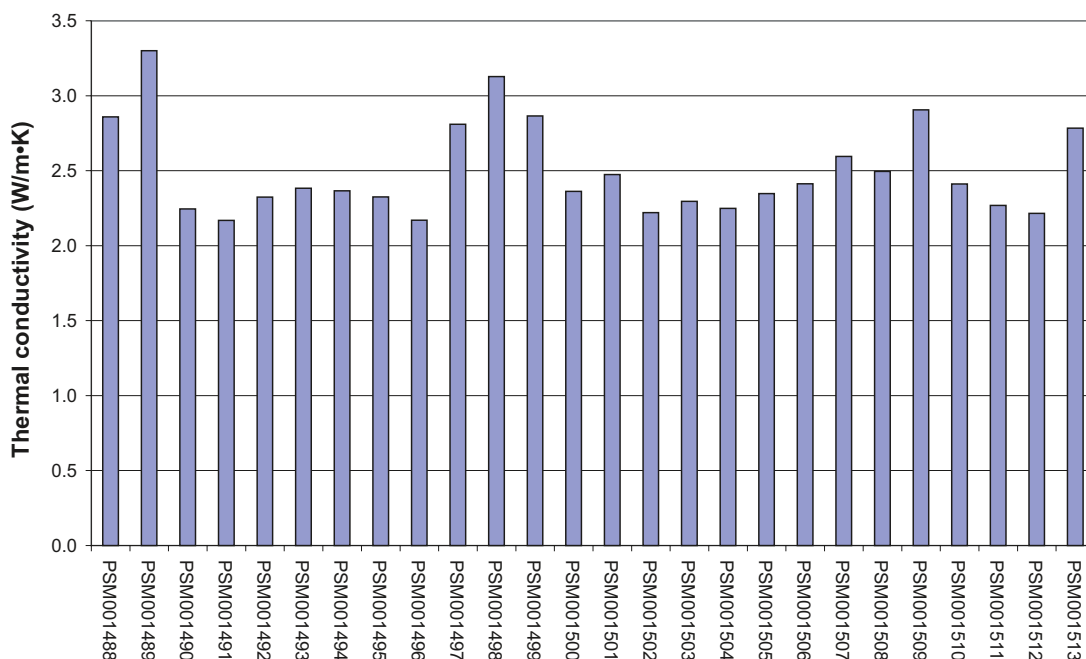


Figure 3-6. Combined results of evaluated thermal conductivity from both the single probe method and the multiprobe methods for the 26 locations where field measurements were carried out /Mossmark and Sundberg 2007/.

A number of uncertainties have been evaluated. For the evaluated thermal conductivity the uncertainties are judged to be small. Uncertainties related to the whole measurement procedure, including installation, gave a standard deviation of 0.03 W/(m·K) for the evaluated thermal conductivity (based on 4 repeated measurements) /Mossmark and Sundberg 2007/.

3.5 Thermal conductivity from mineral composition

3.5.1 Method

The thermal conductivity of rock samples has been calculated by the SCA method (Self Consistent Approximation) using mineral percentages derived from modal analyses and reference values of the thermal conductivity of different minerals, as described in /Sundberg 1988, Sundberg 2003a/. The SCA analyses and the TPS measurements, described in Section 3.3, are approximately at the same scale.

The following data were available for calculations by the SCA-method.

- Modal analyses from samples (c. 200 in total) included in the reporting of site descriptive modelling stage 2.1 for Laxemar /Wrafter et al. 2006/.
- A total of 64 new modal analyses on samples from boreholes KLX03, KLX04, KLX05, KLX07A, KLX08, KLX10, KLX11A, KLX12A, KLX18A and KLX20A. Most of these samples were collected as part of the geological programme /Wahlgren et al. 2006ab, 2007/ and thermal programme /Adl-Zarrabi 2007a/. Some of these samples were taken close to samples for laboratory measurement of thermal properties.

Reference values of thermal conductivity for different minerals, presented in Table 3-11, have been taken from /Horai 1971, Horai and Baldrige 1972/. Values used in the Laxemar modelling stage 2.1 are shown for comparison. The thermal conductivity of plagioclase, olivine and the pyroxenes depends on their chemical composition. For plagioclase, thermal conductivity varies with anorthite content as well as degree and nature of alteration. Therefore, different conductivity values have been used for plagioclase in felsic and mafic rocks, as well as for fresh and altered plagioclase. Based on judgements by /Wahlgren 2007/ and determinations by /Drake and Tullborg 2006b/, an anorthite composition of An 30 is adopted for plagioclase in the granitoid rocks including granites, granodiorites and quartz monzodiorites. For plagioclase in more mafic rocks, for example, diorite and gabbro, an anorthite content of An 50 is assumed.

As a result of alteration, even rock identified and mapped as fresh is generally affected by some degree of alteration; approximately half of the plagioclase in fresh rock is affected by sericitisation/saussuritisation, and approximately 10% of biotite by chloritisation /Drake and Tullborg 2006b/. For samples from drill core mapped as altered (oxidised), plagioclase is almost entirely altered and about half of the biotite is altered to chlorite /Drake and Tullborg 2006ab/. Based on judgements regarding the alteration mineralogy of plagioclase provided by /Drake 2007/ and summarised in Table 3-12, thermal conductivity values of plagioclase in “fresh” granitoid rocks, “fresh” mafic rock and in altered rock have been estimated. For biotite in fresh rock, 10% is assumed to be altered to chlorite. For biotite in altered rock the corresponding figure is 50%. For both plagioclase and biotite, it is obvious that alteration has produced an increase in thermal conductivity. This is particularly the case for chloritised biotite, chlorite (5.15 W/(m·K)) having a much higher thermal conductivity than biotite (2.02 W/(m·K)).

For minerals marked in yellow no reference values of the thermal conductivity have been found and an estimated value of 3.00 W/(m·K) have been used.

Table 3-11. Summary of used thermal conductivity values (W/(m·K)) of minerals used in the modelling /Horai 1971, Horai and Baldrige 1972/.

Mineral	Laxemar 2.1	Laxemar Site
Actinolite	3.45	3.45
Adularia		2.05
Allanite	3.00	3.00
Amphibole	2.81	2.81 ¹
Apatite	1.38	1.38
Biotite	2.02	2.02
Calcite	3.59	3.59
Chlorite	5.15	5.15
Clinopyroxene	4.36	3.82 ²
Epidote	2.83	2.83
Fluorite	9.51	9.51
Garnet	3.35	3.35
Hornblende	2.81	2.81
K-feldspar	2.49	2.49 ³
Magnetite	5.10	5.10
Muscovite	2.32	2.32
Olivine	4.57	4.57
Opaque	3.00	6.6/8.2 ⁵
Orthopyroxene	4.00	4.00 ⁴
Plagioclase: An30	1.70	1.70 ⁶
Plagioclase: An50		1.50 ⁶
Plagioclase: albite (An _{2.5})		2.20 ⁶
Prehnite	3.58	3.58
Pumpellyite	3.00	3.00
Pyroxene	4.00	4.00
Quartz	7.69	7.69
Titanite	2.34	2.34
Topaz	11.24	11.24
Zircon	4.54	4.54
Zoisite	2.15	2.15

¹ Where amphibole is quoted in the modal analyses it is assumed to be hornblende /Wahlgren 2005/.

² Value for augite, the most common forms of clinopyroxene in mafic rocks.

³ Based on microcline, the common form of alkali feldspar in granitoid rocks of Laxemar.

⁴ Mean of Fs 0–Fs 50, the most common compositional range of orthopyroxene in mafic plutonic rocks.

⁵ Mean of values for magnetite and hematite assuming 75% magnetite and 25% hematite in fresh rocks and equal proportions of these minerals in altered rocks (based on interpretation of /Drake and Tullborg 2006b/).

⁶ From curve based on data from Horai 1971. A value of 1.8 for An 30 would be obtained if the curve based on Horai and Baldrige 1972 was used instead.

Yellow: data missing, estimated values.

Orange: unknown chemical composition of the mineral.

Table 3-12. Approximate mineral compositions of altered plagioclase and estimated thermal conductivities.

Rock	Original mineral phase	Altered mineral name	Alteration mineralogy ¹	Estimated λ	λ of original mineral
Fresh granitoid rock	Oligoclase, An 30	Partly saussuritised plagioclase	Oligoclase (54%), albite (27%), adularia (8%), sericite (6%), epidote (2.5%), and prehnite (2.5%)	1.94	1.7 ²
Fresh mafic rock	Andesine-labrador, An 50	Partly saussuritised plagioclase	Andesine-labrador (54%), albite (27%), adularia (8%), sericite (6%), epidote (2.5%), and prehnite (2.5%)	1.82	1.5 ²
Altered rock	Plagioclase	Almost entirely saussuritised plagioclase	Plagioclase (5%), albite (45%), adularia (35%), sericite (10%), epidote (3%), and prehnite (2%)	2.17	1.5–1.7
Altered rock	Plagioclase	Completely saussuritised plagioclase	Albite (47%), adularia (36%), sericite (11%), epidote (3%), prehnite (2%) and hematite (1%).	2.23	1.5–1.7

¹ Based on estimates of the mineral composition of altered plagioclase /Drake 2007/.

² From curve based on data from Horai 1971.

3.5.2 Results

The results of the SCA calculations from mineral composition based on all available modal analyses from the Laxemar and Simpevarp subareas, and arranged according to rock type are presented in Table 3-13. Ävrö granite was divided into two groups based on a quartz content of 18%, which is roughly equivalent to the boundary between granodiorite and quartz monzodiorite on the Streckeisen diagram (20% quartz). It has been shown /Wahlgren et al. 2008/ that the distribution of quartz contents in Ävrö granite is bimodal. Samples with quartz contents between 15% and 20% are relatively uncommon. A plot of the data used in this study is shown in Figure 3-7. Those with contents in this range are generally from the surface in the Simpevarp subarea, and boreholes KLX02 and KLX04 in Laxemar.

Table 3-13. Thermal conductivity (W/(m·K)) calculated from mineralogical compositions (SCA method) for different rock types.

Rock name	Name code	Mean	St. dev	Max	min	Number of samples	Comment
Fine-grained dioritoid	501030	2.64	0.29	3.77	2.16	33	2 altered samples
Quartz monzodiorite	501036	2.74	0.21	3.25	2.40	41	9 altered samples
Ävrö quartz monzodiorite	501046	2.60	0.17	2.27	3.33	68	6 altered samples
Ävrö granodiorite	501056	3.16	0.19	3.76	2.82	96	13 altered samples
Fine-grained diorite-gabbro	505102	2.54	0.15	2.81	2.28	12	
Diorite/gabbro	501033	2.60	0.33	3.72	2.24	20	1 altered sample
Fine-grained granite	511058	3.48	0.32	3.85	2.65	10	
Granite	501058	3.41	0.40	4.02	3.03	6	1 altered sample
Dolerite	501027	2.41				1	

The division of Ävrö granite samples into Ävrö quartz monzodiorite and Ävrö granodiorite is based on a quartz content of 18%.

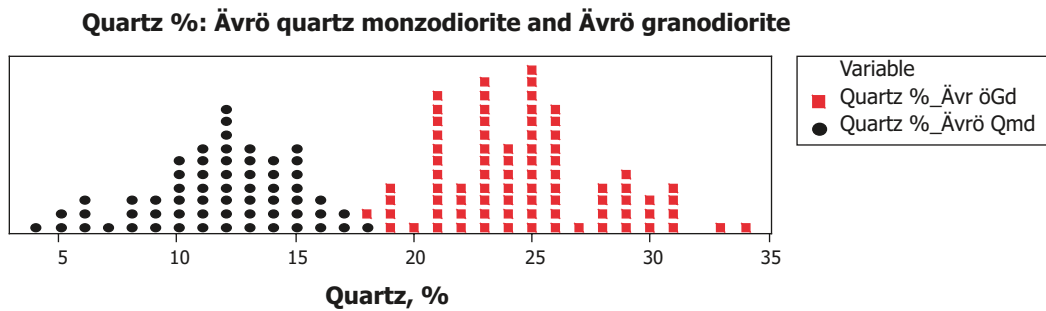


Figure 3-7. Dot plots of quartz content (%) for Ävrö granodiorite and Ävrö quartz monzodiorite. Each dot represents one value.

Figure 3-8 shows the distribution of thermal conductivity values for each variety of Ävrö granite. There is little overlap between the distributions and the overall pattern is similar to that displayed by the TPS data (see Figure 3-1).

Diorite-gabbro displays a wide variation in thermal conductivities measured using the TPS method. SCA calculations from mineral composition show a similar variation. To understand the underlying reasons for this variation, the mineralogy was investigated and compared with calculated thermal conductivities and, where available, even measured thermal conductivities. The results are visualised in Figure 3-9. In Figure 3-10 the plagioclase content is plotted against thermal conductivity values (SCA method). It is concluded that the low conductivity samples are plagioclase-rich, whereas the high-conductivity samples are rich in mafic minerals, such as amphibole (hornblende) and pyroxene.

3.5.3 Influence of alteration on thermal conductivity

Rock affected by alteration makes up approximately 20–25% of the bedrock outside the deformation zones in Laxemar /Wahlgren et al. 2008/. Red staining, referred to as oxidation in the Boremap mapping, is the dominant form of alteration affecting the different types of Ävrö granite (501044), whereas in quartz monzodiorite (501036) alteration classified as saussuritisation and epidotisation are, in addition to oxidation, also abundant. Mineralogical changes associated with alteration can be expected to influence the thermal properties of the rock. As regards the dominant granitoid rocks in Laxemar, i.e. Ävrö granite (501044) and quartz monzodiorite (501036), alteration minerals such as albite, sericite, epidote and chlorite have thermal conductivities that are generally higher than their parent minerals, for example, plagioclase and biotite.

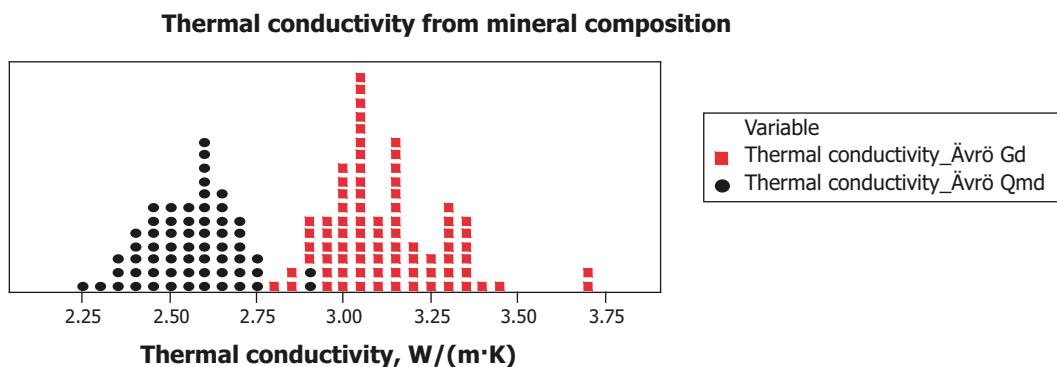


Figure 3-8. Dot plots of thermal conductivity from SCA calculations for Ävrö granodiorite and Ävrö quartz monzodiorite. Each dot represents one value.

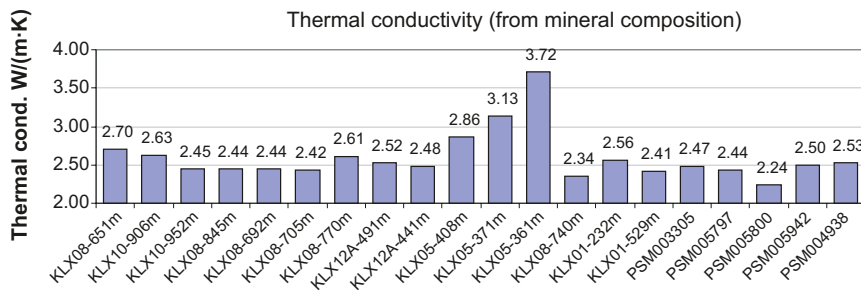
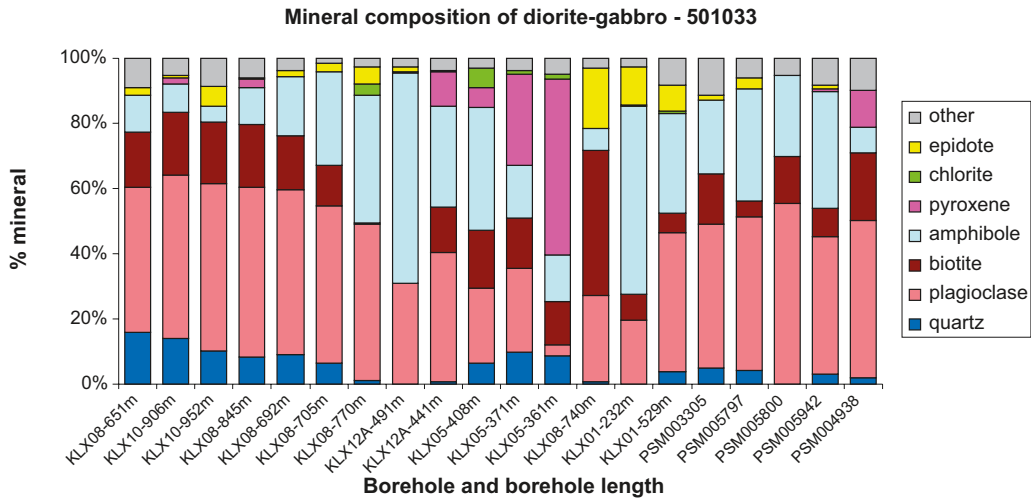


Figure 3-9. Mineral composition of diorite-gabbro samples and (below) thermal conductivity ($W/(m\cdot K)$) calculated by the SCA method for the same samples.

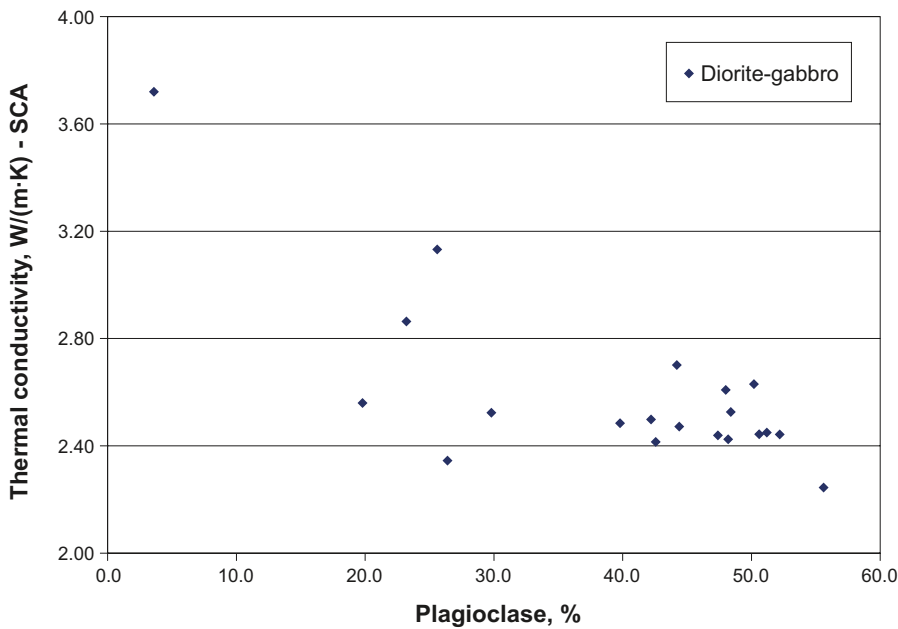


Figure 3-10. Plagioclase content (%) versus thermal conductivity calculated from mineral compositions (SCA method) for diorite-gabbro.

The effect of alteration on rock thermal conductivities was investigated in a couple of different ways. One approach was to compare the calculated thermal conductivity (SCA method) of drill core sample pairs taken in proximity to one another, one of which was fresh the other altered /Drake and Tullborg 2006ab/. Point counting data of altered rock and their unaltered equivalents were evaluated. The calculated thermal conductivities for the altered and unaltered sample pairs comprising rock types Ävrö granite (501044), quartz monzodiorite (501036) and fine-grained dioritoid (501030) are illustrated in Figure 3-11. The rock codes and borehole affinity of each sample are given in Table 3-14. The mean thermal conductivity of the fresh samples is 3.06 W/(m·K), whereas that for the altered samples is 3.22 W/(m·K), which is about 5% higher.

Table 3-14. Boreholes and rock codes for samples in Figure 3-11.

Sample no.	Borehole	Rock code
108	KLX04	501044
137	KLX04	501044
153	KLX04	501044
320	KLX04	501044
630	KLX04	501044
536-2	KSH01A	501030
536-1	KSH01A	501030
100	KSH03A	501036
128	KSH03A	501036
144	KSH03A	501044
172	KSH03A	501036
372	KSH03A	501044
394	KSH03A	501044
661	KSH03A	501044
62	KSH03B	501036
81	KSH03B	501036
82	KSH03B	501036

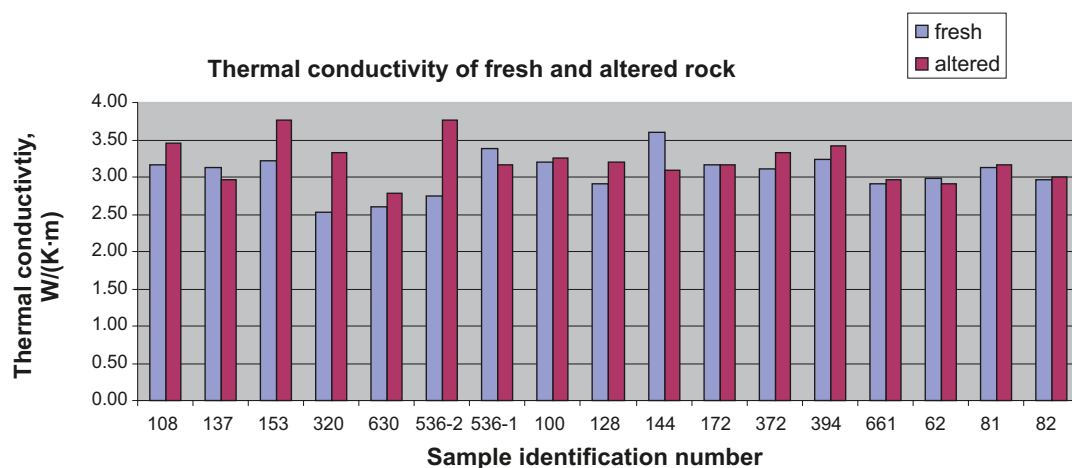


Figure 3-11. Calculated thermal conductivities from mineral composition for fresh and altered sample pairs. Modal analysis data from /Drake and Tullborg 2006ab/.

An alternative approach to evaluating the influence of alteration on thermal conductivity is to compare the mean thermal conductivity of altered samples with that of fresh samples on a rock type basis. In this case all available SCA calculations are used. The thermal conductivity of fresh and altered samples for rock types Ävrö granodiorite (501056), Ävrö quartz monzodiorite (501046) and quartz monzodiorite (501036) are summarised in Table 3-15. According to these SCA calculations, altered rock has between 8 and 14% higher mean thermal conductivity than corresponding fresh rock. These results rely heavily on the assumptions regarding the nature and degree of alteration described in 3.5.1.

Taking into consideration both TPS data (Table 3-9) and SCA data (Table 3-15), and giving both data sets equal weight, altered rock has been estimated to have conductivities that are higher than fresh rock by 6 % for Ävrö granodiorite (501056), 12 % for Ävrö quartz monzodiorite (501046) and 14 % for quartz monzodiorite (501036).

3.5.4 Comparison with laboratory measurements

For several of the drill cores from which samples have been taken for laboratory determination of thermal conductivity (TPS method), sampling for modal analysis and SCA calculations has also been carried out. The objective is to compare determinations from the different methods so as to evaluate the validity of the SCA calculations. In Table 3-16, a comparison of TPS and SCA data is presented on a rock type basis. A comparison of individual samples is illustrated in Figure 3-12. It should be emphasised that the samples are not exactly the same, but come from adjacent sections of the borehole. Therefore, some of the observed differences are probably a result of the sampling.

Table 3-15. Thermal conductivity (W/(m·K)) calculated from mineralogical compositions (SCA method) for fresh and altered samples.

Rock type	Name code	Mean	St. dev	Number of samples	Difference in mean: (altered – fresh)/fresh
Quartz monzodiorite	fresh	2.66	0.13	32	14%
Quartz monzodiorite	altered	3.03	0.19	9	
Ävrö quartz monzodiorite	fresh	2.56	0.13	62	14%
Ävrö quartz monzodiorite	altered	2.93	0.23	6	
Ävrö granodiorite	fresh	3.13	0.17	83	8%
Ävrö granodiorite	altered	3.38	0.18	13	

Table 3-16. Comparison of thermal conductivity of different rock types calculated from mineralogical compositions by the SCA method and measured with the TPS method.

Method	Fine-grained dioritoid (501030)	Quartz monzodiorite (501036)	Ävrö quartz monzodiorite, (501046)	Ävrö granodiorite (501056)	Diorite-gabbro (501033)	Fine-grained diorite-gabbro (505102)
Calculated (SCA): Mean λ , (W/(m·K))	2.69	2.71	2.56	3.16	2.69	2.68
Measured (TPS): Mean λ , (W/(m·K))	2.85	2.78	2.48	3.17	2.72	2.70
Number of sample pairs	5	7	11	19	11	2
Diff. (SCA - TPS)/TPS	-5.7%	-2.5%	3.3%	-0.3%	-1.1%	-0.5%

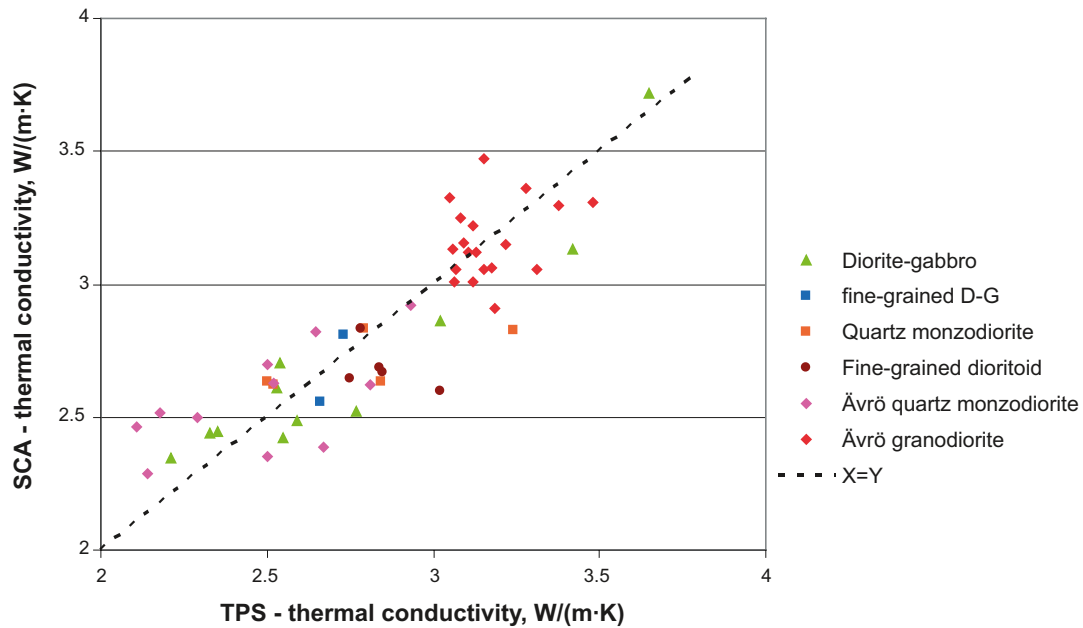


Figure 3-12. TPS versus SCA values for the “same” samples. The line through the data points represents $TPS = SCA$ and is inserted to aid interpretation.

The results indicate a quite a good agreement between the measured (TPS) and calculated thermal conductivity values for most rock types. An exception to this are the samples of Ävrö quartz monzodiorite with thermal conductivities less than 2.3 W/(m·K) as indicated by the TPS data. The SCA values of these four samples overestimate the thermal conductivity by on average 12%. Possible explanations for this are:

1. The degree of alteration assumed in the calculations of “fresh” samples may not be representative for these samples. In other words, they may not have been affected by alteration to the same extent as other Ävrö quartz monzodiorite samples. A lower degree of alteration would mean a lower thermal conductivity for the rock.
2. The anorthite content of plagioclase in this type of Ävrö quartz monzodiorite may be significantly higher than in more quartz rich varieties. This is a reasonable assumption given the quartz poor, mafic-rich nature of some Ävrö quartz monzodiorite. A lower anorthite content would mean a lower thermal conductivity value for plagioclase, and a lower overall thermal conductivity for the rock.

The comparison of SCA results with TPS data indicates that the SCA method yields quite good estimates of the mean thermal conductivities for the different rock types. This is an improvement on previous model versions, when alteration was not taken into account in the SCA determinations.

Table 3-17 presents a comparison of all TPS and SCA data on a rock type basis. The large difference in the mean thermal conductivity determined by the different methods for rock type Ävrö quartz monzodiorite lends further support to the claim made above that the SCA method overestimates the conductivity for this rock type.

Table 3-17. Thermal conductivity (W/(m·K)) of rock types. Comparison of determinations from the TPS and SCA methods.

Rock name	Name code	TPS			SCA		
		Mean	St. dev.	n	Mean	St. dev.	n
Fine-grained dioritoid	501030	2.79	0.16	28	2.64	0.29	33
Quartz monzodiorite	501036	2.74	0.17	63	2.74	0.21	41
Ävrö quartz monzodiorite	501046	2.36	0.20	33	2.60	0.17	68
Ävrö granodiorite	501056	3.17	0.17	60	3.16	0.19	96
Fine-grained granite	511058	3.69	0.08	4	3.48	0.32	10
Granite	501058	3.01		3	3.41	0.40	6
Diorite-gabbro	501033	2.64	0.46	22	2.60	0.33	20
Fine-grained diorite-gabbro	505102	2.49	0.24	4	2.54	0.15	12

3.6 Relationship between thermal conductivity and density

3.6.1 Introduction

A relationship between density and measured (TPS) thermal conductivity for Ävrö granite in Laxemar-Simpevarp are is well established /Sundberg 2003b, Sundberg et al. 2005a, Wrafter et al. 2006, Sundberg et al. 2008a/, and when applied to borehole density logging data, has been used for modelling of thermal conductivity along continuous sections of boreholes /Sundberg et al. 2005a, Sundberg et al. 2006, Wrafter et al. 2006/. A relationship between thermal conductivity and density was also observed for diorite-gabbro /Wrafter et al. 2006/. The observed relationships are consistent with the results of theoretical calculations presented in /Sundberg et al. 2008a/.

Establishing relationships between density and thermal conductivity allows a more reliable use of borehole density data for analysing the spatial correlation structure of thermal properties (Section 5.6.3). In addition, these relationships can be used for deterministically calculating the thermal conductivity of some rock types along continuous sections of borehole (Section 3.7.4).

Laboratory measurements of density have been performed on all the rock samples tested for thermal conductivity reported in Table 3-2. The results of the density measurements are reported in, for example /Liedberg 2007/.

3.6.2 Results

A refined relationship between density and thermal conductivity for Ävrö granite has been developed (Equation 4-1 and Figure 3-13). This relationship is based on all data from the Laxemar subarea as well as two boreholes from the Simpevarp subarea, using both previously reported data together with the results from the recent measurements.

$$y = 3.53E-05x^2 - 0.20146x + 289.810 \quad R^2 = 0.915 \quad \text{Equation 4-1}$$

This equation is valid within the density interval 2,640–2,820 kg/m³.

The relationship between density and thermal conductivity for all other investigated rock types is illustrated in Figure 3-14. For rock types other than Ävrö granite, correlations are not as obviously apparent, perhaps due to the more restricted range of densities. Diorite-gabbro appears to display the reverse relationship between thermal conductivity and density as compared to Ävrö granite. Low density samples have low thermal conductivities (< 2.6 W/[m·K]), whereas high density samples have more variable, but generally higher, conductivities (up to 3.65 W/[m·K]). Furthermore, the marked variation in thermal conductivity displayed by samples with similar

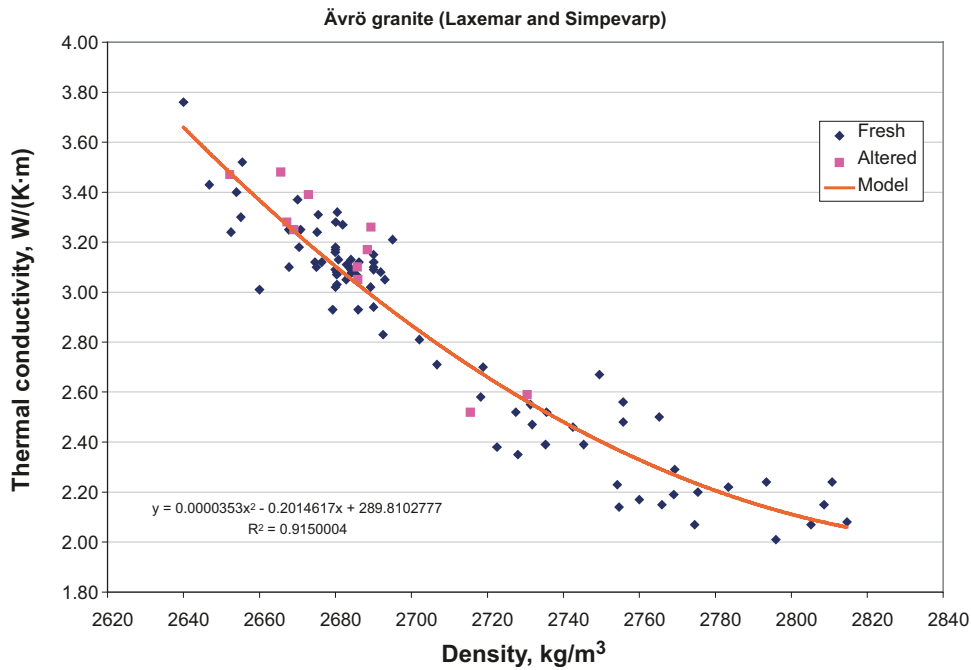


Figure 3-13. Relationships between density and thermal conductivity (TPS measurements) for Ävrö granite. Ävrö granite comprises both Ävrö quartz monzodiorite (density > 2710 kg/m³) and Ävrö granodiorite (density < 2710 kg/m³). Based on linear regression analysis, Equation 4-1 is the relationship used in this study. The model is based on fresh samples only.

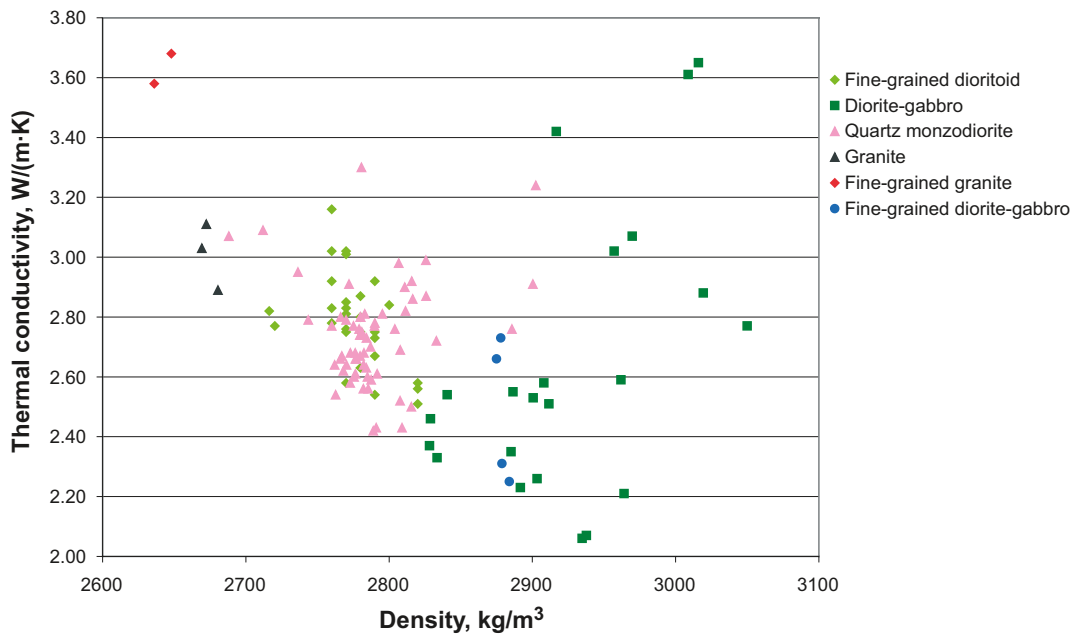


Figure 3-14. Relationships between density and thermal conductivity for rock types other than Ävrö granite.

densities may be partly due to variable degrees of post-magmatic mineralogical changes as a result of, for example, hydrothermal alteration. The observed overall relationship between density and thermal conductivity for all rock types together is consistent with the results of theoretical calculations presented in /Sundberg et al. 2008a/. In their analysis, it was established that, for felsic rocks the thermal conductivity decreases with density, whereas for mafic rocks the opposite relationship applies.

3.7 The use of borehole density logging in thermal modelling

3.7.1 Introduction

Data from borehole logging of density are used to

- Subdivide borehole sections mapped as Ävrö granite into its two constituent rock types: Ävrö granodiorite and Ävrö quartz monzodiorite (Section 3.7.3). The output of this exercise is used as input to the geological simulations.
- Estimate thermal conductivity of rock types for which a relationship with density has been established; see Sections 3.6 and 3.7.4. The thermal conductivity distributions produced by this method are used to provide support for the statistical distribution models (based on much fewer TPS data) used in the simulation of thermal conductivity. The calculations are also used to investigate possible vertical trends in thermal conductivity (Section 3.7.4).
- Investigate the spatial correlation structure of thermal conductivity by variogram analysis (Section 5.6.3). Variogram models are used in the stochastic simulation of thermal conductivity.
- Investigate the representativeness of the thermal data used to characterise and model different rock types (Section 5.6.2).
- Estimate the proportions of subvarieties of some rock types, e.g. diorite-gabbro (Section 5.6.2).

Density logging has been carried out in most cored boreholes in Laxemar. The density logging data described below were re-sampled, calibrated and filtered /Mattsson 2004, 2006abc, Mattsson and Keisu 2005ab, 2006ab, 2007abcde, Mattsson et al. 2005, 2006/.

3.7.2 Quality control of density logs

Because of the importance of density logging data for thermal modelling, the data has been evaluated with regard to their quality. Important aspects are random noise, calibration and bias.

Noise levels vary from as low as 6 kg/m³ to as high as 64 kg/m³ (Table 3-18). Noise levels are above the recommended levels (3–5 kg/m³) for all density logs. Due to the very high noise levels in the data from boreholes KLX02, KLX03 and KLX04, these data have not been used for calculation of thermal conductivity for Ävrö granite (Section 3.7.4) or variogram analysis (Section 5.6.3).

In order to check the quality of the calibration of the density logs, direct density measurements on drill core samples have been compared with density values from borehole loggings for the corresponding borehole positions (Figure 3-15). For thermal modelling purposes, it is primarily for Ävrö granite that accurate calibration is required. To investigate the magnitude of possible bias in the density logs, the difference between the mean measured density and the mean logged density has been calculated on a borehole basis, both for all rock types combined and separately for Ävrö granite (Table 3-19).

The comparison of laboratory measured density with density logs indicates a certain amount of bias in the loggings of the following boreholes: KLX03, 04, 05, 07, 08, 10, 16A and 17A. Some boreholes logs overestimate the “true” density whereas others underestimate the density. At least one borehole, KLX05, displays both types of bias depending on the density range; for densities less than 2,750 kg/m³ the borehole log tends to overestimate the rock densities, whereas the opposite is the case for densities of 2,750 kg/m³ and greater. For boreholes KLX11A, 12A, 13A, and 21B significant bias is not observed. Bias is generally largest in the earlier logged boreholes (up to and including KLX10).

Considering Ävrö granite separately, boreholes KLX02, 03, 04, 05 overestimate the density by about 20 kg/m³, whereas KLX07, 08 and 10 underestimate density by about the same amount. Boreholes 12A, 13A, 17A, 18A and 21B generally show smaller differences between the different methods, although it should be noted that the number of data values is rather low.

Table 3-18. Summary of density loggings in different boreholes.

Borehole	Noise level kg/m ³	Petrophysical data used for calibration ¹	Used for subdivision of Ävrö granite	Comments
KLX02	64	KSH03A,	Yes	Very high noise (not used for variogram analysis or calculation of thermal conductivity for Ävrö granite)
KLX03	23	KLX03	Yes	High noise (not used for variogram analysis or calculation of thermal conductivity for Ävrö granite)
KLX04	21	KSH01A, KSH02, KSH03A, KAV04A	Yes	High noise (not used for variogram analysis or calculation of thermal conductivity for Ävrö granite)
KLX05	14	KLX02, KLX03, KLX04, KSH01A, KSH02, KSH03A, KAV04A	Yes	
KLX07	8	KLX02, KLX03, KLX04, KSH01A, KSH02, KSH03A, KAV04A	Yes	
KLX08	6	KLX10	Yes	
KLX10	6	KLX10	Yes	
KLX11A	9	KFM01D	No	Ävrö granite absent
KLX12A	7	KFM01D	Yes	
KLX13A	13	KLX20A	Yes	
KLX15A	7	KLX20A	No	Ävrö granite absent
KLX16A	8	KLX20A	No	Ävrö granite absent
KLX17A	12	KLX20A	Yes	
KLX18A	12	KLX20A	Yes	
KLX19A	12	KLX20A	No	Ävrö granite absent
KLX20A	18	KLX20A	No	Ävrö granite absent
KLX21B	11	KLX20A	Yes	

¹ the petrophysics data used for calibration given in this table may differ in some cases to those quoted in the geophysical interpretation P-reports /Mattsson 2007/.

3.7.3 Subdivision of Ävrö granite in boreholes on the basis of density logs

Although mapped as a single rock type, Ävrö granite comprises at least two distinct compositional varieties representing magmas which mingled with each other prior to final crystallisation /Wahlgren et al. 2008/. This mingling occurred over a wide range of scales, from the metre scale to a scale of tens or even hundreds of metres. It has been shown that a density value of 2,710 kg/m³ distinguishes the low density Ävrö granodiorite (501056) from the high-density Ävrö quartz monzodiorite (501046) /Wahlgren et al. 2008/. Using this value, density logging data can be used to subdivide Ävrö granite into its constituent types along continuous sections of borehole.

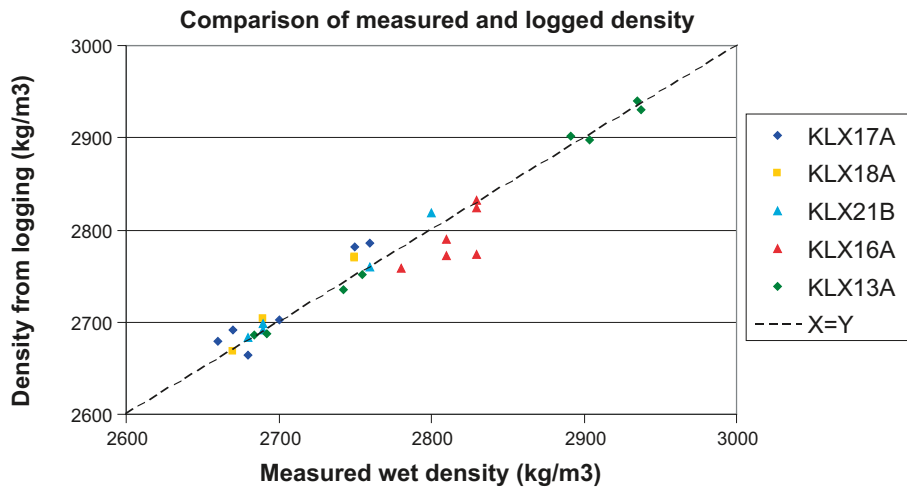
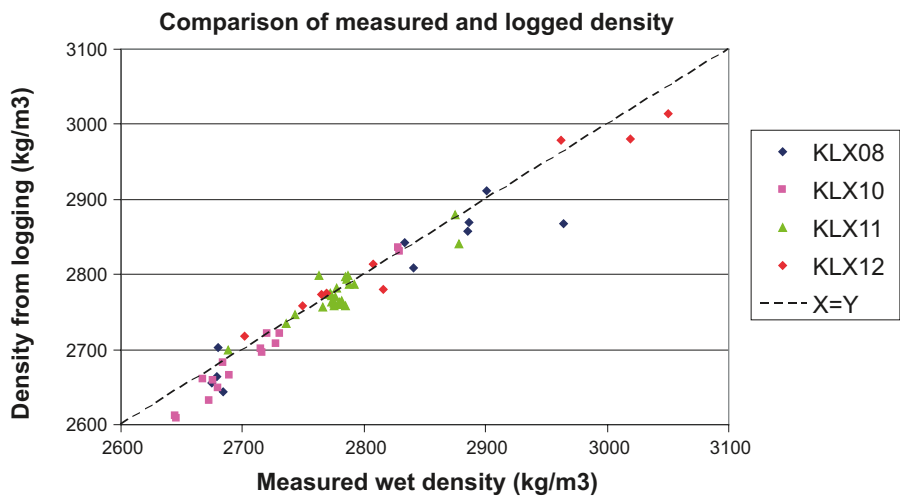
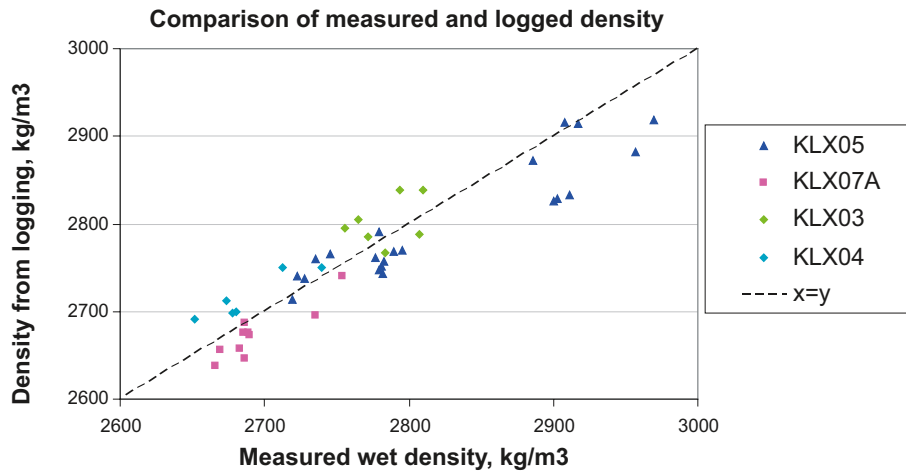


Figure 3-15. Measured density versus logged density for several Laxemar boreholes.

Table 3-19. Comparison of measured density and logged density.

Borehole	Wet density, measured (all rock types)	Density from borehole logs (all rock types)	Number of laboratory samples	Logged density - measured density (all rock types)	Logged density - measured density (Ävrö granite)	Comments on density logs
	mean, kg/m ³	mean, kg/m ³		kg/m ³	kg/m ³ (n - no. of samples)	
KLX02	2,684	2,707	15	23	23 (n=15)	Density logs contain high random noise. Overestimates density. However, based on narrow range of density values.
KLX03	2,784	2,802	18	19	17 (n=13)	Overestimates density. However, based on narrow range of density values.
KLX04	2,689	2,717	15	28	28 (n=15)	Overestimates density
KLX05	2,839	2,812	23	27	14 (n=5)	Overestimates density
KLX07	2,694	2,674	10	-20	-20 (n=10)	Underestimates density
KLX08	2,803	2,782	10	-20	-13 (n=13)	Underestimates density
KLX10	2,709	2,692	15	-16	-18 (n=9)	Underestimates density
KLX11A	2,780	2,775	26	-5		Good correspondence
KLX12A	2,849	2,844	9	-5	10 (n=4)	Good correspondence
KLX13A	2,818	2,816	8	-2	-4 (n=4)	Good correspondence
KLX16A	2,815	2,792	6	-23	(n=0)	Underestimates density. However, based on narrow range of density values.
KLX17A	2,703	2,717	6	14	14 (n=6)	Overestimates density
KLX18A	2,715	2,728	4	13	13 (n=4)	Too few samples to base judgement.
KLX21B	2,724	2,730	5	6	6 (n=5)	Good correspondence

Because of the bias identified in the density logs of some boreholes, adjustments were made to minimise the effect of these errors. These adjustments are listed in Table 3-20. Adjustments were not made to boreholes that showed differences less than 10 kg/m³, had few comparative measured data (< 6), or for which the observed bias was based on a narrow range of density data as, for example, in KLX02 and KLX03.

Table 3-20. Adjustments made to the density logging data for the purpose of dividing Ävrö granite into its different subtypes.

Borehole	Adjustment to density logs – Ävrö granite only	Comment
KLX02	No adjustment made	Density logs contain high random noise.
KLX03	No adjustment made	Bias detected is based on samples having high densities (> 2,750 kg/m ³) which does not imply a similar bias for lower density rocks in the same borehole.
KLX04	Adjustment: -28 kg/m ³	
KLX05	Adjustment: -14 kg/m ³	
KLX07	Adjustment: +20kg/m ³	
KLX08	Adjustment: +15kg/m ³	Adjustment takes even other rock types into account
KLX10	Adjustment: +18kg/m ³	
KLX12A	No adjustments made	
KLX13A	No adjustments made	
KLX17A	Adjustment: -14 kg/m ³	
KLX18A	No adjustments made	
KLX21B	No adjustments made	

In order to perform the subdivision the borehole data required some processing. Three-point moving averages of the 0.1 m density logging data were calculated for Ävrö granite for all boreholes except KLX02 and KLX04. Because of the high random noise present in these boreholes, much stronger filtering was deemed necessary; 15-point for KLX02 and 5-point for KLX04. The purpose of this filtering step is to reduce the frequency of small-scale fluctuations in density caused by random noise. This will reduce the tendency for rocks with densities close to the threshold value of 2,710 kg/m³ to produce small-scale fluctuations between Ävrö quartz monzodiorite and Ävrö granodiorite. Such fluctuations are interpreted as the result of noise in the density data since mingling of the different types of Ävrö granite at the dm-scale is considered very unlikely.

Ävrö granite occurring within large (deterministically modelled) deformation zones has been excluded from the analysis, since the method for dividing Ävrö granite into its two varieties (using a density value of 2,710 kg/m³) is less reliable in rock affected by increased fracturing and porosity, features typical for deformation zones.

The two types of Ävrö granite are assigned the appropriate rock code for each 0.1 m section of borehole. Thereafter, Ävrö quartz monzodiorite and Ävrö granodiorite are treated as separate rock types in the geological simulation work.

3.7.4 Thermal conductivity from density

Based on the relationship between density and thermal conductivity derived for Ävrö granite, as explained in Section 3.6, density values given by the density loggings of boreholes can be used to deterministically assign a thermal conductivity value to each logged decimetre section of Ävrö granite.

Boreholes KLX02, 03 and 04 have been excluded from the analysis because of their high noise levels (Table 3-18). Before calculating thermal conductivity from the density logs, corrections were applied to some borehole density data (KLX05, 07, 08, 10 and 17A) because of bias detected on comparing direct measurements of density with logged density. These corrections are given in Table 3-20. Furthermore, all deformation zones, both major and minor, identified in the extended single-hole interpretation (ESHI) were removed, so as to reduce the risk of introducing bias caused by fractured rock. The relationship shown in Figure 3-13 does not apply to such rock.

For the purposes of calculating thermal conductivity from density loggings, it is assumed that the established relationship, Equation 4-1, is valid for the density interval 2,625–2,850 kg/m³. This range corresponds to the thermal conductivity interval 2.0–3.90 W/(m·K), i.e. slightly outside the interval of measured data. Table 3-21 summarises the results of these calculations on a borehole basis as well as for all boreholes combined.

The results are exemplified by histograms for borehole KLX17A and all boreholes combined in Figure 3-16 and Figure 3-17, respectively. Histograms for the individual boreholes are shown in Appendix A. The histograms display the distribution of thermal conductivity values calculated from density loggings at scale 0.1 m for Ävrö granodiorite and Ävrö quartz monzodiorite separately, as well as both rock types combined. The characteristic bimodality is the most obvious feature of the distributions.

Table 3-21. Thermal conductivity (W/(m·K)) determinations at 0.1 m scale for Ävrö quartz monzodiorite and Ävrö granodiorite from borehole density logging data.

Borehole	Ävrö quartz monzodiorite (501046)		Ävrö granodiorite (501056)	
	Length of borehole, m	Thermal conductivity Mean (st.dev.)	Length of borehole, m	Thermal conductivity Mean (st.dev.)
KLX05	61	2.48 (0.19)	73	3.17 (0.30)
KLX07	179	2.44 (0.16)	302	3.04 (0.17)
KLX08	84	2.55 (0.17)	529	3.10 (0.19)
KLX10	136	2.45 (0.20)	525	3.09 (0.20)
KLX12A	281	2.22 (0.15)	6	3.03 (0.24)
KLX13A	261	2.34 (0.14)	39	3.02 (0.16)
KLX17A	273	2.43 (0.17)	219	3.06 (0.17)
KLX18A	199	2.44 (0.15)	186	3.04 (0.17)
KLX21B	283	2.48 (0.15)	247	3.09 (0.21)
All boreholes	1755	2.40 (0.18)	2,125	3.08 (0.20)

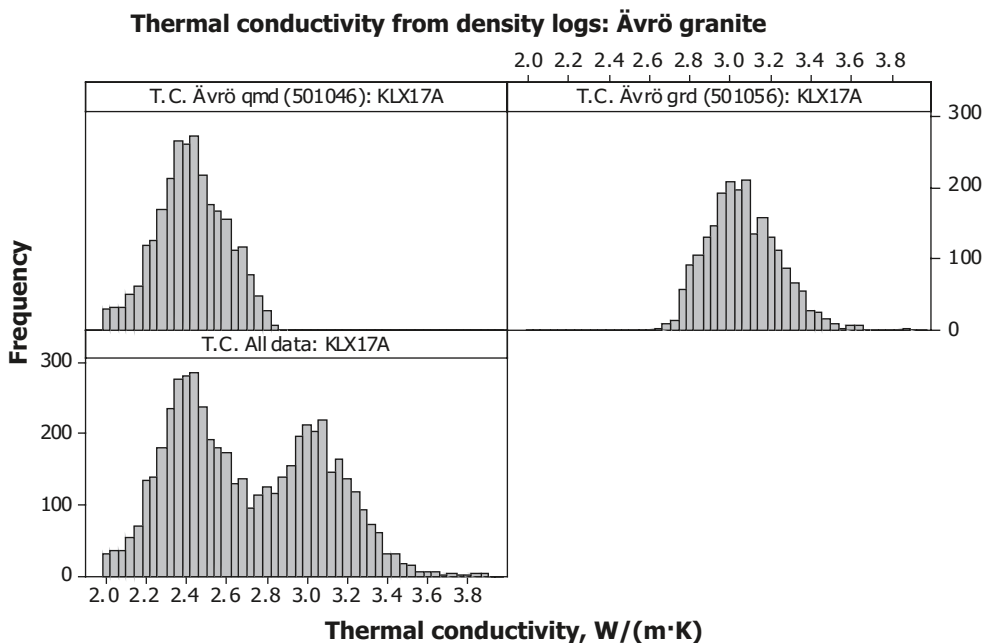


Figure 3-16. Histograms of thermal conductivity for Ävrö quartz monzodiorite (501046), Ävrö granodiorite (501056) and Ävrö granite undifferentiated calculated from density loggings for borehole KLX17A.

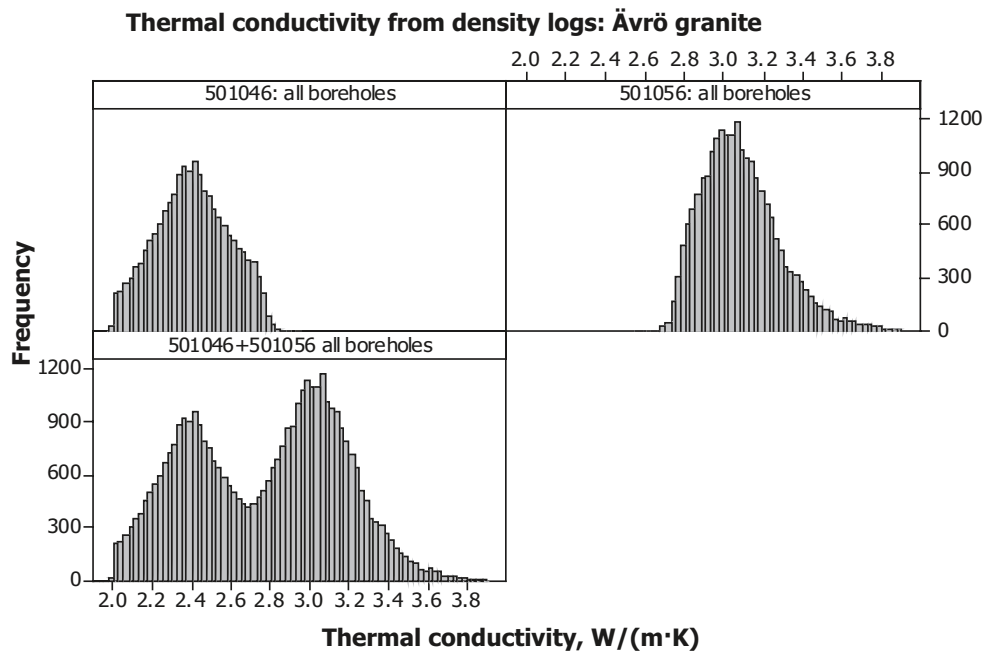


Figure 3-17. Histograms of thermal conductivity for Ävrö quartz monzodiorite (501046), Ävrö granodiorite (501056) and Ävrö granite undifferentiated calculated from density loggings for nine boreholes listed in Table 3-21.

Statistics (mean and standard deviation) of thermal conductivity for Ävrö quartz monzodiorite and Ävrö granodiorite based on density loggings from all boreholes are compared with statistics based on laboratory measurements (TPS) in Table 3-22.

In order to evaluate how well the model in Equation 4-1 reflects the actual thermal conductivity in the borehole, measured samples (TPS) were compared with values estimated from density logging. The results of the comparisons are presented in Figure 3-18. Based on a comparison of data from 44 samples, it was estimated that the calculations from density loggings overestimate the thermal conductivity by on average 0.04 W/(m·K). However, applying the paired t-test to test for a difference in the mean between measured and estimated thermal conductivities showed that the null hypothesis, i.e. that the means are identical, could not be rejected. Thus, based on the available data there is no evidence for any general bias in the thermal conductivity values estimated from density logs. Considering the boreholes separately, there nevertheless appears to be a tendency for some boreholes to either overestimate (e.g. KLX05) or underestimate (e.g. KLX12A) thermal conductivity.

Table 3-22. Thermal conductivity (W/(m·K)) of Ävrö quartz monzodiorite and Ävrö granodiorite based on different methods. Comparison of determinations from the TPS with calculations from density loggings.

Rock name	Name code	TPS: Mean	TPS: St dev.	From density: Mean	From density: St dev.
Ävrö quartz monzodiorite	501046	2.36	0.20	2.40	0.18
Ävrö granodiorite	501056	3.17	0.17	3.08	0.20

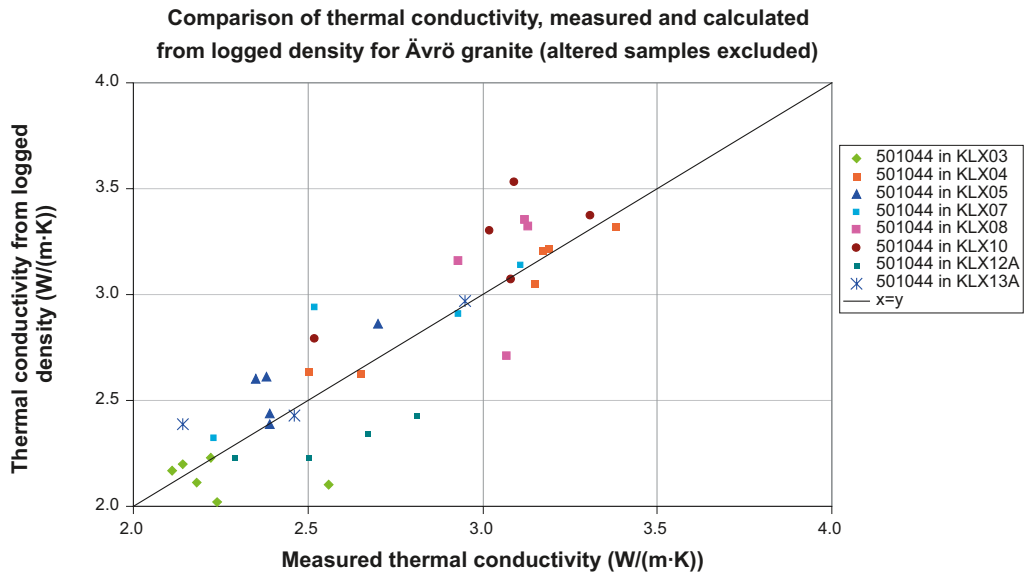


Figure 3-18. Comparison of measured (TPS) thermal conductivity and thermal conductivity calculated from density loggings of Ävrö granite.

Thermal conductivity modelled from density loggings for Ävrö quartz monzodiorite and Ävrö granodiorite has been plotted against vertical depth for several boreholes. The results are exemplified in Figure 3-19 for KLX18A. Plots for other boreholes can be found in Appendix B. The results for all investigated boreholes are plotted together in Figure 3-20. The plotted thermal

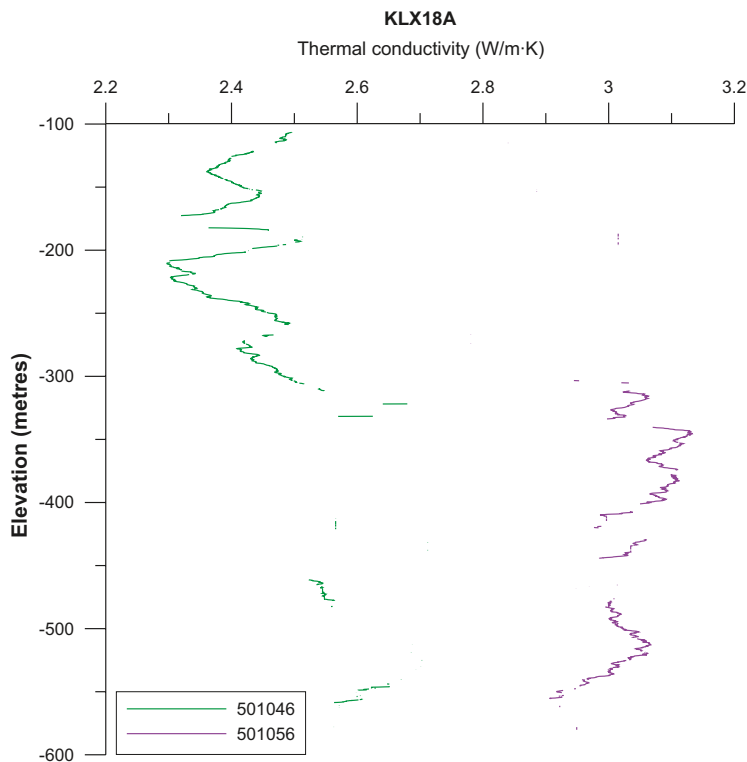


Figure 3-19. Visualisation of large-scale changes in thermal conductivity with depth for Ävrö quartz monzodiorite (501046) and Ävrö granodiorite (501056) in borehole KLX18A. Thermal conductivity is expressed as moving geometric mean calculations for 20 m long borehole sections. Spatial variability is reduced considerably because of this averaging.

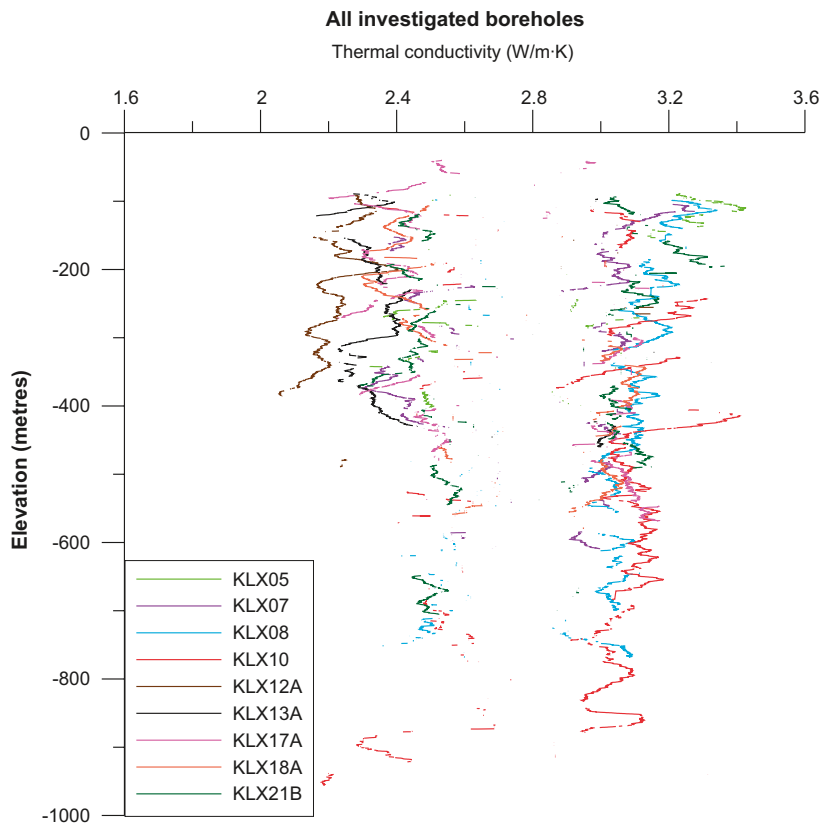


Figure 3-20. Visualisation of large-scale changes in thermal conductivity with depth for Ävrö quartz monzodiorite (501046) and Ävrö granodiorite (501056) in all investigated boreholes. Thermal conductivity is expressed as moving geometric mean calculations for 20 m long borehole sections. Spatial variability is reduced considerably because of this averaging.

conductivity values are geometric mean values for 20 m long borehole sections (moving averages). These plots serve to illustrate large-scale trends in thermal conductivity within the aforementioned rock types. In model stage 2.1, evidence was presented which indicated a possible overall decrease in thermal conductivity with depth with the lowest conductivities found in the depth interval 450 to 600 m /Wrafter et al. 2006/. In that study, the thermal conductivity of all rock types was modelled along the borehole. Data from Ävrö quartz monzodiorite and Ävrö granodiorite in several additional boreholes do not support the previously proposed hypothesis.

3.8 Evaluation of anisotropy of thermal conductivity due to foliation

3.8.1 Introduction

Anisotropy caused by foliation and lineation may occur within a rock type. The foliation and lineation imply a directional orientation of the minerals in the rock mass. The thermal conductivity is generally higher parallel with the mineral foliation and lower perpendicular to the foliation plane. This is because conductive minerals will control the heat flow parallel to the foliation; the minerals extend longer in this plane and are not interrupted to the same extent by less conductive minerals. Perpendicular to the foliation there is a higher density of transitions between different minerals, resulting in less conductive minerals having greater influence. This is accentuated by the crystallographic orientation of the commonly occurring minerals in a rock, such as quartz and biotite. The factor of thermal conductivity anisotropy is defined as thermal conductivity parallel to the foliation divided by thermal conductivity perpendicular to the foliation.

In Laxemar, a faint to weak foliation, which is not uniformly distributed over the area, is commonly present and affects all rock types /Wahlgren et al. 2008/. The intensity of the foliation is significantly less than in the Forsmark area. For this reason measurement of anisotropy on core samples in laboratory have not been included in the thermal investigation programme. The anisotropy has instead been evaluated based on the field measurements with the multi probe method (described in Section 3.4 and in /Mossmark and Sundberg 2007/). However, the primary objective of these measurements was to measure thermal conductivity of rock in the field, at a larger scale compared to laboratory measurements. The measurements were made before a conceptual model was developed of the large scale geometry of the foliation in the Laxemar area. The orientations of the probes in the field measurements are critical to the ability to evaluate anisotropy. However, only at a few sites was the local anisotropy known from AMS (Anisotropy magnetic susceptibility) measurements. At these sites the orientation of the measurements was made according to the strike of the magnetic foliation. At all other sites a general E-W strike of the magnetic foliation was assumed. With the method used here to measure anisotropy, it is not possible to overestimate the anisotropy factor at the scale of measurement.

3.8.2 Analysis

The evaluation of anisotropy of thermal conductivity has been carried using an analytical 3 dimensional equation in a similar way to that described in /Sundberg et al. 2007/. In addition, a simplified 2 dimensional method has been used. Both methods use curve fitting between a measured temperature increase and an analytically calculated temperature curve. The difference between the two methods is small and results presented here are mainly from the evaluation using the 3 dimensional equation.

3.8.3 Results

A presumption for the evaluation of a relevant value of the factor of anisotropy for each location is that the measurements have been carried out parallel and perpendicular to the anisotropy. However, in Laxemar the foliation is weak and hardly visible at the field locations. The orientation of the boreholes for measurements has therefore been made from a general mean value of the strike of the foliation based on measurements of AMS, except for seven locations where a local AMS value is available. The evaluation also assumes that the foliation plane is vertical, parallel to the probes, otherwise the factor of anisotropy is underestimated.

Measurements orientated according to local anisotropy

For the seven locations where thermal measurements in Ävrö granite (Ävrö quartz monzodiorite and Ävrö granodiorite) were carried out where local measurements of AMS have been established reasonably nearby, the mean anisotropy factor for thermal conductivity was 1.10 (Figure 3-21). Some of the measurements have anisotropy factors below one indicating transversal thermal conductivity. At these locations, the boreholes were oriented according to the orientation of the measured AMS (strike of the foliation plane).

Table 3-23 presents the factor of the anisotropy of the thermal conductivity at the seven locations as well as data from the AMS measurements at roughly the same locations, For each location, four AMS measurements had been carried out (except at location PSM007623 where six measurements were conducted). The deviation for the strike and dip in the measurements at each location reflects the degree of local inhomogeneity in the magnetic foliation.

The two locations with the highest factor of anisotropy of thermal conductivity also display the highest degree of AMS. The location with the highest factor of anisotropy of thermal conductivity (PSM001503) has one of the lowest variations for strike and dip of the AMS foliation. The location with the second highest factor of anisotropy (PSM001495) displays dip of the magnetic foliation that for three of the four measurements was steeper than 75 degrees. AMS data for location PSM007623 was not included in /Mattsson et al. 2004/, but were delivered by /Mattsson 2007/.

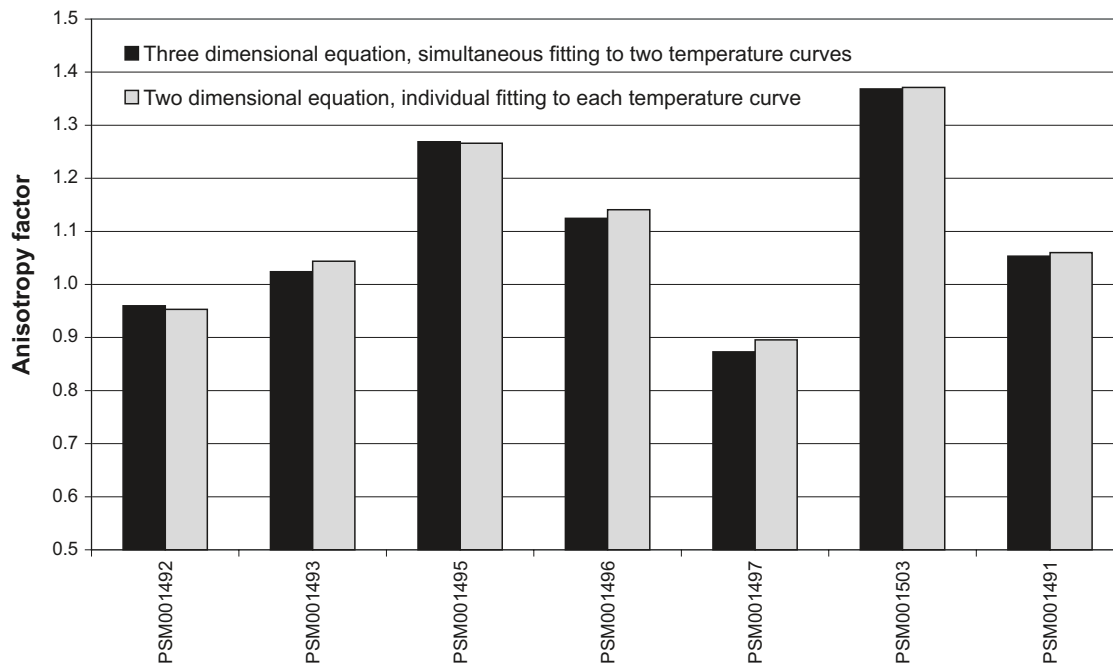


Figure 3-21. Factor of thermal anisotropy for the locations where local measurements of anisotropy of the magnetic susceptibility had been carried out and where the thermal measurements of anisotropy were orientated according to the strike of the foliation plan.

The degree of anisotropy for AMS measurements comprises the foliation and the lineation /Mattsson et al. 2004/. The degree of anisotropy of magnetic foliations was below 1.06 for four of the five measurement locations (Table 3-24). However, at location PSM004310 the degree of anisotropy was 1.158. Near this location, at PSM001503, the highest factor of anisotropy for thermal conductivity was also recorded. The degree of anisotropy of magnetic lineations varied between 1.07 and 1.17 for the five AMS locations. However, there was no evident correlation between the degree of anisotropy of magnetic lineations and the factor of anisotropy for thermal conductivity (Table 3-23 and Table 3-24).

Table 3-23. Factor of anisotropy of thermal conductivity and magnetic susceptibility /Mattsson et al. 2004/ for locations where both thermal conductivity and AMS were measured.

AMS Location ID	Thermal Conductivity Location ID	Factor of anisotropy of thermal conductivity	Degree of anisotropy of the magnetic susceptibility	Range of orientation of foliation	Dip of foliation	Range of dip of foliation
PSM003763	PSM001491	1.05	1.13	132–188	57	42–73
PSM004310	PSM001503	1.37	1.25	243–272	56	51–64
PSM005966	PSM001492	0.96	1.20	8–304	54	25–69
PSM005966	PSM001493	1.02	1.20	8–304	54	25–69
PSM005969	PSM001495	1.27	1.21	116–299	Not determined	35–86
PSM007623*	PSM001496	1.12	1.13	82–268	89	62–88
PSM007623	PSM001497	0.87	1.13	82–268	89	62–88

* No mean is possible to calculate /Mattsson 2008/.

Table 3-24. Degree of anisotropy of magnetic lineations and foliations according to AMS measurements /Mattsson et al. 2004/.

AMS Location ID	Thermal Conductivity Location ID	Degree of anisotropy of magnetic lineation	Degree of anisotropy of magnetic foliation
PSM003763	PSM001491	1.094	1.031
PSM004310	PSM001503	1.077	1.158
PSM005966	PSM001492	1.163	1.033
PSM005966	PSM001493	1.163	1.033
PSM005969	PSM001495	1.153	1.053
PSM007623*	PSM001496	1.088	1.042
PSM007623	PSM001497	1.088	1.042

Measurements orientated according to general anisotropy

For the eleven locations in Ävrö granite which were oriented according to a general direction of the anisotropy of magnetic susceptibility (AMS), the mean anisotropy factor was 0.99. The factor of anisotropy varies between 0.65 and 1.38 for all the twenty locations where anisotropy was evaluated. The mean factor of anisotropy was 1.02.

The variation of the strike of the AMS is considerable according to data presented by /Mattsson et al. 2004/, see Table 3-25. For most of the locations where measurements of the AMS exist, four measurements were carried out (except for PSM007623). The variation between the results of the different determinations of the magnetic foliation plane at each location is also presented in Table 3-25.

The variation in strike of the foliation between the individual measurements (presented as range in Table 3-25) indicates the difficulty to assume a regional direction of the anisotropy. It is anticipated that this difficulty is the reason why the anisotropy factor for thermal conductivity is close to 1.0 for the locations where the general AMS direction was applied.

Table 3-25. Strike and dip of the foliation of the measurements of anisotropy of magnetic susceptibility /Mattsson et al. 2004/. The strike for the foliation of PSM005973 and PSM005974 was not included when calculating the general anisotropy direction.

AMS Location	Foliation			
	Mean strike	Range	Mean Dip	Range
PSM003763	160	132–188	57	42–73
PSM003764	93	78–126	66	52–85
PSM004310	264	243–272	56	51–64
PSM005966	113	8–304	54	25–69
PSM005993	269	254–311	59	55–77
PSM005994	294	126–295	72	61–80
PSM006003	133	124–199	52	10–71
PSM006007	262	256–274	36	33–41
PSM006011	204	196–244	26	20–32
PSM006014	308	141–344	29	29–73
PSM005973*	220	163–254	9	3–19
PSM005974*	107	90–116	48	27–75
PSM007623*	92	82–268	89	62–88

* Data from these locations were not used when calculating a general direction for the foliation strike.

The dip of the foliation varies according to the AMS measurements between 9 and 90 degrees, but in nine of the thirteen locations the foliation is steeper than 45 degrees. Figure 3-22 shows the poles of foliation (minimum axes, perpendicular to the foliation plane) for all the measurements of AMS in Laxemar. The distribution of directions for AMS presented in Figure 3-22 shows the variability in strike and dip for magnetic foliation. The boreholes for the thermal measurements were drilled vertically. However, the dip of the foliation deviates substantially from the vertical for most of the AMS measurements. Consequently, for most locations the boreholes that should represent a perpendicular direction to the foliation plane represent various degrees of intermediate directions. This means that the anisotropy could be underestimated due to deviations in both strike and dip compared to the presumptions in the method (probes situated parallel and perpendicular to the foliation plane).

3.8.4 Summing up

Anisotropy of magnetic susceptibility is governed by the shape and orientation of the magnetite grains, which in turn is considered to reflect the orientation of other more abundant minerals. This preferred orientation of minerals imparts an anisotropy of thermal conductivity to the rock. For seven locations Ävrö quartz monzodiorite and Ävrö granodiorite where measurements of AMS as well as of thermal conductivity have been carried out, the mean anisotropy factor for thermal conductivity was 1.10. The boreholes for measurements of the thermal conductivity had been oriented according to the strike of the AMS measurement at these locations. However, there is an uncertainty in the strike at the site for thermal conductivity since the AMS anisotropy varies locally and the locations for thermal conductivity and AMS measurement may deviate a little from each other.

The two locations with the highest anisotropy factor for thermal conductivity also had the highest degree of anisotropy of the magnetic susceptibility. A correlation between degree of anisotropy of the magnetic foliation and anisotropy for thermal conductivity was observed. However, a correlation between the degree of anisotropy of the magnetic lineation and anisotropy factor for thermal conductivity could not be established (the lineation seems to be weak).

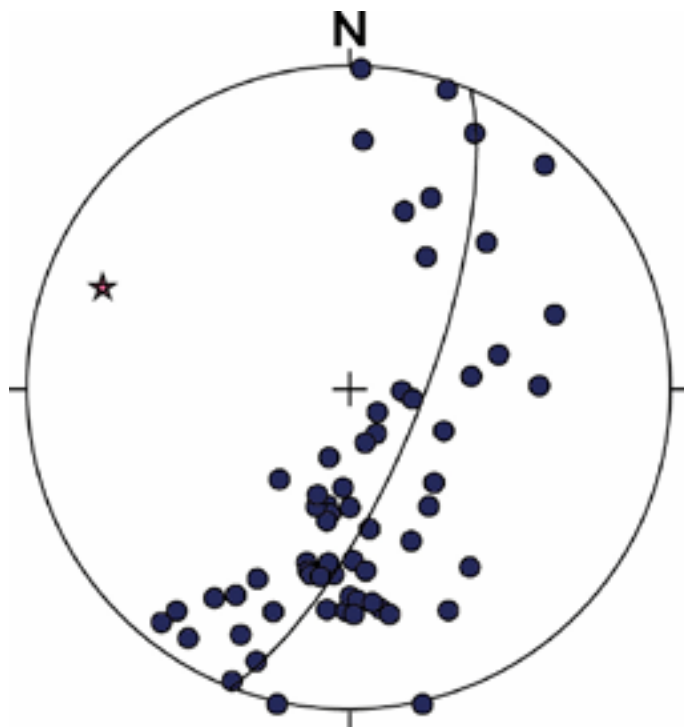


Figure 3-22. Equal area plot (lower hemisphere) of AMS data showing the poles to the magnetic foliation. The star marks the pole to the great circle, i.e. the inferred fold axis. /Wahlgren et al. 2008/.

At each location, four AMS measurements were carried out. At the location with the highest factor of anisotropy for thermal conductivity, the results from the four AMS measurements displayed smaller variations compared to the majority of the AMS locations. A steeper dip of the foliation plane for AMS seemed to correlate with a higher measured anisotropy of thermal conductivity. The boreholes for measurements of thermal conductivity were drilled vertically. If the magnetic foliation deviates from the vertical plane, the measurements of thermal conductivity will correspond to an intermediate orientation (the horizontal) of magnetic foliation (instead of perpendicular to the foliation plane) and the thermal anisotropy will be underestimated. Due to the dip in foliation plane and the uncertainty in strike, the evaluated mean anisotropy factor of 1.10 probably underestimates the real value. Based on the dip of the foliation plane for the different locations a dip-corrected mean anisotropy factor of 1.15 has been estimated, but no compensation has been made for possible uncertainties related to orientation of the strike of the foliation. This factor is of the same order of magnitude as that observed in Forsmark /Back et al. 2007/, a somewhat unexpected result given that the foliation in Forsmark is much more obvious than in Laxemar. The measurements at Laxemar have been made in Ävrö quartz monzodiorite and Ävrö granodiorite only. There are no data available for other rock types. Since the foliation is equally well developed in other rock types, the results relating to anisotropy are judged to be valid for the entire Laxemar area. However, spatially variability in the anisotropy factor can be expected because of the non-uniform distribution of the foliation /Wahlgren et al. 2008/. The foliation generally strikes east-west. The dip of the foliation exhibits an overall trend from shallow to moderate to the north in northern Laxemar (domain RSMA01), to shallow approximately to the south, or subhorizontal, in southern Laxemar (domain RSMD01). In central Laxemar (domain RSMM01) the foliation displays variable dips to the north and south /Wahlgren et al. 2008/. This overall variation in the orientation of the foliation can be expected to produce a corresponding variation in the orientation of anisotropy of thermal conductivity.

For locations of thermal conductivity measurements where no measurements of AMS had been carried out, the boreholes for thermal conductivity had been oriented according to a calculated general AMS direction. At these locations, the mean anisotropy factor for thermal conductivity was 0.99. The direction of AMS varies locally and makes it difficult to assume a general direction of AMS.

3.9 Heat capacity

Heat capacity has been determined indirectly from thermal conductivity and diffusivity measurements using the TPS (Transient Plane Source) method, and directly by calorimetric measurement. Compared to model stage 2.1, the data includes 96 new indirect determinations and 45 direct measurements /Adl-Zarrabi 2006abcdef, 2007ab/. The methods are described in, for example /Adl-Zarrabi 2006d/. For sample locations of the TPS measurements see Table 3-2. Direct calorimetric measurement of heat capacity has been performed on samples from boreholes KLX03, KLX05, KLX07, KLX10, KLX11A, KLX12A and KLX13A.

In Table 3-26 the results from all heat capacity calculations from TPS measurements and from calorimetric measurements are summarised on a rock type basis. Ävrö granite has been divided into Ävrö quartz monzodiorite (501046) and Ävrö granodiorite (501056).

A comparison of direct and indirect methods on the same samples is presented in Table 3-27 and Figure 3-23. Standard deviations are higher for the indirect determinations than for the direct measurement data. Differences in the heat capacity values of up to c. 20% are observed for individual rock samples. However, the average difference between the results of the two methods is less than 1%, which indicates that the calculated values based on TPS determinations, although more uncertain, do not suffer from bias.

Table 3-26. Results of all heat capacity (MJ/m³·K) determinations by the calorimetric method and calculations from TPS measurements.

Rock name	Fine-grained dioritoid	Diorite-gabbro	Quartz monzodiorite	Ävrö quartz monzodiorite	Ävrö granodiorite	Granite	Fine-grained diorite-gabbro	Fine-grained granite
Rock code	501030	501033	501036	501046	501056	501058	505102	511058
TPS								
Mean	2.22	2.34	2.23	2.23	2.20	2.17	2.29	2.04
St. dev.	0.10	0.18	0.102	0.17	0.16		0.12	0.08
N	28	22	63	33	60	3	4	4
Max	2.40	2.65	2.6	2.52	2.50	2.33	2.42	2.12
Min	2.03	1.91	2.00	1.73	1.81	1.89	2.17	1.93
Calorimetric								
Mean		2.44	2.24	2.17	2.12		2.29	
St. dev.		0.04	0.05	0.05	0.10			
N		9	16	9	9		2	
Max		2.52	2.34	2.26	2.25		2.30	
Min		2.38	2.17	2.10	1.91		2.27	

Note that the statistics are based on unweighted data. In other words, no account has been taken of clustered data. However, clustered data is not expected to have a significant effect on the statistics.

Table 3-27. Comparison between heat capacities (MJ/m³·K) calculated from TPS measurement and direct determination by calorimetric method for the same samples.

Rock name	Diorite-gabbro	Quartz monzodiorite	Ävrö quartz monzodiorite	Ävrö granodiorite	Fine-grained diorite-gabbro	All rock types
Rock code	501033	501036	501046	501056	505102	
TPS:						
Mean	2.37	2.22	2.19	2.13	2.20	2.23
St. dev.	0.22	0.10	0.13	0.17		0.164
N	9	16	9	9	2	45
Max	2.63	2.56	2.36	2.42	2.22	2.63
Min	1.91	2.08	1.99	1.89	2.17	1.89
Calorimetric:						
Mean	2.44	2.24	2.17	2.12	2.29	2.24
St. dev.	0.04	0.05	0.05	0.10		0.125
N	9	16	9	9	2	45
Max	2.52	2.34	2.26	2.25	2.3	2.52
Min	2.38	2.17	2.1	1.91	2.27	1.91

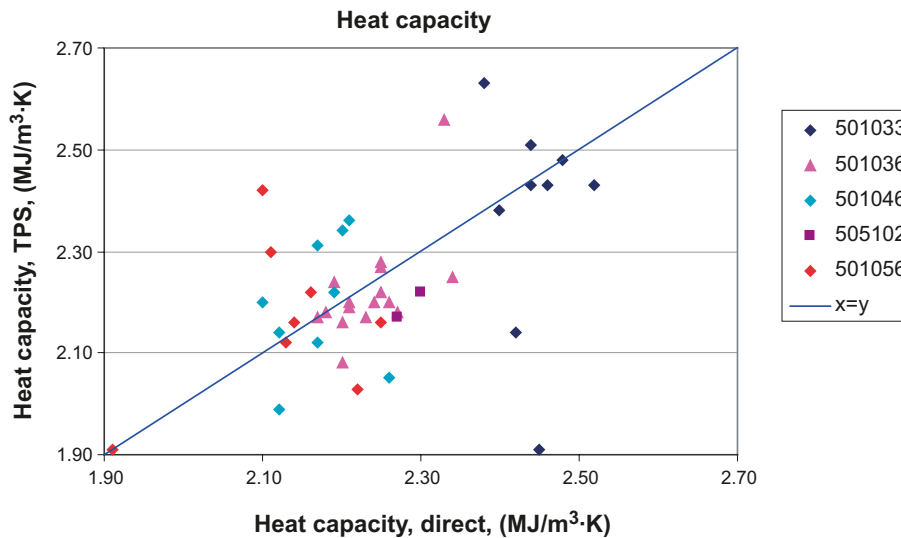


Figure 3-23. Comparison between heat capacities calculated from TPS measurement and direct determination by calorimetric method.

Diorite-gabbro (501033) can be grouped into low and high density types as indicated in Sections 3.6.2 and 5.6.2. Based on results of TPS values, the different types appear to have different heat capacities, see Table 3-28. Given the large uncertainty associated with the TPS determinations (exemplified by the two samples of low density type for which values from both methods are available) it was decided to rely solely on the direct measurements. Based on these data there are no grounds for dividing diorite-gabbro into two groups.

The relationship between thermal conductivity and density was described in Section 3.6. To investigate if a corresponding relationship between heat capacity and density exists, density was plotted against both indirectly and directly determined heat capacity values. Figure 3-24 indicates that individual rock types have a wide range in indirectly determined heat capacity values within a restricted density range. One explanation for this is that these rocks are anisotropic which means that thermal diffusivity determinations vary according to the orientation of the plane of measurement. Figure 3-25 on the other hand shows a more consistent pattern of increasing heat capacity (direct measurements) with increasing density.

Table 3-28. Heat capacities (MJ/m³·K) sub-divided into high and low density variants of diorite-gabbro.

Rock type	Calorimetric		TPS	
	Mean	No. of data	Mean	No. of data
Diorite-gabbro_high dens	2.45	7	2.47	12
Diorite-gabbro_low dens	2.44	2	2.18	10

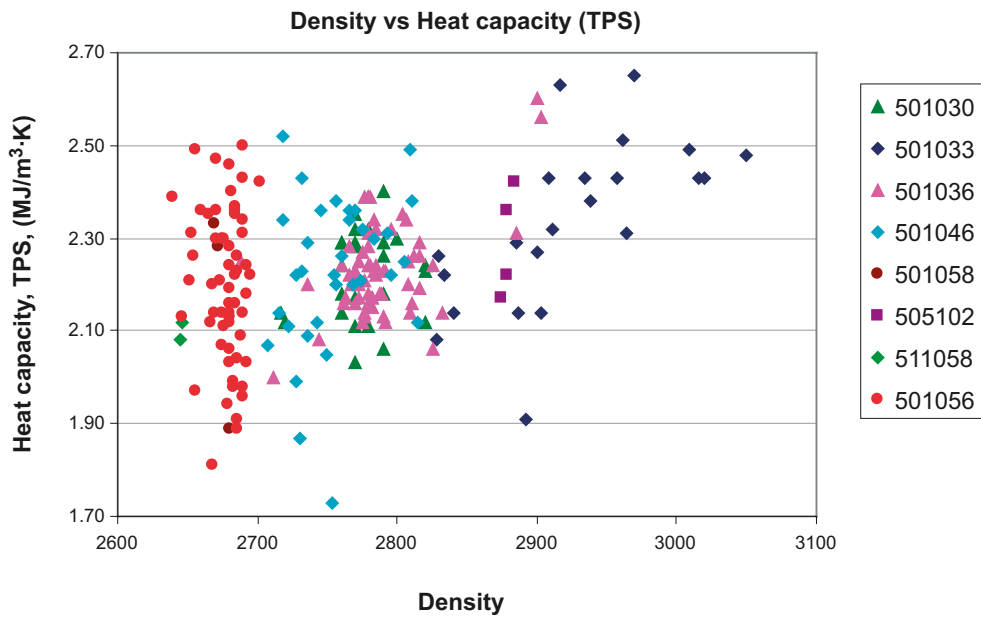


Figure 3-24. Density versus heat capacities calculated from TPS measurement for different rock types.

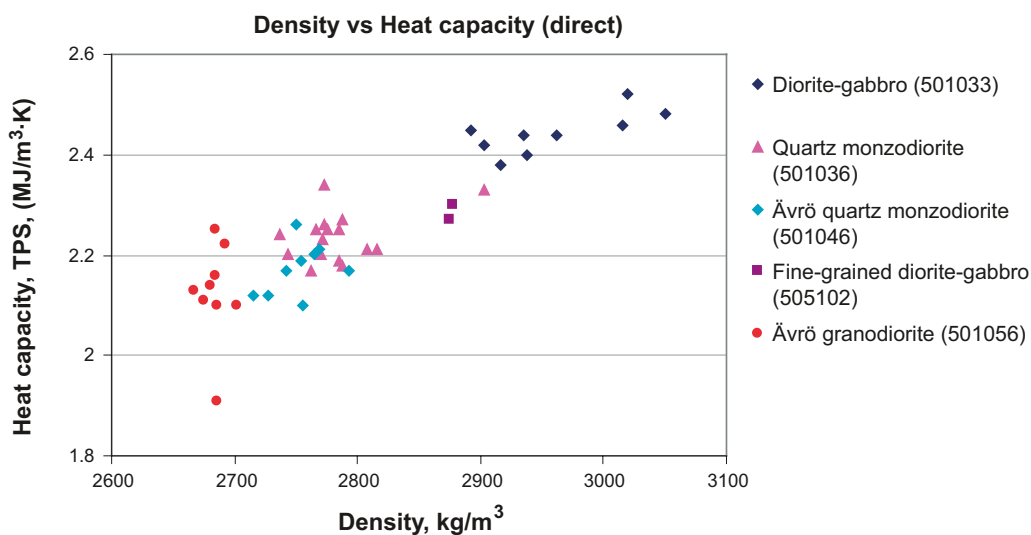


Figure 3-25. Density versus heat capacities (direct measurement) for different rock types.

3.10 Thermal conductivity vs heat capacity

In thermal modelling of Forsmark a relationship between thermal conductivity and heat capacity was established /Sundberg et al. 2008b/. The relationship was described by a second order equation together with a random error component. Applied to the output from simulation of thermal conductivity, heat capacity realisations were created.

However, in Laxemar there are no obvious relationships between thermal conductivity and heat capacity, neither for individual rock types nor for all rock types considered when pooled together (Figure 3-26 and Figure 3-27). Therefore, the approach for modelling heat capacity in Forsmark cannot be mimicked in Laxemar (Section 5.9).

Plots of thermal conductivity versus heat capacity are shown below, both for indirect (Figure 3-26) and direct (Figure 3-27) heat capacity data. In these plots Ävrö granite has been divided into its varieties Ävrö quartz monzodiorite (501046) and Ävrö granodiorite (501056).

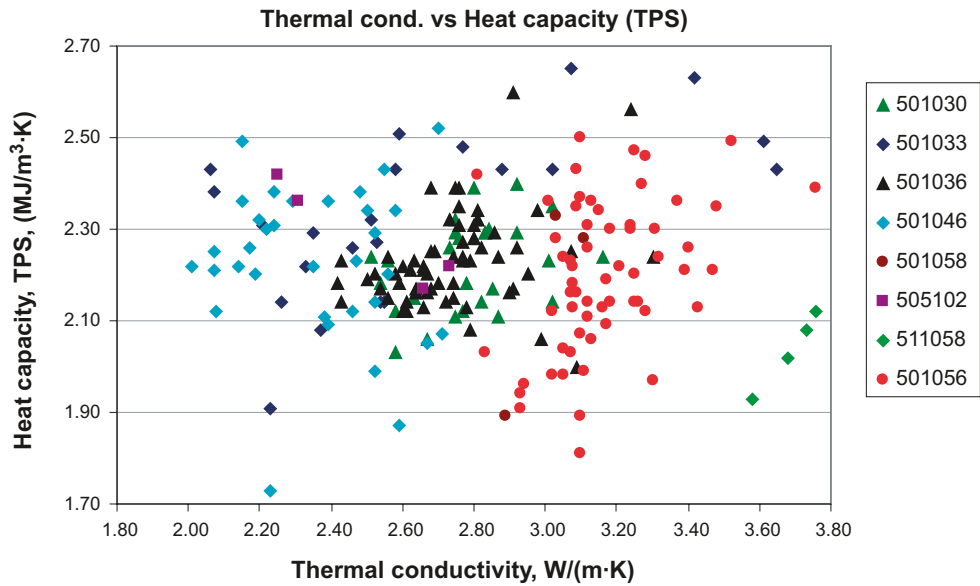


Figure 3-26. Thermal conductivity versus heat capacity. Heat capacity is calculated from TPS determinations.

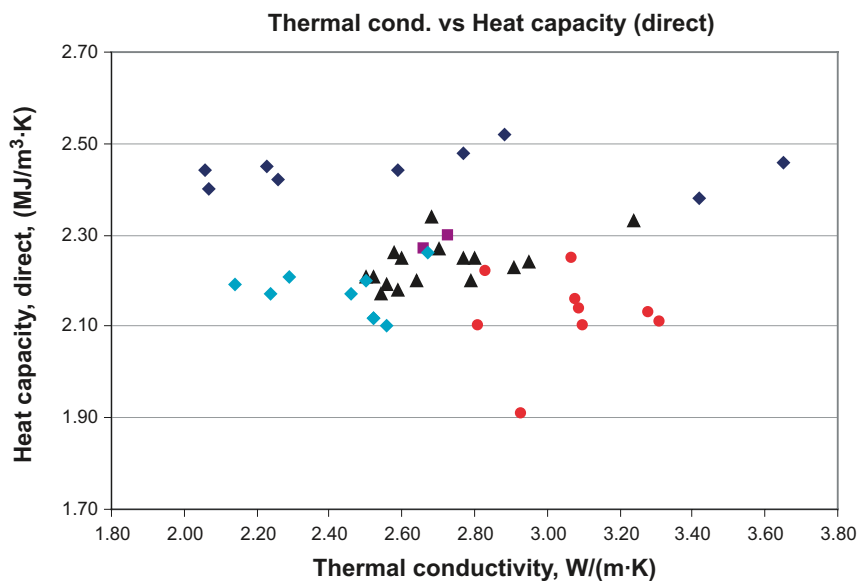


Figure 3-27. Thermal conductivity versus heat capacity. Heat capacity is determined by calorimetric measurements.

3.11 Temperature dependence in thermal properties

The temperature dependence of thermal conductivity and heat capacity has been investigated by laboratory measurements for four rock types: fine-grained dioritoid (501030) and quartz monzodiorite (501036) at three different temperatures (20, 50 and 80°C), Ävrö granodiorite (501056) at three different temperatures (20, 50 and 80°C) for four samples and at four different temperatures (25, 40, 60 and 80°C) for one sample, and Ävrö quartz monzodiorite (501046) at three different temperatures (20, 50 and 80°C) for five samples and four different temperatures (25, 40, 60 and 80°C) for three samples. Results are presented in /Adl-Zarrabi 2004abcd, Sundberg 2002/. All above mentioned measurements have been discussed in earlier site descriptions /Sundberg et al. 2005a, Sundberg et al. 2006/. Rock types Ävrö quartz monzodiorite and Ävrö granodiorite have earlier been named as Ävrö granite.

For the rock type diorite-gabbro (501033) no measurements of site specific samples have been made. However, results from measurements have been found in literature for gabbro /Mottahgy et al. 2005/. In this investigation one sample was used for measuring thermal properties at different temperatures.

Results for temperature dependence of thermal conductivity for fine-grained dioritoid (501030) and quartz monzodiorite (501036) are presented in /Sundberg et al. 2005a/. Figure 3-28– Figure 3-30 presents results for Ävrö granodiorite, Ävrö quartz monzodiorite and gabbro. In Table 3-29 the thermal dependence of thermal conductivity for the five different rock types is summarised.

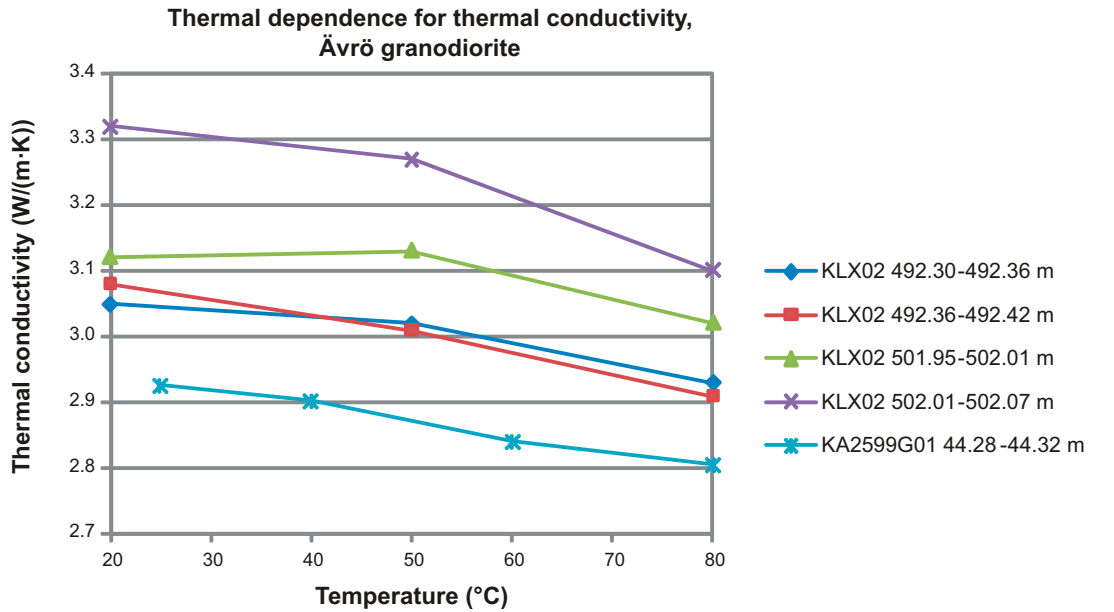


Figure 3-28. Temperature dependence for thermal conductivity, rock type Ävrö granodiorite (501056).

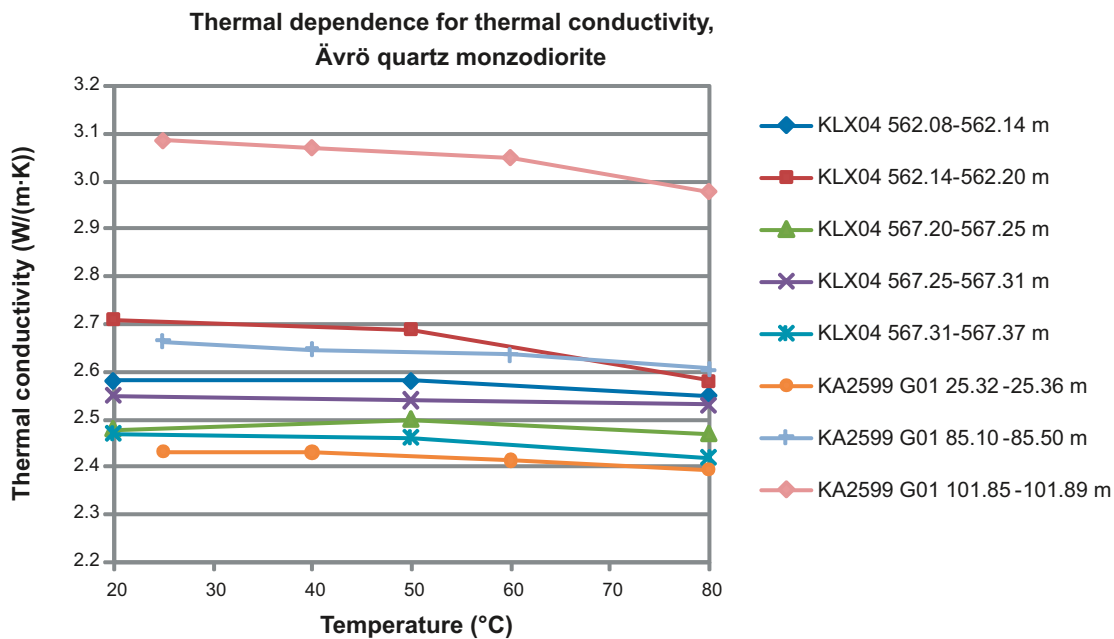


Figure 3-29. Temperature dependence for thermal conductivity, rock type Ävrö quartz monzodiorite (501046).

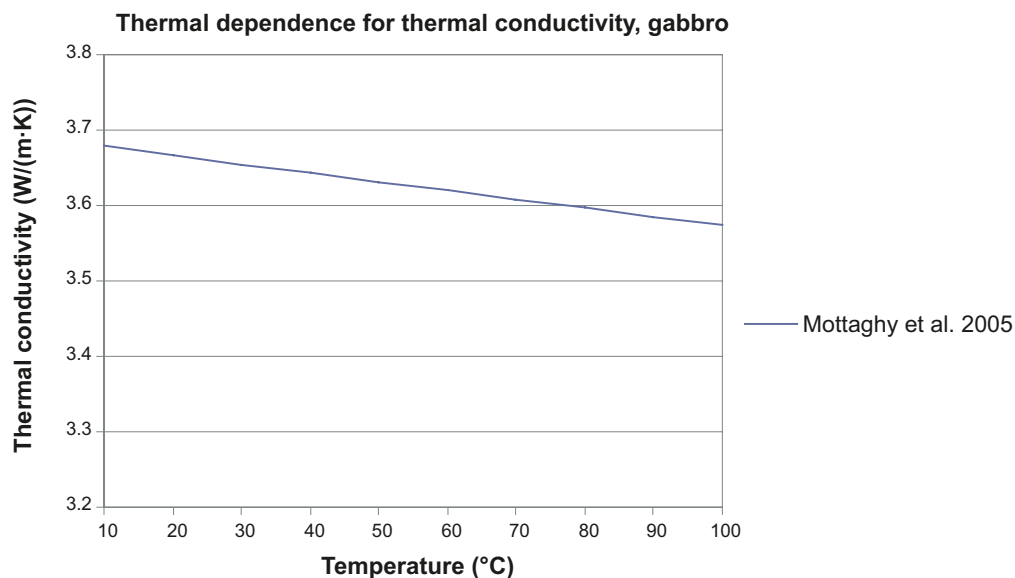


Figure 3-30. Literature data on temperature dependence for thermal conductivity for gabbro /Mottaghy et al. 2005/.

Table 3-29 Temperature dependence of thermal conductivity (per 100°C temperature increase) for different rock types. Mean value of temperature dependence calculated by linear regression.

Rock name	Sample location	Mean	St. dev	Number of samples
Fine-grained dioritoid (501030)	Boreholes KSH01A and KSH02	-3.4%	1.6%	11
Quartz monzodiorite (501036)	Borehole KSH01A	-1.1%	1.1%	5
Ävrö quartz monzodiorite (501046)	Boreholes KLX04 and KA2599G01	-2.9%	3.3%	8
Ävrö granodiorite (501056)	Boreholes KLX02 and KA2599G01	-6.8%	3.6%	5
Fine-grained granite (511058)	Estimated from similar rocktypes in Forsmark /Sundberg et al. 2008b/	-10%	–	–
Gabbro	Literature data /Mottaghy et al. 2005/	-3.1%	–	1

Temperature dependence of heat capacity for fine-grained dioritoid (501030) and quartz monzodiorite (501036) are presented in /Sundberg et al. 2006/. Results for Ävrö quartz monzodiorite (501046), Ävrö granodiorite (501056) and gabbro are shown in Figure 3-31–Figure 3-33. Results for all five rock types are presented in Table 3-30.

Table 3-30. Temperature dependence of heat capacity (per 100°C temperature increase) on samples from different rock types. The mean of the temperature dependence is estimated by linear regression.

Rock name (name code) (sample location)	Mean	St. dev	Number of samples
Fine-grained dioritoid (501030) (boreholes KSH01A and KSH02)	25.6%	3.51%	11
Quartz monzodiorite (501036) (borehole KSH01A)	25.3%	3.30%	5
Ävrö quartz monzodiorite (501046) (Boreholes KLX04 and KA2599G01)	26.0%	7.04%	8
Ävrö granodiorite (501056) (boreholes KLX02 and KA2599G01)	23.8%	2.92%	5
Fine-grained granite (511058) (estimated from similar rocktypes in Forsmark /Sundberg et al. 2008b/)	25%	–	–
Gabbro (litterature data /Mottaghy et al. 2005/)	20.6%	–	1

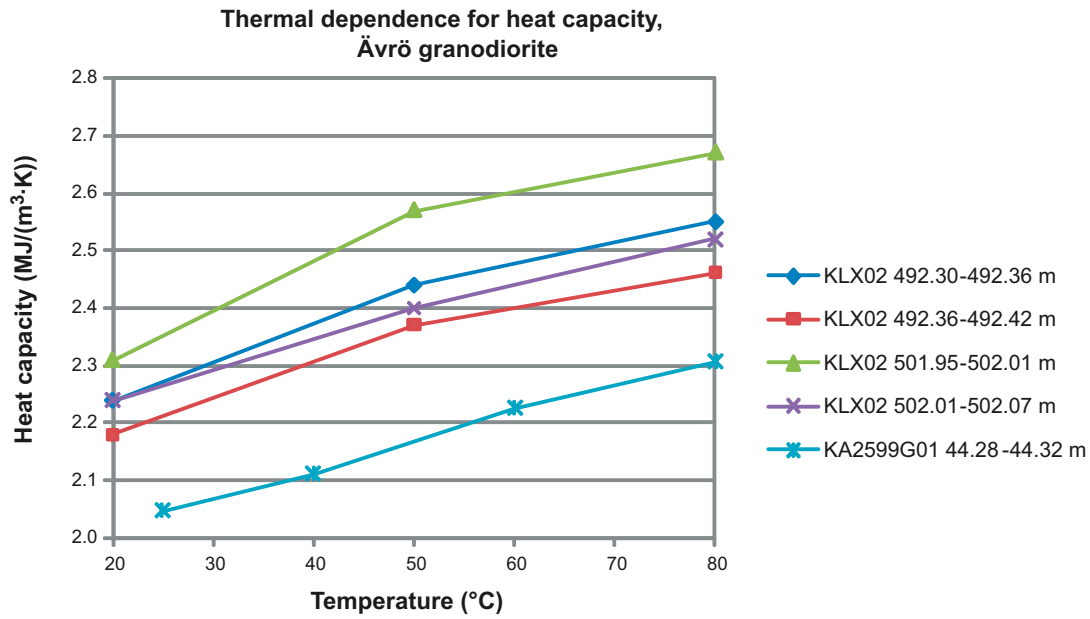


Figure 3-31. Temperature dependence for heat capacity, rock type Ävrö granodiorite (501056).

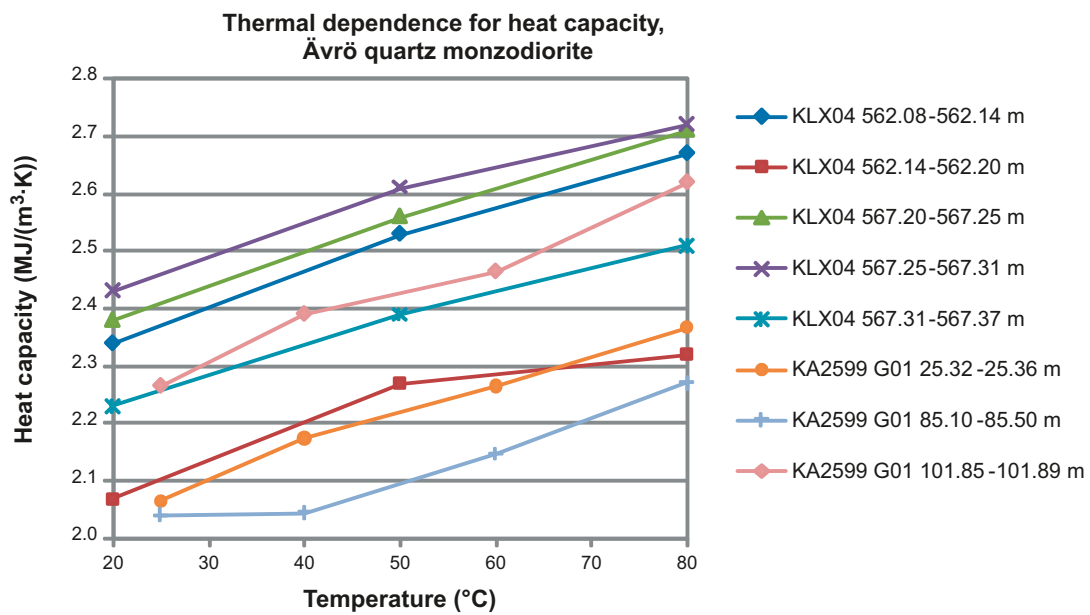


Figure 3-32. Temperature dependence for heat capacity, rock type Ävrö quartz monzodiorite (501046).

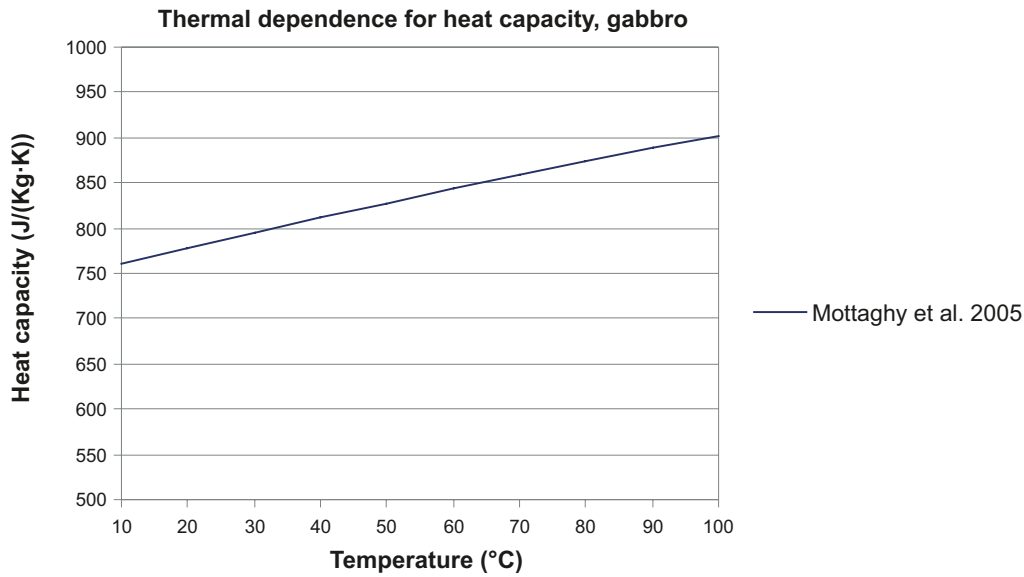


Figure 3-33. Literature data on temperature dependence for heat capacity for gabbro /Mottaghy et al. 2005/. Observe that heat capacity is determined as J/(Kg·K).

Table 3-32 summarises the mean temperature coefficients for different rock types. Thermal conductivity and heat capacity at elevated temperature (above room temperature, approximately 20°–25°C) can be calculated from Equation 3-1 and Equation 3-2.

$$\lambda_1 = \lambda_0(1 + \alpha_\lambda(T_1 - T_0)) \quad \text{Equation 3-1}$$

$$C_1 = C_0(1 + \alpha_C(T_1 - T_0)) \quad \text{Equation 3-2}$$

Where,

- λ_0 Thermal conductivity at room temperature T_0 , W/(m·K)
- λ_1 Thermal conductivity at elevated temperature T_1 , W/(m·K)
- C_0 Heat Capacity at room temperature T_0 , MJ/(m³·K)
- C_1 Heat Capacity at elevated temperature T_1 , MJ/(m³·K)
- α_λ Temperature coefficient for thermal conductivity, 1/°C
- α_C Temperature coefficient for heat capacity, 1/°C

Table 3-31. Summarised mean temperature coefficients for thermal conductivity and heat capacity in different rock types and TRC. TRCs are defined in Table 5-2.

Name code	Rock name	TRC	Thermal conductivity temperature coefficient, α_λ 1/°C	Heat capacity temperature coefficient, α_C 1/°C	Comments
501030	Fine-grained dioritoid	30	$-3 \cdot 10^{-4}$	$2.6 \cdot 10^{-3}$	
501036	Quartz monzodiorite	36	$-1 \cdot 10^{-4}$	$2.5 \cdot 10^{-3}$	
501046	Ävrö quartz monzodiorite	46	$-3 \cdot 10^{-4}$	$2.6 \cdot 10^{-3}$	
501056	Ävrö granodiorite	56	$-7 \cdot 10^{-4}$	$2.4 \cdot 10^{-3}$	
511058	Fine-grained granite	58	$-10 \cdot 10^{-4}$	$2.5 \cdot 10^{-3}$	Estimated from similar rock types in Forsmark /Sundberg et al. 2008b/.
	Gabbro	33 102	$-3 \cdot 10^{-4}$	$2.1 \cdot 10^{-3}$	Literature data /Mottaghy et al. 2005/

3.12 Pressure dependence on thermal conductivity

The thermal conductivity is expected to be lower for stress-released samples compared to determinations at higher pressure (greater depths). The reason is assumed to be the closing of micro cracks. However, the pressure influence up to 50 MPa seems to be low if the samples are water saturated, approximately 1–2% /Walsh and Decker 1966/. The pressure dependence after closing of fractures can be estimated to approximately 0.5–1%/100 MPa, based on data presented in /Seipold and Huenges 1998/. All determinations of thermal conductivity in the site investigation programme have been made on water saturated samples. The pressure dependence has therefore been neglected in the modelling.

3.13 Coefficient of thermal expansion

The coefficient of thermal expansion has been measured on 9 additional samples, three of Ävrö granite (501044) and six of diorite-gabbro (501033) /Åkesson 2007/. These, as well as previously performed measurements reported in /Wrafter et al. 2006/, divided according to rock type, are summarised in Table 3-32. Ävrö granite has been divided into Ävrö quartz monzodiorite (501046) and Ävrö granodiorite (501056). Eight samples from drill core mapped as quartz monzodiorite (501036) have been excluded after consideration of their densities and appearance. These samples are from boreholes in Simpevarp (KSH01A) and Ävrö (KAV04A) and are deemed not to be representative of quartz monzodiorite in Laxemar. Their high densities (2,840–2,910 kg/m³) suggest that they may belong to the diorite-gabbro group of rocks instead.

The mean measured coefficient of thermal expansion for five different rock types varies between $6.9 \cdot 10^{-6}$ and $7.4 \cdot 10^{-6}$ m/(m·K).

Table 3-32. Measured thermal expansion (m/(m·K)) on samples of different rock types from boreholes KSH01A, KSH02, KAV01 and KAV04A (Simpevarp subarea), KLX02, KLX03 and KLX04, KLX05, KLX07A and KLX10 (Laxemar subarea) (interval of temperature: 20–80°C).

Rock code	Rock name	Sample location	Arithmetic mean	St. dev.	Min	Max	Number of samples	Comment
501030	Fine-grained dioritoid	Boreholes KSH01A, KSH02	$6.9 \cdot 10^{-6}$	$1.5 \cdot 10^{-6}$	$4.6 \cdot 10^{-6}$	$9.9 \cdot 10^{-6}$	17	
501033	Diorite-gabbro	Boreholes KLX05, KLX12A,	$7.4 \cdot 10^{-6}$	$1.0 \cdot 10^{-6}$	$5.9 \cdot 10^{-6}$	$8.3 \cdot 10^{-6}$	6	6 new samples
501036	Quartz monzodiorite	Boreholes KSH01A, KLX03	$7.3 \cdot 10^{-6}$	$1.1 \cdot 10^{-6}$	$5.8 \cdot 10^{-6}$	$9.3 \cdot 10^{-6}$	11	8 samples excluded compared to thermal model 2.1
501046	Ävrö quartz monzodiorite	Boreholes KLX02, KLX03, KLX04	$7.1 \cdot 10^{-6}$	$1.4 \cdot 10^{-6}$	$4.3 \cdot 10^{-6}$	$9.1 \cdot 10^{-6}$	12	
501056	Ävrö granodiorite	Boreholes KAV01, KAV04A, KLX02, KLX04, KLX07A, KLX10	$7.3 \cdot 10^{-6}$	$1.9 \cdot 10^{-6}$	$4.5 \cdot 10^{-6}$	$1.2 \cdot 10^{-5}$	37	3 new samples (altered)

3.14 *In situ* temperature

3.14.1 Method

Fluid temperature and vertical temperature gradients have been measured in most cored boreholes in Laxemar. Temperature was measured by fluid temperature loggings at regular 0.1 m intervals. The measured data were filtered and temperature gradients for 9 m sections were calculated.

Large differences in logged temperature for the same depth in different boreholes were noted in earlier model stages /Wrafter et al. 2006/. Uncertainties associated with the data from boreholes KLX01, KLX03, KLX04 and KLX06 were judged to be high and were excluded from further analysis, whereas data from KLX02 and KLX05 were considered to be of satisfactory quality /Wrafter et al. 2006/. For the same reason, the fluid temperature loggings for boreholes logged after data freeze Laxemar 2.1 (KLX07A and onwards) have been evaluated with regard to their reliability. The criteria considered were 1) errors associated with logging probe and 2) time between drilling and logging. The boreholes evaluated are listed in Table 3-33. KLX09 has not been treated because of its location in the northern part of Laxemar, which is outside the area of interest for thermal modelling, i.e. the central and southern parts of Laxemar.

Different probes have been used by Ramböll for temperature logging, Century 8044, Century 8144, Century 9044 and Century 9042. Errors associated with Century 8044, 8144 and 9044 are particularly large, as much as $\pm 2^\circ\text{C}$. Therefore, fluid temperatures logged with these instruments are considered to be unreliable, and are omitted from subsequent analysis. The rejected data are from borehole KLX07A. Boreholes logged using Century 9042 are considerably more accurate, less than $\pm 0.25^\circ\text{C}$ /Stenberg 2006/.

The times between core drilling and temperature logging vary between 2 days and 2 years for the boreholes, see Table 3-33. The period between the end of drilling activity and temperature logging should be sufficiently long in order to allow disturbances of the fluid temperature caused by drilling to stabilise. The drilling activity increases the temperature in the borehole, but a temperature decrease is probably caused by the added drilling fluid. However, the temperature of the drilling fluid may vary. In addition, a temperature equilibration occurs in the borehole when the drilling fluid is transported in the borehole. A rough rule of thumb is that logging should preferably not be carried out within 2 months after the end of drilling, and definitely not within the first 3-4 weeks after drilling. Based on this approximation, it can be deduced that logging data from KLX10, KLX11A, KLX12A, KLX13A, KLX15A, KLX16A, KLX17A, KLX19A and KLX21B may have been collected before the water temperature in the boreholes had stabilised. These data have also been omitted from subsequent calculations.

The temperature and gradient profiles have been investigated for all “approved” boreholes, namely KLX02, KLX05, KLX08, KLX18A and KLX20A. Because of the small number of boreholes available for calculation of *in situ* temperature at repository depth, it was decided to investigate the temperature data obtained during difference flow logging (also called Posiva flow logging or PFL). The temperatures logged in the down-borehole direction, without any pumping, were selected for comparison with the fluid temperature logs described above. Such data is available for three of the “approved” boreholes: KLX05, KLX08 and KLX18A /Sokolnicki and Rouhiainen 2005, Sokolnicki and Pöllänen 2005, Sokolnicki and Kristiansson 2006/. The times between end of drilling and PFL logging for these three boreholes were 3 months, 4 months and 2 months, respectively.

Table 3-33. Evaluation of fluid temperature loggings.

Borehole	Probe	Risk for errors due to design/calibration fault	Core drilling: start-stop	Fluid temperature logging	Period between drilling and logging	Judgement of quality of fluid temp. logging	Comment: main reason(s) for rejecting data
KLX07A	Century 8144	Yes	6 Jan – 4 May, 2005	4 Jul, 2005	2 months	Poor	Unreliable probe
KLX08	Century 9042	Low	4 Apr – 13 Jun, 2005	25 Oct, 2005	4.5 months	Good	
KLX10	Century 9042	Low	18 Jun – 15 Oct, 2005	17 Oct, 2005	2 days	Poor	Short time between drilling and logging
KLX11A	Century 9042	Low	24 Nov, 2005 – 2 Mar 2006	23 Mar, 2006	3 weeks	Poor	Short time between drilling and logging
KLX12A	Century 9042	Low	10 Nov, 2005 – 4 Mar, 2006	22 Mar, 2006	2.5 weeks	Poor	Short time between drilling and logging
KLX13A	Century 9042	Low	19 May – 16 Aug, 2006	7 Sep, 2006	3 weeks	Poor	Short time between drilling and logging
KLX15A	Century 9042	Low	17 Jan – 25 Feb, 2007	21 Mar, 2007	4 weeks	Poor	Rather short time between drilling and logging
KLX16A	Century 9042	Low	28 Nov, 2006 – 9 Jan, 2007	24 Jan, 2007	2 weeks	Poor	Short time between drilling and logging
KLX17A	Century 9042	Low	13 Sep – 23 Oct, 2006	13 Nov, 2006	3 weeks	Poor	Short time between drilling and logging
KLX18A	Century 9042	Low	29 Mar – 2 May, 2006	1 Jun, 2006	4.5 weeks	Fair	
KLX19A	Century 9042	Low	3 Jun – 20 Sep, 2006	12 Oct, 2006	3 weeks	Poor	Short time between drilling and logging
KLX20A	Century 9042	Low	25 Mar – 24 Apr, 2006	31 May, 2006	5 weeks	Fair	
KLX21B	Century 9042	Low	12 Oct – 29 Nov, 2006	21 Dec, 2006	3 weeks	Poor	Short time between drilling and logging

3.14.2 Results

Depth profiles of fluid temperature for boreholes KLX08, KLX18A and KLX20A are presented in Figure 3-34 and Figure 3-35. The y-axis in the figures indicates the elevation (depth above sea level). Corresponding descriptions of fluid temperature in boreholes KLX02 and KLX05 are given in /Sundberg et al. 2006/ and /Wrafter et al. 2006/, respectively. Equations were fitted to the temperature–depth profiles for these five boreholes; see Table 3-35. First-order equations were judged to be satisfactory, as higher order equations did not give better fits to the data. Temperature–depth profiles for all “approved” boreholes are presented in Figure 3-36.

In Table 3-34, the fluid temperature at elevations of –400 m, –500 m and –600 m in all “approved” boreholes are presented. The measured temperatures at –500 m elevation falls within the interval 14.7–14.9°C for the boreholes KLX02, KLX05, KLX08 and KLX18A. Borehole KLX20A does not reach 500 m depth and is therefore not included in this calculation. Temperatures recorded by the Posiva flow logs in boreholes KLX05, KLX08 and KLX18A are also given in this table and indicate a generally good agreement between the two methods. Thus the PFL data do not indicate that the estimated mean fluid temperatures at repository depths suffer from any significant bias.

Table 3-34. Temperature (°C) for the “approved” boreholes at the Laxemar site, at different elevations. Borehole inclinations are also included for the boreholes, given as lowest and highest angles. For KLX02, data are from loggings performed in 2003. These data have not been filtered and resampled. Temperature from Posiva flow logs are given in parentheses.

Borehole	Temperature at –400 m elevation	Temperature at –500 m elevation	Temperature at –600 m elevation	Inclination** (°)
KLX02 (2003)	13.4	14.8	16.3	83–85
KLX05	13.4 (13.1)	14.9 (14.7)	16.4 (16.3)	63–65
KLX08	13.2 (13.2)	14.7 (14.8)	16.3 (16.3)	56–60
KLX18A*	13.1 (13.1)	14.8 (14.7)	–	80–82
KLX20A*	–	–	–	41–51
Arithmetic mean	13.3	14.8	16.3	

* KLX18A and KLX20A reach vertical depths of about 580 m and 309 m, respectively.

** Borehole inclinations are given as lowest and highest angles based on Boremap mapping reports, for example /Mattsson and Eklund 2007/.

Table 3-35. Equations fitted to the temperature profiles for the investigated boreholes.

Borehole	Equation (linear fit)	Calculated from data in elevation interval, m
KLX02 (2003)	$T = -0.0149 z + 7.4786$	– 46 to –1005
KLX05	$T = -0.0148 z + 7.5633$	–80 to –878
KLX08	$T = -0.016482 z + 6.3864$	–63 to –823
KLX18A	$T = -0.015817 z + 6.8625$	–79 to –580
KLX20A	$T = -0.013042 z + 7.6520$	–51 to –309

In Figure 3-36 calculated gradients for the different boreholes are shown. Sections with larger gradient anomalies are commonly associated with deformation zones, where water bearing fractures are likely to be plentiful. Despite the anomalies, the average gradient tends to remain constant with depth, generally lying between 12°C/km and 15°C/km from –200 m to –800 m elevation.

The average annual air temperature recorded at Oskarshamn SMHI meteorological station, the “reference station” for air temperature in the Laxemar area, is 6.4°C /Werner et al. 2006/.

3.15 Geological data

Geological data from boreholes KLX02, KLX03, KLX04, KLX05, KLX07A, KLX08, KLX10, KLX11A, KLX12A, KLX13A, KLX15A, KLX16A, KLX17A, KLX18A, KLX19A, KLX20A and KLX21B have been used for the purposes of thermal modelling. Boreholes located in the northern part of Laxemar (KLX01, KLX06, KLX09) were excluded since they lie outside the area of interest. In addition, boreholes shorter than 200 m, many of them drilled to investigate deformation zones, have been omitted from the analysis.

The following geological borehole data are used in thermal modelling:

1. rock type (> 1 m), rock occurrences (< 1 m), and alteration from the Boremap system,
2. deformation zones defined in boreholes from the extended single hole interpretations (ESHI),
3. geological subdivision of Ävrö granite into rock units Ävrö quartz monzodiorite and Ävrö granodiorite, also taken from ESHI.
4. The lithological domain classification of boreholes as defined in the geological model /Wahlgren et al. 2008/.

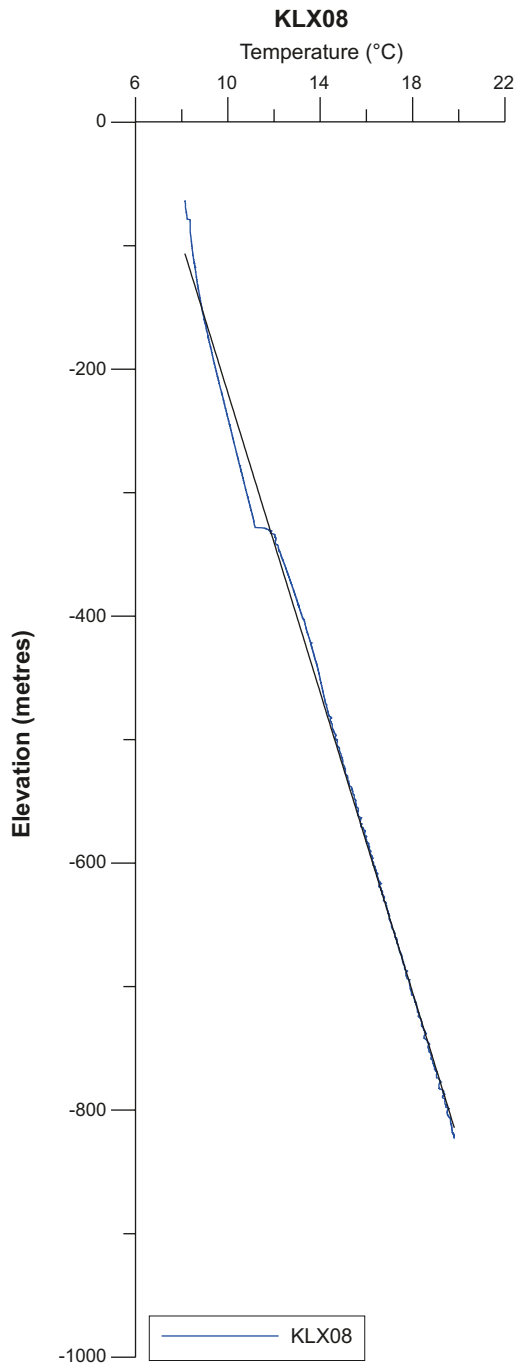


Figure 3-34. Temperature from fluid temperature loggings for KLX08. The black line is the best fit relationship for the temperature–depth profile as defined by the equation in Table 3-35.

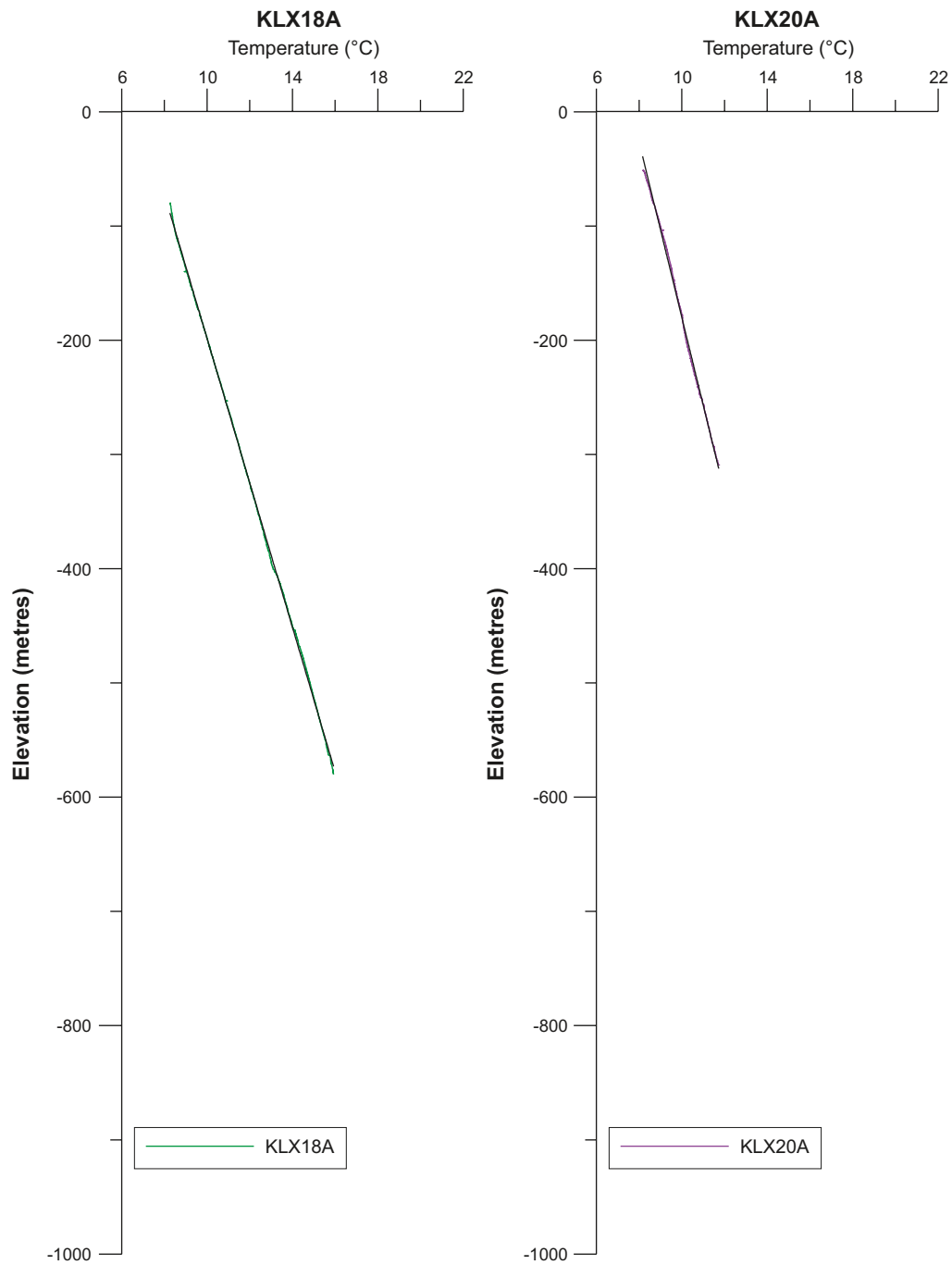


Figure 3-35. Temperature from fluid temperature loggings, for KLX18A and KLX20A. The black lines are the best fit relationships for the temperature–depth profiles as defined by the equations in Table 3-35.

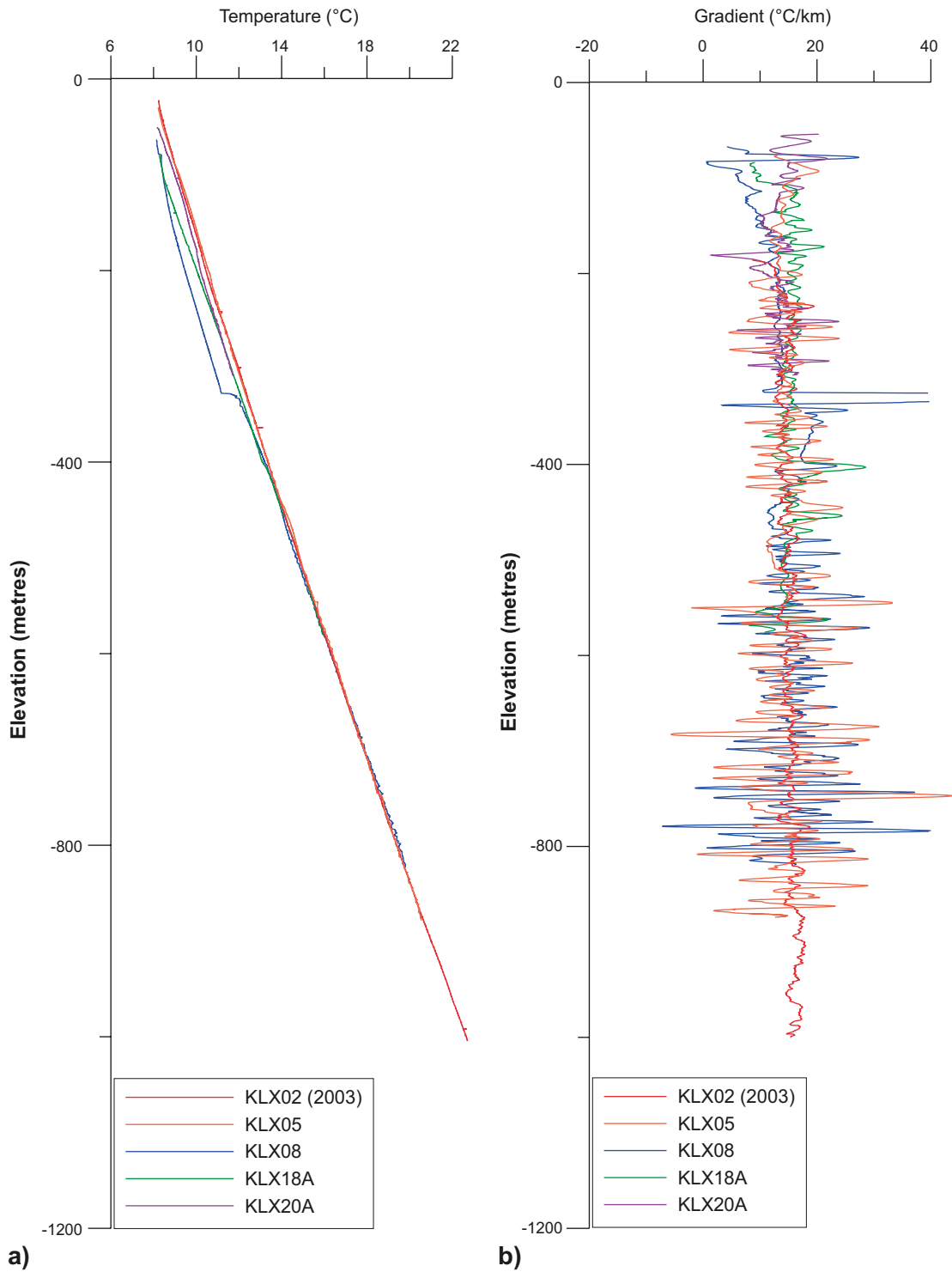


Figure 3-36. Summary of temperature (a) and gradient calculated for nine metre intervals (b) for the four boreholes in Laxemar. Results from “approved” fluid temperature loggings only.

4 Strategy for thermal modelling

4.1 Conceptual model

The methodology employed for thermal modelling in SDM-Site Laxemar has been fundamentally revised compared to previous model versions, and has been documented in a separate strategy report /Back and Sundberg 2007/ and applied in the Forsmark version 2.2 modelling /Back et al. 2007/. The revised strategy for thermal modelling is based on a conceptual model which, for each rock domain, provides a description of the following aspects:

- lithology (including rock alteration),
- thermal properties of different rock types,
- spatial variability and spatial correlation of thermal properties within the various rock types,
- anisotropy in thermal properties.

The rock domain model produced as part of the geological modelling in SDM-Site Laxemar, and described in /Wahlgren et al. 2008/, forms the geometrical basis for the thermal modelling presented here. The definition of rock domains in Laxemar relies almost entirely on lithologies, in particular the dominant rock types.

The conceptual model explains the spatial variability of thermal conductivity within a rock domain in terms of lithological and mineralogical heterogeneity (variability), and also provides an explanation for anisotropy of thermal properties.

Thermal properties, especially thermal conductivity, vary significantly between different rock types but also within individual rock types. The “between rock types” variability is a result of the different compositions of the igneous rock types, resulting from different types of magma. The “within rock type” variability is a result of variations in the mineralogical composition, which too is intimately related to magma composition, but also post-crystallisation processes such as hydrothermal alteration. “Within rock type” variability is also a function of the way rocks have been classified; for example, a particular rock type may include two or more subvarieties or facies.

The total variability in thermal properties within a rock domain thus depends on the lithology and the thermal properties of each rock type. Although the thermal conductivity of a single rock type may be close to normally (Gaussian) distributed, the statistical distribution of thermal conductivity for the domain as a whole is far from normally distributed. Depending on their fraction of the total volume, the low-conductive rock types may determine the lower tail of the thermal conductivity distribution. This lower tail is important for the design of the repository.

The rock mass at Laxemar may have anisotropic thermal properties. There are at least two main types of thermal anisotropy to consider:

1. Anisotropy due to foliation/lineation.
2. Anisotropy due to orientation of subordinate rock bodies.

The first type is a structural anisotropy caused by foliation and lineation which occur within a rock type. The foliation and lineation imply a directional orientation of the minerals in the rock mass. The thermal conductivity is generally higher parallel with the mineral foliation and lower perpendicular to the foliation plane.

The second type of anisotropy is a result of the spatial orientation of magmatic rock bodies, primarily subordinate rocks. These bodies may have preferential directions in space, resulting in anisotropy in the thermal properties. Dykes of e.g. fine-grained diorite-gabbro may result in this type of thermal anisotropy at Laxemar, but only to minor extent.

4.2 Modelling approach

4.2.1 Introduction

The overall strategy for the thermal site descriptive modelling is to produce spatial statistical models of both lithologies and thermal properties and perform stochastic simulations to generate spatial 3D realisations of thermal properties that are representative of the modelled rock domain. These realisations are used to represent the rock domain statistically. The methodology is described in detail in /Back and Sundberg 2007/ and has recently been applied at Forsmark /Back et al. 2007, Sundberg et al. 2008b/.

There are three specific objectives for which the modelling approach can be used:

- Description: statistical description of the thermal properties of a rock domain.
- Prediction: prediction of thermal properties in a specific rock volume.
- Visualisation: visualisation of the spatial distribution of thermal properties.

In this report the focus is on description. Of special interest for the description is to:

- determine the low percentiles of thermal conductivity,
- model how the thermal conductivity varies with scale,
- produce realisations of thermal conductivity that can be used for subsequent modelling work, such as numerical temperature simulations for the thermal design of a repository (distances between canisters and tunnels).

For the thermal description, no consideration is given to specific locations in the rock mass; only the statistics of the rock domain of interest are addressed. The methodology for this type of problem is based on unconditional¹ stochastic simulation. Conditional² stochastic simulation can only be used for small parts of a rock domain because of the large rock volumes involved (computer limitations).

The focus of the modelling approach is on thermal conductivity. In addition, the heat capacity distribution is modelled. The approach is based on the assumption of a Gaussian heat capacity distribution for each rock type (reclassified as TRCs; see below) in the Laxemar area. The overall distribution of heat capacity for the rock domain is a product of the distributions for each rock type and the simulated realisations of the lithology.

4.2.2 Outline of the methodology

The methodology, outlined in Figure 4-1, is applied separately for each rock domain. The simulation scale (1) is defined first. This scale determines how lithological data (2) should be prepared and if a change of support (5) is required for the thermal data (4). The support refers to the volume at which the data apply, whereas a change of support refers to how the distribution changes when passing from one size of support to another. The lithological data acquired from boreholes and mapping of the rock surface need to be reclassified into thermal rock classes, TRCs (3). The main reason is to simplify the lithological simulations as only a limited number of classes can be handled.

The lithological data are used to construct models of the transition between different TRCs, thus describing the spatial statistical structure of each TRC (7). In cases where hard data from boreholes are not sufficient for a full understanding of the geology, expert knowledge regarding, for example, the orientation of subordinate rock types may be a valuable complement (6). The result is a set of transition probability models that are used in the simulation of TRCs (8). The

¹Unconditional simulation is a method that distributes simulated values spatially without honouring measurements at specific locations.

²Conditional simulation is a simulation method where actual observations or measurements are honoured, i.e. the simulated value in a cell will be equal to the measured value.

intermediate result of this first stochastic simulation is a number of realisations of the geology. Both the analysis of the spatial statistical structure of TRCs and the subsequent stochastic simulations are performed using the commercially available software T-PROGS.

Based on the thermal data, a spatial statistical thermal conductivity model is constructed for each TRC (9). It consists of a statistical distribution and a variogram for each TRC. Again, expert judgements regarding, for example, the shape of the distributions may be used to complement the hard data (6). The spatial statistical thermal models are used in the stochastic simulation of thermal conductivity (10) and the result is a number of equally probable realisations of thermal conductivity for the TRC. If required, these realisations can be used to increase the support; see the feedback loop to step 5 in Figure 4-1.

In the next step, the realisations of TRCs (lithology) and thermal conductivity are merged (11), i.e. each realisation of geology is filled with associated simulated thermal conductivity values. The result is a set of realisations of thermal conductivity that considers both the difference in thermal properties between different TRCs, and the variability within each TRC. If the result is desired at a scale different from the simulation scale, upscaling of the realisations can be

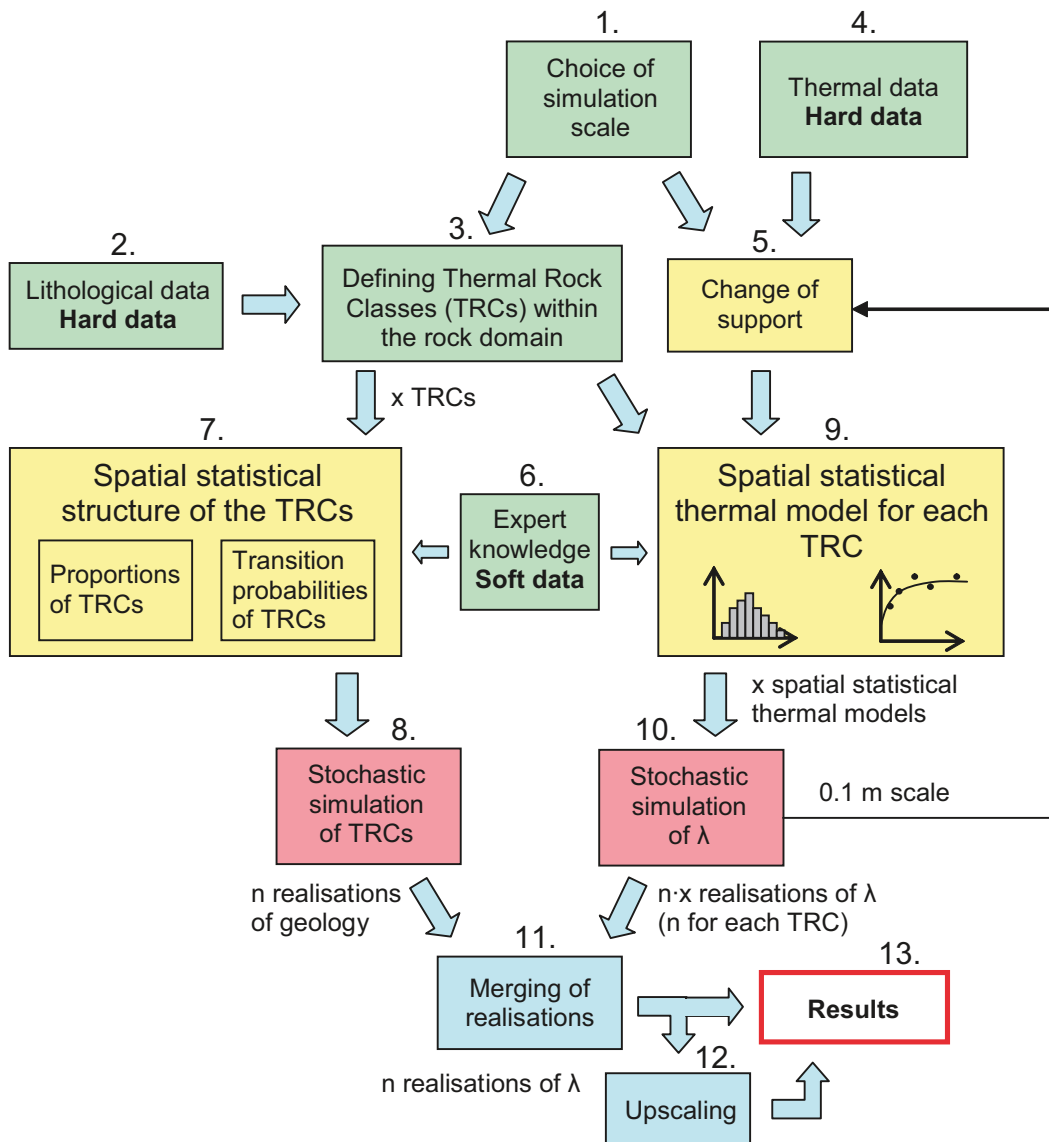


Figure 4-1. Schematic description of the approach for thermal conductivity modelling of a rock domain (λ denotes thermal conductivity).

performed (12). Upscaling can be performed to a scale not larger than the size of the simulation domain. In practice, upscaling should be made to a scale applicable to the problem at hand, preferably the canister scale. The results (13) can be presented in a number of ways, for example as 3D illustrations, histograms and statistical parameters for the rock mass, probabilities of encountering low thermal conductivity values, etc. The described methodology can also be used for other types of rock properties, such as strength in different rocks.

4.2.3 Important adaptations of the modelling approach to Laxemar

The thermal modelling strategy outlined above is described in detail in /Back and Sundberg 2007/. However, there are some aspects of the modelling that need additional comments, primarily related to steps 5-10 in Figure 4-1. These aspects concern the establishment of thermal subdomains of the lithology, the formation of sub-TRCs, a revised procedure for upscaling distribution models, and a further developed methodology for upscaling of variograms.

Thermal subdomains

Spatial statistical analysis of the borehole data (steps 6 and 7 in Figure 4-1) at Forsmark and Laxemar reveals that the rock domains are often not homogeneous in a statistical sense with regards to lithology. However, the stochastic simulations require statistical homogeneity. Therefore, where necessary, rock domains are divided into more lithologically homogeneous subdomains and each subdomain is then modelled and simulated separately. The objective of the division is to create statistically homogeneous subdomains. These subdomains are denoted “thermal subdomains” to emphasise that they are defined from a thermal perspective. A thermal subdomain has no defined spatial boundaries; only its proportion of the rock domain is defined. The proportion is estimated based on borehole lengths and geological expertise. The numbers of realisations produced during simulation for each subdomain corresponds to the relative proportions of the subdomains within the domain.

After simulation, all realisations for all subdomains are combined to form a single set of lithological realisations that represents the rock domain of interest.

Sub-TRCs

Similarly as for lithology, spatial statistical analysis of thermal conductivity indicates that all TRCs (or rock types) are not statistically homogeneous. This is obvious when histograms of calculated thermal conductivity values are compared for different boreholes. In addition, the spatial correlation structure may also differ. In cases where this heterogeneity is believed to have significant effects, the TRC has been divided into sub-TRCs (part of steps 6 and 9 in Figure 4-1). It is then assumed that each sub-TRC is statistically homogeneous. Since the geological borehole mapping does not distinguish between these different types, this issue cannot be dealt with in the lithological simulations by increasing the number of TRCs.

A spatial statistical thermal model is developed for each sub-TRC and stochastic simulation is performed separately for each one. The number of realisations produced during simulation for each sub-TRC corresponds to the proportion of the total TRC that the individual sub-TRCs is estimated to occupy. This proportion is estimated from borehole lengths and expert judgment.

Following simulation, all realisations for all sub-TRCs are combined to form a single set of thermal realisations that represents the TRC of interest.

Upscaling of distribution models

The approach for upscaling of distribution models of thermal conductivity (loop in 9, 10 and 5 in Figure 4-1) has been slightly modified compared to the approach in /Back and Sundberg 2007/. Sequential Gaussian Simulation is no longer used for the upscaling. Instead the LU Decomposition Algorithm /Deutsch and Journel 1998/ is applied. LU decomposition is used

in numerical analysis for rapid solving of complex matrix problems. The algorithm factorises a matrix into a lower triangular matrix L and an upper triangular matrix U. Applied here, LU decomposition provides a very fast solution to the covariance matrix. One important advantage of using this algorithm is that the variance can be more accurately maintained during simulation of small volumes. A drawback is that only a limited number of grid cells can be simulated, in the order of 1,000. Therefore, the following stepwise procedure was applied:

1. Simulation with the LU Decomposition Algorithm at the 0.1 m scale.
2. Upscaling of the distribution from 0.1 to 0.5 m scale with the SCA approach /Back and Sundberg 2007/.
3. Simulation with the LU Decomposition Algorithm at the 0.5 m scale.
4. Upscaling of the distribution from 0.5 to 2 m scale with the SCA approach.
5. Modelling of the upscaled distribution.

The upscaled distribution model was then used for the simulations at the 2 m scale (Sequential Gaussian Simulation), together with the upscaled variogram; see below.

Upscaling of variograms

In the strategy report for thermal modelling /Back and Sundberg 2007/, it was recommended that existing “rules of thumb” for the upscaling of a variogram be used. These rules are usually quite accurate but the approach is not self evident when nested variogram structures are used, as in Laxemar. A nested variogram is a variogram that combines two or more variogram structures in order to model the sample variogram more accurately. Therefore, the methodology was developed so that a variogram can be derived for the desired scale. The approach is described in detail by /Journal and Huijbregts 1978/. Non-fractal behaviour is assumed, which is supported by the sample variograms. For the current thermal modelling the principle is as follows.

If $\gamma(h)$ is the variogram model for the volumes of the measurements (in this case assumed as 0.1 m cubes) and $\gamma_v(h)$ is the variogram for the larger block (i.e. the upscaled variogram for 0.5 m cubes in Laxemar; first step of two in the upscaling, see below) then:

$$\gamma_v(h) = \bar{\gamma}(v, v_h) - \bar{\gamma}(v)$$

where $\bar{\gamma}(v)$ is the mean value of the variogram of measurements within a block of size v and $\bar{\gamma}(v, v_h)$ is the mean value of the variogram between two blocks of size v separated by the distance h . A computer program was constructed to calculate $\bar{\gamma}(v, v_h)$ and $\bar{\gamma}(v)$ based on the code presented by /Journal and Huijbregts 1978/. The code was applied for the upscaling from measurement scale (0.1 m) to the simulation scale (2 m). A two-step procedure was used: first upscaling to 0.5 m and in a second step upscaling from 0.5 m to 2 m; see the previous section of upscaling of distribution models.

4.3 Feedback from other disciplines

The SDM-Site Laxemar rock domain model /Wahlgren et al. 2008/ forms the basis for the description of thermal properties of the rock mass within the local model volume at Laxemar. Three rock domains have been identified within the local model volume. The thermal properties of these three domains are evaluated here. A geological description of these domains is given in Section 5.2.

Valuable cooperation with the geologists of the Laxemar site modelling team has been established and maintained throughout the thermal modelling stages. Integration with geology was particularly comprehensive and important in the case of the geological interpretations used as input in the stochastic simulations of lithologies.

4.4 Modelling assumptions

The modelling approach requires a number of modelling assumptions in various steps of the modelling process. The most important ones are believed to be the following:

- General assumptions:
 - Borehole information from Boremap, and core samples used for thermal property measurements are assumed to be representative of the rock domain, i.e. the statistics derived from this information satisfactorily describe the rock domain. This is an important assumption regarding both lithological information and thermal properties.
 - It is assumed that water movement does not influence the thermal properties of the intact rock volume. Thus water movement is not considered in the modelling. This is a conservative assumption, i.e. thermal conductivity values will be lower than would be the case if water movement was considered.
 - It is assumed that the *in situ* stress field has no influence on the thermal properties
- Assumptions regarding the spatial statistical thermal models:
 - The modelling is performed using effective values of thermal conductivity (isotropic assumption). This also applies to the upscaling methodology where effective values are calculated using the SCA approach; see /Back and Sundberg 2007/. Anisotropy is evaluated separately.
 - Various assumptions regarding the shapes of statistical distributions and variograms for the thermal conductivity of a TRC are required. These are further discussed in Section 5.6.
 - It is assumed that the statistical distribution and the variogram for a TRC is the same for all rock types that belong to that TRC.
 - Spatial correlation in thermal conductivity between different parts of a rock type body is assumed not to be “broken” by the presence of a different type of rock separating these parts.
- Assumptions regarding the spatial statistical structure of TRCs (lithology):
 - Geological interpretations, based on expert opinion, have been used in modelling the spatial statistical structure of a TRC (lithology).
 - It is assumed that the lengths of rock bodies follow a geometric distribution; see Section 5.5.3.
- Assumptions regarding simulation grid and simulation volume:
 - It is assumed that thermal conductivity data (TPS and modal analysis data) represent the 0.1 m scale, which is the scale at which the initial simulations are performed (cells of cubic shape with 0.1 m sides).
 - The 2 m scale is assumed to be sufficiently small to properly represent the subordinate rock types.
 - The simulation volumes ($100 \times 100 \times 100 \text{ m}^3$ for scale 2 m) are assumed to be sufficiently large for the objectives of the simulations (Section 1.2).
 - For the purpose of lithological simulations, a rock domain is divided into thermal subdomains, each of which is assumed to be statistically homogeneous.

Information regarding the assumptions made for the lithological and the spatial statistical thermal models for each TRC is provided in the Chapter 5.

5 Geostatistical analyses and stochastic simulations

5.1 General

The application to Laxemar of the methodology for thermal modelling outlined in Chapter 4 and Figure 4-1 (modelling steps 1 to 10 in Figure 4-1) is presented in this chapter. In Section 5.2, by way of introduction, the aspects of the rock domain model relevant to thermal modelling are described. Then, in Section 5.3, the geological input, both hard and soft data, is presented (steps 2, 3 and 6 in Figure 4-1). Next, in Section 5.4 spatial statistical models of lithologies within each rock domain are established (step 7 in Figure 4-1). This is followed by the results of stochastic simulation of lithologies in 5.5 (step 8 in Figure 4-1). Spatial statistical models for thermal conductivity (step 9 in Figure 4-1) followed by stochastic simulations of thermal conductivity (step 10 in Figure 4-1) are presented in Section 5.6 and Section 5.7 respectively.

The main results of these simulations are:

- the spatial distributions of lithologies in rock domains RSMA01, RSMD01 and RSMM01,
- thermal conductivity distributions of the individual lithologies.

An example of how the methodology can be used to simulate the thermal conductivity within a specific rock volume is described in Section 5.10.

5.2 Conceptual descriptions of the rock domains

5.2.1 Introduction

The Laxemar local model area west of the plastic deformation zones (domains RSMP01 and RSMP02) is characterised by three major rock domains in addition to a small number of volumetrically subordinate domains /Wahlgren et al. 2008/. The three domains that dominate the rock volume are RSMA01, RSMD01 and RSMM01. The thermal properties of these domains south of the important E-W deformation zone EW007 are the focus of the thermal modelling in this report.

The definition of rock domains in Laxemar relies almost entirely on lithologies, in particular the dominant rock types. In the so called single-hole interpretation, a borehole is divided into rock units primarily on the basis of the composition and grain size of the dominant rock type, as well as the degree of lithological homogeneity. Ävrö granite is subdivided into its two subtypes Ävrö quartz monzodiorite and Ävrö granodiorite for the purpose of defining rock units. Rock units having similar characteristics are then assigned to the same rock domain. The lithological characteristics of the three above mentioned domains are given in Table 5-1. The geometrical shape of the rock domains at depth is determined by the rock domain boundaries as defined in the cored boreholes. For a fuller description of the rock domains in Laxemar, the reader is referred to Chapter 4 in /Wahlgren et al. 2008/.

It should be noted that the boundaries between rock domains RSMA01 and RSMM01 and between RSMM01 and RSMD01 have been modified somewhat compared to the previous rock domain model (version 1.2). Therefore, the results presented here are not directly comparable with those of the previous thermal model version (Laxemar 1.2 /Sundberg et al. 2006/ and model stage Laxemar 2.1 /Wrafter et al. 2006/).

Table 5-1. Nomenclature and characteristics of rock domains referred to in this report. Based on /Wahlgren et al. 2008/.

Domain	Description
RSMA01	Dominated by Ävrö granite, in particular the Ävrö granodiorite variety.
RSMB	Dominated by fine-grained dioritoid
RSMBBA	Characterised by a mixture of Ävrö granite and fine-grained dioritoid
RSMD01	Dominated by quartz monzodiorite
RSMM01	Characterised by a high frequency of minor bodies to small enclaves of diorite-gabbro in Ävrö granite, in particular the Ävrö quartz monzodiorite variety.

A number of large deformation zones intersect the rock volume in Laxemar /Wahlgren et al. 2008/. Deformation zones interpreted in the single-hole interpretation work as having a true thickness of >10 m have been modelled deterministically in the 3D RVS model /Wahlgren et al. 2008/. Deformation zones (DZ) of such magnitude will be avoided in a future repository. Thus, the thermal properties of the rock within such zones are not described in the thermal model. It is the intact rock between these deformation zones that are the focus of interest for thermal properties. Minor deformation zones (MDZ), defined as deformation zones with an estimated thickness ≤ 10 m, also occur. While MDZs may be present within a repository, they will be avoided when it comes to selecting positions for deposition holes. No separate analysis of the thermal properties of these zones has been performed.

Between the identified deformation zones, both DZs and MDZs, about 15–30% of the rock domains are interpreted to be altered, usually oxidation (red-staining) or saussuritisation /Wahlgren et al. 2008/. It has been shown (Sections 3.3.2 and 3.5.3) that rock altered to a degree of weak or medium in Laxemar may have thermal conductivities that are on average c. 10% higher than the equivalent fresh or unaltered rock. The available data shows that rock showing only faint alteration does not have significantly different thermal conductivities than rock mapped as fresh. Excluding faint alteration, the proportion of the rock mass affected by alteration to a degree of weak or higher is c. 15% in domain RSMA01, c. 8% in domain RSMD01 and c. 6% in domain RSMM01. Oxidation (red staining) is generally the most abundant type of alteration in rock domains RSMA01 and RSMM01 whereas in domain RSMD01, a high degree of saussuritisation and epidotisation is present in addition to oxidation. Mineralogical changes associated with alteration include the formation of K-feldspar, albite, epidote and sericite from plagioclase, the decomposition of biotite to chlorite and the oxidation of Fe (II) to hematite /Drake and Tullborg 2006ab/. Since alteration has resulted in a different, more variable mineral composition, the thermal properties are likely to have been affected. In most cases the altered minerals have higher thermal conductivities than their original parent minerals. It is also important to note that the observed mineralogical changes extend beyond the zone of visible alteration, e.g. red staining, and are a widespread feature of rock mapped as fresh /Drake and Tullborg 2006ab/.

Because of the tendency for altered rock to have slightly higher thermal conductivities than fresh rock, it was considered unnecessary for thermal modelling purposes to model the thermal properties of altered rock separately.

The rock mechanics modelling team have identified oxidised quartz monzodiorite in rock domain RSMD01 as having lower uniaxial compressive strength than their fresh equivalents /Hakami et al. 2008/. For this reason, it was decided to model oxidised quartz monzodiorite separately in the lithological simulations of domain RSMD01. As can be seen in Figure 5-1, 20–25% of the rock mass in domain RSMD01 (all deformation zones excluded) is altered, mostly to a degree of faint or weak. Just less than half the alteration has been mapped as oxidised.

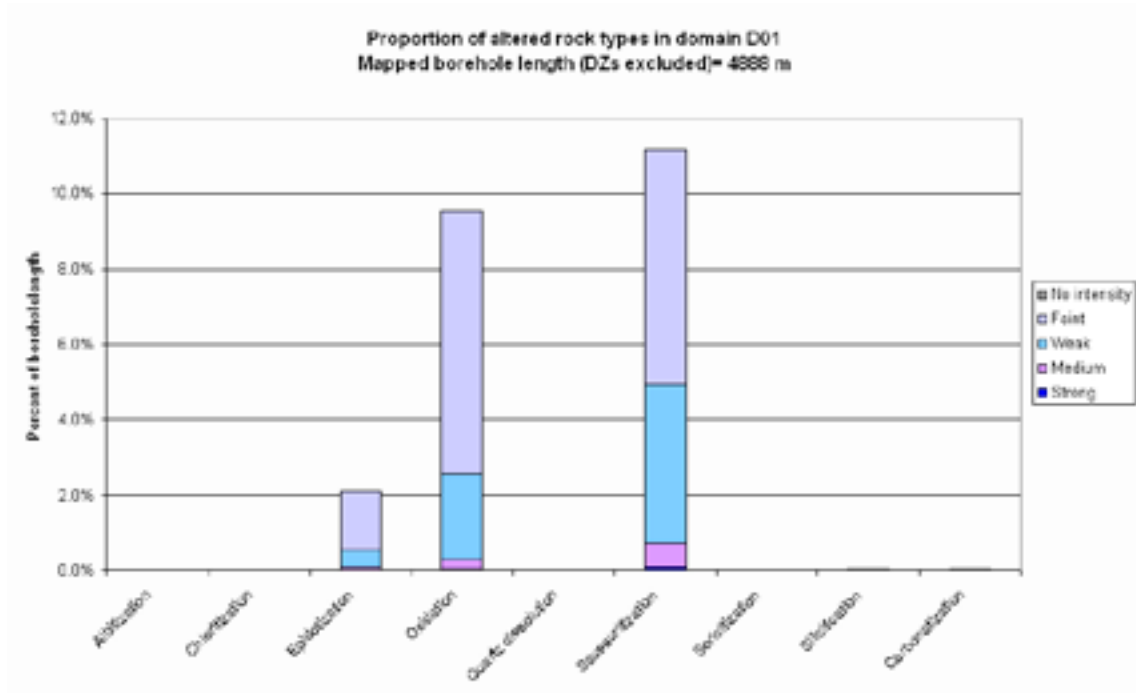


Figure 5-1. Proportion of the rock volume in domain RSMD01 affected by alteration. Estimates based on drill core mapping /Wahlgren et al. 2008/.

Since the size of subordinate rock bodies is of importance for the thermal conductivity distribution at a particular scale an understanding of the true thickness of rock types occurring as dykes or irregular tabular bodies was required. This information was useful for deciding a suitable scale for the stochastic simulations. The scale should be small enough that it can capture the lithological variability. Figure 5-2 shows that a large proportion of fine-grained granite has a thickness less than 1 m. In contrast, bodies of fine-grained diorite-gabbro are commonly thicker than 1 m. Since fine-grained granite and pegmatite are by definition quartz rich and are characterised by high thermal conductivities, modelling of small bodies of these rock types was considered unnecessary. Instead the simulations could be optimised to capture the size distribution of the fine-grained diorite-gabbro, which is characterised by much lower thermal conductivity. Due to the different thermal conductivities and their dyke-like appearance, the fine-grained diorite-gabbro may cause anisotropy in the thermal properties. For this reason, the orientation of the above-mentioned subordinate rock types has been investigated.

5.3 Geological input

The preparation of geological data, both hard and soft, for each rock domain for the purposes of lithological simulations is described in the following four sections.

5.3.1 Thermal Rock Classes (TRC) – Definition, properties and proportions

The geological simulations of rock domains can deal with a maximum of five lithological classes. For this reason, the rock types are grouped into classes, called thermal rock classes (TRC) – step 3 in Figure 4-1. Rock types with similar thermal and lithological properties were assigned to the same class. The TRCs were defined primarily on the basis of their thermal properties, e.g. thermal conductivity, of the rock types. However, consideration was also taken of a rock type's geological properties, such as overall composition (felsic, intermediate or mafic) and mode of occurrence. A description of the eight TRCs defined is given in Table 5-2.

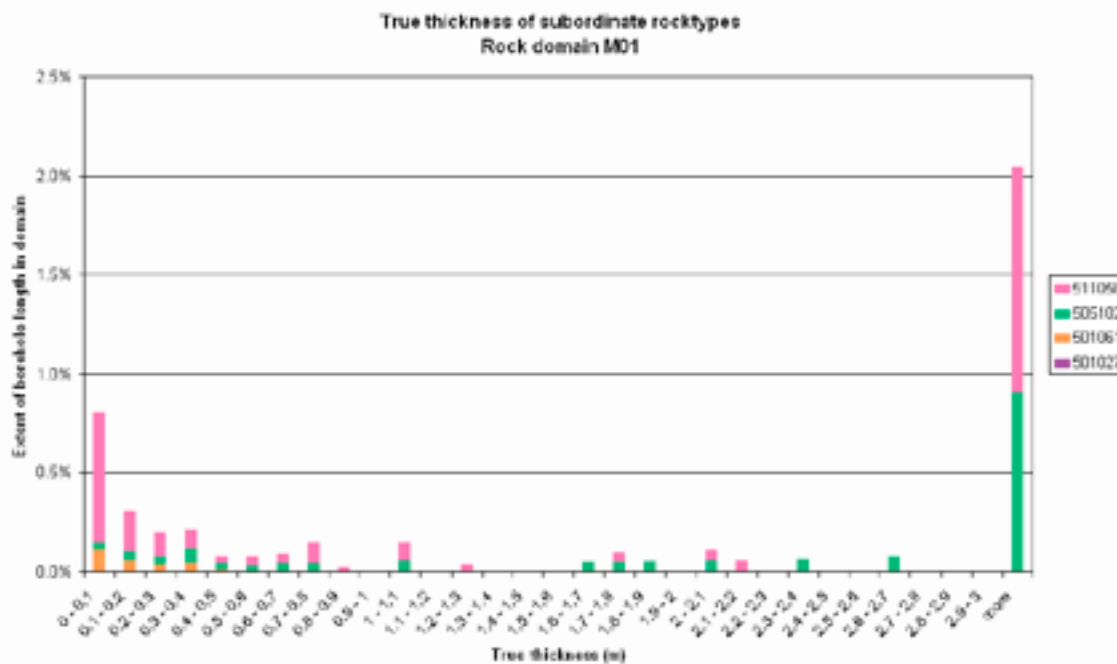


Figure 5-2. Proportion of subordinate rock types in different thickness classes /Wahlgren et al. 2008/

Table 5-2. Classification of rock types into thermal rock classes (TRC). Dominant rock type in bold. For a more complete summary of thermal conductivity statistics, see Table 3-2.

TRC	Rock name/code	Mean thermal conductivity (TPS)	Composition, mode of occurrence, etc	Present in rock domain
30	Fine-grained dioritoid (501030)	2.79	Intermediate composition (Both rock types occur in roughly equal proportions with borehole lengths varying between 2– 25 m)	A
	Quartz monzodiorite (501036)	2.74		
33	Diorite-gabbro (501033)	2.64	Intermediate- mafic composition	M
	Fine-grained diorite-gabbro (505102)	2.49		
36	Quartz monzodiorite (501036)	2.70	Intermediate. Quartz monzodiorite dominates	D
	Fine-grained dioritoid (501030)	2.79		
56	Ävrö granodiorite (501056)	3.16	Both felsic in composition.	A, M
	Granite (501058)	3.01		
46	Ävrö qtz monzodiorite (501046)	2.36	Intermediate composition	A, M
58	Fine-grained granite (511058)	3.69	Felsic composition; occur as dykes and small irregular bodies	A, D, M
	Pegmatite (501061)			
102	Fine-grained diorite-gabbro (505102)	2.49	Intermediate- mafic (fine-grained diorite-gabbro occurs as dykes)	A, D
	Diorite-gabbro (501033)	2.64		
	Dolerite (501027)			
136	Oxidised Quartz monzodiorite (501036)		Intermediate composition. Oxidised quartz monzodiorite (501036) rock.	D

The code for a TRC is defined by using the two or three last digits of the rock code for the dominating rock type in that class. An exception to this is TRC 136 which is comprised of oxidised quartz monzodiorite, a rock class primarily defined in order to facilitate stochastic simulation of rock mechanic properties. This particular subdivision of quartz monzodiorite into different TRCs for geological simulation purposes will have no implications for thermal modelling. In other words both TRC 36 and TRC 136 in domain RSMD01 will be assigned identical thermal models. Ävrö granite has been divided into its constituent varieties, namely Ävrö quartz monzodiorite and Ävrö granodiorite, and forms the basis for two TRCs, 46 and 56 respectively. Dolerite, which occurs in domain RSMD01 only, has been observed in only three boreholes, namely KLX14A, KLX19A and KLX20A. It is not considered to be evenly distributed throughout the RSMD01 domain, and seems to be associated with deformation zones /Wahlgren et al. 2008/.

The TRCs defined for domains RSMA01, RSMD01 and RSMM01 together with the proportions of rock types are presented in Table 5-3, Table 5-4 and Table 5-5. Each domain consists of five TRCs. However, only four TRCs are selected for modelling of domain RSMD01 and domain RSMM01 since TRCs making up less than 1% of the volume are excluded. This can be justified by the fact that none of these rocks types are considered critical to the statistical description of the low conductive rock in these domains, since they typically are characterised by intermediate to relatively high thermal conductivity values. Furthermore, their low frequency provides a poor basis for calculating transition probabilities, one of the key model parameters used in stochastic simulation of lithologies. Some TRCs are common to more than one rock domain; an example of this is TRC 58, which is characterised by fine-grained granite (511058).

5.3.2 Orientation and geometry of subordinate rock types

A preferred orientation of subordinate rock types may produce anisotropy in thermal conductivity. The results of the analysis of the orientation of subordinate dyke rocks (fine-grained granite and fine-grained diorite-gabbro) were evaluated together with the geology team in order to decide whether or not it was necessary to model the orientation of these rock types (Step 6 in Figure 4-1).

Table 5-3. Division of rock types into thermal rock classes (TRCs) for domain RSMA01. Proportions of different rock types are modified from /Wahlgren et al. 2008/.

TRC	Rock name/code	Proportion of rock type in domain RSMA01, %	Proportion of TRC in domain RSMA01, %
56	Ävrö granodiorite (501056)	62	63
	Granite (501058)	1.0	
46	Ävrö qtz monzodiorite (501046)	26	26
58	Fine-grained granite (511058)	3.3	3.6
	Pegmatite (501061)	0.3	
30	Fine-grained dioritoid (501030)	2.7	5.2
	Quartz monzodiorite (501036)	2.5	
102	Fine-grained diorite-gabbro (505102)	2.3	2.5
	Diorite-gabbro (501033)	0.2	

With the exception of the two Ävrö granite varieties, the rock type proportions are based on boreholes KLX02, KLX04, KLX07A and B, KLX08, KLX10, KLX18A and KLX21B /Wahlgren et al. 2008/ with deformation zones included. Boreholes located within domain RSMA01 in the northern part of Laxemar outside the area of focus for the present model stage have been excluded from the calculations of the rock type proportions. These comprise boreholes KLX01, KLX06 and boreholes drilled from drill site KLX09. Proportions of Ävrö quartz monzodiorite and Ävrö granodiorite are based on an analysis of density logging data (see Section 3.7.3).

Table 5-4. Division of rock types into thermal rock classes (TRCs) for domain RSMM01. Proportions of different rock types are modified from /Wahlgren et al. 2008/.

TRC	Rock types/rock code	Proportion of rock type in domain RSMM01, %	Proportion of TRC in domain RSMM01 %
46	Ävrö qtz monzodiorite (501046)	52	52
56	Ävrö granodiorite (501056)	23	25
	Granite (501058)	2.0	
33	Diorite-gabbro (501033)	16.4	18.2
	Fine-grained diorite-gabbro (505102)	1.8	
58	Fine-grained granite (511058)	4.7	5.2
	Pegmatite (501061)	0.5	
30	Quartz monzodiorite (501036)	0.4	0.8
	Fine-grained dioritoid (501030)	0.4	

With the exception of the two Ävrö granite varieties, the rock type proportions are based on boreholes KLX03, KLX05, KLX08, KLX10, KLX13A, KLX17A and KLX18A /Wahlgren et al. 2008/ with deformation zones included. Proportions of Ävrö quartz monzodiorite and Ävrö granodiorite are based on an analysis of density logging data. TRC 30 is excluded from lithological simulations since rock types together they make up less than 1% of domain RSMM01.

Table 5-5. Division of rock types into thermal rock classes (TRCs) for domain RSMD01. Proportions of different rock types are modified from /Wahlgren et al. 2008/.

TRC	Rock types/rock code	Proportion of rock type in domain RSMD01, %	Proportion of TRC in domain RSMD01, %
36	Quartz monzodiorite (501036)	79	79.3
	Fine-grained dioritoid (501030)	0.3	
136	Oxidised quartz monzodiorite (501036)	10	10
102	Fine-grained diorite-gabbro (505102)	1.8	4.6
	Diorite-gabbro (501033)	0.1	
	Ävrö qtz monzodiorite (501046)	0.6	
	Dolerite (501027)	2.1	
58	Fine-grained granite (511058)	5.0	6.4
	Pegmatite (501061)	1.4	
56	Ävrö granodiorite (501056)	0.5	0.9
	Granite (501058)	0.4	

Proportions are based on boreholes KLX03, KLX05, KLX08, KLX10, KLX11A, KLX12A, KLX14A, KLX15A, KLX16A, KLX19A, KLX20A and KLX21B /Wahlgren et al. 2008/ with deformation zones included. Proportions of Ävrö quartz monzodiorite and Ävrö granodiorite are based on an analysis of density logging data. The proportions of quartz monzodiorite and oxidised quartz monzodiorite are approximations based on an analysis of different types of alteration /Wahlgren et al. 2008/. TRC 56 excluded from lithological simulations since both rocks together make up less than 1% of the total borehole length.

Although fine-grained granite shows a predominance of subhorizontal to moderately dipping occurrences in each of the three domains, it was not considered justified to model this rock type as anisotropic for the following reasons:

1. there is a high degree of variation in orientation especially in domains RSMA01 and RSMM01 /Wahlgren et al. 2008/,
2. at the surface fine-grained granite is observed in many cases to occur as irregular-shaped bodies rather than dykes /Wahlgren et al. 2008/,
3. fine-grained granite has high thermal conductivity and is not of critical importance for the thermal model.

Fine-grained diorite-gabbro, however, shows much less variation in orientation in all domains. A predominance of flat-lying bodies is indicated by stereoplots /Wahlgren et al. 2008/. These features are exemplified in Figure 5-3 for domain RSMD01. Any preferred orientation of fine-grained diorite-gabbro in domain RSMM01 is unlikely to produce anisotropy in thermal conductivity since this rock type has similar thermal conductivity to Ävrö quartz monzodiorite, the dominant rock type in domain RSMM01. Even in domain RSMA01, the abundance of low conductive Ävrö quartz monzodiorite means that any anisotropy caused by the preferred orientation of fine-grained diorite-gabbro is unlikely to have any influence on the lower tail of the distribution of thermal conductivity values. In domain RSMD01, fine-grained diorite-gabbro is the rock type with the lowest mean thermal conductivity, and therefore the way in which this rock type is modelled in the geological simulations will influence the lower tail of the thermal conductivity distribution produced by thermal modelling.

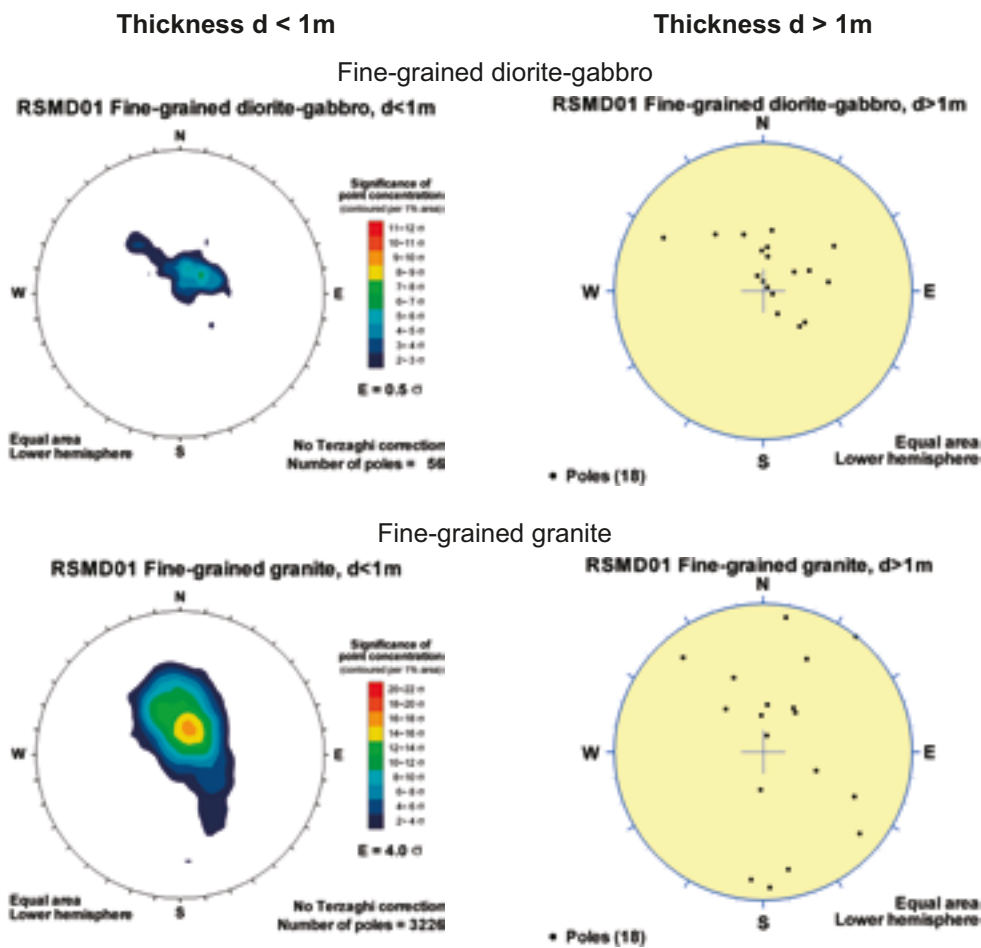


Figure 5-3. Stereoplots showing the orientation of fine-grained diorite-gabbro (top) and fine-grained granite (below) in domain RSMD01 /Wahlgren et al. 2008/.

Expert judgements regarding the geometry of fine-grained diorite-gabbro were elicited from the geological modelling team. Based on impressions gained in the field these bodies have a limited extension although the low degree of outcrop exposure means that one seldom sees the limits of these “dykes” /Wahlgren et al. 2008/. Thus, it was assumed that, for the purposes of lithological simulations, fine-grained diorite-gabbro (TRC 102) in domain RSMD01 occurs as horizontal sheets having an extension in the x-y plane ten times longer than their thickness or vertical direction.

Potential anisotropy in the geometry of other rock types has not been modelled due to lack of knowledge.

5.3.3 Characterisation of domains and division into thermal subdomains

Geological borehole data form the basis for the stochastic simulations of lithologies. This section presents the initial work involved in the processing of the lithological borehole data (steps 2 and 6 in Figure 4-1). Borehole sections used to represent each rock domain in the geological simulations follow the domain classification of boreholes described in the geological model /Wahlgren et al. 2008/. A total of 16 boreholes were used. A summary is presented in Table 5-6. Boreholes or borehole sections belonging to a domain were excluded from the analysis if their length was less than 200 m and 100 m, respectively. Boreholes in the northern part of Laxemar belonging to domain RSMA01 (KLX01, KLX06, KLX09) were also excluded, as they are located well outside the area of focus.

Table 5-6. Domain classification of boreholes according to the geological model /Wahlgren et al. 2008/.

Domain	Borehole	Borehole intervals (Sec up – Sec low) used as input for modelling (from geological model /Wahlgren et al. 2008/)	Comment
RSMA01	KLX02	200–540 m,	Boreholes sections belonging to domain RSMA01 in KLX07B,, KLX10C, KLX18A were excluded because shorter than 200 m.
	KLX04	101–991 m	
	KLX07A	102–842 m	
	KLX08	101–587 m	
	KLX10	102–857 m	
	KLX21B	101–768 m	
RSMD01	KLX03	621–998 m	Borehole sections belonging to domain RSMD01 in KLX08, KLX10, KLX12A and KLX21B were excluded because shorter than 200 m.
	KLX05	473–995 m	
	KLX11A	101–990 m	
	KLX15A	78–980 m	Borehole KLX20A excluded because not considered representative.
	KLX16A	1–434 m	
	KLX19A	100–796 m	
RSMM01	KLX03	101–620 m	
	KLX05	108–473 m	
	KLX08	587–924 m	
	KLX10	857–981 m	
	KLX12A	102–528 m	
	KLX13A	102–593 m	
	KLX17A	66–697 m	
	KLX18A	119–611 m	

An examination of the lithologies in the boreholes reveals that the rock domains are not homogeneous in a statistical sense. This is confirmed by spatial statistical analysis. However, the stochastic simulations assume statistical homogeneity. By subdividing the borehole data into groups, greater homogeneity can be obtained within each group or “thermal subdomain” (see Section 4.2.3). By simulating each “subdomain” separately more of the overall lithological heterogeneity within the rock domain can be captured.

The subdivision of boreholes into thermal subdomains was based on geological criteria and is described below for domains RSMA01 (Table 5-7 and Table 5-8) and RSMM01 (Table 5-9 and Table 5-10). Domain RSMD01 has not been divided into subdomains. The proposed subdomain classification of boreholes was examined by the geological modelling team to ensure it was consistent with their overall understanding of the geology. It should be noted that a thermal subdomain has no defined spatial boundaries; only its proportion of the rock domain is defined.

The geological simulations produce a set of realisations, where the number of realisations for each subdomain is chosen so that it is proportional to the borehole length assigned to each subdomain (Table 5-22). The rock domain as a whole is described by combining the realisations from each thermal subdomain (see Section 6.1). In this way, the realisations honour the borehole data as closely as possible, thus avoiding introducing bias in, for example, rock type proportions.

Domain RSMA01

Three thermal subdomains were defined for domain RSMA01. These are summarised in Table 5-7.

The minimum length of a borehole section assigned to a subdomain is set at 100 m. The motive for this is that it is desirable to retain the lithological variability that appears at scales smaller than 100 m, which corresponds to the length of the sides of the simulation volume. Borehole sections belonging to domain RSMA01 were divided into two main groups or subdomains. Sections dominated by Ävrö granodiorite were distinguished from sections dominated by Ävrö quartz monzodiorite. Boundaries between these subdomains within individual boreholes are based on the extended single-hole interpretations (ESHI). The transition between sections dominated by Ävrö quartz monzodiorite and sections dominated by Ävrö granodiorite are normally on a scale of 100 m or more. It is these boundaries that are used to define the subdomains. Smaller scale transitions, where they are defined in ESHI, are ignored. A consequence of this approach is that lithological realisations of a particular subdomain will be dominated by one or the other type of Ävrö granite, but with a component of the subordinate type occurring as smaller bodies. Large scale transitions between the different Ävrö granite varieties will not be simulated. A third subordinate subdomain was defined by the very heterogeneous section in borehole KLX04 from 470 m to 720 m. Table 5-8 describes the borehole characterisation of the subdomains in detail.

Table 5-7. Thermal subdomains defined in rock domain RSMA01. A subdomain’s proportion of the domain is based on the borehole length assigned to each subdomain.

Subdomain	Characteristic rock type(s)	Dominant TRC	Proportion of domain, %
A1	Ävrö granodiorite	56	74%
A2	Ävrö quartz monzodiorite	46	18%
A3	Very heterogenous	30	8%

Table 5-8. Borehole sections used to characterise subdomains in domain RSMA01.

Subdomain	Borehole	Borehole length, from-to, m ¹	Approximate borehole length per subdomain (DZ included), m
A1	KLX02	202–400 m	3,000 m
	KLX04	100–470 m	
	KLX04	728–990 m	
	KLX07A	100–450 m	
	KLX07A	586–816 m	
	KLX08	100–586 m	
	KLX10	102–856 m	
	KLX21B	408–768 m	
A2	KLX02	402–540 m	580 m
	KLX07A	450–584 m	
	KLX21B	100–406 m	
A3	KLX04	472–726 m	250 m

¹based on domain classification of boreholes, ESHI (extended single-hole interpretations) and interpretation of density logging data.

Domain RSMM01

Domain RSMM01 is the most lithologically heterogeneous of all the modelled rock domains and required division into 5 subdomains to adequately simulate this heterogeneity. These are summarised in Table 5-9.

The dominant type of Ävrö granite was used, in the same way as described for domain RSMA01, to make the first subdivision. Each borehole section was further classified according to the proportion of diorite-gabbro present, less than 15% or higher than 15%. In this way, four groups or subdomains were defined. Borehole KLX05 between 108 m and 292 m borehole length with its large proportion of fine-grained granite cannot be assigned to any of the above groups, and forms a fifth subdomain. Table 5-10 describes the borehole characterisation of subdomains in detail.

Table 5-9. Thermal subdomains defined in rock domain RSMM01. A subdomain's proportion of the domain is based on the borehole length assigned to each subdomain.

Thermal subdomain	Characteristic rock type(s)	Dominant TRC	Proportion of domain, %
M1	Ävrö quartz monzodiorite,	46	38%
M2	Ävrö quartz monzodiorite + high proportion diorite-gabbro	46	35%
M3	Ävrö granodiorite	56	11%
M4	Ävrö granodiorite + high proportion diorite-gabbro	56	10%
M5	Ävrö granodiorite + high proportion fine grained granite	56	6%

Table 5-10. Borehole sections used to characterise subdomains in domain RSMM01.

Thermal subdomain	Borehole	Borehole length, from-to, m ¹	Approximate borehole length per subdomain (DZ included), m
M1	KLX03	101–620 m	1,200 m
	KLX17A	66–588 m	
	KLX18A	119–336 m	
M2	KLX05	292–473 m	1,050 m
	KLX10	857–981 m	
	KLX12A	102–528 m	
	KLX13A	102–456 m	
M3	KLX13A ²	458–593 m	500 m
	KLX17A	590–697 m	
	KLX18A	338–611 m	
M4	KLX08	587–924 m	350 m
M5	KLX05	108–290 m	200 m

¹based on domain classification of boreholes, ESHI (extended single-hole interpretations). ² excluded because of the presence of a deformation zone between 486 m and 593 m

Domain RSMD01

All of rock domain RSMD01 is assigned to the one thermal domain as summarised in Table 5-11.

In contrast to domains RSMA01 and RSMM01, domain RSMD01 is lithologically quite homogenous, and subdivision into subdomains was judged to be unnecessary. The proportion of TRC 136 (oxidised Quartz monzodiorite) in different boreholes does show considerable variation, however. All boreholes in domain RSMD01 with the exception of KLX20A have between 2 and 14% oxidised quartz monzodiorite. In contrast, about 40% of the borehole length in KLX20A is made up of such rock. Instead of creating a separate subdomain based on KLX20A, it was decided to exclude the borehole from the input to the geological simulations, for the following reasons:

- This borehole is situated in the western periphery of domain RSMD01 where it intersects a larger regional deformation zone (NS001). The large occurrence of alteration in KLX20A is associated with this deformation zone.
- A future deep repository is unlikely to be situated in areas close to this type of large deformation zone, which means that this borehole is considered to be less representative of the repository volume in domain RSMD01.

The remaining boreholes characterising the domain were treated as a single domain. The borehole sections, approximately 3,500 m in total, used to characterise domain RSMD01 are listed in Table 5-6.

Table 5-11. Thermal domain defined in rock domain RSMD01.

Thermal domain	Chatacteristic rock type(s)	Dominant TRC	Proportion of domain, %
D	Quartz monzodiorite	36	100%

5.3.4 Lithological data preparation

Geological borehole data were processed into a format suitable for spatial statistical analysis (Step 2 in Figure 4-1). The data were prepared to match the resolution used in the simulations, which is defined as the size of a grid cell in the simulation, in this case 2 m. This required assigning a TRC to each position along a borehole at 2 m intervals.

The borehole data was processed according to the following steps:

1. Data from rock type (> 1 m borehole length) and rock occurrence (< 1 m borehole length) in the Boremap system were merged. The resolution in the Boremap system is 1 cm. Fine-grained granite and pegmatite having borehole lengths less than 1 m were removed. This is justified since a large proportion, approximately 50%, of these rock types occur as very small bodies, often as veins and thin dykes (< 0.2 m borehole length). This is illustrated for domain RSMM01 in Figure 5-2. Since 2 m cubes (grid cells) is the smallest size that can be represented in the geological simulations, retaining these occurrences would lead to an overestimation of larger bodies of fine-grained granite, creating a so called discretisation error. By excluding these minor occurrences, the overall proportion of this TRC is reduced. Since both fine grained granite and pegmatite are quartz rich felsic rock with relatively high thermal conductivities, this decision is not considered critical for the modelling of thermal properties, in which the focus is on accurate description of the low-conductive rock mass.
2. Each 0.1 m section of borehole was assigned a rock type according to the dominant lithology.
3. A data column indicating the presence of large (deterministically modelled) deformation zones was created using data from ESHI.
4. Ävrö granite was reclassified as either Ävrö quartz monzodiorite or Ävrö granodiorite by means of borehole density logging data, which has a resolution of 0.1 m. The subdivision, based on borehole density logging data, uses a threshold density value of 2,710 kg/m³. The procedure for this step is described in Section 3.7.3.
5. Boreholes and parts of boreholes were grouped according to the domain classification of boreholes /Wahlgren et al. 2008/.
6. The appropriate TRC code was assigned to each 0.1 m section. Borehole sections within identified large (deterministically modelled) deformation zones were not assigned a TRC and have been excluded from the analysis. The main reason for this is that the rock mass within such deformation zones will not be utilised for deposition holes in a possible future repository. Another reason is that the method for dividing Ävrö granite into its two varieties (using a density value of 2,710 kg/m³) is less reliable in rock affected by increased fracturing and porosity which is typical for deformation zones. Minor deformation zones (MDZ), which are not modelled deterministically, have not been excluded from the borehole data. Such zones, although not allowed to intersect a deposition hole, may be close enough to have an effect on the temperature field surrounding a deposition hole /SKB 2006c/, which means that the rock in the zones is relevant for thermal properties. Ävrö granite also occurs in some of these deformation zones, but generally speaking the densities recorded by density logging do not appear to be influenced to the extent that it renders the method for dividing Ävrö granite into its two types ineffective.
7. At regular 2 m intervals along the borehole a TRC code was randomly selected from the 0.1 m codes within a 2 m section. This selected TRC is assumed to represent the lithology at each 2 m interval. This probabilistic approach was considered appropriate in order to avoid underestimating the proportions of rock types occurring as small bodies, i.e. 1–2 m borehole length.
8. Coordinates (northing, easting and elevation) were assigned to each 2 m section. These coordinates were obtained from geophysical logging data files in the SICADA database.

5.4 Spatial statistical structure of the TRCs (lithology)

5.4.1 Establishment of lithological models

In this section the models of the spatial distribution of lithologies are presented (Step 7 in Figure 4-1). The models are based on an analysis of the borehole data described in 5.3.4. Since the resolution of the borehole data was 2 m, the spatial properties also apply to 2 m resolution. Typical (mean) lens length and interactions of TRCs were calculated by transition probability analysis of the borehole data using T-PROGS software /Carle 1999, Carle and Fogg 1997/. Length refers to the dimensions of a TRC in a particular direction, often the borehole direction. Model parameters derived from this statistical analysis were modified in order to take geological interpretations into account (Step 6 in Figure 4-1), for example, anisotropy due to subordinate rock bodies as described in Section 5.3.2. In the context of the lithological simulations, anisotropy refers to subordinate rock types having dimensions in one particular direction that are different to another direction. Only domain RSMD01 was modelled with anisotropy. The other domains were modelled with the presumption of isotropy for reasons outlined in Section 5.3.2.

The typical lens lengths estimated for TRC 58 (fine-grained granite) have been adjusted downwards in most subdomains. The reason for this adjustment is that fine-grained granite generally occurs as dykes, with a true thickness that is lower than the apparent thickness indicated by borehole intersections. An exception is subdomain M5 where bodies of fine-grained granite are much larger than normal. No adjustment was made for this subdomain.

Some borehole sections were omitted for purposes of estimating typical lengths and transition probabilities, but were included for calculation of thermal subdomain proportions as well as the proportions of TRCs. The main reason for excluding data is that some sections were statistically anomalous compared to other sections assigned to the subdomain. For example, a 125 m long borehole section in KLX10 belonging to subdomain M2 was omitted for this reason. However, the number of realisations run for this subdomain, which is directly related to its relative proportion, acknowledges the presence of this section. Likewise for domain RSMD01, typical lens lengths for TRC 102 were calculated without KLX19A, whereas proportions and transition probabilities were based on all boreholes including KLX19A. This adjustment was introduced to prevent the large dolerite occurrence in KLX19A from influencing the typical lens length. Instead, the lens lengths are based on the more evenly distributed fine-grained diorite-gabbro. Dolerite, on the other hand, is a rather anomalous rock, with isolated occurrences generally associated with deformation zones.

Spatial properties of TRCs for the 2 m resolution were scaled up to provide model parameters for 4 m and 8 m resolution. The up-scaling was made through standard transition probability analysis, as described by e.g. /Davis 1986/. This was performed for rock domain RSMM01 only for the purpose of describing the size distribution of subordinate rocks.

Domain RSMA01

The results of the spatial analysis for domain RSMA01 for 2 m data are given in Table 5-12 to Table 5-14. Transition probabilities are presented as embedded probabilities of passing from one TRC to other TRCs irrespective of the lag distance; see /Davis 1986, Carle and Fogg 1997, Back and Sundberg 2007/ for more details.

Table 5-12. Proportions, transition probabilities and typical lengths for domain RSMA01, thermal subdomain A1 for 2 m data. Transition probabilities are shown as embedded probabilities of going from one TRC to other TRCs. Diagonal terms show the typical lengths of TRCs based on all boreholes.

TRC	Proportion	Isotropic transition probabilities to TRCs (embedded) and typical lengths (m). (Lengths shown in bold)				
		<i>TRC30</i>	<i>TRC 46</i>	<i>TRC 56</i>	<i>TRC 58</i>	<i>TRC 102</i>
<i>TRC 30</i>	0.02	6.17	0.17	0.83	0.00	0.00
<i>TRC 46</i>	0.19	0.04	7.51	0.93	0.01	0.02
<i>TRC 56</i>	0.76	0.09	0.74	24.02	0.05	0.12
<i>TRC 58</i>	0.01	0.00	0.33	0.67	3.50*	0.00
<i>TRC 102</i>	0.01	0.00	0.21	0.79	0.00	2.73

* Based on geological interpretations, the typical length of TRC58 was estimated to be half the length calculated in the transition analysis of borehole data.

Table 5-13. Proportions, transition probabilities and typical lengths for domain RSMA01, subdomain A2 for 2 m data. See also text in Table 5-12.

TRC	Proportion	Isotropic transition probabilities to TRCs (embedded) and typical lengths (m). (Lengths shown in bold)			
		<i>TRC 30</i>	<i>TRC 46</i>	<i>TRC 56</i>	<i>TRC 102</i>
<i>TRC 30</i>	0.01	3.00	0.50	0.00	0.50
<i>TRC 46</i>	0.61	0.04	14.54	0.97	0.00
<i>TRC 56</i>	0.37	0.05	0.91	8.80	0.05
<i>TRC 102</i>	0.01	0.00	0.50	0.50	2.00

Table 5-14. Proportions, transition probabilities and typical lengths for domain RSMA01, subdomain A3 for 2 m data. See also text in Table 5-12.

TRC	Proportion	Isotropic transition probabilities to TRCs (embedded) and typical lengths (m). (Lengths shown in bold)				
		<i>TRC30</i>	<i>TRC 46</i>	<i>TRC 56</i>	<i>TRC 58</i>	<i>TRC 102</i>
<i>TRC 30</i>	0.35	22.49	0.00	0.13	0.13	0.73
<i>TRC 46</i>	0.24	0.08	5.00	0.92	0.00	0.00
<i>TRC 56</i>	0.22	0.00	0.91	4.67	0.00	0.09
<i>TRC 58</i>	0.10	1.00	0.00	0.00	6.50*	0.00
<i>TRC 102</i>	0.09	0.25	0.50	0.00	0.25	5.50

* Based on geological interpretations, the typical length of TRC58 was estimated to be half the length calculated in the transition analysis of borehole data.

Domain RSMD01

The results of the spatial analysis for domain RSMA01 for 2 m data are given in Table 5-15 for the vertical direction and in Table 5-16 for the horizontal direction. Transition probabilities are presented as embedded probabilities.

Table 5-15. Proportions, transition probabilities and typical lengths for domain RSMD01 in z-direction for 2 m data. See also text in Table 5-12.

TRC	Proportion	Isotropic transition probabilities to TRCs (embedded) and typical lengths (m). (Lengths shown in bold)			
		TRC 36	TRC 58	TRC 102	TRC 136
TRC 36	0.83	17.10	0.16	0.15	0.69
TRC 58	0.03	0.89	4.01	0.00	0.11
TRC 102	0.03	0.74	0.00	3.71	0.26
TRC 136	0.10	0.93	0.02	0.05	2.68

* Based on geological interpretations, the typical length of TRC58 was estimated to be two-thirds the length (5.99 m) calculated in the transition analysis of borehole data.

The results of the transition probability analysis for the vertical (z) direction, presented in Table 5-15, were adjusted for the horizontal (xy) plane, due to the geological interpretation of anisotropic conditions for TRC102. This TRC was interpreted to occur as thin discs in the x,y-plane with length ratio 10:10:1 in the x,y,z directions as described in Section 5.3.2. The typical length in the x-y-plane was therefore adjusted to 10 times the length in z direction, i.e. to 37.1 metres. Due to the relationship between proportions, typical lengths and transition probabilities, the transition probabilities and typical lengths for other TRCs changed as the lengths for TRC102 were adjusted. The transition probabilities and typical lengths after adjusting for the anisotropy of TRC102 are shown in Table 5-16.

Domain RSMM01

The results of the spatial analysis for domain RSMM01 for 2 m data are given in Table 5-17 to Table 5-19. Transition probabilities are presented as embedded probabilities. The spatial properties for the 4 m and 8 m lag resolution (i.e. 4 m and 8 m lag distances) were estimated by up-scaling of the 2 m data. The results of the spatial analysis for each subdomain for 4 m and 8 m data are given in Appendix L.

Table 5-16. Proportions, transition probabilities and typical lengths for domain RSMD01 in x,y-directions for 2 m data, after adjusting for anisotropy in TRC102. See also text in Table 5-12.

TRC	Proportion	Isotropic transition probabilities to TRCs (embedded) and typical lengths (m). (Lengths shown in bold)			
		TRC 36	TRC 58	TRC 102	TRC 136
TRC 36	0.83	19.55	0.17	0.00	0.83
TRC 58	0.03	0.89	4.01	0.00	0.11
TRC 102	0.03	0.74	0.00	37.11	0.26
TRC 136	0.10	0.93	0.02	0.05	2.68

* Based on geological interpretations, the typical length of TRC58 was estimated to be two-thirds the length (5.99 m) calculated in the transition analysis of borehole data.

Table 5-17. Proportions, transition probabilities and typical lengths for subdomain M1 for 2 m data. See also text in Table 5-12.

TRC	Proportion	Isotropic transition probabilities to TRCs (embedded) and typical lengths (m). (Lengths shown in bold)			
		TRC 33	TRC 56	TRC 46	TRC 58
TRC 33	0.09	4.61	0.04	0.96	0.00
TRC 56	0.10	0.07	4.04	0.90	0.03
TRC 46	0.80	0.38	0.59	18.69	0.04
TRC 58	0.01	0.33	0.00	0.67	3.00*

* Typical length of TRC58 was estimated to 4.67 m in the transition analysis, but adjusted to 3 m based on geological interpretations.

Table 5-18. Proportions, transition probabilities and typical lengths for subdomain M2 for 2 m data. See also text in Table 5-12.

TRC	Proportion	Isotropic transition probabilities to TRCs (embedded) and typical lengths (m). (Lengths shown in bold)			
		TRC 33	TRC 56	TRC 46	TRC 58
TRC 33	0.29	10.77	0.16	0.81	0.08
TRC 56	0.05	0.14	3.06	0.86	0.00
TRC 46	0.64	0.61	0.30	17.07	0.08
TRC 58	0.02	0.40	0.20	0.40	3.00*

* Typical length of TRC58 was estimated to 4 m in the transition analysis, but adjusted to 3 m based on geological interpretations.

Table 5-19. Proportions, transition probabilities and typical lengths for subdomain M3 for 2 m data. See also text in Table 5-12.

TRC	Proportion	Isotropic transition probabilities to TRCs (embedded) and typical lengths (m). (Lengths shown in bold)			
		TRC 33	TRC 56	TRC 46	TRC 58
TRC 33	0.05	6.67	0.67	0.33	–
TRC 56	0.81	0.27	26.51	0.73	–
TRC 46	0.14	0.00	1.00	5.40	–
TRC 58	–	–	–	–	–

Table 5-20. Proportions, transition probabilities and typical lengths for subdomain M4 for 2 m data. Se also text in Table 5-12.

TRC	Proportion	Isotropic transition probabilities to TRCs (embedded) and typical lengths (m). (Lengths shown in bold)			
		TRC 33	TRC 56	TRC 46	TRC 58
TRC 33	0.25	8.26	0.89	0.11	–
TRC 56	0.61	0.47	10.45	0.53	–
TRC 46	0.14	0.08	0.92	4.17	–
TRC 58	–	–	–	–	–

Table 5-21. Proportions, transition probabilities and typical lengths for subdomain M5 for 2 m data. See also text in Table 5-12.

TRC	Proportion	Isotropic transition probabilities to TRCs (embedded) and typical lengths (m). (Lengths shown in bold)			
		TRC 33	TRC 56	TRC 46	TRC 58
TRC 33	0.01	2.00	1.00	0.00	0.00
TRC 56	0.68	0.12	14.10	0.64	0.24
TRC 46	0.13	0.00	0.71	3.43	0.29
TRC 58	0.18	0.00	0.75	0.25	8.00

5.5 Stochastic simulation of TRCs (lithology)

5.5.1 Introduction

Stochastic unconditional simulations of the spatial distribution of TRCs at 2 m resolution were performed for each thermal subdomain or domain using the spatial properties derived from the analysis described in Section 5.4.1 (Step 8 in Figure 4-1). Simulations were performed using the T-PROGS software. The model dimensions were 100 m x 100 m x 100 m, i.e. a total of 125,000 cells. A total of 1,000 realisations were produced for each rock domain. These were divided among the subdomains in proportion to the borehole length making up each subdomain (Table 5-22).

In addition, a total of 200 realisations were produced for the 4 m and 8 m resolution simulations performed for rock domain RSMM01. These were divided among the subdomains following the same principle as for the 2 m simulations (Table 5-22).

5.5.2 Example results

Figure 5-4, Figure 5-5 and Figure 5-6 gives examples of realisations of the distribution of TRCs for the three modelled rock domains.

Table 5-22. Division of realisations for each rock domain.

Rock domain	Thermal subdomain	Number of realisations, 2 m simulations	Number of realisations, 4 m and 8 m simulations
RSMA01	A1	741	
	A2	179	
	A3	80	
RSMD01	D	1,000	
RSMM01	M1	383	76
	M2	347	70
	M3	109	22
	M4	105	20
	M5	56	12

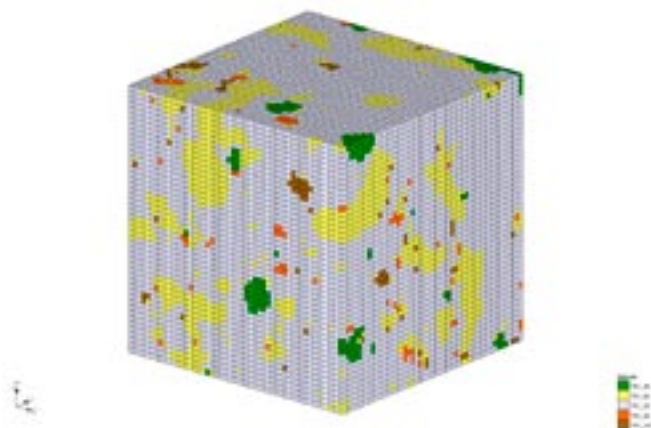


Figure 5-4. A visualisation of one realisation of the distribution of TRCs in subdomain A1 with 2 m resolution (cell size). The simulated rock volume has dimensions 100x100x100 metres. The simulated TRCs are TRC30 (green), TRC46 (yellow), TRC56 (white), TRC58 (red) and TRC102 (brown). Simulations were performed using the T-PROGS software.

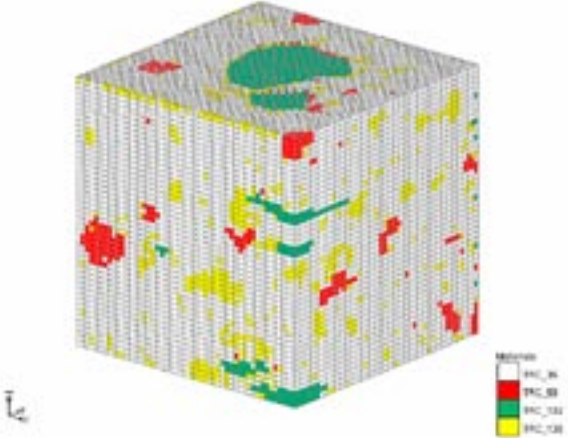


Figure 5-5. A visualisation of one realisation of the distribution of TRCs in domain RSMD01 with 2 m resolution (cell size). The simulated rock volume has dimensions 100x100x100 metres. The simulated TRCs are TRC36 (white), TRC58 (red), TRC102 (green) and TRC136 (yellow). Simulations were performed using the T-PROGS software.

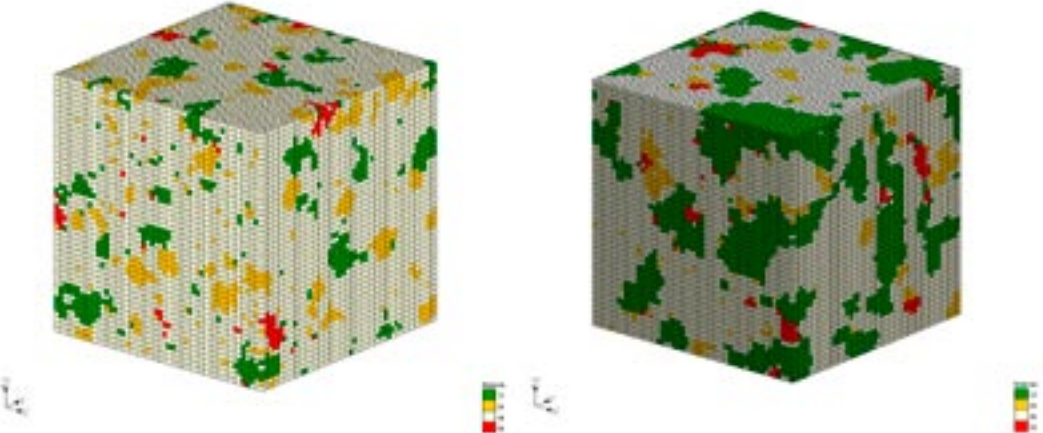


Figure 5-6. Two visualisations of realisations of the distribution of TRCs in subdomain M1 (left) and subdomain M2 (right) with 2 m resolution (cell size). The simulated rock volume has dimensions 100x100x100 metres. The simulated TRCs are TRC33 (green), TRC46 (white), TRC56 (yellow) and TRC58 (red). Simulations were performed using the T-PROGS software.

5.5.3 Analysis and verification of results

Methodology

The statistical properties, i.e. the proportions of categories (TRCs), the typical lengths of categories and the spatial properties of categories are assumed to be stationary for all realisations. The relevance of the results of the simulations have been analysed and verified by means of statistical analysis with respect to the ability of T-PROGS to reproduce:

- The proportions of the TRCs,
- Typical (mean) lengths of TRCs calculated by transition probability analysis, and
- The distribution of TRC lengths observed in borehole data.

The simulations were used for the verification analysis, which was made as follows:

- The proportions of TRCs were calculated for 10 randomly selected realisations and compared to the proportions calculated from borehole data. The reproducibility of proportions was assumed to be equal for all subdomains.
- The typical lengths were calculated from 36 “simulated boreholes” along each direction (x, y and z) for each of 10 randomly selected realisations for all scales and all subdomains. Typical lengths were calculated for x, y and z directions for all TRCs.
- Histograms of the lengths of the TRCs were produced from the 36 “simulated boreholes” along each direction (x, y and z) for each of the 10 randomly selected realisations in each subdomain.
- For all subdomains a comparison was made between simulated typical lengths (mean values) and the typical lengths (mean values) estimated from the transition analysis (referred to as “nominal” lengths below). The mean values of simulated TRC lengths were estimated assuming a geometric distribution, which is a fundamental assumption in the approach to geological simulation used here. The transitions between categories (TRCs) are assumed to follow a Markov process, in which the lengths of the categories have a geometric distribution. The geometric distribution is the discrete analogue of the continuous exponential distribution, and has a probability function $P(X = n) = (1-p)^{n-1} p$. In the geological model application used here, the probability function describes the probability of leaving TRC X after taking n steps, each step having a probability p for leaving X . The mean of the geometric distribution is $1/p$. For further description of geometric distributions see e.g. /Evans et al. 2000/. It can be seen in the histograms from both simulations and from boreholes that the geometric distribution is a relevant model in most cases (see Appendix J). The comparison of the mean simulated lengths and mean lengths (nominal) from the transition analysis – both estimated assuming geometric distribution – was therefore considered as a relevant measure of performance.
- Histograms of the lengths of the TRCs observed in boreholes were produced.
- A qualitative comparison was made between the histograms produced from the simulations and the histograms produced from the actual borehole data.

Proportions

The simulated proportions for the TRCs have been analysed for domain RSMD01 and thermal subdomains A1, A2, A3 and M1. T-PROGS nearly exactly reproduces the proportions of the TRCs for all realisations and for all domains. Table 5-23 shows example results of the proportions of TRCs in 10 randomly selected realisations for subdomain A1. The corresponding tables for the other simulations can be found in Appendix I.

Table 5-23. Proportions of TRCs in 10 randomly selected realisations for subdomain A1.

Category	Proportions from input borehole data (%)	Proportions of randomly selected realisation (%)									
		1	2	3	4	5	6	7	8	9	10
TRC 30	2.4	2.4	2.4	2.4	2.4	2.4	2.4	2.4	2.4	2.4	2.4
TRC 46	19.2	19.2	19.2	19.2	19.2	19.2	19.2	19.2	19.2	19.2	19.2
TRC 56	76.0	75.9	75.9	75.9	75.9	75.9	75.9	75.9	75.9	75.9	75.8
TRC 58	1.3	1.3	1.3	1.3	1.3	1.3	1.3	1.3	1.3	1.3	1.3
TRC 102	1.2	1.2	1.2	1.2	1.2	1.2	1.2	1.2	1.2	1.2	1.2

Typical lengths – General

Calculations of typical lengths of TRCs were made from “simulated boreholes” through 10 randomly selected realisations for each of the subdomains. The “borehole length” of each borehole is 100 metres and 36 “simulated boreholes” were made in each direction. The total “borehole length” for the statistical analysis were thus $100 \times 36 \times 10 = 36,000$ metres for each direction. Although the simulations were made assuming isotropic conditions, it was interesting to compare the typical simulated lengths for the different directions to the isotropic nominal length to investigate whether the simulations were biased in any of the principal directions. The typical lengths of the TRCs in the data obtained from the “simulated boreholes” were calculated by transition probability analysis. TRCs that constitute the “background” in the simulations were not relevant to include in the analysis and were therefore omitted.

Typical lengths – Domain RSMA01

Results of the calculations of the typical length (m) for directions x, y and z are exemplified here by subdomain A1 in Table 5-24 to Table 5-27. Results for the other subdomains can be found in Appendix I.

Table 5-24. Typical lengths of TRC30 in subdomain A1.

Typical simulated length (m)*	Nominal value (m)*	Comment on simulated values
$\mu_x = 6.88$	6.17	OK
$\mu_y = 7.00$	6.17	OK
$\mu_z = 6.34$	6.17	OK

* The typical simulated length is the mean lengths estimated from “simulated boreholes” through the simulated rock volumes. The nominal value is the typical length estimated from the transition analysis in T-PROGS.

Table 5-25. Typical lengths of TRC46 in subdomain A1.

Typical simulated length (m)*	Nominal value (m)*	Comment on simulated values
$\mu_x = 8.38$	7.51	OK
$\mu_y = 7.88$	7.51	OK
$\mu_z = 8.28$	7.51	OK

* The typical simulated length is the mean lengths estimated from “simulated boreholes” through the simulated rock volumes. The nominal value is the typical length estimated from the transition analysis in T-PROGS.

Table 5-26. Typical lengths of TRC58 in subdomain A1.

Typical simulated length (m)*	Nominal value (m)*	Comment on simulated values
$\mu_x=4.98$	3.50	Somewhat high
$\mu_y=4.92$	3.50	Somewhat high
$\mu_z=4.50$	3.50	Somewhat high

* The typical simulated length is the mean lengths estimated from “simulated boreholes” through the simulated rock volumes. The nominal value is the typical length estimated from the transition analysis in T-PROGS.

Table 5-27. Typical lengths of TRC102 in subdomain A1.

Typical simulated length (m)*	Nominal value (m)*	Comment on simulated values
$\mu_x=3.94$	2.73	Somewhat high
$\mu_y=3.52$	2.73	Somewhat high
$\mu_z=3.66$	2.73	Somewhat high

* The typical simulated length is the mean lengths estimated from “simulated boreholes” through the simulated rock volumes. The nominal value is the typical length estimated from the transition analysis in T-PROGS.

It can be seen from the analysis that T-PROGS does not produce any directional bias for subdomain A1. T-PROGS produces reasonable estimates of typical lengths. The shorter lengths of TRC58 and TRC102 are somewhat overestimated. This may be due to the discretisation of the model, where the shortest possible length that can be simulated is 2 meters, i.e. equal to the cell size of the model. Even for other subdomains and domains it is commonly observed that T-PROGS overestimates TRCs having short model lengths.

Typical lengths – Domain RSMD01

Results of the calculations of the typical lengths (m) for directions x, y and z for domain RSMD01 are presented in Appendix I. Table 5-28 shows the typical lengths for TRC102 in domain RSMD01. The very strong anisotropy of TRC102 could not be reproduced as strongly as suggested by the geological interpretation of the area.

Typical lengths – Domain RSMM01

Results of the calculations of the typical lengths (m) for directions x, y and z for subdomain RSMM01 are presented in Appendix I. Table 5-28 shows the typical lengths for TRC33 in subdomains M1 and M3, respectively. It can be seen from the analysis that T-PROGS does not produce any significant directional bias. Typical lengths for TRC33 are reproduced well, although there is a tendency towards slight overestimations.

Table 5-28. Typical lengths of TRC102 in domain RSMD01.

Typical simulated length (m)*	Nominal value (m)*	Comment on simulated values
$\mu_x= 13.91$	37.1	Low
$\mu_y=9.67$	37.1	Low
$\mu_z=4.68$	3.71	OK

* The typical simulated length is the mean lengths estimated from “simulated boreholes” through the simulated rock volumes. The nominal value is the typical length estimated from the transition analysis in T-PROGS.

Table 5-29. Typical lengths of TRC33 in subdomain M1 for the 2 metre scale.

Typical simulated length (m)*	Nominal value (m)*	Comment on simulated values
$\mu_x = 5.34$	4.61	Somewhat high
$\mu_y = 5.60$	4.61	Somewhat high
$\mu_z = 5.88$	4.61	Somewhat high

* The typical simulated length is the mean lengths estimated from “simulated boreholes” through the simulated rock volumes. The nominal value is the typical length estimated from the transition analysis in T-PROGS.

Table 5-30. Typical lengths of TRC33 in subdomain M3 for the 2 metre scale.

Typical simulated length (m)*	Nominal value (m)*	Comment on simulated values
$\mu_x = 7.20$	6.67	OK
$\mu_y = 6.92$	6.67	OK
$\mu_z = 7.04$	6.67	OK

* The typical simulated length is the mean lengths estimated from “simulated boreholes” through the simulated rock volumes. The nominal value is the typical length estimated from the transition analysis in T-PROGS.

It can be concluded that T-PROGS is able to realistically reproduce the typical lengths calculated from transition analyses, but that there is in general a slight, in the order of 10%, overestimation of lengths. For shorter lengths close to the model resolution, overestimations are often greater and are believed to be due to discretisation effects.

Distribution of lengths

Due to the large number of “simulated boreholes” in the simulated volumes it is assumed that the histograms in Appendix J give a good representation of the simulated lengths of TRCs. A visual comparison was made of the histograms from the “simulated boreholes” with lengths observed in the actual borehole data, see Appendix K. The borehole information is rather limited compared to the number of data used for the simulation histograms. The visual comparison indicates, however, that T-PROGS is able to reproduce – for all TRCs – the TRC lengths registered in the borehole data.

5.5.4 Modelling of size distribution of TRCs

Based on the results of stochastic simulations of lithologies, it is possible to calculate the size distribution of subordinate rock types. However, a large number of simulations are required at several scales for this analysis. This work is on-going and will be reported in the near future. A summary of the results of the analysis carried out thus far is presented here.

To illustrate the information that can be obtained from a size-distribution analysis, the results of simulations at three scales, 2 m, 4 m and 8 m, have been analysed for TRC 33 in domain RSMM01. This was performed by using an algorithm that calculates the volume of individual rock bodies in the lithological realisations created by the stochastic simulations.

A set of rock volume classes were defined, and the number of TRC bodies belonging to each volume class were calculated. The statistics for the smaller scales are corrected for the smaller volumes so that the different scales can be compared.

According to the method used for determining the size distribution for a rock type, bodies in contact with the boundary of the simulation volume are removed. Retaining the boundary bodies would introduce a bias, since the volume of boundary bodies would be underestimated due to truncation, and the number of bodies would be overestimated because the boundary bodies occur in two or more simulation volumes. An alternative approach to tackling this problem is to count all the bodies, even those truncated by the sides of the simulation cube, followed by applying correction factors to compensate for the bias mentioned above. However, this approach has not been tested.

In Figure 5-7, the size distributions of TRC 33 (mainly diorite-gabbro) are shown. In the first plot, the average number of bodies in each volume class per realisation is shown. A realisation is a cube with sides 100 m long corresponding to a rock volume of 1,000,000 m³. The second plot is a cumulative probability plot showing the relative volume of a TRC that is comprised of bodies with a size less than or equal to a volume class. As regards the cumulative graphs, each scale is normalised to the volume for the largest scale. A simple approach is used: if the larger simulation scale is x times larger than the smaller scale, the size distribution for the smaller scale is multiplied by x. This scaling assumption will be tested in future work.

Since the true shape of rock bodies are uncertain (due to the existence of essentially vertical boreholes) or difficult to model, the isotropic assumption used in the simulations influences the computed size distribution.

Due to discretisation into 2 m, 4 m and 8 m cells respectively, the size distribution results for the lower part of the curve for each scale are not well resolved. Even the data for the largest bodies, i.e. “the upper end”, are uncertain, due to limited simulation volumes, as well as the removal of boundary bodies. In future work, determining the type of distribution, e.g. power-law, that describes these data will be central to the understanding of the size distribution. To obtain a better description of smaller bodies, simulation at a smaller scale than 2 m is required. It is proposed that 0.5 m is a suitable scale.

5.5.5 Uncertainties in estimates of TRC proportions

Introduction

Since thermal properties are closely correlated to rock type, the uncertainties in the estimated proportions of different rock types in rock domains are directly translated to uncertainties in the resulting thermal models. An intermediate step in thermal modelling of Laxemar was stochastic simulations of rock types (or TRCs). Input to these simulations was borehole data based on the domain classification of boreholes /Wahlgren et al. 2008/. The uncertainties associated with the estimates of volume proportions of different TRCs are quantified here.

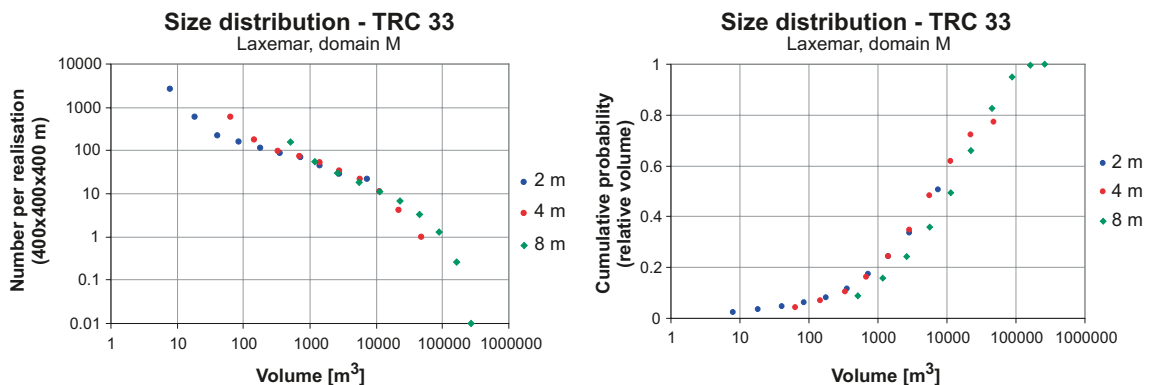


Figure 5-7. Size distribution of bodies of TRC 33, domain RSMM01 in Laxemar, based on stochastic simulation at 2 m, 4 m and 8 m scales. A single realisation at 8 m scale represents a rock volume of 64,000,000 m³. Note that the number of rock bodies in the figure on the left is underestimated because bodies located at the boundaries of the simulation volume are ignored.

There are some minor differences between the borehole data used for lithological simulations and the corresponding data used by the geological modelling team for characterisation of rock domains. Therefore, the proportions of thermal rock classes (TRC) estimated for each rock domain in the thermal model differ somewhat from the corresponding estimates given in the geological model.

Data treatment and assumptions

The mean proportions of TRCs and their confidence intervals have been determined based on borehole data selected as input for lithological simulations (see Table 5-31). The way in which the borehole data has been processed and the assumptions made are described in Section 5.3.4. The main differences between this and the data used by the geological modelling team in their volumetric estimates /Wahlgren et al. 2008/ are described below:

1. For purposes of lithological simulations, Ävrö granite in boreholes was divided into Ävrö quartz monzodiorite and Ävrö granodiorite. It should be noted that the estimated proportions of these rock types in each borehole are also uncertain because of the method used to make the subdivision, i.e. using density logs (Section 3.7.3). In the geological model, volume estimates of Ävrö quartz monzodiorite and Ävrö granodiorite have not been estimated, but are grouped under Ävrö granite.
2. Fine-grained granite and pegmatite having borehole lengths less than 1 m have been excluded from the analysis. By excluding these minor occurrences, the overall proportion of TRC 58 is reduced by about half.
3. Rock types belonging to a TRC making up less than 1% of the borehole length of a domain have been omitted.
4. Borehole sections occurring within large (deterministically modelled) deformation zones have been excluded. Proportions given in the geological model are based on borehole data with all deformation zones included.
5. Fewer boreholes were used in the input for lithological simulations. Boreholes were excluded if they were shorter than 200 m and borehole sections in a domain were excluded if they were shorter than 100 m.
6. The calculations for domain RSMA01 are based only on KLX02, KLX04, KLX07A, KLX08, KLX10 and KLX21B, since these boreholes are considered to be more representative for the bedrock in the central and southern part of the domain RSMA01 /Wahlgren et al. 2008/. KLX01, KLX06 and KLX09 in the northern part of Laxemar are excluded. The calculations for domain RSMD01 exclude borehole KLX20A.
7. Data from SICADA tables *p_rock* (> 1 m borehole length) and *p_rock_occurrence* (< 1 m borehole length) in the Boremap system are merged in such a way that that occurrences less than 5 cm are excluded, which may lead to underestimation of the proportions of some rock types. The geological modelling team have used somewhat different approach for merging the above mentioned tables /Wahlgren et al. 2008/.
8. The borehole data is weighted to take account of the different lengths of each borehole; longer boreholes contribute more data than short boreholes (this is consistent with the way the borehole data has been used in the lithological simulations – and by the geological modelling team).

Method for estimating confidence intervals

Each borehole or borehole section is seen as a sample (random data value) with a certain proportion of a rock type or TRC. First, the proportion of each TRC in each borehole is calculated. If there are 8 boreholes, this gives 8 different proportions for each TRC. In this calculation, the

Table 5-31. Boreholes used to characterise rock domains in the geological simulations.

Domain	Borehole	Borehole intervals (Sec up – Sec low) used as input for lithological simulations (based on geological rock domain model /Wahlgren et al. 2008/)
RSMA01	KLX02	200–540 m,
	KLX04	101–991 m
	KLX07A	102–842 m
	KLX08	101–587 m
	KLX10	102–857 m
	KLX21B	101–768 m
RSMD01	KLX03	621–998 m
	KLX05	473–995 m
	KLX11A	101–990 m
	KLX15A	78–980 m
	KLX16A	1–434 m
	KLX19A	100–796 m
RSMM01	KLX03	101–620 m
	KLX05	108–473 m
	KLX08	587–924 m
	KLX10	857–981 m
	KLX12A	102–528 m
	KLX13A	102–593 m
	KLX17A	66–697 m
	KLX18A	119–611 m

value for each borehole is weighted according to the length of the borehole. Then the bootstrapping method is applied to these data values. This involves randomly selecting 8 values with replacement from the original set of 8. The bootstrap resampling is performed 50,000 times. For each resample a new mean proportion is calculated, and a distribution of mean proportions for each TRC is produced. For each TRC, confidence intervals for the statistic of interest can be determined. No assumptions regarding the nature of the data distributions are required, as confidence limits can be determined directly from the simulated data. In the case presented below, the 95% two-sided confidence limits for the mean volume proportions of TRCs are estimated.

The confidence intervals estimated here are valid for the borehole scale.

Results

Domain RSMA01

The mean volume proportions and the 95% upper and lower confidence limits for TRCs in domain RSMA01 are presented in Table 5-32. The results are based on boreholes KLX02, KLX04, KLX07A, KLX08, KLX10 and KLX21B, that is the six boreholes used for lithological simulations of domain RSMA01. Bootstrapping was applied to TRC proportions per borehole based on data with different resolutions, both 0.1 m and 2 m. The 0.1 m data, with its higher resolution, can be considered to be more reliable. However, the 2 m data has been used in the lithological simulations, which form the basis for thermal modelling. A comparison of the mean proportions and estimated confidence intervals for the different data sets show only minor differences. The distributions generated by the bootstrap method for the 2 m data can be found in Appendix M.

Table 5-32. Proportions and confidence intervals for TRCs in domain RSMA01. Proportions based on geological model are from /Wahlgren et al. 2008/.

TRC	Rock name/ code	Mean proportion of TRC in domain RSMA01, %. From 2 m data	95% confidence intervals. Calculated from boot- strapping results, 2 m data	Mean proportion of TRC in domain RSMA01, %. From 0.1 m data	95% confidence intervals. Calculated from boot- strapping results, 0.1 m data	Proportion of TRC in 1,000 realisations, 2 m simulations, % %	Proportions based on geological model /Wahlgren et al. 2008/*
56	Ävrö granodiorite (501056), Granite (501058)	64.6%	55–76%	64.6%	55–76%	64.6%	} 88.7%
46	Ävrö Qtz monzodiorite (501046)	26.2%	15–40%	25.9%	15–40%	27.1%	
58	Fine-grained granite (511058) Pegmatite (501061)	1.8%	0.6–2.8%	1.9%	0.6–3.1%	1.8%	3.6%
30	Fine-grained dioritoid (501030) Quartz monzodiorite (501036)	5.4%	0.3–11.3%	5.6%	0.4–11.7%	4.8%	5.2%
102	Fine-grained diorite-gabbro (505102) Diorite-gabbro (501033)	2.0%	1.2–2.8%	2.0%	1.3–2.8%	1.7%	2.5%

* Boreholes located within domain RSMA01 in the central and southern part of Laxemar

The distribution of mean values for some TRCs shows a "clustering" pattern; certain values are very common while other values between these clusters occur more seldom, or not at all. This effect arises as a result of a combination of few values (boreholes) and one or more of the boreholes deviating strongly from the others. TRC 46 is an example of this (see Appendix M).

Domain RSMD01

The mean volume proportions and the 95% upper and lower confidence limits for TRCs in domain RSMD01 are presented in Table 5-33. The results are based on boreholes KLX03, KLX05, KLX11A, KLX15A, KLX16A and KLX19A, that is the six boreholes used for lithological simulations of domain RSMD01. Bootstrapping was applied to TRC proportions per borehole based on data with a resolution of 2 m. The distributions generated by the bootstrap method can be found in Appendix M.

Table 5-33. Proportions and confidence intervals for TRCs in domain RSMD01. Proportions based on geological model are from /Wahlgren et al. 2008/.

TRC	Rock name/code	Mean proportion of TRC in domain RSMD01, From 2 m data	95% confidence intervals. Calculated from bootstrapping results, 2 m data	Proportion of TRC in 1,000 realisations, 2 m simulations,	Proportions based on geological model /Wahlgren et al. 2008/
36	Quartz monzodiorite (501036)	84.6%	80–89%	82.9%	} 89.1%
136	Oxidised quartz monzodiorite (501036)	8.4%	5.9–10.8%	9.9%	
58	Fine-grained granite (511058) Pegmatite (501061)	3.6%	1.1–8.9%	3.5%	6.4%
102	Fine-grained diorite-gabbro (505102), Diorite-gabbro (501033), Ävrö quartz monzodiorite (501046), Dolerite (501027)	3.4%	1.1–6.0%	3.7%	c. 4%
36+136	Quartz monzodiorite (501036)	93.0%	89–96%		Other: < 1% 89.1%

Domain RSMM01

The mean volume proportions and the 95% upper and lower confidence limits for TRCs in domain RSMM01 are presented in Table 5-34. The results are based on boreholes KLX03, KLX05, KLX08, KLX10A, KLX12A, KLX13A, KLX17A and KLX18A, that is the eight boreholes used for lithological simulations of domain RSMM01. Bootstrapping was applied to TRC proportions per borehole based on data with a resolution of 2 m. The distributions generated by the bootstrap method can be found in Appendix M.

Table 5-34. Proportions and confidence intervals for TRCs in domain RSMM01. Proportions based on geological model are from /Wahlgren et al. 2008/.

TRC	Rock name/code	Mean proportion of TRC in domain RSMM01. From 2 m data	95% confidence intervals. Calculated from bootstrapping results, 2 m data	Proportion of TRC in 1,000 realisations, 2 m simulations,	Proportions based on geological model /Wahlgren et al. 2008/
33	Diorite-gabbro (501033), Fine-grained diorite-gabbro (505102),	16.9%	11.2–24.0%	16.7%	} 77%
56	Ävrö granodiorite (501056), Granite (501058)	27.7%	15.4–41.4%	24.7%	
46	Ävrö qtz monzodiorite (501046)	53.2%	35.6–68.0%	56.4%	
58	Fine-grained granite (511058) Pegmatite (501061)	2.2%	0.5–4.7%	2.2%	5.2%
					Other: < 1%

Conclusions

- The proportions of each TRC estimated from the borehole data used for lithological simulations deviate somewhat from the proportions of different rock types estimated by the geological team /Wahlgren et al. 2008/. The main reasons for the observed discrepancies are: 1) slightly different sets of boreholes were used by the different modelling teams, and 2) the borehole data was processed in slightly different ways. The confidence intervals presented here for the TRCs are valid given the assumptions made in the preparation of the data for lithological simulations. The most noticeable difference concerns TRC 58. The main reason for this is the exclusion from the lithological simulation data of fine-grained granite (511058) and pegmatite (501061) having borehole occurrences less than 1 m length. For all other TRCs the estimates by the geological modelling team fall within the calculated 95% certainty limits.
- Despite the relatively large number of boreholes in each domain, the high degree of lithological heterogeneity results in rather large uncertainties in the estimated proportions of TRCs. For example, the mean proportion of TRC 46 (Ävrö quartz monzodiorite) in domain RSMA01 lies between 15% and 40% with 95% confidence.
- The proportions estimated from the output of the simulations deviate slightly from the proportions in the input data. It was shown in Section 5.5.3 that the simulations nearly exactly reproduce the proportions of the TRCs used as input. Therefore, the discrepancies observed here are related to the way in which T-PROGS, the program used for lithological simulations, interpreted the borehole data. On calculating the proportions of TRCs from the borehole data, T-PROGS has interpreted short gaps in the data (brought about by removal of very minor rock types and deterministically modelled deformation zones) incorrectly. The effect of this error, largest for domain RSMM01, is, however, small compared to the estimated uncertainties.
- The same method can obviously be applied to rock type proportions instead of TRCs.

5.6 Spatial statistical models of thermal conductivity

5.6.1 Approach

Spatial statistical thermal conductivity models at the 0.1 m scale are required for each TRC in order to perform simulations at the scale at which the measurement data applies (Step 9 in Figure 4-1). Upscaling is performed in two steps in order to define thermal models for the 2 m scale, which is the same scale as that used in the geological simulations. Two types of model are required for each TRC: a statistical distribution model and a model describing spatial correlation, i.e. a variogram model; see 5.6.2 and 5.6.3. The statistical distribution model represents heterogeneity in thermal conductivity, without consideration of anisotropy.

Once the thermal models for the 0.1 m scale are defined, the thermal models for the 2 m scale are fairly easily determined (Step 5 in Figure 4-1). Therefore, the focus of the presentation below is on the thermal models for the 0.1 m scale.

Spatial statistical models of thermal conductivity are based on the following data (Step 4 in Figure 4-1):

- Thermal conductivity data consist of TPS measurements (Section 3.3), calculations from modal analysis by the SCA method (Section 3.5), field measurements at larger scales (Section 3.4), and calculations from density logging data (Section 3.7.4). The first two data types are the main source of information for defining histograms for TRCs.
- data for describing spatial correlation by means of variogram models are primarily density logging data (Sections 3.7.1 and 5.6.3) supported by TPS data.

5.6.2 Statistical distribution models – 0.1 m scale

For TRCs for which TPS data is plentiful or the SCA data may be biased, only the more reliable TPS data were used in defining the distribution models. For other TRCs, SCA values were used together with TPS data to create the data distributions. Declustering was applied to most rock types to ensure that spatially clustered data does not produce a bias in the statistics.

The statistical distribution models for each TRC are constructed from data values from the constituent rock types. For example, TRC 56 combines data from both Ävrö granodiorite (501056) and granite (501058). The data are weighted according to the relative proportions of each rock type as well as the number of data values available for each rock type.

For TRCs common to both domain RSMA01 and RSMM01, namely TRC 56 and TRC 58, the data are weighted according to the proportions of each rock type in domain RSMM01, which is broadly similar to those in domain RSMA01. A thermal model has not been defined for TRC 136 since this rock class was defined solely for the purpose of rock mechanic modelling. In the thermal modelling, TRC 136 is synonymous with TRC 36.

Thermal conductivity values determined from altered samples of the different rock types have been included in the data sets. For the common rock types, the relative amount of data on altered samples is roughly equivalent to the proportion of the rock mass outside the deformation zones which has been mapped as altered to a degree of weak or higher; i.e. faint alteration excluded /Wahlgren et al. 2008/. Approximately 20–30% of the rock mass, lowest in domain RSMM01, highest in domain RSMA01, has been mapped as altered. Excluding faint alteration reduces the figure to between 7 and 15% /Wahlgren et al. 2008/.

Standard distribution models, e.g. normal, lognormal, were not used to describe the probability distributions of thermal conductivity since for most TRCs such models were not supported by the data. Distribution models are instead based on smoothing of the sample histograms, performed using an algorithm in the geostatistical software GSLIB /Deutsch and Journel 1998/. This algorithm uses a simulated annealing procedure that honours the sample data statistics, such as the mean and standard deviation. Smoothing is required because of relatively small data sets. The smoothing operation requires input regarding the maximum and minimum values. Changing these values has a slight, but noticeable, effect on the shape of the distribution model. The principles for setting lower and upper limits of thermal conductivity in the distribution models for each thermal rock class (TRC) are given below.

1. The first and most important criterion is that the distribution model covers the range of the data for each TRC (both TPS and SCA data).
2. Theoretical lower limits of thermal conductivity were approximated from SCA calculations based on “extreme”, but possible, mineral compositions of each rock type. By “extreme” it is meant mineral compositions which produce the lowest rock thermal conductivities. These estimates were made in cooperation with the geological modelling team /Wahlgren 2008/. The upper limits were chosen more arbitrarily.
3. For rock types for which the judgements of extreme, but possible, compositions are difficult or impossible to make, the maximum and minimum limits set for compositionally similar rock types were used as guidelines.

TRC 30

TRC 30 occurs in domain RSMA01 and is comprised mainly of quartz monzodiorite (501036) and fine-grained dioritoid (501030) in roughly equal amounts. This TRC constitutes approximately 5% of the rock mass in domain RSMA01. The statistical distribution model is based on both rock types combined. Both TPS and SCA data are available, but only the more reliable TPS data is used. There are 63 TPS values for quartz monzodiorite and 28 for fine-grained dioritoid. Altered samples are included in the data sets.

Histograms and statistics for the two rock types are shown in Appendix C. Figure 5-8 shows the data for the two rock types combined. A statistical distribution model is produced by fitting a smoothed histogram to the weighted data, see Figure 5-9. The minimum value chosen is 2.3 W/(m·K), and is based on an extreme but possible mineral composition for quartz monzodiorite. Adopting a minimum value of 2.3 W/(m·K), the smoothing algorithm in GSLIB produces a distribution that does not taper off towards zero. To create a model that tapers off to zero at 2.3 W/(m·K), the smoothed histogram generated by GSLIB was modified. The lower tail between 2.3 and 2.4 W/(m·K) was adjusted as shown in Figure 5-9. This has the effect of producing a model with a slightly different mean and standard deviation compared with the data. But compared to other uncertainties, this adjustment is considered unimportant.

TRC 33

TRC 33 is present in domain RSMM01 only, where it makes up almost 20% of the rock volume. This TRC is dominated by diorite-gabbro (501033), but also includes subordinate amounts of fine-grained diorite-gabbro (505102). An analysis of various types of data from diorite-gabbro reveals a wide variation in properties and indicates, as the rock name suggests, that more than one distinct rock type is present. These data include:

1. Modal analyses. Mineralogy varies from plagioclase-rich compositions to mafic-mineral-rich compositions.
2. Density measurements on drill core samples. Density values of about 22 samples vary from 2,820 kg/m³ to 3,050 kg/m³.
3. Thermal conductivity measurements on the same samples as in 2. Thermal conductivities vary from 2.0 to 3.7 W/(m·K).
4. Borehole density logging data.

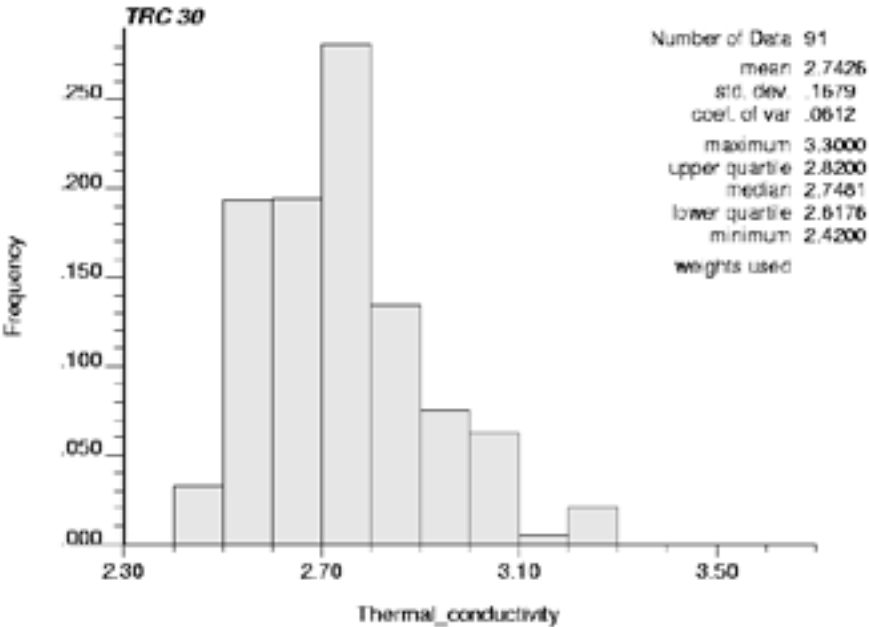


Figure 5-8. Histogram of TPS values for fine-grained dioritoid (501030) and quartz monzodiorite (501036). Data weighted to take account of clustering, the number of data values available for each rock type, and the relative proportions of the rock types in the TRC 30.

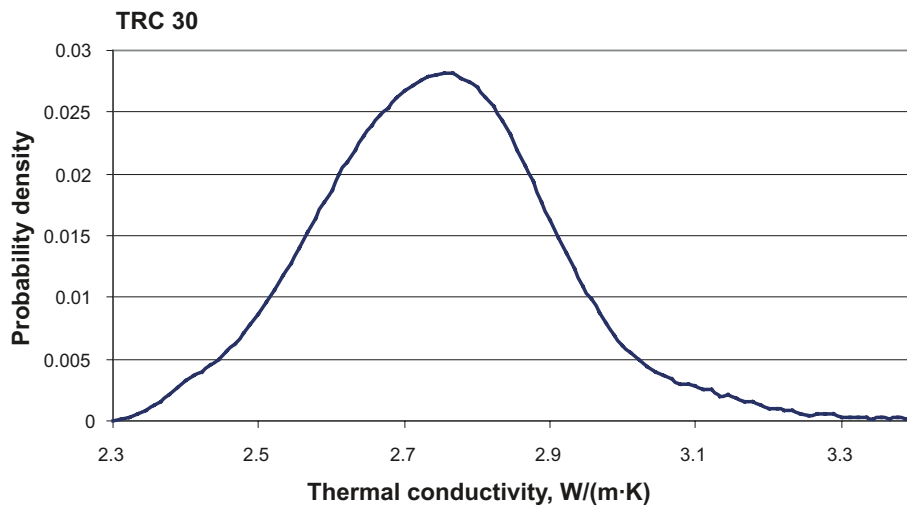


Figure 5-9. Statistical distribution model of thermal conductivity for TRC 30 based on smoothing of the data histogram: TPS values for fine-grained dioritoid (501030) and quartz monzodiorite (501036). Minimum value of 2.3 W/(m·K) based on calculations for a theoretical extreme composition.

Figure 5-10 indicates that diorite-gabbro with densities lower than 2,925 kg/m³ have generally low thermal conductivities, whereas rock having densities higher than 2,925 kg/m³ have very variable thermal conductivities. On the basis of density loggings, bodies of diorite-gabbro can be divided into two main compositional varieties. Bodies having low density (generally < 2,925 kg/m³) occur mainly in boreholes KLX03, KLX08, KLX10 and KLX18A. This type is referred to as type A. Bodies displaying high densities (generally > 2,925 kg/m³) are found mainly in boreholes KLX05, KLX12A, KLX13A and KLX17A. These bodies are referred to as type B. There is a certain degree of overlap in density values between two types. Although this is somewhat of a simplification it allows the rock to be characterised more accurately for thermal modelling purposes. A thermal model is erected for each type.

Thermal conductivity data for diorite-gabbro is provided by 22 TPS values and 8 SCA values. In order to assign the data values to the two different types of diorite-gabbro, the following procedure was followed:

1. TPS values were divided on the basis of the type of diorite-gabbro identified using density logging data. Samples belonging to diorite-gabbro bodies with densities predominantly < 2,925 kg/m³ were assigned to type A, and samples, diorite-gabbro bodies with densities that are predominantly > 2,925 kg/m³ were assigned to type B. The principle is exemplified by the four samples from borehole KLX13A sampled from two separate diorite-gabbro bodies; see Figure 5-10. Two samples belong to a low density body and are placed in type A. The other two were taken from a high density body and were thus placed in type B.
2. SCA values were also divided between types A and B but for most samples density logging data is not available. A study of mineralogy and its relationship with density indicates that samples dominated by felsic minerals (plagioclase, ± quartz) or having roughly equal amounts of felsic and mafic minerals have densities less than 2,950 kg/m³. Samples dominated by mafic minerals have densities greater than 2,920 kg/m³. These two groups correspond closely to the low (type A) and high density (type B) varieties of diorite-gabbro identified in boreholes by density logging. Not all modal analyses are accompanied by density determinations, but it is assumed that the above relationship holds for all samples. Data values based on the same samples as the laboratory measurements were excluded from the data distribution.

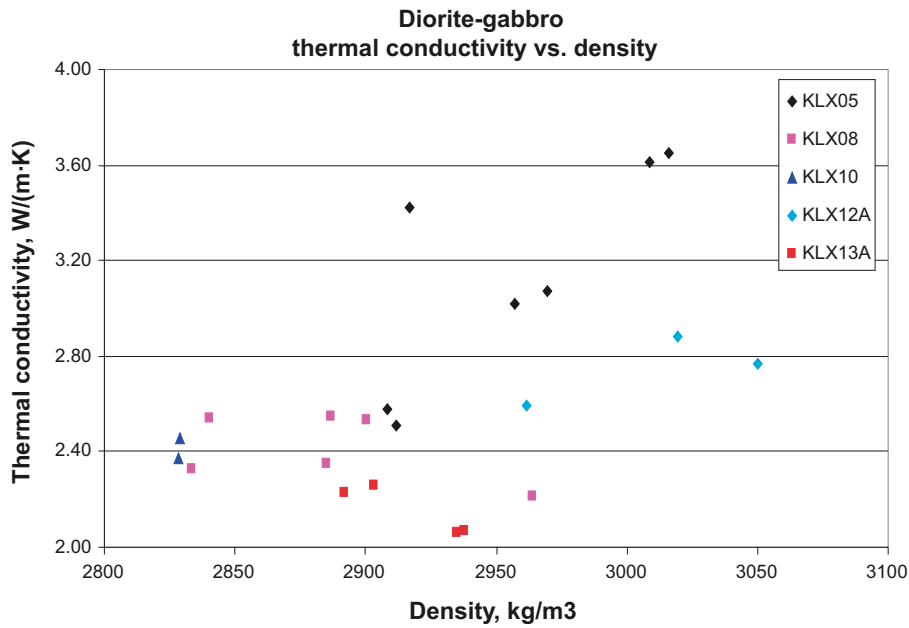


Figure 5-10. Density versus thermal conductivity (TPS) for diorite-gabbro samples.

Histograms and statistics for the two types of diorite-gabbro are presented in Figure 5-11. Type A is characterised by low thermal conductivities (2.2–2.6 W/(m·K)). Type B is characterised by a wide range of thermal conductivity values from low to high (2.1–3.7 W/(m·K)).

Thermal conductivity data for fine-grained diorite-gabbro (505102) is provided by 4 TPS values and 10 SCA values; see Figure 5-12. The distribution of thermal conductivity values is similar to that for diorite-gabbro Type A. All four TPS samples have densities lower than 2,925 kg/m³, again similar to the low-density diorite-gabbro type.

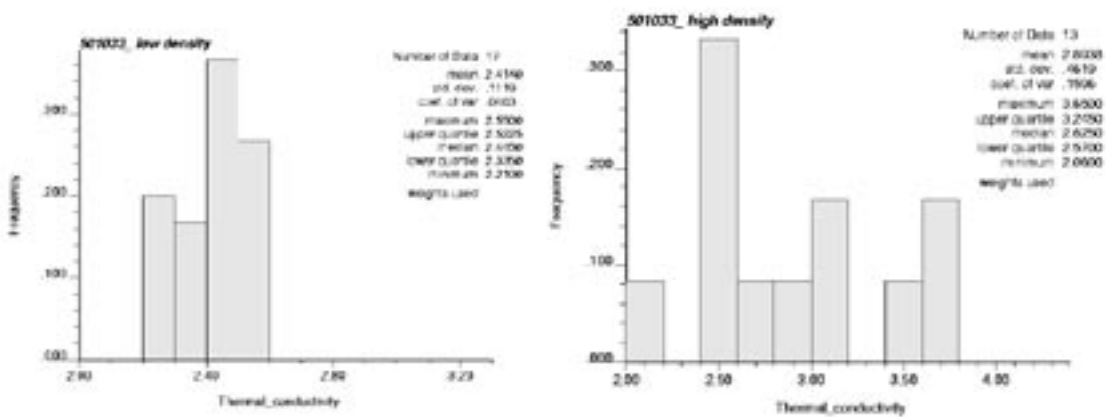


Figure 5-11. Histograms of thermal conductivity for diorite-gabbro (501033), type A (low density) and type B (high density) based on TPS and SCA values.

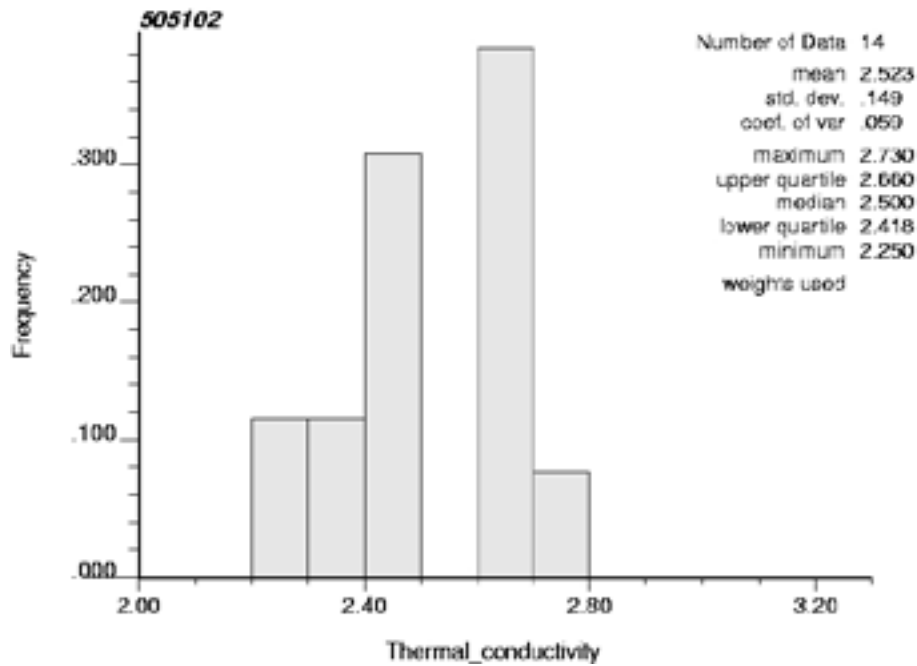


Figure 5-12. Histogram of TPS and SCA values for fine-grained diorite-gabbro (505102).

Both fine grained diorite-gabbro and diorite-gabbro type A are combined to form TRC 33A, the data distribution for which is shown in Figure 5-13. A distribution model is produced by fitting a smoothed histogram to the data, see Figure 5-14.

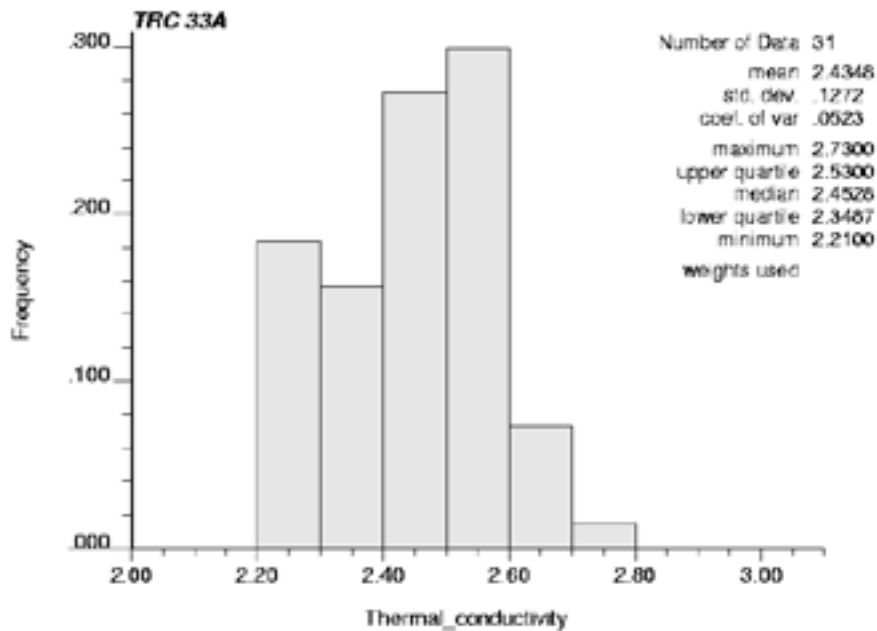


Figure 5-13. Histogram of thermal conductivity for TRC 33A based on TPS and SCA data for diorite-gabbro (501033) type A and fine grained diorite-gabbro (505102).

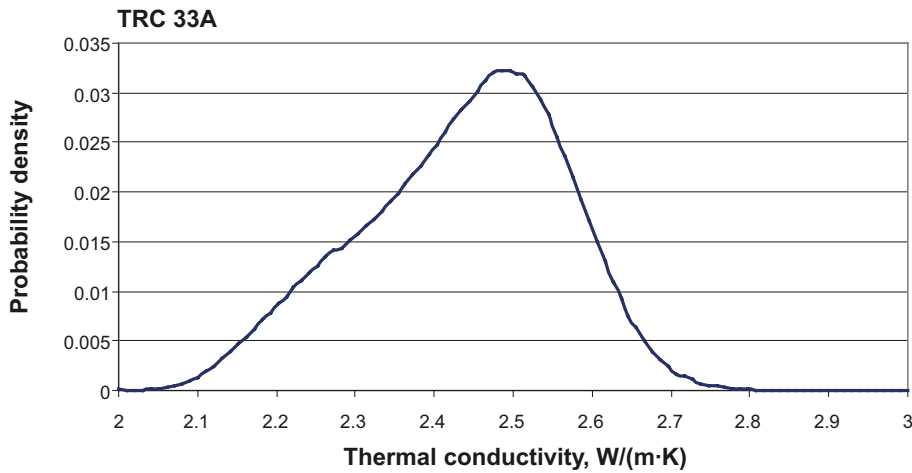


Figure 5-14. Statistical distribution model of thermal conductivity for TRC 33A based on smoothing of the data histogram: TPS and SCA values for diorite-gabbro (501033) type A and fine grained diorite-gabbro (505102). Minimum value of 2.0 W/(m·K) based on calculations for a theoretical extreme composition.

TRC 33B is represented by high-density diorite-gabbro. The large spread in data values coupled with a small number of data ($n=13$) (Figure 5-11) means that any distribution model based on these data will be associated with a high degree of uncertainty. Therefore, it was decided to create a triangular distribution which honours the mean and the standard deviation of the data; see Figure 5-15. Note that the minimum value of the distribution model is only slightly lower than the lowest TPS data value encountered; 2.06 in Figure 5-11.

Based on the relative proportions of diorite-gabbro (501033) and fine-grained diorite-gabbro (505102) in domain RSMM01, as well as density logging data for diorite-gabbro, it is estimated that TRC 33A and TRC 33B are present in domain RSMM01 in approximately equal amounts. Therefore, the thermal realisations for TRC 33 will be divided equally between TRC 33A and TRC 33B.

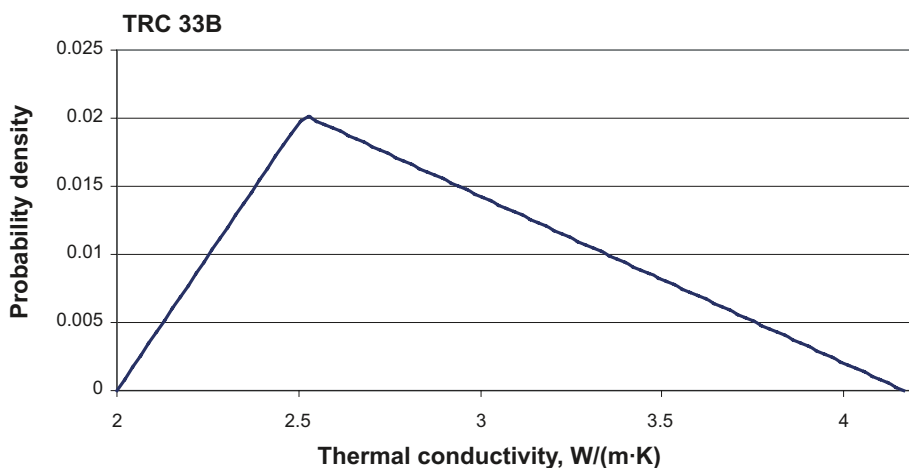


Figure 5-15. Statistical distribution model of thermal conductivity for TRC 33B assuming a triangle distribution based on statistics of TPS and SCA values for diorite-gabbro (501033) type B. The choice of 2.0 W/(m·K) for the minimum value is based on calculation of thermal conductivity for an extreme but possible mineral composition.

TRC 36

TRC 36 occurs in domain RSMD01 and is comprised mainly of rock type quartz monzodiorite (501036), but also very minor amounts of fine-grained dioritoid (501030). Although in the lithological simulations a separate TRC is defined by oxidised quartz monzodiorite (TRC 136), for thermal modelling purposes TRC 136 is assumed to be synonymous with TRC 36, so that both can be described by the same spatial statistical model of thermal conductivity (Section 5.3.1).

The statistical distribution model for TRC 36 is based on quartz monzodiorite (501036) only. Both TPS and SCA data are available. A comparison of TPS data with SCA data indicates that the latter may be underestimating thermal conductivity slightly. Thus the SCA values are not used. The number of TPS values (n=63) is considered to be sufficient to describe the distribution. These data are presented in Figure 5-16.

Five of the total of 63 data values for quartz monzodiorite represent altered rock (weak or higher), which have been shown to have higher thermal conductivity than fresh rock (Section 3.3.2). These values, which correspond to 8% of the total number of data values, are included in the data set on which the distribution model is based. This is similar to the proportion of the rock mass (deformation zones excluded) in domain RSMD01 altered to a degree of weak or higher as indicated by estimates from the borehole data /Wahlgren et al. 2008/.

A statistical distribution model produced by fitting a smoothed histogram to the data is shown in Figure 5-17. The smoothed distribution model generated by GSLIB was modified to create a model that tapers off to zero at 2.3 W/(m·K). The minimum value of 2.3 W/(m·K) was chosen based on an extreme but possible mineral composition for quartz monzodiorite. The lower tail between 2.3 W/(m·K) and 2.4 W/(m·K) was adjusted as shown in Figure 5-18. This has the affect of producing a model with a slightly different mean and standard deviation compared with the data. But compared to other uncertainties, this adjustment is considered unimportant.

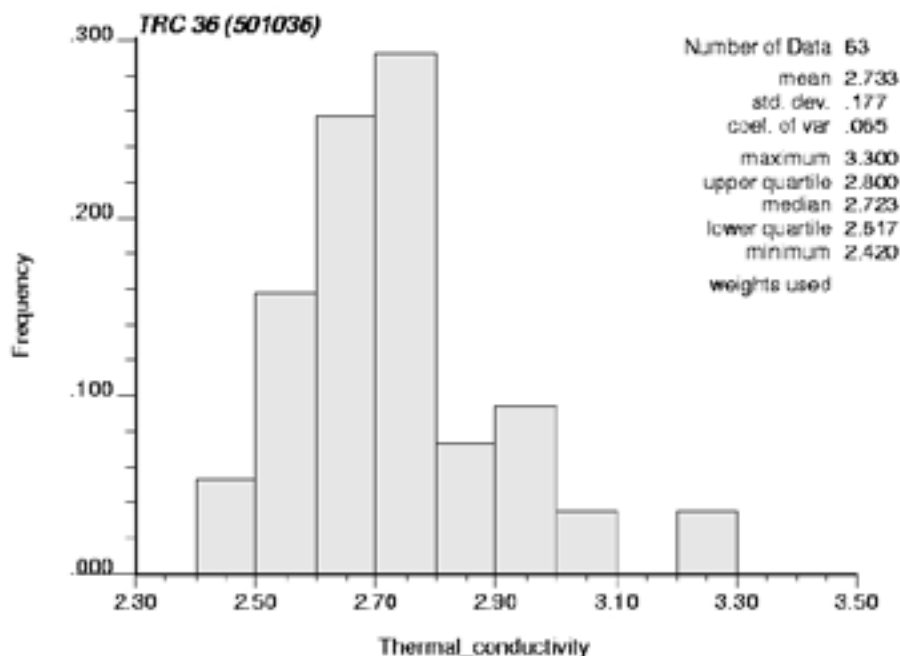


Figure 5-16. Histogram of TPS values for quartz monzodiorite (501036). Data weighted to take account of clustering.

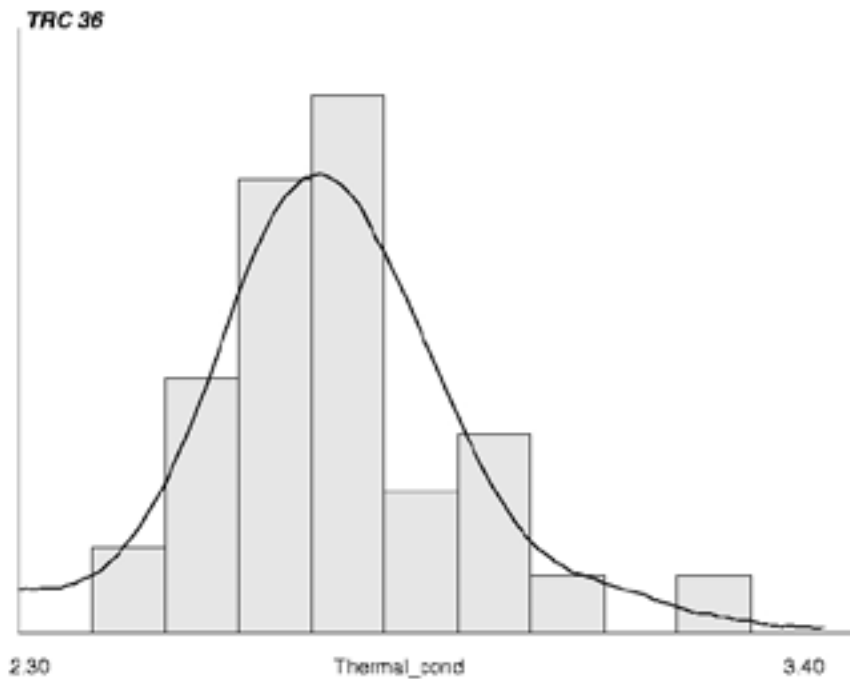


Figure 5-17. Statistical distribution model of thermal conductivity for TRC 36 based on smoothing of the TPS data histogram.

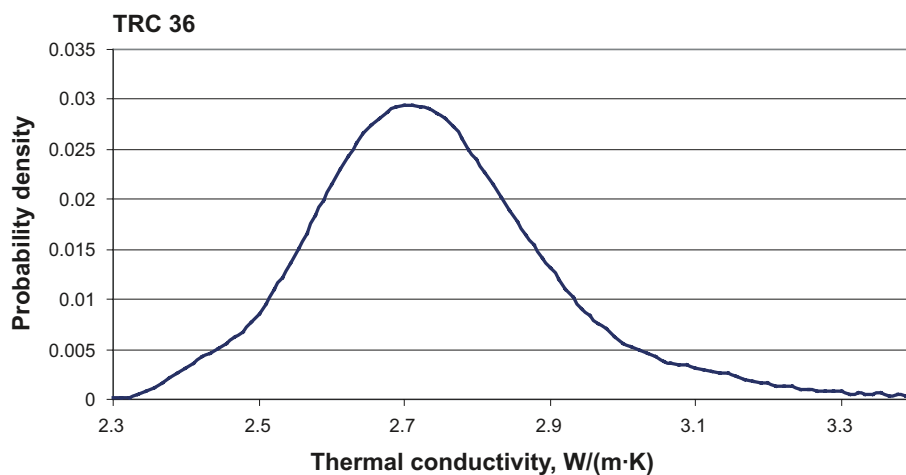


Figure 5-18. Modified statistical distribution model of thermal conductivity for TRC 36 based on smoothing of the data histogram: TPS values for quartz monzodiorite (501036). Minimum value of 2.3 W/(m·K) based on calculations for a theoretical extreme composition.

TRC 46

TRC 46, present in domains RSMMA01 and RSMM01, is comprised of one rock type, namely Ävrö quartz monzodiorite (501046).

TPS data are the most reliable type of data available but suffer from being few in number. Although there are 33 TPS data values, almost half of them come from spatial clusters of rock samples at four different borehole locations. This reduces the overall representativeness of the data. Histograms and statistics for declustered data are presented in Figure 5-19. The declustered TPS statistics are slightly different to the uncensored data statistics. The irregular shape of the histogram suggests that more data would be required to define the shape of the distribution with greater certainty.

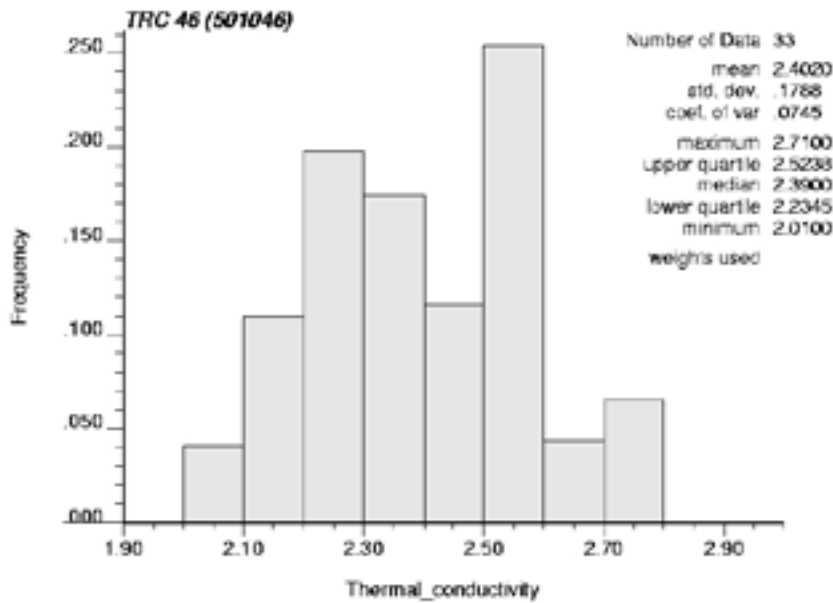


Figure 5-19. Histogram of thermal conductivity for TRC 46 based on 33 TPS data for Ävrö quartz monzodiorite.

One alternative is to complement the TPS data with values calculated from mineral composition (SCA data). A comparison of TPS and SCA data for Ävrö quartz monzodiorite indicates quite a good correspondence between the two methods, for all but the lowest thermal conductivities (Figure 3-12). For low thermal conductivity rocks, the SCA method overestimates the thermal conductivity, which reduces the benefit of considering this data significantly. For discussion of this point, see Section 3.5.4.

Another alternative for increasing the representativeness of the data is to use the calculations from density loggings. Thermal conductivity calculations from density loggings (Figure 5-20) show similar mean and standard deviation to the TPS data (Figure 5-19). Because of the large amount of data based on density logs, the calculated values give a smoother distribution than that based on TPS data. However, there are uncertainties associated with the calculated data, due to bias and noise in density loggings, and errors introduced when calculating thermal conductivity from density.

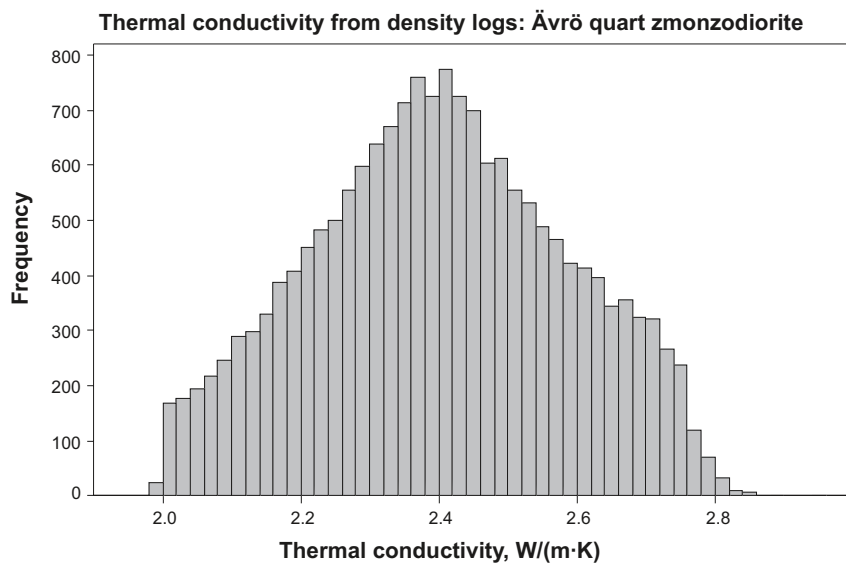


Figure 5-20. Histogram of thermal conductivity for Ävrö quartz monzodiorite based on calculations from density logging for several boreholes combined.— see Table 3-21. Mean = 2.40 W/(m·K), std. dev. = 0.18 W/(m·K) (n=17554).

Having considered the data from the different methods, it was decided that the more reliable TPS data should be used as the basis for the distribution model. A model is fitted to the data by using a smoothing algorithm, see Figure 5-21. The minimum and maximum values were set to 1.9 W/(m·K) and 2.9 W/(m·K), respectively. The minimum value was based on an extreme but possible mineral composition.

To gain an appreciation of the how representative the TPS data are, the laboratory measured density data (same samples as the TPS data) were compared with the density data from borehole logging, see Figure 5-24 and Figure 5-23. This comparison indicates that the samples selected for TPS measurement may be somewhat biased. Low density samples are slightly overrepresented, which in turn indicates the possibility of a bias towards higher thermal conductivities. The smoothing operation used on the TPS data tends to correct this bias, by reducing the probability of lambda values between 2.5 and 2.7 at the same time increasing the probability between 2.4 W/(m·K) and 2.5 W/(m·K).

In conclusion, the statistical distribution model for TRC 46 is based on the relatively reliable TPS data. The histogram is smoothed so as to even out the irregularities caused by the small number of data. Relative to the TPS data, the smoothing operation has the greatest effect on the middle part of the distribution. In contrast, the lower tail of the data distribution is influenced little by the smoothing procedure; the model follows the data closely and thus can be considered quite reliable for this part of the distribution. This is important for evaluating the results of the simulations; see Section 5.7.

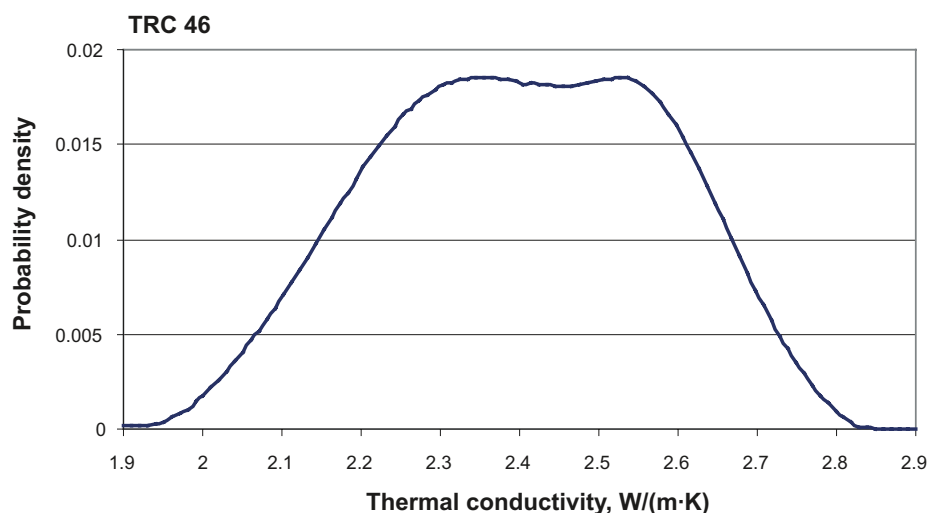


Figure 5-21. Statistical distribution model of thermal conductivity for TRC 46 based on smoothing of the TPS data histogram. Minimum value of 1.9 W/(m·K) based on calculations for a theoretical extreme composition.

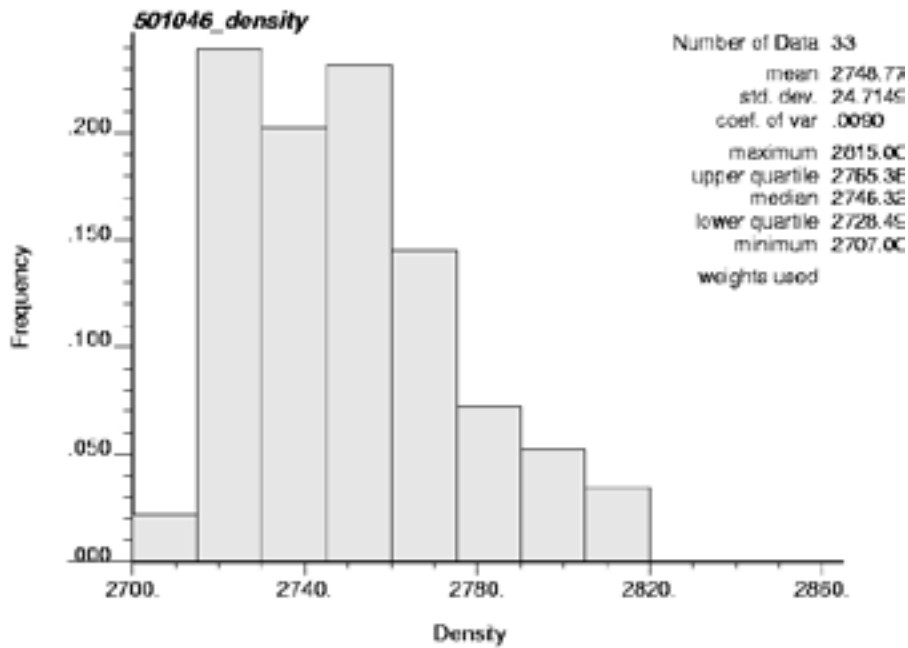


Figure 5-22. Histograms of density for Ävrö quartz monzodiorite (501046) from laboratory measurements.

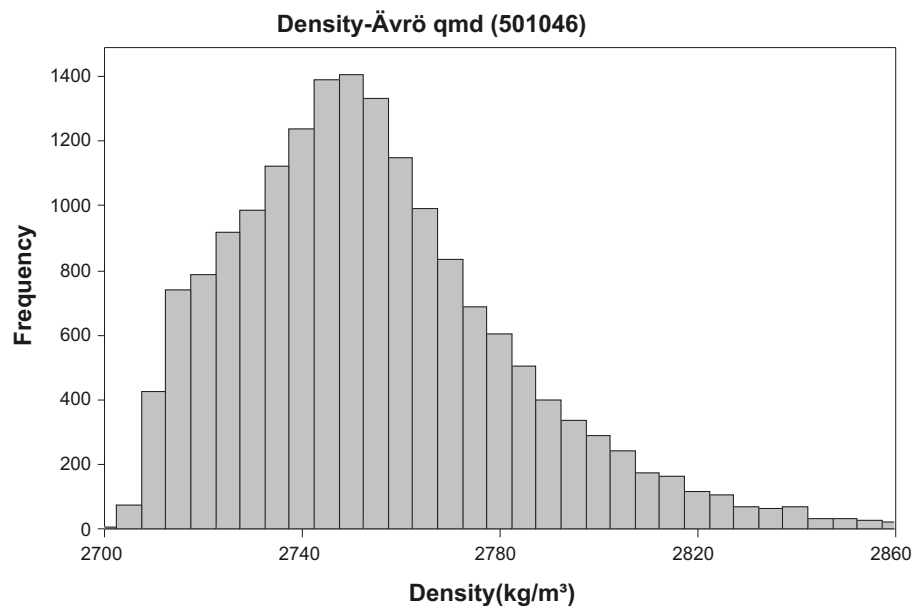


Figure 5-23. Histograms of density for Ävrö quartz monzodiorite (501046): from density logging of boreholes KLX05, 07A, 08, 10, 12A, 13A, 17A, 18A and 21B. Mean density from logs = 2,755 kg/m³; standard deviation = 30 kg/m³.

TRC 56

TRC 56 occurs in domains RSMMA01 and RSMM01. It is comprised of two rock types, Ävrö granodiorite (501056) and granite (501058). The latter is very subordinate in all both rock domains. For granite, SCA data has been used to complement the few TPS values. Data distribution for both Ävrö granodiorite and granite are presented in Appendix C.

The most reliable thermal conductivity data is provided by the TPS data, which is rather plentiful (60 for Ävrö granodiorite and 3 for granite, altered samples included). The Ävrö granodiorite data is based on samples from 10 boreholes in Laxemar and two in the Simpevarp subarea. Therefore, representativeness is considered to be good. Samples taken in groups from short sections of borehole may result in bias. To investigate if this is the case declustering has been performed on data for Ävrö granodiorite. The declustered (weighted) data give a higher standard deviation than the uncensored data, while the mean is more or less the same. The SCA data yields a similar mean and standard deviation to the TPS data.

The distribution model for TRC 56 is based on the TPS data for Ävrö granodiorite as well as the TPS and SCA data (n=8) for granite (501058), see Figure 5-24. The values are weighted relative to the proportion of these rock types in the TRC in domain RSMM01 (c. 25% 501056 and 2% 501058) but the model is assumed to apply to TRC 56 in domain RSMA01, even though the relative proportions of these rock types are slightly different. This is of little importance since the distributions are quite similar. A smoothed histogram is applied to these data to produce a model for TRC 56, see Figure 5-25.

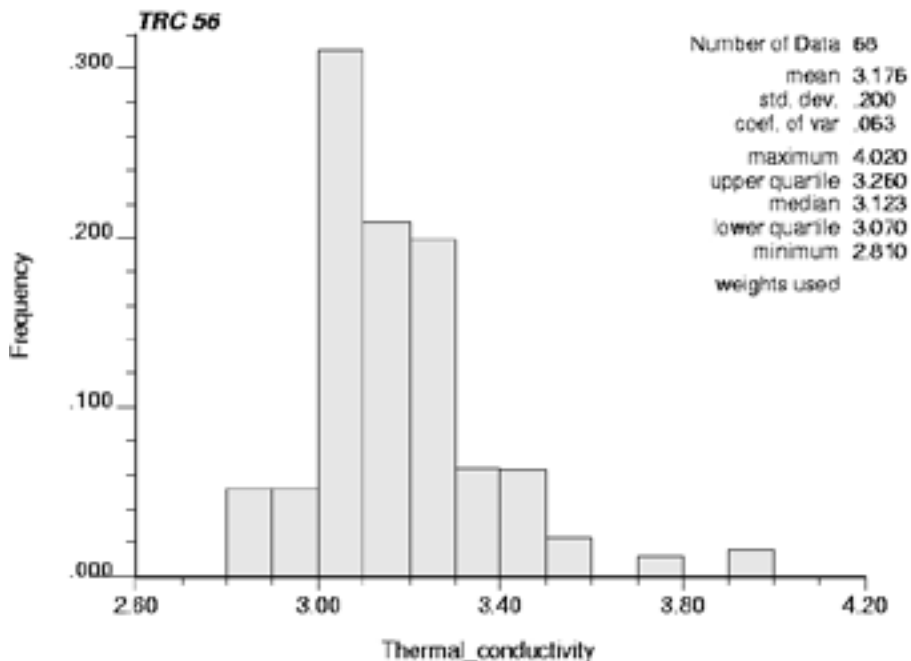


Figure 5-24. Histogram of thermal conductivities for TRC 56 based on data for Ävrö granodiorite (501056) and granite (501058); data values weighted.

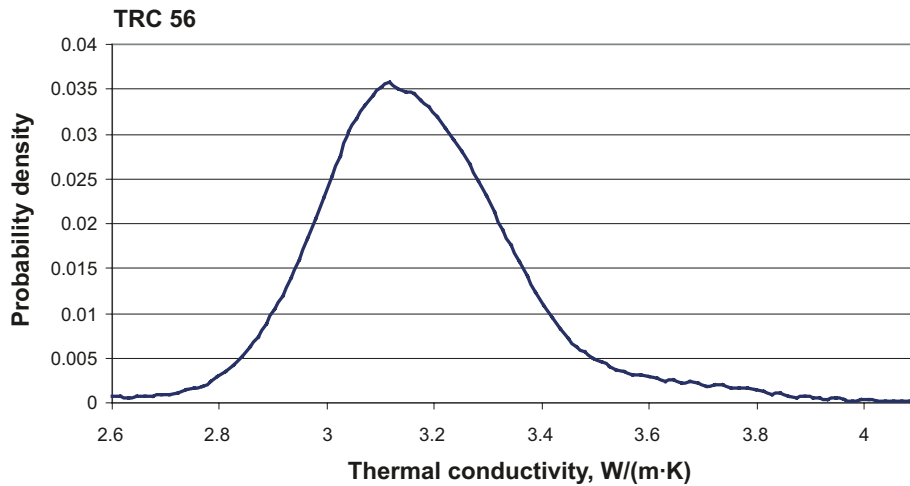


Figure 5-25. Statistical distribution model of thermal conductivity for TRC 56 based on smoothing of the data histogram (Ävrö granodiorite (501056) and granite (501058)). Minimum value of 2.6 W/(m·K) based on rounded-off lowest value from calculations from density.

TRC 58

TRC 58 is defined in all three rock domains and comprises two rock types, the more common fine grained granite (511058) and subordinate pegmatite (501061). Both rock types occur as dykes, veins and minor irregular bodies.

Thermal conductivity data for fine-grained granite is provided by 4 TPS values and 9 SCA values. At least two of the TPS samples have been identified as altered. A histogram of the data and statistics are presented in Figure 5-26. Declustering of the data was not required. No data is available for pegmatite, but data on pegmatite in Forsmark indicates a thermal conductivity of about 3.5 W/(m·K), which is similar to the mean thermal conductivity for fine-grained granite.

A distribution model is produced by fitting a smoothed histogram to the data, see Figure 5-27. The small number of data values (n=13) gives a rather uncertain model.

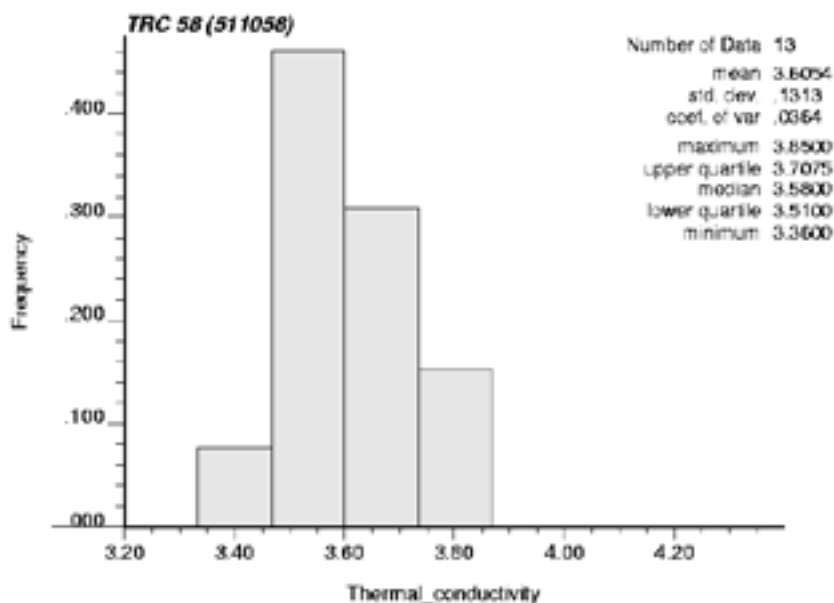


Figure 5-26. Histogram of thermal conductivity for TRC 58 based on TPS and SCA values for fine-grained granite (511058).

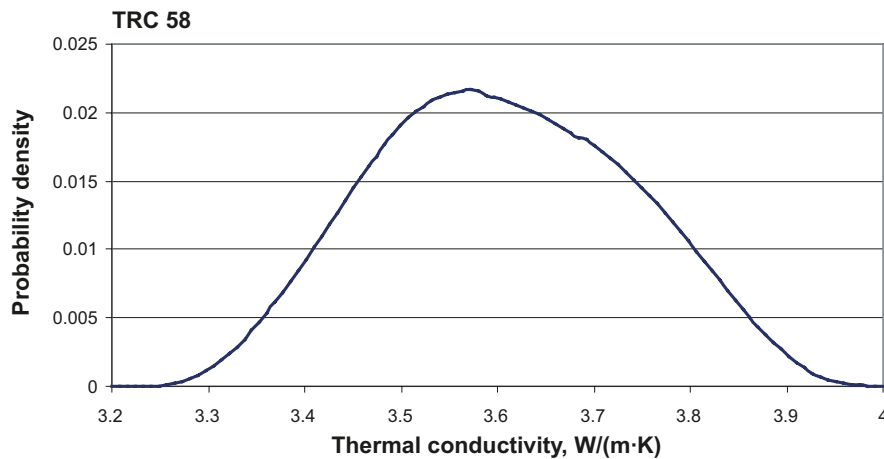


Figure 5-27. Statistical distribution model of thermal conductivity for TRC 58 based on smoothing of the data histogram. The choices of minimum and maximum values have only a minor effect on the shape of the distribution.

TRC 102

TRC 102, present in both domains RSMA01 and RSMD01, is comprised mainly of rock type fine-grained diorite-gabbro (505102). In domain RSMA01, minor amounts of diorite-gabbro have been assigned to this TRC. In domain RSMD01, Ävrö quartz monzodiorite and dolerite are also included in this TRC, because of their similar thermal properties.

For purposes of thermal modelling, however, only data from the main rock type is used as the basis for the TRC model. The motives for using only fine-grained diorite-gabbro to represent this TRC this are the low proportions of the other rock types, or in the case of dolerite, lack of data.

Thermal conductivity data for fine-grained diorite-gabbro is provided by 4 TPS values and 10 SCA values. A histogram and statistics are presented in Figure 5-28. An attempt was made to fit a distribution model to the data using the smoothed algorithm in GSLIB. However, the resulting model had a very unsatisfactory appearance due to the small number of data values (n=14). For this reason, it was decided to create a triangle distribution which honours the mean and the standard deviation of the data quite closely; see Figure 5-29. The choice of such a distribution is a reflection of the considerable uncertainty associated with this model.

Summary of thermal distribution models

Table 5-35 summarises the thermal conductivity statistics for each TRC.

5.6.3 Variogram models – 0.1 m scale

The spatial correlation of thermal conductivity within each TRC is modelled by a variogram. This involves two main steps. First, a sample variogram is constructed from data. Secondly, a variogram model is fitted to the sample variogram. Where possible TPS data are used to construct the sample variograms, but for most TRCs these data are not sufficiently abundant to enable construction of reliable variograms. Therefore, borehole density logs were used to study spatial correlation of thermal conductivity.

A relationship between thermal conductivity and density has been established for some rock types (Section 3.6, Figure 3-13). Even for rock types where no relationship is obvious, due to, for example, the narrow range in density, a relationship may still exist. In any case, it is reasonable to assume that any spatial dependence in density, as indicated by a variogram, also reflects spatial dependence in thermal conductivity /Sundberg et al. 2007/. The primary purpose of calculating variograms based on density loggings is to estimate the range, i.e. the separation distance over which spatial dependence is apparent.

Table 5-35. Statistics for each TRC of the distribution models used for simulation and the thermal conductivity data on which the models are based.

TRC	Data			Model	
	Mean (W/m·K)	Standard deviation (W/m·K)	No. of data	Mean (W/m·K)	Standard deviation (W/m·K)
TRC 30	2.74	0.17	91	2.75	0.16
TRC 33A	2.43	0.13	31	2.43	0.13
TRC 33B	2.89	0.46	13	2.89	0.46
TRC 36	2.73	0.18	63	2.73	0.17
TRC 46	2.40	0.18	33	2.40	0.18
TRC 56	3.18	0.20	68	3.18	0.20
TRC 58	3.60	0.13	13	3.60	0.13
TRC 102	2.52	0.15	14	2.50	0.16

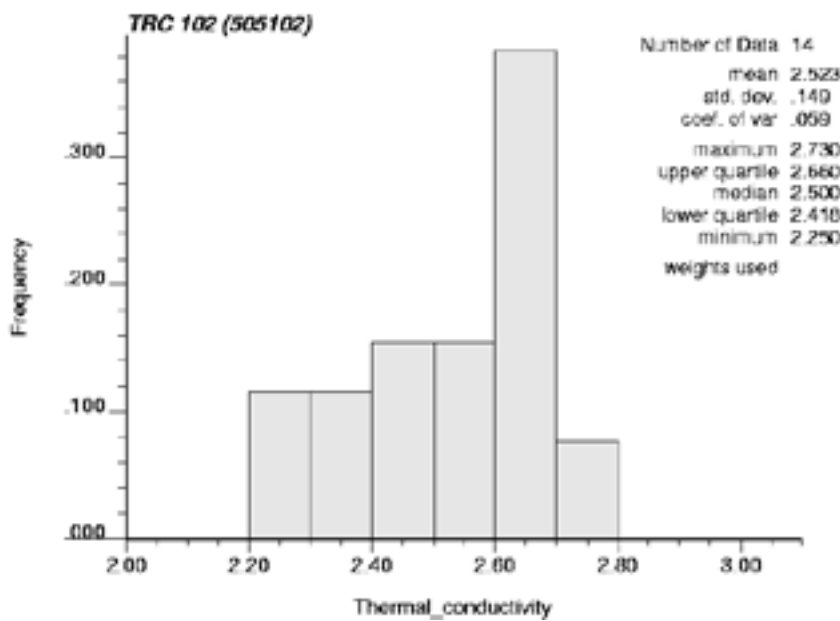


Figure 5-28. Histogram of thermal conductivity for TRC 10 based on TPS and SCA values for fine-grained diorite-gabbro (505102).

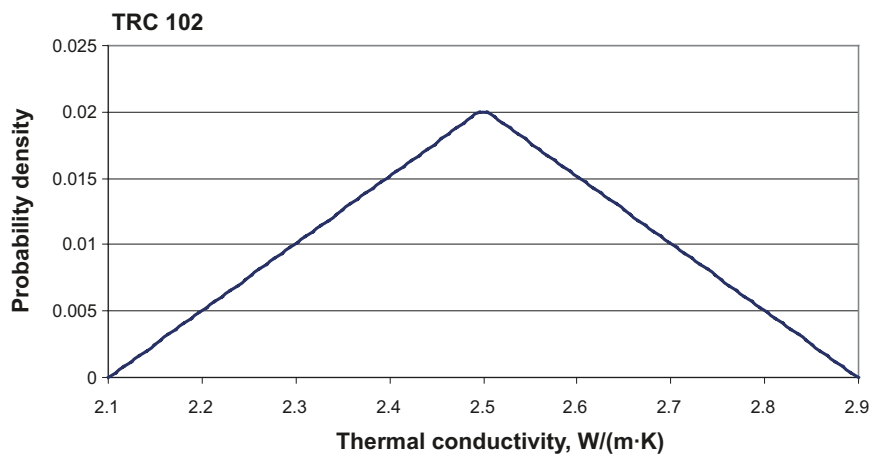


Figure 5-29. Statistical distribution model of thermal conductivity for TRC 102 assuming a triangle distribution based on statistics of TPS and SCA values for diorite-gabbro (505102). The choice of 2.0 W/(m·K) for the minimum value is based on a consideration of the data for similar rock types, namely the low density variety of diorite-gabbro.

The procedure followed in order to construct sample variograms for each TRC is described below.

1. Data were selected for the rock type representing each TRC. The model of the spatial correlation structure for each TRC is based on the dominant rock type within the TRC. For example, the variogram model for TRC 56 is based on Ävrö granodiorite (501056). Variograms based on density logging data could be constructed for all TRCs. For TRCs 36, 46 and 56, sufficient TPS data was available to warrant variogram analysis. For other TRCs, insufficient TPS data are available. Data values from altered samples were removed, since they may disturb the overall patterns of spatial correlation.
2. Before the density logging data could be analysed, it was necessary to first process the data into a format suitable for analysis:
 - Borehole data with high noise ($> 20 \text{ kg/m}^3$) were excluded from the analysis. These included data from boreholes KLX02, KLX03 and KLX04.
 - Density logs have not been corrected for the bias indicated in Section 3.7.2. This has little or no effect on the variograms as long as data from more than one borehole are not grouped together.
 - Data from all deformation zones, as defined in the geological model (ESHI), /Wahlgren et al. 2008/ were removed so as not to capture spatial variability caused by alteration, fracturing, etc.
 - The borehole data were sorted according to rock type and a separate file was created for the rock type to be analysed.
 - Uncharacteristically low or high density logging values (different for different rock types) were removed, as such values are a result of interference from adjacent rock types. This is particularly important for rock types which occur as small bodies or dykes.
3. Normal scores transformation of the data was performed and variograms were calculated and plotted for different lag distances and lag tolerances; see /Deutsch and Journel 1998/. The variograms are standardised to the total variance which means that all variances are normalised to the total variance, and implies that the sill of the variogram is equal to one.

Because the data are restricted to boreholes, it is not possible to calculate reliable variograms in any directions other than in the direction of the boreholes, i.e. “down-hole” variograms /Dowd 2007/. For this reason, directional variograms cannot be constructed. It is assumed that the spatial correlation within a particular rock type is isotropic. This is a reasonable assumption for most of the rocks at Laxemar given their lack of layered characteristics.

A number of principles were defined for fitting suitable variogram models:

1. If possible, the variogram structures should have a physical/geological explanation. The variogram model should be guided, where possible, by the geological knowledge of the phenomenon /Journel and Huijbregts 1978/. For example, for very short lag distances (dm) and for small support volumes, coarse-grained rocks such as granites can be expected to show larger variance compared to fine-grained rocks, thus giving a higher nugget effect. This is because of the greater heterogeneity within small volumes in coarse-grained rocks. If there is no physical explanation for a feature of a variogram, an artefact of measurement should be suspected. In this case it may be best to ignore the feature and adopt the simplest model instead. Some generalisations can be made.
2. The variogram model for each TRC was chosen after an overall judgement of the sample variograms from individual boreholes. Given a choice between alternative variogram models, the one chosen was that giving the higher degree of spatial correlation, i.e. a lower nugget and a longer range
3. Three types of standard models (variogram structures) were considered: spherical, exponential and Gaussian (although the Gaussian model was not used). In addition, the nugget can also be considered to be a variogram structure. The type selected was the one that best fitted the sample variogram. If required, a combination of variogram structures, a so-called “nested” variogram model, can be used in order to obtain a better fit to the sample variogram.

4. The nugget (small-scale variability at a scale smaller than measurement scale) should be based, where possible, on TPS-data.
5. The range (correlation length) should be based, where possible, on density log data and if such data are not available, on correlation lengths of similar rock types. TPS data are usually too few to produce reliable estimates of range. If the range is uncertain, a higher value in the indicated interval was chosen in order not to underestimate spatial continuity.
6. The nugget constant is estimated by extrapolating the average linear behaviour of the first sample variogram points to the ordinate axis /Journel and Huijbregts 1978/.

In the absence of sufficient TPS data, density variograms may also be used to roughly approximate the nugget. It is difficult to say whether the nugget estimated from density variograms underestimate or overestimate the nugget. The relatively high measurement error in the density logging data would give a higher nugget. On the other hand, the overlapping measurement volumes and the filtering procedure applied to the density logging data in order to dampen the random noise, means that the spatial dependence at distances less than about 0.4 m is strongly overestimated, giving a nugget which is too low. Compared to TPS values, the support of the density data is higher, which should give a lower nugget effect. The combined effect of these different phenomena is very difficult to evaluate. To reduce the effects of these phenomena, more reliance was placed on density logs with low random noise, and the semi-variance values for lag distances up to 0.4 m were ignored.

It is assumed that density exhibits maximum variance within individual boreholes. In reality, the total variance may not always be captured in individual boreholes, which suggests that the principle of stationarity is not always fulfilled. A consequence of this is that large-scale heterogeneity cannot be successfully modelled. This would require dividing the data into separate more homogenous groups and constructing models (statistical distribution and variogram models) for each group in much the same way as is done for TRC 33 (type A and B). However, for the purpose of describing thermal conductivity distributions of domains at scales up to at least 10–20 m, this shortcoming has little effect.

TRC 30

The variogram model for TRC 30 is based on quartz monzodiorite (501036), one of two common rock types making up this thermal rock class. The model is described below under TRC 36, in which quartz monzodiorite is the dominant rock type.

TRC 33A

Laboratory measurement data (TPS) are far too few to calculate variograms. Therefore, variograms were calculated from density logging data only. The largest bodies of the low density variety of diorite-gabbro are intersected by borehole KLX08, which makes it the obvious candidate for the analysis of spatial correlation. Plotted for lag distances up to 200 m (Figure 5-30), the variogram shows a cyclic behaviour. This repetitive behaviour could be a so called “hole effect” indicating that, geologically, there are areas with similar properties occurring regularly, in this case every 50 m. An investigation of the density log for KLX08 reveals that bodies of diorite-gabbro occur at on average 50 m intervals along part of the borehole. A similar pattern of spatial variability within individual bodies may explain the observed variogram.

Whether these large-scale structures have a geological explanation or not is, however, not particularly relevant, since correlation structures on the same scale or larger than the simulation volume cannot be modelled. Nor are they important to the study at hand. For the purpose of thermal simulations it is important to model the spatial dependence up to the sill (representing the total sample variance). Since the variogram reaches a sill (representing the total sample variance) at less than 25 m, a sample variogram for lag distances up to 25 m was plotted (Figure 5-31). A variogram model was fitted using a nugget of 0.1 and two separate structures with different variances and ranges, i.e. the variogram model is made up by so-called “nested” variogram structures (see the summary section below for a more thorough discussion of nested variograms).

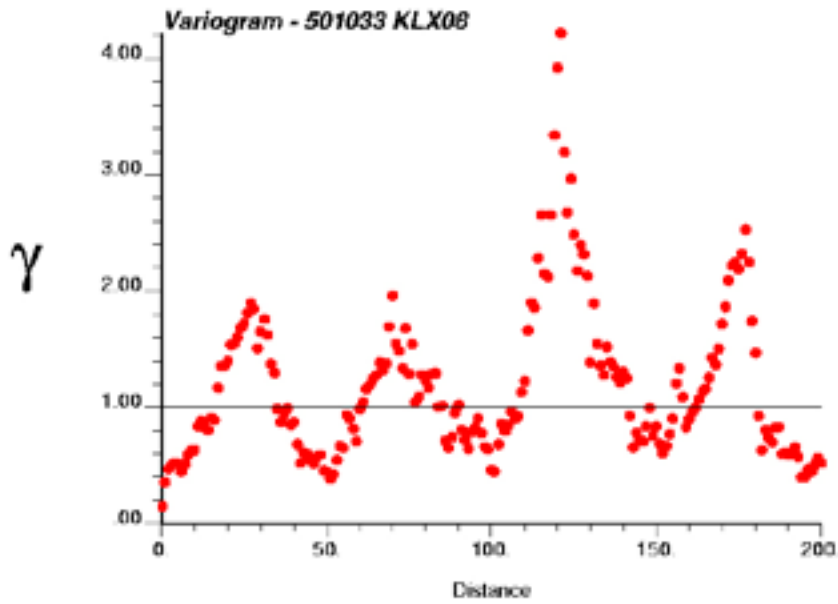


Figure 5-30. Variogram for diorite-gabbro (501033) produced from density logging data from borehole KLX08. Lag distance (x axis) in metres (m). Variogram is standardised to the variance of the measured data.

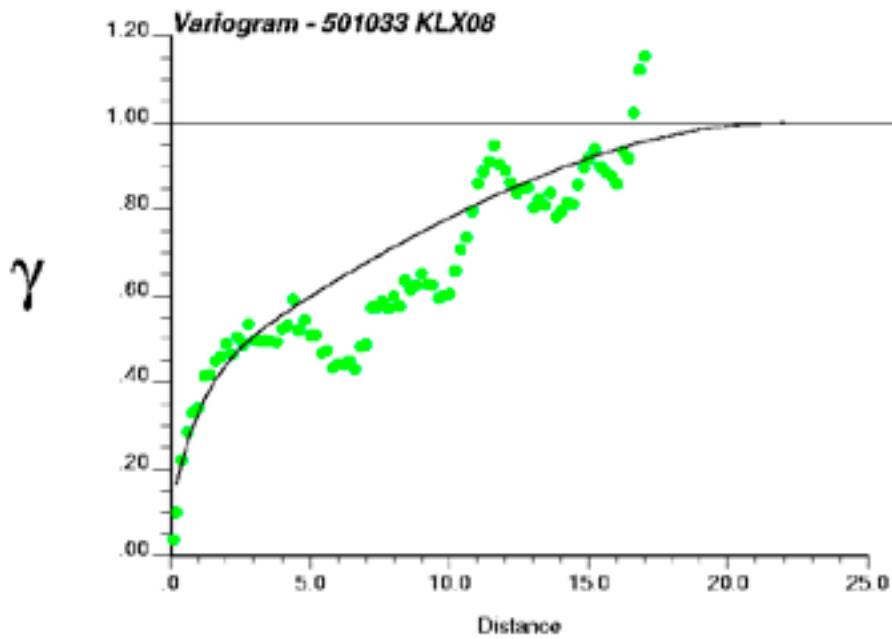


Figure 5-31. Variogram model for TRC 33A based on sample variograms for diorite-gabbro (501033) produced from density logging data from borehole KLX08. A nested variogram model was fitted. Lag distance (x axis) in metres (m). Variogram is normalised to the variance of the measured data.

TRC 33B

For TRC 33B, variograms were also based solely on density logging data. Two boreholes are particularly suitable for variogram analysis of this high-density variety of diorite-gabbro because of the presence of large bodies of this rock type. These are KLX05 and KLX12A; see Figure 5-32. As with diorite-gabbro in borehole KLX08 described above, there are large-scale structures apparent which are neither relevant nor possible to model. Variograms for shorter distances display a very clear spatial correlation with a low nugget and a range of less than 20. A model was chosen based on an overall judgement of both borehole variograms. Again, a nested variogram model was fitted to the sample variogram.

TRC 36

Variogram analysis of TPS data for quartz monzodiorite (501036) indicates the presence of long spatial correlation structures, in the order of several hundred metres. This pattern, shown in Figure 5-33, is also observed for density measurements on the same samples as the TPS data.

Variograms for quartz monzodiorite based on density loggings for 5 boreholes have been calculated. Individual boreholes indicate variable, but often long, correlation structures. Boreholes KLX11A and KLX15A (Figure 5-34) display large-scale correlation structures (100–300 m) similar to that shown by the laboratory data (cf. Figure 5-33). However, it is not possible to simulate a range that is large compared to the simulation field (100 x 100 x 100 m). For this reasons, a range of 75 m was chosen, which corresponds to the range observed in two of the other boreholes, KLX05 and KLX16A (Figure 5-35).

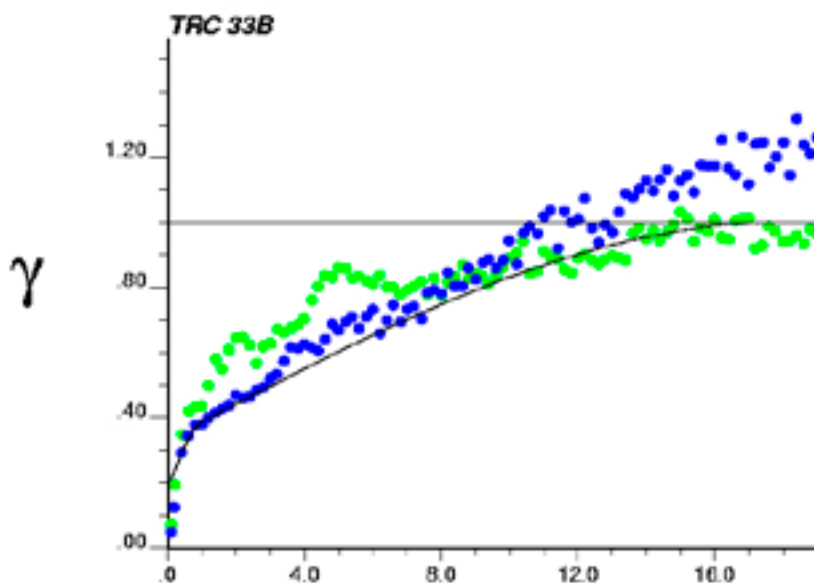


Figure 5-32. Variogram model for TRC 33B based on sample variograms for diorite-gabbro (501033) produced from density logging data from borehole KLX05 (green) and KLX12A (blue). A nested variogram model was fitted. Lag distance (x axis) in metres (m). Variogram is standardised to the variance of the measured data. Semi-variance values (γ) for lag distances below 0.4 m are unreliable (see section 5.6.3).

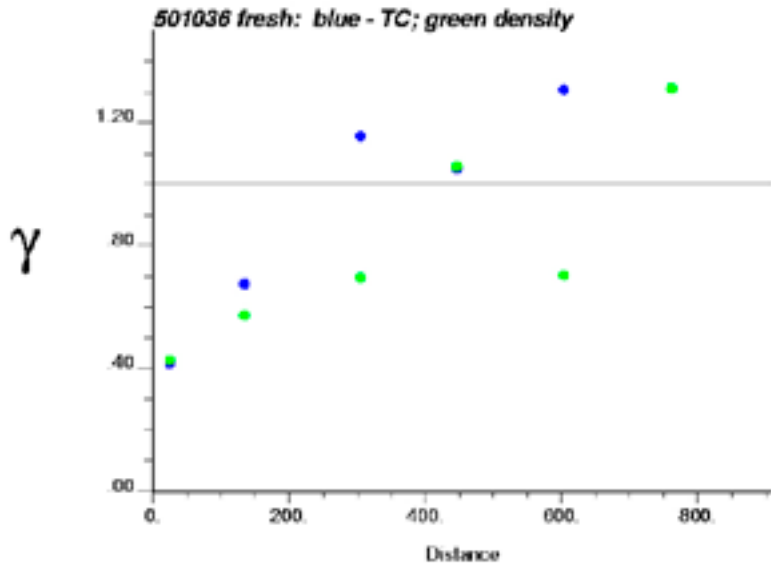


Figure 5-33. Variograms of density (green) and thermal conductivity (blue) for quartz monzodiorite (501036) based on laboratory measurement data (n=58). Lag distance (x axis) in metres (m). Variogram is standardised to the variance of the measured data.

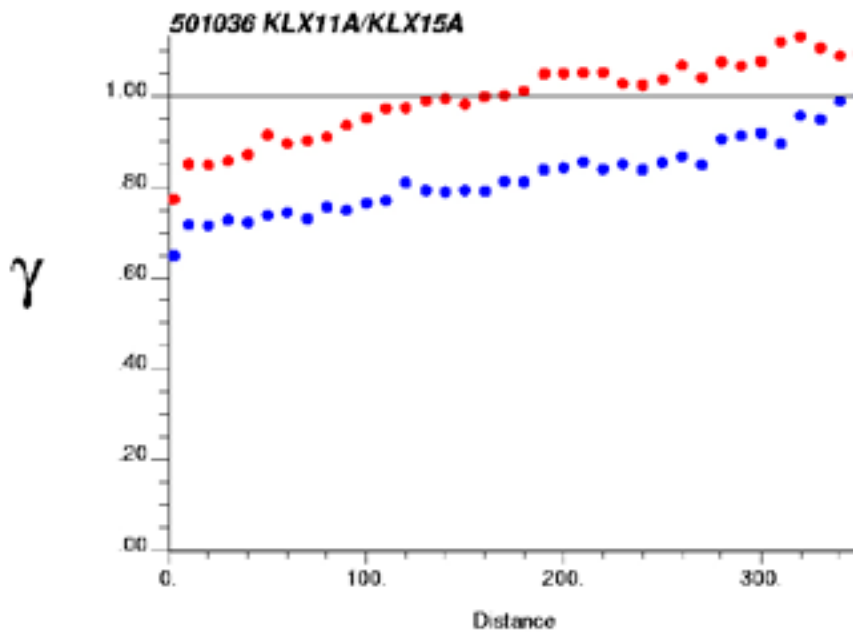


Figure 5-34. Variogram for quartz monzodiorite produced from density logging data from boreholes KLX11A (blue) and KLX15A (red). Lag distance (x axis) in metres (m). Variogram is standardised to the variance of the measured data.

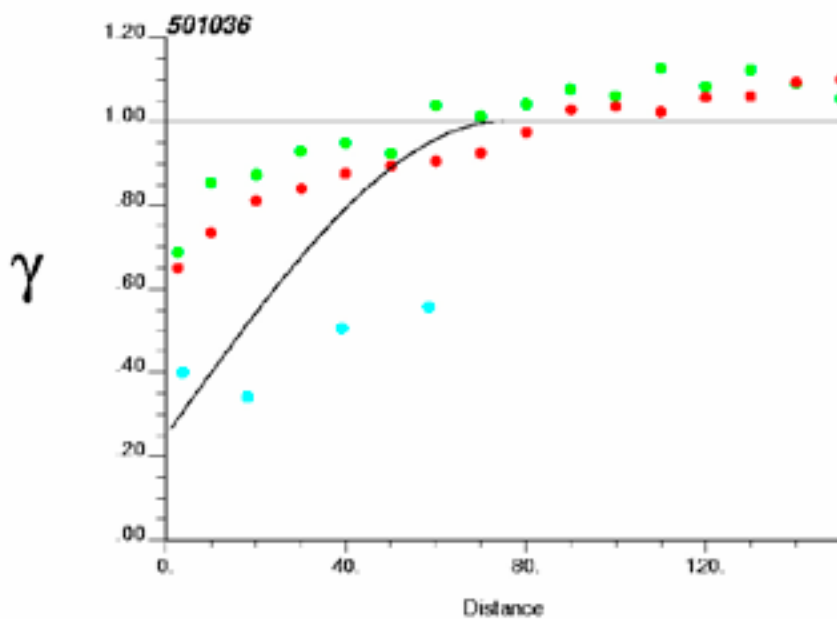


Figure 5-35. Variogram model for TRC 36 based on sample variograms for quartz monzodiorite produced from density logging data from borehole KLX05 (red) and KLX16A (green), as well as TPS data (blue). Lag distance (x axis) in metres (m). Variogram is standardised to the variance of the measured data.

The TPS data indicate a considerably lower nugget than the density logging data. A nugget of 0.33 is chosen based on the TPS data.

Plots of density versus borehole length (Figure 5-36) provide an explanation for the very different variograms calculated from different boreholes. In KLX11A, for example, the density generally increases down the borehole, which means very long correlation distances. The same pattern is seen in KLX15A. These two boreholes differ from KLX19A, in which large-scale trends are not obvious, see Figure 5-36.

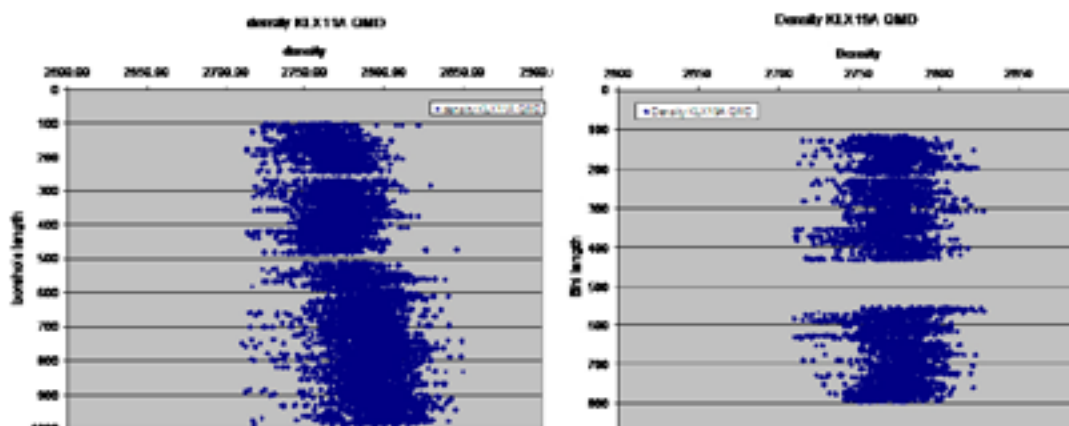


Figure 5-36. Density versus borehole length for quartz monzodiorite (501036) in boreholes KLX11A (left) and KLX19A (right). Density from borehole density logging.

Variogram analysis of both TPS data and density logging data for quartz monzodiorite indicates the presence of long spatial correlation structures, in the order of several hundred metres. In relation to the simulation volume (a cube with sides of 100 m), this spatial correlation can be described in terms of a trend or “drift”. The presence of drift in relation to the scale of the simulation implies that the assumption of stationarity is not fulfilled, which in the context of the present study means that the mean and variance should be constant within each 100*100*100 m cube.

However, the principle of stationarity is a key assumption of geostatistical modelling. In order to adhere to the principles of stationarity, any spatial correlation or trends which are longer than can be incorporated by the simulation volume cannot be reproduced. In practice, this means assuming that the total variance is present within the simulation volume, despite evidence to the contrary. In the case of Quartz monzodiorite, it is probable that such a relatively small volume compared to the size of the rock domain has a variance that is lower than the total variance for this rock type. Moreover, in reality the mean is expected to vary between each 100 m cube but is held relatively constant in the simulations. The constant mean and the total variance within each realisation are achieved by using a spatial correlation length of about 70–80 m, slightly shorter than the sides of the simulation cube. This assumption does not have an adverse influence on the simulation results and the overall thermal modelling, given the objective of description of domain statistics. This is because the results are scaled up to a maximum of 5 m. The choice of range for the variogram does not significantly affect the modelling of spatial variability at such short distances. In other words, the spatial variability at the 5 m scale can be reproduced satisfactorily. However, the assumption of stationarity means that we are unable to reproduce the variability which exists at the scale of the simulation volume, i.e. the difference in mean and variance between individual realisations is much lower than is expected in reality.

TRC 46

The variogram model for TRC 46 is based on Ävrö quartz monzodiorite (501046), the sole rock type in this thermal rock class. A variogram based on TPS data for Ävrö quartz monzodiorite is very unreliable. There are only 18 data pairs for the first lag distance of 0.2 m (average) which gives a standardised variance of 0.2. Although this value is not very reliable, it does indicate that spatial correlation may be very strong for short distances. This was kept in mind when interpreting the density variograms for Ävrö quartz monzodiorite.

Density variograms for boreholes KLX12A, KLX13A, KLX17A and KLX18A were calculated; see Figure 5-37.

The following variogram model (nested) is proposed for TRC 46 based on an overall judgement of the variogram analyses. A nugget value of 0.25 is based on a consideration of TPS data and density data from borehole KLX17A. A range of 35 m is based on density variograms for boreholes KLX17A and KLX18A. The selected model comprises two spherical variogram structures and is illustrated in Figure 5-38 together with the density variogram for KLX17A. It can be concluded that the variogram model for TRC 46 to a large extent is based on a small set of TPS data at small separation distances, and density loggings from subjectively selected boreholes.

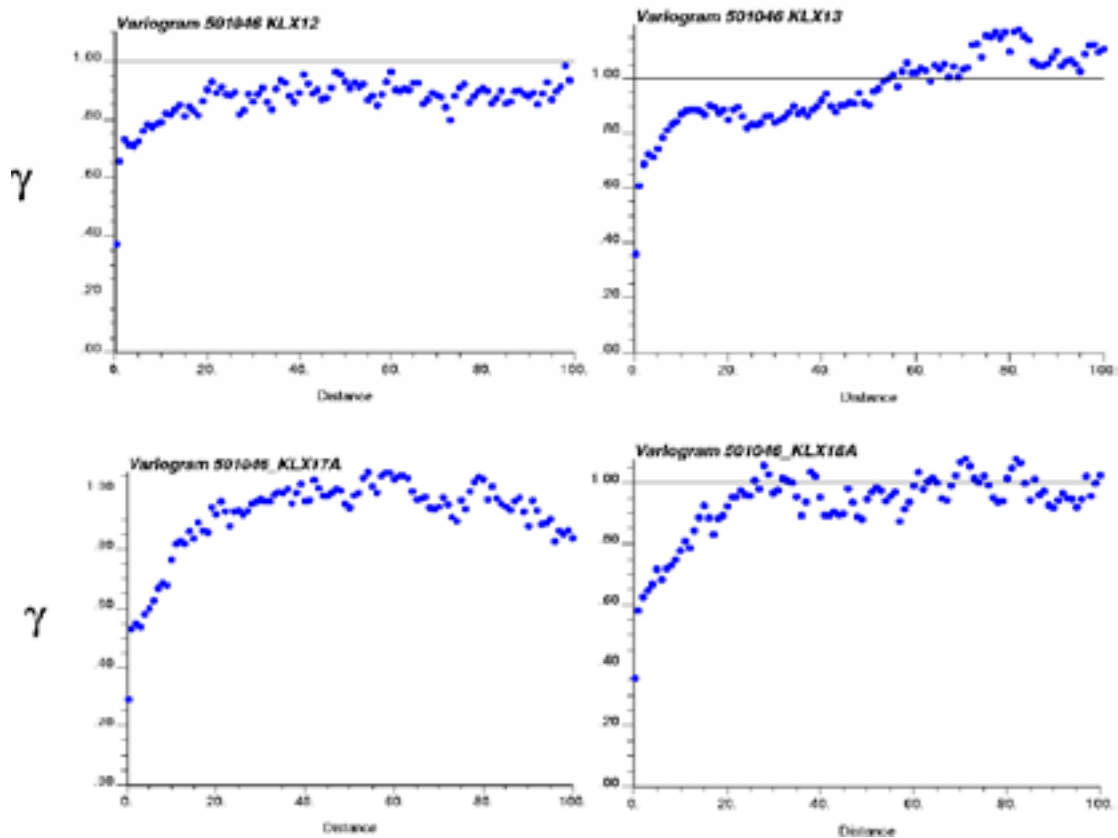


Figure 5-37. Variograms for Åvrö quartz monzodiorite (501046) produced from density logging data from boreholes KLX12A, 13A, 17A and 18A. Lag distance (x axis) in metres (m). Variograms are standardised to the variance of the measured data.

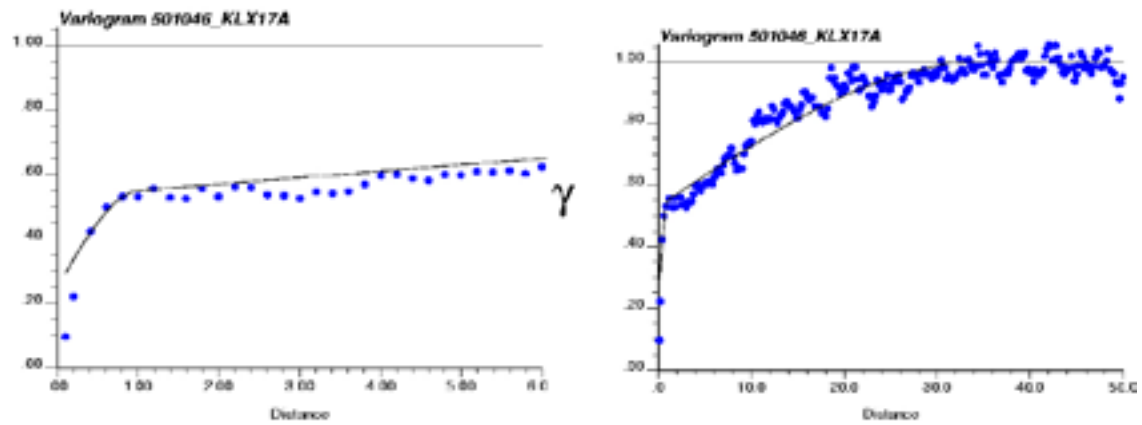


Figure 5-38. Variogram model for TRC 46 shown at two different scales. Model based on sample variograms for Åvrö quartz monzodiorite (501046) produced from density logging data from borehole KLX17A and a consideration of the TPS data. A nested variogram model was fitted. Lag distance (x axis) in metres. Variogram is standardised to the variance of the measured data. Semi-variance values (γ) for lag distances below 0.4 m are unreliable (see Section 5.6.3).

TRC 56

The variogram model for TRC 56 is based on Ävrö granodiorite (501056), the dominant rock type making up this thermal rock class. A variogram based on TPS data for Ävrö granodiorite constrains the nugget quite well. For a lag distance of 0.1 m the standardised semivariance based on 35–40 data pairs is approximately 0.65. Density variograms were calculated for 6 boreholes: KLX07A, KLX08, KLX10, KLX17A, KLX18A and KLX21B. Variograms for KLX08, KLX17A and KLX18A reach the sill within 10 indicating little spatial continuity. This is exemplified for KLX17A in Figure 5-39. Boreholes KLX07A, KLX10 and KLX21B produce rather similar variograms with correlation lengths of 25–50 m, see Figure 5-40. The selected nested model, with a nugget of 0.6 and a range of 50 m for the large-scale structure, is shown in Figure 5-40 and Figure 5-41.

TRC 58

The variogram model for TRC 58 is based on fine-grained granite (501058), the dominant rock type making up this thermal rock class. Borehole KLX05 is one of the few boreholes with large bodies of fine-grained granite, which makes it the obvious choice as the basis for a variogram model for TRC 58. The density variogram for this borehole and the fitted model are shown in Figure 5-42. The fitted model reflects the behaviour of the variogram very closely up to lag distances of 2.5 m. For longer distances, the model deviates quite a lot from the data variogram. An alternative model, with a longer range, could arguably have been chosen. However, given the high thermal conductivity of fine-grained granite, and the fact that it occurs in relatively minor amounts, accurate modelling of spatial continuity for this TRC is not critical to the overall modelling results.

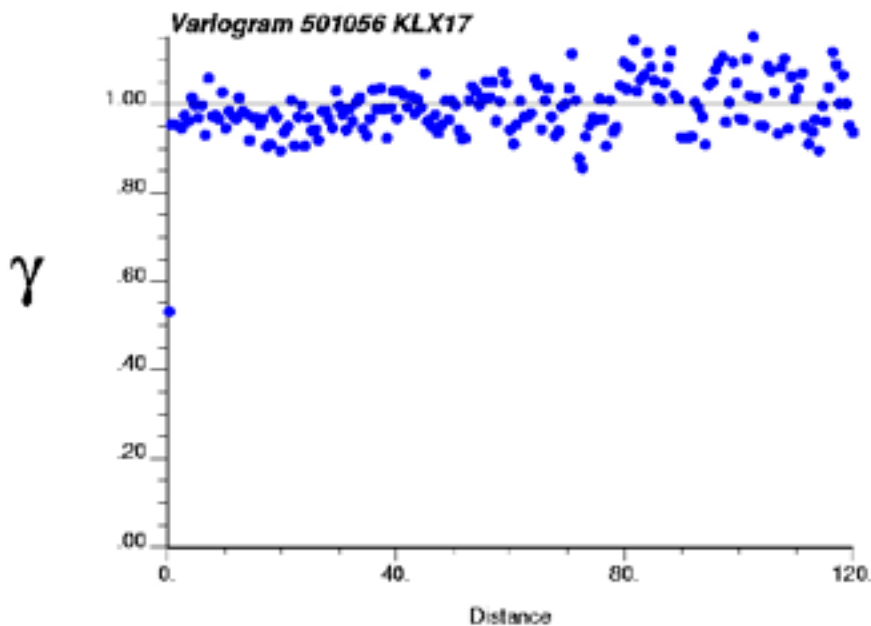


Figure 5-39. Variogram for Ävrö granodiorite (501056) produced from density logging data from borehole KLX17A. Lag distance (x axis) in metres (m). Variogram is standardised to the variance of the measured data.

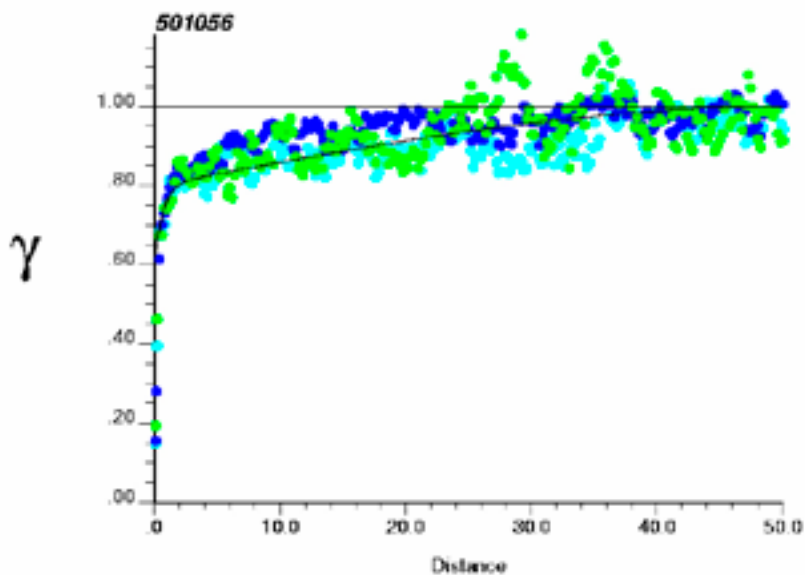


Figure 5-40. Variograms for Ävrö granodiorite (501056) calculated from density logging data from borehole KLX07A (light blue), KLX10 (dark blue) and KLX21B (green). A nested variogram model was fitted. Nugget based on TPS data and range on density variogram for KLX07A. Lag distance (x axis) in metres (m). Variogram is standardised to the variance of the measured data. Semi-variance values (γ) for lag distances below 0.4 m are unreliable (see Section 5.6.3).

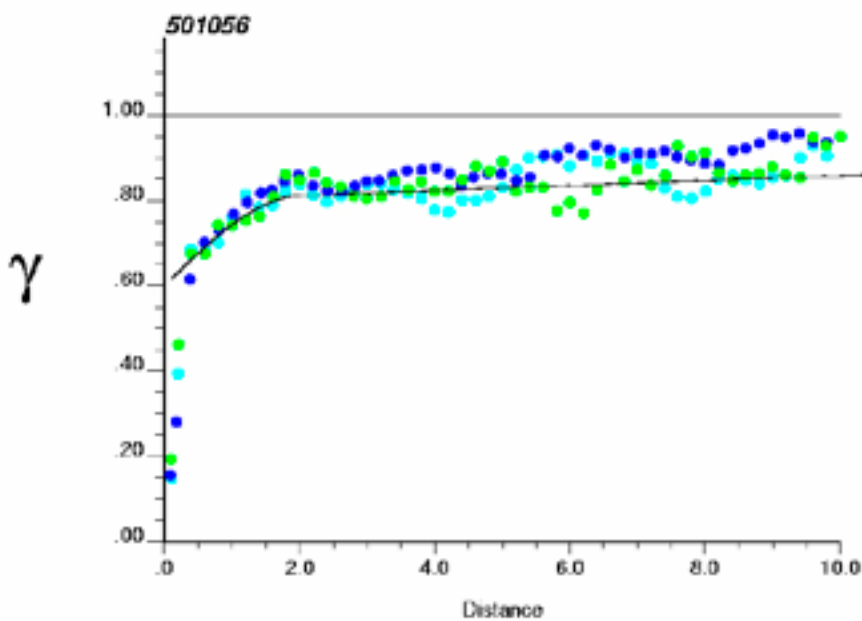


Figure 5-41. Variograms with lag distances up to 10 m for Ävrö granodiorite (501056) calculated from density logging data from borehole KLX07A (light blue), KLX10 (dark blue) and KLX21B (green). Lag distance (x axis) in metres (m). Variogram is standardised to the variance of the measured data.

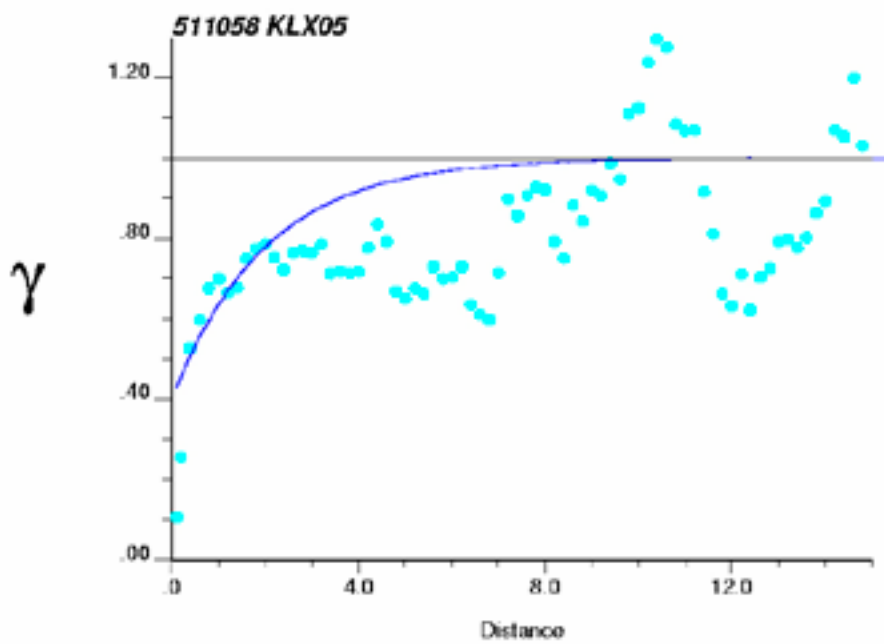


Figure 5-42. Variogram for fine-grained granite (511058) calculated from density logging data from borehole KLX05. Nugget and range based on this variogram. Shape of model based on first part of density variogram, i.e. lag distances up to 2.5 m. Lag distance (x axis) in metres (m). Variogram is standardised to the variance of the measured data.

TRC 102

The variogram model for TRC 102 is based on fine-grained diorite-gabbro (505102), the dominant rock type making up this thermal rock class. Boreholes KLX10 and KLX11A were employed to calculate variograms of density logging data for fine-grained diorite-gabbro (Figure 5-43). Fine-grained diorite-gabbro generally occurs as flat-lying dykes 1–5 m thick. Therefore, spatial correlation for distances longer a couple of metres is not to be expected in the borehole direction. The variogram model was based on the density variogram for KLX10.

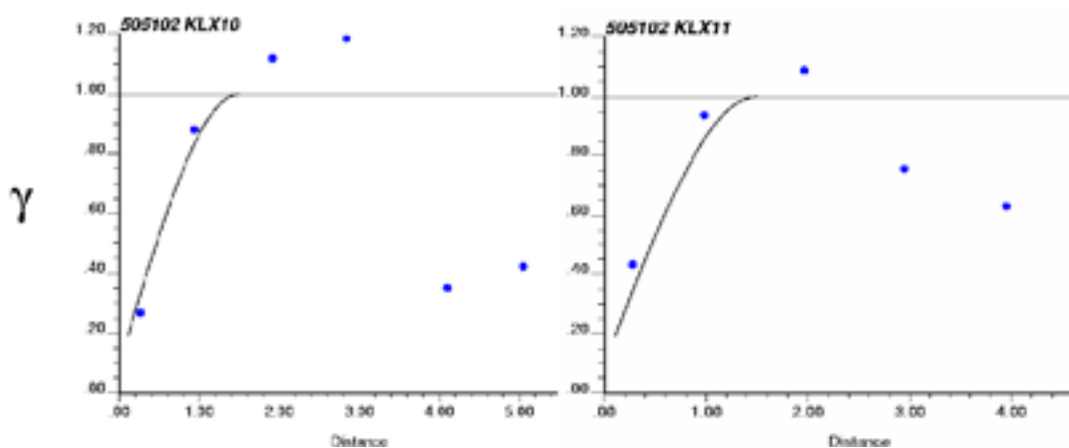


Figure 5-43. Variogram model for TRC 102 shown in relation to variograms of density logging data from fine-grained diorite-gabbro (505102) in boreholes KLX10 and KLX11A. Model based on variogram from KLX10. Lag distance (x axis) in metres (m). Variogram is standardised to the variance of the measured data.

Summary of variogram models – 0.1 m

The variogram models for each TRC are summarised in Table 5-36. Variogram models with more than one structure, in addition to the nugget, are referred to as nested variograms. The column “Structure” in Table 5-36 indicates the type of variogram structure being used. The variogram models consist of up to three variogram structures (when nugget is counted as a separate structure). The complete variogram model is a linear combination of the variogram structures. The different basic structures that have been used are nugget, spherical and exponential models. The equations for these models can be found in any geostatistical textbook, e.g. /Deutsch and Journel 1997/. Each structure is completely defined by the parameters in Table 5-36. The semi-variance parameter, also denoted “contribution”, is a measure of how much a structure contributes to the complete variogram model. Thus, this parameter could be regarded as a weighting factor. These factors should add to 1 for the complete variogram model, as in the table. The second parameter that defines the shape of a variogram structure is the range. The nugget can be regarded as always having a range equal to zero.

It should be noted that the variogram models are applicable at the 0.1 m scale only. For simulation at larger scales, the variogram models have to be scaled up appropriately as outlined in Section 5.7.2.

The variable ranges between different TRCs can be explained by different degrees of spatial continuity. A rock crystallised from magma that is well mixed and homogenous will have long range. The rather homogenous quartz monzodiorite is a good example of this. More heterogeneous rock types such as Ävrö quartz monzodiorite and diorite-gabbro have shorter ranges.

Table 5-36. Variogram model parameters for modelling spatial correlation of thermal conductivity at 0.1 m scale for each TRC. Semi-variance of variogram structures standardised to the variance of the measured data so that the sum of the semi-variance values for all structures is 1. The nugget is treated as a separate variogram structure with no range.

TRC	Rock type, code	Structure	Semi-variance (contribution, weight)	Range, m
TRC 30	501036	Nugget	0.33	
		Spherical	0.67	75
TRC 33A	501033 A	Nugget	0.10	
		Exponential	0.30	3
		Spherical	0.60	22
TRC 33B	501033 B	Nugget	0.18	
		Spherical	0.15	1
		Spherical	0.67	18
TRC 36	501036	Nugget	0.33	
		Spherical	0.67	75
TRC 46	501046	Nugget	0.25	
		Spherical	0.28	1
		Spherical	0.47	35
TRC 56	501056	Nugget	0.60	
		Spherical	0.20	2
		Spherical	0.20	50
TRC 58	511058	Nugget	0.40	
		Exponential	0.60	6
TRC 102	505102	Nugget	0.10	
		Spherical	0.90	1.5

5.7 Stochastic simulation of thermal conductivity

5.7.1 Procedure

Stochastic simulation of thermal conductivity was performed for each TRC (Step 10 in Figure 4-1). Unconditional simulation was performed at three scales: 0.1 m, 0.5 m and 2 m. The purpose of the first two simulations was to perform change-of-support (upscaling) from the scale of thermal measurements (c. 0.1 m) to the 2 m scale (Step 5 in Figure 4-1). After change of support, unconditional simulations were performed at the 2 m scale with the objective of describing the rock domains statistically.

The simulation volume for the 2 m scale simulations was $100 \times 100 \times 100$ m, i.e. a total number of 125,000 cells in each realisation. This is the same scale and simulation volume as used in the geological simulations. The numbers of thermal realisations run for the 2 m scales were 1,000 for each TRC. In the case of TRC 33, which is comprised of sub-TRCs, the 1,000 thermal realisations are divided equally between the TRC33A and TRC33B.

Each TRC is simulated at the 0.1 m scale using the statistical distribution and variogram models defined in Sections 5.6.2 and 5.6.3, and at 0.5 and 2 m scales by the upscaled models described in Sections 5.7.2 and 5.7.3 below. The software used to perform the simulations is GSLIB. Simulation using this program requires selecting a number of search options that require a great deal of trial and error in order to produce satisfactory simulation results. This is described in some detail by /Deutsch and Journel 1998/.

Verification of simulations was performed by analysing the extent to which the results could reproduce:

1. Variogram models: the variograms produced by the individual realisations should fit closely to the input variogram model /Deutsch and Journel 1998/. However, some fluctuations of the realisation variograms is to be expected.
2. Distribution models: a large number of realisations combined should reproduce the statistics (histogram) of the model. However, each individual realisation should not be expected to do so /Deutsch and Journel 1998/.

5.7.2 Spatial statistical thermal models – 2 m scale

Simulations at scale 2 m require a thermal model (statistical distribution and variogram models) for each TRC determined for this particular scale. In order to obtain a statistical distribution for the 2 m scale, upscaling of the simulation results at 0.1 m scale is performed in two stages for each TRC, first from 0.1 m to 0.5 m, and then from 0.5 m to 2 m. The histogram of the upscaled values (2 m scale), plotted for each TRC in Appendix F, provides the basis for the statistical distribution model for simulations at the 2 m scale. Details on how this was performed for the various TRCs are given in Section 4.2.3.

The variogram models for the 0.5 m and 2 m scales are modified from the model used for the 0.1 m scale by an upscaling algorithm (see Section 4.2.3). The variogram parameters for modelling at 0.5 m and 2 m scale are summarised in Table 5-37 for each TRC, and plotted in Appendix D. Note that on upscaling from 0.1 m to 0.5 m scale, and from 0.5 m to 2 m scale, the nugget is essentially eliminated (cf. Table 5-36 and related text).

5.7.3 Upscaling and results of simulation of thermal conductivity

For each TRC (and sub-TRCs) the following plots and diagrams have been produced to illustrate the upscaling steps and the simulation results.

Table 5-37. Variogram parameters for modelling spatial correlation of thermal conductivity at 0.5 m and 2 m scales for each TRC. The nugget is treated as a separate variogram structure with no range. Semi-variance of variogram structures is standardised to the variance of the data so that the sum of the semi-variance values for all structures is 1.

TRC	Rock type, code	Structure	0.5 m Semi-variance (contribution, weight)	Range	2 m Semi-variance (contribution, weight)	Range
TRC 30	501036	Nugget	0		0	
		Spherical	1	75	1	75
TRC 33A	501033 A	Nugget	0		0	
		Spherical	0.22	3	1	22
		Spherical	0.78	22		
TRC 33B	501033 B	Nugget	0		0	
		Spherical	0.07	1.4	1	20
		Spherical	0.93	18		
TRC 36	501036	Nugget	0		0	
		Spherical	1	75	1	75
TRC 46	501046	Nugget	0		0	
		Spherical	0.2	1.3	1	36
		Spherical	0.8	35		
TRC 56	501056	Nugget	0		0	
		Spherical	0.4	2	0.12	3
		Spherical	0.6	50	0.88	50
TRC 58	511058	Nugget	0		0	
		Spherical	1	7	1	9
TRC 102	505102	Nugget	0		0	
		Spherical	1	1.9	1	3.8

Upscaling

1. Histogram of thermal conductivity values from simulations at 0.1 m scale (Figure 5-44, Figure 5-46, Figure 5-48, Figure 5-50, Figure 5-52, Figure 5-54, Figure 5-56, and Figure 5-58). The statistics should be similar to those of the distribution models given in Table 5-35.
2. Histograms of simulated 0.5 m values upscaled to 2 m (Appendix F). Together with the histogram of 0.1 m simulation results, these histograms show the degree to which variability within each TRC is evened out on upscaling from 0.1 m to 2 m.
3. Histograms for the intermediate 0.5 m scale (Appendix F).

Simulation results

1. Histogram of simulated values from 1,000 realisations combined for simulations at 2 m scale (Figure 5-45, Figure 5-47, Figure 5-49, Figure 5-51, Figure 5-53, Figure 5-55, Figure 5-57, Figure 5-59).
2. Histogram of simulated values from individual realisations for simulations at 2 m scale (Appendix F).
3. Variogram reproduction plots for the 2 m scale based on individual realisations (Appendix E).
4. Visual representation of simulation results at 2 m scale. 2D slice through a 3D realisation (Appendix G).

TRC 30

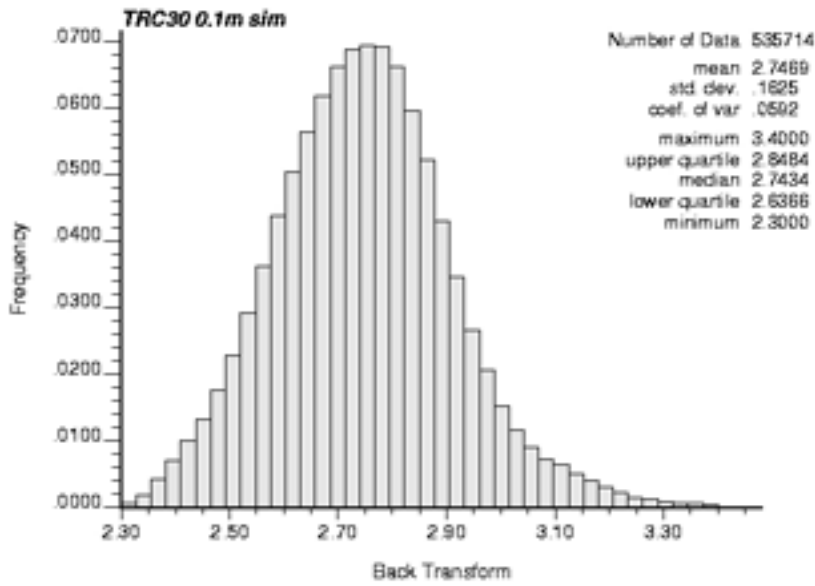


Figure 5-44. Histogram of simulated values at 0.1 m scale before upscaling for TRC 30.

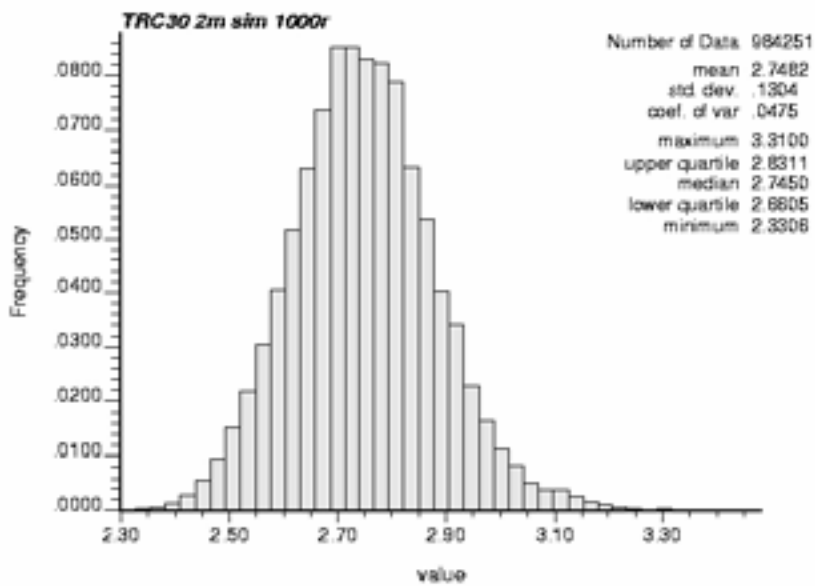


Figure 5-45. Histogram of simulation results at 2 m scale for TRC 30.

TRC 33A

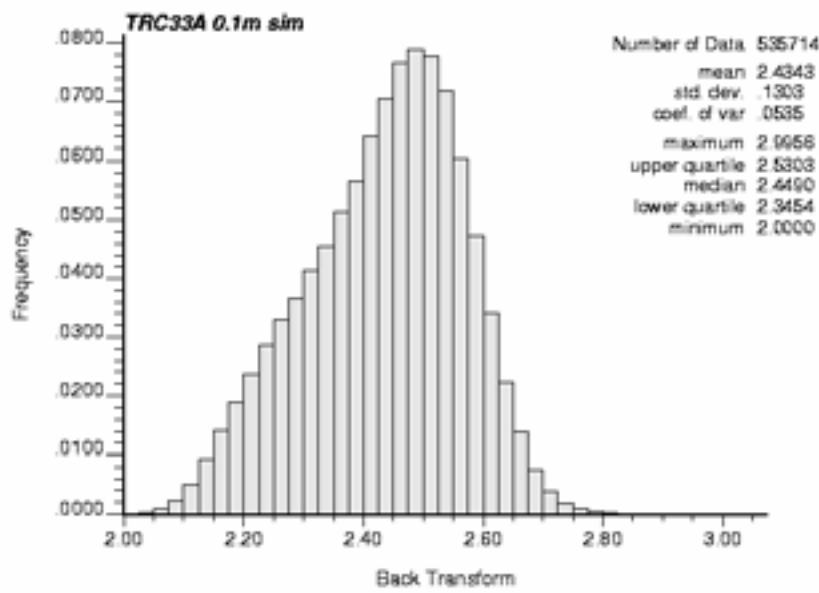


Figure 5-46. Histogram of simulated values at 0.1 m scale before upscaling for TRC 33A.

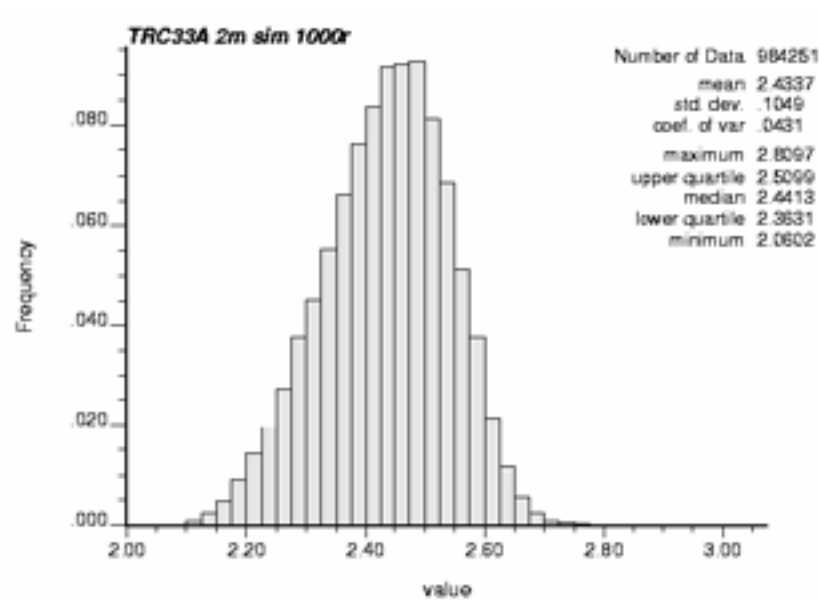


Figure 5-47. Histogram of simulation results at 2 m scale for TRC 33A.

TRC 33B

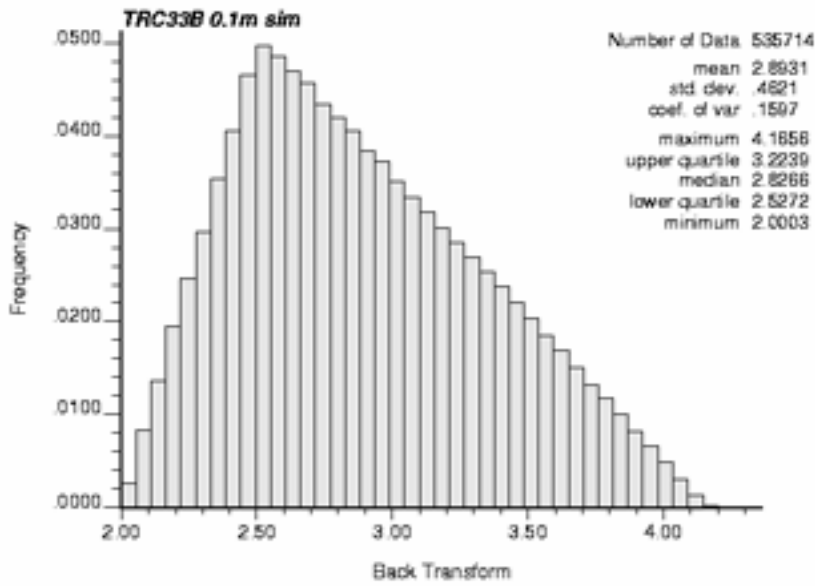


Figure 5-48. Histogram of simulated values at 0.1 m scale before upscaling for TRC 33B.

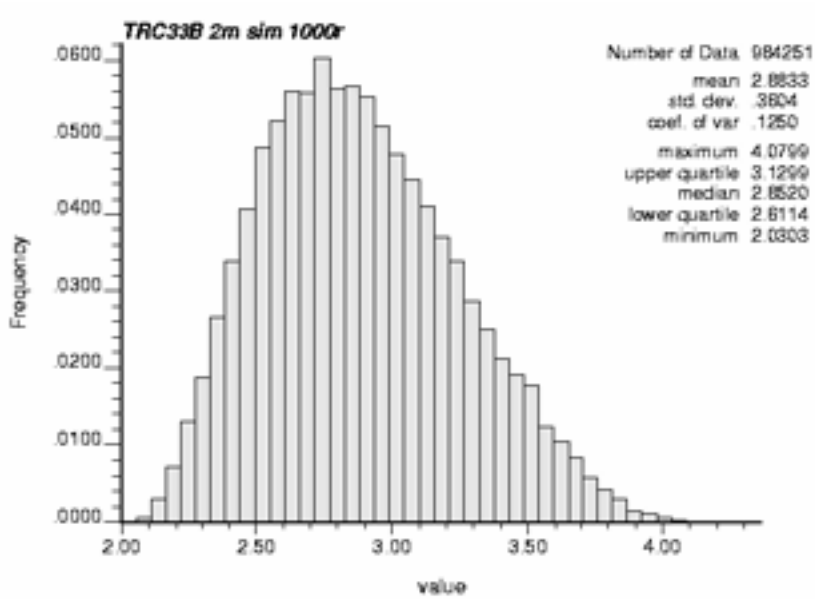


Figure 5-49. Histogram of simulation results at 2 m scale for TRC 33B.

TRC 36

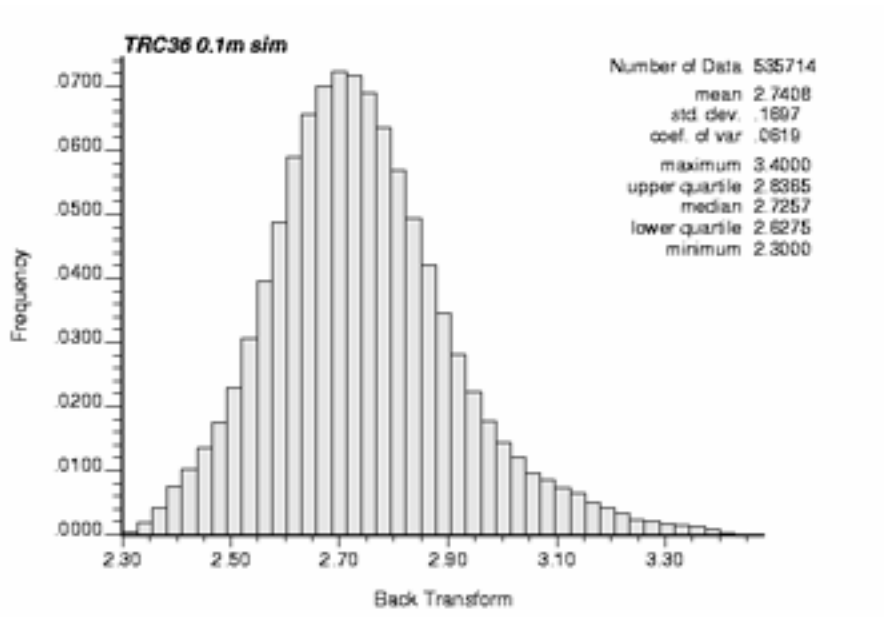


Figure 5-50. Histogram of simulated values at 0.1 m scale before upscaling for TRC 36.

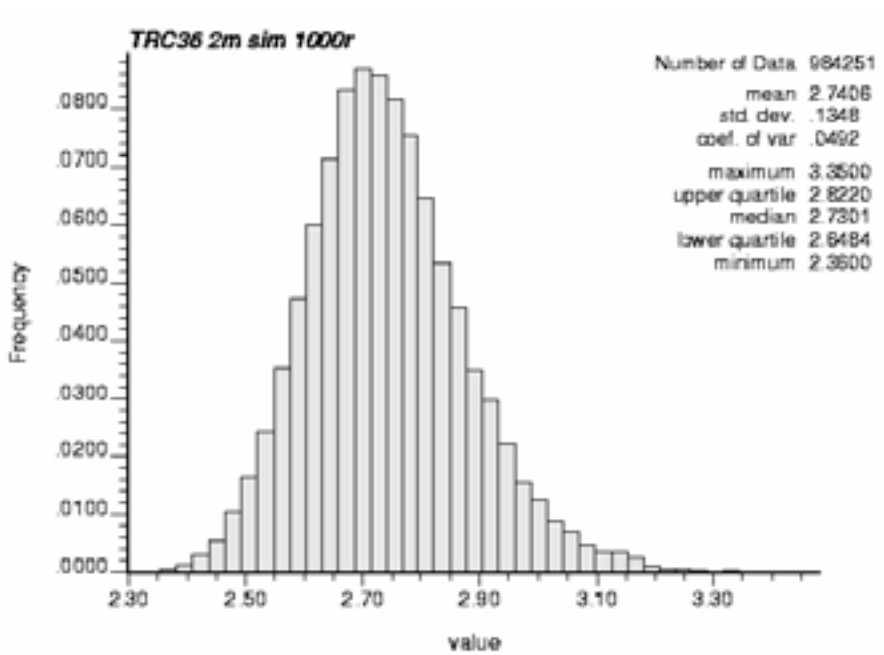


Figure 5-51. Histogram of simulation results at 2 m scale for TRC 36.

TRC 46

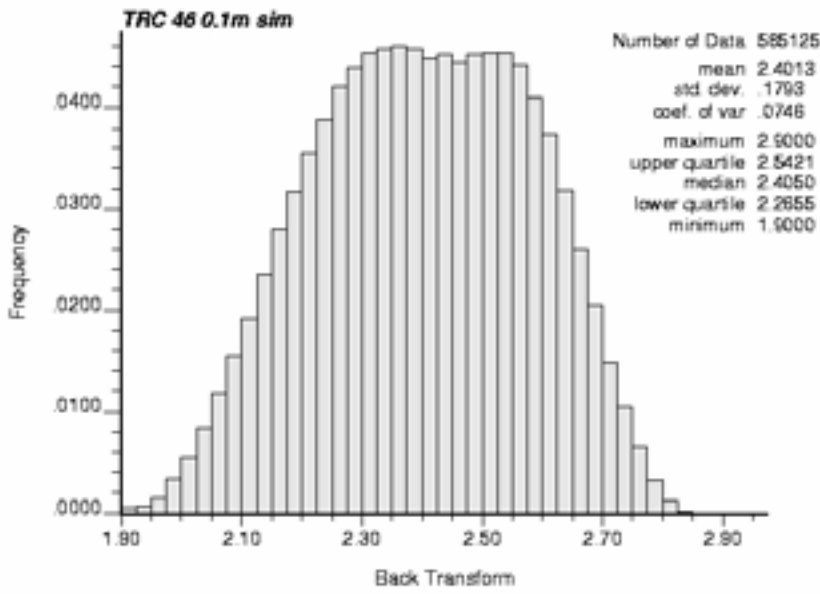


Figure 5-52. Histogram of simulated values at 0.1 m scale before upscaling for TRC 46.

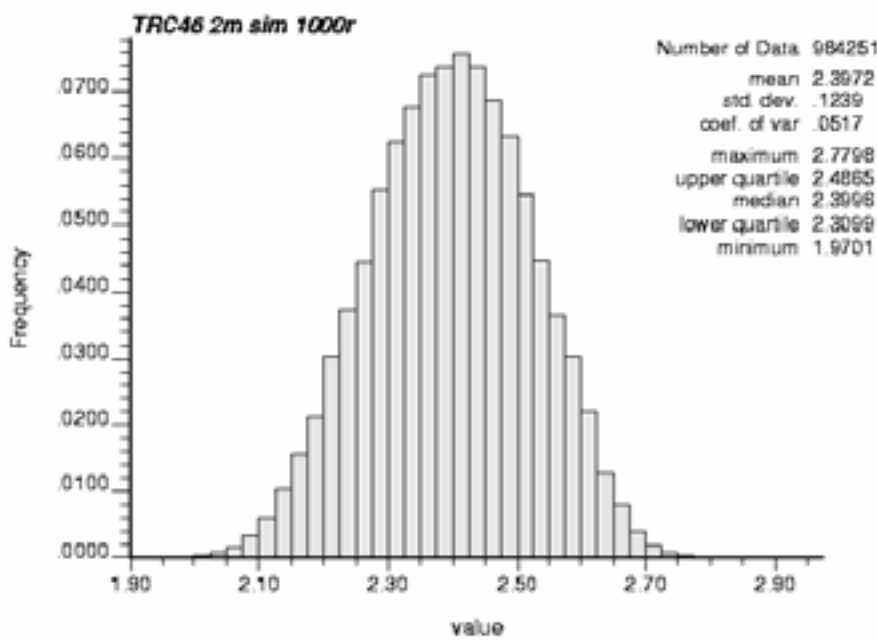


Figure 5-53. Histogram of simulation results at 2 m scale for TRC 46.

TRC 56

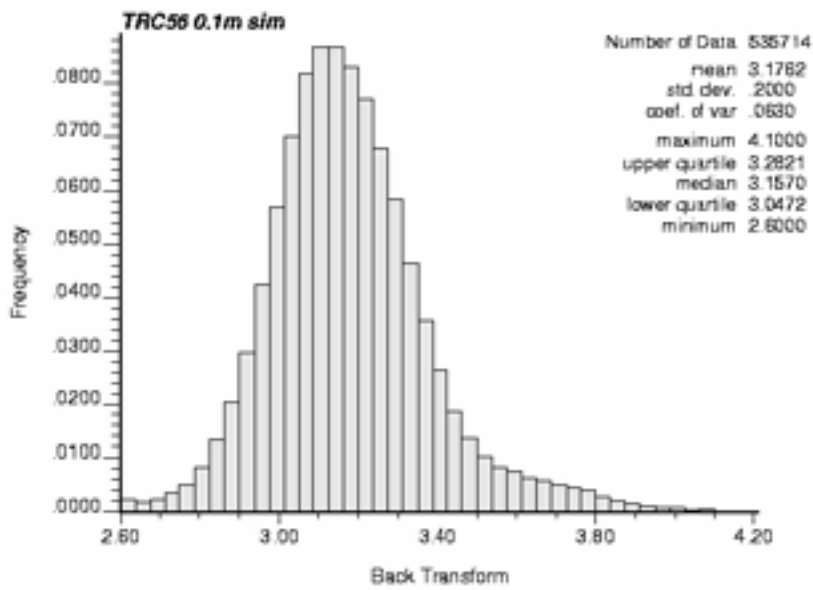


Figure 5-54. Histogram of simulated values at 0.1 m scale before upscaling for TRC 56.

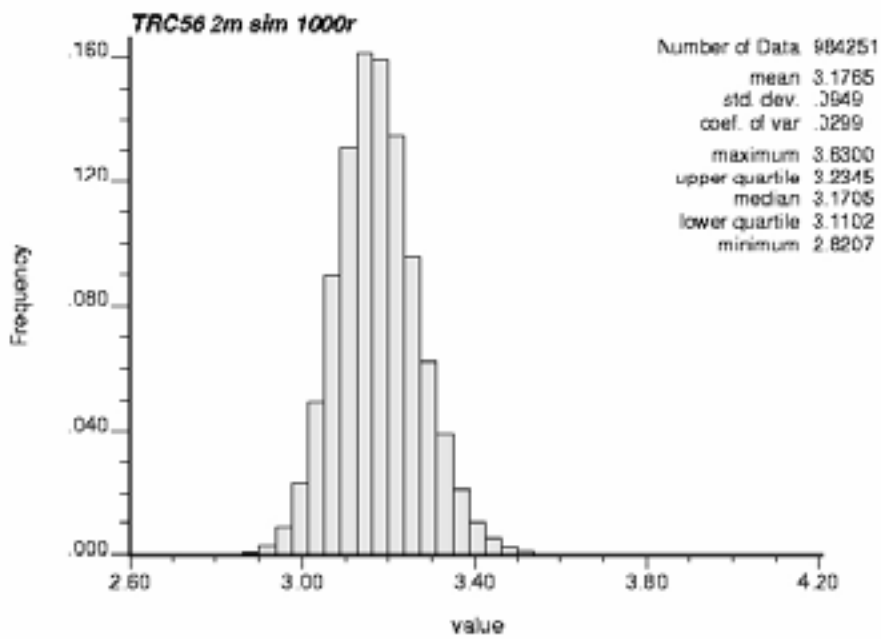


Figure 5-55. Histogram of simulation results at 2 m scale for TRC 56.

TRC 58

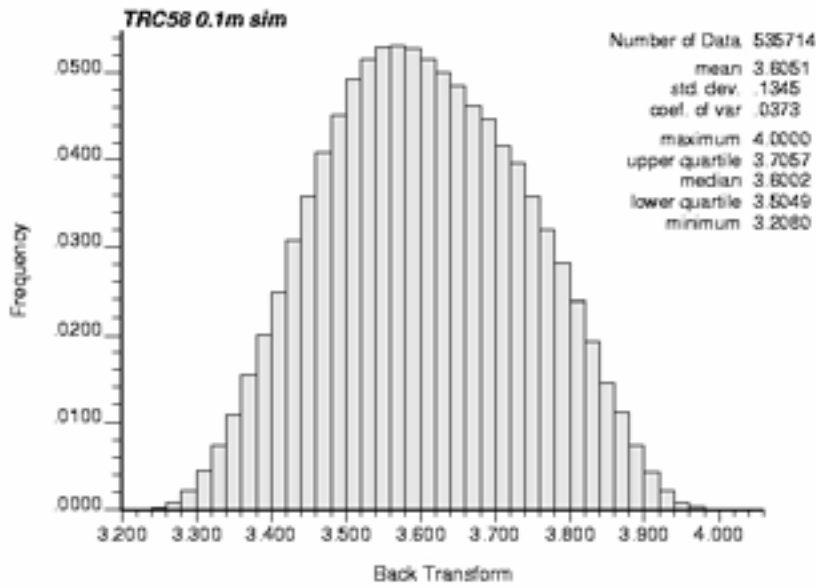


Figure 5-56. Histogram of simulated values at 0.1 m scale before upscaling for TRC 58.

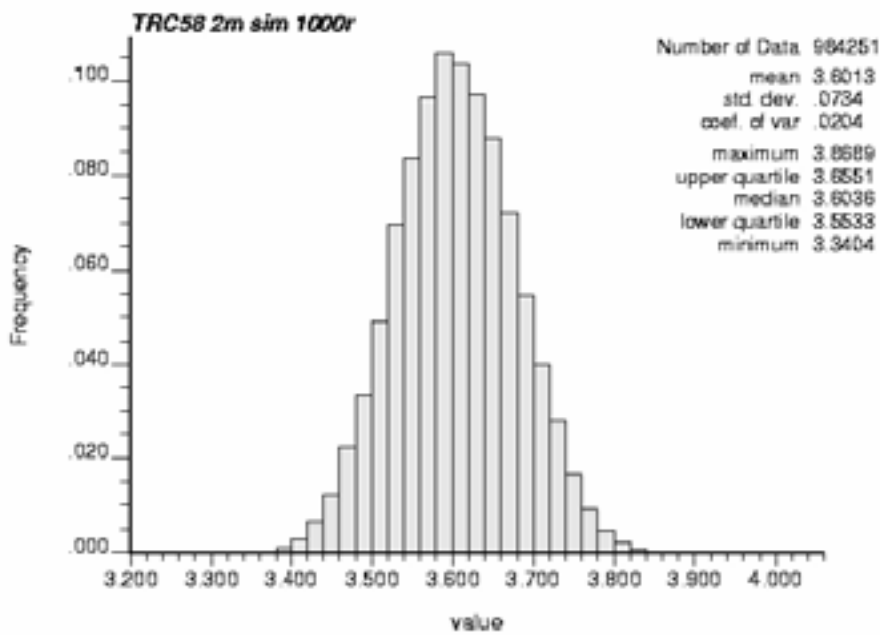


Figure 5-57. Histogram of simulation results at 2 m scale for TRC 58.

TRC 102

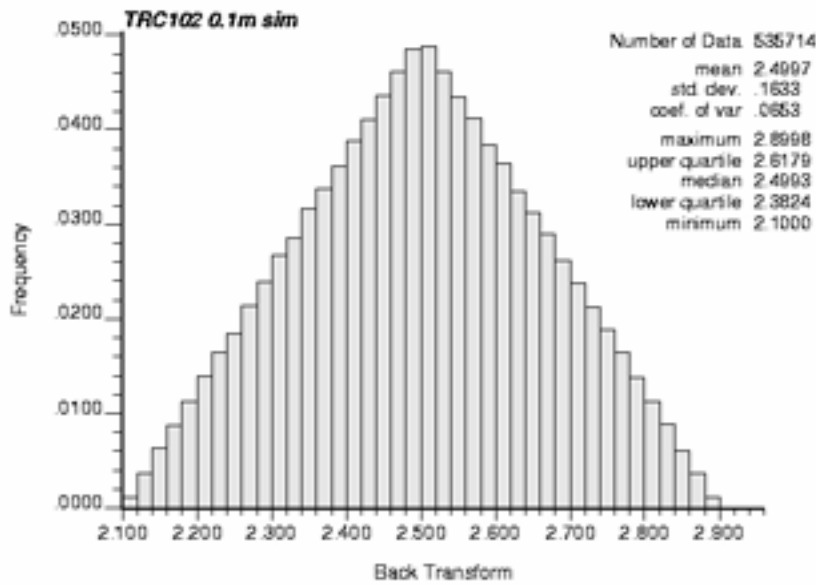


Figure 5-58. Histogram of simulated values at 0.1 m scale before upscaling for TRC 102.

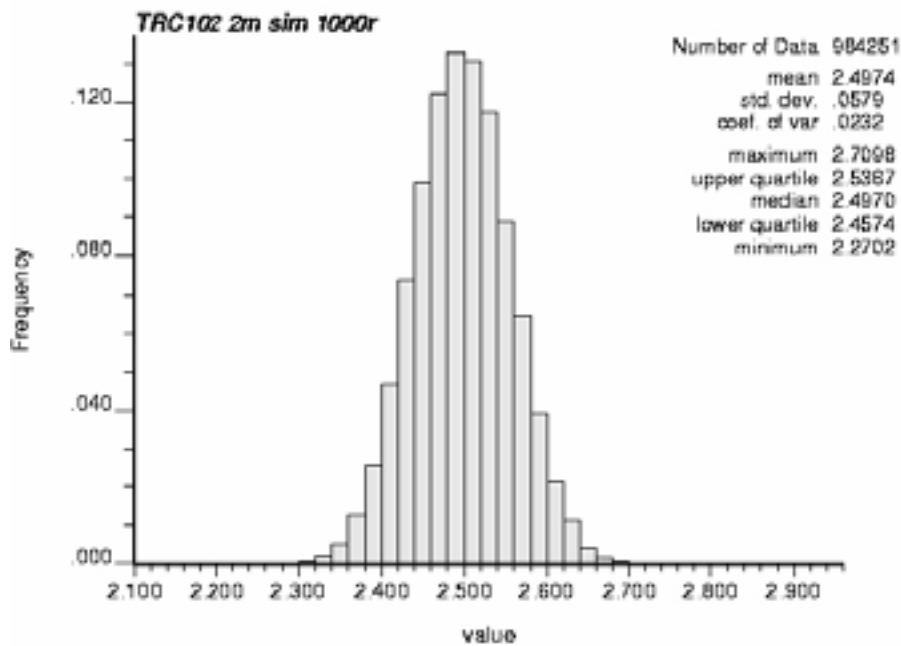


Figure 5-59. Histogram of simulation results at 2 m scale for TRC 102.

Statistics of the results of thermal simulations for all TRCs and sub-TRCs are summarised in Table 5-38. The histograms based on the upscaled realisations define the statistical distribution models for simulations at the 0.5 m and 2 m scales. These results are discussed and evaluated in Section 5.8.

Table 5-38. Thermal conductivity statistics for all simulated TRCs. Simulation at 2 m scale uses the distribution of upscaled 0.5 m values as a distribution model.

TRC	Scale (m)	Source of data	Mean (W/m·K)	Standard deviation (W/m·K)	Variance reduction due to upscaling (%)
30	0.1	Simulations	2.747	0.163	
	0.5	Upscaled 0.1 m realisations	2.746	0.132	34
	0.5	Simulations	2.746	0.132	
	2	Upscaled – 0.5 m realisations	2.746	0.130	36*
	2	Simulations – 1,000 realisations	2.748	0.130	
33A	0.1	Simulations	2.434	0.130	
	0.5	Upscaled 0.1 m realisations	2.434	0.117	19
	0.5	Simulations	2.434	0.118	
	2	Upscaled – 0.5 m realisations	2.433	0.105	35*
	2	Simulations – 1,000 realisations	2.434	0.105	
33B	0.1	Simulations	2.893	0.462	
	0.5	Upscaled 0.1 m realisations	2.887	0.393	28
	0.5	Simulations	2.886	0.395	
	2	Upscaled – 0.5 m realisations	2.884	0.361	39*
	2	Simulations – 1,000 realisations	2.883	0.360	
36	0.1	Simulations	2.741	0.170	
	0.5	Upscaled 0.1 m realisations	2.740	0.138	34
	0.5	Simulations	2.740	0.137	
	2	Upscaled – 0.5 m realisations	2.740	0.136	36*
	2	Simulations – 1,000 realisations	2.741	0.135	
46	0.1	Simulations	2.401	0.179	
	0.5	Upscaled 0.1 m realisations	2.400	0.141	38
	0.5	Simulations	2.400	0.141	
	2	Upscaled – 0.5 m realisations	2.399	0.124	52*
	2	Simulations – 1,000 realisations	2.397	0.124	
56	0.1	Simulations	3.176	0.200	
	0.5	Upscaled 0.1 m realisations	3.173	0.117	66
	0.5	Simulations	3.174	0.118	
	2	Upscaled – 0.5 m realisations	3.173	0.096	77*
	2	Simulations – 1,000 realisations	3.177	0.095	
58	0.1	Simulations	3.605	0.135	
	0.5	Upscaled 0.1 m realisations	3.604	0.097	48
	0.5	Simulations	3.605	0.097	
	2	Upscaled – 0.5 m realisations	3.604	0.074	70*
	2	Simulations – 1,000 realisations	3.601	0.073	
102	0.1	Simulations	2.500	0.163	
	0.5	Upscaled 0.1 m realisations	2.498	0.128	38
	0.5	Simulations	2.500	0.128	
	2	Upscaled – 0.5 m realisations	2.497	0.058	87*
	2	Simulations – 1,000 realisations	2.497	0.058	

* Variance reduction due to upscaling from 0.1 m to 2 m.

5.8 Evaluation of models of thermal conductivity and simulation results

Statistics of realisations

The statistics of the combined thermal conductivity realisations for a TRC honour the model statistics very well. There is a very close correspondence between the means and variances of the realisations (Table 5-38) and the underlying models (Table 5-35 and Table 5-38).

The statistics, e.g. the mean, of individual realisations may deviate somewhat from the model statistics (Appendix F). For individual realisations it is acceptable, and to a certain degree even desirable, that the statistics deviate slightly from the model, as long as the statistics of all realisations combined are very similar to the models.

Variogram reproduction

The results of variogram reproduction are presented in Appendix E. Plots compare the variograms calculated from the realisations with the model variograms on which simulations were based. Generally speaking, the fit of the variograms to the models are good; the observed fluctuations are symmetric around the models. These fluctuations indicate that a certain amount of heterogeneity has been produced. Variograms for TRCs with short correlation lengths (range) relative to the simulation volume exhibit a better fit to the model. For TRCs with long ranges, e.g. TRC 36, the fluctuations of the realisation variograms are seen to be larger. This was expected /Deutsch and Journel 1998/.

Upscaling

Upscaling of simulation results at 0.1 m scale to 2 m produces a marked reduction in variance for TRCs that show a low degree of spatial continuity, e.g. TRC 56, TRC 58 and TRC 102. For TRCs with a high degree of spatial continuity, e.g. TRC 36, the variance reduction is considerably lower. For example, TRC 46 shows a 52% reduction in variance on upscaling from 0.1 m to 2 m. In other words, approximately half of the spatial variability present at the cm–dm scale is evened out at the 2 m scale.

Despite the observed reduction in variance as a result of upscaling, a comparison of the 0.1 m and 2 m histograms indicates that for some TRCs (33A, 33B and 46) the lower tails have become “lighter” but have not disappeared; in other words extremely low values are much less frequent but still exist at the 2 m scale. Taking TRC 46 as an example, the proportion of values lower than 2.1 W/(m·K) after upscaling to 2 m is not insignificant.

Comparison between upscaled simulation results with field measurements of thermal conductivity for TRC 46 (Table 5-39) show both lower mean and standard deviation for field measurements. The mean for the simulation results is outside the confidence interval for the field measurements. The corresponding standard deviation is inside the interval. The differences probably reflect lower representativeness for the field measurements. The simulation results represent much more data. However, it is interesting to see that the mean minus two standard deviations is close to each other.

Table 5-39. Comparison between thermal conductivity (W/(m·K)) derived from field measurements of Ävrö quartz monzodiorite and simulation results for TRC 46. The two distributions represent about the same scale, 0.5 m. Confidence intervals for means and standard deviations of field measurements.

TRC 46	Simulation results, 0.5 m	Field measurement	95% confidence intervals
Mean	2.40	2.31	2.27–2.36
St dev	0.14	0.09	0.07–0.14
Mean – 2 st dev	2.12	2.13	

Impact of thermal models on simulation results

The observation about upscaling made above emphasises the importance of the thermal models on which the simulations are based. Having reliable models is of greatest importance for those TRCs that a) occur as large geological bodies, b) have low thermal conductivities, and c) display strong spatial continuity. The reason is that, for these TRCs, low thermal conductivity values persist to a high degree even after upscaling to 2 m blocks. It is the lower tails of the thermal conductivity distributions that will affect the canister spacing in a future waste repository. Thus, how these TRCs are modelled is crucial to the overall rock domain thermal model presented in Chapter 6 and its future application. Again TRCs 33A, 33B and 46 are the most important in this respect, TRC 46 particularly so, as it is volumetrically important in both domains RSMA01 and RSMM01.

In Section 5.6.2, it was pointed out that the TPS data for Ävrö quartz monzodiorite produced a somewhat unsatisfactory distribution model for TRC 46, perhaps because of too few data values. The fitted model deviates somewhat from the irregular data distribution. However, it was also pointed out that the lower tail of the data distribution was mimicked closely by the model produced by the smoothing operation, and consequently that the model could be considered quite reliable for this part of the distribution.

The variogram model for TRC 46 model was also considered reasonable, although there are uncertainties in both the nugget and the ranges. The first part of variogram model (0–10 m) model is to a large extent based on a small set of TPS data at small separation distances, and density loggings from borehole KLX17A. If other boreholes were selected as the basis of the variogram model, simulation results would have been slightly different. This is illustrated in Figure 5-60 by the variograms for three different boreholes. In this figure only the lag distances up to 6 m are shown. If the model had been fitted to either KLX13A or KLX18A, a slightly larger variance reduction would have been obtained on upscaling to 2 m.

The distribution model for TRC 33B is particularly uncertain due to the small number (13) of data values and high variability in thermal conductivity. The triangular distribution model used to describe this sub-TRC has a rather heavy low-tail with a minimum value of 2.06 W/(m·K). On the other hand, individual values down to 2.06 W/(m·K) indicate that such a distribution may not be unreasonable. The nugget and range of the variogram model are based solely on density logging data; see Figure 5-32. The very low nugget (standardised) of 0.1, which was based on borehole KLX12A, means that upscaling to 2 m scale does not produce a large reduction in variance. This clearly has a profound effect on the overall simulation results for rock domain RSMM01. Again, basing the first part of variogram model (0–5 m) on another borehole, for example KLX05, would have produced a slightly higher variance reduction as a result of upscaling; see Figure 5-61.

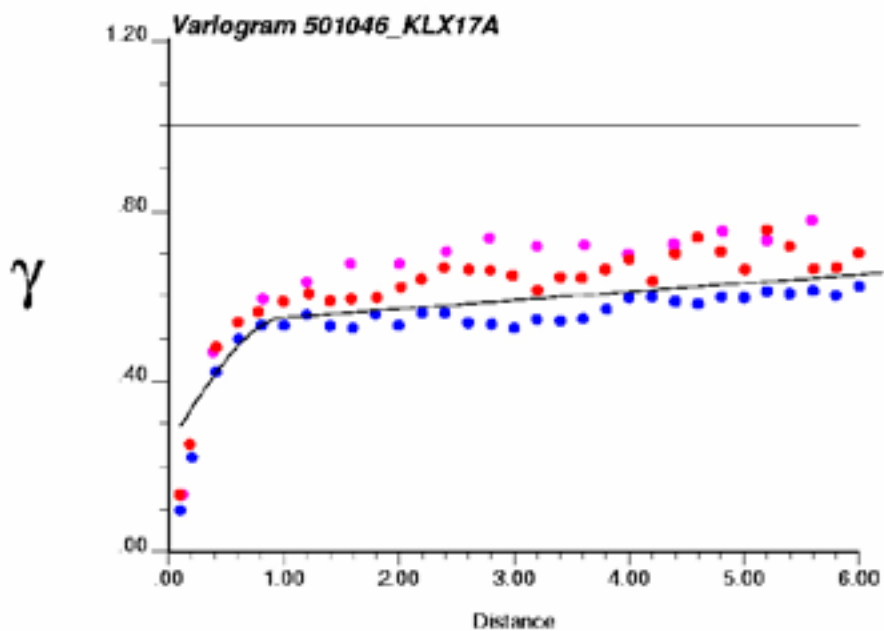


Figure 5-60. Variograms for Ävrö quartz monzodiorite (501046) produced from density logging data from borehole KLX13A (pink), 17A (blue) and 18A (red). The model used in simulations is represented by the black line. Lag distance (x axis) in metres (m). Variogram is standardised to the variance of the measured data. Semi-variance values (γ) for lag distances below 0.4 m are unreliable (see Section 5.6.3).

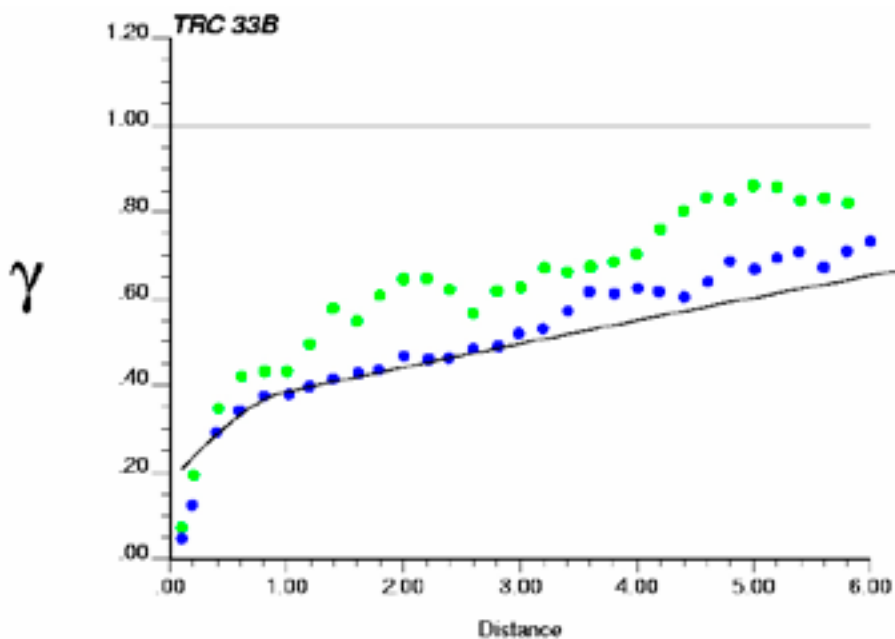


Figure 5-61. Variogram model for TRC 33B based on sample variograms for diorite-gabbro (501033) produced from density logging data. Borehole KLX05 (green) and KLX12A (blue). Nested variogram model fitted – black line. Lag distance (x axis) in metres (m). Variogram is standardised to the variance of the measured data. Semi-variance values (γ) for lag distances below 0.4 m are unreliable (see Section 5.6.3).

5.9 Statistical models of heat capacity

In thermal modelling of Forsmark a relationship between thermal conductivity and heat capacity was established /Sundberg et al. 2008b/. The relationship was described by a second order equation together with a random error component. Applied to the output from simulation of thermal conductivity, heat capacity realisations were created.

However, in Laxemar there are no obvious relationships between thermal conductivity and heat capacity, neither for individual rock types nor for all rock types considered when pooled together (Figure 3-26 and Figure 3-27). Therefore, the approach for modelling heat capacity in Forsmark cannot be mimicked in Laxemar.

In Laxemar the heat capacity has been modelled based on the TRC-distribution in each realisation together with a statistical distribution model for heat capacity for each TRC (Table 5-40). The statistical models of heat capacity assigned to each TRC are generally based on direct (calorimetric) measurement data from the dominant rock type in each TRC (Table 3-26). For TRC 58 calculations from TPS measurements on fine-grained granite (511058) are used instead since direct measurements have not been performed. However, the standard deviation is adjusted downwards to a more realistic level. For TRC 30, which comprises both fine-grained dioritoid (501030) and quartz monzodiorite (501036) in equal proportions, the model is based on direct measurements from the latter rock type since such data is not available for fine-grained dioritoid. Calculations from TPS indicate, however, similar heat capacity distributions for both these rock types (Table 3-26). The standard deviation for TRC 102 is based on a judgement of both the direct and indirect determinations on fine-grained diorite-gabbro (505102).

The models, which apply at the 2 m scale, are normal distributions truncated at the mean \pm two standard deviations. Since upscaling from measurement scale (0.1 m) to simulation scale (2 m) has not been performed, this truncation step gives a variability which is considered to be more realistic for the 2 m scale. Each cell in a rock domain realisation is randomly assigned a heat capacity value from the appropriate truncated normal distribution. This produces heat capacity distributions at rock domain level.

5.10 Conditional stochastic simulation of thermal conductivity

5.10.1 Introduction

The strategy for thermal modelling, described in /Back and Sundberg 2007/, can also be used for predicting the thermal properties of a specific volume of rock or at specific locations. This contrasts with the main objective of the thermal modelling presented in the current report, which is to provide a spatial statistical description of the thermal properties at domain level. Prediction of thermal conductivity at specific locations may be relevant during the construction phase of a repository, in particular, in the deposition tunnel and around the deposition holes. For this purpose, the type of geostatistical simulation used is referred to as conditional stochastic simulation. With conditional simulation, the data at specific locations, both TRCs and thermal conductivities, are honoured.

The objective of the simulations performed here is to illustrate how the methodology can be used to predict the spatial distribution of thermal conductivity in a specific volume of rock. Conditional simulation can provide the following results:

- A set of equally probable realisations of thermal conductivity in the rock mass of interest.
- The most likely thermal conductivity value at a specific location, and a statistical distribution of possible values (uncertainty).
- The probability that the thermal conductivity will be lower than a specified threshold value at a specific location.

Table 5-40. Statistical distribution models of heat capacities (MJ/m³·K). Apart from TRC 58, models are based on determinations by calorimetric method. For TRC 58, TPS measurement are used.

TRC	TRC 30	TRC 33	TRC 36	TRC 46	TRC 56	TRC 102	TRC 58
Rock type	501036	501033	501036	501046	501056*	505102	511058
Mean value	2.236	2.443	2.236	2.171	2.151	2.285	2.038
Std dev	0.049	0.042	0.049	0.051	0.056	0.05	0.05
+ 2 std dev	2.33	2.53	2.33	2.27	2.26	2.39	2.14
- 2 std dev	2.14	2.36	2.14	2.07	2.04	2.19	1.94

* One outlier excluded

Conditional simulation was performed for a volume of rock at depth below the Oxhagen area. Boreholes KLX05 and KLX12A were drilled from a site in Oxhagen (Figure 1-2). The simulations were conditioned on data from a section of borehole KLX05, corresponding to an elevation of between -247 m and -407 m. This section of KLX05 is lithologically heterogenous and was therefore considered particularly suitable for simulation. The section belongs to thermal sub-domain M2 within rock domain RSMM01 (Section 5.3.3), and is therefore comprised mainly of diorite-gabbro (TRC 33) and Ävrö quartz monzodiorite (TRC 46) with minor amounts of Ävrö granodiorite (TRC 56) and fine-grained granite (TRC 58). The dimensions of the simulation volume are 100 m, 100 m, and 160 m in the x, y and z directions respectively, and the resolution (simulation scale) is 2 m.

Detailed descriptions of the stochastic simulations of thermal conductivity for each TRC and the TRCs (lithologies) can be found in Appendix N and O, respectively.

5.10.2 Model for simulated volume

The realisations of TRCs (lithology) (Appendix O) were merged with the realisations of thermal conductivity (Appendix N) in a similar way as described in Section 4.2.2 and Figure 4-1. The result is a set of 100 realisations of thermal conductivity at the 2 m scale for the simulation volume. Histograms of the simulated thermal conductivity values based on all realisations for the 2 m scale and the 5 m scale (upscaled from 2 m) are presented in Figure 5-62. Upscaling of the realisations to 5 m has the effect of smoothing the histogram. Summary statistics of the realisations are given in Table 5-41. Of particular interest is how the statistical parameters vary between the different realisations. Therefore, 95% confidence limits are estimated for the mean and the low-tail percentiles. The lower tail is a result of the low-conductive rocks, mainly Ävrö quartz monzodiorite and diorite-gabbro.

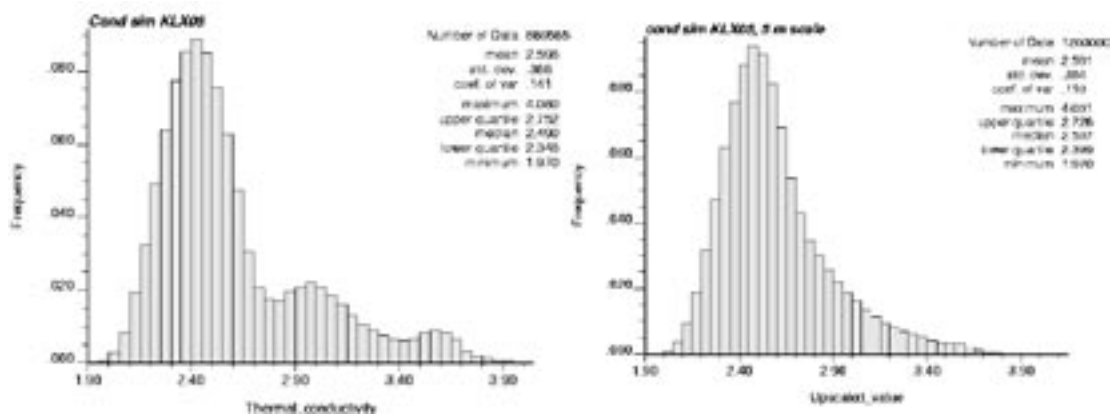


Figure 5-62. Histogram of thermal conductivity values at the 2 m scale (left) and upscaled to the 5 m scale (right) for the simulated volume based on 100 realisations.

Table 5-41. Summary statistics for the simulated volume based on 100 realisations at the 2 m scale and upscaled to 5 m. The calculated statistical parameters for each scale refer to the means of 100 realisations. The indicated uncertainties for the means and percentiles (in brackets) are calculated as two-sided 95% confidence intervals based on the variability between the 100 realisations.

Statistical parameter	2 m	5 m	Unit
Mean	2.60 (-0.04/+0.05)	2.59 (-0.04/+0.05)	W/(m·K)
Variance	0.133	0.081	[W/(m·K)] ²
Standard deviation	0.364	0.283	W/(m·K)
Min	1.98	2.03	W/(m·K)
Max	4.07	3.86	W/(m·K)
0.1-percentile (0.001-quantile)	2.04 (±0.06)	2.07 (±0.08)	W/(m·K)
1-percentile (0.01-quantile)	2.10 (-0.07/+0.08)	2.14 (±0.09)	W/(m·K)
2.5-percentile (0.025-quantile)	2.15 (-0.09/+0.07)	2.19 (-0.09/+0.08)	W/(m·K)

An example of a 2D-slice through a 3D thermal realisation for the simulated volume is visualised in Figure 5-63. The corresponding realisation of lithologies is also presented.

The results can be compared with the results of unconditional simulation of subdomain M2. The mean thermal conductivities both at 2 m and 5 m scales are slightly higher for the simulated volume than for the thermal subdomain M2 (c.f. Figure 6-17).

5.10.3 Evaluation of simulation results

Each realisation provides an alternative equiprobable representation of the distribution of thermal conductivity in the simulated rock volume. The differences between the realisations are a reflection of the spatial uncertainty.

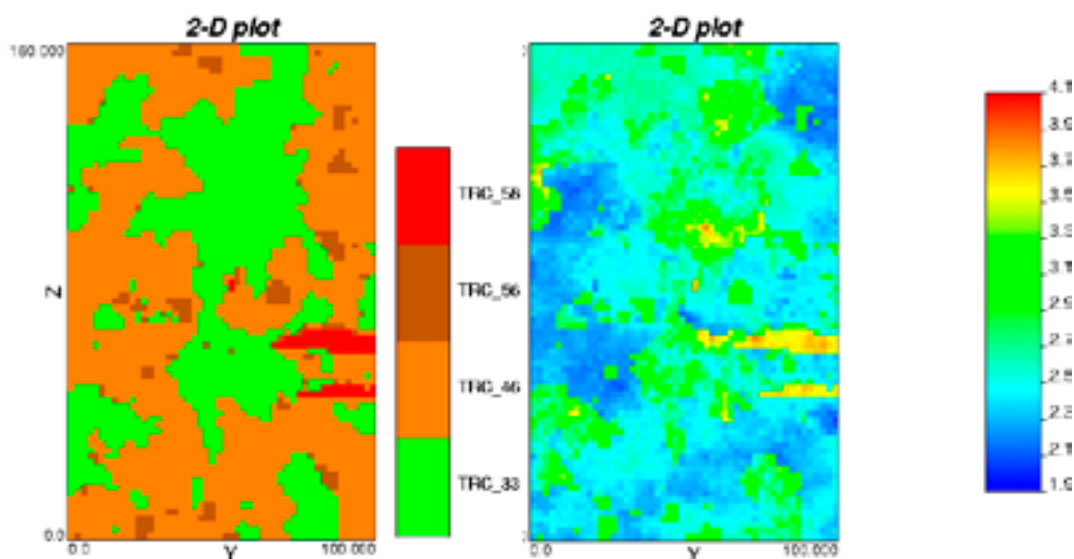


Figure 5-63. Example realisation of thermal conductivity (slices in yz-plane) for the simulated volume (right) and corresponding realisation of lithology (TRC) (left). The resolution of the simulation is 2 m. Slice no. 25 of 50, $x = 50$ m.

The best estimate of thermal conductivity at each position can be determined by calculating the average of the same cell in all 100 realisations (Figure 5-64). Averaging provides the best estimate at a particular location, but because of the smoothing effect, it underestimates the “true” spatial variability between points. The individual realisations reproduce the “true” variability both with respect to the histogram and spatially through the variogram.

From the 100 realisations we have access, at each point, to a distribution (histogram) of possible thermal conductivity values. Based on these histograms, the probability that the thermal conductivity will be lower or higher than a specified threshold can be estimated at each location. In Figure 5-65, the probability of thermal conductivity in each 2 m cell having a value lower than 2.3 W/(m·K) is illustrated. In a similar way, probability distributions higher than a specific value can be determined.

An evaluation of the distribution of simulated values at individual locations also allows the degree of confidence in the predictions to be calculated. To illustrate this, seven points have been chosen at different distances, ranging from 2 m to 36 m, from a known data point along a line in a direction from east to west. The known data point has the following properties:

- borehole length = 302 m,
- lithology = TRC 46, and
- thermal conductivity = c. 2.42 W/(m·K).

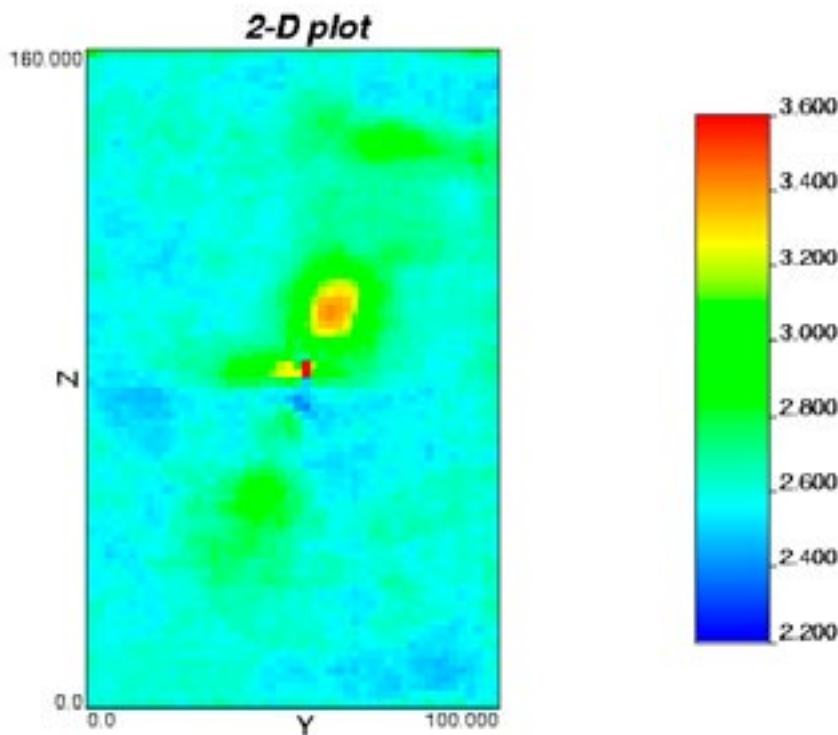


Figure 5-64. A 2D slice (yz plane) through the simulated volume showing the best estimate of thermal conductivity at each point estimated by averaging the 100 realisations. Note that the variance is reduced significantly. Slice no. 25 of 50, $x = 50$ m.

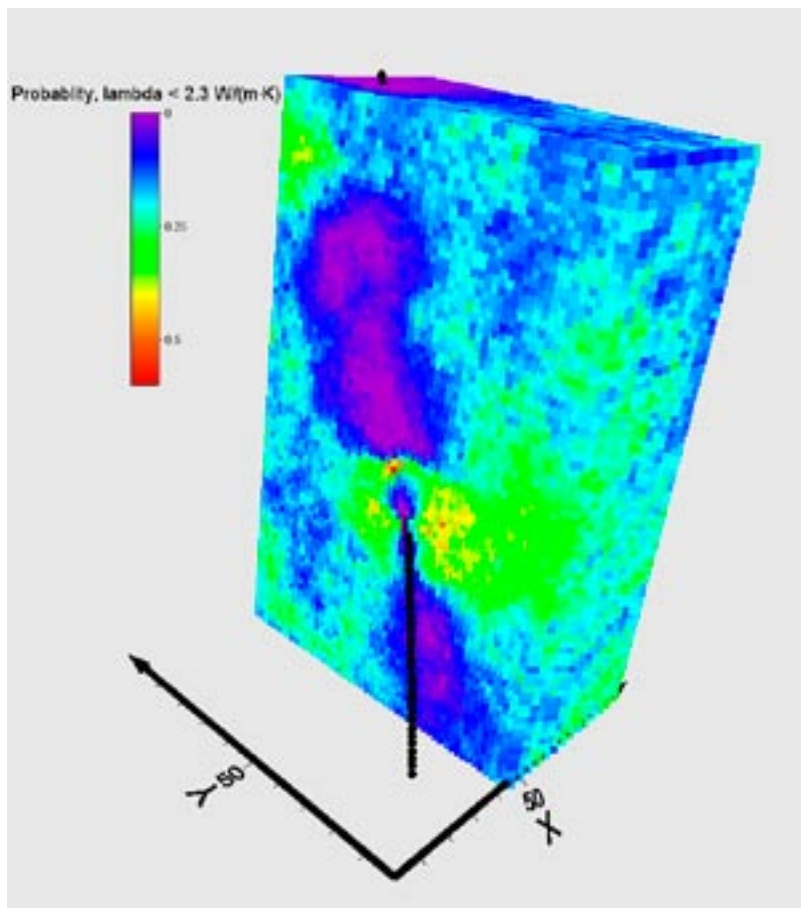


Figure 5-65. The probability of a cell having a thermal conductivity lower than 2.3 W/(m·K). Note that close to the borehole the probability of thermal conductivity being lower than 2.3 is generally low. However, locally the probability of values below 2.3 is higher. Borehole KLX05 is indicated by the black line.

For each unknown point, the most likely value as well as two standard deviations both below and above the mean have been plotted (Figure 5-66). Although strictly speaking, confidence intervals for thermal conductivity should be determined directly from the histograms for each location, the upper and lower limits of thermal conductivity as expressed by the two standard deviations were an effective way of getting an indication of the reliability of the predictions. It can be seen from the example that the predicted values up to 6–7 m away from known data have rather high confidence whereas confidence is much lower for longer distances.

Typical correlation lengths of lithologies for the two dominant TRCs, TRC 46 and TRC 33, are 10 and 17 m, respectively. For thermal conductivity, the corresponding correlation lengths are 20 and 35 m, respectively. This means that for locations situated at distances longer than 10 to 17 m from known data points (includes both lithology and thermal conductivity), the predictions will be poorly conditioned and the variability of the predicted thermal conductivity will be inevitably high. Such a conclusion is supported by Figure 5-66.

If more local data were available, for example another borehole in close proximity to the existing one, the models of the correlation structure would be improved and the uncertainties in the simulations would be reduced. In the geological simulations only TRC 58 was modelled with anisotropy. It was assumed to occur as flat-lying dyke-like bodies. Other TRCs are modelled as isotropic in geometry. New geological interpretations based on additional information acquired, for example, during the underground excavations could be used to revise the spatial models for TRCs.

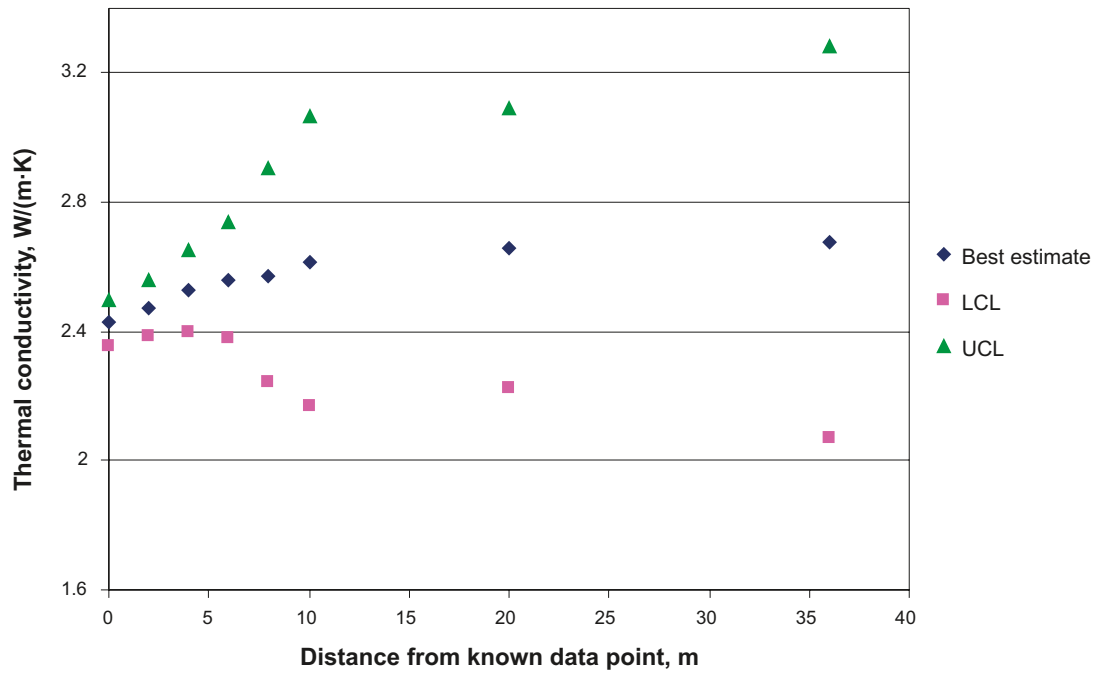


Figure 5-66. Example of the relationship between the variance of simulated values at specific locations and the distance from a known data point in the borehole. The variability is expressed by \pm two standard deviations; Upper Confidence Limit (UCL) and Lower Confidence Limit (LCL). The simulated values at each location may not be normally distributed because of rock type changes.

The results of the simulations described in this section illustrate the potential of conditional simulation in modelling the properties of a specific rock volume using known data points for conditioning. The results are not relevant for the thermal model at domain level, which is presented in Chapter 6, and will not be discussed further in this report.

6 Thermal domain model

6.1 Domain modelling results

The results of the final modelling steps (11, 12 and 13 in Figure 4-1) are presented below for three rock domains, RSMA01, RSMM01 and RSMD01; see Figure 2-1. The results for thermal conductivity is presented in Section 6.2 and the results for heat capacity is presented in Section 6.3. First, the output of the lithological simulations and the thermal conductivity simulations are merged. Then upscaling to larger scales is performed. Histograms and tables are used to illustrate the results of the thermal modelling for different scales. For domains with thermal subdomains, the proportions of the different subdomains are important for the domain properties (see Table 6-1 and Table 6-2) is the basis for the number of realisations in each subdomain.

6.2 Thermal conductivity

6.2.1 Rock domain RSMA01

Domain RSMA01 consist of three thermal subdomains, described in Section 5.3.3. Below, both the domain results and the results for the different thermal subdomains are presented.

Domain results

The main output of the thermal modelling for domain RSMA01 is the set of 1,000 realisations of thermal conductivity from the 2 m-simulations. A histogram of these realisations combined is shown in Figure 6-1. Summary statistics of the realisations are presented in Table 6-3. The lower tail is a result of the low-conductive rocks, mainly Ävrö quartz monzodiorite. Upscaling of the realisations to 5 m has the effect of smoothing the histogram, i.e. the bimodal distribution becomes unimodal, as illustrated in Figure 6-2.

Table 6-1 Proportions of the simulations in the different thermal subdomains that together form the domain RSMA01 realisations.

Domain RSMA01	No. of lithological realisations	Percent of domain	Thermal realisations used
Sub domain A1	741	74.1	1–741
Sub domain A2	179	17.9	742–920
Sub domain A3	80	8.0	921–1,000

Table 6-2 Proportions of the simulations in the different thermal subdomains that together form the domain RSMM01 realisations.

Domain RSMM01	No. of lithological realisations	Percent of domain	Thermal realisations used
Sub domain M1	383	38.3	1–383
Sub domain M2	347	34.7	384–730
Sub domain M3	109	10.9	731–839
Sub domain M4	105	10.5	840–944
Sub domain M5	56	5.6	945–1,000

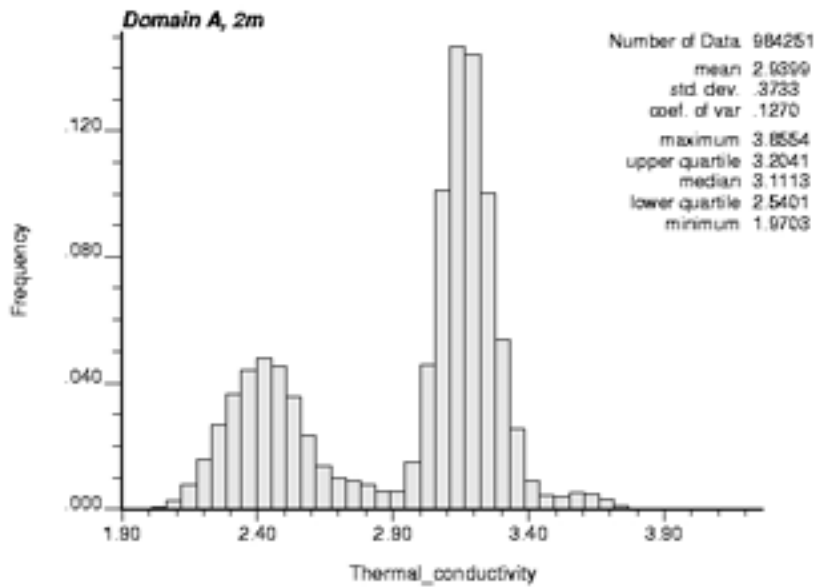


Figure 6-1. Histogram of thermal conductivity for domain RSMA01 simulated at the 2 m scale.

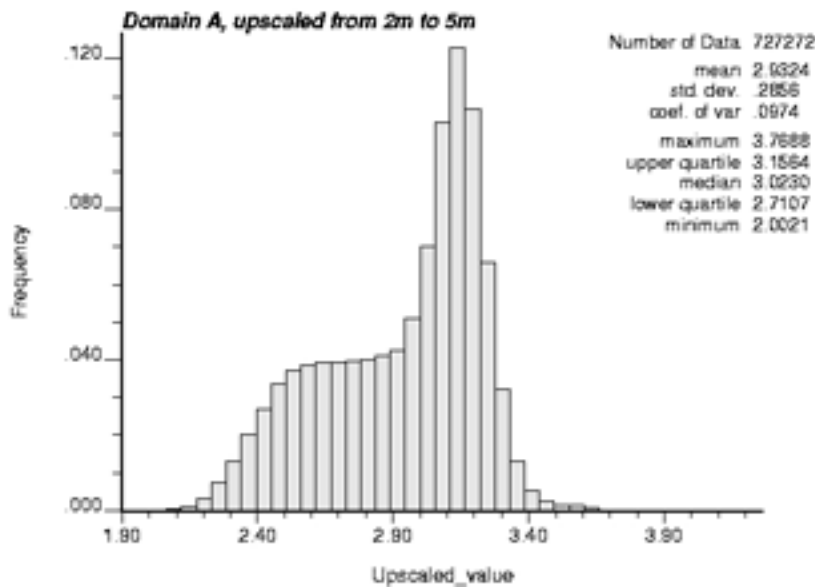


Figure 6-2. Histogram of thermal conductivity for domain RSMA01 simulated at the 2 m scale but upscaled to 5 m.

Table 6-3. Summary statistics for domain RSMA01 based on simulations at the 2 m scale and upscaled to 5 m.

Statistical parameter	2 m	5 m	Unit
Mean	2.940	2.933	W/(m·K)
Variance	0.139	0.082	[W/(m·K)] ²
Standard deviation	0.373	0.286	W/(m·K)
Min	1.970	1.973	W/(m·K)
Max	3.870	3.789	W/(m·K)
0.1-percentile (0.001-quantile)	2.085	2.160	W/(m·K)
1-percentile (0.01-quantile)	2.174	2.272	W/(m·K)
2.5-percentile (0.025-quantile)	2.228	2.339	W/(m·K)

Subdomain results

Domain RSMA01 comprises three thermal subdomains, as described in Section 5.3.3. Examples of 2D-slices of the 3D realisations for the subdomains are visualised in Figure 6-3 to Figure 6-5. Subdomain A1 is dominated by the medium-high conductive Ävrö granodiorite. In subdomain A2 the low conductive Ävrö quartz monzodiorite dominates. Subdomain A3 is mixed.

Histograms of thermal conductivity for thermal subdomains are shown in Figure 6-6 to Figure 6-8 for the 2 m and 5 m scales. The proportions of high and low conductive rocks in each subdomain characterise the shape of the histograms.

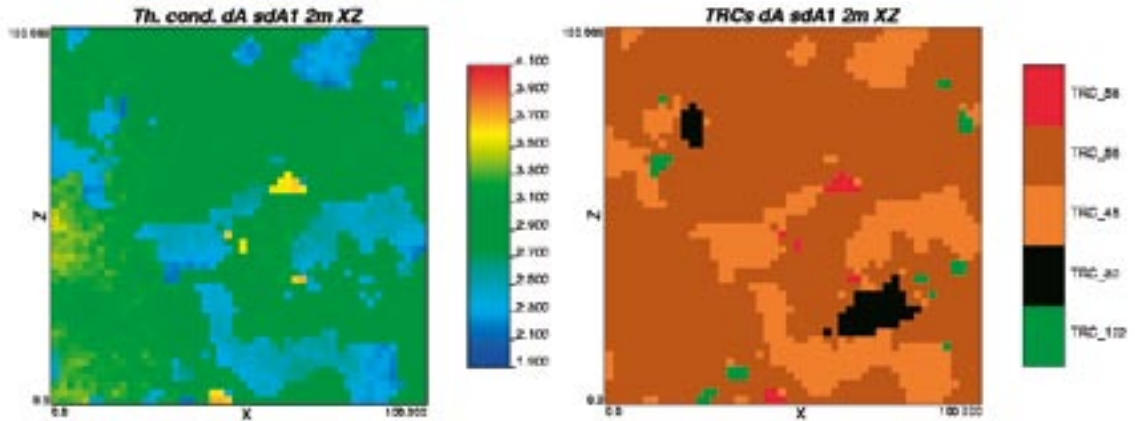


Figure 6-3. An example 2D visualisation of a realisation of thermal conductivity (slices in xz-plane) for thermal subdomain A1 simulated at the 2 m scale (left) and corresponding realisation of lithology (TRC) (right).

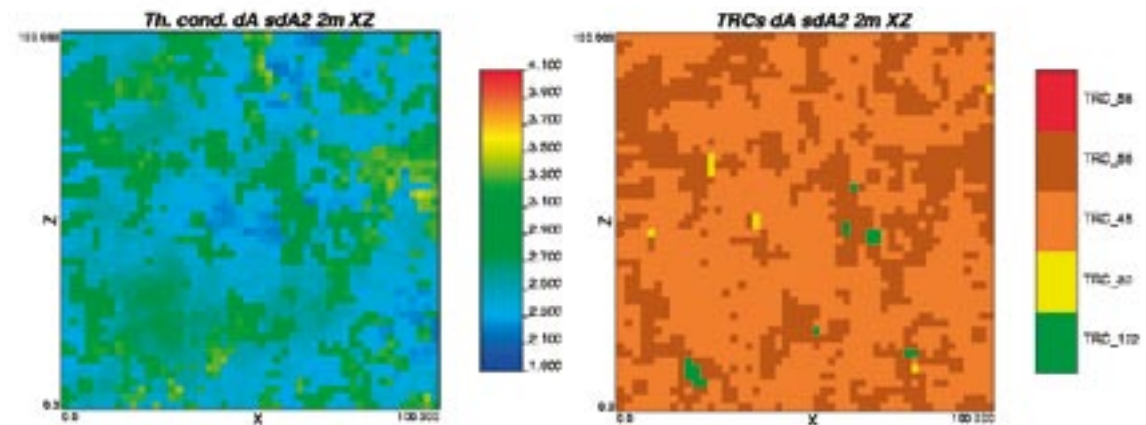


Figure 6-4. An example 2D visualisation of a realisation of thermal conductivity (slices in xz-plane) for thermal subdomain A2 simulated at the 2 m scale (left) and corresponding realisation of lithology (TRC) (right).

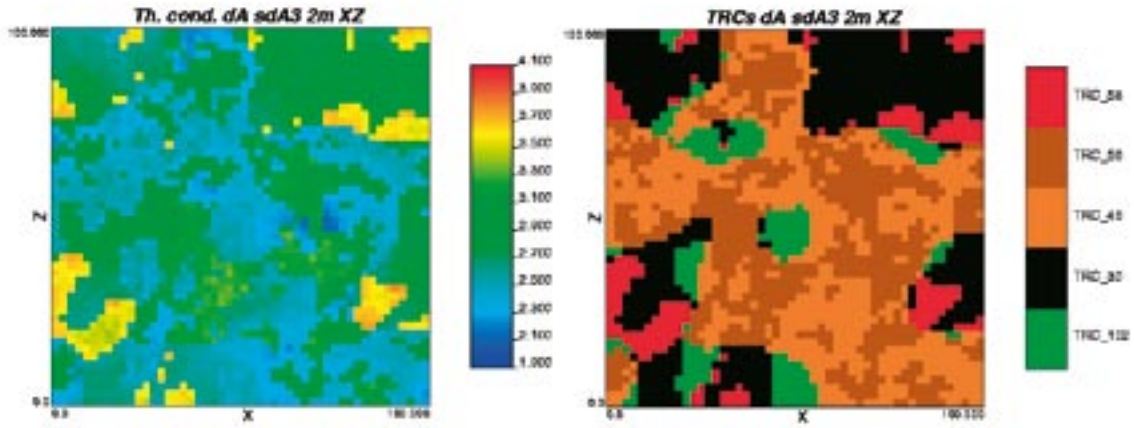


Figure 6-5. An example 2D visualisation of a realisation of thermal conductivity (slices in xz-plane) for thermal subdomain A3 simulated at the 2 m scale (left) and corresponding realisation of lithology (TRC) (right).

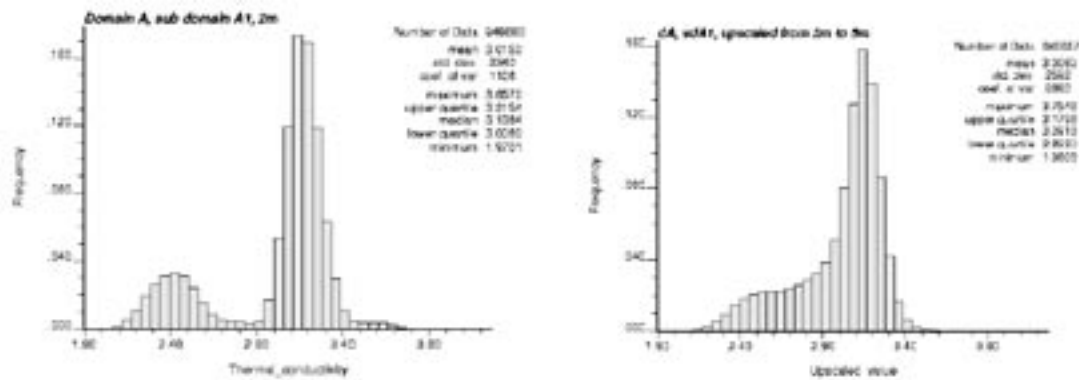


Figure 6-6. Histogram of thermal conductivity for thermal subdomain A1 in domain RSMA01 at the 2 m (left) and 5 m (right) scales.

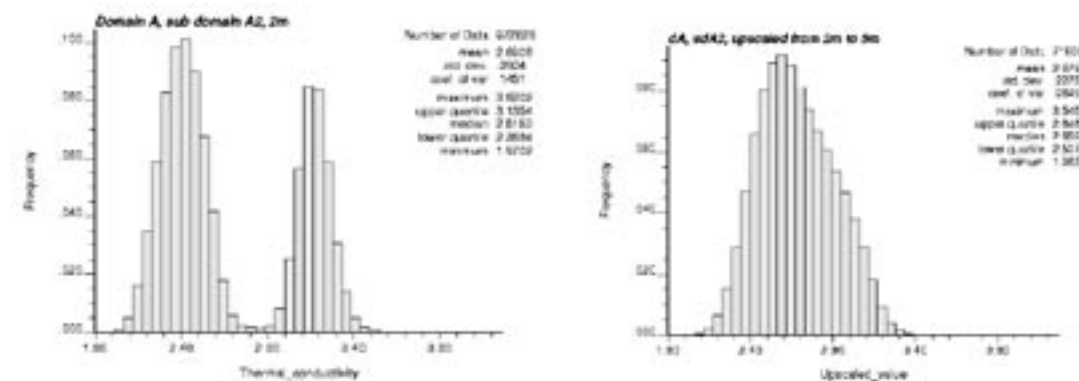


Figure 6-7. Histogram of thermal conductivity for thermal subdomain A2 in domain RSMA01 at the 2 m (left) and 5 m (right) scales.

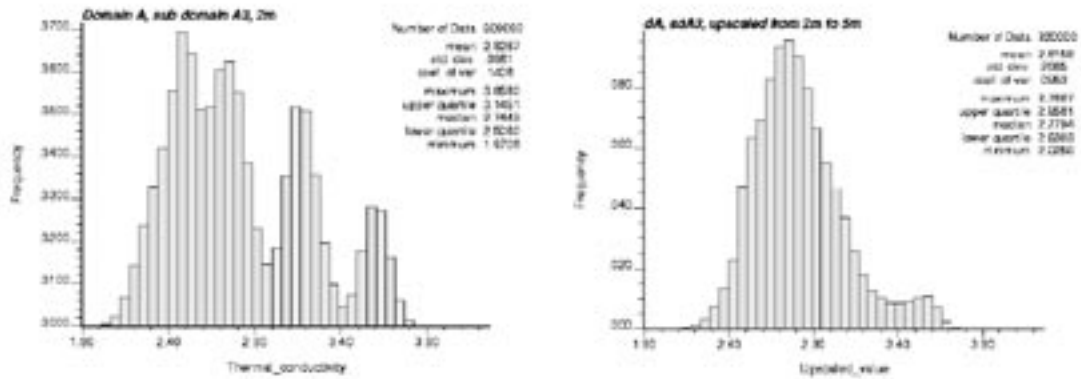


Figure 6-8. Histogram of thermal conductivity for thermal subdomain A3 in domain RSMA01 at the 2 m (left) and 5 m (right) scales.

6.2.2 Rock domain RSMM01

Domain RSMM01 consist of five thermal subdomains, described earlier. Below, both the domain results and the results for the different thermal subdomains are presented.

Domain results

The main result of the thermal modelling for domain RSMM01 is the set of 1,000 realisations of thermal conductivity from the 2 m-simulations. A histogram of these realisations combined is presented in Figure 6-9. Summary statistics of the realisations are given in Table 6-4. The lower tail is a result of the low-conductive rocks, mainly Ävrö quartz monzodiorite and diorite-gabbro. Upscaling of the realisations to 5 m has the effect of smoothing the histogram, as illustrated in Figure 6-10.

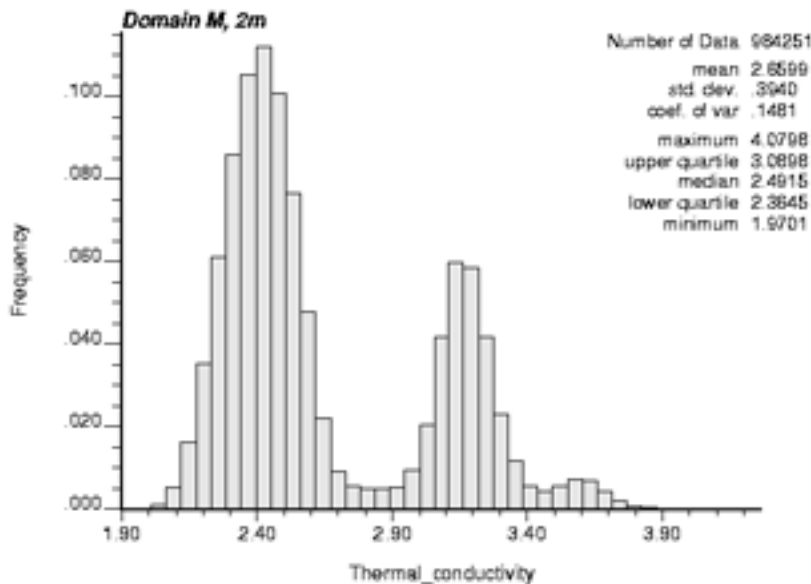


Figure 6-9. Histogram of thermal conductivity for domain RSMM01 simulated at the 2 m scale.

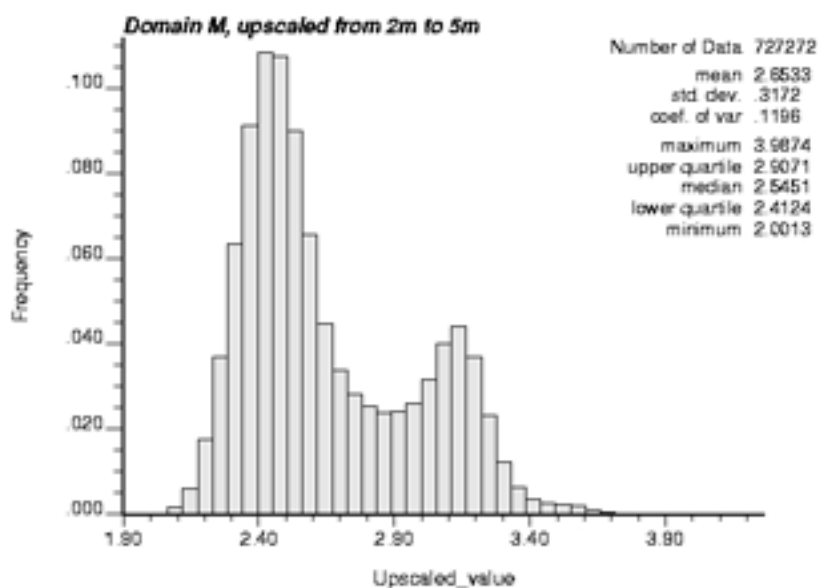


Figure 6-10. Histogram of thermal conductivity for domain RSMM01 simulated at the 2 m scale but upscaled to 5 m.

Table 6-4. Summary statistics for domain RSMM01 based on simulations at the 2 m scale and upscaled to 5 m.

Statistical parameter	2 m	5 m	Unit
Mean	2.660	2.653	W/(m·K)
Variance	0.155	0.101	[W/(m·K)] ²
Standard deviation	0.394	0.317	W/(m·K)
Min	1.970	1.975	W/(m·K)
Max	4.080	4.029	W/(m·K)
0.1-percentile (0.001-quantile)	2.064	2.105	W/(m·K)
1-percentile (0.01-quantile)	2.140	2.185	W/(m·K)
2.5-percentile (0.025-quantile)	2.181	2.230	W/(m·K)

Subdomain results

Domain RSMM01 is subdivided into five thermal subdomains. Examples of 2D-slices of the 3D realisations for the subdomains are visualised in Figure 6-11 to Figure 6-15. Subdomains 1 and 2 are dominated by low conductive Ävrö quartz monzodiorite (TRC 46) and have low and high proportions of diorite-gabbro (TRC 33), respectively. Subdomains 3 and 4 are dominated by medium-high conductive Ävrö granodiorite (TRC 56) and have low and high amounts of diorite-gabbro (TRC 33), respectively. Subdomain 5 is also dominated by Ävrö granodiorite (TRC 56) but has a rather high content of fine grained granite (TRC 58).

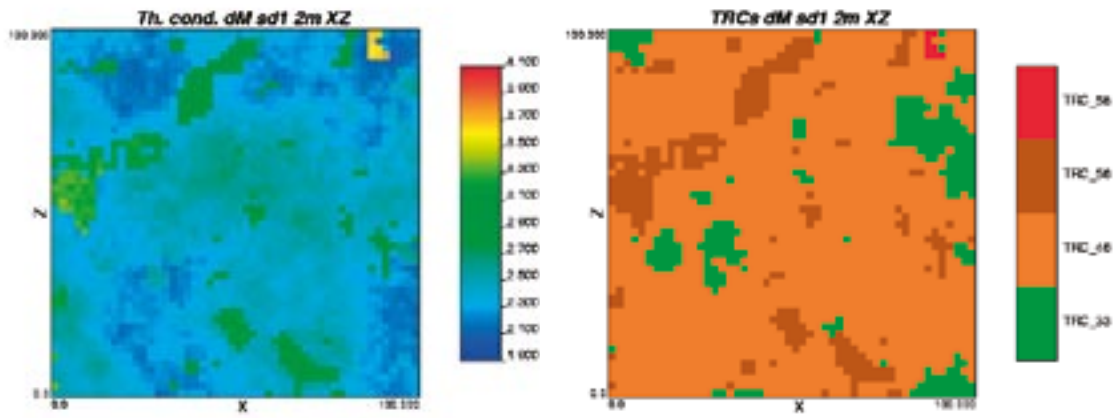


Figure 6-11. An example 2D visualisation of a realisation of thermal conductivity (slices in xz-plane) for thermal subdomain M1 simulated at the 2 m scale (left) and corresponding realisation of lithology (TRC) (right).

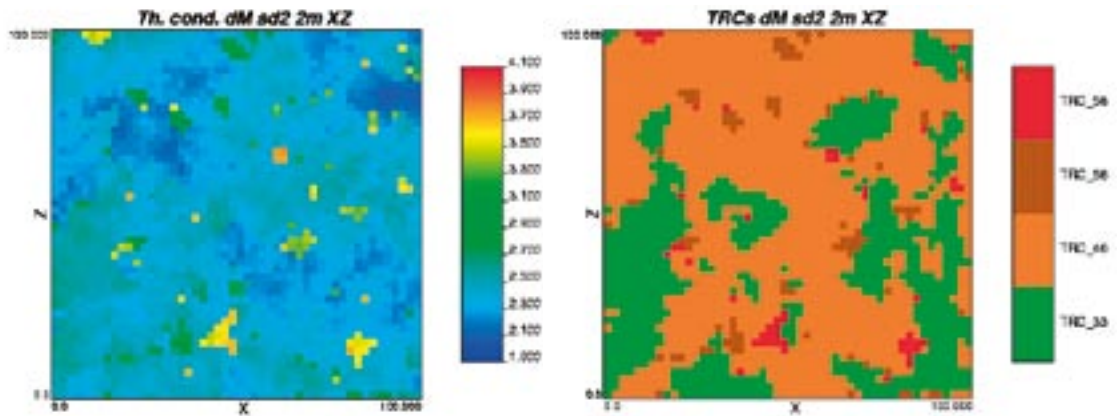


Figure 6-12. An example 2D visualisation of a realisation of thermal conductivity (slices in xz-plane) for thermal subdomain M2 simulated at the 2 m scale (left) and corresponding realisation of lithology (TRC) (right).

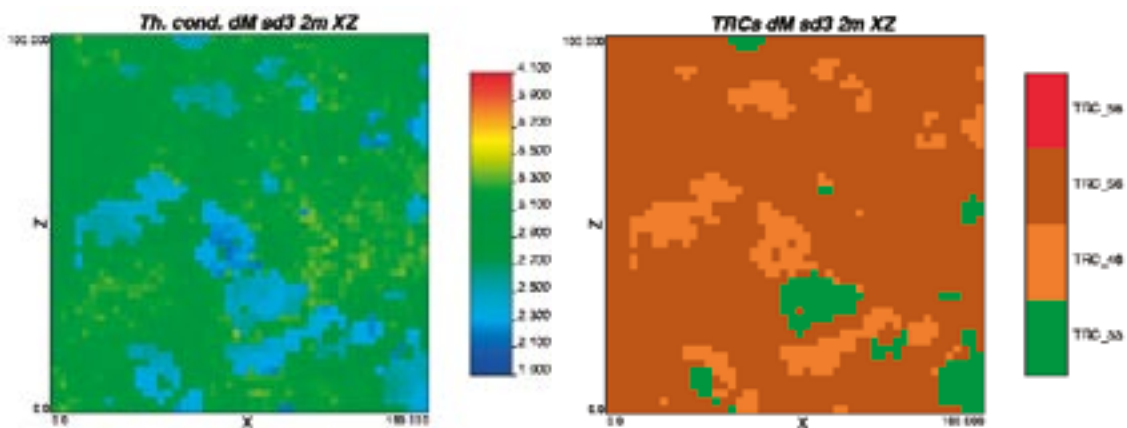


Figure 6-13. An example 2D visualisation of a realisation of thermal conductivity (slices in xz-plane) for thermal subdomain M3 simulated at the 2 m scale (left) and corresponding realisation of lithology (TRC) (right).

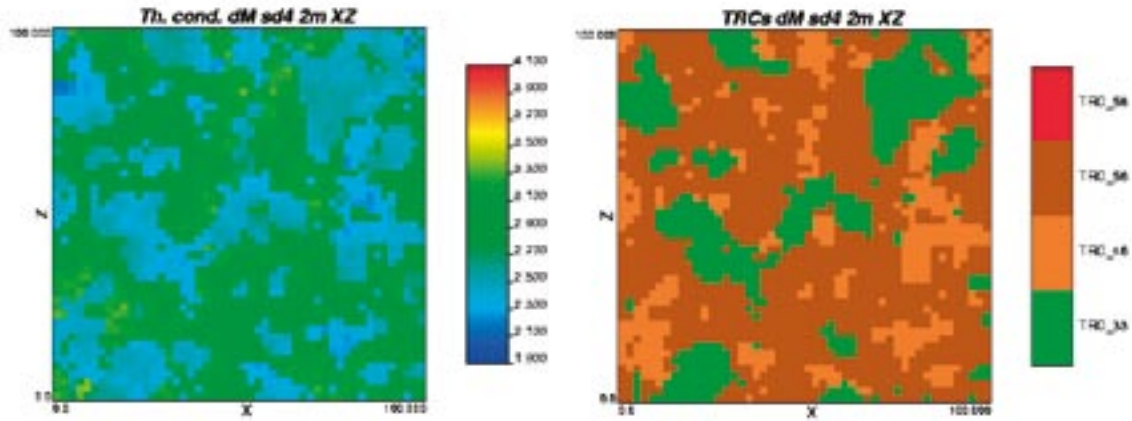


Figure 6-14. An example 2D visualisation of a realisation of thermal conductivity (slices in xz-plane) for thermal subdomain M4 simulated at the 2 m scale (left) and corresponding realisation of lithology (TRC) (right).

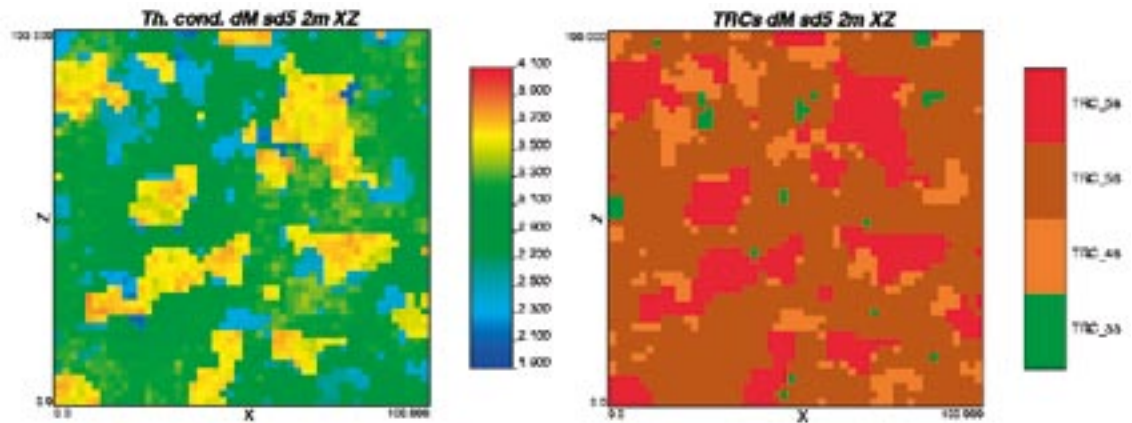


Figure 6-15. An example 2D visualisation of a realisation of thermal conductivity (slices in xz-plane) for thermal subdomain M5 simulated at the 2 m scale (left) and corresponding realisation of lithology (TRC) (right).

Histograms of thermal conductivity of the five thermal subdomains are shown in Figure 6-16 to Figure 6-20 for the 2 m and 5 m scales.

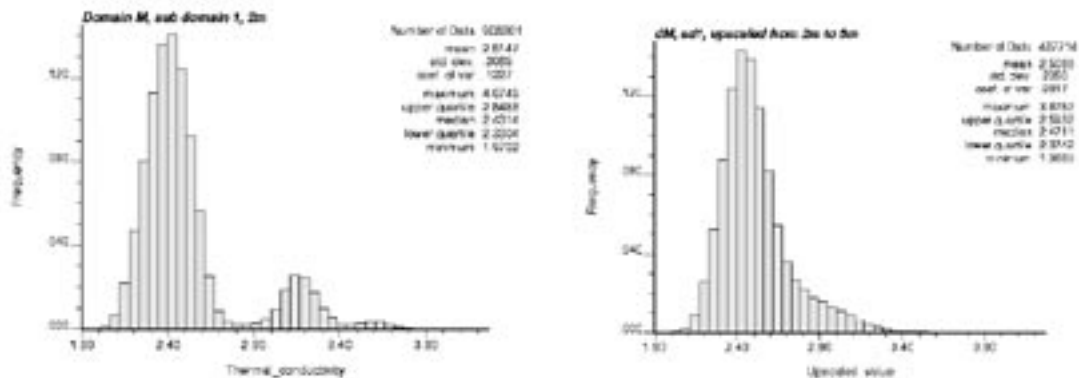


Figure 6-16. Histogram of thermal conductivity for thermal subdomain M1 in domain RSMM01 at the 2 m and 5 m scales.

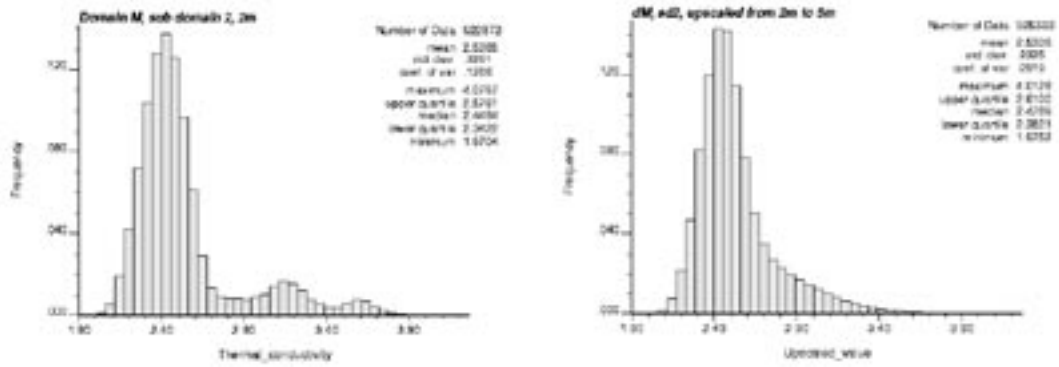


Figure 6-17. Histogram of thermal conductivity for thermal subdomain M2 in domain RSMM01 at the 2 m and 5 m scales.

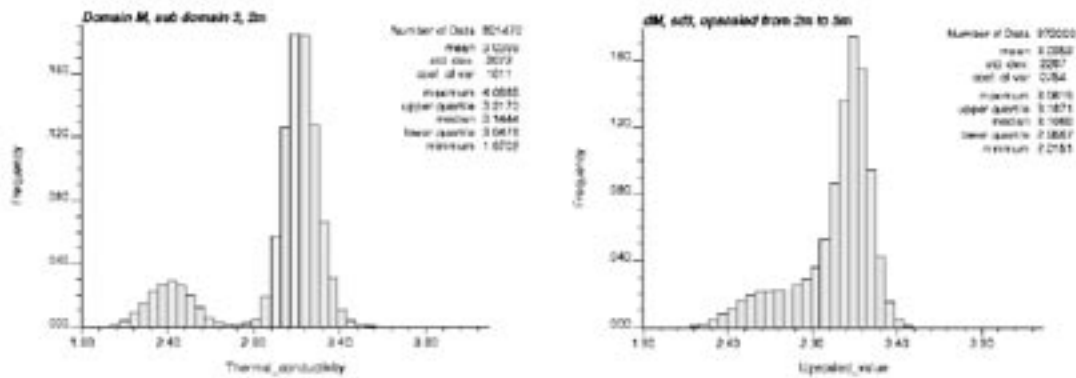


Figure 6-18. Histogram of thermal conductivity for thermal subdomain M3 in domain RSMM01 at the 2 m and 5 m scales.

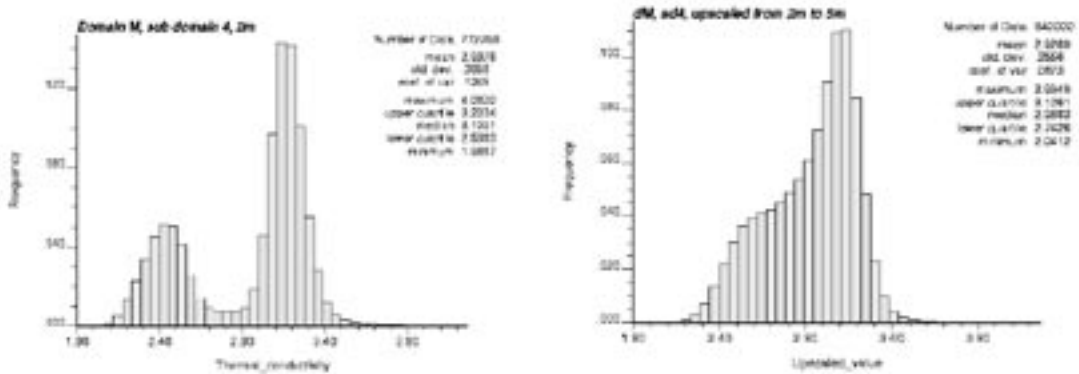


Figure 6-19. Histogram of thermal conductivity for thermal subdomain M4 in domain RSMM01 at the 2 m and 5 m scales.

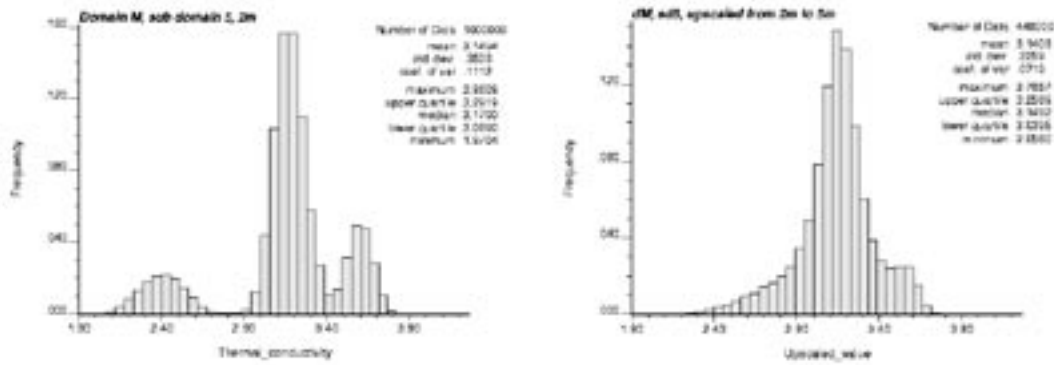


Figure 6-20. Histogram of thermal conductivity for thermal subdomain M5 in domain RSMM01 at the 2 m and 5 m scales.

6.2.3 Rock domain RSMD01

Domain results

The main result of the thermal modelling for domain RSMD01 is the set of 1,000 realisations of thermal conductivity from the 2 m-simulations. Examples of 2D-slices of the 3D realisations for the domain are visualised in Figure 6-21. No thermal subdomain was defined for domain RSMD01.

A histogram of all realisations is shown in Figure 6-22. Upscaling of the realisations to 5 m has the same effect of smoothing the histogram as for all the other domains; see Figure 6-23. Summary statistics of the realisations are presented in Table 6-5.

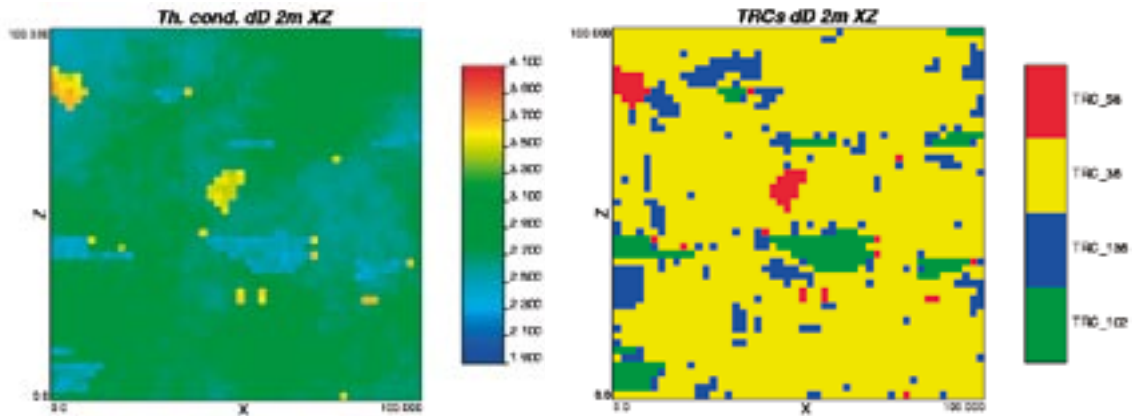


Figure 6-21. An example 2D visualisation of a realisation of thermal conductivity (slices in xz-plane) for domain RSMD01 simulated at the 2 m scale (left) corresponding realisation of lithology (TRC) (right).

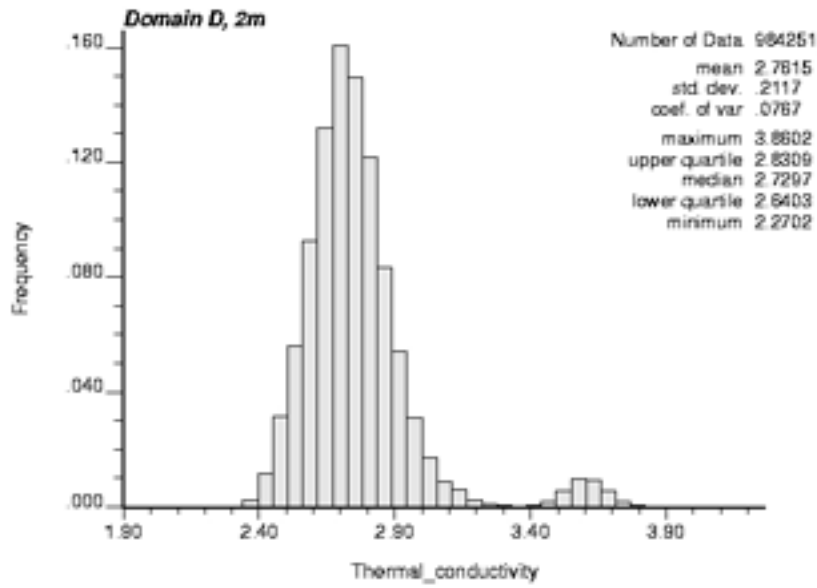


Figure 6-22. Histogram of thermal conductivity for domain RSMD01 simulated at the 2 m scale.

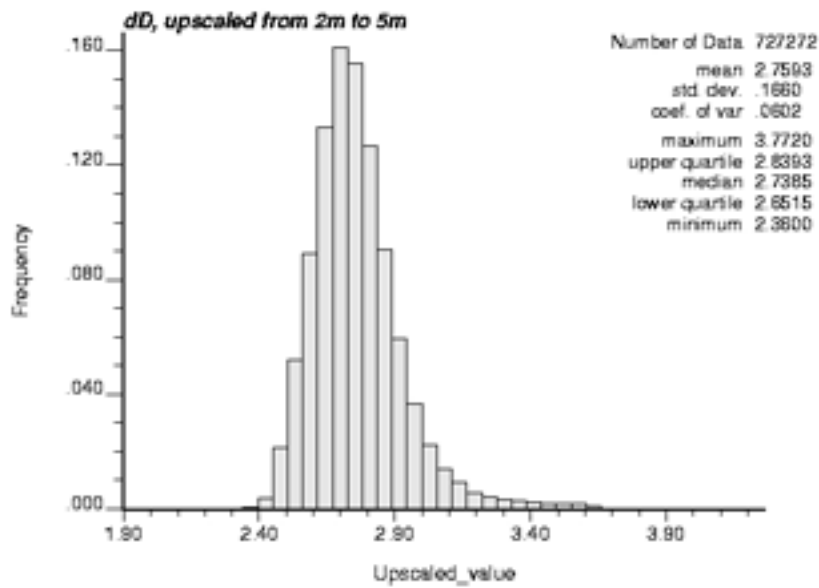


Figure 6-23. Histogram of thermal conductivity for domain RSMD01 simulated at the 2 m scale but upscaled to 5 m.

Table 6-5. Summary statistics for domain RSMD01 based on simulations at the 2 m scale and upscaled to 5 m.

Statistical parameter	2 m	5 m	Unit
Mean	2.761	2.759	W/(m·K)
Variance	0.045	0.028	[W/(m·K)] ²
Standard deviation	0.212	0.166	W/(m·K)
Min	2.270	2.360	W/(m·K)
Max	3.870	3.786	W/(m·K)
0.1-percentile (0.001-quantile)	2.377	2.412	W/(m·K)
1-percentile (0.01-quantile)	2.436	2.475	W/(m·K)
2.5-percentile (0.025-quantile)	2.474	2.504	W/(m·K)

6.3 Heat capacity

The heat capacity has been modelled based on the TRC-distribution in each realisation together with a statistical distribution model for heat capacity for each TRC (Section 5.9).

The resulting distributions of heat capacity at the 2 m scale for domains and thermal subdomains are shown below, together with example visualisation of the distribution of heat capacities. There are no dramatic differences in the mean heat capacity in the different domains. However, domain RSMM01 (Figure 6-27) has a bimodal distribution and domain RSMD01 (Figure 6-32) has an evident lower tail. The different subdomains show larger variations, especially in domain RSMM01 (Figure 6-28–Figure 6-31). The mean and standard deviations are summarised in Table 6-6.

Domain RSMA01

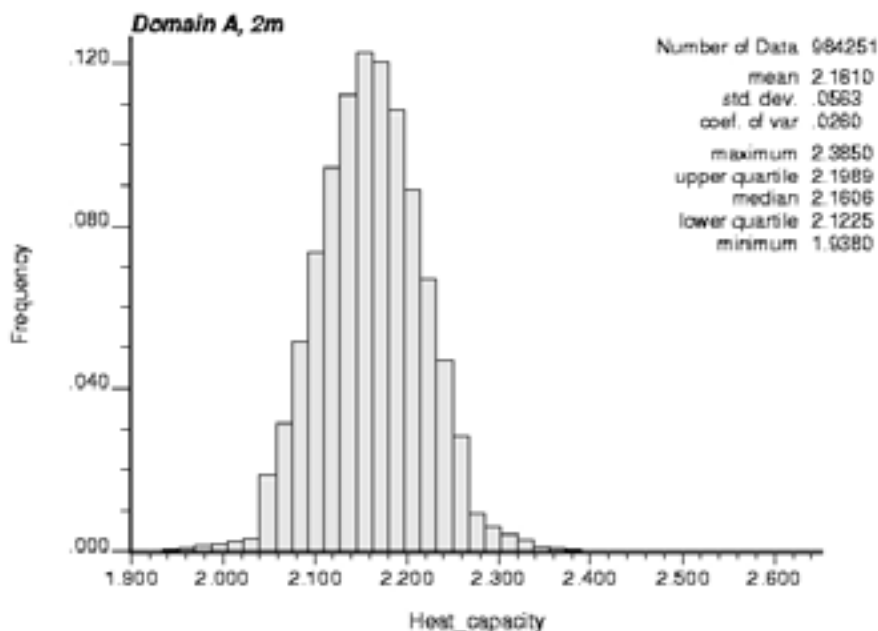


Figure 6-24. The distribution of heat capacities for domain RSMA01.

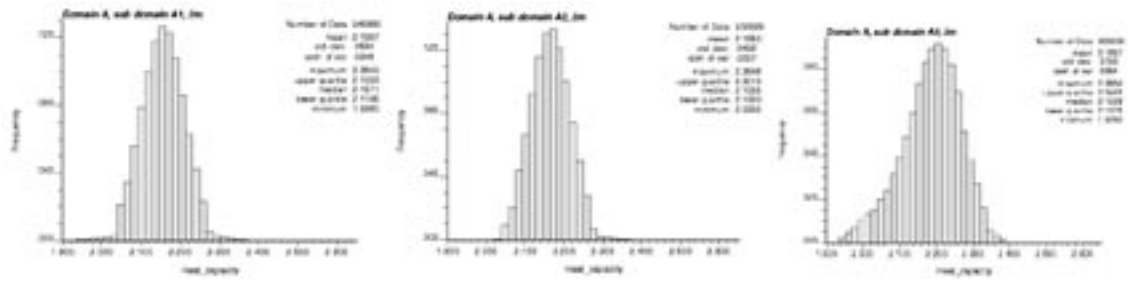


Figure 6-25. The distribution of heat capacities for thermal subdomains in domain RSMA01; A1 (left), A2 (middle), A3 (right).

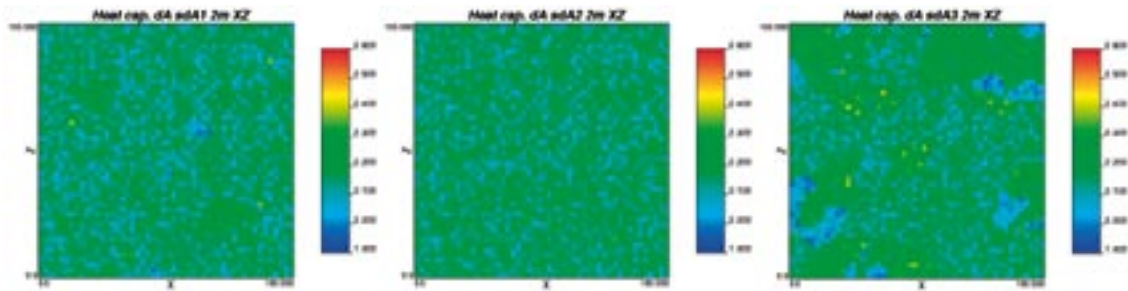


Figure 6-26. Example visualisations of the spatial distribution of heat capacities for thermal subdomains belonging to domain RSMA01; A1 (left), A2 (middle), A3 (right).

Domain RSMM01

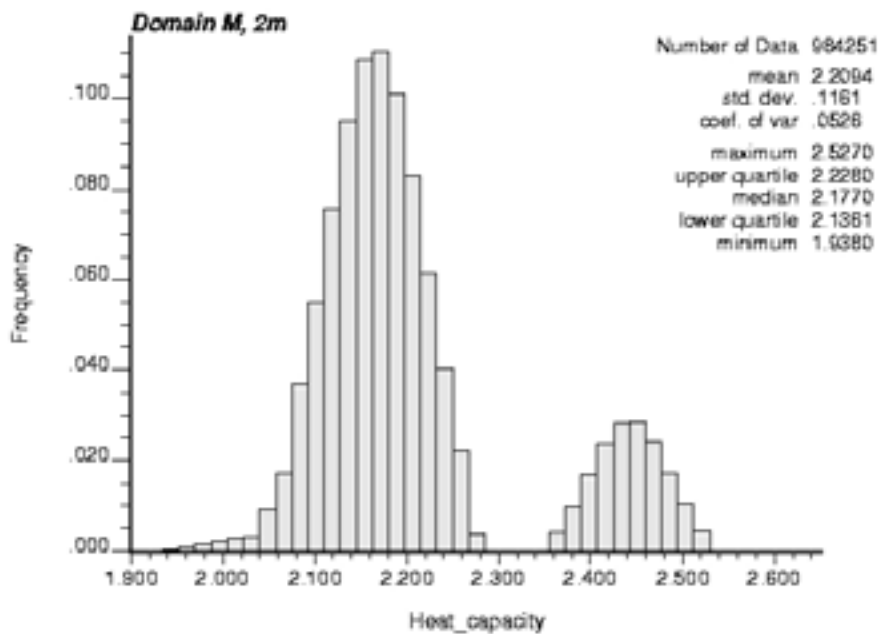


Figure 6-27. The distribution of heat capacities for domain RSMM01.

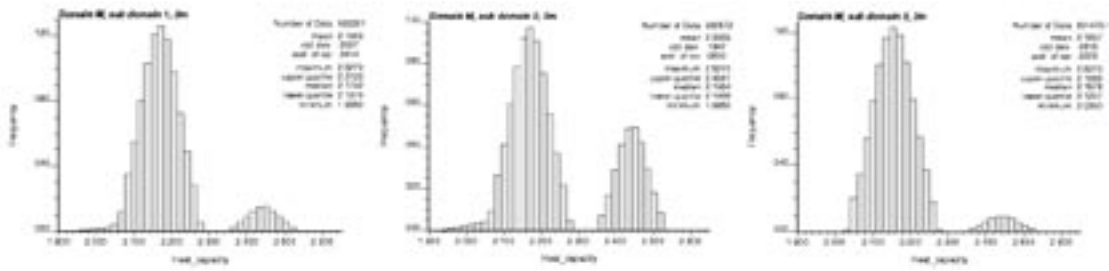


Figure 6-28. The distribution of heat capacities for thermal subdomains to domain RSMM01; M1 (left), M2 (middle), M3 (right).

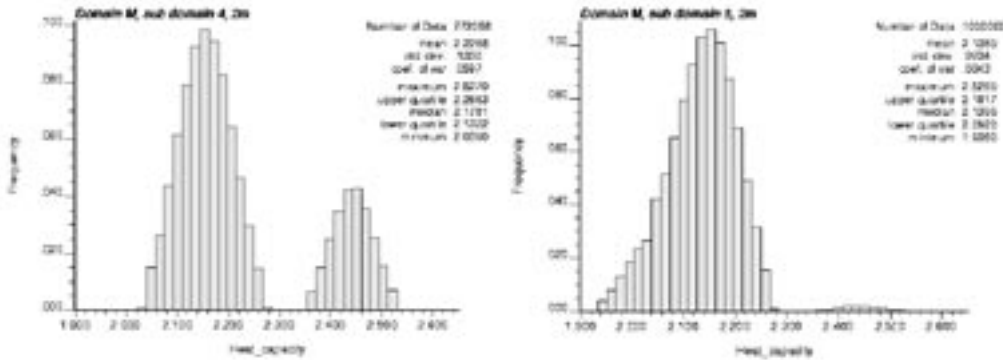


Figure 6-29. The distribution of heat capacities for thermal subdomains to domain RSMM01; M4 (left), M5 (right).

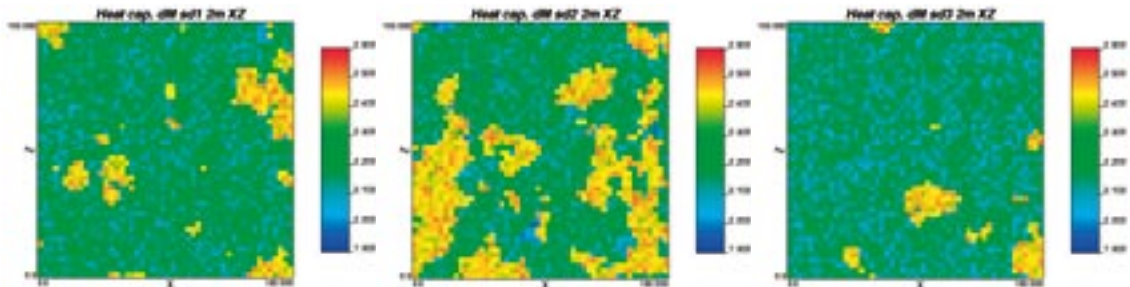


Figure 6-30. Example visualisations of the spatial distribution of heat capacities for thermal subdomains in domain RSMM01; M1 (left), M2 (middle), M3 (right).

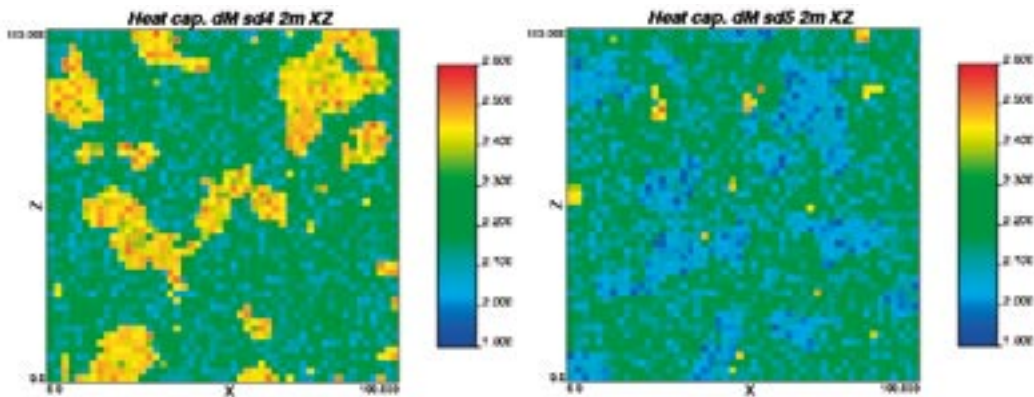


Figure 6-31. Example visualisations of the spatial distribution of heat capacities for thermal subdomains in domain RSMM01; M4 (left), M5 (right).

Domain RSMD01

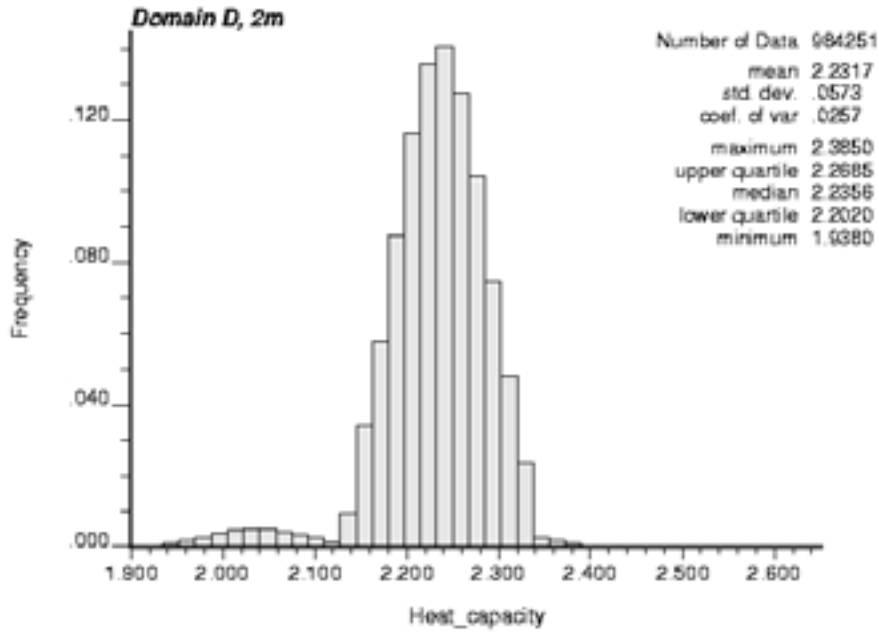


Figure 6-32. The distribution of heat capacities for domain RSMD01.

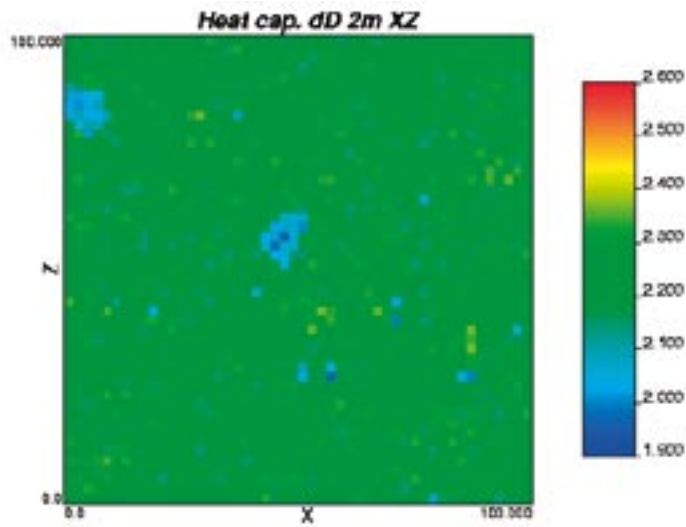


Figure 6-33. Example visualisation of the spatial distribution of heat capacities for domain RSMD01.

Table 6-6. Heat capacity for different domains.

Domain	Mean (MJ/(m ³ ·K))	St. dev (MJ/(m ³ ·K))
RSMA01	2.16	0.06
RSMM01	2.21	0.12
RSMD01	2.23	0.06

6.4 Evaluation of domain modelling results

6.4.1 Rock domain RSMA01

The lower tail of the thermal conductivity distribution for each rock domain is of great importance for the design of a repository. The modelling results were therefore analysed in detail in this respect. The analysis was performed on the 0.1-percentile, 1-percentile and 2.5-percentile of the thermal conductivity distribution for each domain. In addition, a range of scales, from 2 m to 5 m, was analysed. However, the repository design will be based on thermal numerical simulation with the realisations of thermal properties as input, see Section 6.5.1. The lower tail is analysed mainly for understanding and comparative purposes.

The results are presented in Figure 6-34 to Figure 6-36 for the three percentiles, respectively. The plots illustrate how the lower percentiles increase when the scale increases, both for the domain as a whole, as well as for the different thermal subdomains. This is a way of describing how the variance reduction affects the lower percentiles and how sensitive they are to the choice of scale.

Values for larger scales than the simulation scale 2 m are calculated (upscaled) using the Self-Consistent Approximation (SCA) approach; see /Sundberg 1988, Appendix A in Back and Sundberg 2007/. It is evident from Figure 6-34 to Figure 6-36 that the variance reduction when the scale increases is relatively weak. The plateau between 3 and 4 m scale is probably an effect of the discretisation of the simulations into 2 m cells, and the way upscaling is performed. The 2 m discretisation implies that the most of the variance reduction from 2 m to 4 m occurs already at 3 m. In other words, there is a discretisation error that the upscaling is unable to eliminate.

Thermal subdomain A2 has considerably lower thermal conductivity for the low-percentiles compared to the domain as a whole. However, subdomain A2 has a rather minor influence on the low-percentiles of the whole domain since this subdomain A2 is present in low proportions. The proportions of the thermal subdomains A1, A2 and A3 in the whole domain are 74, 18 and 8%, respectively.

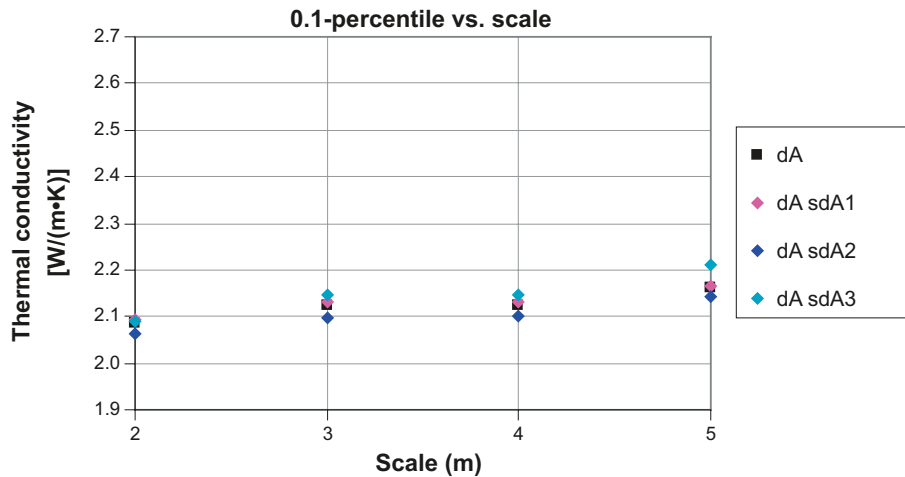


Figure 6-34. The 0.1-percentile (0.001 quantile) versus scale for domain RSMA01 and the corresponding three thermal subdomains. Upscaling was performed on simulated values at the 2 m scale.

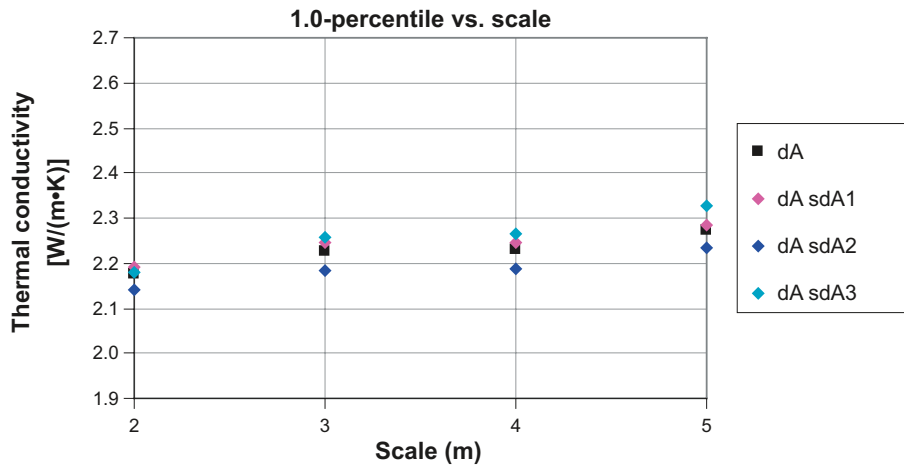


Figure 6-35. The 1-percentile (0.01 quantile) versus scale for domain RSMA01 and the corresponding three thermal subdomains. Upscaling was performed on simulated values at the 2 m scale.

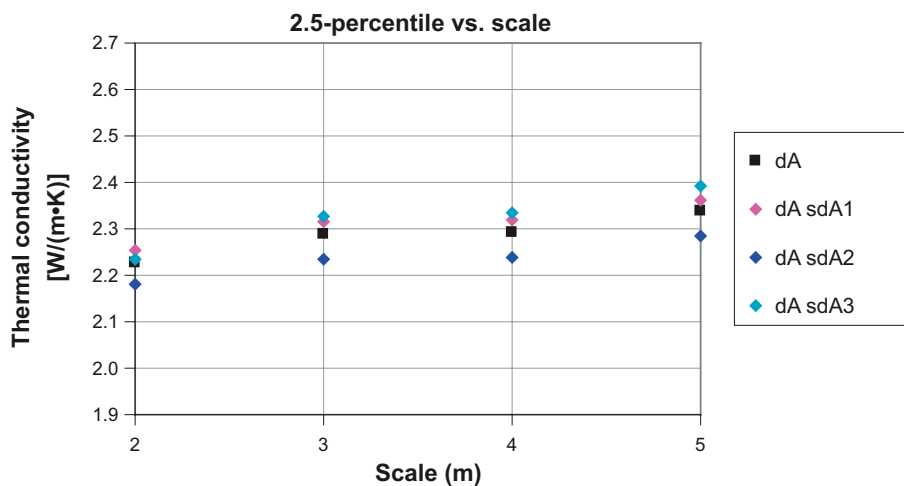


Figure 6-36. The 2.5-percentile (0.025 quantile) versus scale for domain RSMA01 and the corresponding three thermal subdomains. Upscaling was performed on simulated values at the 2 m scale.

6.4.2 Rock domain RSMM01

The lower tail of the thermal conductivity distribution were analysed in detail in the same way as for Domain RSMA01. The results are presented in Figure 6-37 to Figure 6-39 for the three percentiles, respectively. The plots illustrate how the lower percentiles increase when the scale increases, both in the domain and the different thermal subdomains.

Values for larger scales than the simulation scale 2 m are calculated (upscaled) using the Self-Consistent Approximation (SCA) approach. In Figure 6-34 to Figure 6-36 it is shown that there are quite large differences between the different subdomains. Subdomains 3 to 5 have much larger variance reduction compared to subdomain 1 and 2. However, these more high-conductive parts have only a minor influence on the different percentiles for the whole domain since they are present in low proportions. The proportions of the thermal subdomains M1, M2, M3, M4 and M5 in the whole domain are 38, 35, 11, 10 and 5%, respectively.

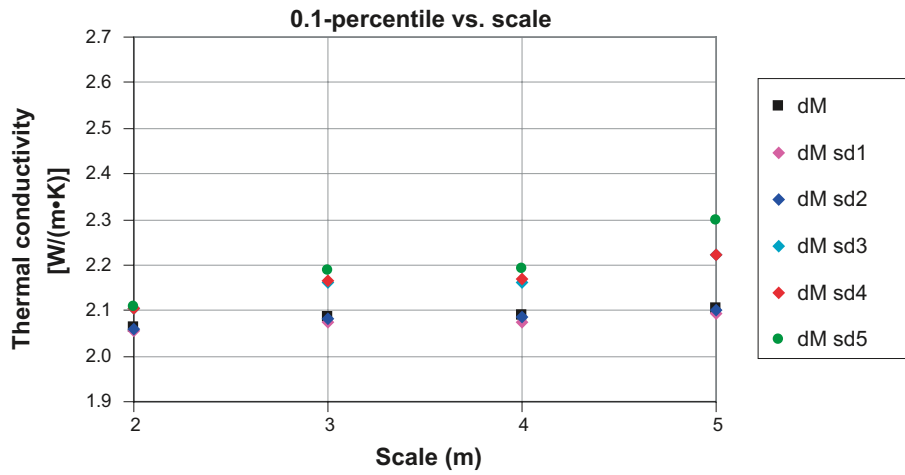


Figure 6-37. The 0.1-percentile (0.001 quantile) versus scale for domain RSMM01 and the corresponding five thermal subdomains. Upscaling was performed on simulated values at the 2 m scale.

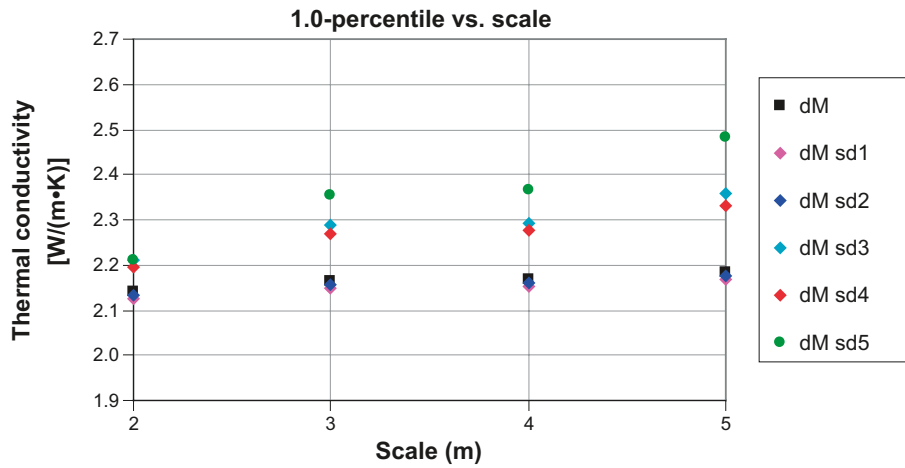


Figure 6-38. The 1-percentile (0.01 quantile) versus the scale for domain RSMM01 and the corresponding five thermal subdomains. Upscaling was performed on simulated values at the 2 m scale.

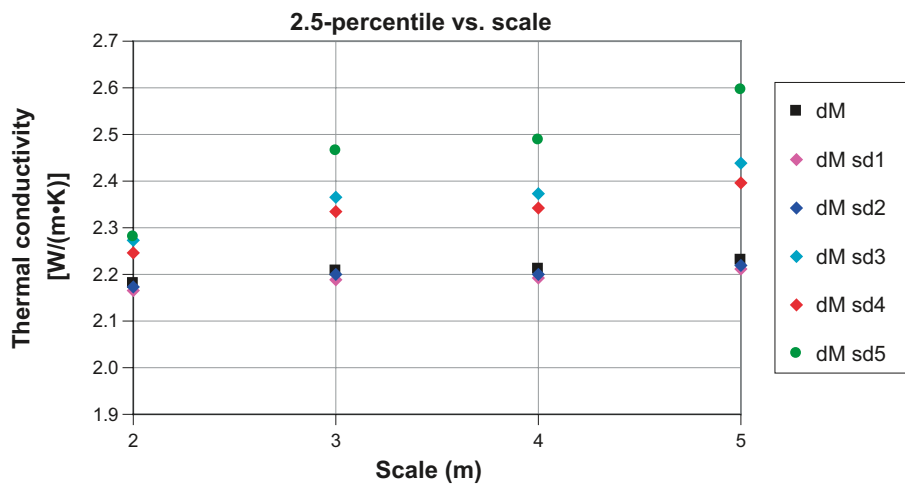


Figure 6-39. The 2.5-percentile (0.025 quantile) versus scale for domain RSMM01 and the corresponding five thermal subdomains. Upscaling was performed on simulated values at the 2 m scale.

6.4.3 Rock domain RSMD01

The lower tail of the thermal conductivity distribution was analysed in the same way as for the previously described domains. The results are presented in Figure 6-40 to Figure 6-42 for the three percentiles, respectively. The plots illustrate how the lower percentiles increase when the scale increases. It is evident from Figure 6-40 to Figure 6-42 that the effect of upscaling is very small.

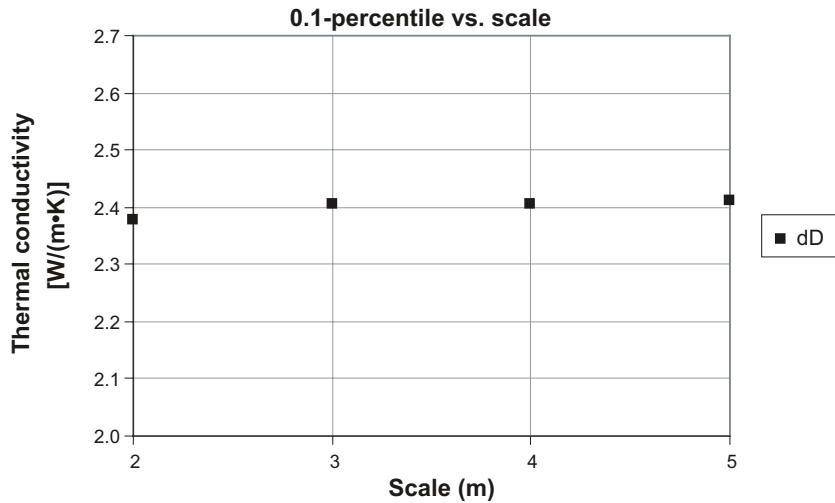


Figure 6-40. The 0.1-percentile (0.001 quantile) versus scale for domain RSMD01. Upscaling was performed on simulated values at the 2 m scale.

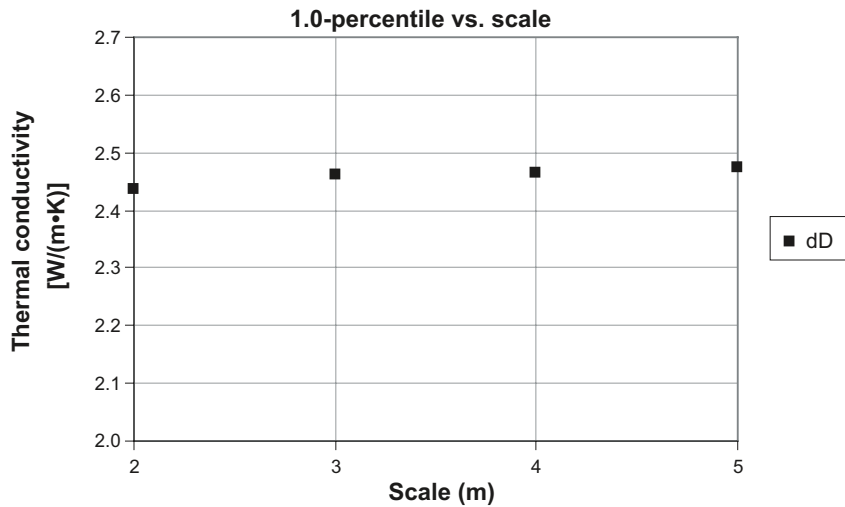


Figure 6-41. The 1-percentile (0.01 quantile) versus scale for domain RSMD01. Upscaling was performed on simulated values at the 2 m scale.

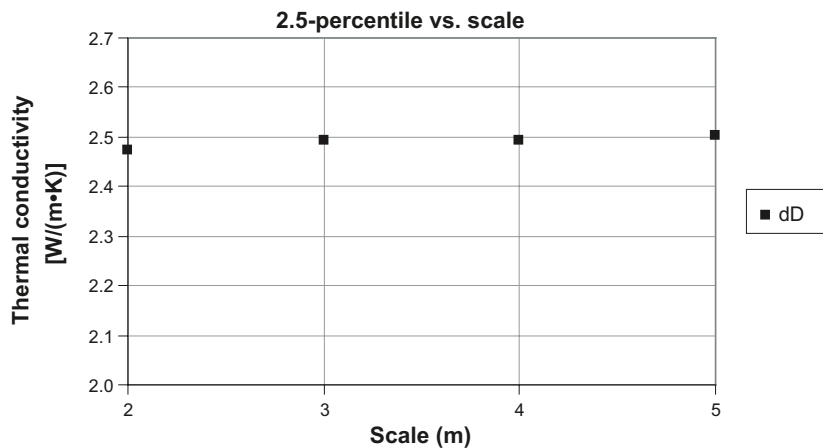


Figure 6-42. The 2.5-percentile (0.025 quantile) versus scale for domain RSMD01. Upscaling was performed on simulated values at the 2 m scale.

6.4.4 Anisotropy due to subordinate rock bodies

Domain RSMD01 is the only domain in Laxemar that has been modelled with anisotropy in the geological simulations. In Forsmark, stage 2.2 /Back et al. 2007/ the anisotropy due to subordinate rock types was analysed. The effect was found to be small for the thermal conductivity in different directions. There are good reasons to expect that the anisotropy effect is even smaller at Laxemar depending on the inferred smaller geological anisotropy. For this reason, no further analysis of effects of anisotropy has been made in the current analysis for Laxemar.

6.4.5 Impact of rock type (TRC) proportions on lower tail percentiles

Because of the high degree of lithological heterogeneity present, particularly high in domain RSMM01, the estimated TRC proportions may deviate somewhat from the true proportions. Based on confidence intervals for TRC proportions at borehole scale (see Section 5.5.5), this uncertainty is estimated to have only a minor effect on the lower thermal conductivity tail. For domain RSMA01, the 1 percentile for the 2 m scale may be up to 0.02 W/(m·K) lower than the best estimate of 2.17 W/(m·K). This applies to the case where TRC 46 (Ävrö quartz monzodiorite) makes up 40% of the domain which is the estimated upper 95% confidence limit for this TRC, and can be compared to the best estimate of 27%. For domains RSMD01 and RSMM01, the corresponding uncertainty is less than 0.01 W/(m·K). In other words, as a result of uncertainties in rock type (TRC) proportions, the 1 percentile may be up to 0.01 W/(m·K) lower than predicted by the thermal model.

6.5 Summary of domain thermal properties

6.5.1 Introduction

The main result of the thermal modelling is a set of realisations describing the spatial distribution of thermal properties in the 2 m scale for each of the three rock domains, namely RSMA01, RSMM01 and RSMD01. There are 1,000 realisations made for each domain with 125,000 cells in each realisation. Each cell in the realisation contains information about thermal conductivity, heat capacity and the TRC code. From the histograms of simulated thermal conductivity values representing the rock mass within a domain, the lower percentiles of thermal conductivity have been determined, as these are of special interest for design of a repository. The scale dependence of thermal conductivity has also been evaluated. In future design work, the realisations (illustrated in Section 6.2) can be used, most importantly as input for numerical temperature simulations for design of repository layout (e.g. distances between deposition holes). The strategy for thermal dimensioning is described in /Hökmark et al. 2009/.

6.5.2 Thermal conductivity

The thermal conductivity at domain level is summarised in Table 6-7 to Table 6-9 for rock domains RSMA01, RSMM01 and RSMD01, respectively. Domain RSMA01 has the highest mean thermal conductivity, RSMM01 the lowest. In spite of the clear difference in mean thermal conductivity between domains RSMA01 and RSMM01, the low percentiles are rather similar for these two domains, both having 1-percentiles less than 2.2 W/(m·K). This is largely an effect of the presence of low-conductive Åvrö quartz monzodiorite in both domains. However, the difference increases on upscaling to 5 m. The lithologically more homogeneous domain RSMD01 shows less variation in thermal conductivity and has low-percentiles that are significantly higher compared to the other two domains. Domain RSMM01 is the most heterogeneous domain.

The values above are valid at 20°C. With increasing temperature the thermal conductivity of the dominant granitoid rock decreases by about 10 %/100°C temperature increase, calculated as the mean value.

The thermal conductivity distributions in each domain are schematically represented in a N-S cross-section through the Laxemar local model volume (Figure 6-43). Although the variations in thermal conductivity within each domain are not to scale, the fundamental differences between the domains are clearly illustrated.

Table 6-7. Thermal conductivity of domain RSMA01 based on simulations at the 2 m scale.

Statistical parameter	2 m scale, W/(m·K)	5 m scale, W/(m·K)
Mean	2.94	2.93
Standard deviation	0.373	0.286
0.1-percentile	2.09	2.16
1-percentile	2.17	2.27
2.5-percentile	2.23	2.34

Table 6-8. Thermal conductivity of domain RSMM01 based on simulations at the 2 m scale.

Statistical parameter	2 m scale, W/(m·K)	5 m scale, W/(m·K)
Mean	2.66	2.65
Standard deviation	0.394	0.317
0.1-percentile	2.06	2.11
1-percentile	2.14	2.19
2.5-percentile	2.18	2.23

Table 6-9. Thermal conductivity of domain RSMD01 based on simulations at the 2 m scale.

Statistical parameter	2 m scale, W/(m·K)	5 m scale, W/(m·K)
Mean	2.76	2.76
Standard deviation	0.212	0.166
0.1-percentile	2.38	2.41
1-percentile	2.44	2.48
2.5-percentile	2.47	2.50

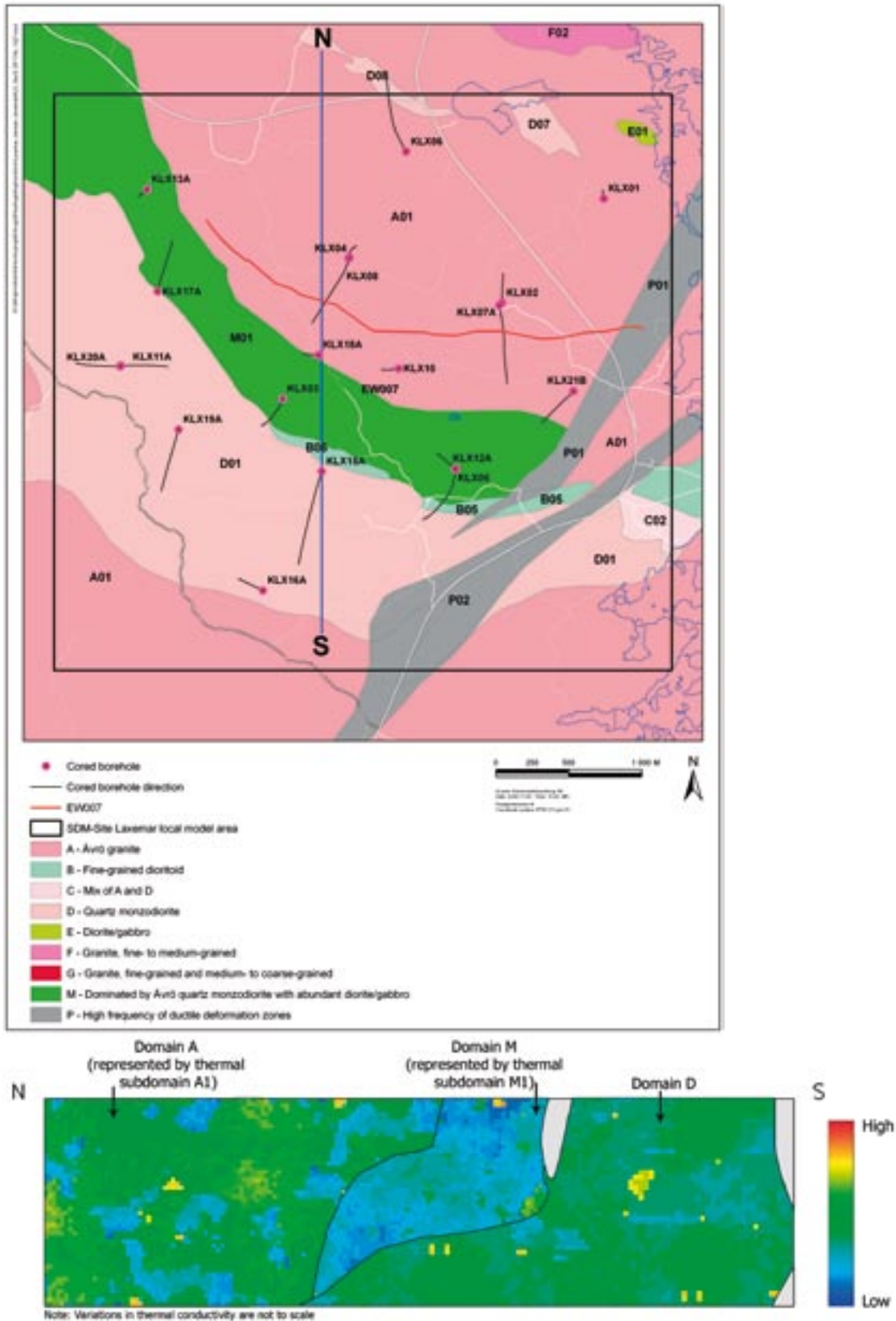


Figure 6-43. Schematic representation of the thermal conductivity distribution in rock domains RSMA01, RSMM01 and RSMD01. The figure represents a N-S oriented vertical cross-section (as indicated on the map) through the Laxemar local model volume. The vertical extension is 2 km. The spatial variability of thermal conductivity represents the 2 m scale.

The above results for the different domains can be compared with previously reported results. In Table 6-10, results presented in version 1.2 /Sundberg et al. 2006/ and version 2.1 /Wrafter et al. 2006/ are compared with the results of the latest modelling work. The mean thermal conductivities are generally higher in the site version, but estimates of the 2.5 percentiles are lower for domain RSMA01 and RSMM01, despite the larger scale in the current site version. It should be noted, however, that the results presented here are not directly comparable with those of previous model versions, because:

- the domain boundaries have been redefined since modelling stage 2.1 /Wahlgren et al. 2008/,
- in the current thermal model only the southern and western parts of domain RSMA01 within the local model volume are described, not the entire domain as was the case in previous versions /Sundberg et al. 2006, Wrafter et al. 2006/.

Between model stages 1.2 and 2.1, investigations of thermal properties as part of the Focusing Laxemar work /SKB 2005/ resulted in a simplified thermal model, comprising four thermal domains which deviated somewhat from the rock domains defined in the geological model version 1.2 /SKB 2006b/. However, three of these thermal domains correspond quite closely to the rock domains of the revised 2.2 geological model (version Site) /Wahlgren et al. 2008/ on which the present study is based. Table 6-11 compares the mean thermal conductivities for each thermal domain estimated as part of the Focusing Laxemar study with the results of the present study. The results are rather similar.

Table 6-10. Comparison of modelling results for thermal conductivity (W/(m·K)) with previous model version/stage.

Domain	Mean W/(m·K)			St. dev. W/(m·K)			2.5% percentile W/(m·K)		
	1.2	2.1	SDM-Site	1.2	2.1	SDM-Site	1.2	2.1	SDM-Site
Model version/ stage	1.2	2.1	SDM-Site	1.2	2.1	SDM-Site	1.2	2.1	SDM-Site
Scale, m	0.8	0.8	2	0.8	0.8	2	0.8	0.8	2
Domain RSMA01	2.82	2.75	2.94	0.29	0.36	0.37	2.32	< 2.22	2.23
Domain RSMM01	2.58 ¹	2.56 ¹	2.66			0.39	2.3 ¹		2.18
Domain RSMD01	2.70	2.77	2.76	0.17	0.28	0.21	2.44	< 2.41	2.47

¹ Estimations based on simulations in 0.1 m scale

Table 6-11. Comparison of modelling results for thermal conductivity (W/(m·K)) in this study and Focusing Laxemar investigations /SKB 2005/.

Focusing Laxemar		Site	
Thermal domain	Mean W/(m·K)	Rock domain	Mean W/(m·K)
	Scale 0.8 m		2 m
TA1	2.93	Domain RSMA01	2.94
TA3	2.58	Domain RSMM01	2.66
TD	2.74	Domain RSMD01	2.76

6.5.3 Thermal anisotropy

Based on field measurements, the mean thermal conductivity anisotropy factor due to foliation is estimated to be 1.15. The orientation of the foliation, as well as its degree of development, varies throughout the Laxemar area which implies that the orientation and magnitude of anisotropy of thermal conductivity will also vary accordingly.

6.5.4 Heat capacity

The results for different domains are summarised in Table 6-12.

6.5.5 Temperature dependence in thermal properties

With increasing temperature the thermal conductivity of the main rock types decreases by 0–7% /100°C temperature increase. The heat capacity increases by approximately 25% /100°C temperature increase (see Table 3-31).

6.5.6 Thermal expansion coefficient

The mean measured coefficient of thermal expansion for five different rock types varies between $6.9 \cdot 10^{-6}$ and $7.4 \cdot 10^{-6}$ m/(m·K).

6.5.7 *In situ* temperature

The mean *in situ* temperatures measured at –400 m, –500 m and –600 m elevation, based on 4–5 boreholes, are estimated at 13.3°C, 14.8°C, and 16.3°C, respectively. The uncertainties reported in earlier model version/stages regarding the quality of *in situ* temperature measurements have now been identified. The mean values reported here are based on borehole loggings that are considered to be reliable.

Table 6-12 Heat capacity for different domains.

Domain	Mean (MJ/(m ³ ·K))	Std (MJ/(m ³ ·K))
RSMA01	2.16	0.06
RSMM01	2.21	0.12
RSMD01	2.23	0.06

7 Evaluation of uncertainties

7.1 Data uncertainty

The main data uncertainties are described below.

7.1.1 Thermal conductivity and heat capacity

Assuming the samples are isotropic, the TPS measurements are considered to be quite reliable, especially the thermal conductivity. The measurement of thermal conductivity and thermal diffusivity take different volumes into account. This has no influence on the results when the samples are isotropic. However, if the samples have anisotropic thermal behaviour, which to some degree is the case in the Laxemar area, there may be impact on the results. The largest error is assumed to be in the determination of thermal diffusivity. This has an impact on the determined heat capacity calculated from the thermal conductivity and diffusivity from the TPS measurements. However, the heat capacity has also been determined directly by a calorimetric method and these measurements are considered to be more reliable. The uncertainty in thermal conductivity associated with SCA data is significantly larger than for TPS data.

Uncertainties are also associated with the determined anisotropic thermal conductivity of the Ävrö granodiorite and Ävrö quartz monzodiorite. The anisotropy factor is uncertain due to the field measurement procedure with vertical boreholes, uncertain strike, a dipping foliation plane, the possible presence of a lineation in combination with few determinations (see Section 3.8). Uncertainties in the strike and dip of foliation in relation to the experimental configuration results in a potential underestimation of the anisotropy factor. However, after correction for the effect of dipping foliation plane the mean value is judged to be quite reliable. The spatial variability of the thermal anisotropy factor is particularly uncertain.

7.1.2 Thermal expansion coefficient

Given the small number of sample locations, the representativeness of samples selected for thermal expansion measurements can be questioned. However the variability both within and between different rock types are low.

7.1.3 Temperature

In earlier model versions, the temperature loggings were associated with rather large uncertainties. In the current model version, the reliability of temperature loggings has been evaluated in relation to calibration errors and disturbances from drilling. As a result of this evaluation, only “approved” boreholes have been used in the description. Although there are only a small number of reliable boreholes, the uncertainties are much smaller than in earlier model versions. The reliability of the estimated mean temperatures is strengthened by the temperature data from the Posiva flow logging in the same boreholes.

7.1.4 Boremap data

The uncertainties in the orientation of the boreholes and in the orientation of geological objects in the boreholes, documented by /Munier and Stigsson 2007/, are judged to have little or no effect on the results of the thermal modelling.

Fine-grained diorite-gabbro (505102), which occurs as dyke-like bodies throughout Laxemar, is commonly mixed with fine-grained granite, the latter making up between 5 and 50% of the total. However, in the Boremap data, which is the basis for the lithological simulations, these

occurrences have been recorded as simply fine-grained diorite-gabbro. This means that bodies of fine-grained diorite-gabbro (TRC 102) have in reality a higher thermal conductivity than indicated by the model used here. The impact of this simplification on the thermal modelling results is that the lower tail percentiles of thermal conductivity in domain RSMD01 may be slightly underestimated. The lower tail in domain RSMD01 is determined by TRC 36 (quartz monzodiorite) as well as TRC 102 (which comprises mainly fine-grained diorite-gabbro), so the impact on the lower tail percentiles is unlikely to be large. This could be evaluated by adopting an alternative distribution model for TRC 102 which takes into account the mixed lithological nature of the fine-grained diorite-gabbro. The implication of this simplification in borehole mapping for the thermal results of rock domains RSMA01 and RSMM01 is negligible.

7.2 Model uncertainty

7.2.1 Major model uncertainties

The thermal stochastic modelling primarily concerns thermal conductivity. There are several uncertainties associated with the different steps of this modelling. Here, a description is given of the five uncertainties that are believed to be most important for the results at rock domain level, i.e. uncertainties associated with:

1. the simulation scale,
2. the simulation volume,
3. the spatial statistical structure of TRCs (lithology),
4. the spatial statistical thermal models, and
5. the simulation technique.

Uncertainties 1 and 2 are associated with the representativeness of boreholes and samples, as well as lack of data. Uncertainties 3, 4 and 5 are related to each other and concern the simulation methodology as a whole.

7.2.2 The simulation scale

The effect of using a simulation scale of 2 m to represent subordinate rock types is not fully known. A discretisation error will affect results for domain properties in domains with rock bodies smaller than the simulation scale. However, in domain RSMA01 and RSMM01, TRCs critical to the lower tail of the thermal conductivity distribution are generally present at sizes much larger than the simulation scale. In domain RSMD01, one of the rock types impacting on the low tail of the distribution is fine-grained diorite-gabbro (TRC 102), which occurs as dyke-like bodies, a significant proportion of which have a true thickness less than 2 m. Thus, the discretisation error produces too many rock bodies of size 2 m (or larger) which in turn gives a slightly conservative estimate of the lower percentiles for rock domain RSMD01. However, the effect of discretisation diminishes rapidly on upscaling, and have more or less disappeared in the results presented for the 5 m scale.

7.2.3 The simulation volume

Theoretically, the limited simulation volumes affect the simulation results but the effect decreases when the simulation volume increases. In the Forsmark site descriptive model, the simulation volumes were $50 \times 50 \times 50 \text{ m}^3$ /Back et al. 2007/. In this description for Laxemar the simulation volume has been increased to $100 \times 100 \times 100 \text{ m}^3$. There are three reasons for this; larger bodies of subordinate rock types occur in Laxemar, long correlation lengths have been observed for some TRCs, and the need for repository design to have thermal realisations representing a larger volume.

There are two situations when the limited volume could be a problem for the objective of describing a rock domain statistically:

1. When the lithological simulation volume is so small that the true properties of this limited rock volume deviate from the true domain or subdomain statistics. This is only a problem if upscaling to large blocks is performed, which is not the case in the model presented here. The limited simulation volumes also seem to be related to difficulties in fully reproducing anisotropy of subordinate rock bodies, as described by the model parameters, in the lithological simulations. This is exemplified by the underestimation of anisotropy of TRC102 in domain RSMD01.
2. When the correlation lengths of thermal properties are similar to or longer than the length of the simulation volume. The latter may result in the thermal conductivity simulations being unable to reproduce the spatial variability seen in data (experience indicates that variograms are difficult to reproduce when simulation volumes are small /Dowd 2007/).

For simulations at the 2 m scale, the first type of uncertainty is believed to be of minor importance. The second type of uncertainty is believed to be important mainly for domain RSMD01. Quartz monzodiorite (TRC 36), the main rock type in this domain, displays correlation lengths that are long in relation to the simulation volume. However, this is not believed to be critical for the simulation results.

There is an additional important uncertainty related to the simulation volume and associated with stochastic simulation in general. Histograms of data and the corresponding statistical distribution models represent a rock domain as a whole. However, simulations are performed using a much smaller simulation volume (100 m cube) than the total volume of the rock domain. Some of the rock types exhibit a small but noticeable trend in the thermal conductivity values within the rock domain. This implies that a slightly smaller variance is expected within a real 100 m cube of rock compared to the entire rock domain. The performed simulations however, assume stationarity and do not recognise different statistics in different parts of the rock domain. Instead, the total variance of the domain is assumed to be found in every simulated 100 m cube. Thus, the assumption of stationarity is associated with uncertainty at the scale of the simulated cube, but has little impact on the descriptive statistics at domain level, which is the focus of this report.

It can be concluded that although there are uncertainties associated with the simulation volume, none of these are believed to have had any major impact on the thermal modelling results. However, care must be taken if the produced realisations are used for purposes other than statistical description of a rock domain.

7.2.4 The spatial statistical structure of TRCs (lithology)

The models used for the lithological simulations are largely based on “best estimates” of uncertain parameters. There are several uncertainties associated with the developed models of the proportions and the spatial statistical structure of the TRCs (lithology). Most of these are coupled to the lack of knowledge concerning detailed geological information, such as typical lengths of rock bodies, the true shape and orientation of rock bodies, trends in the statistics of the lithology within the rock domain etc. These uncertainties could in principle be evaluated by including different sets of soft data (expert opinion) and studying the variation in output. However, no such structured analysis has been performed. Instead, “best estimates” have been determined in cooperation with the geologists. Thus, potential bias in the expert knowledge is transferred to the simulations of the lithology. This uncertainty may be significant for the lower tail of the thermal conductivity distribution in domain RSMD01 where one of the critical rock types is fine-grained diorite-gabbro (included in TRC 102). Because this rock type is present as relatively small bodies, its true size distribution and anisotropy is particularly important.

There are also uncertainties linked to the degree to which geological inhomogeneity has been reproduced in the lithological simulations. In the simulation volume, the proportions of TRCs

are held constant in each realisation. In reality, the proportions are variable at the scale of the simulation volume due to lithological heterogeneity. Geological heterogeneities within the domains RSMM01 and RSMA01 were dealt with by dividing the domains into subdomains, according to the strategy outlined in /Back and Sundberg 2007/. This is believed to have reduced the uncertainty significantly.

Uncertainties concerning the true proportions of TRCs in the rock domains produce uncertainties in the lower tail of the thermal conductivity distribution at rock domain level (Section 6.4.5). As a result of these uncertainties, the 1 percentile for the 2 m scale may be up to 0.02 W/(m·K) lower than predicted by the thermal model. This uncertainty is highest for domain RSMA01.

Due to the uncertainties in the TRC proportions, the uncertainties in the overall distribution (the main body of the distribution, tails excluded) of thermal conductivity are likely to be larger than in the lower tails of these distributions. This type of uncertainty is least for the lithologically homogenous RSMD01 domain and largest for the lithologically heterogeneous RSMA01 and RSMM01 domains.

Finally the estimated proportions of the different subdomains in a rock domain have rather large uncertainties as they are primarily based on the assumption that existing boreholes are representative. It should also be observed that the thermal subdomains are not geometrically bounded. If this could be achieved, it would allow more optimal canister spacing in the different subdomains.

7.2.5 The spatial statistical thermal models

Limited data for some TRCs result in uncertain spatial statistical thermal models. When data are few and show large variability, the shape of a statistical distribution cannot only be based on hard data. The distribution models are particularly uncertain regarding the tails of the distributions. Moreover, the lower limit of thermal conductivity for a TRC is usually not known and must be determined based on expert opinion. Therefore, the uncertainties in the shapes of the lower tails of the distribution models are translated into uncertainties in the estimates of low percentiles for the domains. This is only of importance for the TRCs with low thermal conductivities, in particular TRC 33A, 33B and 46.

The variograms require even more data than the distribution models. It has been assumed that thermal conductivity exhibits a similar correlation structure as density. This is a reasonable assumption that allows the construction of variograms, but the associated uncertainty is not known, at least not for all TRCs. Moreover, it is not clear whether the spatial correlation models used are applicable to the whole thermal conductivity distribution for a TRC. However, there are reasons to believe that these uncertainties have only a minor effect on the domain results. Although the correlation structure influences the simulation results after upscaling, the absolute values of thermal conductivity are more important for the tails of the distributions. Potentially, the impact of uncertainties in the variogram models on the domain results is largest for TRC 102. This is due to the low thermal conductivity in combination with a short range. If the range was longer, a lower reduction in variance with upscaling would result, thus giving more lower thermal conductivity values in the tail of the domain distribution.

The above uncertainties could be handled by performing simulations using alternative distribution and spatial correlation models for the critical TRCs. Due to the time-consuming nature of the simulations, this has not been feasible. Another way of tackling these uncertainties would be to divide rock types into subpopulations, e.g. by separating data from different boreholes, and to model each subtype separately. However, this would require much more data than currently exist.

An assessment of the spatial statistical thermal models for the dominant TRCs (TRC 46, 56 and 36) indicates that they are based on rather plentiful data and, if anything, err on the conservative side. TRC 46 is critical to the lower tails of the distributions for domains RSMA01 and RSMM01 whereas TRC 36 is important for domain RSMD01. The spatial statistical models of

thermal conductivity for diorite-gabbro (TRC 33 – both 33A and 33B), which also contributes to the lower tail of the distribution in domain RSMM01, are less certain because of the smaller amount of data and larger heterogeneity in thermal properties. However, the volumetric importance of TRC 46 in domain RSMM01 means that uncertainties in the lower tail related to TRC 33 are not as important as they would otherwise have been.

In spite of the uncertainties, the spatial statistical thermal conductivity models are believed to be more reliable than in previous versions of the thermal site descriptive modelling. They do not rely on any particular statistical distribution and the correlation structure is explicitly included in the model, which was not the case in previous model versions.

7.2.6 The simulation technique

The simulation technique is a source of uncertainty. This uncertainty is closely related to the simulation scale and the simulation volume. The advantage of this uncertainty compared to the others is that it can easily be identified. The principle is simple: The result of a simulation is compared against the input models. Deviations indicate that there is uncertainty. This type of verification was performed both for the lithological and the thermal simulations. The conclusion is that the output of the thermal simulations resembles the input very well but for the lithological simulations there is not an exact match; for example as regards the length distribution of rock types. The reasons for this are the restricted simulation volumes (see above) and the simulation algorithms. This uncertainty is believed to have only a minor influence on the results.

7.3 Summary of uncertainties

Small uncertainties in the lower tail of the thermal conductivity distributions will have a significant impact on canister spacing in layout D2. For this reason, the uncertainties in the thermal model listed in this chapter focus on the lower tail of the thermal conductivity distribution.

As regards the overall distribution (the main body of the distribution, tails excluded) of thermal conductivities for each rock domain, the highest confidence is placed in the results for rock domain RSMD01, because of its higher degree of homogeneity in geology and thermal properties compared to rock domains RSMM01 and RSMA01. The rather large uncertainties associated with the output of the geological simulations for rock domains RSMM01 and RSMA01, in particular the proportions of rock types and proportions of thermal subdomains, imply that the overall statistical distribution of thermal conductivity is also uncertain for these domains. This is the aspect of the thermal model with the lowest confidence. This uncertainty is intimately related to the heterogeneity in the geology present in domain RSMA01 and, in particular, domain RSMM01.

Confidence in the lower tails of the thermal conductivity distributions is generally high, although slightly higher for rock domains RSMA01 and RSMM01 than for rock domain RSMD01. The uncertainties that do exist are primarily associated with uncertainties in the spatial statistical thermal models (distribution models and spatial correlation models) for the critical TRCs. In contrast, the lower tails of the thermal conductivity distributions are not very sensitive to uncertainties in the rock type proportions and the spatial statistical structure of lithology (TRCs), as was discussed in Section 7.2.4, although some impact on rock domain RSMD01 can be suspected.

More specifically, the lower tail for domain RSMD01 has been evaluated with respect to how the fine-grained diorite-gabbro is modelled. Fine-grained diorite-gabbro (TRC 102) is the rock type in domain RSMD01 having the lowest thermal conductivities (data as low as 2.25 W/(m·K)) but its impact on the tail of the thermal conductivity distribution at 5 m scale is limited for the following reasons. Firstly, upscaling from measurement scale to 2 and 5 m scales leads to a rapid evening out of the spatial variability in thermal conductivity; most of the variance present

at measurement scale (cm-dm) is eliminated at the 2 m scale (see Table 5-38). Secondly, both the realisations and the borehole data indicate that fine grained diorite-gabbro occurs as relatively small rock bodies, the majority having a thickness of less than 4 m. Thus at larger scales their impact is reduced. Thirdly, the lower tail is also defined by quartz monzodiorite (TRC 36), the dominant rock type in domain RSMD01. In contrast to fine-grained diorite-gabbro, upscaling within quartz monzodiorite produces only a small reduction in spatial variability (see Table 5-38) due to its longer spatial correlation. In conclusion, uncertainties regarding the spatial statistical models (both lithology and thermal) of TRC 102, have a rather limited impact on the lower tail of the thermal conductivity distributions in domain RSMD01.

Furthermore, as pointed on in Section 7.1.4, fine-grained diorite-gabbro (505102) commonly occurs with fine-grained granite (511058) as composite intrusions, the latter making up between 5 and 50% of the total. This implies that in reality the thermal conductivity of bodies mapped as fine-grained diorite-gabbro (TRC 102) is higher than indicated by the model used in the thermal modelling, which in turn implies that the thermal conductivity modelling results for domain RSMD01, in particular the low percentiles, can be considered to be slightly underestimated.

Overall confidence in the thermal model is reinforced by the mutual consistency between understanding as expressed by the geology and the thermal properties descriptions.

8 Conclusions

The performed modelling has provided valuable insight into the thermal properties at Laxemar. The presented models are judged to represent the modelled rock domains and their variability in a proper way. The modelling results are more realistic and reliable than previous model versions and uncertainties are easier to identify.

Because the lower tail of the thermal conductivity distribution is of central importance to the decision of canister spacing in layout D2, a lot of effort has been placed on estimating the low percentiles of thermal conductivity at different scales.

The main conclusions of the thermal modelling are:

- The thermal model SDM-site for Laxemar provides a spatial statistical description of the rock mass thermal conductivity and its uncertainties for the needs of repository design and safety assessment.
- The methodology employed for thermal modelling, involving stochastic simulation of both lithologies and thermal conductivity, takes into account the spatial variability of thermal conductivity both within and between different rock types.
- The thermal properties of three rock domains, RSMA01, RSMM0101 and RSMD01 have been successfully modelled. The main output result of the modelling is a set of realisations generated by stochastic simulation that can be used for various purposes, e.g. statistical analysis and numerical temperature simulations. However, the presented approach provides almost unlimited possibilities for different types of analyses and evaluations of the domain results. Only the most straight-forward analyses have been presented in this report. For example, the low percentiles of thermal conductivity were estimated and the impact of scale was determined.
- Rock domain RSMA01 has the highest mean thermal conductivity of the modelled rock domains. However, the lower tail percentiles of thermal conductivity at 2 m scale for domain RSMA01 are significantly lower than for domain RSMD01 and only slightly higher than those for domain RSMM01, the latter rock domain showing the lowest mean thermal conductivity. The reason for the low 0.1, 1 and 2.5 percentiles of thermal conductivity in domain RSMA01 is the presence of significant amounts of the low-conductive Ävrö quartz monzodiorite. The statistics of thermal conductivity at domain level are summarised in Table 6-3, Table 6-4 and Table 6-5 for rock domains RSMA01, RSMM01 and RSMD01, respectively.
- The choice of scale has an influence on the distribution of thermal conductivity values. The variance decreases and the lower tail percentiles increase as the scale of observation increases from 2 to 5 m. The scale dependence is greatest for domain RSMA01 and least for domain RSMD01.
Best estimates of the 0.1 percentile of thermal conductivity are:
 - Domain RSMA01: 2.09 W/(m·K) for the 2 m scale and 2.16 W/(m·K) for the 5 m scale.
 - Domain RSMM01: 2.06 W/(m·K) for the 2 m scale and 2.11 W/(m·K) for the 5 m scale.
 - Domain RSMD01: 2.38 W/(m·K) for the 2 m scale and 2.41 W/(m·K) for the 5 m scale.
 - Corresponding estimates for 1 and 2.5 percentiles are given in Table 6-7, Table 6-8 and Table 6-9.
- Confidence in the lower tails of the thermal conductivity distributions for the modelled rock domains is generally high, although slightly higher for rock domains RSMA01 and RSMM01 than for rock domain RSMD01. The uncertainties that do exist are primarily associated with uncertainties in the spatial statistical thermal models (distribution models and spatial correlation models) for the certain TRCs.

- The aspect of the model with the highest confidence is the overall distribution (the main body of the distribution, tails excluded) of thermal conductivities for domain RSMD01, because of its higher degree of homogeneity in geology and thermal properties. The aspect of the model with the lowest confidence is the overall distribution of thermal conductivities for domain domains RSMA01 and RSMM01, which is related to the higher degree of geological heterogeneity present. However, the lower percentiles of thermal conductivity are not very sensitive to the uncertainties linked to geological heterogeneity for any of the domains.
- The uncertainties in the thermal model SDM-site have been reduced considerably when compared to the results of previous model stages. Some of the most important are:
 - 1) The spatial statistical thermal models for the major thermal rock classes (TRCs) represent a large improvement on previous work. Models of spatial correlation within each TRC (variograms), permits spatial variability to be modelled, something that was not possible with the approach used in previous model versions.
 - 2) In model stage 2.1, there were still considerable uncertainties associated with the thermal models for some of the rock types, in particular diorite-gabbro (501033). Although there are still uncertainties, diorite-gabbro (501033) is now understood to consist of at least two distinct rock types having different thermal properties.
 - 3) The geology of the rock domains, in particular domain RSMM01, is much better understood as a result of more boreholes.
 - 4) In contrast to the previous modelling approach, the upscaling procedure used in the present approach is theoretically robust.
 - 5) Knowledge of the impact of alteration on thermal conductivity has improved by measurements of thermal properties on altered rock.
 - 6) Poor precision in heat capacity determinations from thermal conductivity and diffusivity measurements was recognised during model stage 2.1 and has been rectified by carrying out direct measurements.
- The use of density borehole logging data to subdivide borehole sections mapped as Ävrö granite into its subtypes, Ävrö quartz monzodiorite and Ävrö granodiorite, proved to be a very effective method for distinguishing between two distinct rock types with very different thermal properties.
- An overall trend towards significantly lower thermal conductivity at depths of 450 m to 600 m indicated in model stage 2.1 is not supported by the new data.
- Any anisotropy in thermal conductivity caused by the preferred orientation of subordinate rock bodies is considered to be small.
- Anisotropy in thermal conductivity resulting from foliation has been established. Field measurements in Ävrö granite indicate that thermal conductivity parallel to the foliation plane are higher, by a factor of approximately 1.15, than conductivity perpendicular to the foliation. The spatial variability of this anisotropy is not known.
- The thermal conductivity of altered rock is approximately 5–15% higher than fresh rock. The impact of alteration has been incorporated into the thermal modelling and is therefore reflected in the domain results.
- The mean heat capacity at the 2 m scale for the modelled rock domains varies between 2.16 and 2.23 MJ/(m³·K).
- The temperature variation with depth is rather well established. The mean *in situ* temperatures at –400 m, –500 m and –600 m elevation are estimated at 13.3°C, 14.8°C, and 16.3°C, respectively.
- The mean thermal expansion coefficient for the dominant granitoid rock types varies between $6.9 \cdot 10^{-6}$ and $7.4 \cdot 10^{-6}$ m/(m·K).
- There is good mutual consistency between the understanding of geology and the thermal properties description.

References

- Adl-Zarrabi B, 2004a.** Drill hole KSH01A: Thermal properties: heat conductivity and heat capacity determined using the TPS method and mineralogical composition by modal analysis. SKB P-04-53, Svensk Kärnbränslehantering AB.
- Adl-Zarrabi B, 2004b.** Drill hole KSH02: Thermal properties: heat conductivity and heat capacity determined using the TPS method and mineralogical composition by modal analysis. SKB P-04-54, Svensk Kärnbränslehantering AB.
- Adl-Zarrabi B, 2004c.** Drill hole KLX02: Thermal properties: heat conductivity and heat capacity determined using the TPS method and mineralogical composition by modal analysis. SKB P-04-258, Svensk Kärnbränslehantering AB.
- Adl-Zarrabi B, 2004d.** Drill hole KLX04: Thermal properties: heat conductivity and heat capacity determined using the TPS method and mineralogical composition by modal analysis. SKB P-04-267, Svensk Kärnbränslehantering AB.
- Adl-Zarrabi B, 2006a.** Borehole KLX07. Thermal conductivity and thermal diffusivity determined using the TPS method. Oskarshamn site investigation. SKB P-05-208, Svensk Kärnbränslehantering AB.
- Adl-Zarrabi B, 2006b.** Borehole KLX08. Thermal conductivity and thermal diffusivity determined using the TPS method. Oskarshamn site investigation. SKB P-06-31, Svensk Kärnbränslehantering AB.
- Adl-Zarrabi B, 2006c.** Borehole KLX10. Thermal conductivity and thermal diffusivity determined using the TPS method. Oskarshamn site investigation. SKB P-06-36, Svensk Kärnbränslehantering AB.
- Adl-Zarrabi B, 2006d.** Borehole KLX11A. Thermal properties of rocks using calorimeter and TPS method. Oskarshamn site investigation. SKB P-06-269. Svensk Kärnbränslehantering AB.
- Adl-Zarrabi B, 2006e.** Borehole KLX12A. Thermal properties of rocks using calorimeter and TPS method. Oskarshamn site investigation. SKB P-06-72. Svensk Kärnbränslehantering AB.
- Adl-Zarrabi B, 2006f.** Borehole KLX13A. Thermal properties of rocks using calorimeter and TPS method. Oskarshamn site investigation. SKB P-06-275. Svensk Kärnbränslehantering AB.
- Adl-Zarrabi B, 2007a.** Boreholes KLX03, KLX05, KLX07, KLX10 and KLX11A. Thermal properties of rocks using calorimeter and TPS method, and mineralogical composition by modal analysis. Oskarshamn site investigation. SKB P-07-62. Svensk Kärnbränslehantering AB.
- Adl-Zarrabi B, 2007b.** Borehole KLX16A. Thermal properties of rocks using TPS method. Oskarshamn site investigation. SKB P-07-144. Svensk Kärnbränslehantering AB.
- Back P-E, Sundberg J, 2007.** Thermal Site Descriptive Model. A Strategy for the Model Development during Site Investigations. Version 2.0. SKB R-07-42, Svensk Kärnbränslehantering AB.
- Back P E, Wrafter J, Sundberg J, Rosén L, 2007.** Thermal properties. Site descriptive modeling Forsmark – stage 2.2. SKB R-07-47, Svensk Kärnbränslehantering AB.
- Carle S F, 1999.** T-PROGS: Transition Probability Geostatistical Software. Version 2.1. Hydrologic Sciences Graduate Group. University of California.

- Carle S F, Fogg G E, 1997.** Modeling spatial variability with one- and multi-dimensional Markov chains. *Mathematical Geology*, v. 28, no. 7.
- Davis J C, 1986.** *Statistics and data analysis in geology*. Wiley & Sons.
- Deutsch C, Journel A, 1998.** *GS-LIB: Geostatistical Software Library and User's Guide*. Second edition. Oxford University Press, New York.
- Dowd P A, 2007.** University of Adelaide. Personal communication.
- Drake H, Tullborg E-L, 2006a.** Mineralogical, chemical and redox features of red-staining adjacent to fractures – Results from drill core KSH01A+B and KSH03A+B. P-06-01, Svensk Kärnbränslehantering AB.
- Drake H, Tullborg E-L, 2006b.** Mineralogical, chemical and redox features of red-staining adjacent to fractures – Results from drill core KLX04. P-06-02, Svensk Kärnbränslehantering AB.
- Drake H, 2007.** Personal communication.
- Drake H, Page L, Tullborg E-L, 2007.** 40Ar/39Ar dating of fracture minerals. Oskarshamn site investigation. P-07-27, Svensk Kärnbränslehantering AB.
- Evans M, Hastings N, Peacock B. 2000.** *Statistical distributions*, third edition, John Wiley & Sons Inc..
- Hakami E, Lanaro F, Fredriksson A, 2008.** Rock Mechanics Laxemar. Site descriptive modelling. SDM-Site Laxemar. SKB R-08-57, Svensk Kärnbränslehantering AB.
- Horai K, 1971.** Thermal conductivity of rock-forming minerals. *J. Geophys. Res.* 76, p 1278–1308.
- Horai and Baldrige, 1972.** Thermal conductivity of nineteen igneous rocks, Application of the needle probe method to the measurement of the thermal conductivity of rock. Estimation of the thermal conductivity of rock from the mineral and chemical compositions. *Phys. Earth Planet. Interiors* 5, p 151.
- Hökmark H, Sundberg J, Kristensson O, Lönnqvist M, Hellström G, 2009.** Strategy for thermal dimensioning of the final repository for spent nuclear fuel. SKB R-09-04, Svensk Kärnbränslehantering AB.
- Journel A G and Huijbregts C J, 1978.** *Mining geostatistics*. Academic Press, London.
- Liedberg L, 2007.** Borehole KLX03, KLX05, KLX07A, KLX10 and KLX11A. Determination of porosity by water saturation and density by buoyancy technique. Oskarshamn site investigation. SKB P-07-61, Svensk Kärnbränslehantering AB.
- Mattsson H, 2004.** Interpretation of geophysical borehole data and compilation of petrophysical data from KSH03A (100–1,000 m), KSH03B, HAV09, HAV10 and KLX02 (200–1,000 m). Oskarshamn site investigation. SKB P-04-214, Svensk Kärnbränslehantering AB.
- Mattsson H, Thunehed H, Triumf C-A, 2004.** Compilation of petrophysical data from rock samples and in situ gamma-ray spectrometry measurements. Stage 2 – 2004 (including 2002). Oskarshamn site investigation Revised September 2006. SKB P-04-294. Svensk Kärnbränslehantering AB.
- Mattsson H, Keisu M, 2005a.** Interpretation of geophysical borehole measurements from KLX05. Oskarshamn site investigation. SKB P-05-189, Svensk Kärnbränslehantering AB.
- Mattsson H, Keisu M, 2005b.** Interpretation of geophysical borehole measurements from KLX07A, KLX07B, HLX20, HLX32, HLX34 and HLX35. Oskarshamn site investigation. SKB P-05-259, Svensk Kärnbränslehantering AB.

Mattsson H, Thunehed H, Keisu M, 2005. Interpretation of geophysical borehole measurements and compilation of petrophysical data from KLX01, KLX03, KLX04, HLX21, HLX22, HLX23, HLX24, HLX25, HLX26, HLX27 and HLX28. Oskarshamn site investigation. SKB P-05-34, Svensk Kärnbränslehantering AB.

Mattsson H, 2006a. Interpretation of geophysical borehole measurements from KLX11A. Oskarshamn site investigation. SKB P-06-157, Svensk Kärnbränslehantering AB.

Mattsson H, 2006b. Interpretation of geophysical borehole measurements from KLX10. Oskarshamn site investigation. SKB P-06-162, Svensk Kärnbränslehantering AB.

Mattsson H, 2006c. Interpretation of geophysical borehole measurements from KLX12A. Oskarshamn site investigation. SKB P-06-253, Svensk Kärnbränslehantering AB.

Mattsson H, Keisu M, 2006a. Interpretation of geophysical borehole measurements from KLX08, HLX30, HLX31 and HLX33. Oskarshamn site investigation. SKB P-06-65, Svensk Kärnbränslehantering AB.

Mattsson H, Keisu M, 2006b. Interpretation of geophysical borehole measurements from KLX18A, KLX20A, KLX09B, KLX09D, KLX09F, KLX11B, HLX38, HLX39, HLX40, HLX41 and interpretation of petrophysical data from KLX20A. Oskarshamn site investigation. SKB P-06-292, Svensk Kärnbränslehantering AB.

Mattsson H, Keisu M, Thunehed H, 2006. Interpretation of geophysical borehole measurements from KLX13A, KLX14A, KLX22A, KLX22B, KLX23A, KLX23B, KLX24A, KLX25A, KLX26A and KLX26B. Oskarshamn site investigation. SKB P-06-317, Svensk Kärnbränslehantering AB.

Mattsson H, 2007. Geo Vista AB. Personal communication.

Mattsson KJ, Eklund S, 2007. Boremap mapping of core drilled borehole KLX18A.

Mattsson H, Keisu M, 2007a. Interpretation of geophysical borehole measurements from KLX19A, KLX28A, and KLX29A. Oskarshamn site investigation. SKB P-07-21, Svensk Kärnbränslehantering AB.

Mattsson H, Keisu M, 2007b. Interpretation of geophysical borehole measurements from KLX17A and HLX43. Oskarshamn site investigation. SKB P-07-25, Svensk Kärnbränslehantering AB.

Mattsson H, Keisu M, 2007c. Interpretation of geophysical borehole measurements from KLX21B. Oskarshamn site investigation. SKB P-07-75, Svensk Kärnbränslehantering AB.

Mattsson H, Keisu M, 2007d. Interpretation of geophysical borehole measurements from KLX16A. Oskarshamn site investigation. SKB P-07-97, Svensk Kärnbränslehantering AB.

Mattsson H, Keisu M, 2007e. Interpretation of geophysical borehole measurements from KLX15A. Oskarshamn site investigation. SKB P-07-114, Svensk Kärnbränslehantering AB.

Mattsson H, 2008. Geo Vista AB. Personal communication.

Mossmark F, Sundberg J, 2007. Oskarshamn site investigation. Field Measurements of Thermal Properties. Multi Probe Measurements in Laxemar. SKB P-07-77, Svensk Kärnbränslehantering AB.

Mottaghy D, Schellschmidt R, Popov YA, Clauser C, Kukkonen IT, Nover G, Milanovsky S and Romushkevich RA, 2005. New heat flow data from the immediate vicinity of the Kola super-deep borehole. Vertical variation in heat flow confirmed and attributed to advection. *Tectonophysics* 401, 119–142.

- Munier R, Stenberg L, Stanfors R, Milnes A G, Hermanson J, Triumf C-A, 2003.** Geological Site Descriptive Model. A strategy for the model development during site investigations. SKB R-03-07, Svensk Kärnbränslehantering AB.
- Munier R, Stigsson M, 2007.** Implementation of uncertainties in borehole geometries and geological orientation data in Sicada. SKB R-07-19, Svensk Kärnbränslehantering AB.
- Seipold U, Huenges E, 1998.** Thermal properties of gneisses and amphibolites high pressure and high temperature investigations of KTB-rock samples. *Tectonophysics* 291, 173–178.
- SKB, 2005.** Program för fortsatta undersökningar av berggrund, mark, vatten och miljö inom delområde Laxemar. SKB R-05-37, Svensk Kärnbränslehantering AB.
- SKB, 2006a.** Long-term safety for KBS-3 repositories at Forsmark and Laxemar – a first evaluation. Main Report of the SR-Can project. SKB TR-06-09, Svensk Kärnbränslehantering AB.
- SKB, 2006b.** Preliminary Site Description Laxemar subarea – version 1.2. SKB R-06-10, Svensk Kärnbränslehantering AB, Stockholm, Sweden.
- SKB, 2006c.** Preliminary safety evaluation for the Laxemar subarea – Based on data and site descriptions after the initial site investigation stage. SKB TR-06-06, Svensk Kärnbränslehantering AB.
- SKB, 2006d.** Preliminary Site Description Laxemar stage 2.1. Feedback for completion of the site investigation including input from safety assessment and repository engineering. SKB R-06-110, Svensk Kärnbränslehantering AB.
- SKB, 2009.** Site description of Laxemar at completion of the site investigation phase (SDM-Site Laxemar) SKB TR-09-01 Svensk Kärnbränslehantering AB. (In prep).
- Sokolnicki M, Rouhiainen P, 2005.** Difference flow logging in borehole KLX05 – subarea Laxemar. SKB R-05-160. Svensk Kärnbränslehantering AB.
- Sokolnicki M, Pöllänen J, 2005.** Difference flow logging in borehole KLX08 – subarea Laxemar. SKB R-05-267. Svensk Kärnbränslehantering AB.
- Sokolnicki M, Kristiansson S, 2006.** Difference flow logging in borehole KLX18A – subarea Laxemar. SKB R-06-184. Svensk Kärnbränslehantering AB.
- Stenberg L, 2006.** SKB. Personal communication.
- Sundberg J, 1988.** Thermal Properties of Soils and Rocks. Publ. A 57, Dissertation. Geologiska institutionen, Chalmers University of Technology, and University of Göteborg.
- Sundberg J, 2002.** Determination of thermal properties at Äspö HRL. Comparison and evaluation of methods and methodologies for borehole KA 2599 G01. SKB R-02-27, Svensk Kärnbränslehantering AB.
- Sundberg J, 2003a.** A strategy for the model development during site investigations version 1.0. SKB R-03-10, Svensk Kärnbränslehantering AB.
- Sundberg J, 2003b.** Thermal properties at Äspö HRL. Analysis of distribution and scale factors. SKB R-03-17, Svensk Kärnbränslehantering AB.
- Sundberg J, Back P-E, Bengtsson A, Ländell M, 2005a.** Oskarshamn site investigation. Thermal modelling of the Simpevarp Area – Supporting document for thermal model version 1.2. SKB R-05-24, Svensk Kärnbränslehantering AB.
- Sundberg J, Back P-E, Hellström G, 2005b.** Scale dependence and estimation of rock thermal conductivity. Analysis of upscaling, inverse thermal modelling and value of information with the Äspö HRL prototype repository as an example. SKB R-05-82, Svensk Kärnbränslehantering AB.

Sundberg J, Wrafter J, Back P-E, Ländell M, 2006. Thermal modelling. Preliminary site description Laxemar subareas – version 1.2. R-06-13, Svensk Kärnbränslehantering AB.

Sundberg J, Wrafter J, Sundberg A, 2007. Forsmark site investigation. Anisotropy of thermal properties in granite at Forsmark. Large-scale field measurements and comparison with small-scale field measurements and laboratory measurements. SKB P-07-194, Svensk Kärnbränslehantering AB.

Sundberg J, Back P-E, Ericsson L O, Wrafter J, 2008a. A method for estimation of thermal conductivity and its spatial variability in igneous rocks from in situ density logging. (Submitted to International Journal of Rock Mechanics and Mining Sciences, Elsevier).

Sundberg J, Wrafter J, Ländell M, Back P E, Rosén L, 2008b. Thermal properties Forsmark. Modelling stage 2.3: Complementary analysis and verification of the thermal bedrock model. SKB R-08-65, Svensk Kärnbränslehantering AB.

Wahlgren C-H, 2005. Geological Survey of Sweden. Personal communication.

Wahlgren C-H, Bergman T, Ahl M, 2006a. Modal and geochemical analyses of drill core samples 2005. Classification of rock types in KLX03, KLX04, KLX06, KLX07A, KLX07B, KLX08 and KLX10. SKB R-06-07, Svensk Kärnbränslehantering AB.

Wahlgren C-H, Bergman T, Ahl M, Ekström M, 2006b. Modal and geochemical analyses of drill core samples 2006 and updated bedrock map of the Laxemar subarea. Classification of rock types in KLX08, KLX10, KLX11A, KLX12A, KLX18A and KLX20A. SKB P-06-279. Svensk Kärnbränslehantering AB.

Wahlgren C-H, Hermanson J, Curtis P, Forsberg O, Triumf C-A, Tullborg E-L, Drake H, 2006c. Geological description of rock domains and deformation zones in the Simpevarp and Laxemar subareas. Preliminary site description, Laxemar subarea, version 1.2. SKB R-05-69, Svensk Kärnbränslehantering AB.

Wahlgren C-H, 2007. Geological Survey of Sweden. Personal communication.

Wahlgren C-H, Bergman T, Ahl M, Ekström M, Page L, Söderlund A, 2007. Modal and geochemical analyses of drill core samples 2007 and $^{40}\text{Ar}/^{39}\text{Ar}$ dating of a dolerite. Classification of rock types in KLX15A, KLX16A, KLX19A, KLX20A and KLX21B. SKB P-07-191. Svensk Kärnbränslehantering AB.

Wahlgren C-H, 2008. Geological Survey of Sweden. Personal communication.

Wahlgren C-H, Curtis P, Hermanson J, Forssberg O, Öhman J, Fox A, La Pointe P, Drake H, Triumf C-A, Mattsson H, Thunehed H, Juhlin C, 2008. Geology Laxemar. Site descriptive modelling SDM-Site Laxemar. SKB R-08-54, Svensk Kärnbränslehantering AB.

Walsh J B, Decker E R, 1966. Effect of pressure and saturating fluid on the thermal conductivity of compact rock. *J. Geophys. Res.*, 71, 12.

Werner K, Bosson E, Berglund S, 2006. Description of climate, surface hydrology, and near-surface hydrogeology. Preliminary site description Laxemar subarea – version 1.2. SKB R-05-61, Svensk Kärnbränslehantering AB.

Wrafter J, Sundberg J, Ländell M, Back P, 2006. Thermal modelling. Site descriptive modelling. Laxemar 2.1. SKB R-06-84, Svensk Kärnbränslehantering AB.

Åkesson U, 2007. Boreholes KLX07A, KLX10, KLX05 and KLX12A. Extensometer measurements of the coefficient of thermal expansion of rock. SKB P-07-63, Svensk Kärnbränslehantering AB.

Thermal conductivity from density logs – histograms

Based on the relationship between density and thermal conductivity derived for Ävrö granite, as explained in Section 3.6, density values given by the density loggings of boreholes have been used to deterministically assign a thermal conductivity value to each logged decimetre section of Ävrö granite in nine boreholes. As explained in Section 3.6 Ävrö granite has been divided into two varieties, namely Ävrö quartz monzodiorite (501046) and Ävrö granodiorite (501056).

Histograms of calculated thermal conductivity are presented below on a borehole basis, as well as for all boreholes combined. The histograms display the distribution of thermal conductivity values calculated from density loggings at scale 0.1 m for Ävrö granodiorite and Ävrö quartz monzodiorite separately, as well as both rock types combined.

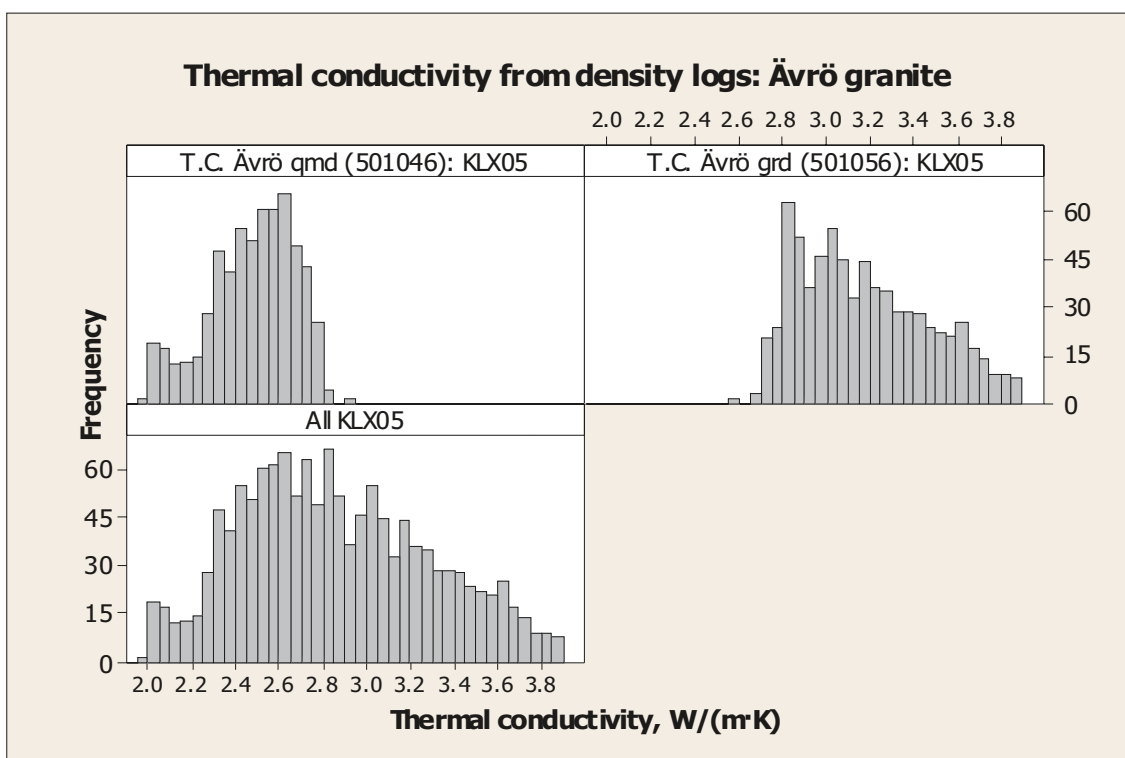


Figure A-1. Histograms of thermal conductivity for Ävrö quartz monzodiorite (501046), Ävrö granodiorite (501056) and Ävrö granite undifferentiated calculated from density loggings for borehole KLX05.

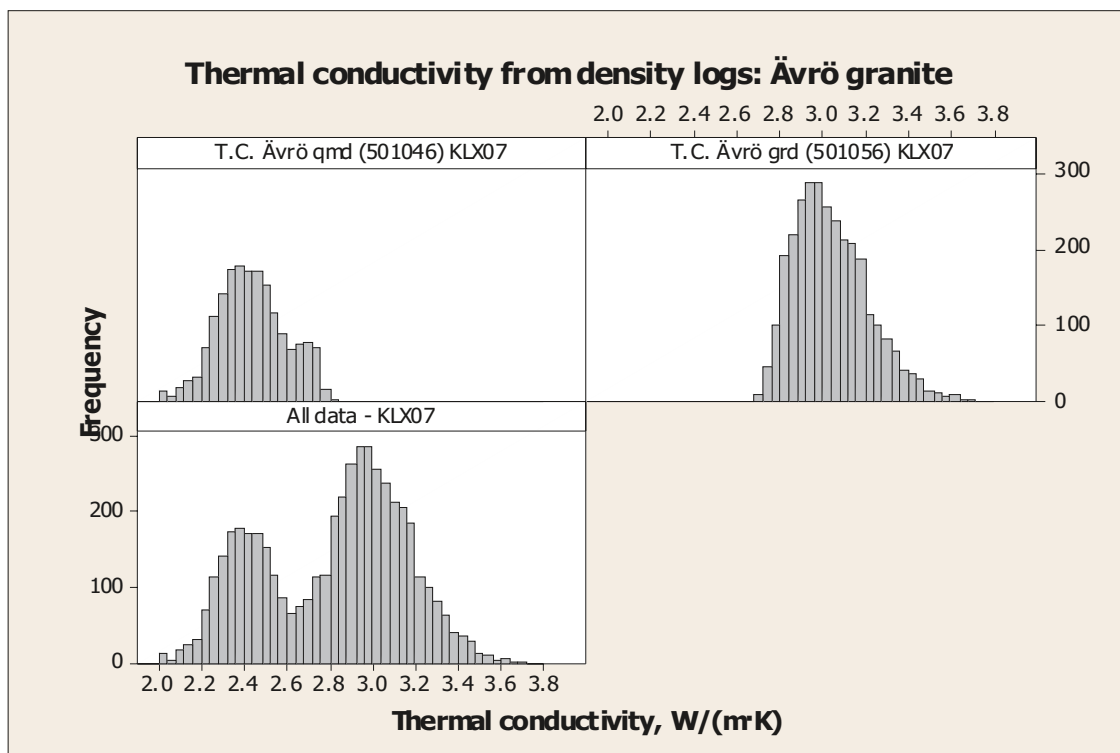


Figure A-2. Histograms of thermal conductivity for Ävrö quartz monzodiorite (501046), Ävrö granodiorite (501056) and Ävrö granite undifferentiated calculated from density loggings for borehole KLX07.

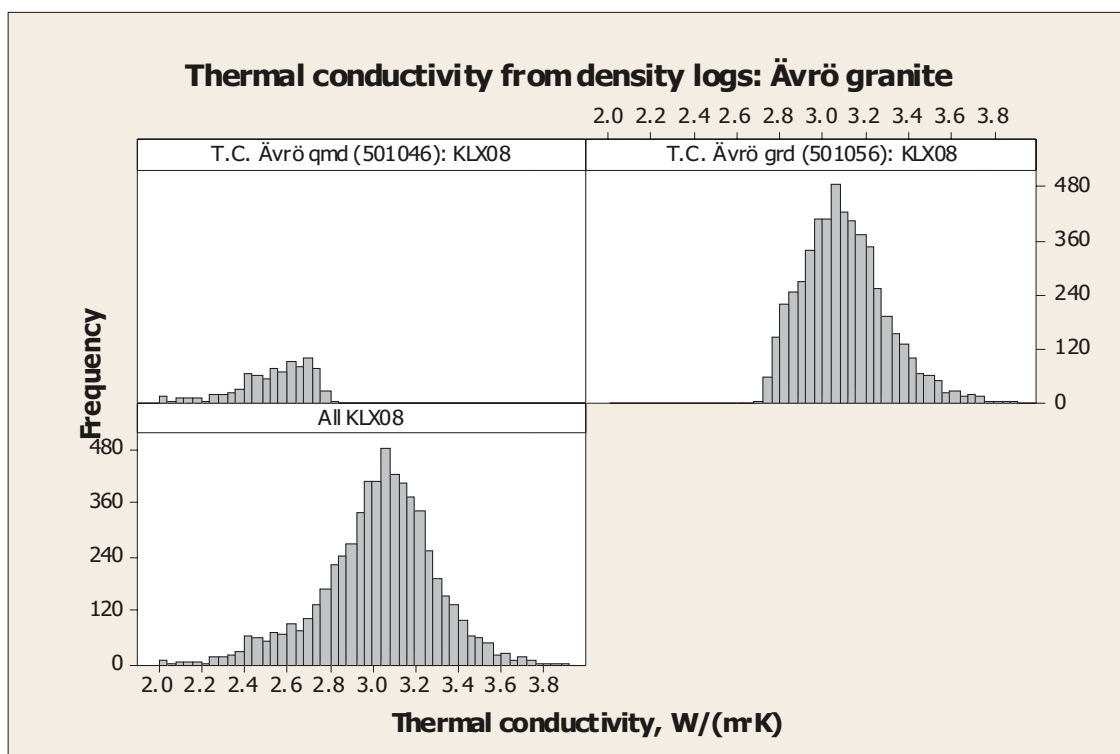


Figure A-3. Histograms of thermal conductivity for Ävrö quartz monzodiorite (501046), Ävrö granodiorite (501056) and Ävrö granite undifferentiated calculated from density loggings for borehole KLX08.

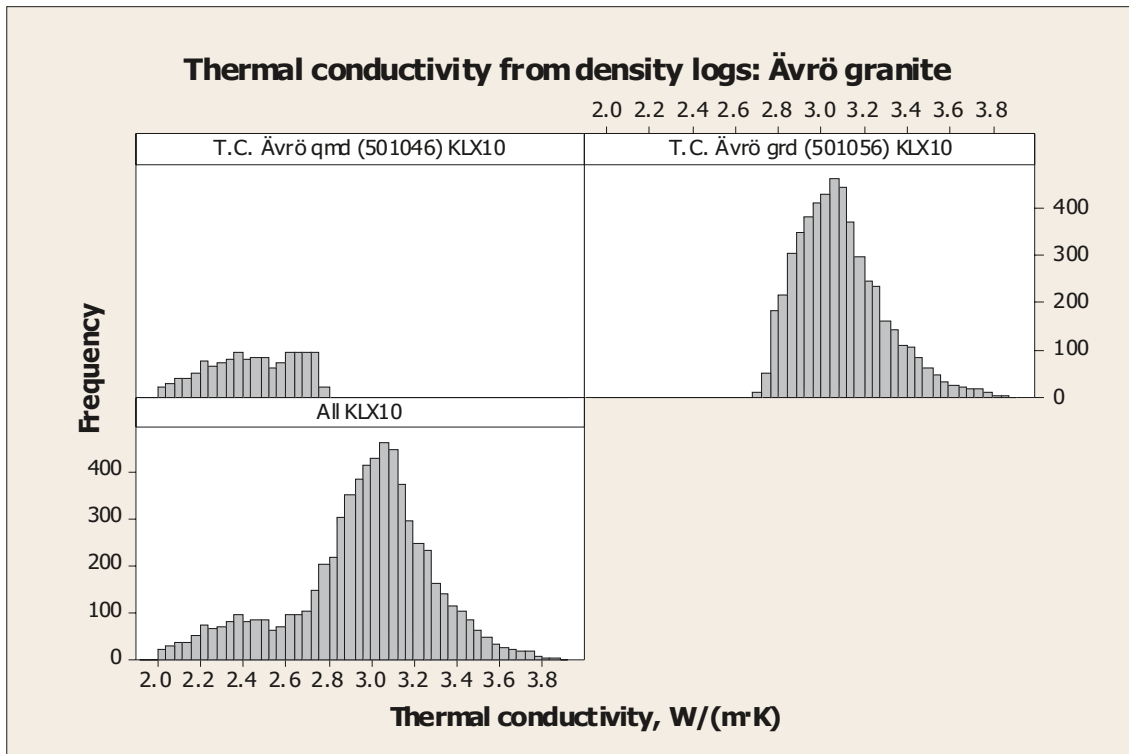


Figure A-4. Histograms of thermal conductivity for Ävrö quartz monzodiorite (501046), Ävrö granodiorite (501056) and Ävrö granite undifferentiated calculated from density loggings for borehole KLX10.

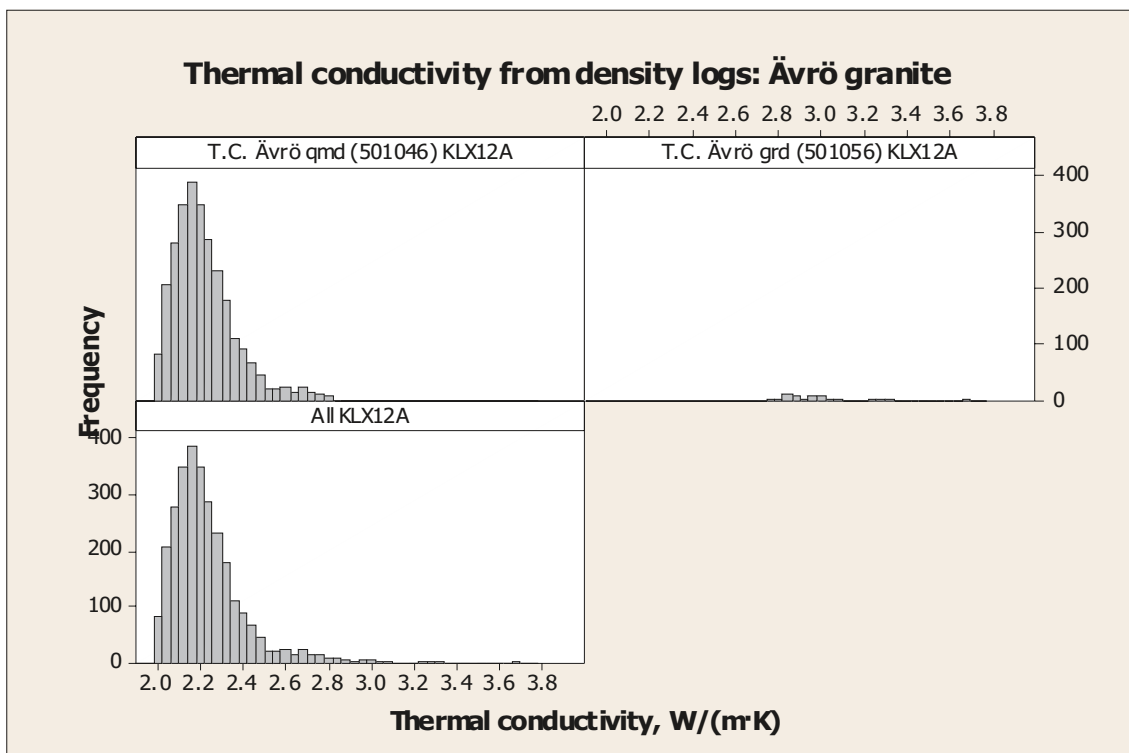


Figure A-5. Histograms of thermal conductivity for Ävrö quartz monzodiorite (501046), Ävrö granodiorite (501056) and Ävrö granite undifferentiated calculated from density loggings for borehole KLX12A.

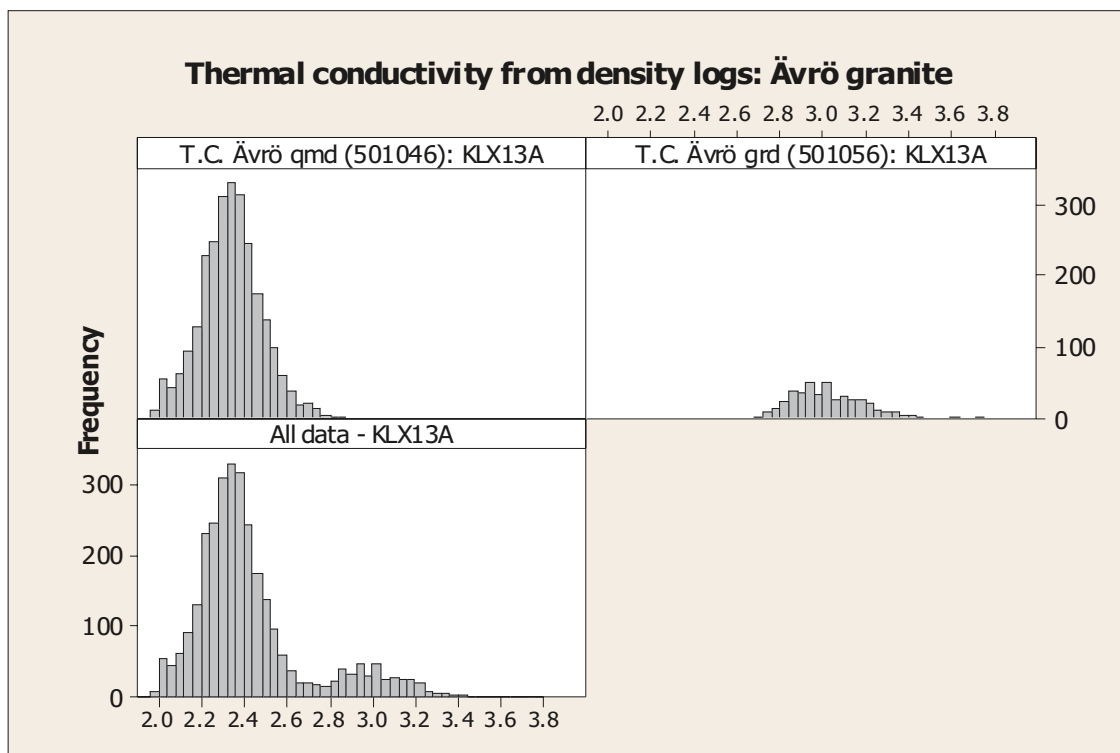


Figure A-6. Histograms of thermal conductivity for Ävrö quartz monzodiorite (501046), Ävrö granodiorite (501056) and Ävrö granite undifferentiated calculated from density loggings for borehole KLX13A.

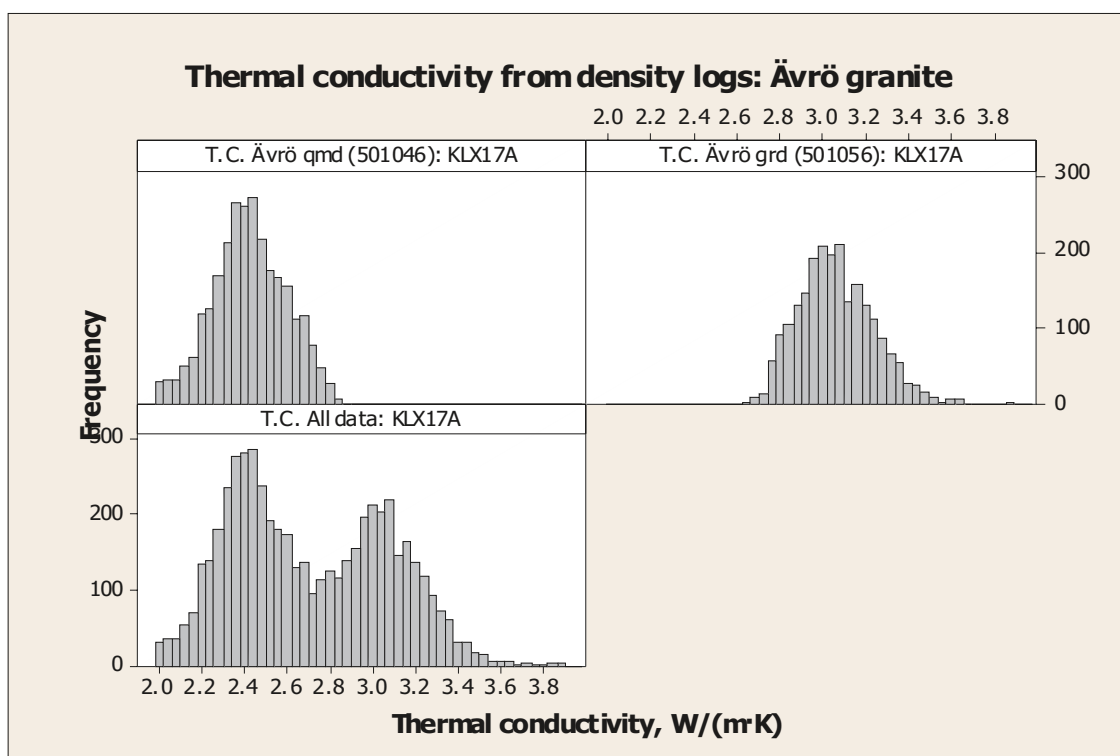


Figure A-7. Histograms of thermal conductivity for Ävrö quartz monzodiorite (501046), Ävrö granodiorite (501056) and Ävrö granite undifferentiated calculated from density loggings for borehole KLX17A.

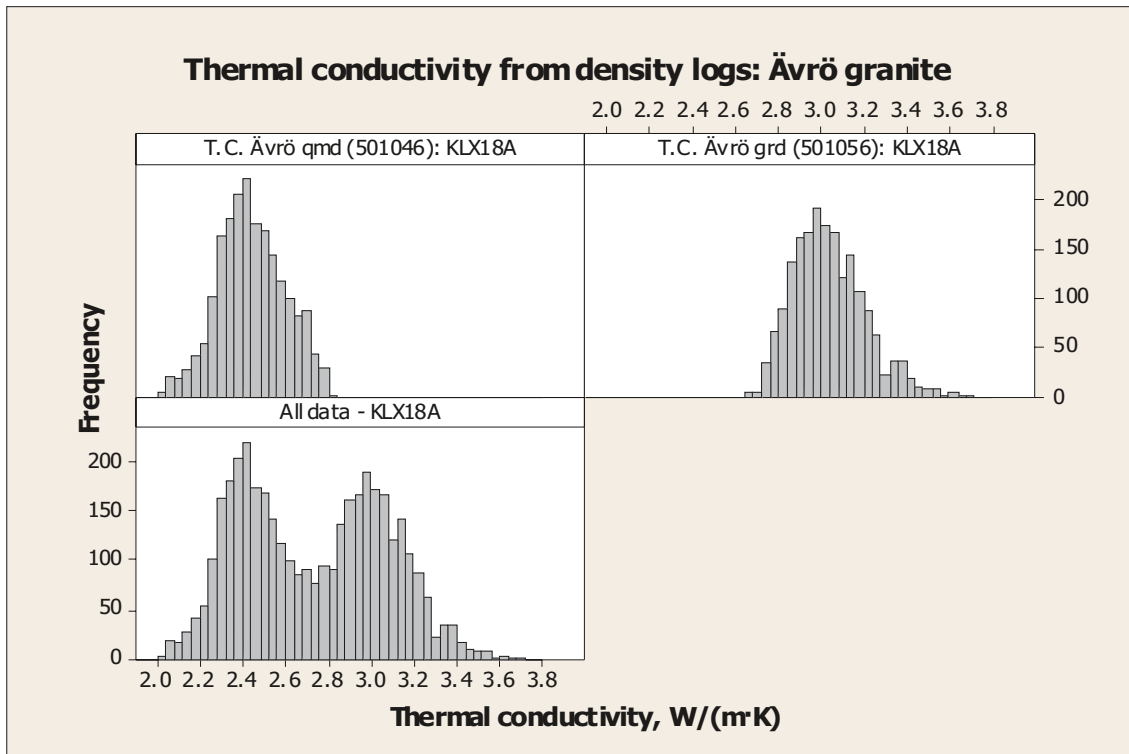


Figure A-8. Histograms of thermal conductivity for Ävrö quartz monzodiorite (501046), Ävrö granodiorite (501056) and Ävrö granite undifferentiated calculated from density loggings for borehole KLX18A.

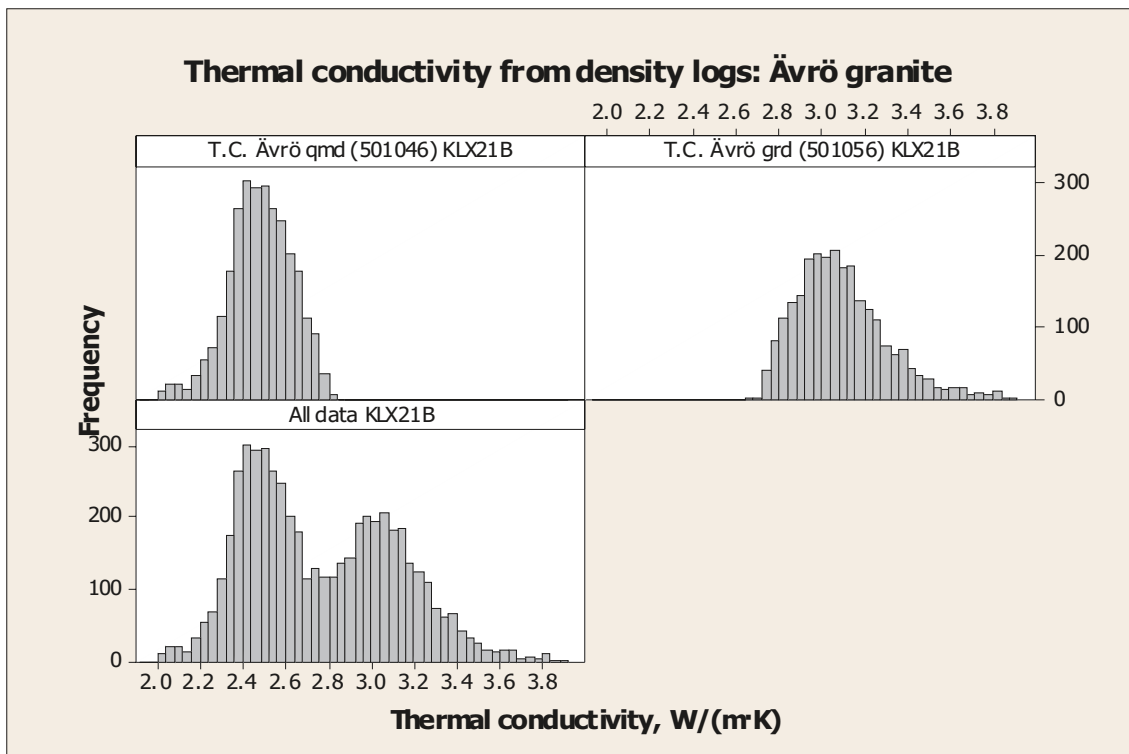


Figure A-9. Histograms of thermal conductivity for Ävrö quartz monzodiorite (501046), Ävrö granodiorite (501056) and Ävrö granite undifferentiated calculated from density loggings for borehole KLX21B.

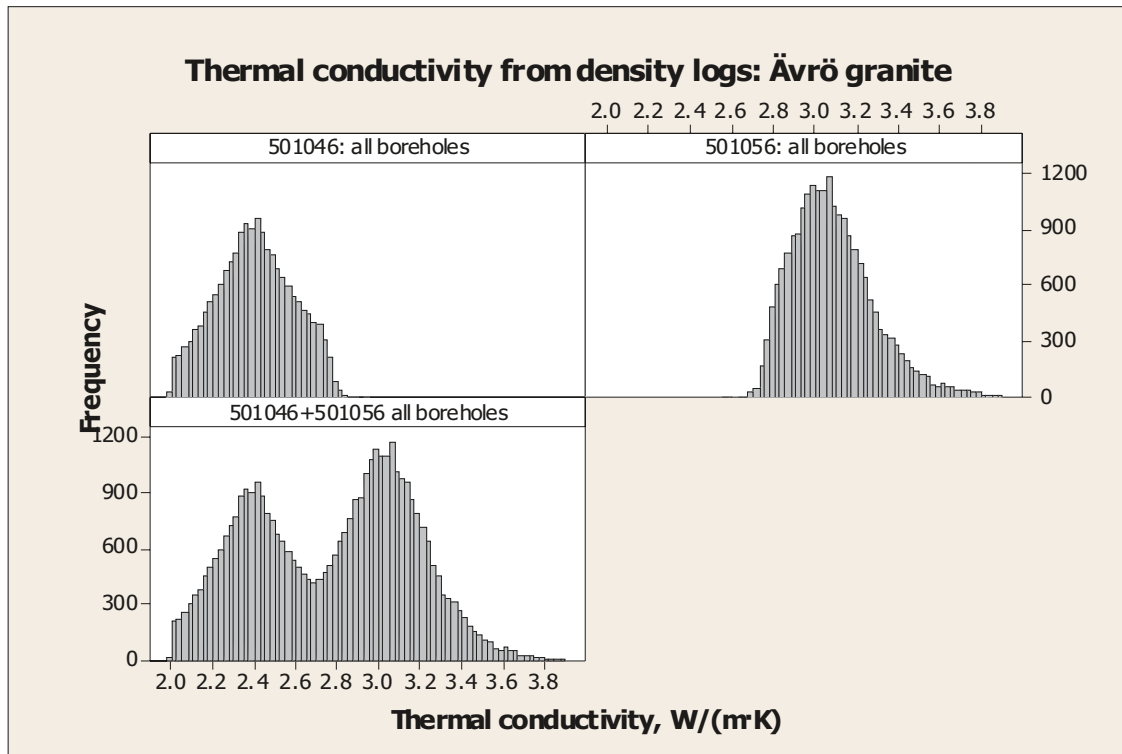


Figure A-10. Histograms of thermal conductivity for Ävrö quartz monzodiorite (501046), Ävrö granodiorite (501056) and Ävrö granite undifferentiated calculated from density loggings for nine boreholes, KLX05,07, 08, 10, 12A, 13A, 17A, 18A and 21B.

Thermal conductivity from density logs – borehole profiles

Based on the relationship between density and thermal conductivity derived for Ävrö granite, as explained in Section 3.6, density values given by the density loggings of boreholes have been used to deterministically assign a thermal conductivity value to each logged decimetre section of Ävrö granite in nine boreholes. As explained in Section 3.6 Ävrö granite has been divided into two varieties, namely Ävrö quartz monzodiorite (501046) and Ävrö granodiorite (501056).

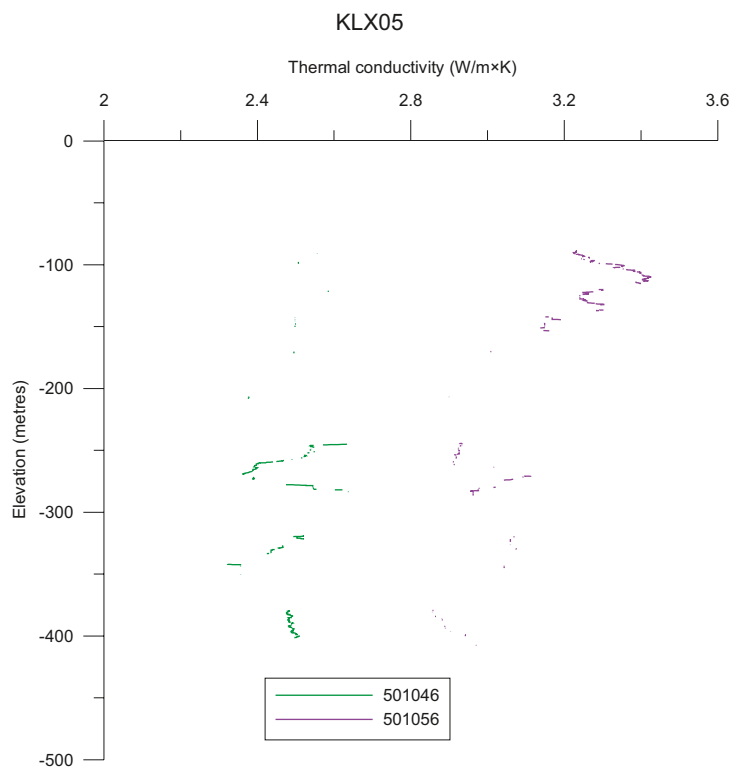


Figure B-1. Visualisation of large-scale changes in thermal conductivity with depth for Ävrö quartz monzodiorite (501046) and Ävrö granodiorite (501056) in borehole KLX05. Thermal conductivity is expressed as moving geometric mean calculations for 20 m long borehole sections. Spatial variability is reduced considerably because of this averaging.

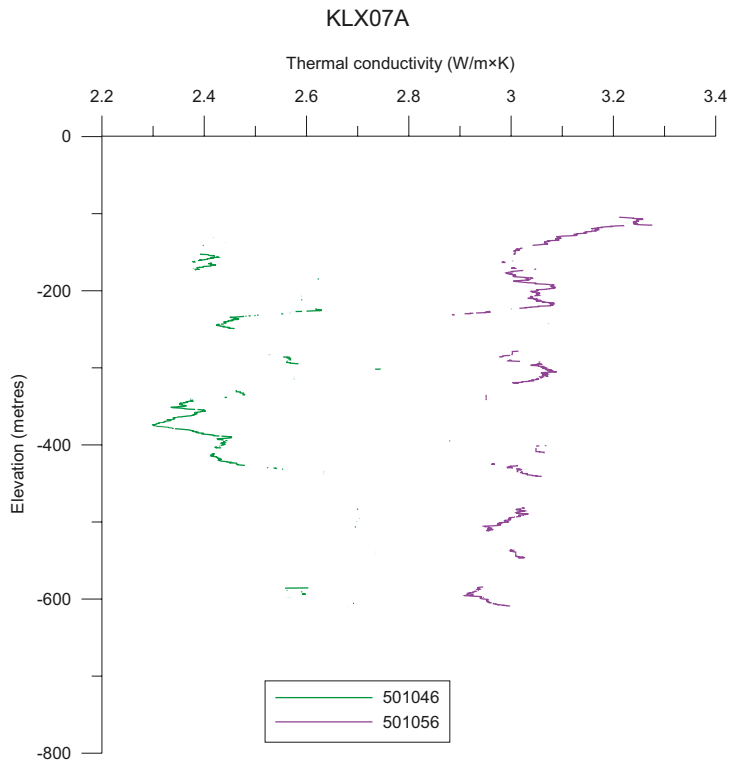


Figure B-2. Visualisation of large-scale changes in thermal conductivity with depth for Ävrö quartz monzodiorite (501046) and Ävrö granodiorite (501056) in borehole KLX07. Thermal conductivity is expressed as moving geometric mean calculations for 20 m long borehole sections. Spatial variability is reduced considerably because of this averaging.

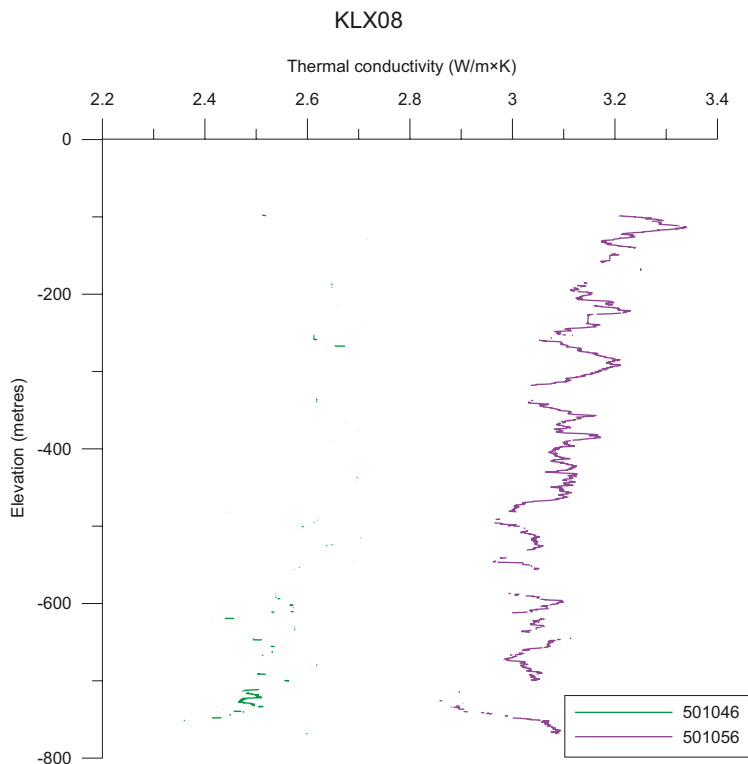


Figure B-3. Visualisation of large-scale changes in thermal conductivity with depth for Ävrö quartz monzodiorite (501046) and Ävrö granodiorite (501056) in borehole KLX08. Thermal conductivity is expressed as moving geometric mean calculations for 20 m long borehole sections. Spatial variability is reduced considerably because of this averaging.

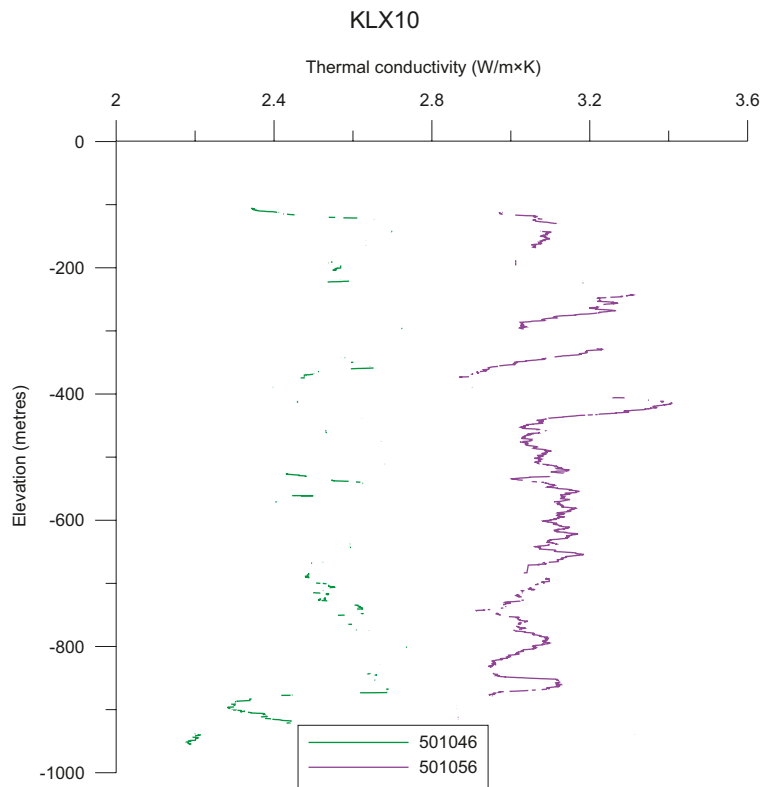


Figure B-4. Visualisation of large-scale changes in thermal conductivity with depth for Ävrö quartz monzodiorite (501046) and Ävrö granodiorite (501056) in borehole KLX10. Thermal conductivity is expressed as moving geometric mean calculations for 20 m long borehole sections. Spatial variability is reduced considerably because of this averaging.

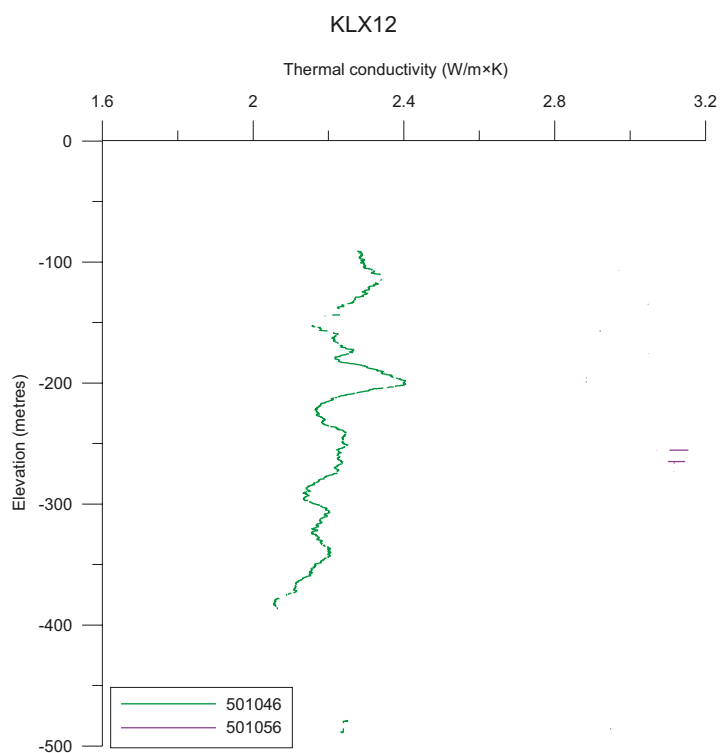


Figure B-5. Visualisation of large-scale changes in thermal conductivity with depth for Ävrö quartz monzodiorite (501046) and Ävrö granodiorite (501056) in borehole KLX12A. Thermal conductivity is expressed as moving geometric mean calculations for 20 m long borehole sections. Spatial variability is reduced considerably because of this averaging.

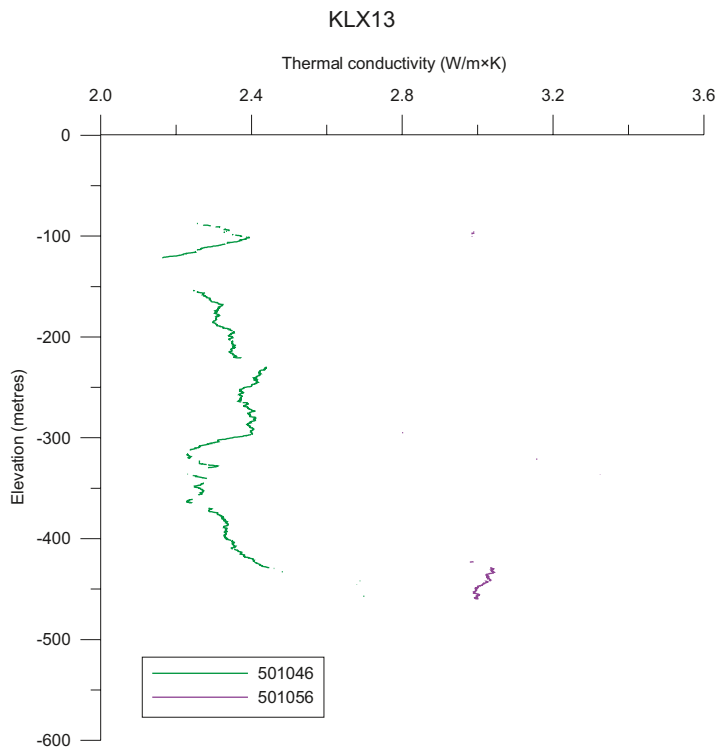


Figure B-6. Visualisation of large-scale changes in thermal conductivity with depth for Ävrö quartz monzodiorite (501046) and Ävrö granodiorite (501056) in borehole KLX13A. Thermal conductivity is expressed as moving geometric mean calculations for 20 m long borehole sections. Spatial variability is reduced considerably because of this averaging.

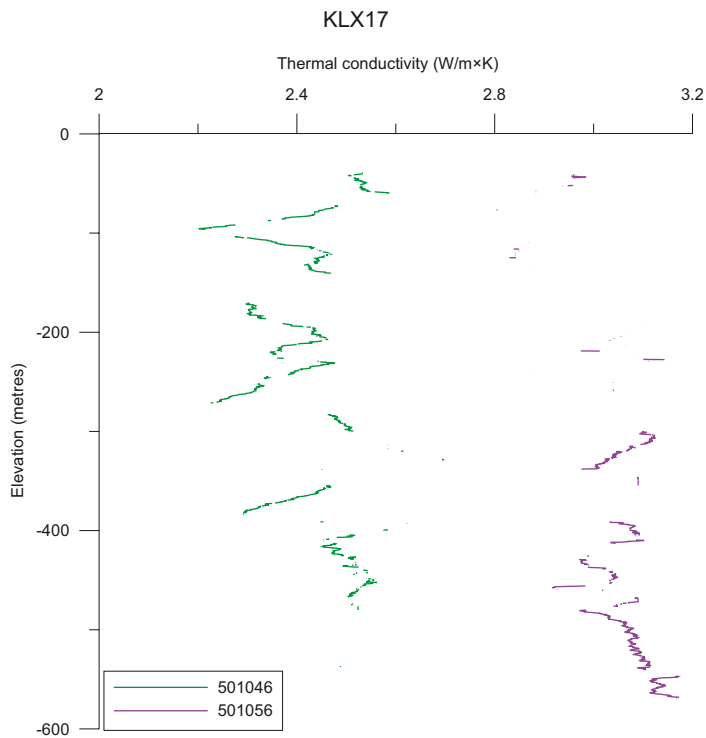


Figure B-7. Visualisation of large-scale changes in thermal conductivity with depth for Ävrö quartz monzodiorite (501046) and Ävrö granodiorite (501056) in borehole KLX17A. Thermal conductivity is expressed as moving geometric mean calculations for 20 m long borehole sections. Spatial variability is reduced considerably because of this averaging.

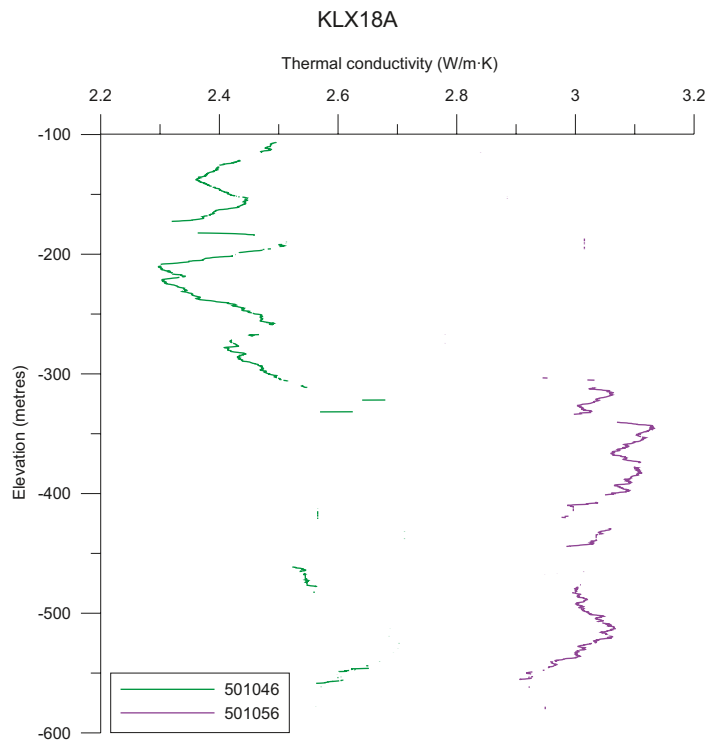


Figure B-8. Visualisation of large-scale changes in thermal conductivity with depth for Ävrö quartz monzodiorite (501046) and Ävrö granodiorite (501056) in borehole KLX18A. Thermal conductivity is expressed as moving geometric mean calculations for 20 m long borehole sections. Spatial variability is reduced considerably because of this averaging.

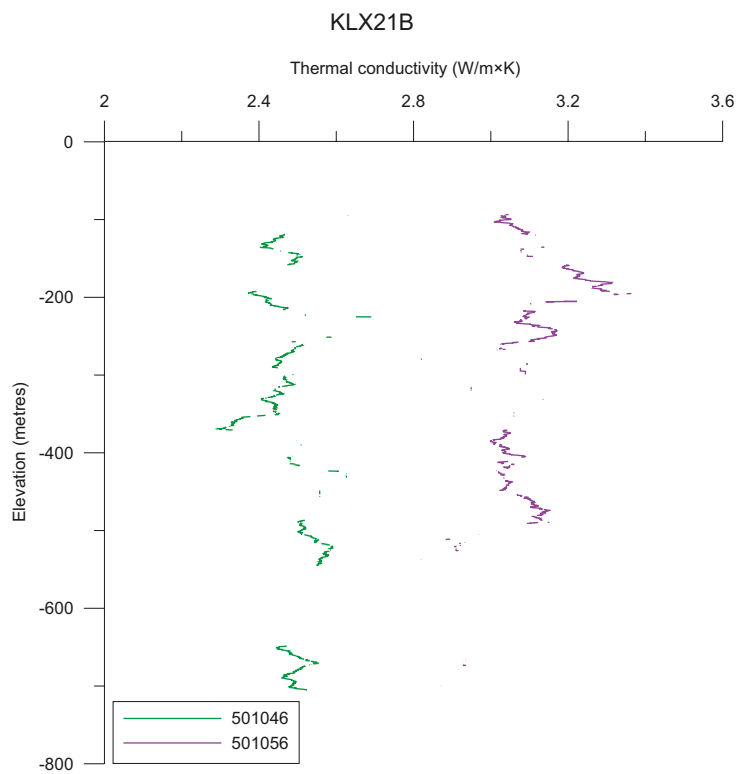
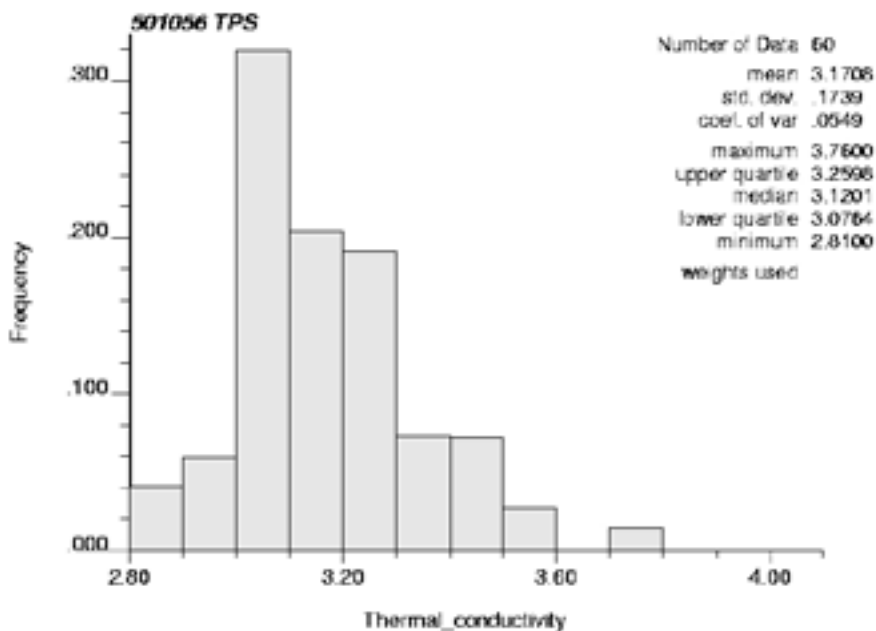


Figure B-9. Visualisation of large-scale changes in thermal conductivity with depth for Ävrö quartz monzodiorite (501046) and Ävrö granodiorite (501056) in borehole KLX21B. Thermal conductivity is expressed as moving geometric mean calculations for 20 m long borehole sections. Spatial variability is reduced considerably because of this averaging.

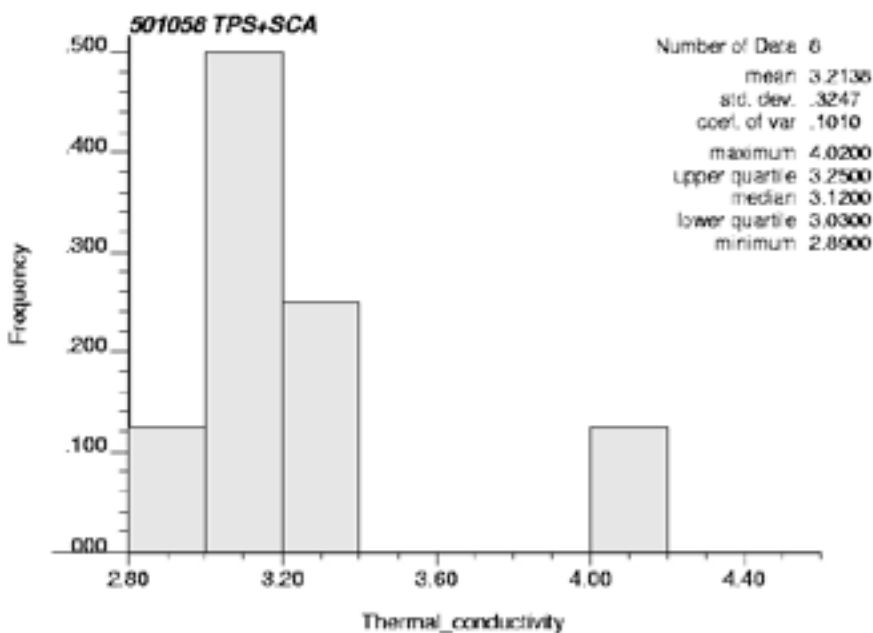
Histograms of thermal conductivity

Histograms of thermal conductivity for individual rock types based on TPS data alone or TPS and SCA data combined. Rock types not shown here can be found in the main report in Section 5.6.2.



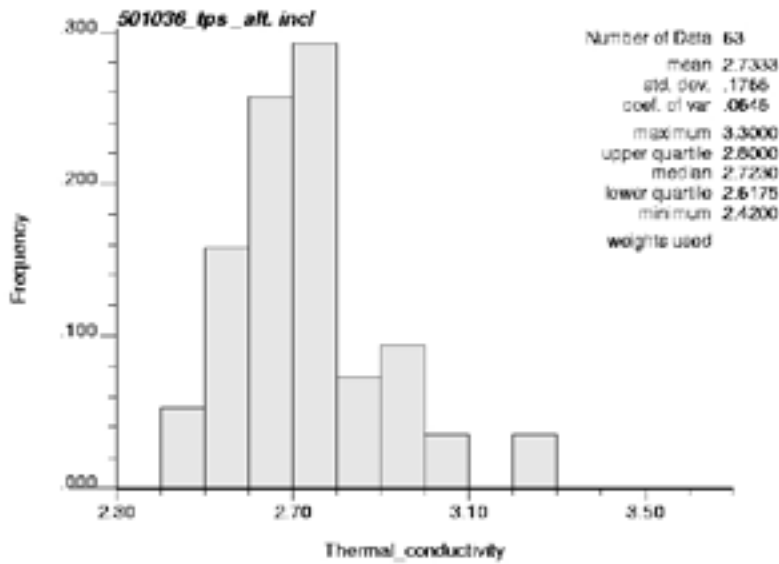
Ävrö granodiorite

Figure C-1. Histogram of thermal conductivity for Ävrö granodiorite (501056) based on TPS and SCA data. Altered samples included. Declustering weights used.



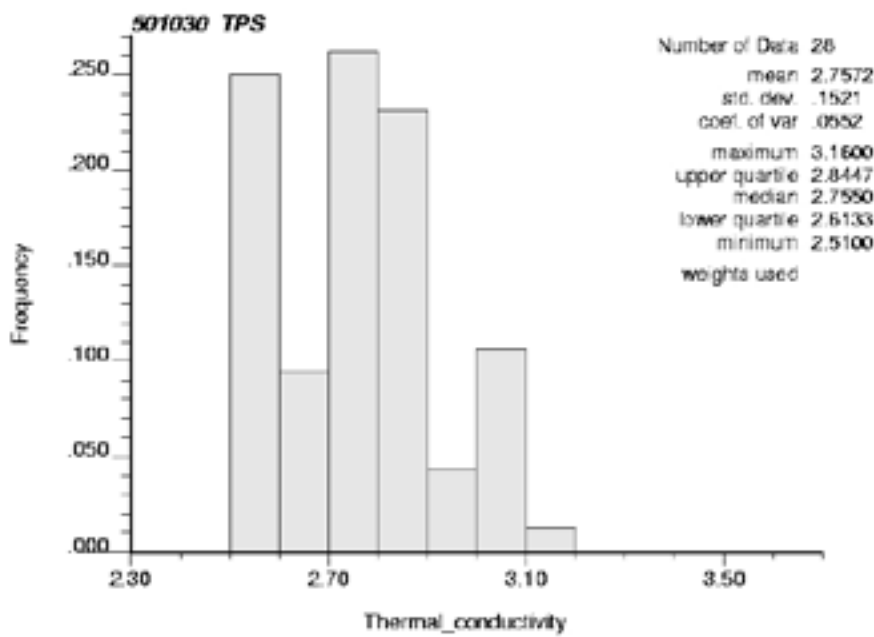
Fine-grained granite

Figure C-2. Histogram of thermal conductivity for granite (501058) based on TPS and SCA data.



Quartz monzodiorite

Figure C-3. Histogram of thermal conductivity for Quartz monzodiorite (501036) based on TPS data. Altered samples included. Declustering weights used.

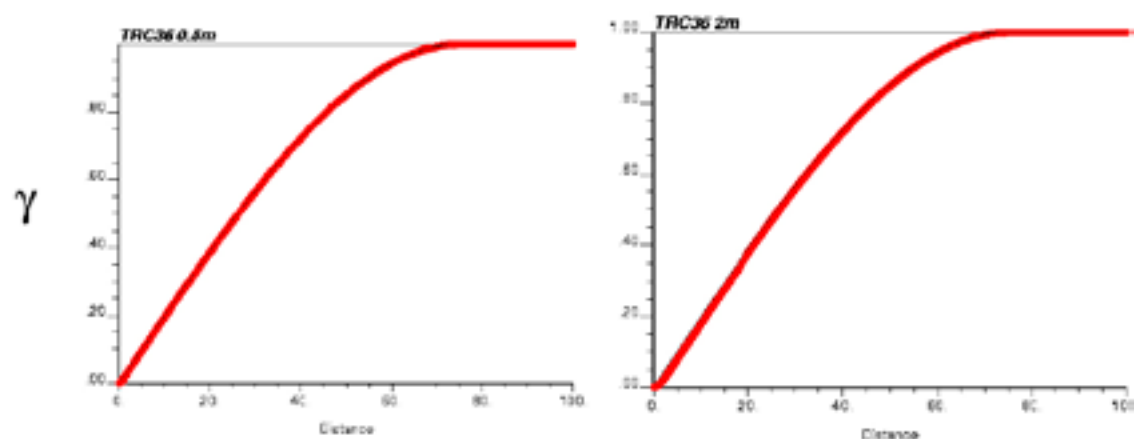


Fine-grained dioritoid

Figure C-4. Histogram of thermal conductivity for Fine-grained dioritoid (501030) based on TPS data. Declustering weights used.

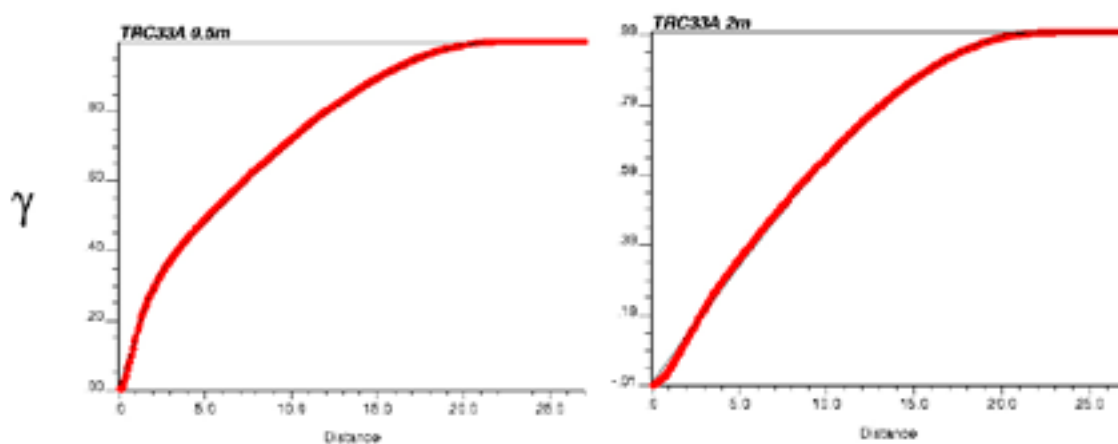
Variogram models

Variograms for scale 0.5 m and 2 m for each TRC are presented below. These models are based on upscaled 0.1 m models.



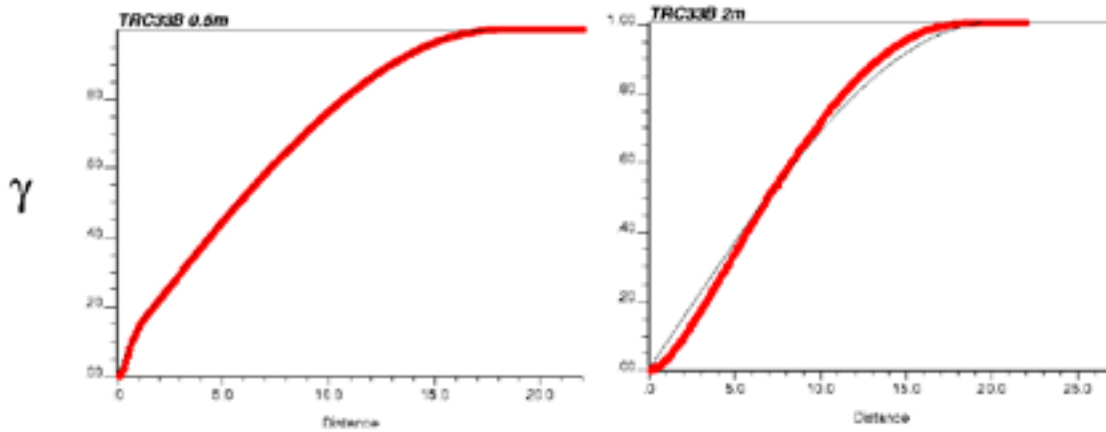
TRC 30 and TRC 36

Figure D-1. Variograms for TRC 30 and TRC 36 for 0.5 m and 2 m scales. Red dots represent the upscaled variogram from 0.1m to 0.5m and from 0.5 m to 2 m. Black lines are the fitted models.



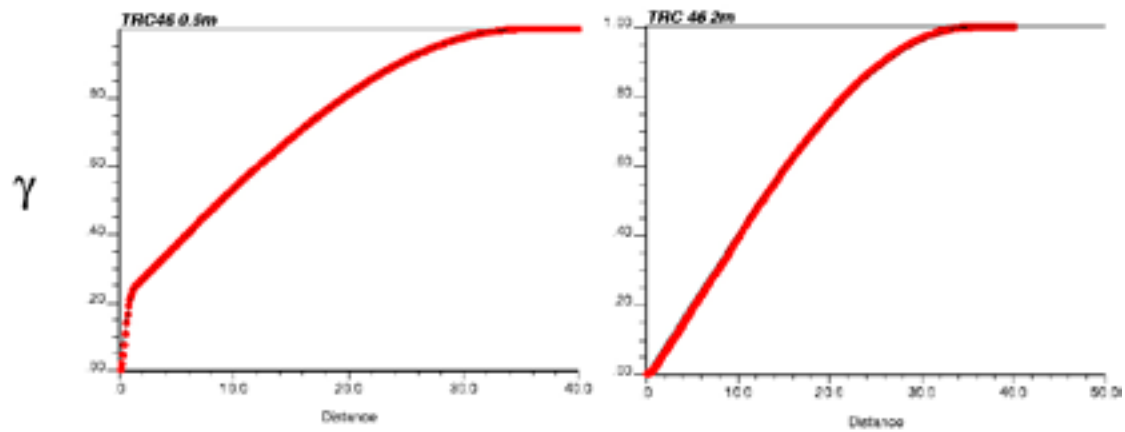
TRC 33A

Figure D-2. Variograms for TRC 33A for 0.5 m and 2 m scales. Red dots represent the upscaled variogram from 0.1m to 0.5m and from 0.5 m to 2 m. Black lines are the fitted models.



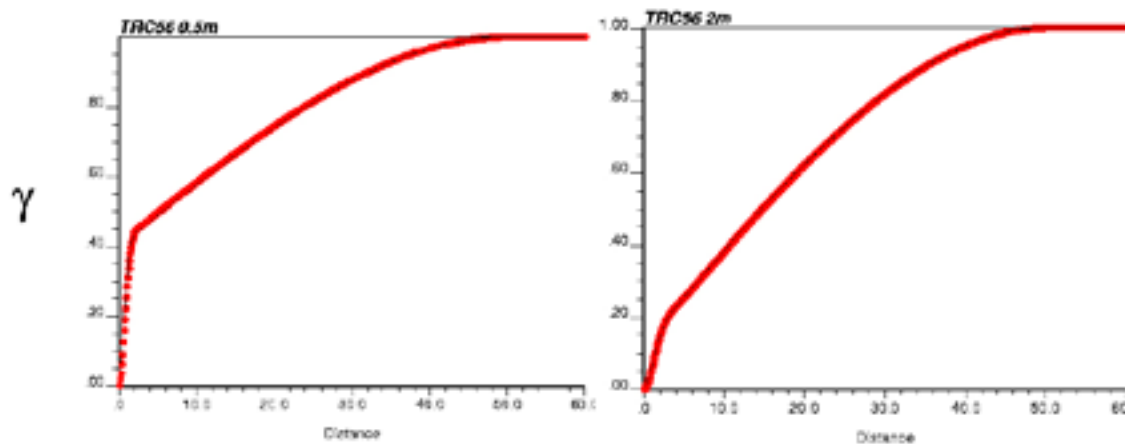
TRC 33B

Figure D-3. Variograms for TRC 33B for 0.5 m and 2 m scales. Red dots represent the upscaled variogram from 0.1m to 0.5m and from 0.5 m to 2 m. Black lines are the fitted models.



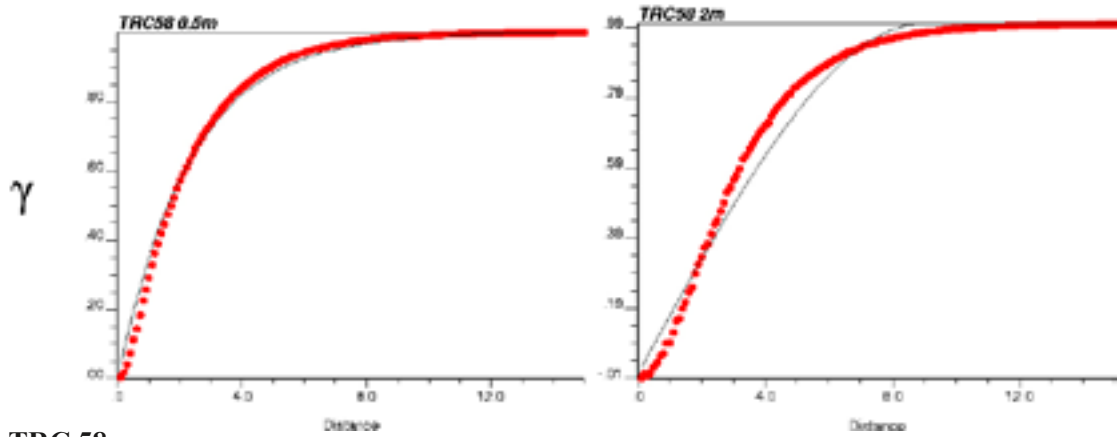
TRC 46

Figure D-4. Variograms for TRC 46 for 0.5 m and 2 m scales. Red dots represent the upscaled variogram from 0.1m to 0.5m and from 0.5 m to 2 m. Black lines are the fitted models.



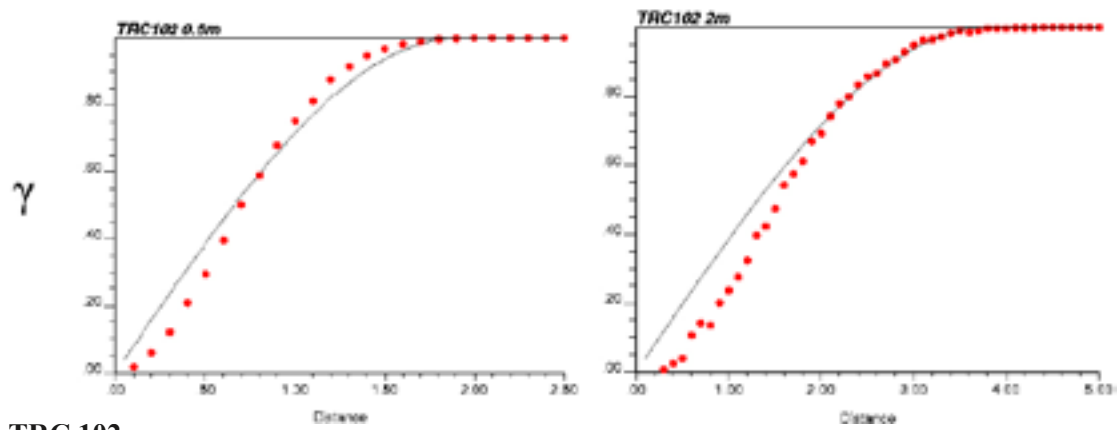
TRC56

Figure D-5. Variograms for TRC 56 for 0.5 m and 2 m scales. Red dots represent the upscaled variogram from 0.1m to 0.5m and from 0.5 m to 2 m. Black lines are the fitted models.



TRC 58

Figure D-6. Variograms for TRC 58 for 0.5 m and 2 m scales. Red dots represent the upscaled variogram from 0.1m to 0.5m and from 0.5 m to 2 m. Black lines are the fitted models.



TRC 102

Figure D-7. Variograms for TRC 102 for 0.5 m and 2 m scales. Red dots represent the upscaled variogram from 0.1m to 0.5m and from 0.5 m to 2 m. Black lines are the fitted models.

Variogram model reproduction

2 m simulations

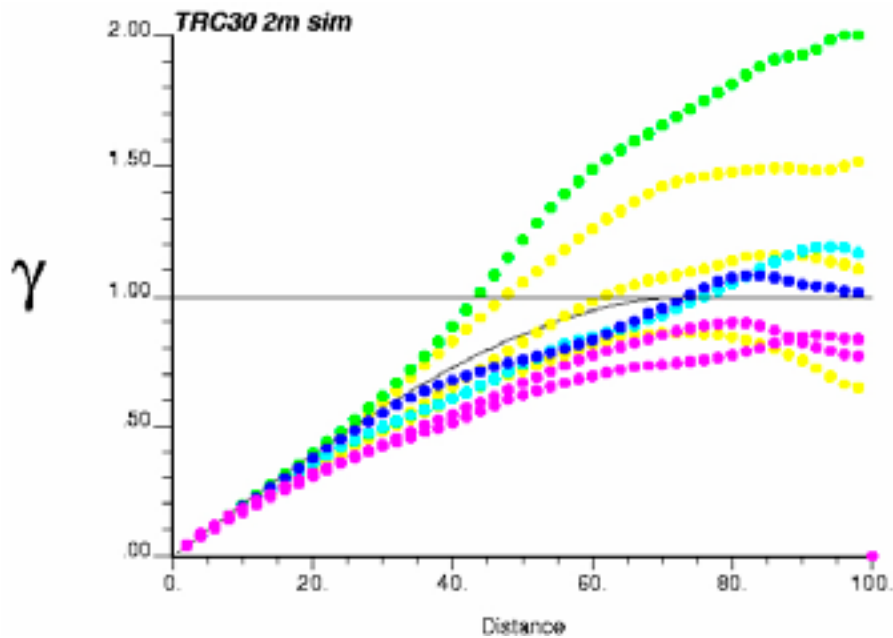


Figure E-1. Comparison of the variogram model and variograms of 8 independent realisations for TRC 30. Search options used in simulating: search radii – 60 m; no. of simulated nodes – 32; multiple grid search – yes; no of multiple grid refinements – 3. Lag distance (x axis) in metres (m). Variogram is standardised to the variance of the simulated values.

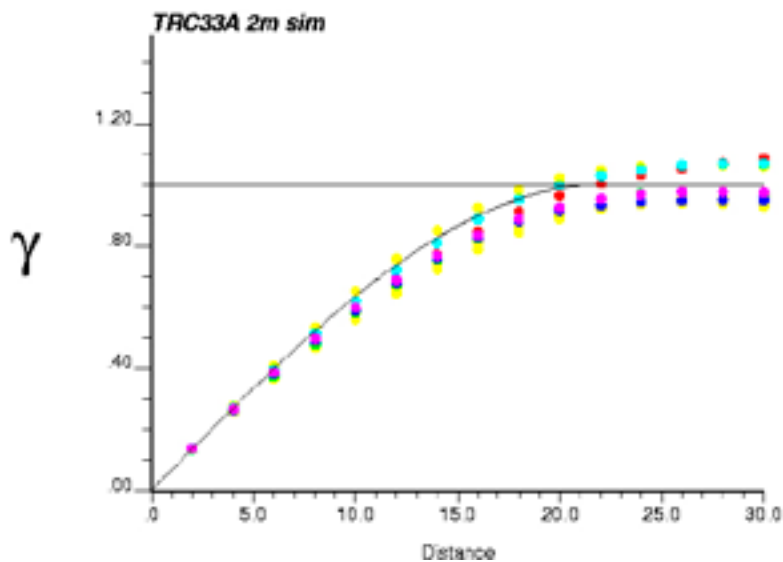


Figure E-2. Comparison of the variogram model and variograms of 8 independent realisations for TRC 33A. Search options used in simulating: search radii – 20 m; no. of simulated nodes – 32; multiple grid search – yes; no of multiple grid refinements – 3. Lag distance (x axis) in metres (m). Variogram is standardised to the variance of the simulated values.

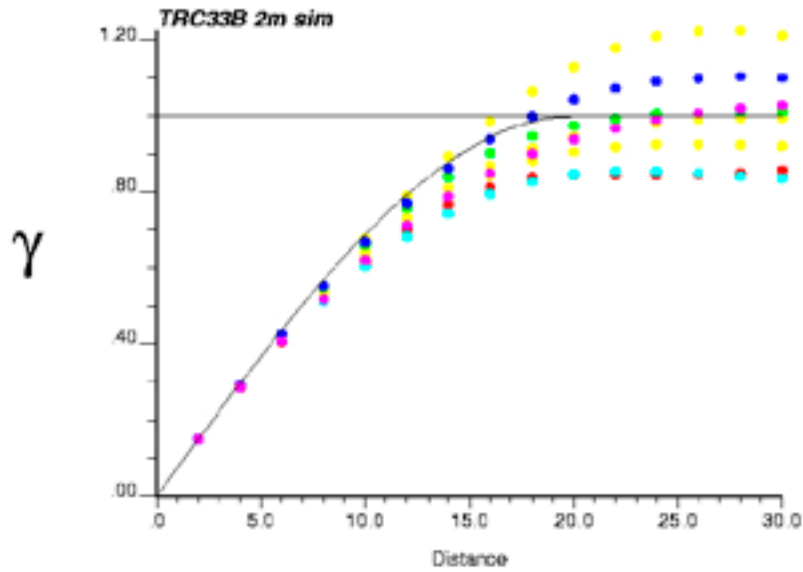


Figure E-3. Comparison of the variogram model and variograms of 8 independent realisations for TRC 33B. Search options used in simulating: search radii – 20 m; no. of simulated nodes – 32; multiple grid search – yes; no of multiple grid refinements – 3. Lag distance (x axis) in metres (m). Variogram is standardised to the variance of the simulated values.

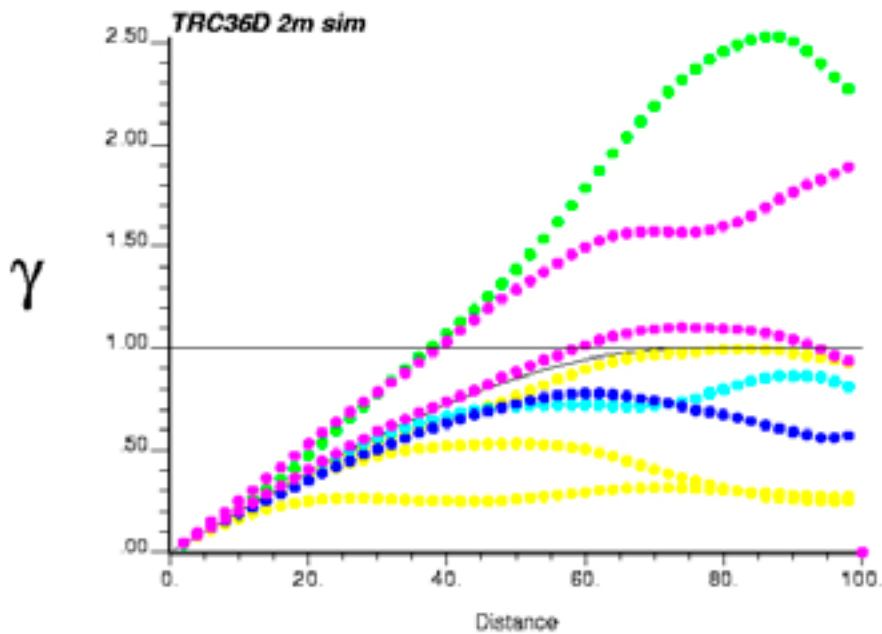


Figure E-4. Comparison of the variogram model and variograms of 8 independent realisations for TRC 36. Search options used in simulating: search radii – 60 m; no. of simulated nodes – 32; multiple grid search – yes; no of multiple grid refinements – 3. Lag distance (x axis) in metres (m). Variogram is standardised to the variance of the simulated values.

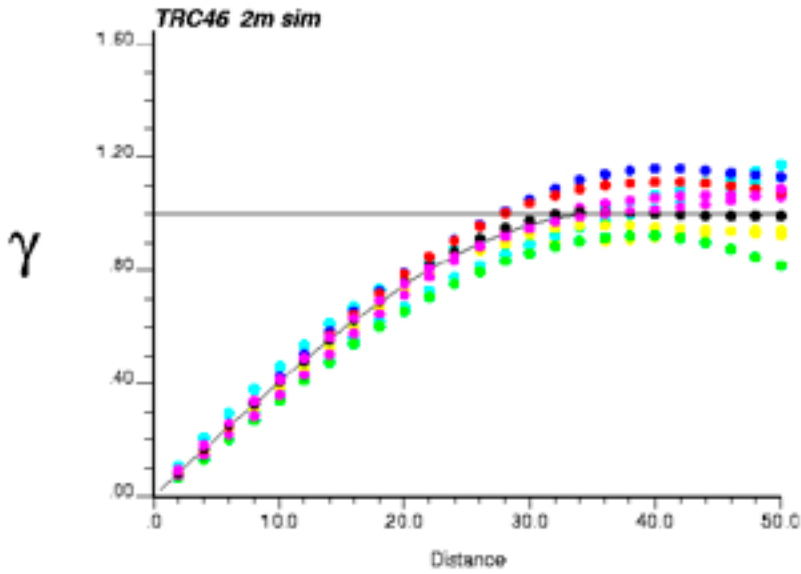


Figure E-5. Comparison of the variogram model and variograms of 8 independent realisations for TRC 46. Search options used in simulating: search radii – 36 m; no. of simulated nodes – 32; multiple grid search – yes; no of multiple grid refinements – 3. Lag distance (x axis) in metres (m). Variogram is standardised to the variance of the simulated values.

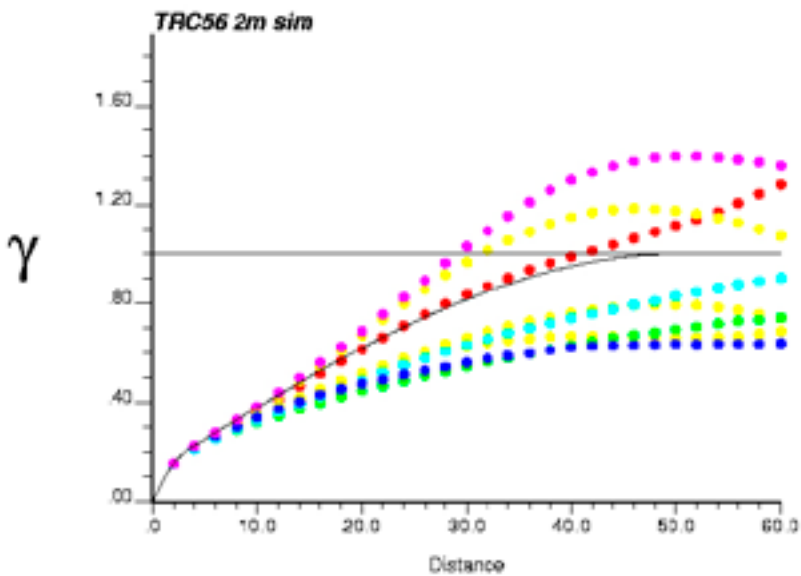


Figure E-6. Comparison of the variogram model and variograms of 8 independent realisations for TRC 56. Search options used in simulating: search radii – 30 m; no. of simulated nodes – 32; multiple grid search – yes; no of multiple grid refinements – 3. Lag distance (x axis) in metres (m). Variogram is standardised to the variance of the simulated values.

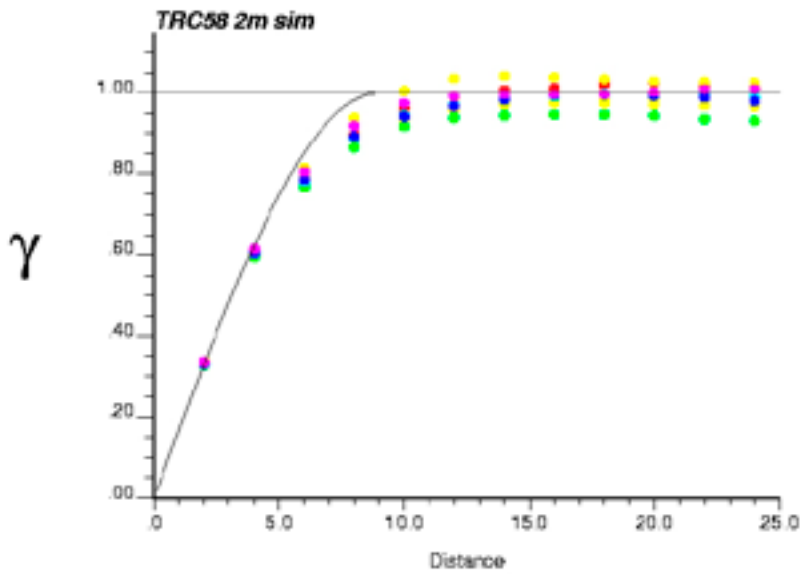


Figure E-7. Comparison of the variogram model and variograms of 8 independent realisations for TRC 58. Search options used in simulating: search radii – 6 m; no. of simulated nodes – 32; multiple grid search – yes; no of multiple grid refinements – 3. Lag distance (x axis) in metres (m). Variogram is standardised to the variance of the simulated values.

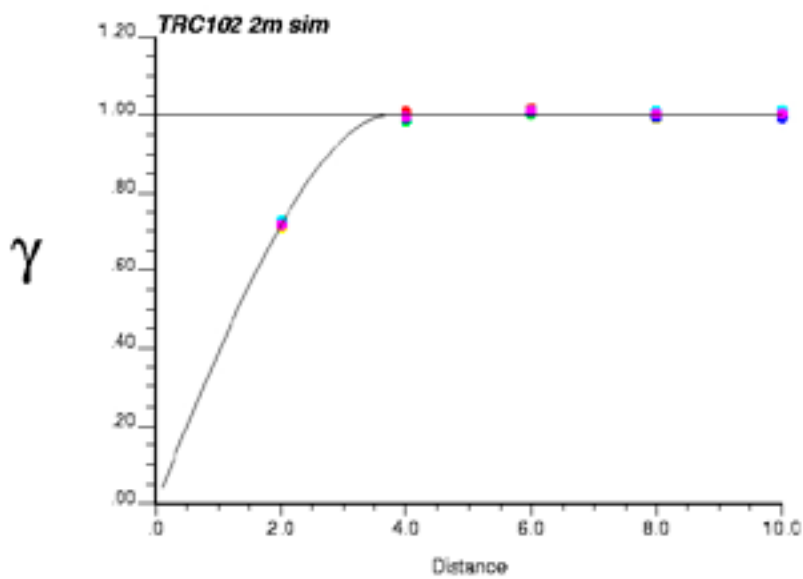


Figure E-8. Comparison of the variogram model and variograms of 8 independent realisations for TRC 102. Search options used in simulating: search radii – 4 m; no. of simulated nodes – 32; multiple grid search – yes; no of multiple grid refinements – 3. Lag distance (x axis) in metres (m). Variogram is standardised to the variance of the simulated values.

Histograms of thermal conductivity – simulations for each TRC
TRC 30

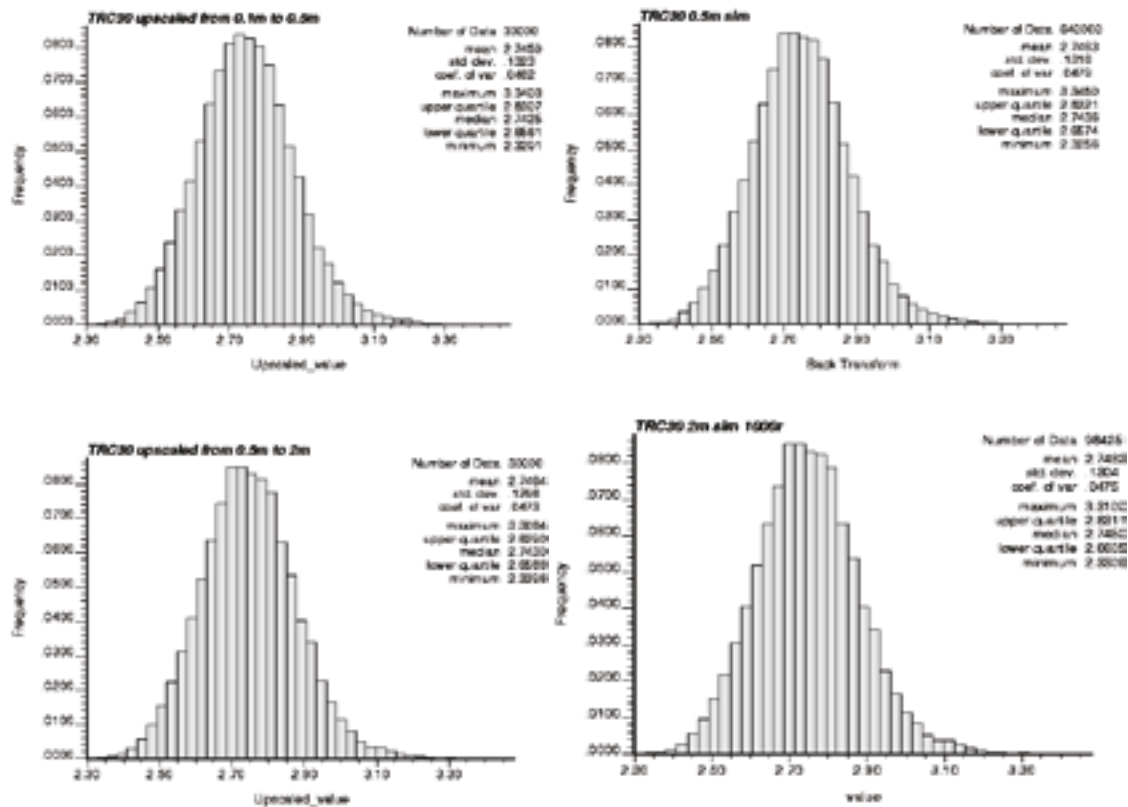


Figure F-1. Histograms of simulation results for TRC 30: 0.1 m simulations upscaled to 0.5 m, 0.5 m simulations, 0.5 m simulations upscaled to 2 m, and 2 m simulations. The histogram of the 2 m simulations are based on 1,000 realisations. The lower left histogram is used as a distribution model in the 2 m simulations.

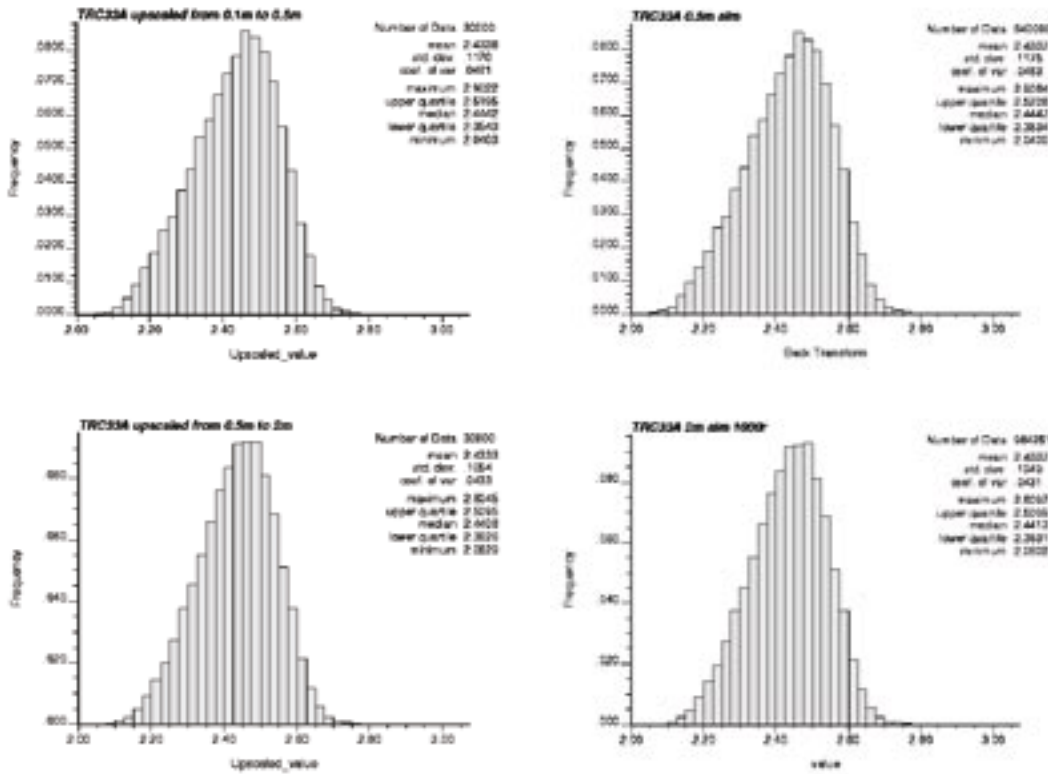


Figure F-2. Histograms of simulation results for TRC 33A: 0.1 m simulations upscaled to 0.5 m, 0.5 m simulations, 0.5 m simulations upscaled to 2 m, and 2 m simulations. The histogram of the 2 m simulations are based on 1,000 realisations. The lower left histogram is used as a distribution model in the 2 m simulations.

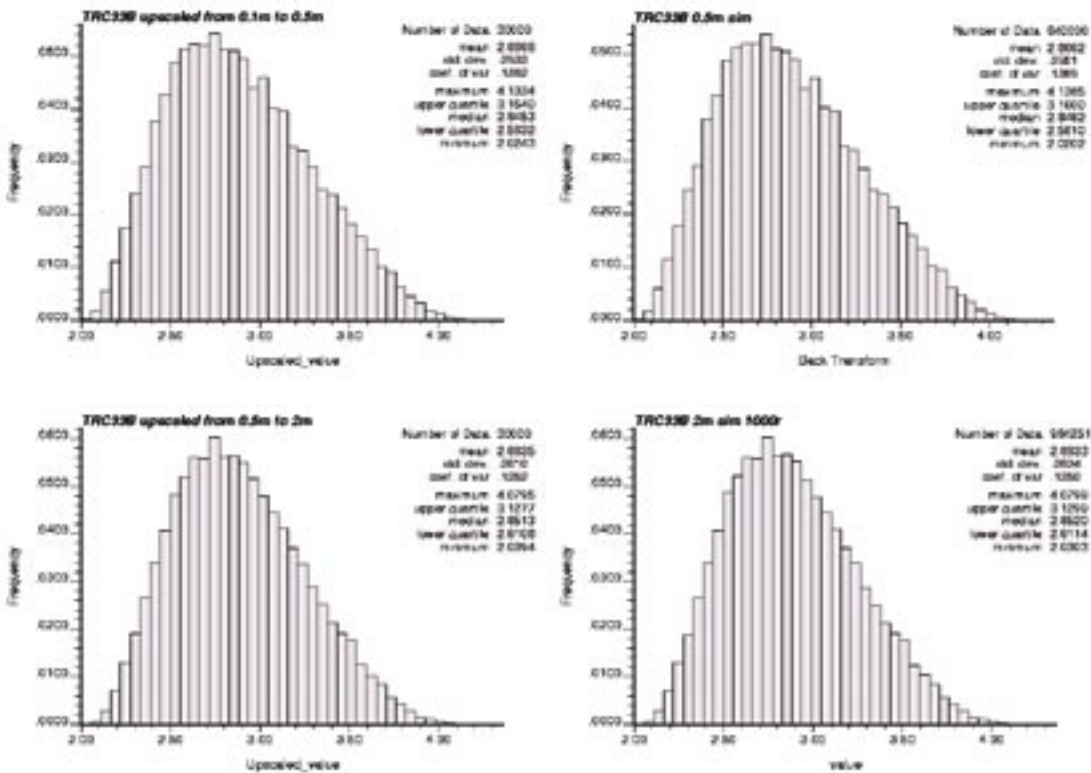


Figure F-3. Histograms of simulation results for TRC 33B: 0.1 m simulations upscaled to 0.5 m, 0.5 m simulations, 0.5 m simulations upscaled to 2 m, and 2 m simulations. The histogram of the 2 m simulations are based on 1,000 realisations. The lower left histogram is used as a distribution model in the 2 m simulations.

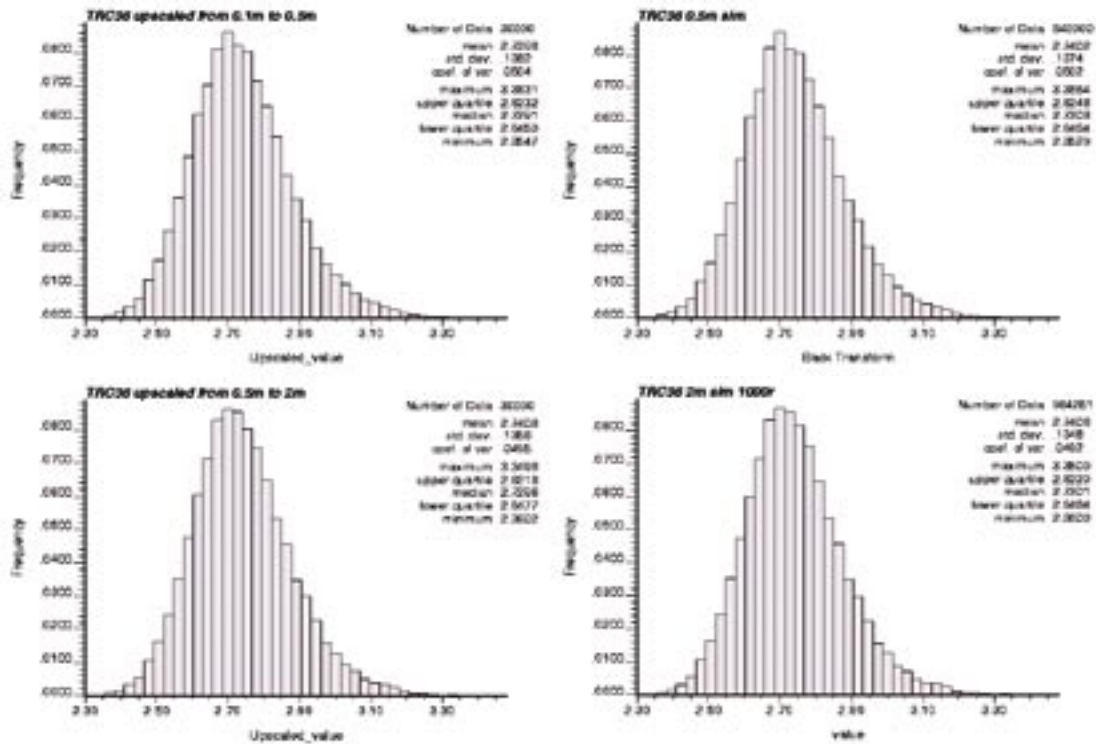


Figure F-4. Histograms of simulation results for **TRC 36**: 0.1 m simulations upscaled to 0.5 m, 0.5 m simulations upscaled to 2 m, and 2 m simulations. The histogram of the 2 m simulations are based on 1,000 realisations. The lower left histogram is used as a distribution model in the 2 m simulations.

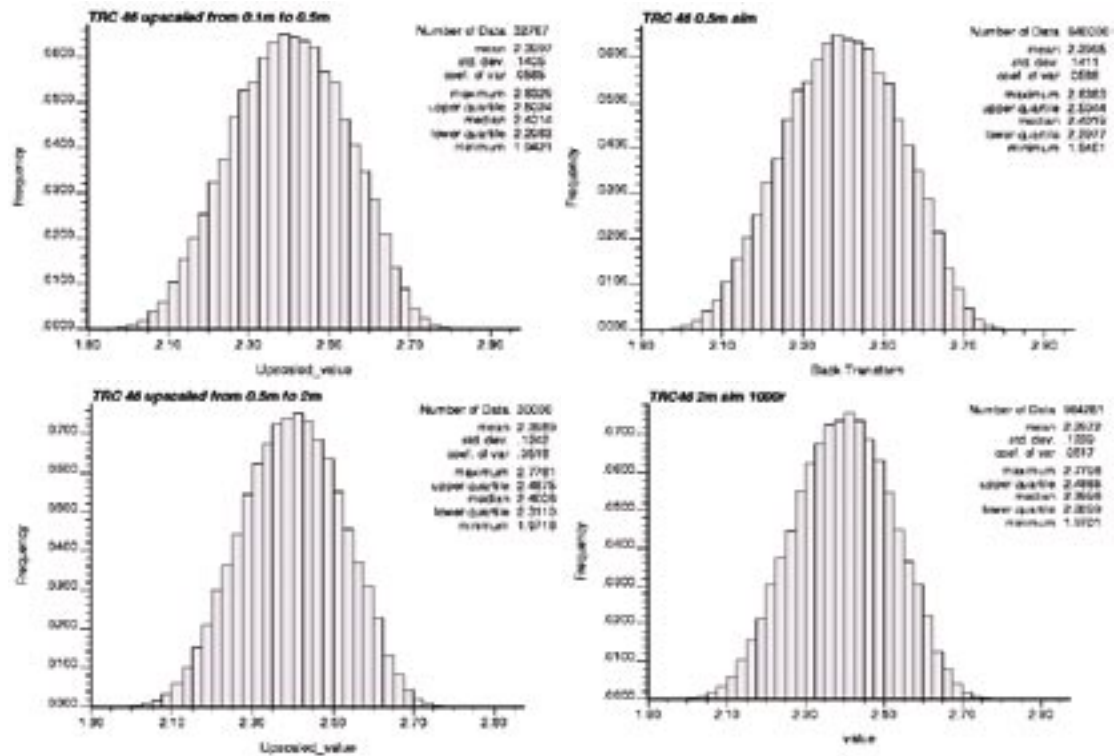


Figure F-5. Histograms of simulation results for **TRC 46**: 0.1 m simulations upscaled to 0.5 m, 0.5 m simulations upscaled to 2 m, and 2 m simulations. The histogram of the 2 m simulations are based on 1,000 realisations. The lower left histogram is used as a distribution model in the 2 m simulations.

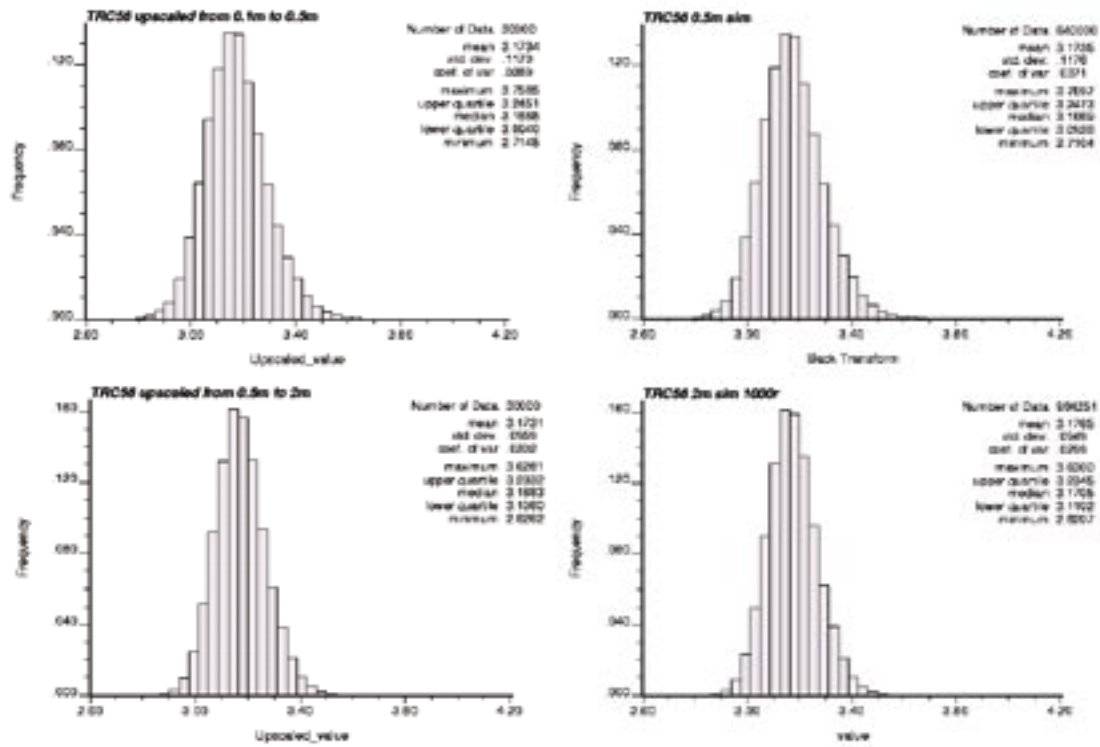


Figure F-6. Histograms of simulation results for TRC 56: 0.1 m simulations upscaled to 0.5 m, 0.5 m simulations, 0.5 m simulations upscaled to 2 m, and 2 m simulations. The histogram of the 2 m simulations are based on 1,000 realisations. The lower left histogram is used as a distribution model in the 2 m simulations.

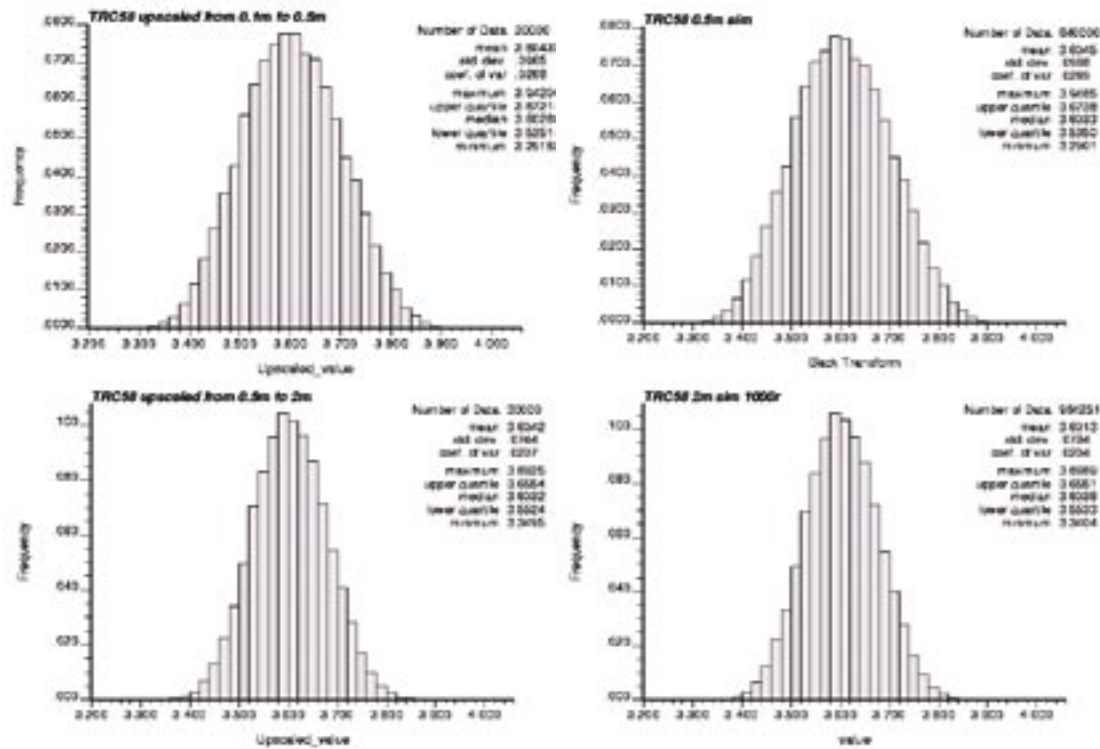


Figure F-7. Histograms of simulation results for TRC 58: 0.1 m simulations upscaled to 0.5 m, 0.5 m simulations, 0.5 m simulations upscaled to 2 m, and 2 m simulations. The histogram of the 2 m simulations are based on 1,000 realisations. The lower left histogram is used as a distribution model in the 2 m simulations.

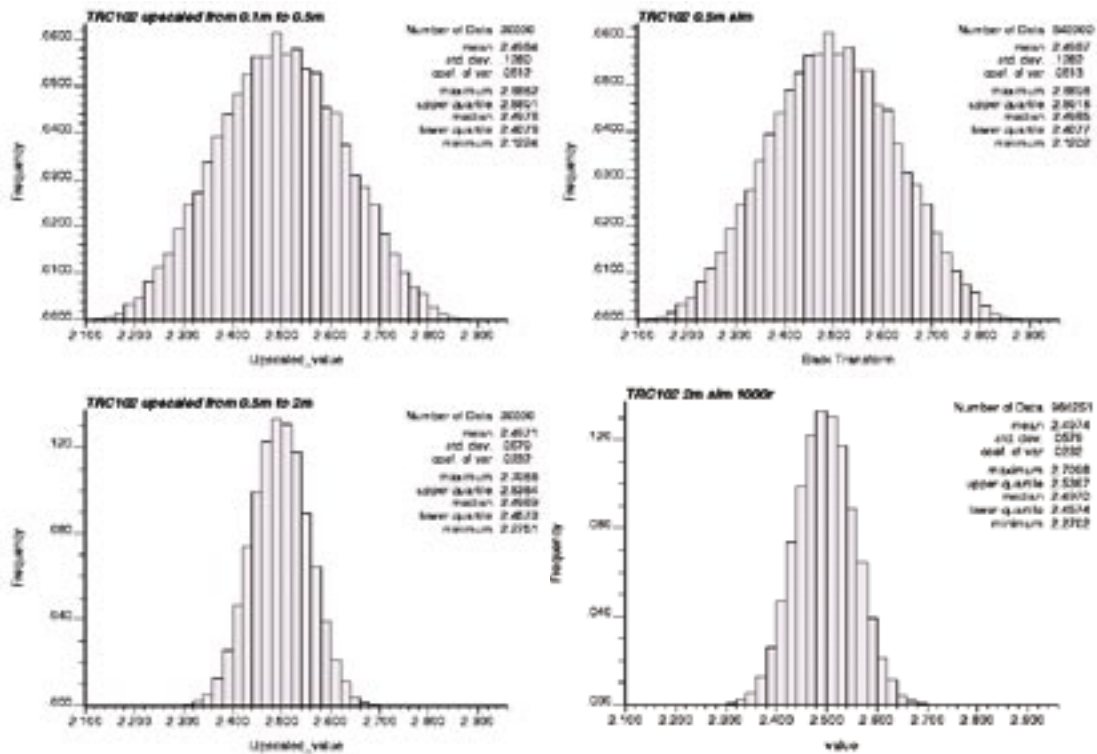


Figure F-8. Histograms of simulation results for TRC 102: 0.1 m simulations upscaled to 0.5 m, 0.5 m simulations, 0.5 m simulations upscaled to 2 m, and 2 m simulations. The histogram of the 2 m simulations are based on 1,000 realisations. The lower left histogram is used as a distribution model in the 2 m simulations.

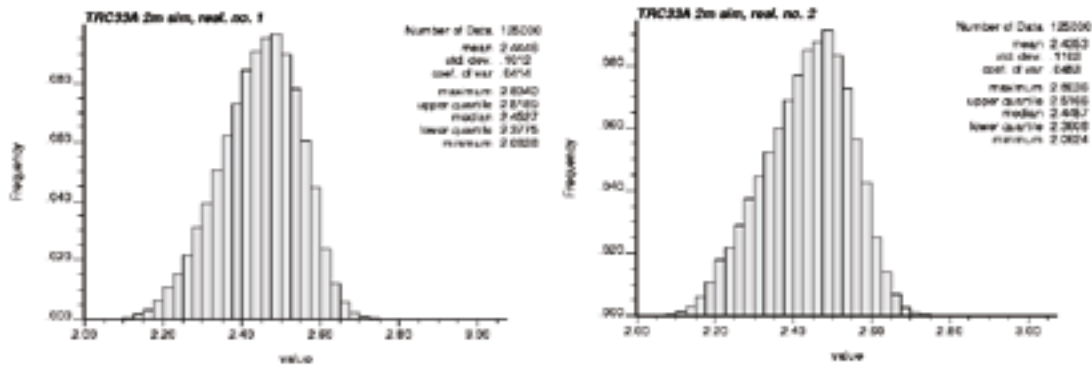


Figure F-9. Histograms of two individual realisations at 2 m scale for TRC 33A.

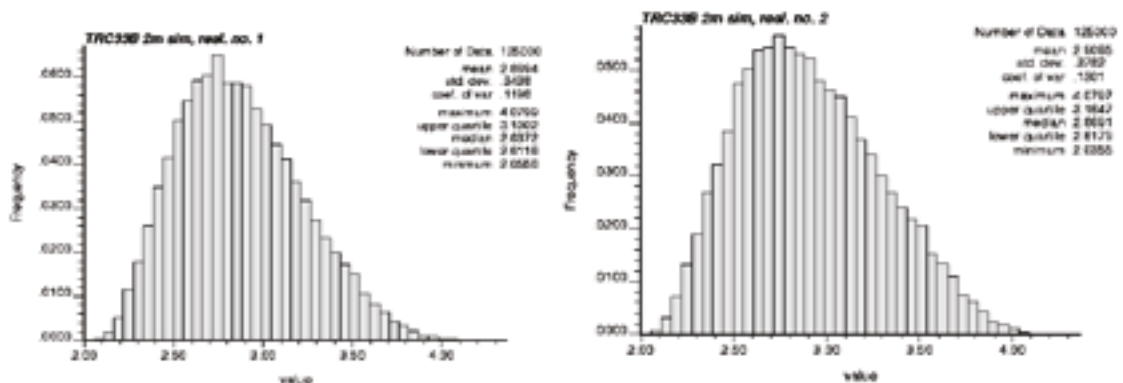


Figure F-10. Histograms of two individual realisations at 2 m scale for TRC 33B.

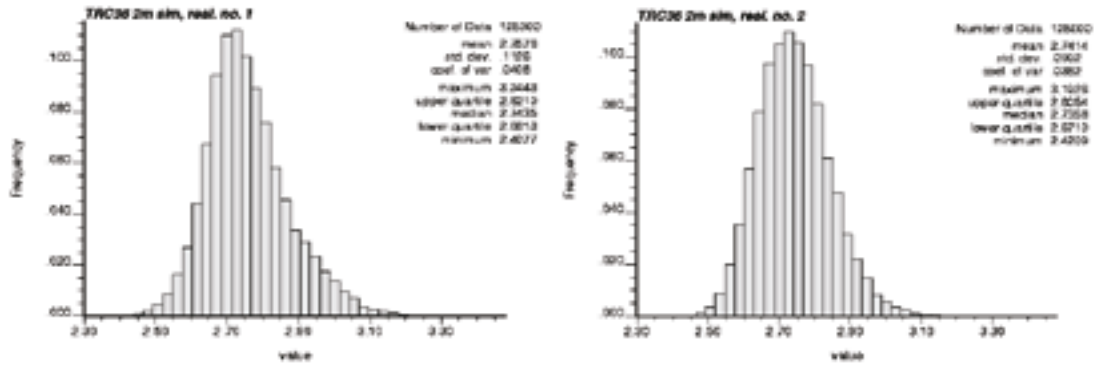


Figure F-11. Histograms of two individual realisations at 2 m scale for TRC 36.

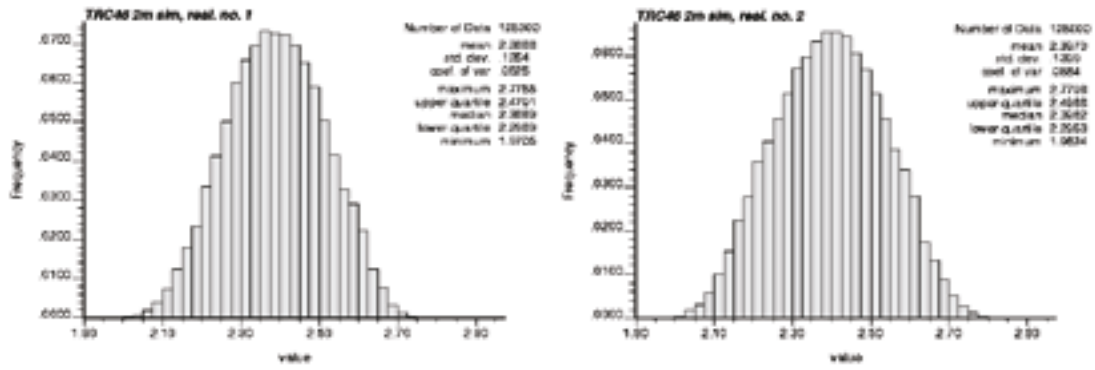


Figure F-12. Histograms of two individual realisations at 2 m scale for TRC 46.

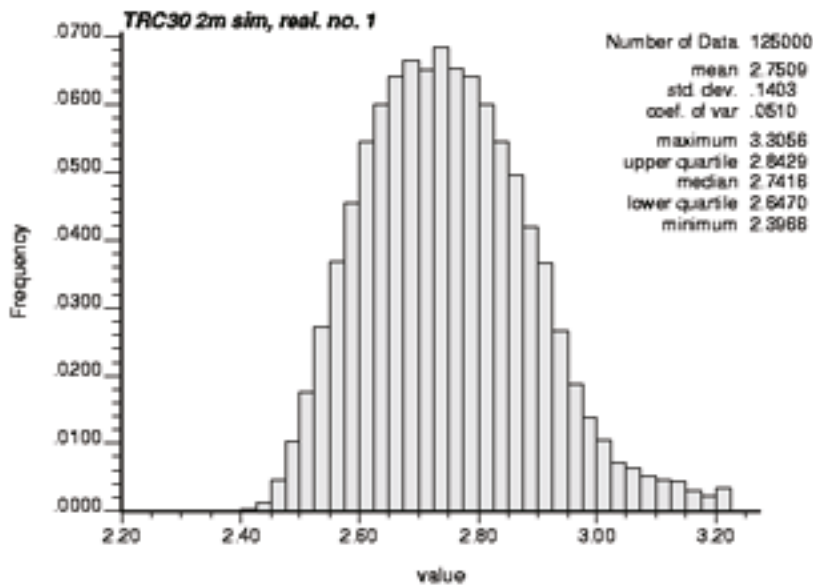


Figure F-13. Histogram of individual realisations at 2 m scale for TRC 30.

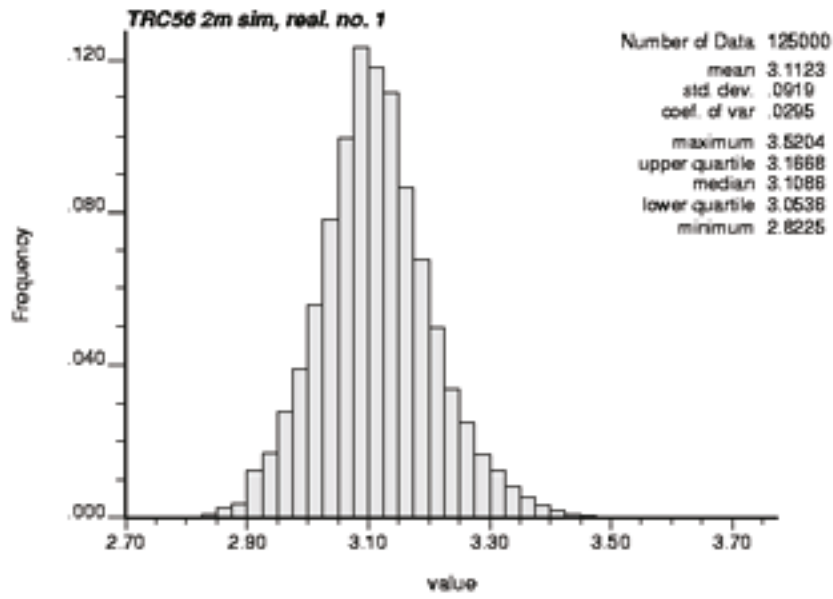


Figure F-14. Histogram of one realisation at 2 m scale for TRC 56.

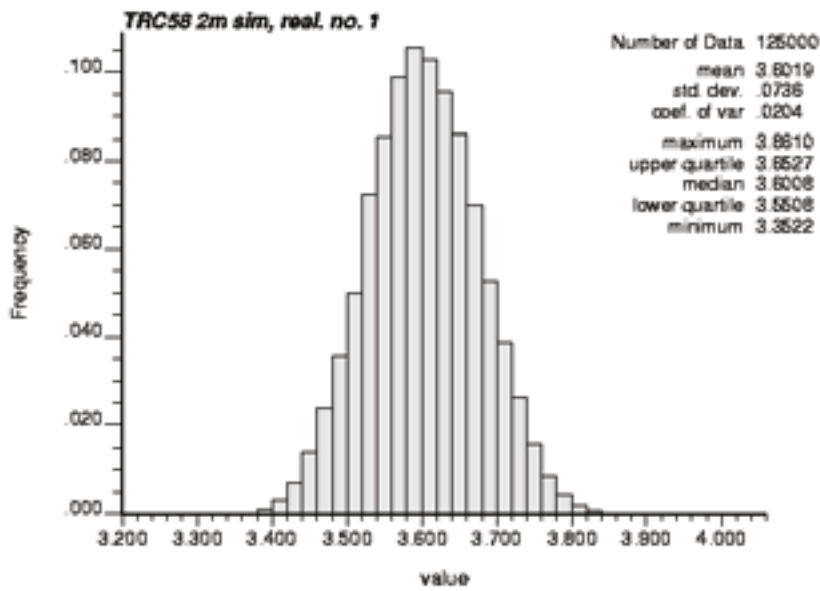


Figure F-15. Histogram of one realisation at 2 m scale for TRC 58.

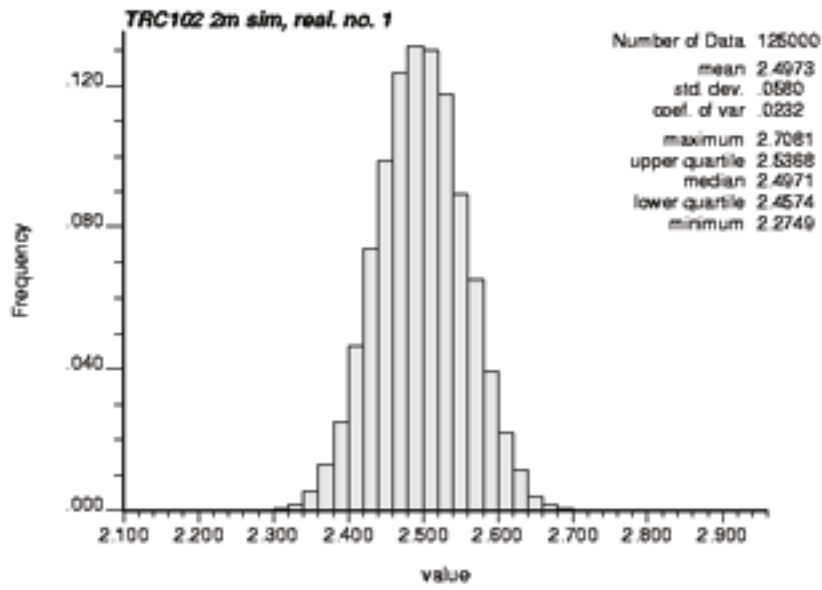


Figure F-16. Histogram of one realisation at 2 m scale for TRC 102.

Visualisations of TRC thermal realisations

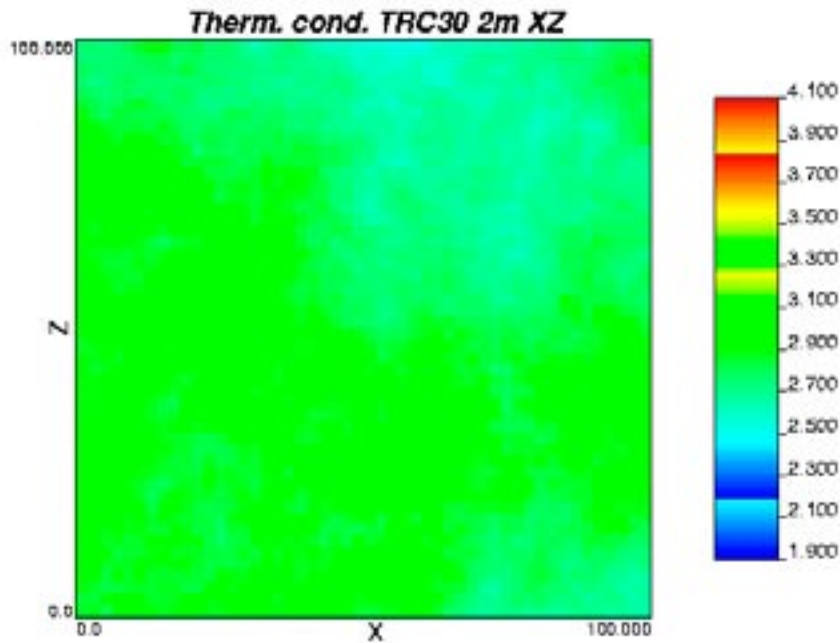


Figure G-1. 2D slice from one 3D realisation (simulation scale = 2 m) illustrating the distribution of thermal conductivity values in TRC 30. $R=1$, Slice=25, xz -plane.

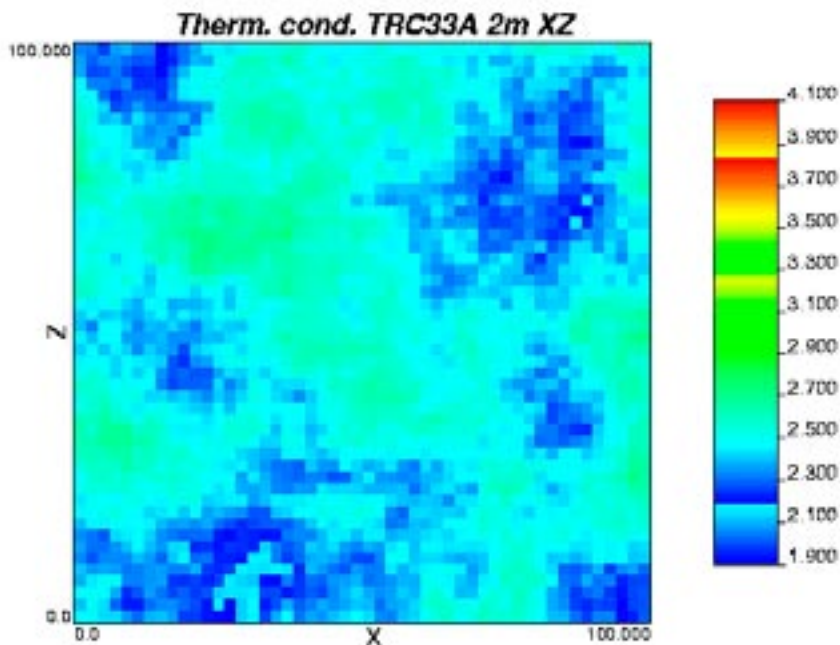


Figure G-2. 2D slice from one 3D realisation (simulation scale = 2 m) illustrating the distribution of thermal conductivity values in TRC 33A. $R=1$, Slice=25, xz -plane.

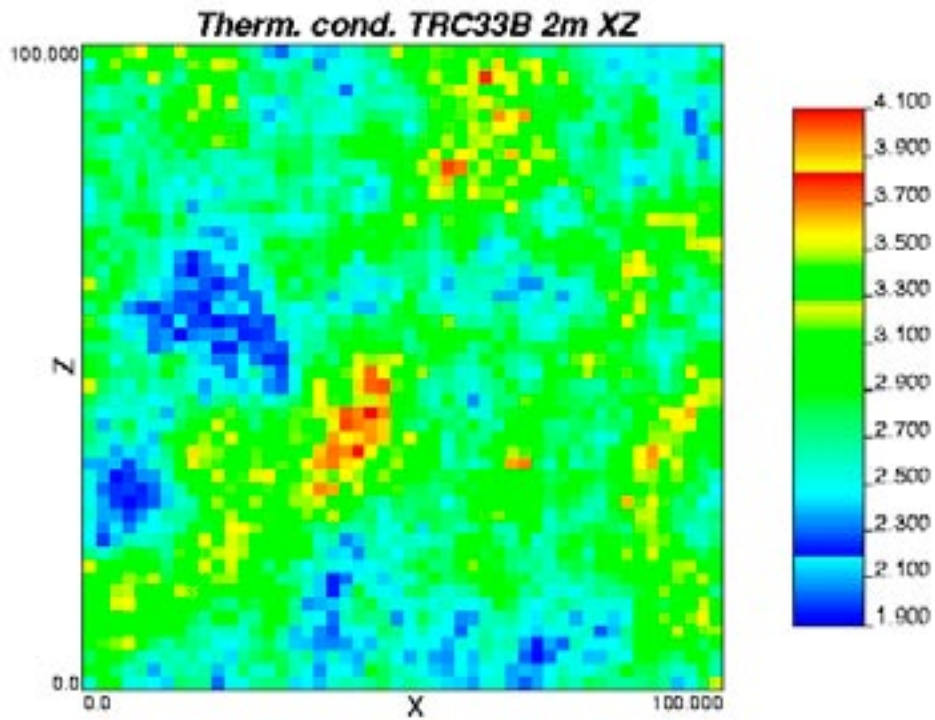


Figure G-3. 2D slice from one 3D realisation (simulation scale = 2 m) illustrating the distribution of thermal conductivity values in TRC 33B. R=1, Slice=25, xz-plane.

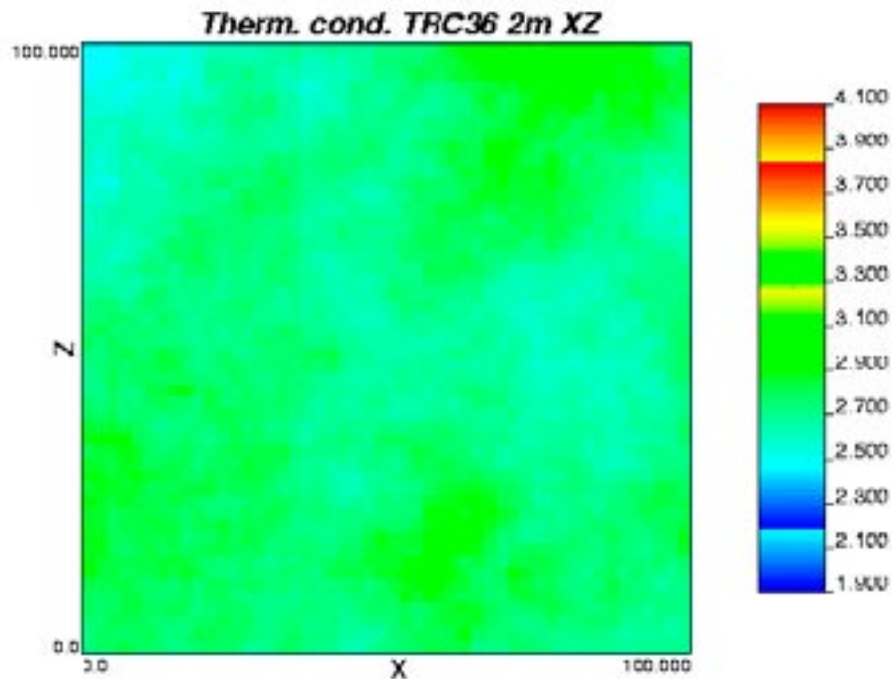


Figure G-4. 2D slice from one 3D realisation (simulation scale = 2 m) illustrating the distribution of thermal conductivity values in TRC 36. R=1, Slice=25, xz-plane.

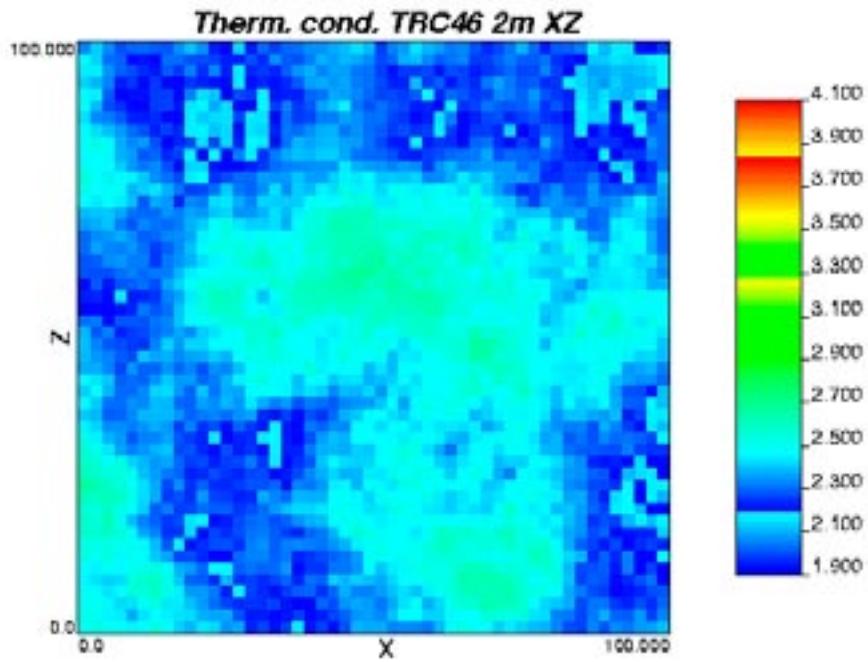


Figure G-5. 2D slice from one 3D realisation (simulation scale = 2 m) illustrating the distribution of thermal conductivity values in TRC 46. $R=1$, Slice=25, xz-plane.

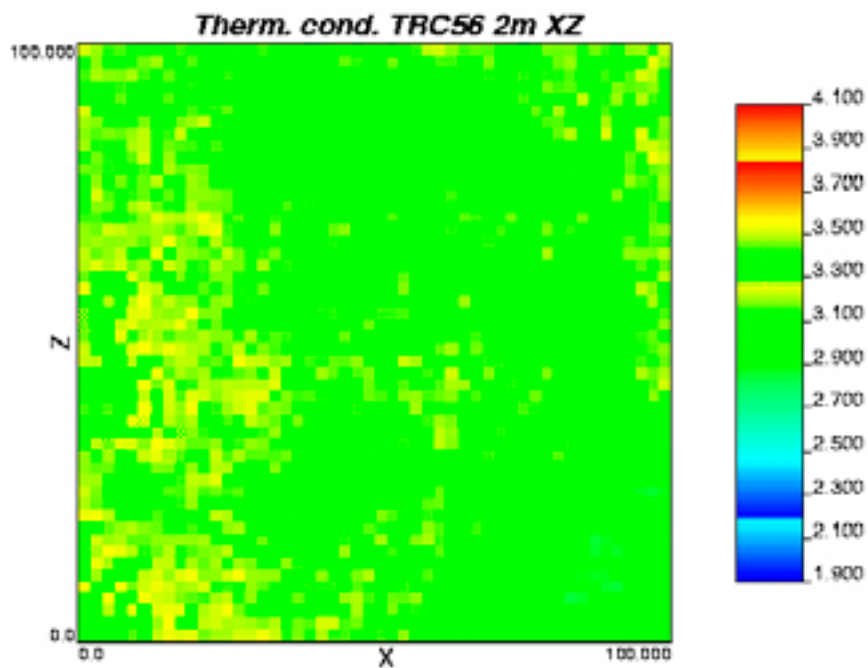


Figure G-6. 2D slice from one 3D realisation (simulation scale = 2 m) illustrating the distribution of thermal conductivity values in TRC 56. $R=1$, Slice=25, xz-plane.

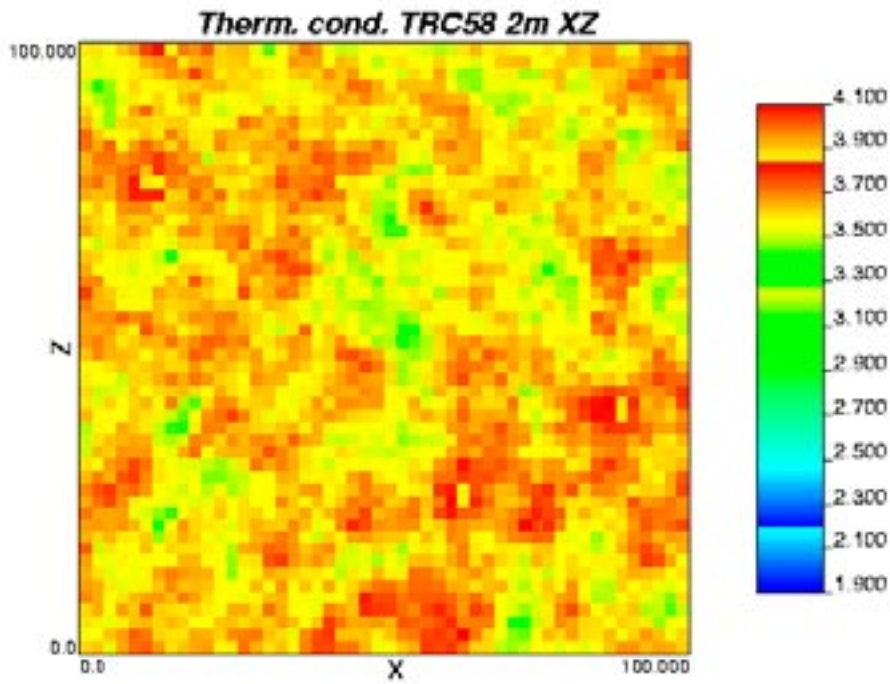


Figure G-7. 2D slice from one 3D realisation (simulation scale = 2 m) illustrating the distribution of thermal conductivity values in TRC 58. R=1, Slice=25, xz-plane.

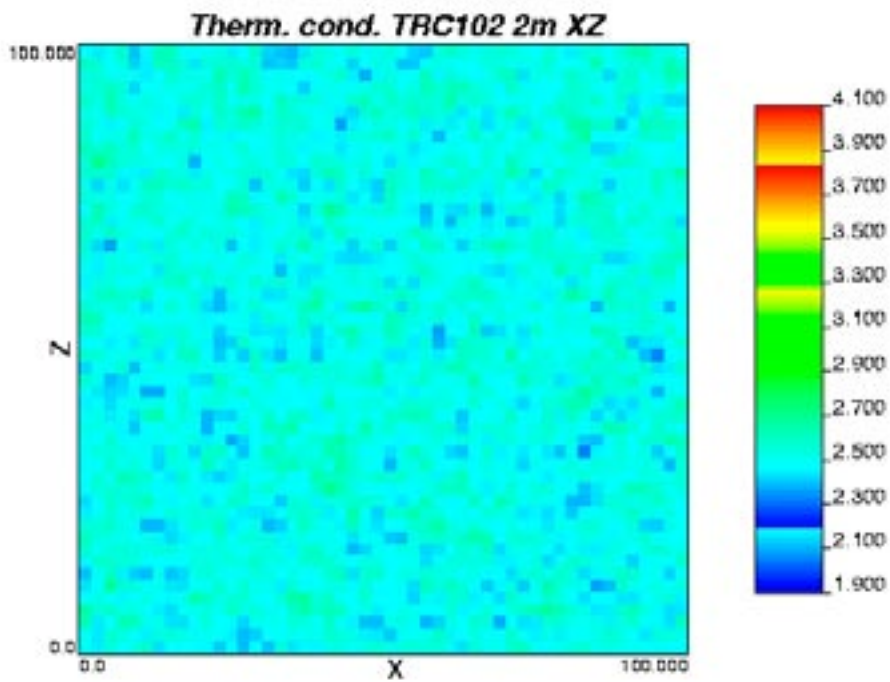


Figure G-8. 2D slice from one 3D realisation (simulation scale = 2 m) illustrating the distribution of thermal conductivity values in TRC 102. R=1, Slice=25, xz-plane.

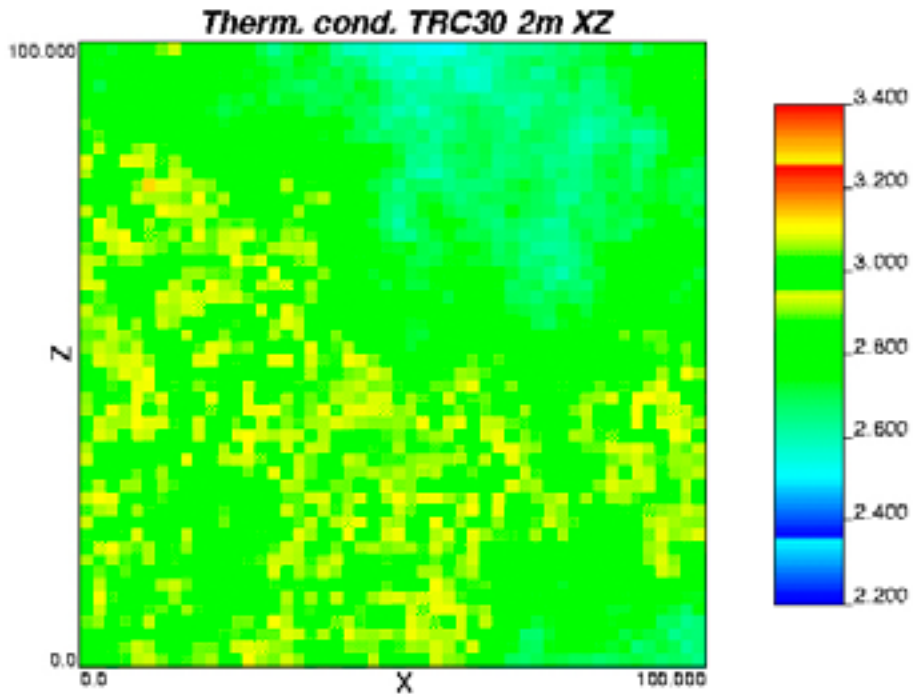


Figure G-9. 2D slice from one 3D realisation (simulation scale = 2 m) illustrating the distribution of thermal conductivity values in TRC 30. R=1, Slice=25, xz-plane. TRC-unique legend scale.

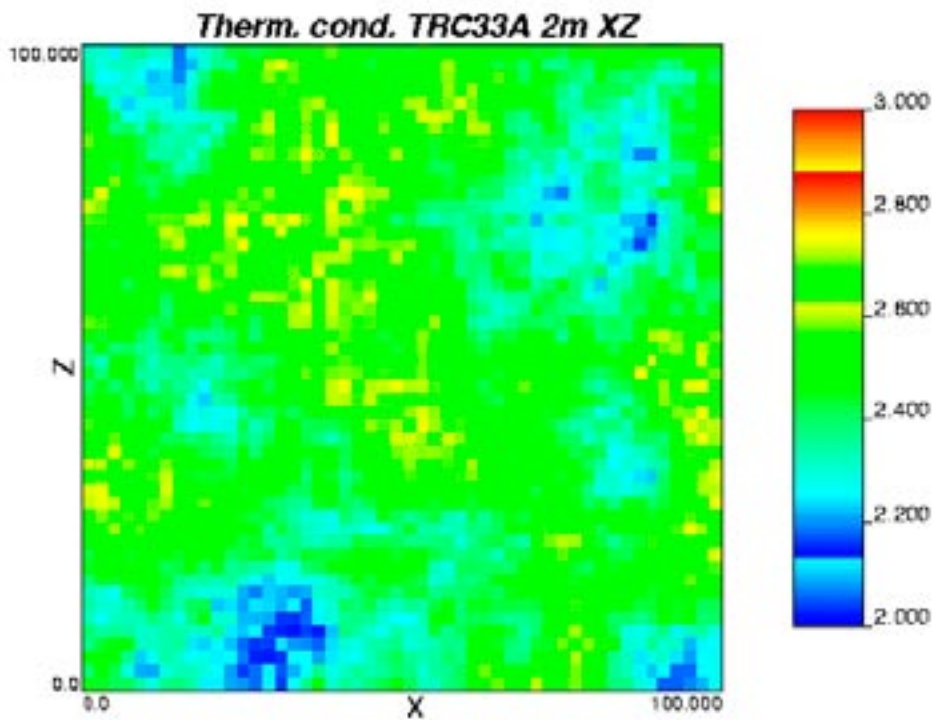


Figure G-10. 2D slice from one 3D realisation (simulation scale = 2 m) illustrating the distribution of thermal conductivity values in TRC 33A. R=1, Slice=25, xz-plane. TRC-unique legend scale.

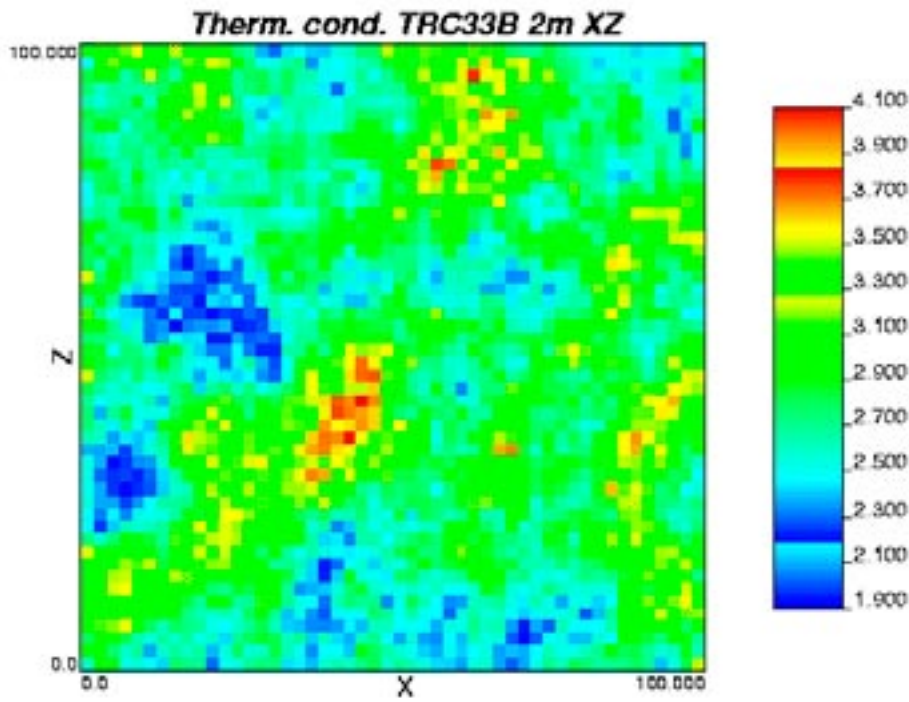


Figure G-11. 2D slice from one 3D realisation (simulation scale = 2 m) illustrating the distribution of thermal conductivity values in TRC 33B. R=1, Slice=25, xz-plane. TRC-unique legend scale.

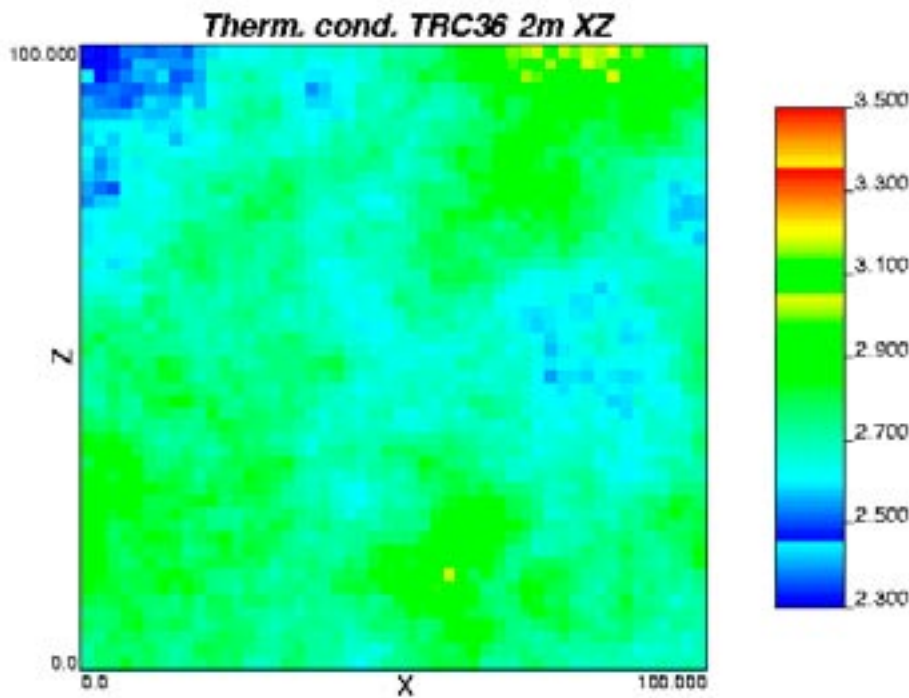


Figure G-12. 2D slice from one 3D realisation (simulation scale = 2 m) illustrating the distribution of thermal conductivity values in TRC 36. R=1, Slice=25, xz-plane. TRC-unique legend scale.

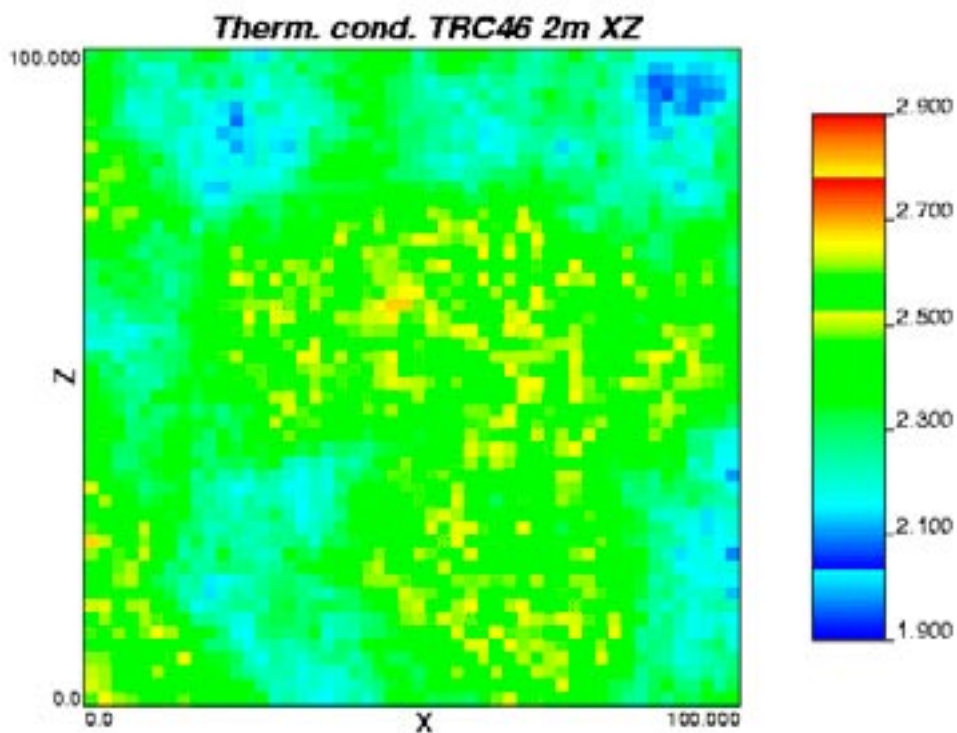


Figure G-13. 2D slice from one 3D realisation (simulation scale = 2 m) illustrating the distribution of thermal conductivity values in TRC 46. $R=1$, Slice=25, xz -plane. TRC-unique legend scale.

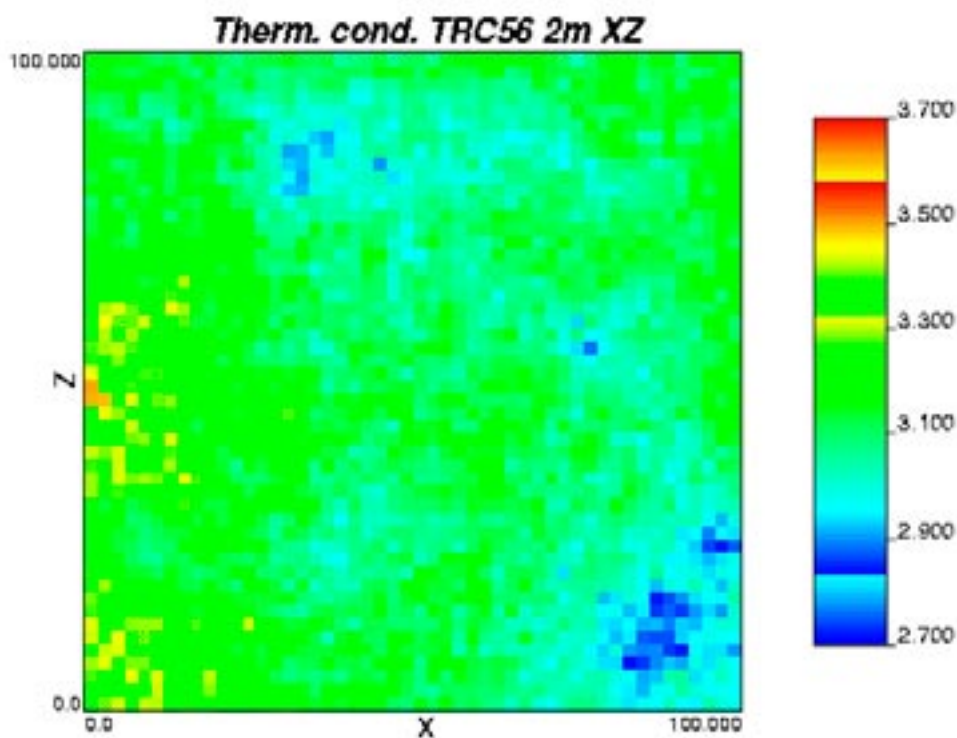


Figure G-14. 2D slice from one 3D realisation (simulation scale = 2 m) illustrating the distribution of thermal conductivity values in TRC 56. $R=1$, Slice=25, xz -plane. TRC-unique legend scale.

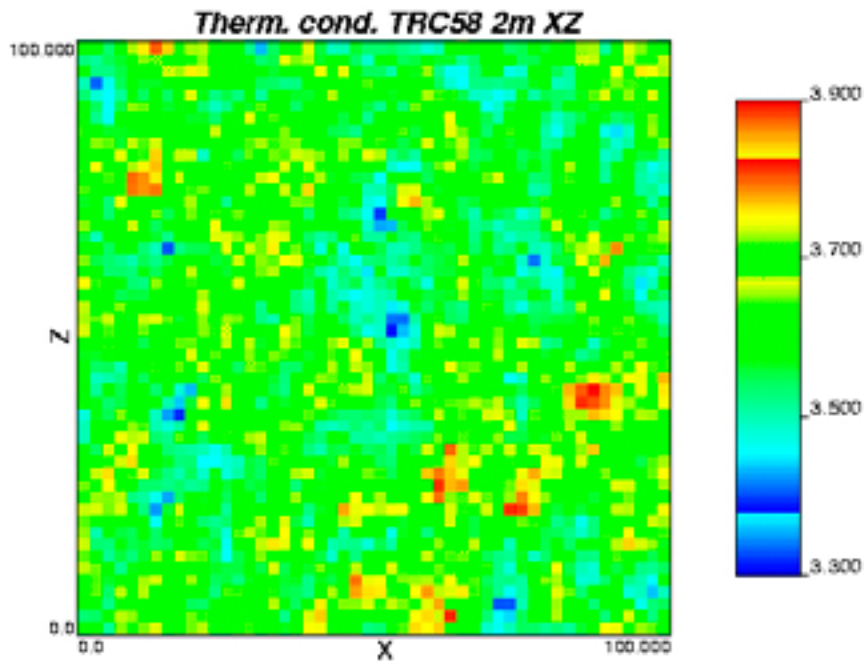


Figure G-15. 2D slice from one 3D realisation (simulation scale = 2 m) illustrating the distribution of thermal conductivity values in TRC 58. R=1, Slice=25, xz-plane. TRC-unique legend scale.

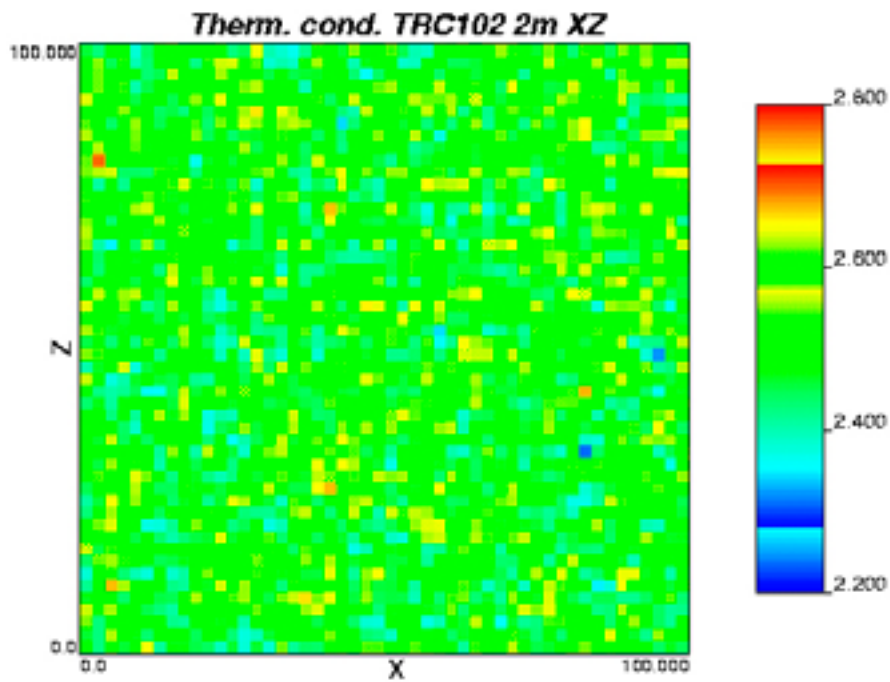


Figure G-16. 2D slice from one 3D realisation (simulation scale = 2 m) illustrating the distribution of thermal conductivity values in TRC 102. R=1, Slice=25, xz-plane. TRC-unique legend scale.

Visualisations of domain thermal realisations

Example thermal realisations and the corresponding geological realisations are presented in 2D for all three modelled rock domains and all thermal subdomains.

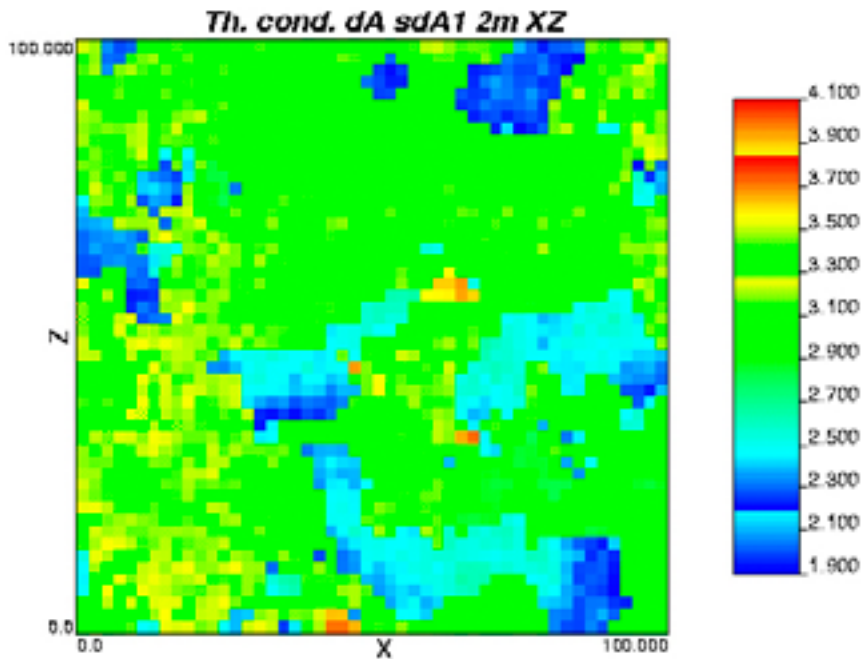


Figure H-1. 2D slice from one 3D realisation (simulation scale = 2 m) illustrating the distribution of thermal conductivity values for domain RSMA01, sub domain A1. R=1, Slice=25, xz-plane.

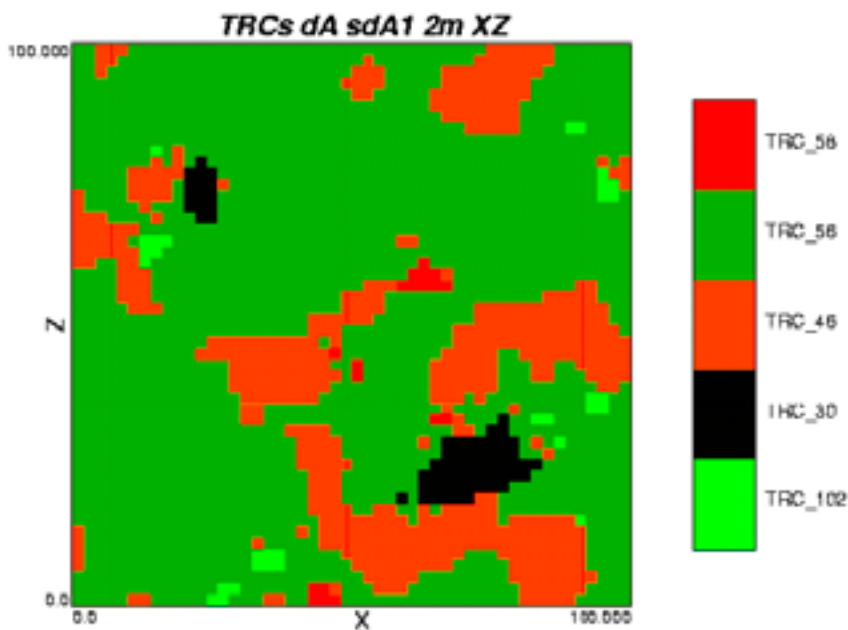


Figure H-2. 2D slice from one 3D realisation (simulation scale = 2 m) illustrating the distribution of TRCs for domain RSMA01, sub domain A1. R=1, Slice=25, xz-plane.

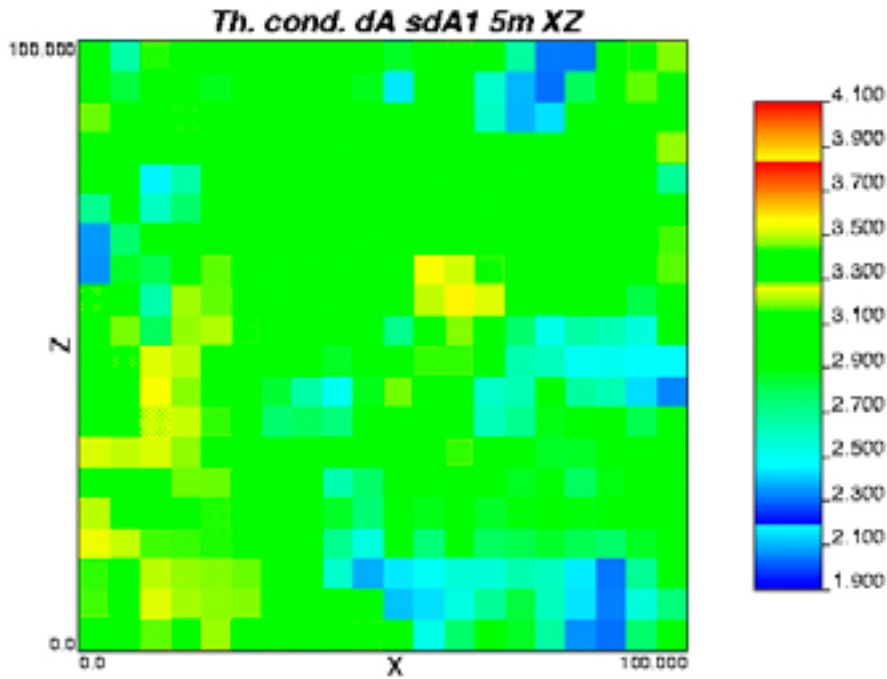


Figure H-3. 2D slice from one 3D realisation (simulation scale = 5 m) illustrating the distribution of thermal conductivity values for domain RSMA01, sub domain A1. R=1, Slice=10, xz-plane.

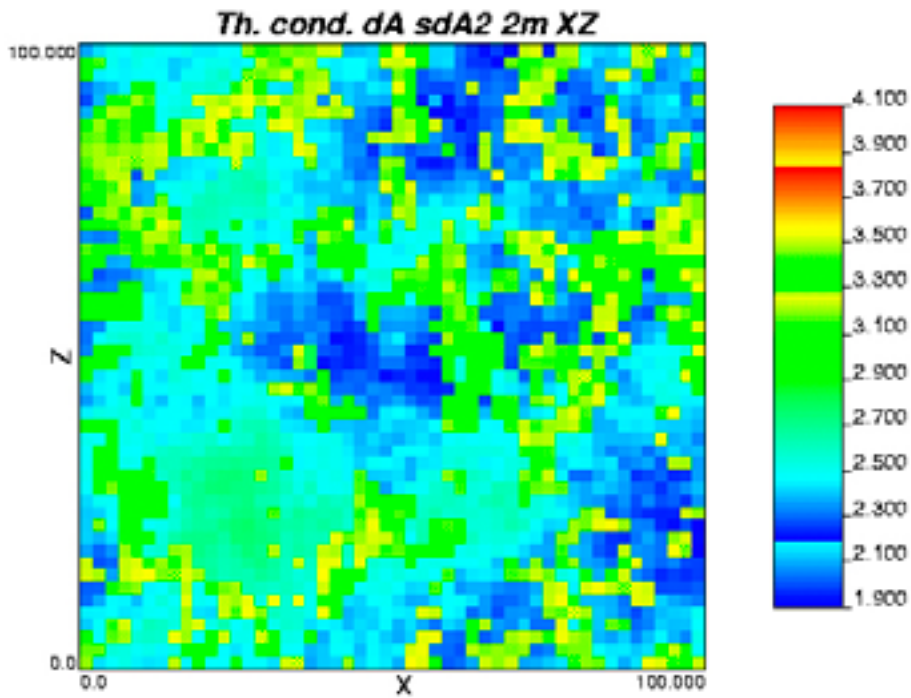


Figure H-4. 2D slice from one 3D realisation (simulation scale = 2 m) illustrating the distribution of thermal conductivity values for domain RSMA01, sub domain A2. R=1, Slice=25, xz-plane.

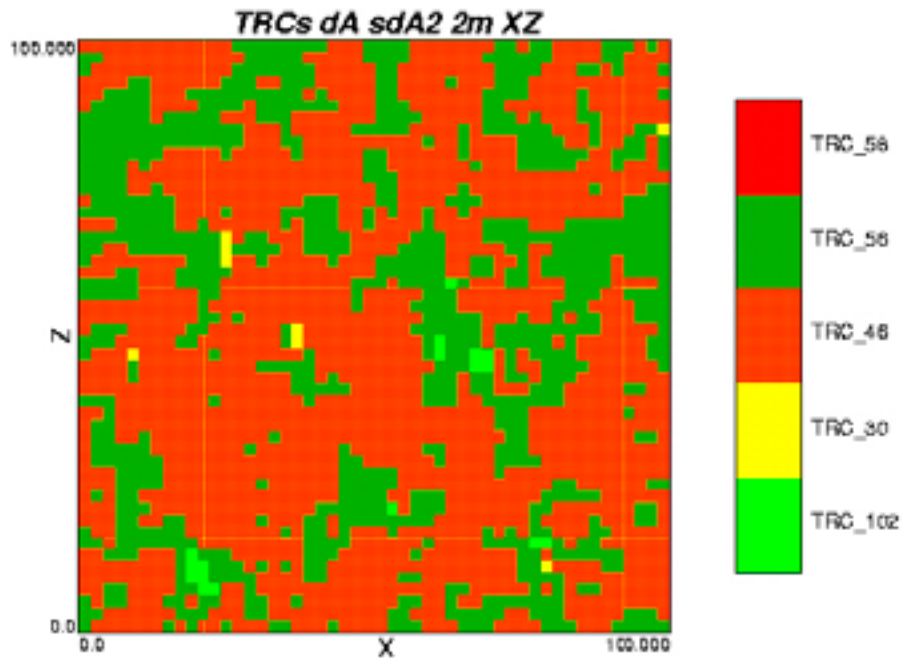


Figure H-5. 2D slice from one 3D realisation (simulation scale = 2 m) illustrating the distribution of TRCs for domain RSMA01, sub domain A2. $R=1$, Slice=25, xz-plane.

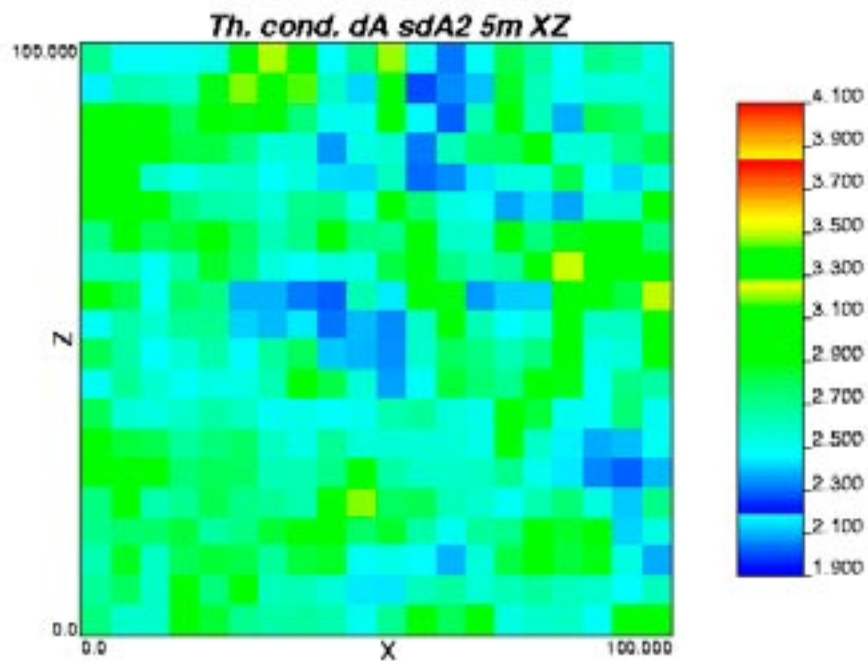


Figure H-6. 2D slice from one 3D realisation (simulation scale = 5 m) illustrating the distribution of thermal conductivity values for domain RSMA01, sub domain A2. $R=1$, Slice=10, xz-plane.

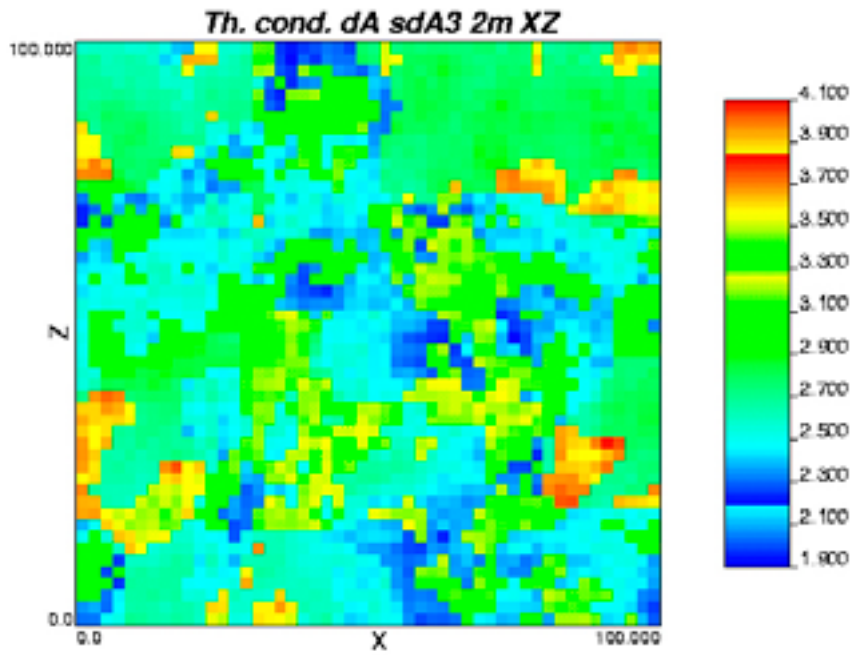


Figure H-7. 2D slice from one 3D realisation (simulation scale = 2 m) illustrating the distribution of thermal conductivity values for domain RSMA01, sub domain A3. R=1, Slice=25, xz-plane.

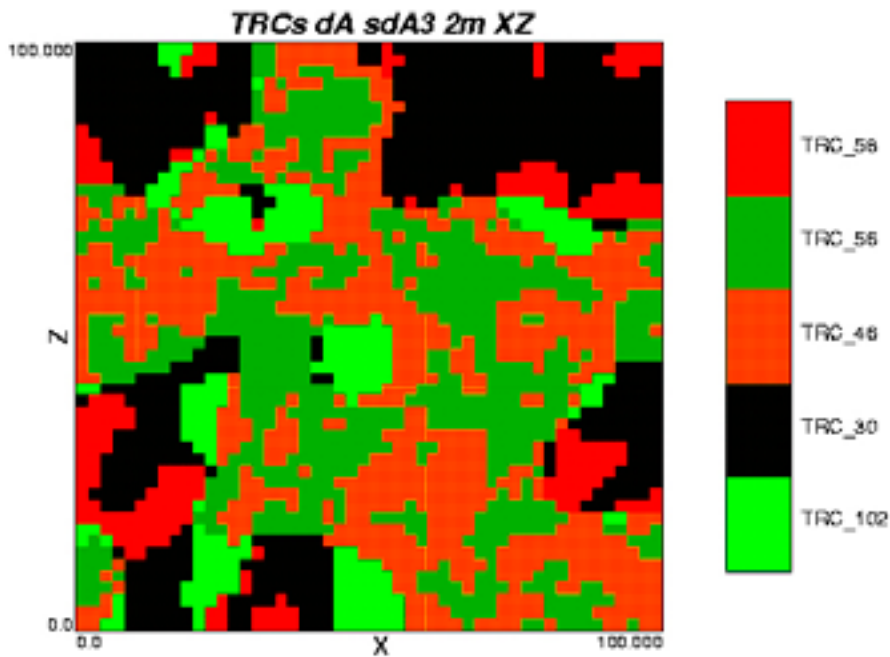


Figure H-8. 2D slice from one 3D realisation (simulation scale = 2 m) illustrating the distribution of TRCs for domain RSMA01, sub domain A32. R=1, Slice=25, xz-plane.

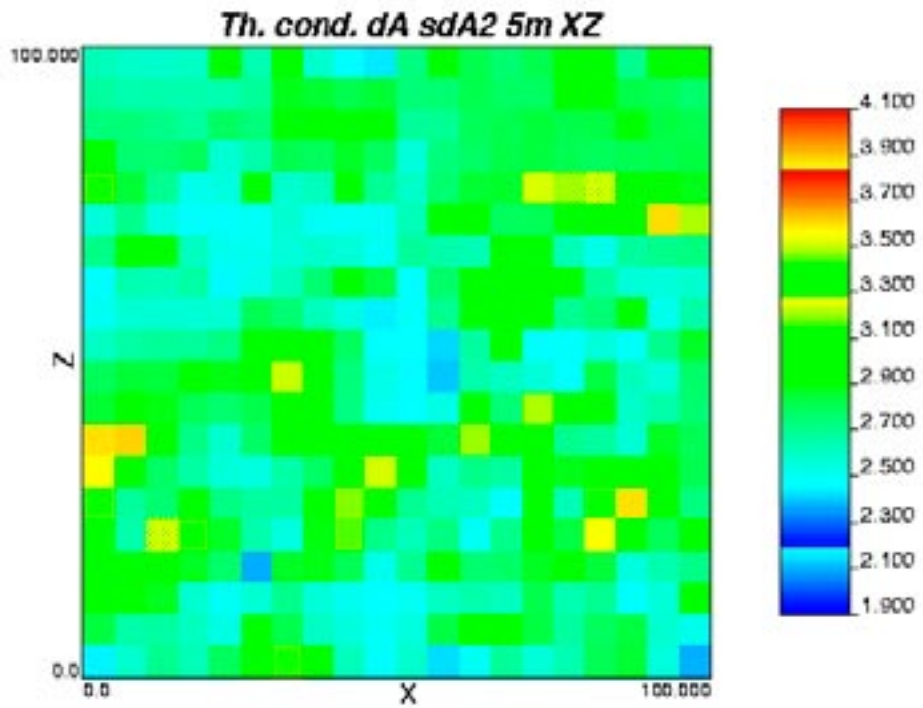


Figure H-9. 2D slice from one 3D realisation (simulation scale = 5 m) illustrating the distribution of thermal conductivity values for domain RSMA01, sub domain A3. R=1, Slice=10, xz-plane.

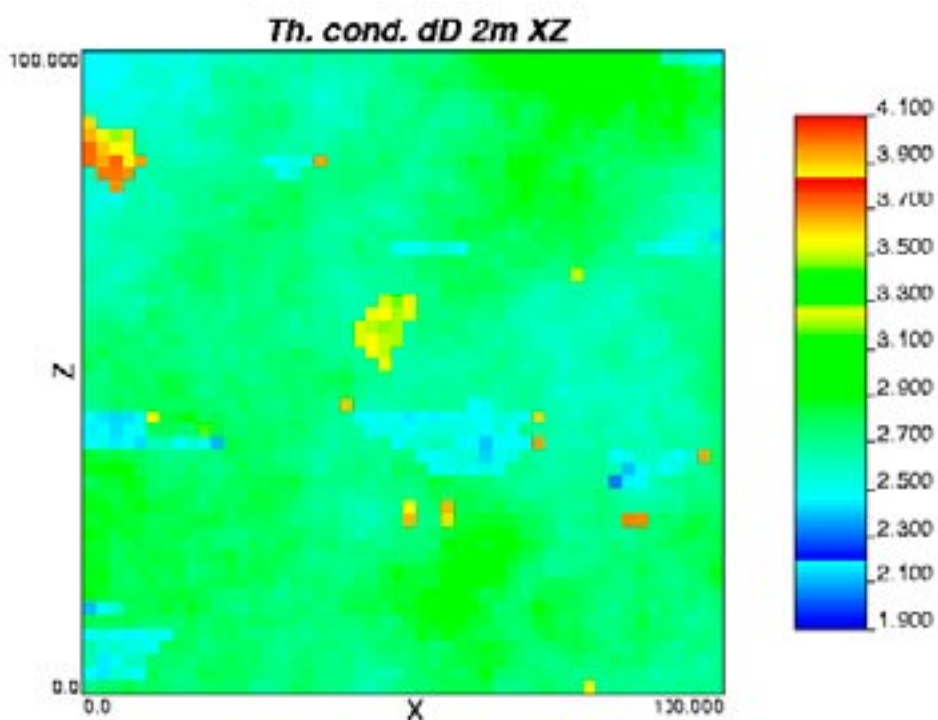


Figure H-10. 2D slice from one 3D realisation (simulation scale = 2 m) illustrating the distribution of thermal conductivity values for domain RSMD01. R=1, Slice=25, xz-plane.

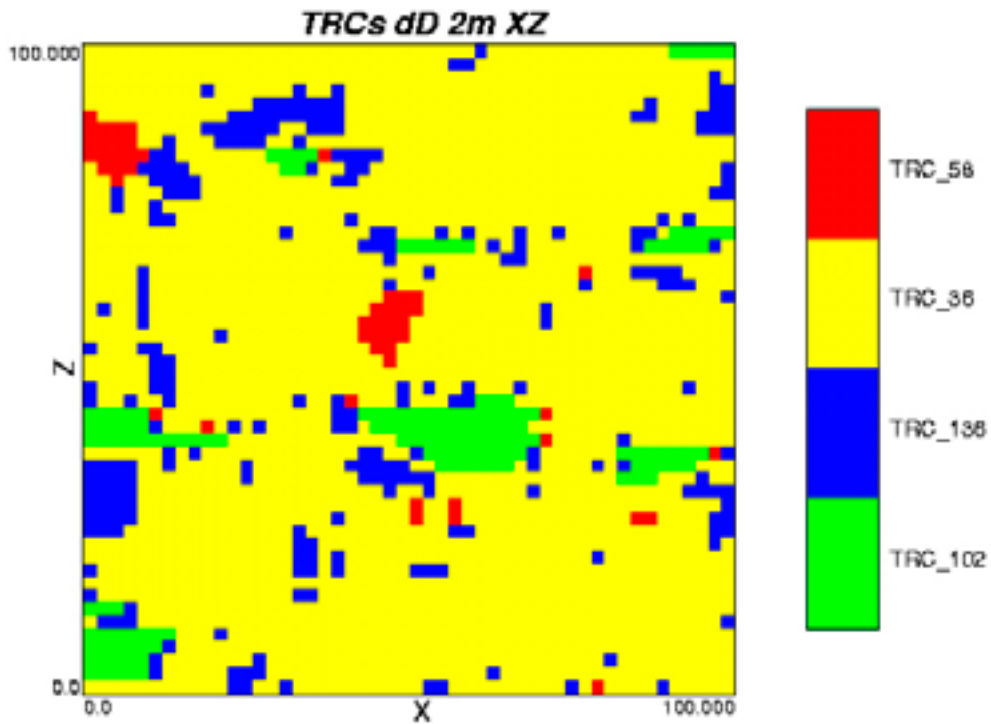


Figure H-11. 2D slice from one 3D realization (simulation scale = 2 m) illustrating the distribution of TRCs for domain RSMD01. R=1, Slice=25, xz-plane.

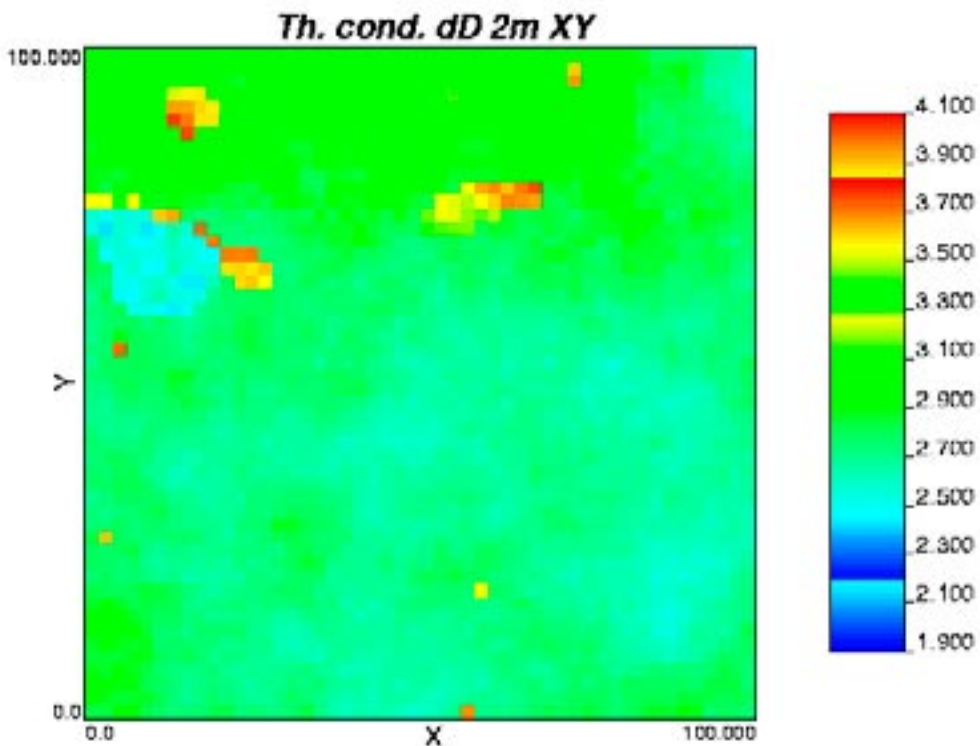


Figure H-12. 2D slice from one 3D realization (simulation scale = 2 m) illustrating the distribution of thermal conductivity values for domain RSMD01. R=1, Slice=25, xy-plane.

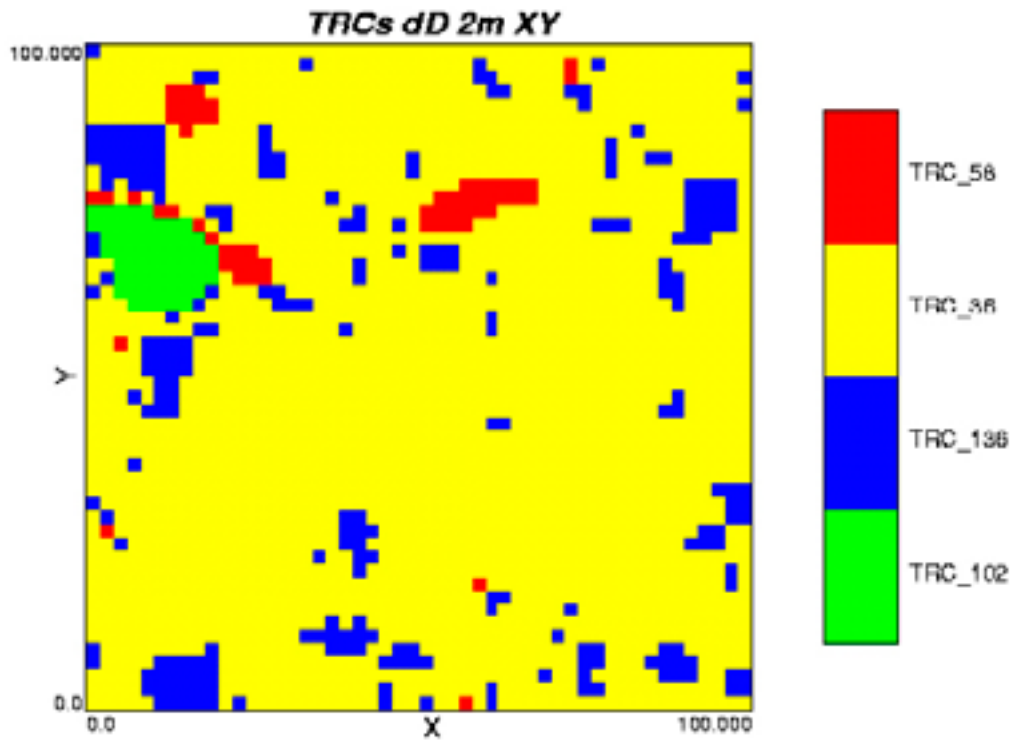


Figure H-13. 2D slice from one 3D realisation (simulation scale = 2 m) illustrating the distribution of TRCs for domain RSMD01. R=1, Slice=25, xy-plane.

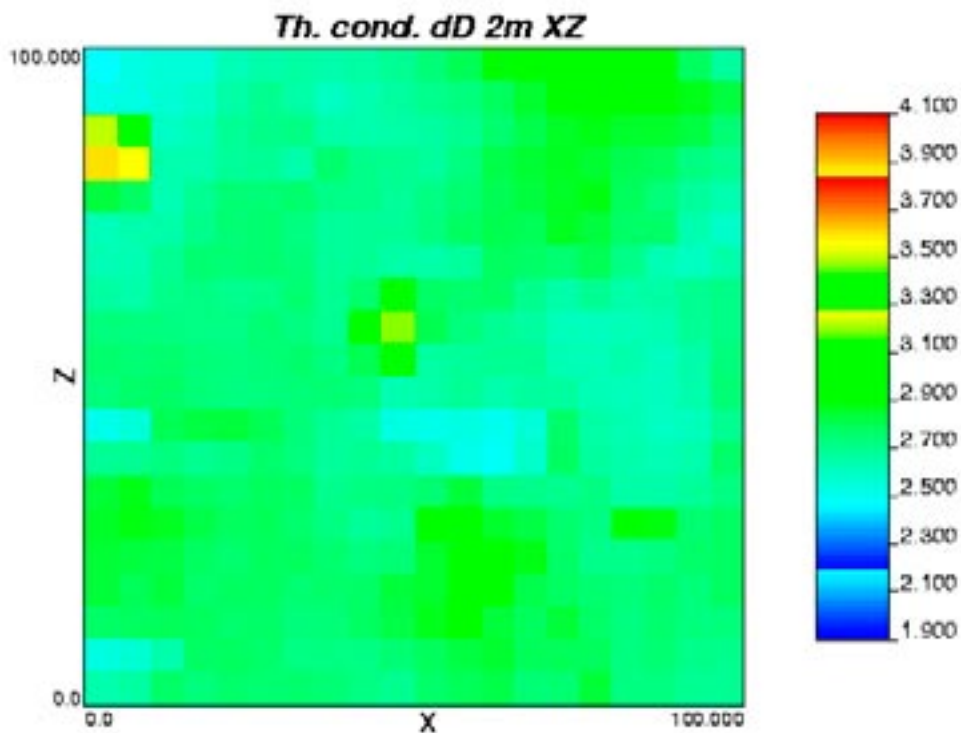


Figure H-14. 2D slice from one 3D realisation (simulation scale = 5 m) illustrating the distribution of thermal conductivity values for domain RSMD01. R=1, Slice=10, xz-plane.

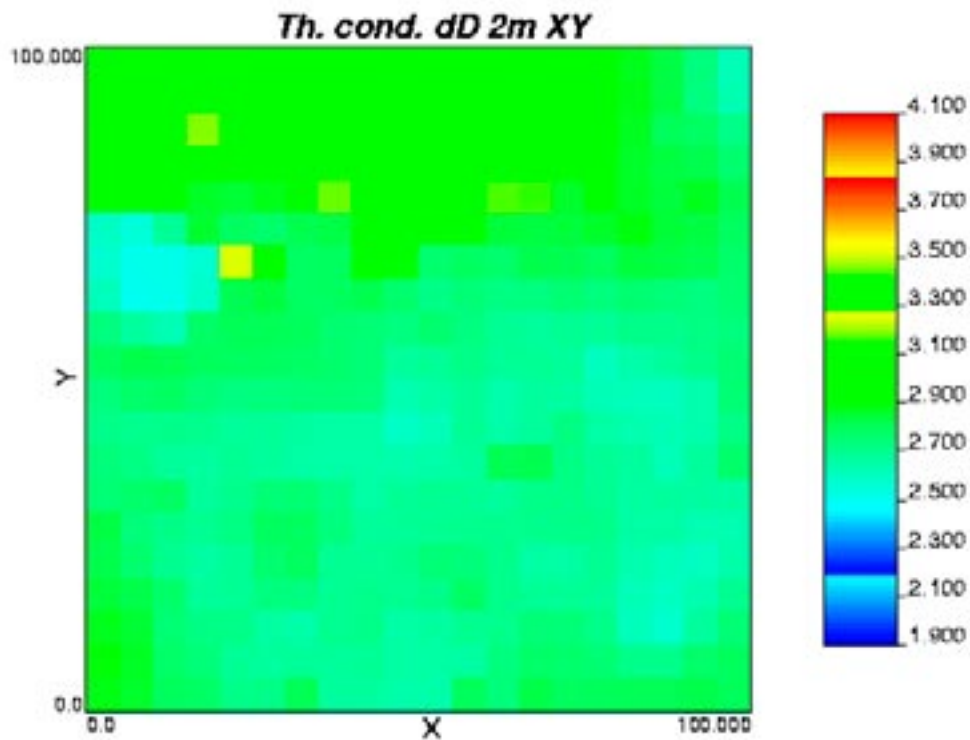


Figure H-15. 2D slice from one 3D realisation (simulation scale = 5 m) illustrating the distribution of thermal conductivity values for domain RSMD01. $R=1$, Slice=10, xy -plane.

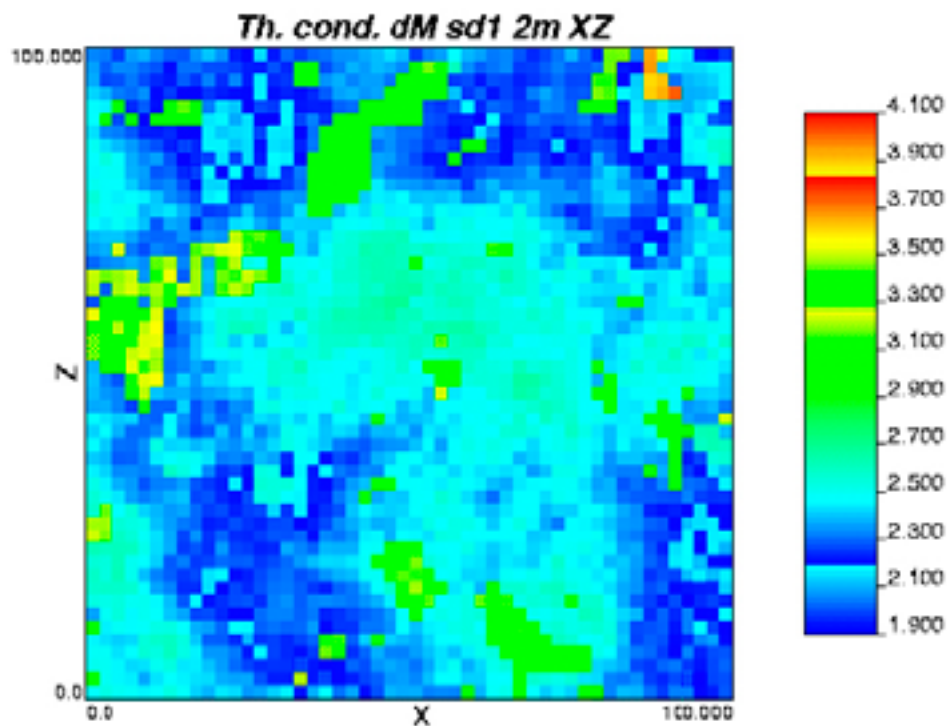


Figure H-16. 2D slice from one 3D realisation (simulation scale = 2 m) illustrating the distribution of thermal conductivity values for domain RSMM01, sub domain 1. $R=1$, Slice=25, xz -plane.

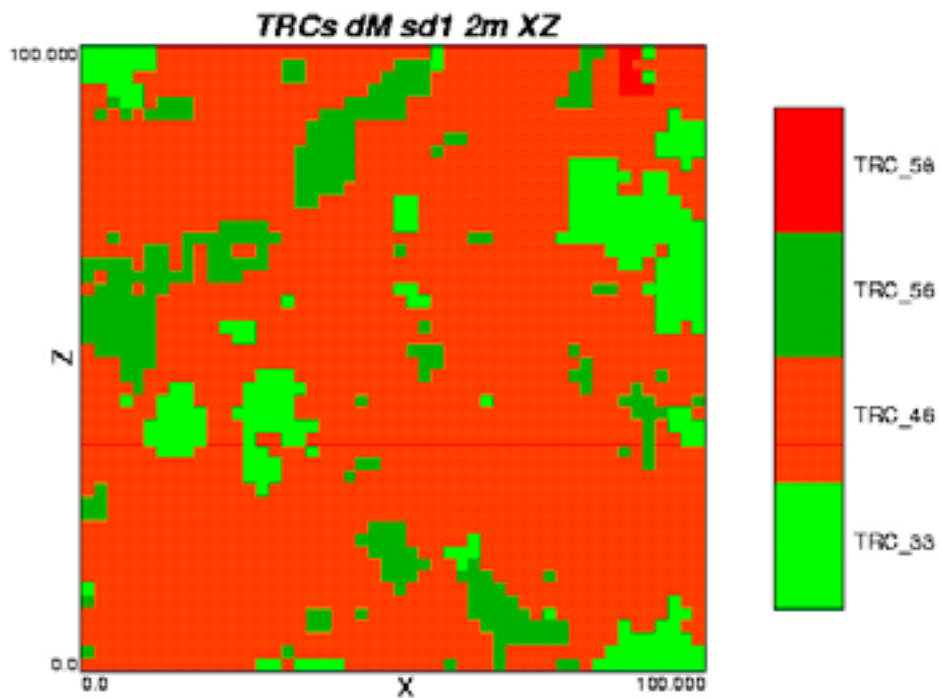


Figure H-17. 2D slice from one 3D realisation (simulation scale = 2 m) illustrating the distribution of TRCs for domain RSMA01, sub domain A32. R=1, Slice=25, xz-plane.

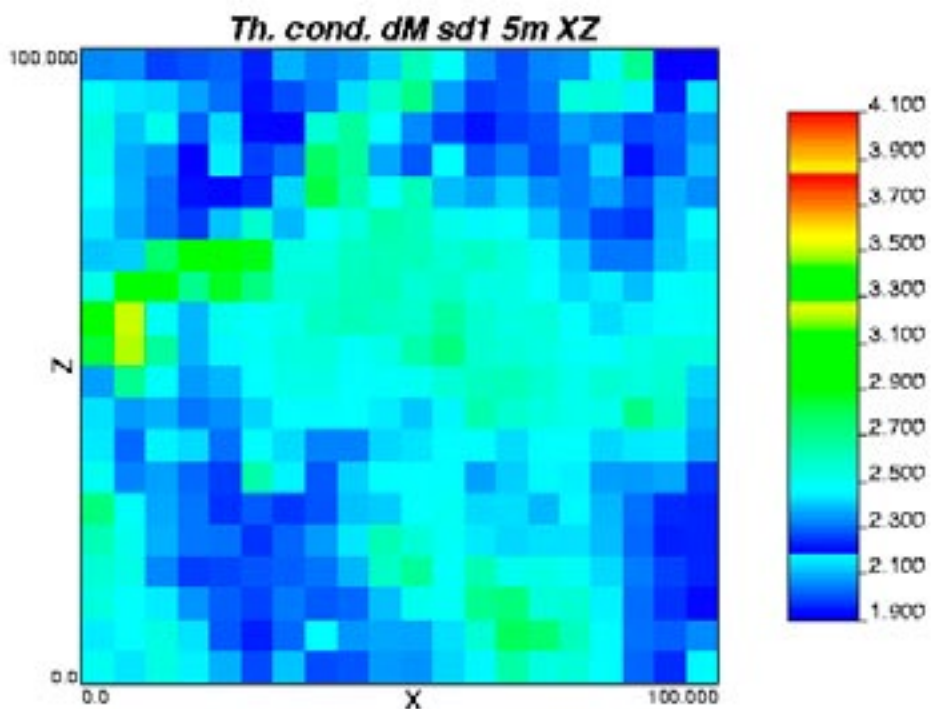


Figure H-18. 2D slice from one 3D realisation (simulation scale = 5 m) illustrating the distribution of thermal conductivity values for domain RSMM01, sub domain 1. R=1, Slice=10, xz-plane.

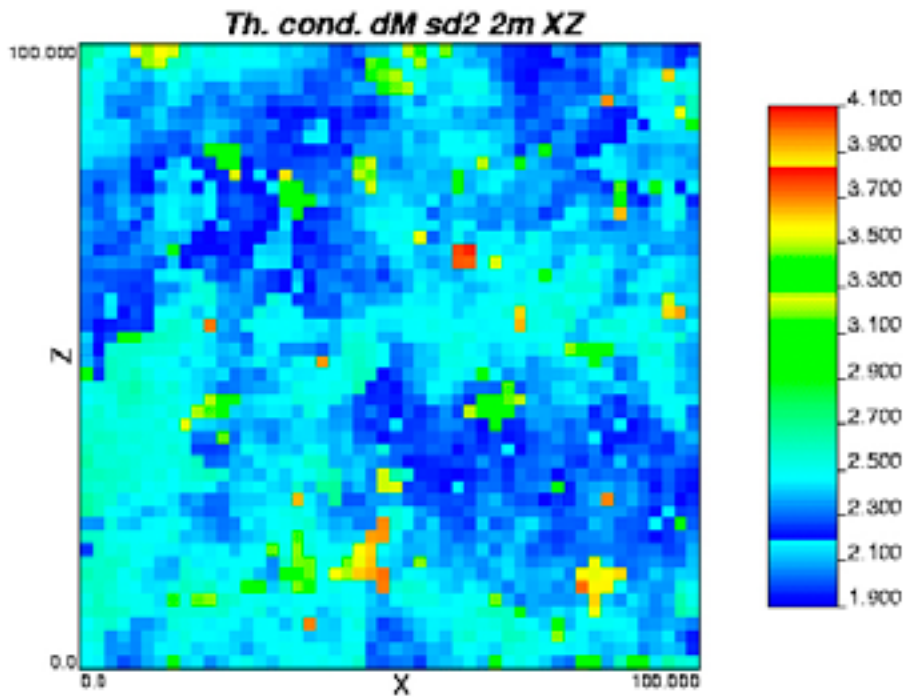


Figure H-19. 2D slice from one 3D realisation (simulation scale = 2 m) illustrating the distribution of thermal conductivity values for domain RSMM01, sub domain 2. R=1, Slice=25, xz-plane.

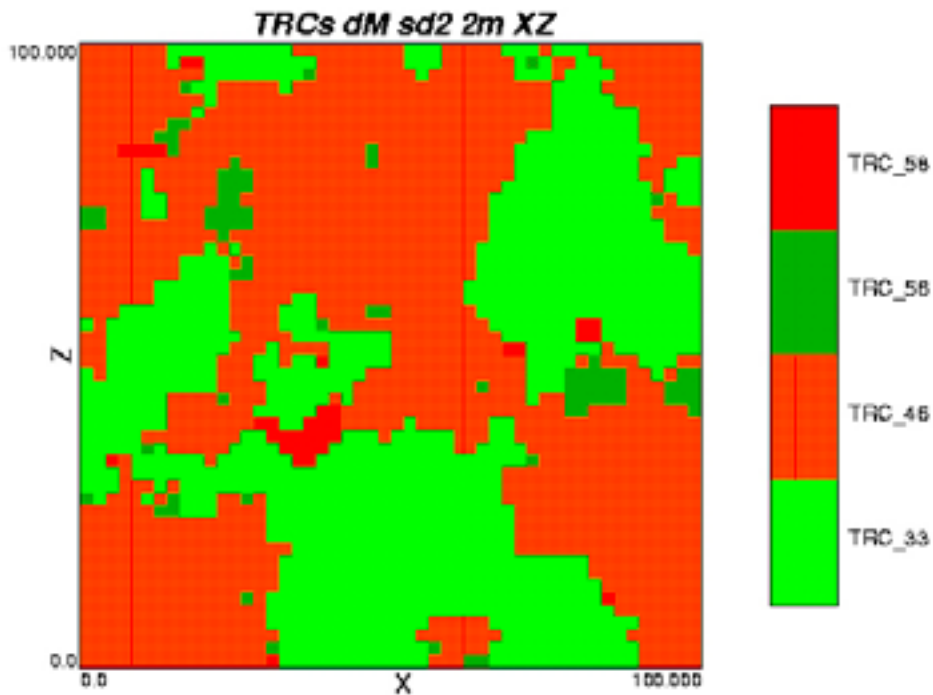


Figure H-20. 2D slice from one 3D realisation (simulation scale = 2 m) illustrating the distribution of TRCs for domain RSMM01, sub domain 2. R=1, Slice=25, xz-plane.

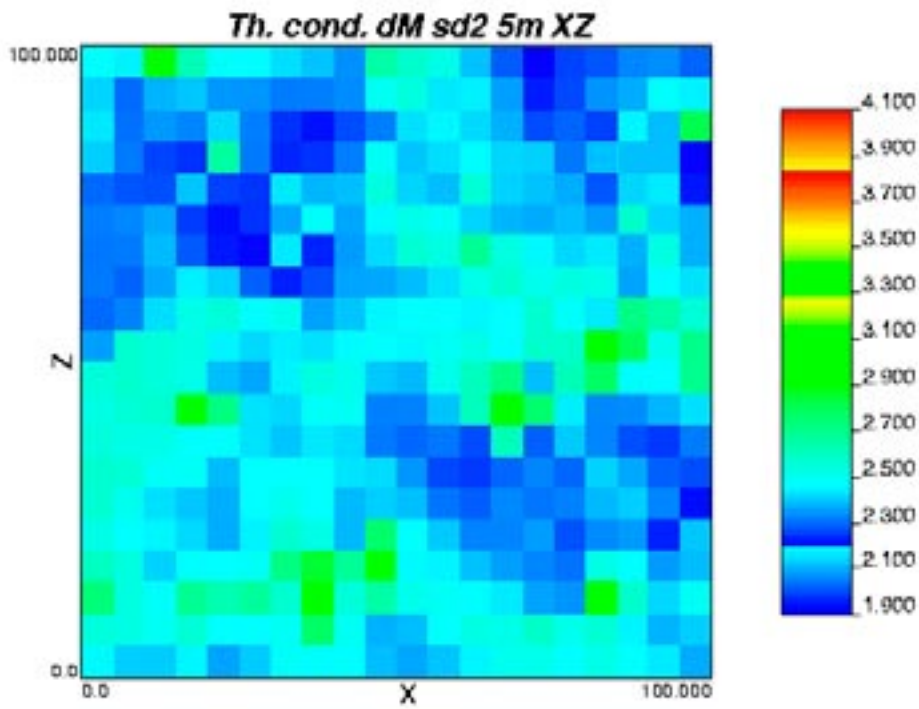


Figure H-21. 2D slice from one 3D realisation (simulation scale = 5 m) illustrating the distribution of thermal conductivity values for domain RSMM01, sub domain 2. R=1, Slice=10, xz-plane.

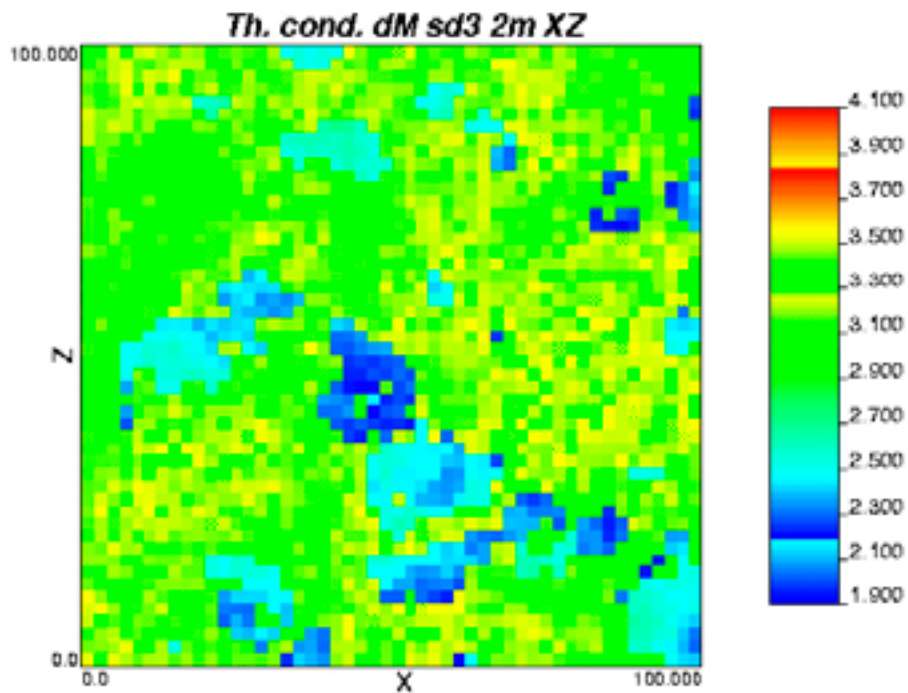


Figure H-22. 2D slice from one 3D realisation (simulation scale = 2 m) illustrating the distribution of thermal conductivity values for domain RSMM01, sub domain 3. R=1, Slice=25, xz-plane.

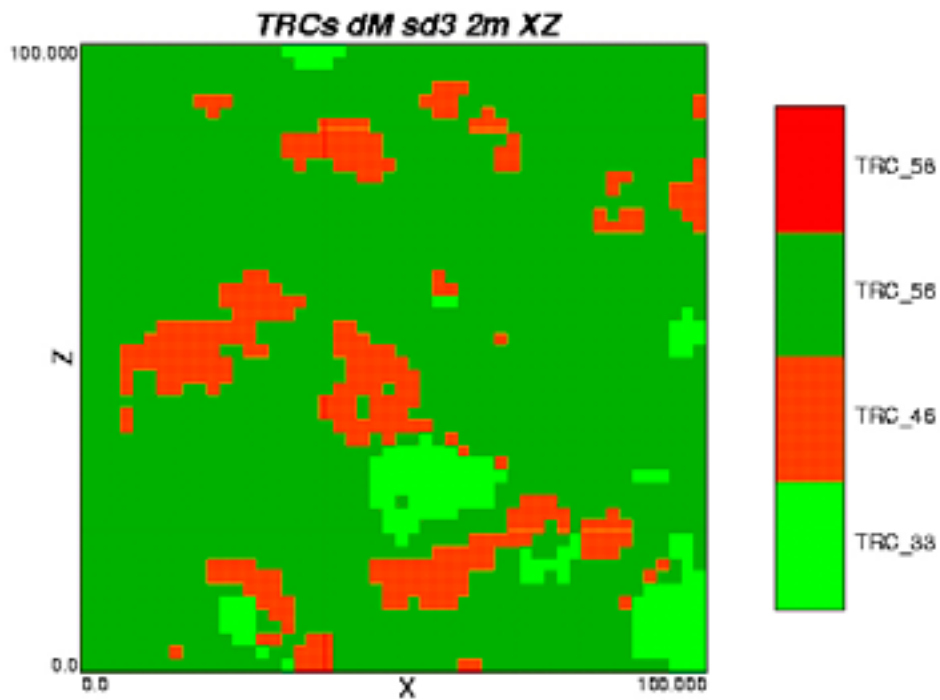


Figure H-23. 2D slice from one 3D realisation (simulation scale = 2 m) illustrating the distribution of TRCs for domain RSMM01, sub domain 3. R=1, Slice=25, xz-plane.

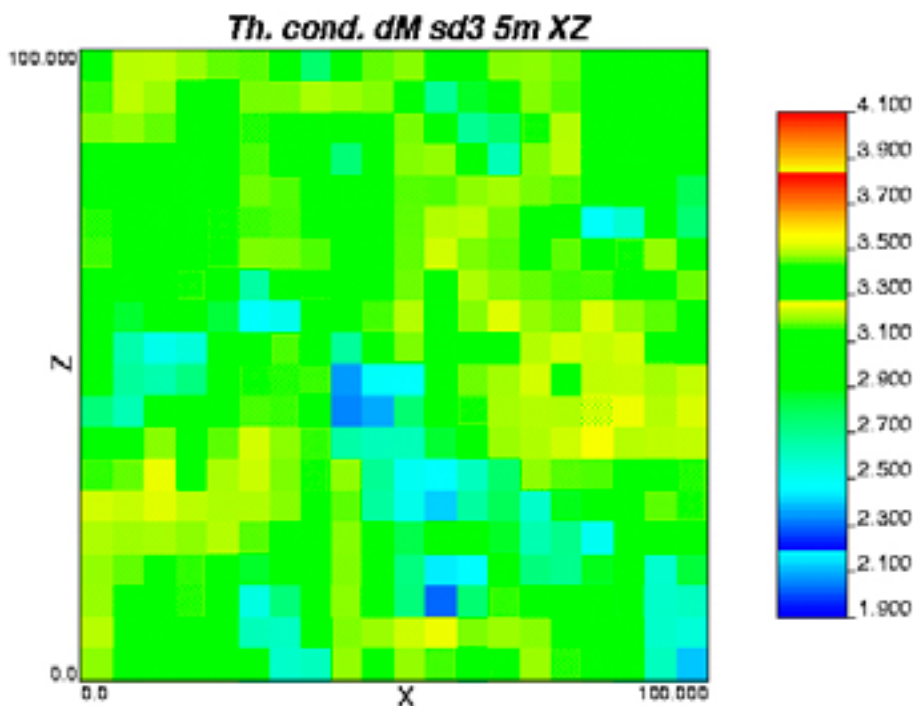


Figure H-24. 2D slice from one 3D realisation (simulation scale = 5 m) illustrating the distribution of thermal conductivity values for domain RSMM01, sub domain 3. R=1, Slice=10, xz-plane.

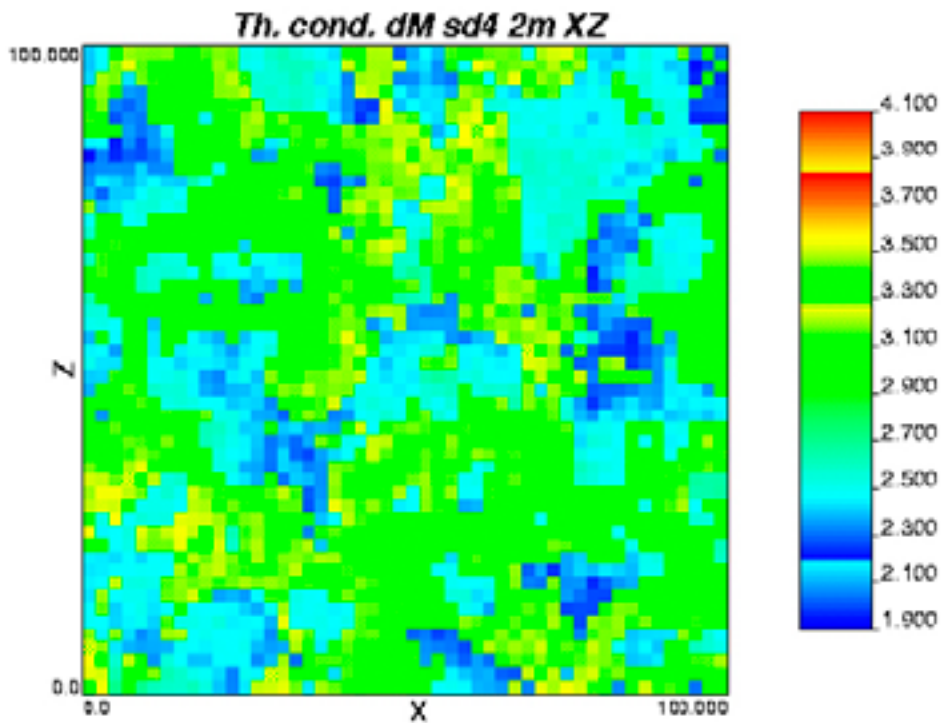


Figure H-25. 2D slice from one 3D realisation (simulation scale = 2 m) illustrating the distribution of thermal conductivity values for domain RSMM01, sub domain 4. R=1, Slice=25, xz-plane.

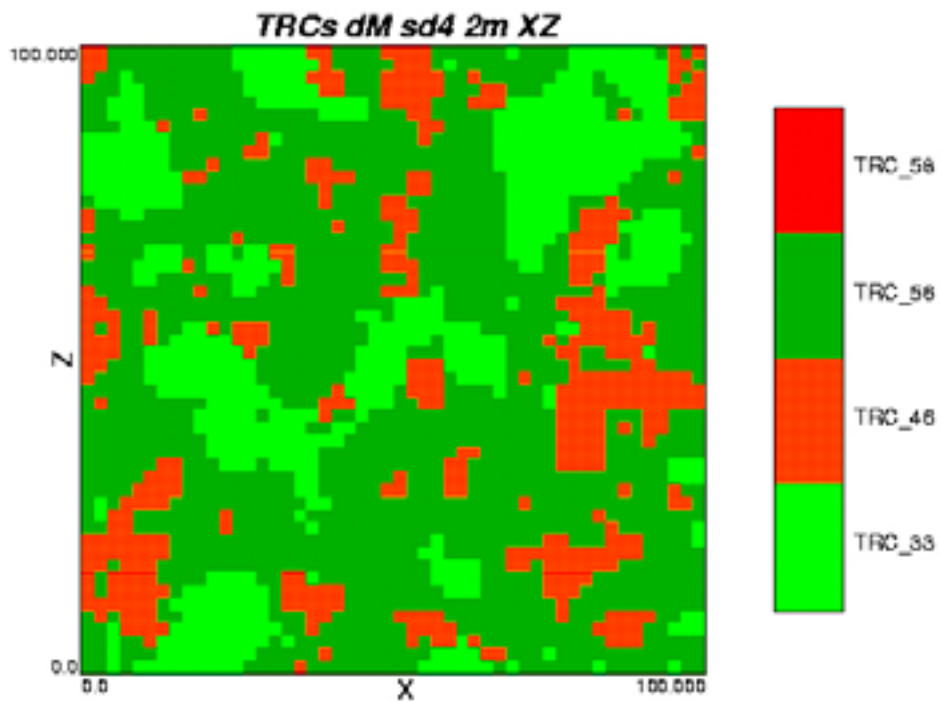


Figure H-26. 2D slice from one 3D realisation (simulation scale = 2 m) illustrating the distribution of TRCs for domain RSMM01, sub domain 4. R=1, Slice=25, xz-plane.

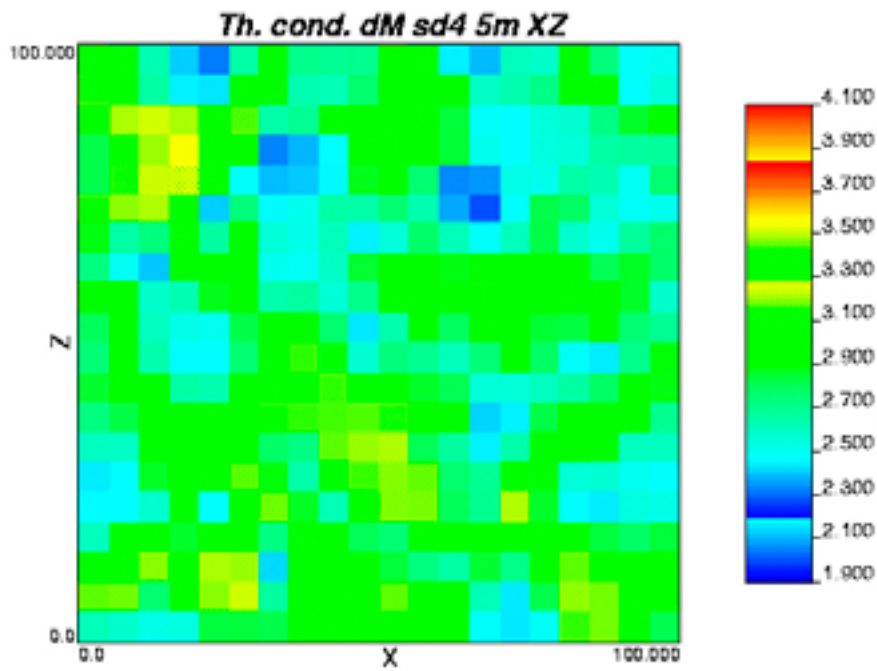


Figure H-27. 2D slice from one 3D realisation (simulation scale = 5 m) illustrating the distribution of thermal conductivity values for domain RSMM01, sub domain 4. $R=1$, Slice=10, xz -plane.

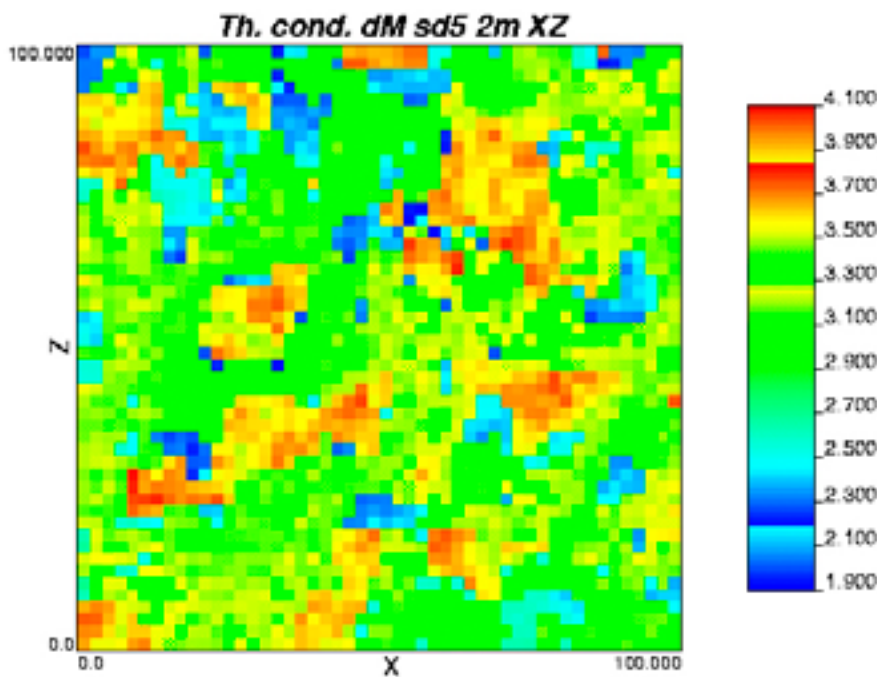


Figure H-28. 2D slice from one 3D realisation (simulation scale = 2 m) illustrating the distribution of thermal conductivity values for domain RSMM01, sub domain 5. $R=1$, Slice=25, xz -plane.

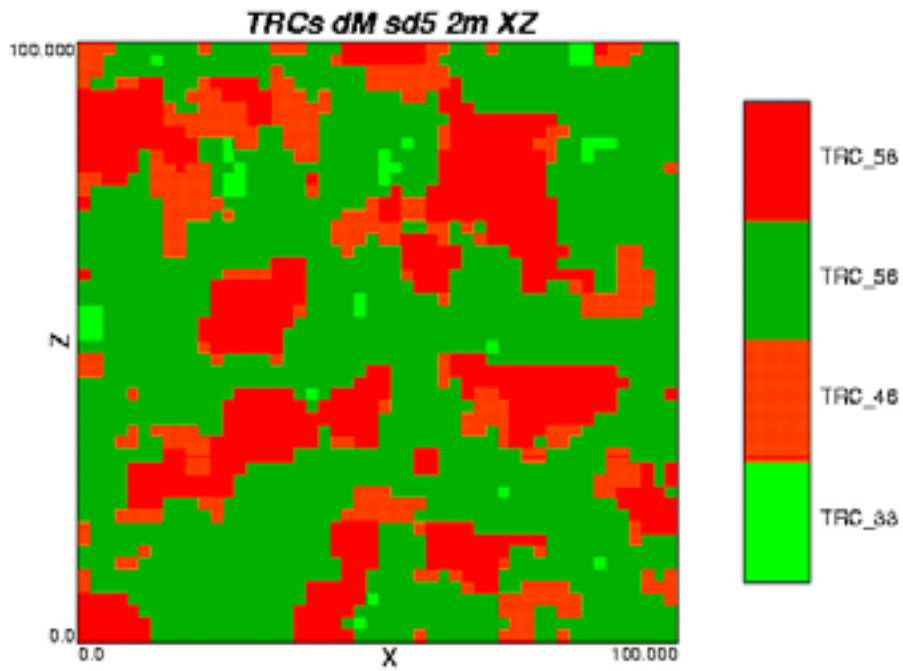


Figure H-29. 2D slice from one 3D realisation (simulation scale = 2 m) illustrating the distribution of TRCs for domain RSMM01, sub domain 5. $R=1$, Slice=25, xz -plane.

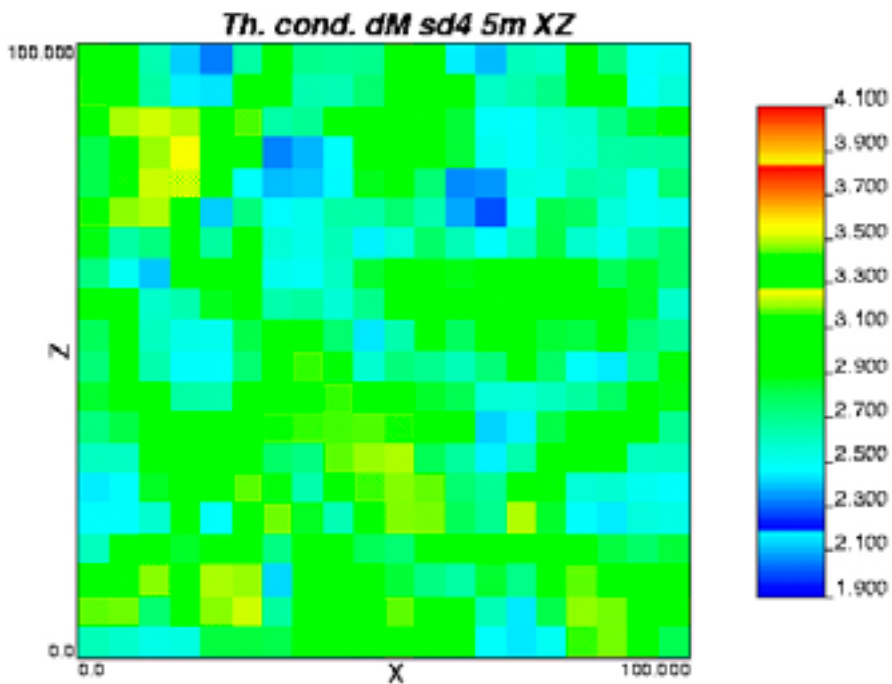


Figure H-30. 2D slice from one 3D realisation (simulation scale = 5 m) illustrating the distribution of thermal conductivity values for domain RSMM01, sub domain 5. $R=1$, Slice=10, xz -plane.

Verification of stochastic simulations of TRCs

Proportions

The tables below show the proportions of TRCs in 10 randomly selected realisations for selected subdomains or domain. As can be seen from Table I-1 to Table 5, T-PROGS nearly exactly reproduces the proportions of the TRCs for all realisations and for all scales.

Table I-1. Proportions of TRCs in 10 randomly selected realisations for subdomain A1.

Category	Proportions from borehole (%)	Proportions of randomly selected realisation (%)									
		1	2	3	4	5	6	7	8	9	10
TRC 30	2.4	2.4	2.4	2.4	2.4	2.4	2.4	2.4	2.4	2.4	2.4
TRC 46	19.2	19.2	19.2	19.2	19.2	19.2	19.2	19.2	19.2	19.2	19.2
TRC 56	76.0	75.9	75.9	75.9	75.9	75.9	75.9	75.9	75.9	75.9	75.8
TRC 58	1.3	1.3	1.3	1.3	1.3	1.3	1.3	1.3	1.3	1.3	1.3
TRC 102	1.2	1.2	1.2	1.2	1.2	1.2	1.2	1.2	1.2	1.2	1.2

Table I-2. Proportions of TRCs in 10 randomly selected realisations for subdomain A2.

Category	Proportions from borehole (%)	Proportions of randomly selected realisation (%)									
		1	2	3	4	5	6	7	8	9	10
TRC 30	1.1	1.1	1.1	1.1	1.1	1.1	1.1	1.1	1.1	1.1	1.1
TRC 46	61.0	61.0	61.1	61.0	61.1	61.0	61.1	61.1	61.0	61.0	61.1
TRC 56	37.2	37.1	37.1	37.1	37.1	37.2	37.1	37.1	37.2	37.2	37.1
TRC 102	0.7	0.7	0.7	0.8	0.7	0.7	0.7	0.7	0.7	0.7	0.7

Table I-3. Proportions of TRCs in 10 randomly selected realisations for subdomain A3.

Category	Proportions from borehole (%)	Proportions of randomly selected realisation (%)									
		1	2	3	4	5	6	7	8	9	10
TRC 30	35.4	35.4	35.0	35.6	35.0	34.9	35.0	35.3	35.1	35.5	35.1
TRC 46	23.6	23.7	23.9	23.6	23.9	24.0	23.9	23.7	23.9	23.7	23.8
TRC 56	22.1	21.9	22.2	21.9	22.1	22.2	22.1	21.9	22.1	22.0	22.1
TRC 58	10.2	10.4	10.3	10.3	10.3	10.2	10.3	10.3	10.2	10.3	10.3
TRC 102	8.7	8.6	8.7	8.6	8.6	8.7	8.6	8.8	8.7	8.5	8.6

Table I-4. Proportions of TRCs in 10 randomly selected realisations for domain RSMD01.

Category	Proportions from borehole (%)	Proportions of randomly selected realisation (%)									
		1	2	3	4	5	6	7	8	9	10
TRC 36	83.2	82.9	83.0	82.9	83.0	82.9	83.0	83.0	82.9	83.0	83.0
TRC 58	3.5	3.5	3.5	3.5	3.5	3.5	3.5	3.5	3.5	3.5	3.5
TRC 102	3.4	3.7	3.6	3.8	3.7	3.7	3.7	3.6	3.7	3.7	3.7
TRC 136	9.9	9.9	9.9	9.9	9.9	9.9	9.9	9.9	9.9	9.9	9.9

Table I-5. Proportions of TRCs in 10 randomly selected realisations for subdomain M1.

Category	Proportions from borehole (%)	Proportions of randomly selected realisation (%)									
		1	2	3	4	5	6	7	8	9	10
TRC33	8.6	8.6	8.6	8.6	8.6	8.6	8.6	8.6	8.6	8.6	8.6
TRC56	10.5	10.5	10.5	10.5	10.5	10.5	10.5	10.5	10.5	10.5	10.5
TRC46	79.8	79.8	79.8	79.8	79.8	79.8	79.8	79.8	79.8	79.8	79.8
TRC58	1.1	1.1	1.2	1.1	1.1	1.2	1.2	1.2	1.1	1.2	1.2

Typical lengths

Calculations of typical lengths of TRCs were made from “simulated boreholes” through 10 randomly selected realisations for each of the subdomains. The “borehole length” of each borehole is 100 metres and 36 “simulated boreholes” were made in each direction. The typical lengths of the TRCs in the data obtained from the “simulated boreholes” were calculated by transition probability analysis. TRCs that constitute the “background” in the simulations were not relevant to include in the analysis and were therefore omitted.

Domain RSMA01

The results of the calculations of the typical lengths (m) for subdomain A1 are presented in Section 5.5.3. The results of the calculations of the typical length (m) for directions x, y and z for subdomain A2 are presented in Table I-6 to Table I-8.

It can be seen from the analysis that T-PROGS does not reproduce any directional bias for subdomain A2. T-PROGS somewhat overestimates typical lengths for TRC102. Nominal lengths for TRC102 are very short in subdomain A2 and equal to the model resolution. The reason for overestimation of shorter lengths is the discretisation of the model, where 2 metres is the shortest length that can be represented. The reason for the slight overestimations of TRC56 is not known.

Table I-6. Typical lengths of TRC30 in subdomain A2.

Typical simulated length (m)*	Nominal value (m)*	Comment on simulated values
$\mu_x=3.86$	3.00	OK
$\mu_y=3.94$	3.00	OK
$\mu_z=3.86$	3.00	OK

* The typical simulated length is the mean lengths estimated from “simulated boreholes” through the simulated rock volumes. The nominal value is the typical length estimated from the transition analysis in T-PROGS.

Table I-7. Typical lengths of TRC56 in subdomain A2.

Typical simulated length (m)*	Nominal value (m)*	Comment on simulated values
$\mu_x = 5.98$	8.80	Low
$\mu_y = 5.98$	8.80	Low
$\mu_z = 6.00$	8.80	Low

* The typical simulated length is the mean lengths estimated from “simulated boreholes” through the simulated rock volumes. The nominal value is the typical length estimated from the transition analysis in T-PROGS.

Table I-8. Typical lengths of TRC102 in subdomain A2.

Typical simulated length (m)*	Nominal value (m)*	Comment on simulated values
$\mu_x = 3.50$	2.00	Somewhat high
$\mu_y = 2.97$	2.00	Somewhat high
$\mu_z = 3.22$	2.00	Somewhat high

* The typical simulated length is the mean lengths estimated from “simulated boreholes” through the simulated rock volumes. The nominal value is the typical length estimated from the transition analysis in T-PROGS.

The results of the calculations of the typical lengths (m) for directions x, y and z for subdomain A3 are presented in Table I-9 to Table I-12.

Table I-9. Typical lengths of TRC46 in subdomain A3.

Typical simulated length (m)*	Nominal value (m)*	Comment on simulated values
$\mu_x = 6.34$	5.00	Somewhat high
$\mu_y = 6.31$	5.00	Somewhat high
$\mu_z = 6.31$	5.00	Somewhat high

* The typical simulated length is the mean lengths estimated from “simulated boreholes” through the simulated rock volumes. The nominal value is the typical length estimated from the transition analysis in T-PROGS.

Table I-10. Typical lengths of TRC56 in subdomain A3.

Typical simulated length (m)*	Nominal value (m)*	Comment on simulated values
$\mu_x = 6.46$	4.67	Somewhat high
$\mu_y = 6.31$	4.67	Somewhat high
$\mu_z = 6.31$	4.67	Somewhat high

* The typical simulated length is the mean lengths estimated from “simulated boreholes” through the simulated rock volumes. The nominal value is the typical length estimated from the transition analysis in T-PROGS.

Table I-11. Typical lengths of TRC58 in subdomain A3.

Typical simulated length (m)*	Nominal value (m)*	Comment on simulated values
$\mu_x = 6.90$	6.50	OK
$\mu_y = 7.10$	6.50	OK
$\mu_z = 6.96$	6.50	OK

* The typical simulated length is the mean lengths estimated from “simulated boreholes” through the simulated rock volumes. The nominal value is the typical length estimated from the transition analysis in T-PROGS.

Table I-12. Typical lengths of TRC102 in subdomain A3.

Typical simulated length (m)*	Nominal value (m)*	Comment on simulated values
$\mu_x = 6.30$	5.50	OK
$\mu_y = 6.12$	5.50	OK
$\mu_z = 6.10$	5.50	OK

* The typical simulated length is the mean lengths estimated from “simulated boreholes” through the simulated rock volumes. The nominal value is the typical length estimated from the transition analysis in T-PROGS.

It can be seen from the analysis that T-PROGS does not reproduce any directional bias for subdomain A3. T-PROGS slightly overestimates the shorter lengths of TRC46 and TRC56. The typical lengths for TRC58 and TRC 102 are reproduced realistically.

Domain RSMD01

The results of the calculations of the typical lengths (m) for directions x, y and z for domain RSMD01 are presented in Table 13 to Table 15.

It can be seen from the analysis that T-PROGS does not reproduce any directional bias for domain RSMD01. T-PROGS gives reasonable estimations of TRC58 and TRC136, although the latter is somewhat overestimated, which is assumed to be due to the discretisation of the model. The very strong anisotropy of TRC102 could not be reproduced as strongly as suggested by the geological interpretations.

Table I-13. Typical lengths of TRC58 in domain RSMD01.

Typical simulated length (m)*	Nominal value (m)*	Comment on simulated values
$\mu_x = 4.77$	4.01	OK
$\mu_y = 4.87$	4.01	OK
$\mu_z = 4.40$	4.01	OK

* The typical simulated length is the mean lengths estimated from “simulated boreholes” through the simulated rock volumes. The nominal value is the typical length estimated from the transition analysis in T-PROGS.

Table I-14. Typical lengths of TRC102 in domain RSMD01.

Typical simulated length (m)*	Nominal value (m)*	Comment on simulated values
$\mu_x = 13.91$	37.1	Low
$\mu_y = 9.67$	37.1	Low
$\mu_z = 4.68$	3.71	OK

* The typical simulated length is the mean lengths estimated from “simulated boreholes” through the simulated rock volumes. The nominal value is the typical length estimated from the transition analysis in T-PROGS.

Table I-15. Typical lengths of TRC136 in domain RSMD01.

Typical simulated length (m)*	Nominal value (m)*	Comment on simulated values
$\mu_x = 3.99$	2.68	Somewhat high
$\mu_y = 4.04$	2.68	Somewhat high
$\mu_z = 3.93$	2.68	Somewhat high

* The typical simulated length is the mean lengths estimated from “simulated boreholes” through the simulated rock volumes. The nominal value is the typical length estimated from the transition analysis in T-PROGS.

Domain RSMM01

The results of the calculations of the typical length (m) for directions x, y and z for subdomain M1 are presented in Table 16 to Table 18.

It can be seen from the analysis that T-PROGS does not reproduce any directional bias for subdomain M1. T-PROGS somewhat overestimates typical lengths. Nominal lengths for all TRCs are relatively short in subdomain M1 and for TRC58 only 1.5 times the model resolution. The reason for overestimation of shorter lengths is the discretisation of the model, where 2 metres is the shortest length that can be represented.

The results of the calculations of the typical lengths (m) for directions x, y and z for subdomain M2 are presented in Table 19 to Table 21.

Table I-16. Typical lengths of TRC33 in subdomain M1 for the 2 metre scale.

Typical simulated length (m)*	Nominal value (m)*	Comment on simulated values
$\mu_x=5.34$	4.61	Somewhat high
$\mu_y=5.60$	4.61	Somewhat high
$\mu_z=5.88$	4.61	Somewhat high

* The typical simulated length is the mean lengths estimated from “simulated boreholes” through the simulated rock volumes. The nominal value is the typical length estimated from the transition analysis in T-PROGS.

Table I-17. Typical lengths of TRC56 in subdomain M1 for the 2 metre scale.

Typical simulated length (m)*	Nominal value (m)*	Comment on simulated values
$\mu_x=5.38$	4.04	Somewhat high
$\mu_y=5.14$	4.04	Somewhat high
$\mu_z=5.16$	4.04	Somewhat high

* The typical simulated length is the mean lengths estimated from “simulated boreholes” through the simulated rock volumes. The nominal value is the typical length estimated from the transition analysis in T-PROGS.

Table I-18. Typical lengths of TRC58 in subdomain M1 for the 2 metre scale.

Typical simulated length (m)*	Nominal value (m)*	Comment on simulated values
$\mu_x=3.84$	3.00	Somewhat high
$\mu_y=3.86$	3.00	Somewhat high
$\mu_z=4.14$	3.00	Somewhat high

* The typical simulated length is the mean lengths estimated from “simulated boreholes” through the simulated rock volumes. The nominal value is the typical length estimated from the transition analysis in T-PROGS.

Table I-19. Typical lengths of TRC33 in subdomain M2 for the 2 metre scale.

Typical simulated length (m)*	Nominal value (m)*	Comment on simulated values
$\mu_x=11.0$	10.77	OK
$\mu_y=10.8$	10.77	OK
$\mu_z=11.4$	10.77	OK

* The typical simulated length is the mean lengths estimated from “simulated boreholes” through the simulated rock volumes. The nominal value is the typical length estimated from the transition analysis in T-PROGS.

Table I-20. Typical lengths of TRC56 in subdomain M2 for the 2 metre scale.

Typical simulated length (m)*	Nominal value (m)*	Comment on simulated values
$\mu_x = 4.08$	3.06	Somewhat high
$\mu_y = 4.39$	3.06	Somewhat high
$\mu_z = 4.00$	3.06	Somewhat high

* The typical simulated length is the mean lengths estimated from “simulated boreholes” through the simulated rock volumes. The nominal value is the typical length estimated from the transition analysis in T-PROGS.

Table I-21. Typical lengths of TRC58 in subdomain M2 for the 2 metre scale.

Typical simulated length (m)*	Nominal value (m)*	Comment on simulated values
$\mu_x = 4.39$	3.00	Somewhat high
$\mu_y = 4.10$	3.00	Somewhat high
$\mu_z = 4.18$	3.00	Somewhat high

* The typical simulated length is the mean lengths estimated from “simulated boreholes” through the simulated rock volumes. The nominal value is the typical length estimated from the transition analysis in T-PROGS.

It can be seen from the analysis that T-PROGS does not reproduce any directional bias for subdomain M2. T-PROGS somewhat overestimates typical lengths for TRC56 and TRC 58. Nominal lengths for these TRCs are relatively short in subdomain M2 and only 1.5 times the model resolution. The reason for overestimation of shorter lengths is the discretisation of the model, where 2 metres is the shortest length that can be represented.

The results of the calculations of the typical lengths (m) for directions x, y and z for subdomain M3 are presented in Table 22 and Table 23.

It can be seen from the analysis that T-PROGS does not reproduce any directional bias for subdomain M3. T-PROGS reproduces typical lengths for TRC33 well, but provides slight overestimations of TRC56 lengths. The reason for the slight overestimations of TRC46 is not known.

Table I-22. Typical lengths of TRC33 in subdomain M3 for the 2 metre scale.

Typical simulated length (m)*	Nominal value (m)*	Comment on simulated values
$\mu_x = 7.20$	6.67	OK
$\mu_y = 6.92$	6.67	OK
$\mu_z = 7.04$	6.67	OK

* The typical simulated length is the mean lengths estimated from “simulated boreholes” through the simulated rock volumes. The nominal value is the typical length estimated from the transition analysis in T-PROGS.

Table I-23. Typical lengths of TRC46 in subdomain M3 for the 2 metre scale.

Typical simulated length (m)*	Nominal value (m)*	Comment on simulated values
$\mu_x = 6.20$	5.40	Somewhat high
$\mu_y = 6.20$	5.40	Somewhat high
$\mu_z = 6.20$	5.40	Somewhat high

* The typical simulated length is the mean lengths estimated from “simulated boreholes” through the simulated rock volumes. The nominal value is the typical length estimated from the transition analysis in T-PROGS.

The results of the calculations of the typical lengths (m) for directions x, y and z for subdomain M4 are presented in Table I-24 to Table I-25.

It can be seen from the analysis that T-PROGS does not reproduce any directional bias for subdomain M4. T-PROGS somewhat overestimates typical lengths for TRC33 and TRC46. Nominal lengths for all TRC46 are relatively short in subdomain M2 and only 2 times the model resolution. An overestimation of shorter lengths is expected due to discretisation effects, where 2 metres is the shortest length that can be represented. The reason for the slight overestimations of TRC33 is not known.

The results of the calculations of the typical lengths (m) for directions x, y and z for subdomain M5 are presented in Table 26 to Table 28.

Table I-24. Typical lengths of TRC33 in subdomain M4 for the 2 metre scale.

Typical simulated length (m)*	Nominal value (m)*	Comment on simulated values
$\mu_x = 9.22$	8.26	Somewhat high
$\mu_y = 9.03$	8.26	Somewhat high
$\mu_z = 9.19$	8.26	Somewhat high

* The typical simulated length is the mean lengths estimated from “simulated boreholes” through the simulated rock volumes. The nominal value is the typical length estimated from the transition analysis in T-PROGS.

Table I-25. Typical lengths of TRC46 in subdomain M4 for the 2 metre scale.

Typical simulated length (m)*	Nominal value (m)*	Comment on simulated values
$\mu_x = 5.56$	4.17	Somewhat high
$\mu_y = 5.08$	4.17	Somewhat high
$\mu_z = 5.32$	4.17	Somewhat high

* The typical simulated length is the mean lengths estimated from “simulated boreholes” through the simulated rock volumes. The nominal value is the typical length estimated from the transition analysis in T-PROGS.

Table I-26. Typical lengths of TRC33 in subdomain M5 for the 2 metre scale.

Typical simulated length (m)*	Nominal value (m)*	Comment on simulated values
$\mu_x = 3.11$	2.00	Somewhat high
$\mu_y = 2.94$	2.00	Somewhat high
$\mu_z = 3.12$	2.00	Somewhat high

* The typical simulated length is the mean lengths estimated from “simulated boreholes” through the simulated rock volumes. The nominal value is the typical length estimated from the transition analysis in T-PROGS.

Table I-27. Typical lengths of TRC46 in subdomain M5 for the 2 metre scale.

Typical simulated length (m)*	Nominal value (m)*	Comment on simulated values
$\mu_x = 4.51$	3.45	Somewhat high
$\mu_y = 4.44$	3.45	Somewhat high
$\mu_z = 4.45$	3.45	Somewhat high

* The typical simulated length is the mean lengths estimated from “simulated boreholes” through the simulated rock volumes. The nominal value is the typical length estimated from the transition analysis in T-PROGS.

Table I-28. Typical lengths of TRC58 in subdomain M5 for the 2 metre scale.

Typical simulated length (m)*	Nominal value (m)*	Comment on simulated values
$\mu_x = 8.95$	8.00	Somewhat high
$\mu_y = 8.59$	8.00	OK
$\mu_z = 8.90$	8.00	Somewhat high

* The typical simulated length is the mean lengths estimated from “simulated boreholes” through the simulated rock volumes. The nominal value is the typical length estimated from the transition analysis in T-PROGS.

It can be seen from the analysis that T-PROGS does not reproduce any directional bias for subdomain M5. T-PROGS somewhat overestimates typical lengths. Nominal lengths for TRC33 and TRC46 are short in subdomain M5 and for TRC33 has a nominal value equal to the model resolution. The reason for overestimation of shorter lengths is the discretisation of the model, where 2 metres is the shortest length that can be represented.

Histograms of TRC length distributions in realisations

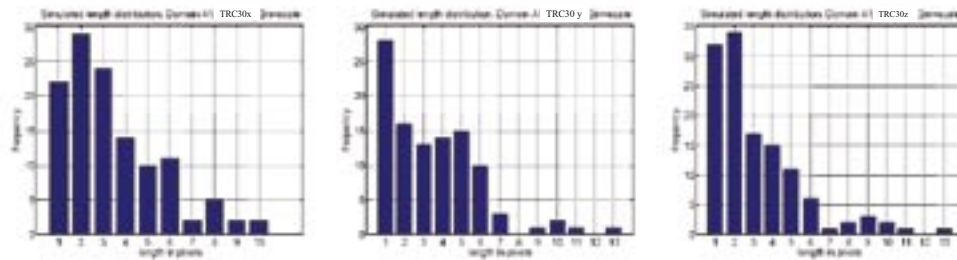


Figure 1. Histogram from 36 "borings" in 10 randomly selected realisations of TRC30 in x-, y- and z-direction. Domain A1. X-axis in pixels (px); 1 px = 2m.

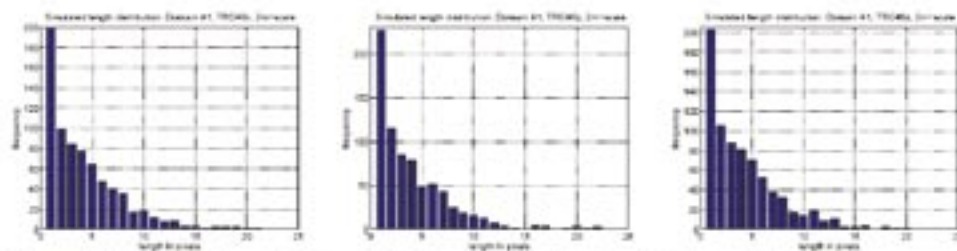


Figure 2. Histogram from 36 "borings" in 10 randomly selected realisations of TRC 46 in x-, y- and z-direction. Domain A1. X-axis in pixels (px); 1px = 2m.

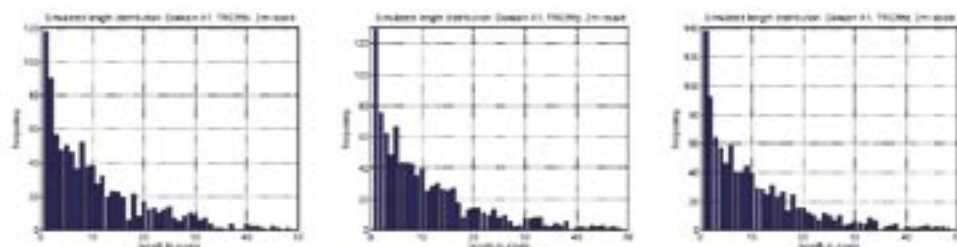


Figure 3. Histogram from 36 "borings" in 10 randomly selected realisations of TRC 56 in x-, y- and z-direction. Domain A1. X-axis in pixels (px); 1px = 2m.

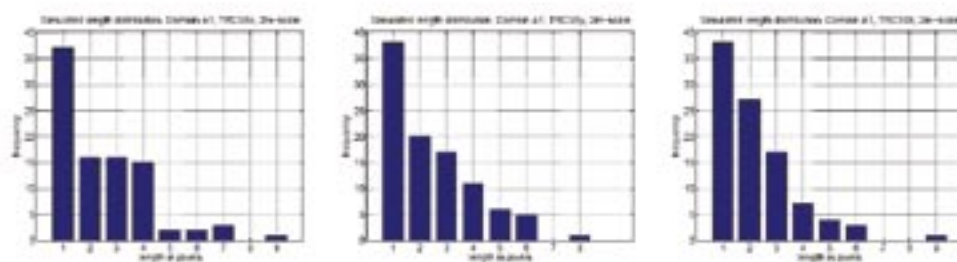


Figure 4. Histogram from 36 "borings" in 10 randomly selected realisations of TRC 58 in x-, y- and z-direction. Domain A1. X-axis in pixels (px); 1px = 2m.

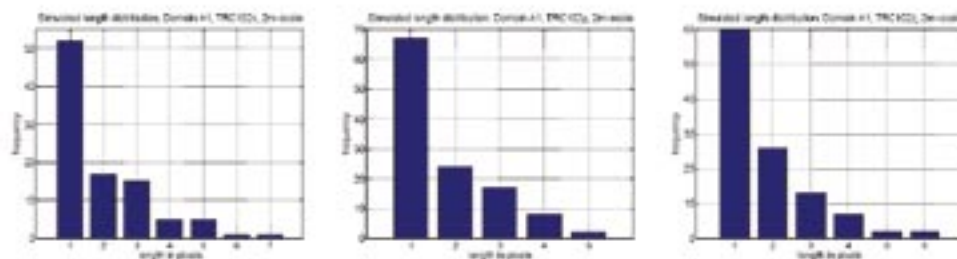


Figure 5. Histogram from 36 "borings" in 10 randomly selected realisations of TRC 102 in x-, y- and z-direction. Domain A1. X-axis in pixels (px); 1px = 2m.

Figure J-1. Histograms of TRC length distributions in realisations at 2 m scale, Subdomain A1.

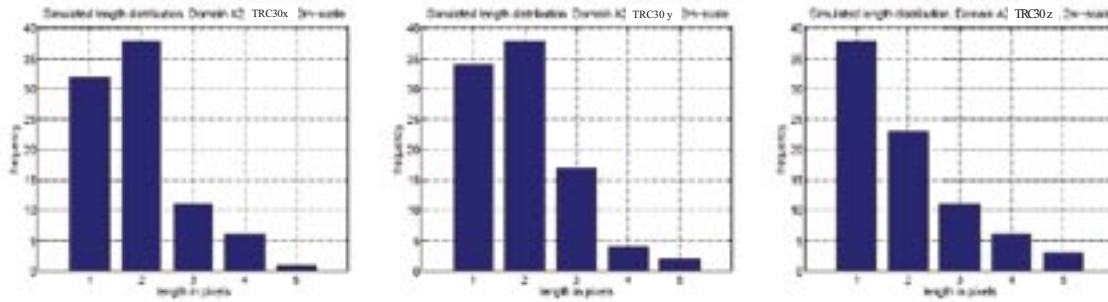


Figure 1. Histogram from 36 "borings" in 10 randomly selected realisations of TRC30 in x-, y- and z-direction. Domain A2. X-axis in pixels (px); 1 px = 2m.

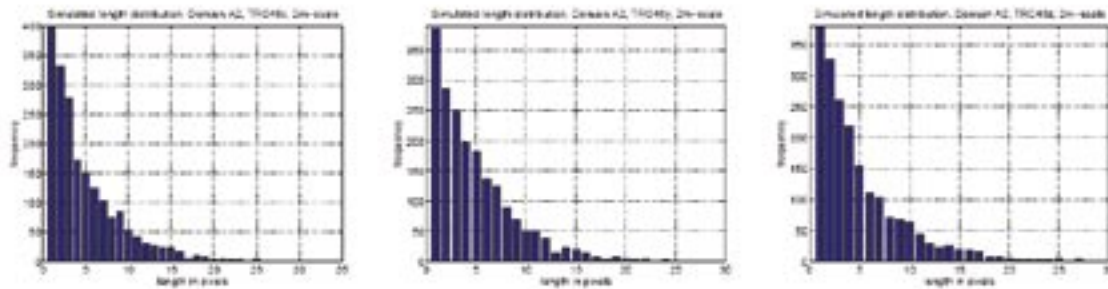


Figure 2. Histogram from 36 "borings" in 10 randomly selected realisations of TRC 46 in x-, y- and z-direction. Domain A2. X-axis in pixels (px); 1px = 2m.

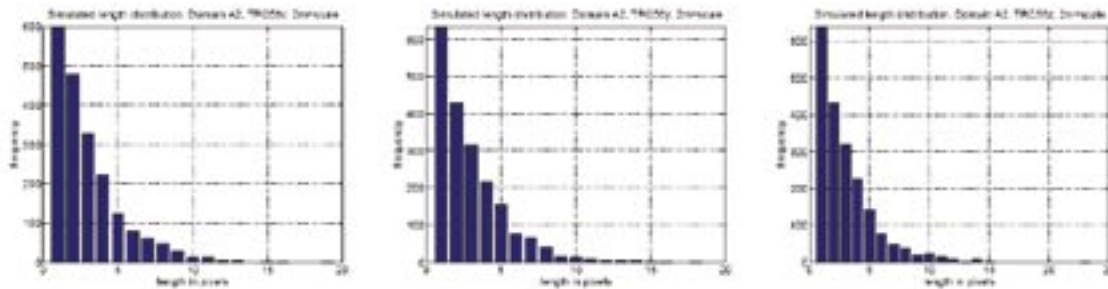


Figure 3. Histogram from 36 "borings" in 10 randomly selected realisations of TRC 56 in x-, y- and z-direction. Domain A2. X-axis in pixels (px); 1px = 2m.

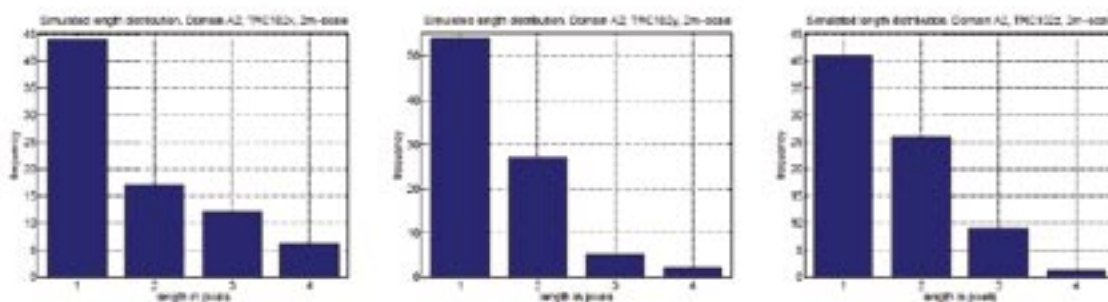


Figure 4. Histogram from 36 "borings" in 10 randomly selected realisations of TRC 58 in x-, y- and z-direction. Domain A2. X-axis in pixels (px); 1px = 2m.

Figure J-2. Histograms of TRC length distributions in realisations at 2 m scale, Subdomain A2.

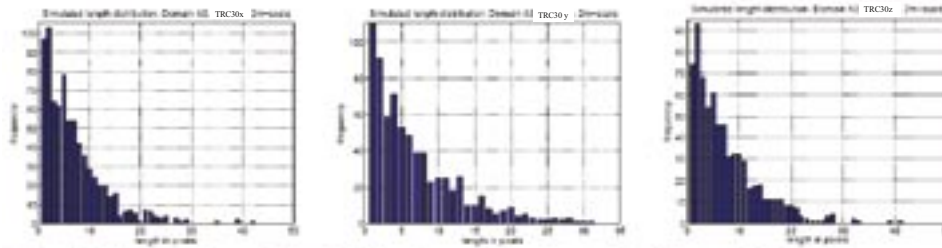


Figure 1. Histogram from 36 "borings" in 10 randomly selected realisations of TRC30 in x-, y- and z-direction. Domain A3. X-axis in pixels (px); 1 px = 2m.

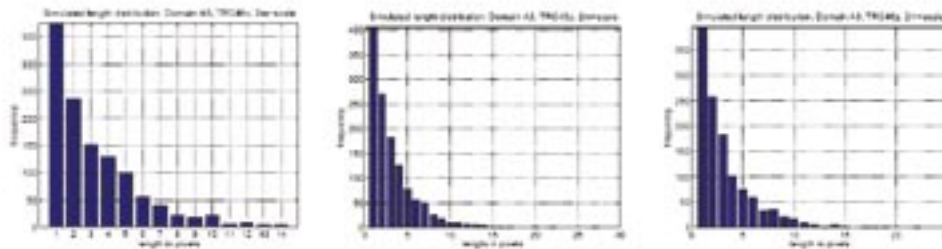


Figure 2. Histogram from 36 "borings" in 10 randomly selected realisations of TRC 46 in x-, y- and z-direction. Domain A3. X-axis in pixels (px); 1px = 2m.

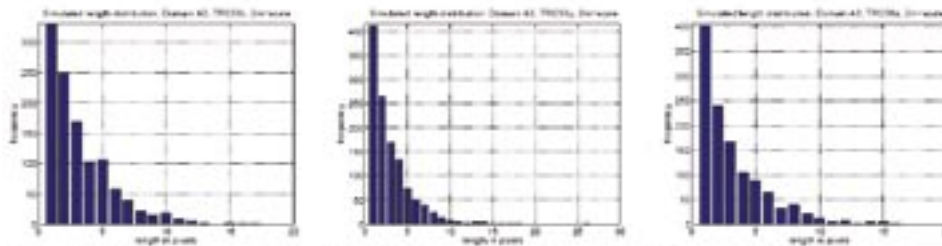


Figure 3. Histogram from 36 "borings" in 10 randomly selected realisations of TRC 56 in x-, y- and z-direction. Domain A3. X-axis in pixels (px); 1px = 2m.

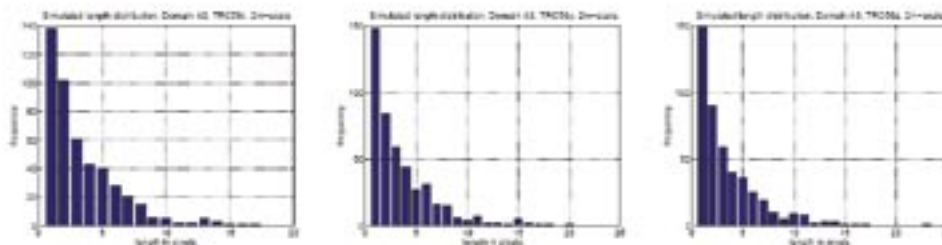


Figure 4. Histogram from 36 "borings" in 10 randomly selected realisations of TRC 58 in x-, y- and z-direction. Domain A3. X-axis in pixels (px); 1px = 2m.

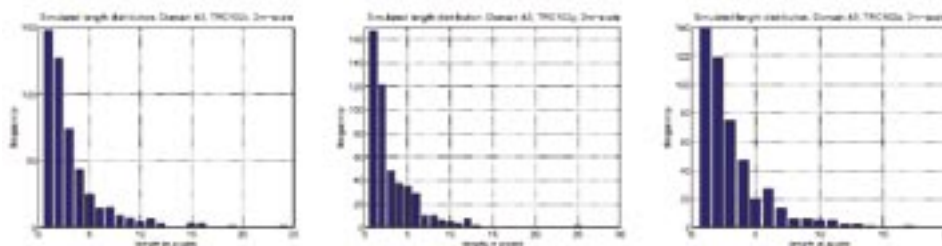


Figure 5. Histogram from 36 "borings" in 10 randomly selected realisations of TRC 102 in x-, y- and z-direction. Domain A3. X-axis in pixels (px); 1px = 2m.

Figure J-3. Histograms of TRC length distributions in realisations at 2 m scale, Subdomain A3.

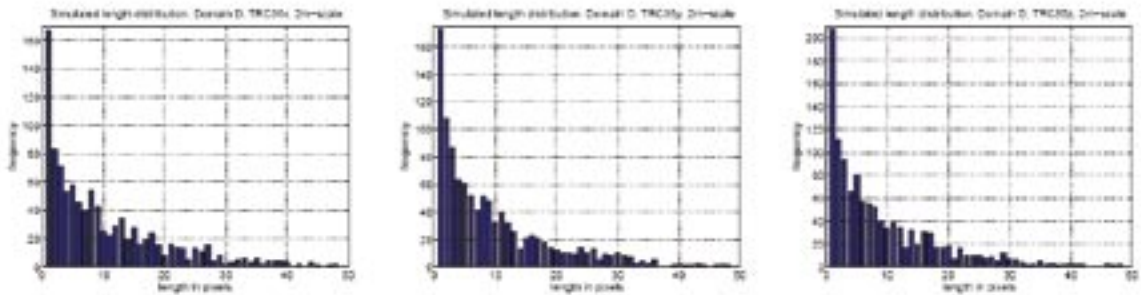


Figure 1. Histogram from 36 "borings" in 10 randomly selected realisations of TRC 36 in x -, y - and z -direction. Domain D. X -axis in pixels (px); 1px = 2m.

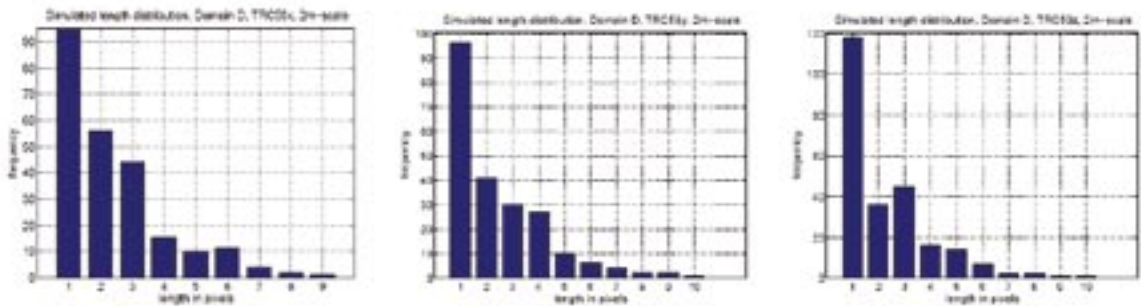


Figure 2. Histogram from 36 "borings" in 10 randomly selected realisations of TRC 58 in x -, y - and z -direction. Domain D. X -axis in pixels (px); 1px = 2m.

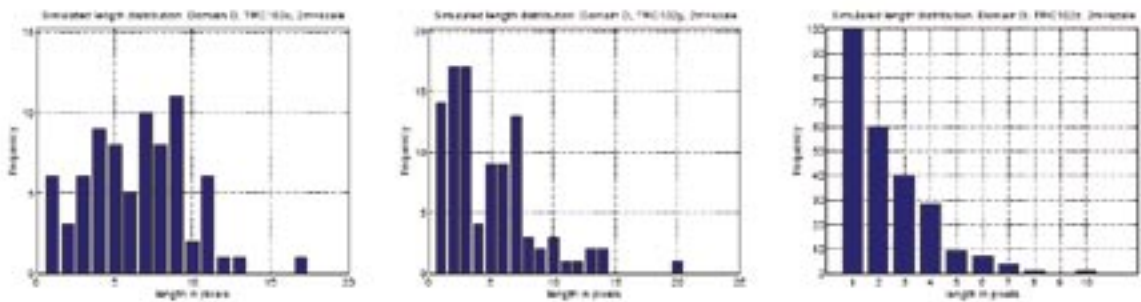


Figure 3. Histogram from 36 "borings" in 10 randomly selected realisations of TRC 102 in x -, y - and z -direction. Domain D. X -axis in pixels (px); 1px = 2m.

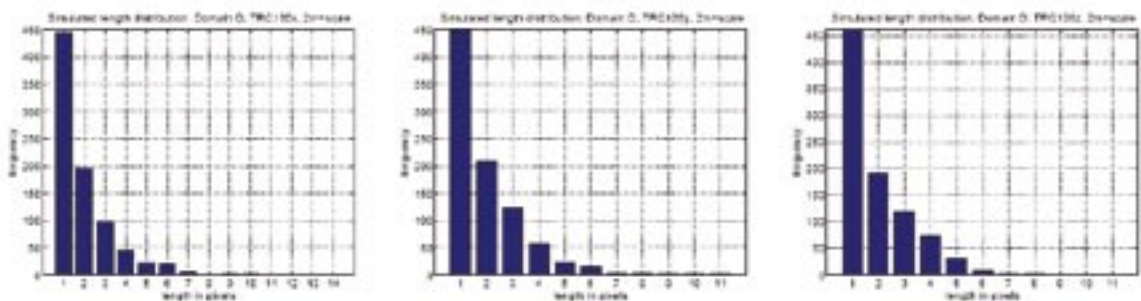


Figure 4. Histogram from 36 "borings" in 10 randomly selected realisations of TRC 136 in x -, y - and z -direction. Domain D. X -axis in pixels (px); 1px = 2m.

Figure J-4. Histograms of TRC length distributions in realisations at 2 m scale, Domain RSMD01.

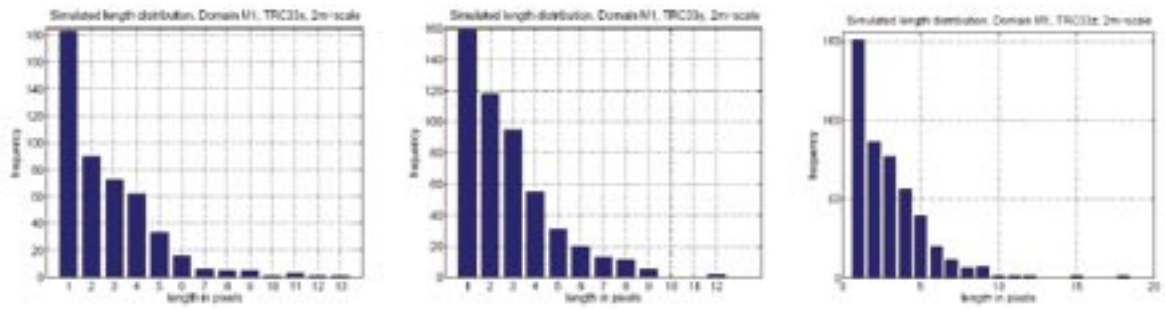


Figure 1. Histogram from 36 "borings" in 10 randomly selected realisations of TRC 33 in x -, y - and z -direction. Domain M1. X-axis in pixels (px); 1px = 2m.

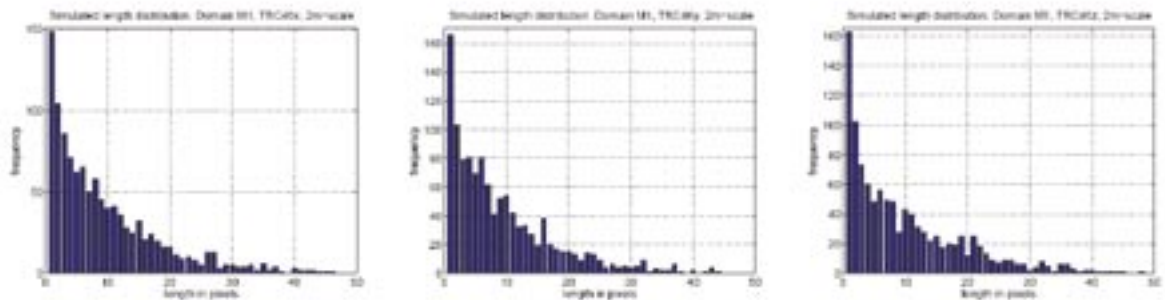


Figure 2. Histogram from 36 "borings" in 10 randomly selected realisations of TRC 46 in x -, y - and z -direction. Domain M1. X-axis in pixels (px); 1px = 2m.

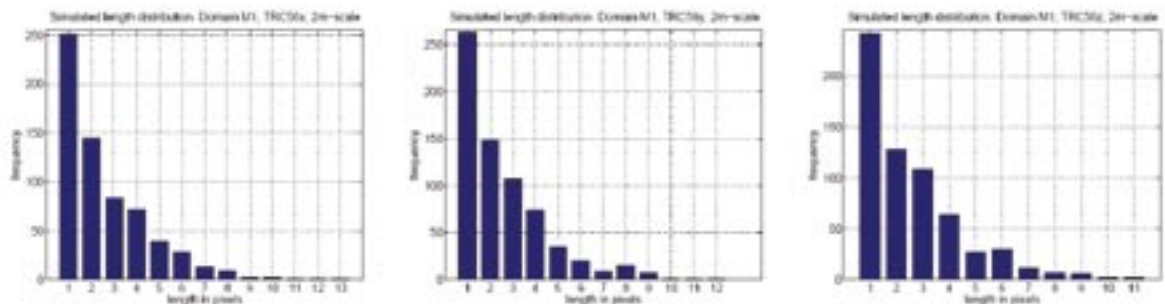


Figure 3. Histogram from 36 "borings" in 10 randomly selected realisations of TRC 56 in x -, y - and z -direction. Domain M1. X-axis in pixels (px); 1px = 2m.

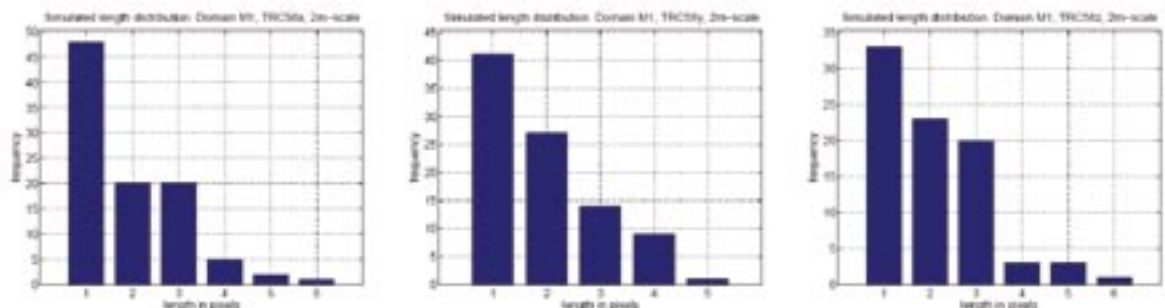


Figure 4. Histogram from 36 "borings" in 10 randomly selected realisations of TRC 58 in x -, y - and z -direction. Domain M1. X-axis in pixels (px); 1px = 2m.

Figure J-5. Histograms of TRC length distributions in realisations at 2 m scale, Subdomain M1.

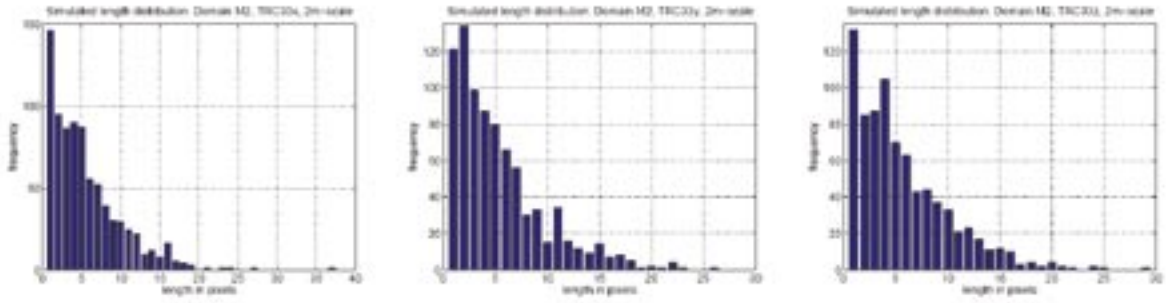


Figure 1. Histogram from 36 "borings" in 10 randomly selected realisations of TRC 33 in x -, y - and z -direction. Domain M2. X -axis in pixels (px); 1px = 2m.

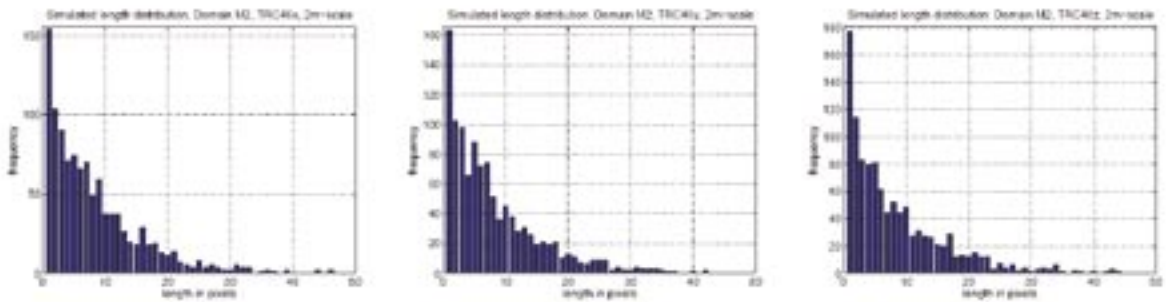


Figure 2. Histogram from 36 "borings" in 10 randomly selected realisations of TRC 46 in x -, y - and z -direction. Domain M2. X -axis in pixels (px); 1px = 2m.

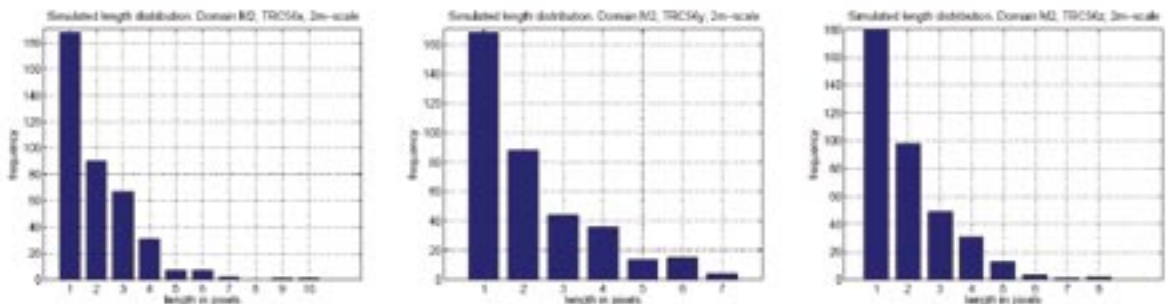


Figure 3. Histogram from 36 "borings" in 10 randomly selected realisations of TRC 56 in x -, y - and z -direction. Domain M2. X -axis in pixels (px); 1px = 2m.

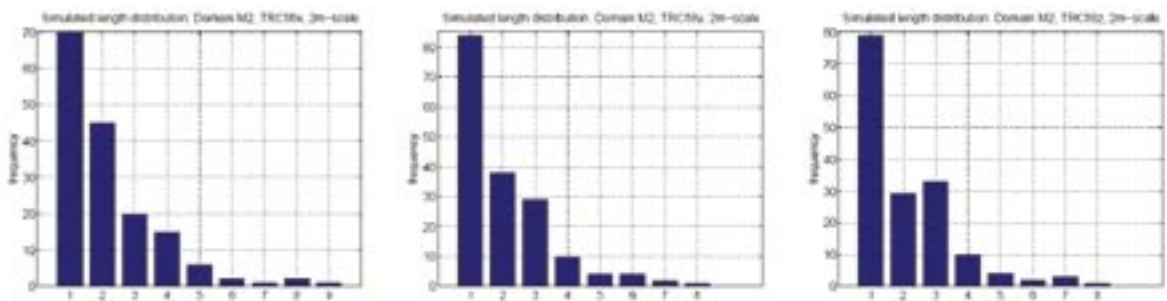


Figure 4. Histogram from 36 "borings" in 10 randomly selected realisations of TRC 58 in x -, y - and z -direction. Domain M2. X -axis in pixels (px); 1px = 2m.

Figure J-6. Histograms of TRC length distributions in realisations at 2 m scale, Subdomain M2.

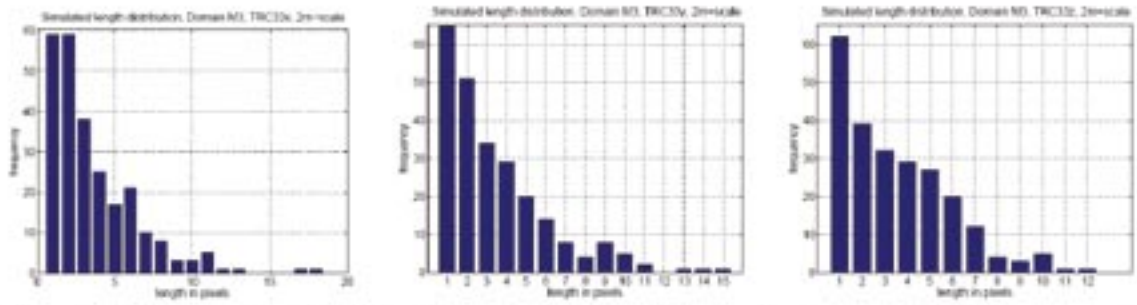


Figure 1. Histogram from 36 "borings" in 10 randomly selected realisations of TRC 33 in x -, y - and z -direction. Domain M3. X -axis in pixels (px); $1\text{px} = 2\text{m}$.

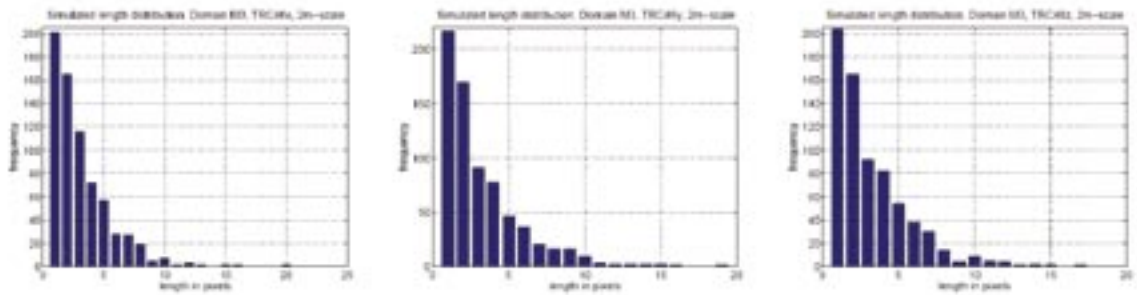


Figure 2. Histogram from 36 "borings" in 10 randomly selected realisations of TRC 46 in x -, y - and z -direction. Domain M3. X -axis in pixels (px); $1\text{px} = 2\text{m}$.

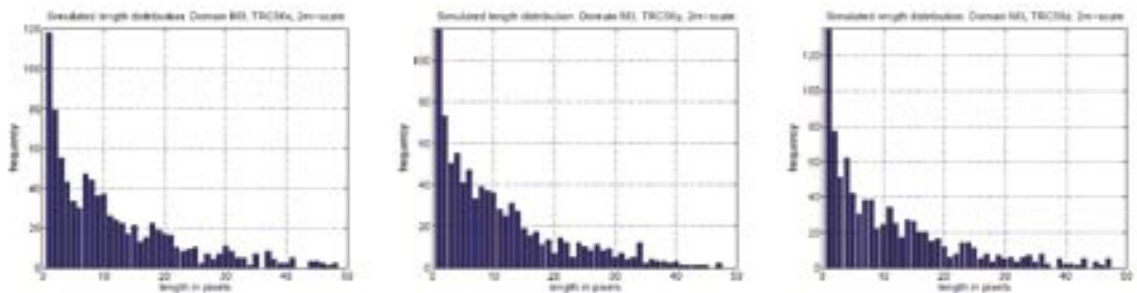


Figure 3. Histogram from 36 "borings" in 10 randomly selected realisations of TRC 56 in x -, y - and z -direction. Domain M3. X -axis in pixels (px); $1\text{px} = 2\text{m}$.

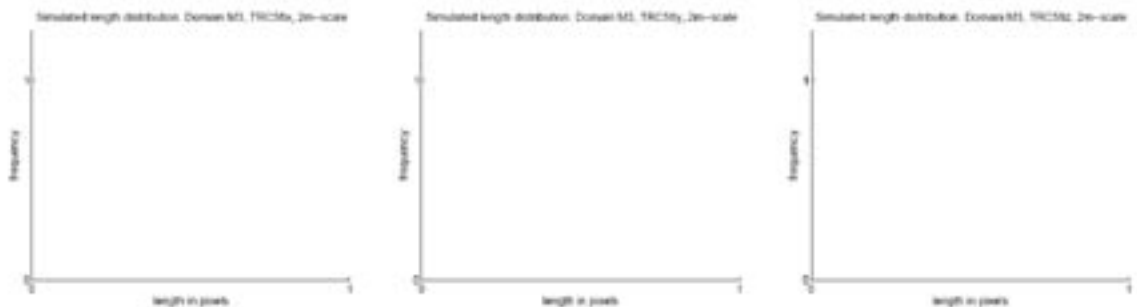


Figure 4. Histogram from 36 "borings" in 10 randomly selected realisations of TRC 58 in x -, y - and z -direction. Domain M3. X -axis in pixels (px); $1\text{px} = 2\text{m}$.

Figure J-7. Histograms of TRC length distributions in realisations at 2 m scale, Subdomain M3.

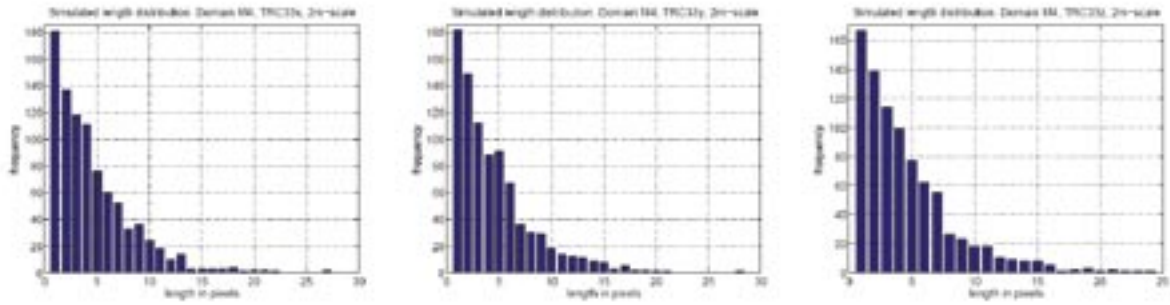


Figure 1. Histogram from 36 "borings" in 10 randomly selected realisations of TRC 33 in x -, y - and z -direction. Domain M4. X -axis in pixels (px); 1px = 2m.

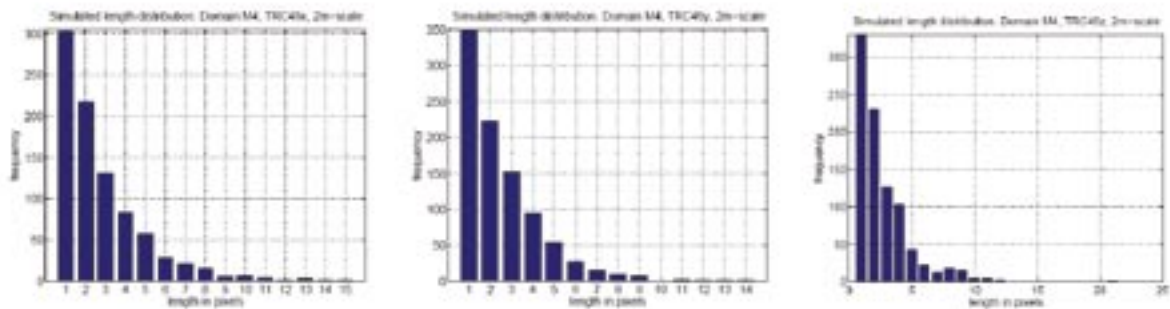


Figure 2. Histogram from 36 "borings" in 10 randomly selected realisations of TRC 46 in x -, y - and z -direction. Domain M4. X -axis in pixels (px); 1px = 2m.

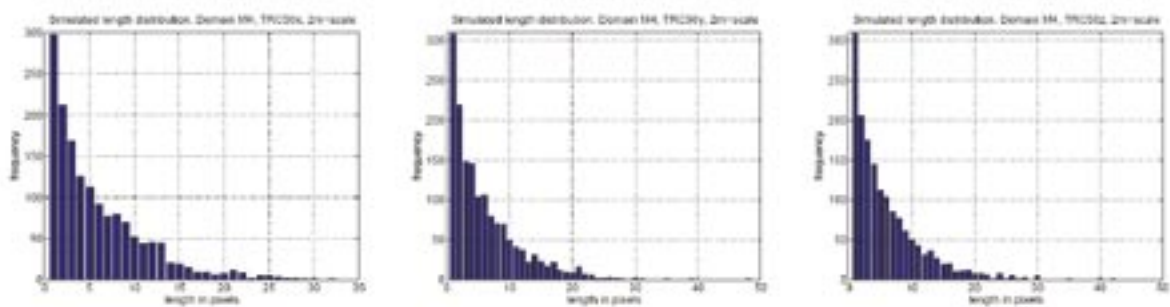


Figure 3. Histogram from 36 "borings" in 10 randomly selected realisations of TRC 56 in x -, y - and z -direction. Domain M4. X -axis in pixels (px); 1px = 2m.

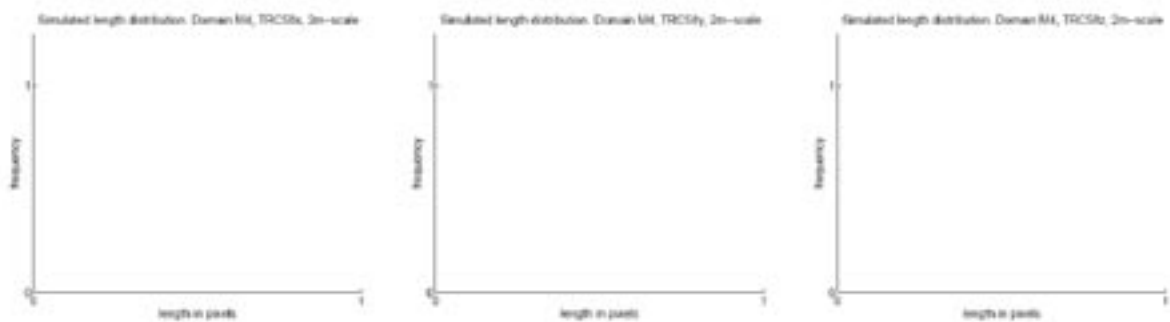


Figure 4. Histogram from 36 "borings" in 10 randomly selected realisations of TRC 58 in x -, y - and z -direction. Domain M4. X -axis in pixels (px); 1px = 2m.

Figure J-8. Histograms of TRC length distributions in realisations at 2 m scale, Subdomain M4.

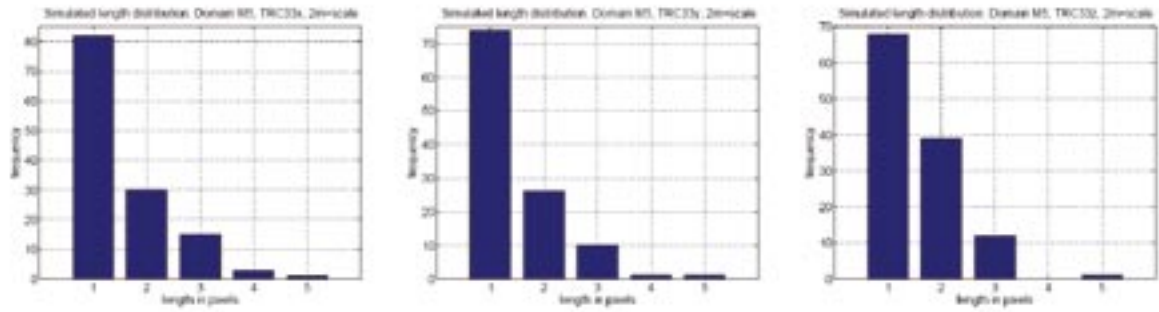


Figure 1. Histogram from 36 "borings" in 10 randomly selected realisations of TRC 33 in x -, y - and z -direction. Domain M5. X -axis in pixels (px); 1px = 2m.

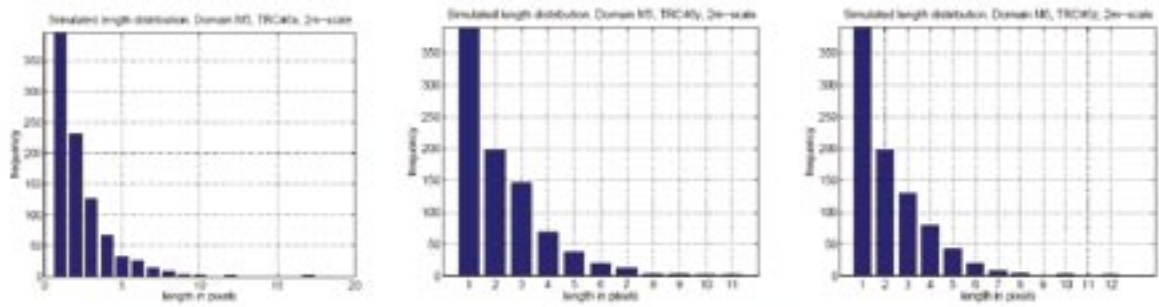


Figure 2. Histogram from 36 "borings" in 10 randomly selected realisations of TRC 46 in x -, y - and z -direction. Domain M5. X -axis in pixels (px); 1px = 2m.

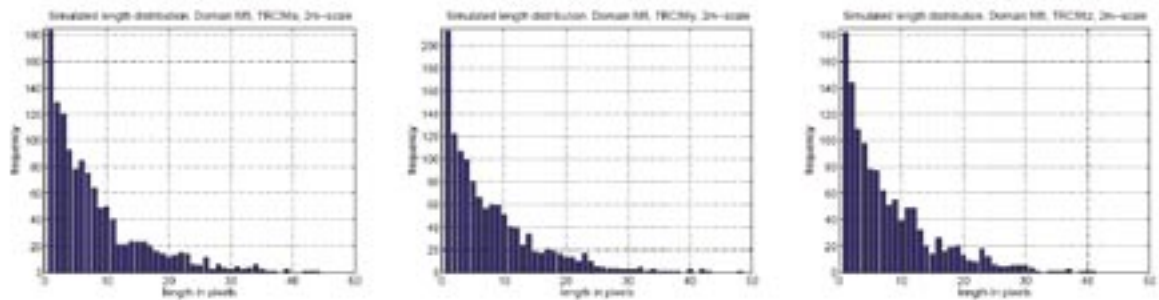


Figure 3. Histogram from 36 "borings" in 10 randomly selected realisations of TRC 56 in x -, y - and z -direction. Domain M5. X -axis in pixels (px); 1px = 2m.

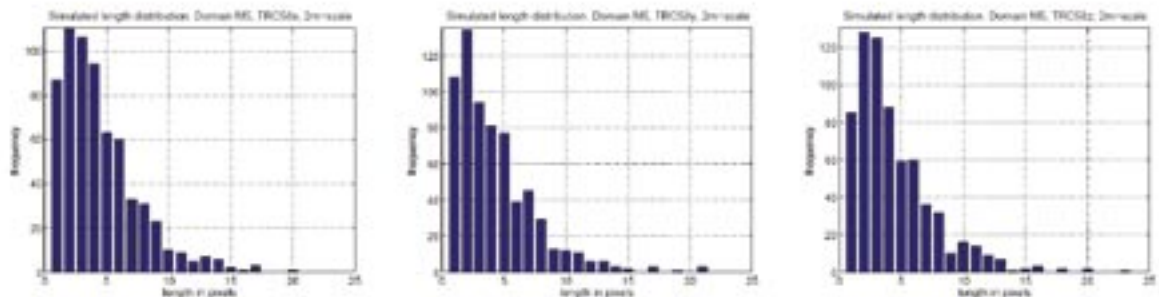


Figure 4. Histogram from 36 "borings" in 10 randomly selected realisations of TRC 58 in x -, y - and z -direction. Domain M5. X -axis in pixels (px); 1px = 2m.

Figure J-9. Histograms of TRC length distributions in realisations at 2 m scale, Subdomain M5.

Histograms of TRC length distributions in boreholes

Histograms of TRC length distributions in boreholes, Domain RSMA01

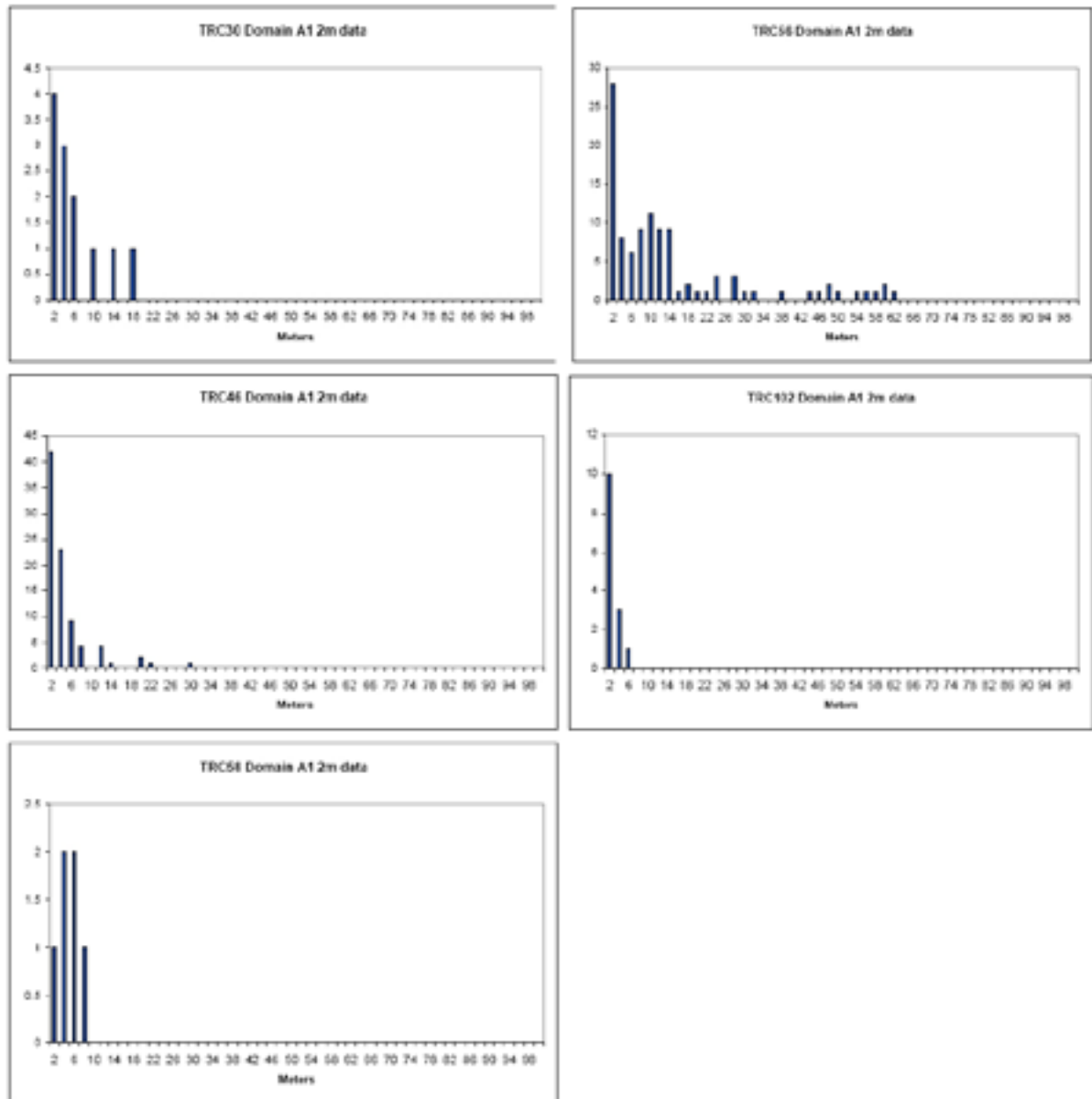


Figure K-1. Histograms of TRC lengths observed in borehole data in subdomain A1.

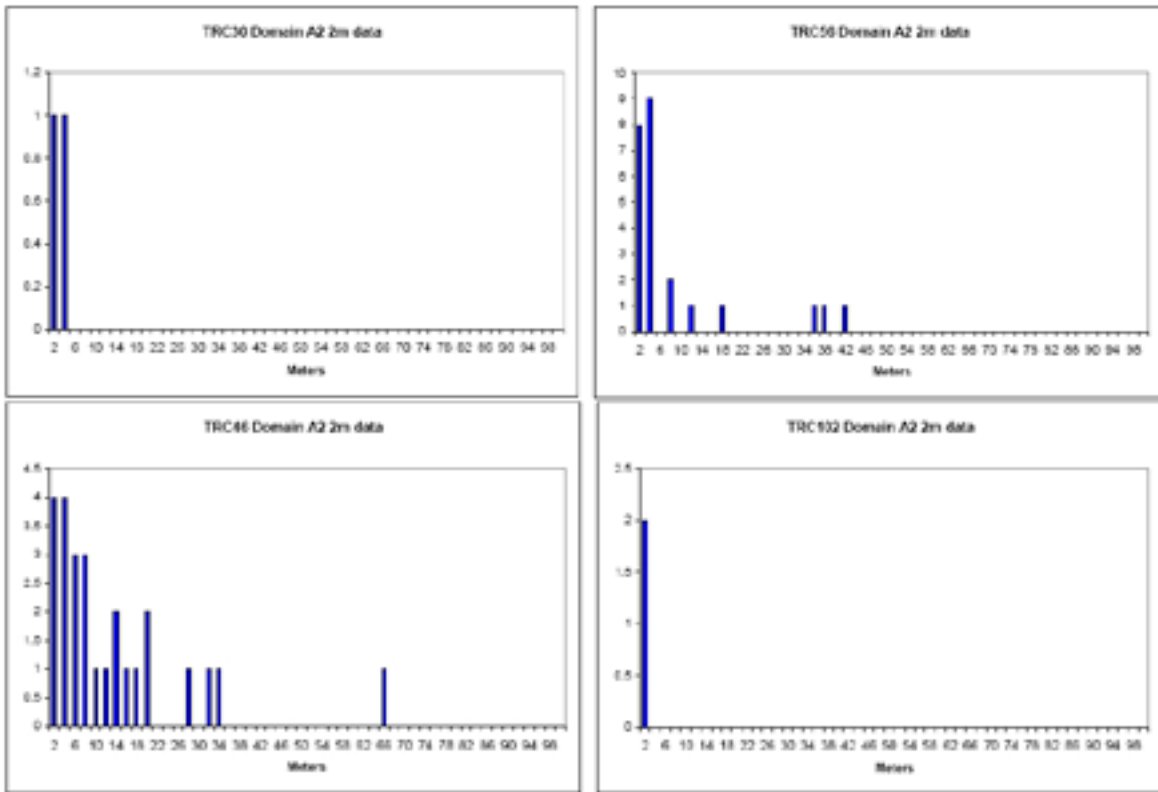


Figure K-2. Histograms of TRC lengths observed in borehole data in subdomain A2.

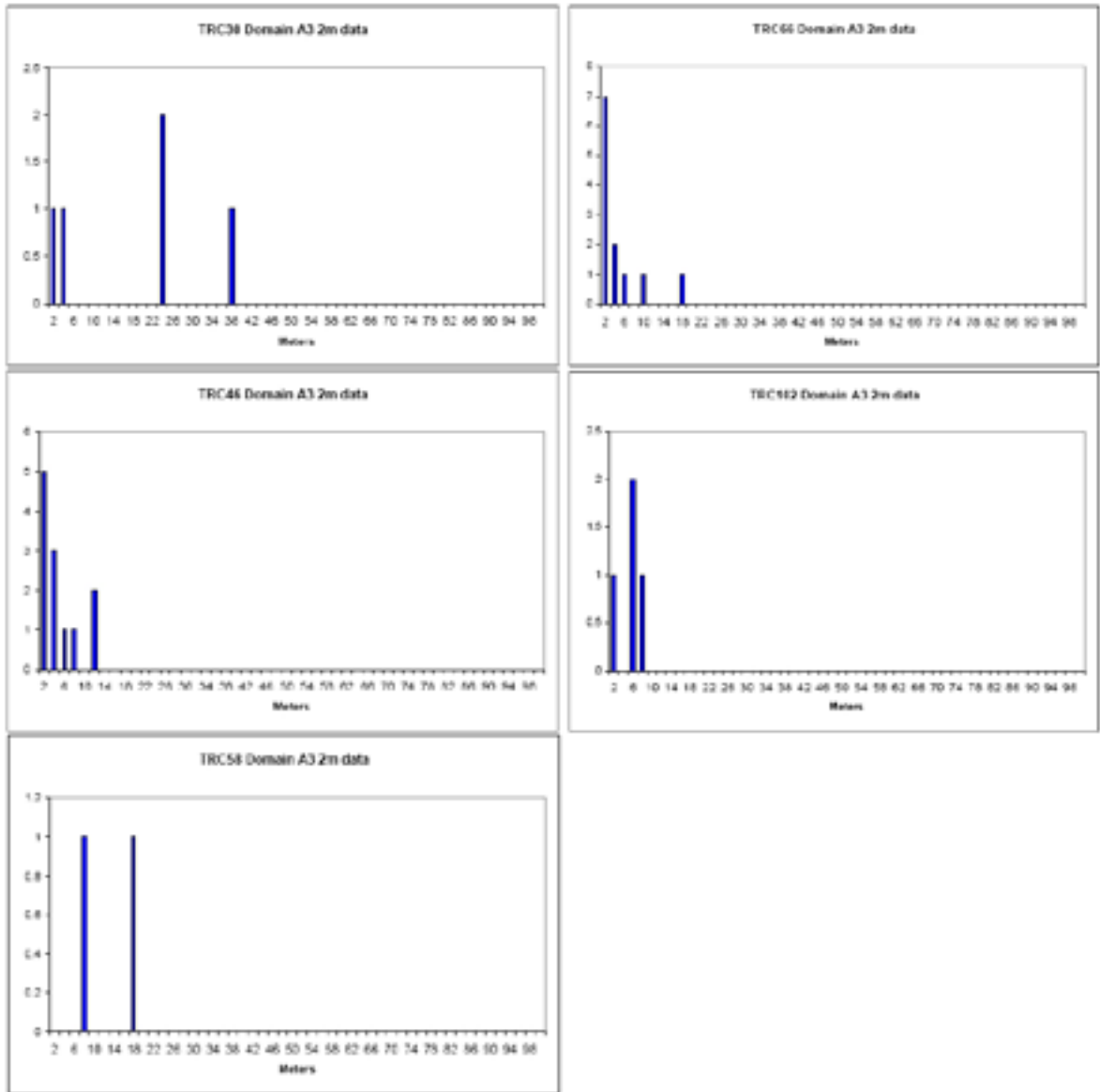


Figure K-3. Histograms of TRC lengths observed in borehole data in subdomain A3.

Histograms of TRC length distributions in boreholes Domain RSMD01

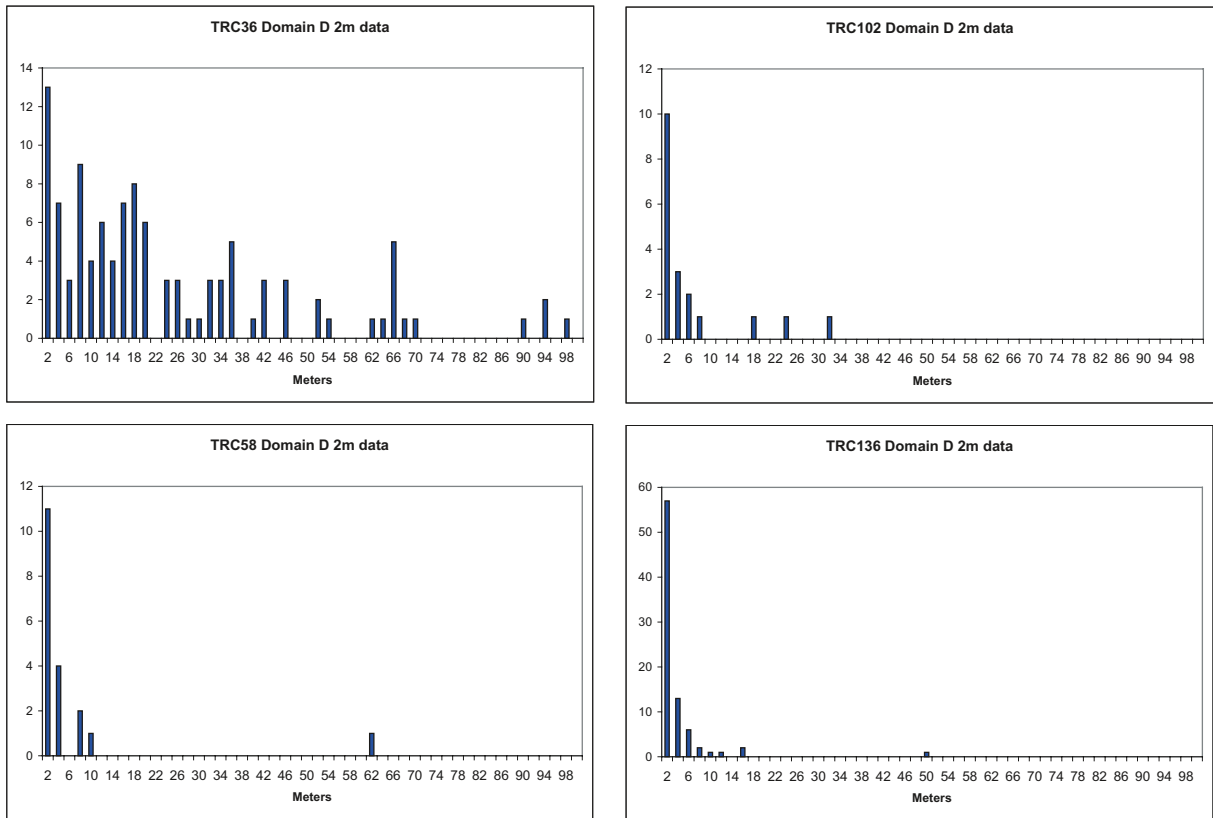


Figure K-4. Histograms of TRC lengths observed in borehole data in domain RSMD01.

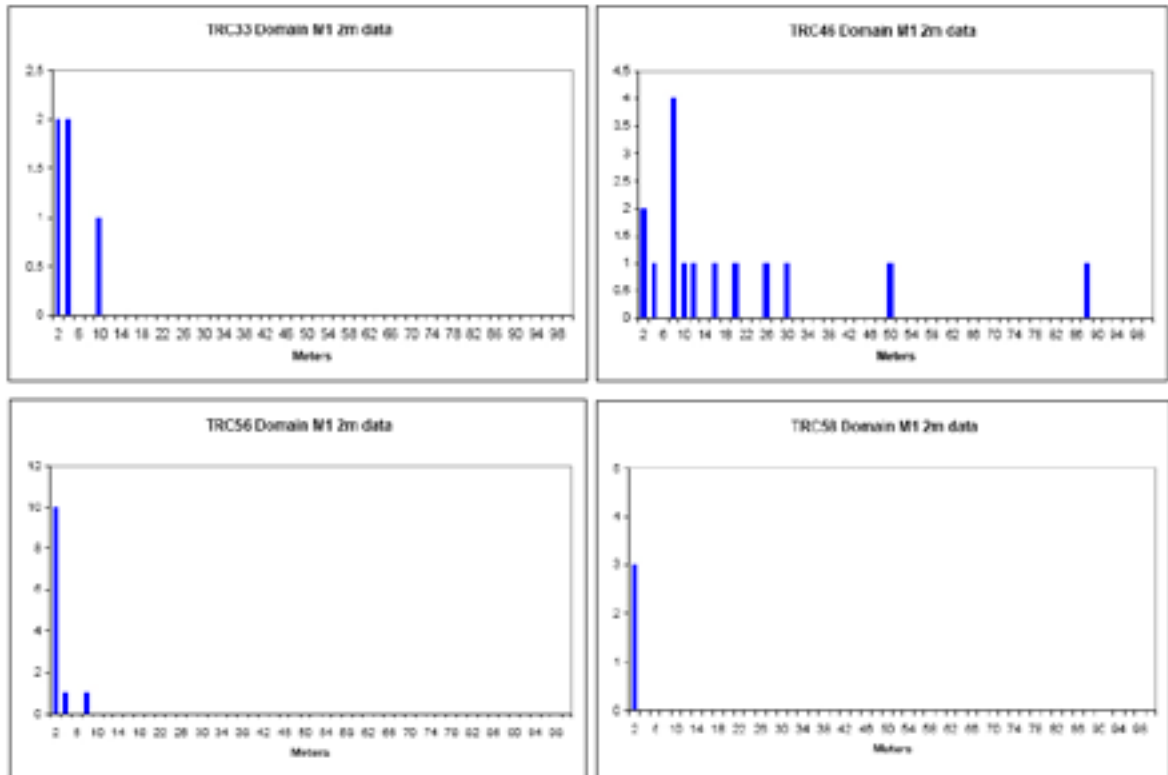


Figure K-5. Histograms of TRC lengths observed in borehole data in subdomain M1.

Histograms of TRC length distributions in boreholes Domain RSMM01

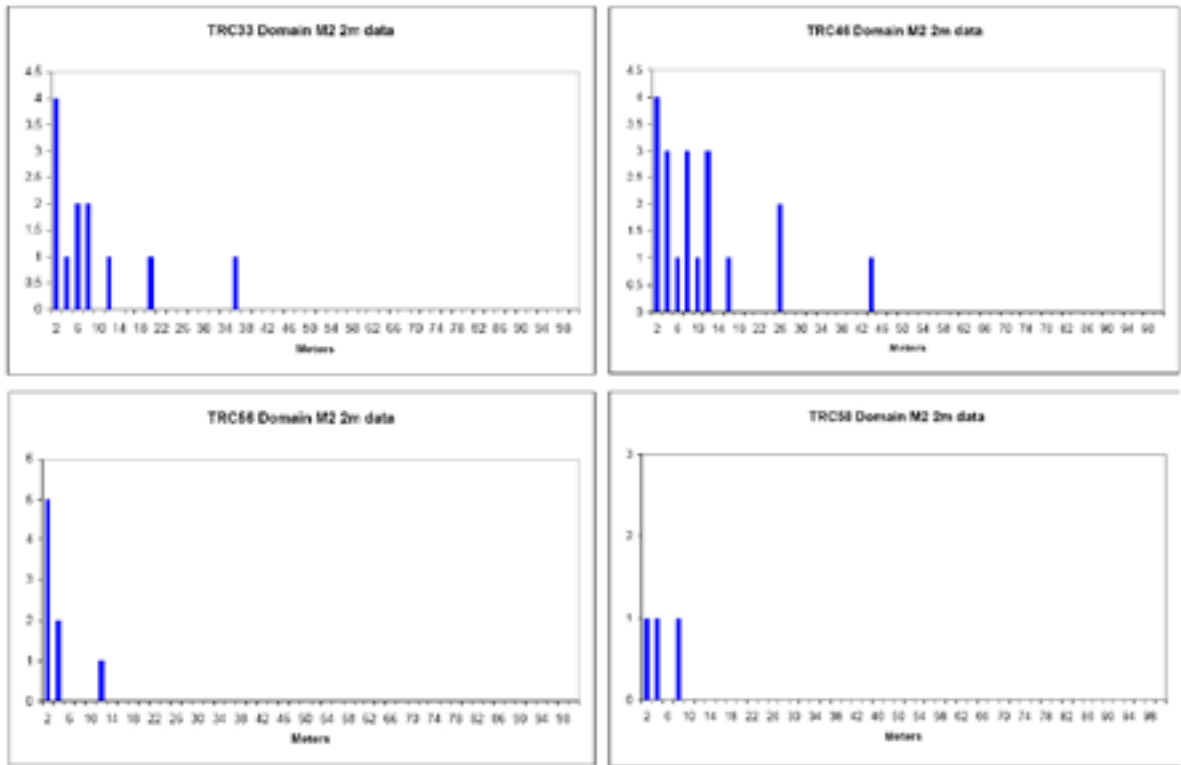


Figure K-6. Histograms of TRC lengths observed in borehole data in subdomain M2.

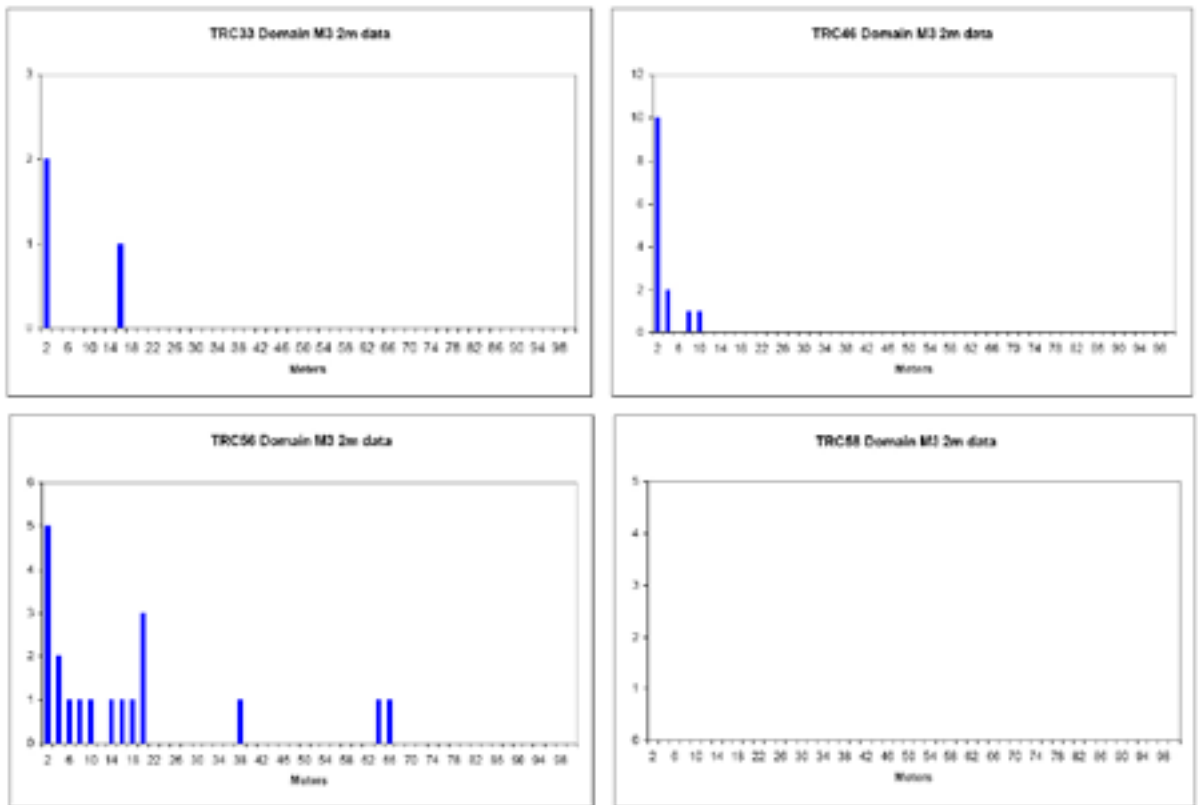


Figure K-7. Histograms of TRC lengths observed in borehole data in subdomain M3.

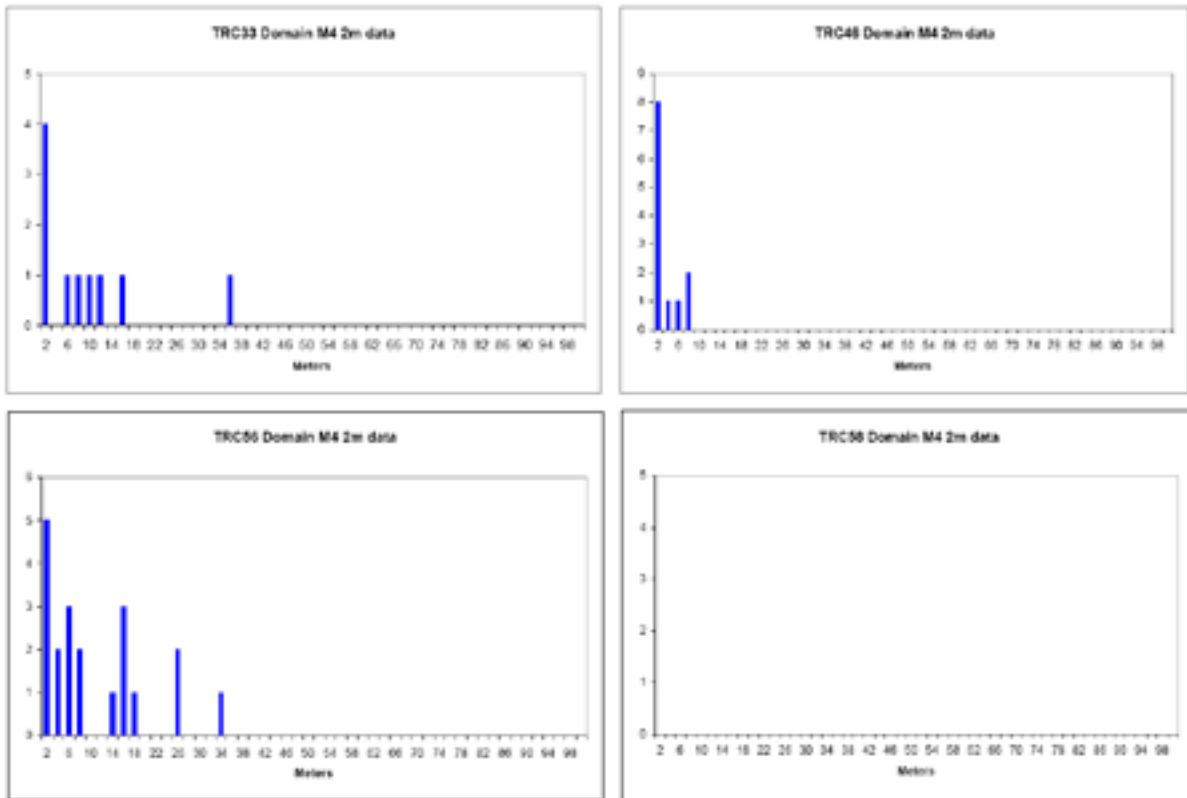


Figure K-8. Histograms of TRC lengths observed in borehole data in subdomain M4.

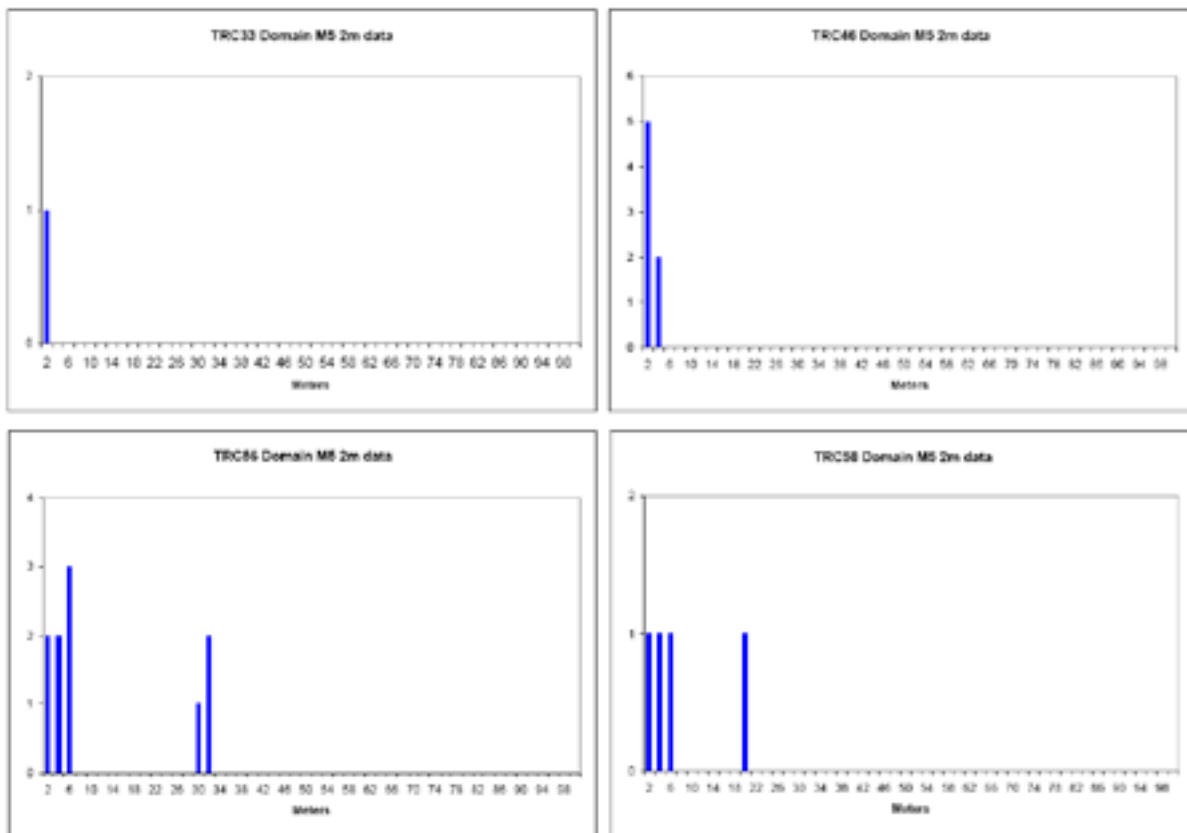


Figure K-9. Histograms of TRC lengths observed in borehole data in subdomain M5.

Spatial analysis for 4 m and 8 m data.

The spatial properties for the 4 m and 8 m lag resolution (i.e. 4 m and 8 m lag distances) were estimated by up-scaling of the 2 m data. The up-scaling was made through standard transition probability analysis, as described by e.g. Davis (1986). The results of the spatial analysis for each domain for 4 m and 8 m data are given in the tables below. Transition probabilities are presented as embedded probabilities.

Table L-1. Proportions, transition probabilities and typical lengths for subdomain M1 for 4 m data. Transition probabilities are shown as embedded probabilities of going from one TRC to other TRCs. Diagonal terms show the typical lengths of TRCs based on all boreholes.

TRC	Proportion	Isotropic transition probabilities to TRCs (embedded) and typical lengths (m). (Lengths shown in bold)			
		TRC 33	TRC 56	TRC 46	TRC 58
TRC 33	0.09	6.03	0.07	0.93	0.01
TRC 56	0.10	0.08	5.58	0.90	0.02
TRC 46	0.80	0.38	0.56	25.14	0.06
TRC 58	0.01	0.24	0.04	0.72	4.51

Table L-2. Proportions, transition probabilities and typical lengths for subdomain M2 for 4 m data. See also text in Table L-1.

TRC	Proportion	Isotropic transition probabilities to TRCs (embedded) and typical lengths (m). (Lengths shown in bold)			
		TRC 33	TRC 56	TRC 46	TRC 58
TRC 33	0.29	12.47	0.10	0.84	0.06
TRC 56	0.09	0.17	4.66	0.82	0.01
TRC 46	0.60	0.66	0.24	21.99	0.10
TRC 58	0.02	0.39	0.12	0.50	4.54

Table L-3. Proportions, transition probabilities and typical lengths for subdomain M3 for 4 m data. See also text in Table L-1.

TRC	Proportion	Isotropic transition probabilities to TRCs (embedded) and typical lengths (m). (Lengths shown in bold)			
		TRC 33	TRC 56	TRC 46	TRC 58
TRC 33	0.05	7.91	0.72	0.28	–
TRC 56	0.81	0.27	33.14	0.73	–
TRC 46	0.14	0.01	0.99	6.86	–
TRC 58	–	–	–	–	–

Table L-4. Proportions, transition probabilities and typical lengths for subdomain M4 for 4 m data. See also text in Table L-1.

TRC	Proportion	Isotropic transition probabilities to TRCs (embedded) and typical lengths (m). (Lengths shown in bold)			
		<i>TRC 33</i>	<i>TRC 56</i>	<i>TRC 46</i>	<i>TRC 58</i>
<i>TRC 33</i>	0.25	9.87	0.86	0.14	–
<i>TRC 56</i>	0.61	0.51	14.18	0.49	–
<i>TRC 46</i>	0.14	0.13	0.87	5.85	–
<i>TRC 58</i>	–	–	–	–	–

Table L-5. Proportions, transition probabilities and typical lengths for subdomain M5 for 4 m data. See also text in Table L-1.

TRC	Proportion	Isotropic transition probabilities to TRCs (embedded) and typical lengths (m). (Lengths shown in bold)			
		<i>TRC 33</i>	<i>TRC 56</i>	<i>TRC 46</i>	<i>TRC 58</i>
<i>TRC 33</i>	0.01	4.07	0.87	0.09	0.04
<i>TRC 56</i>	0.68	0.07	19.72	0.58	0.35
<i>TRC 46</i>	0.13	0.01	0.72	5.14	0.27
<i>TRC 58</i>	0.18	0.01	0.78	0.21	9.51

Table L-6. Proportions, transition probabilities and typical lengths for subdomain M1 for 8 m data. See also text in Table L-1.

TRC	Proportion	Isotropic transition probabilities to TRCs (embedded) and typical lengths (m). (Lengths shown in bold)			
		<i>TRC 33</i>	<i>TRC 56</i>	<i>TRC 46</i>	<i>TRC 58</i>
<i>TRC 33</i>	0.09	9.46	0.10	0.89	0.01
<i>TRC 56</i>	0.10	0.09	9.30	0.89	0.16
<i>TRC 46</i>	0.80	0.41	0.53	45.57	0.06
<i>TRC 58</i>	0.01	0.14	0.08	0.78	8.17

Table L-7. Proportions, transition probabilities and typical lengths for subdomain M2 for 8 m data. See also text in Table L-1.

TRC	Proportion	Isotropic transition probabilities to TRCs (embedded) and typical lengths (m). (Lengths shown in bold)			
		<i>TRC 33</i>	<i>TRC 56</i>	<i>TRC 46</i>	<i>TRC 58</i>
<i>TRC 33</i>	0.29	16.2	0.08	0.88	0.04
<i>TRC 56</i>	0.09	0.22	8.49	0.75	0.02
<i>TRC 46</i>	0.60	0.74	0.18	29.61	0.08
<i>TRC 58</i>	0.02	0.35	0.06	0.59	8.24

Table L-8. Proportions, transition probabilities and typical lengths for subdomain M3 for 8 m data. Se also text in Table L-1.

TRC	Proportion	Isotropic transition probabilities to TRCs (embedded) and typical lengths (m). (Lengths shown in bold)			
		<i>TRC 33</i>	<i>TRC 56</i>	<i>TRC 46</i>	<i>TRC 58</i>
<i>TRC 33</i>	0.05	10.77	0.78	0.22	–
<i>TRC 56</i>	0.81	0.28	48.66	0.72	–
<i>TRC 46</i>	0.14	0.03	0.97	10.33	–
<i>TRC 58</i>	–	–	–	–	–

Table L-9. Proportions, transition probabilities and typical lengths for subdomain M4 for 8 m data. Se also text in Table L-1.

TRC	Proportion	Isotropic transition probabilities to TRCs (embedded) and typical lengths (m). (Lengths shown in bold)			
		<i>TRC 33</i>	<i>TRC 56</i>	<i>TRC 46</i>	<i>TRC 58</i>
<i>TRC 33</i>	0.25	13.54	0.83	0.17	–
<i>TRC 56</i>	0.61	0.57	22.70	0.43	–
<i>TRC 46</i>	0.14	0.21	0.79	9.83	–
<i>TRC 58</i>	–	–	–	–	–

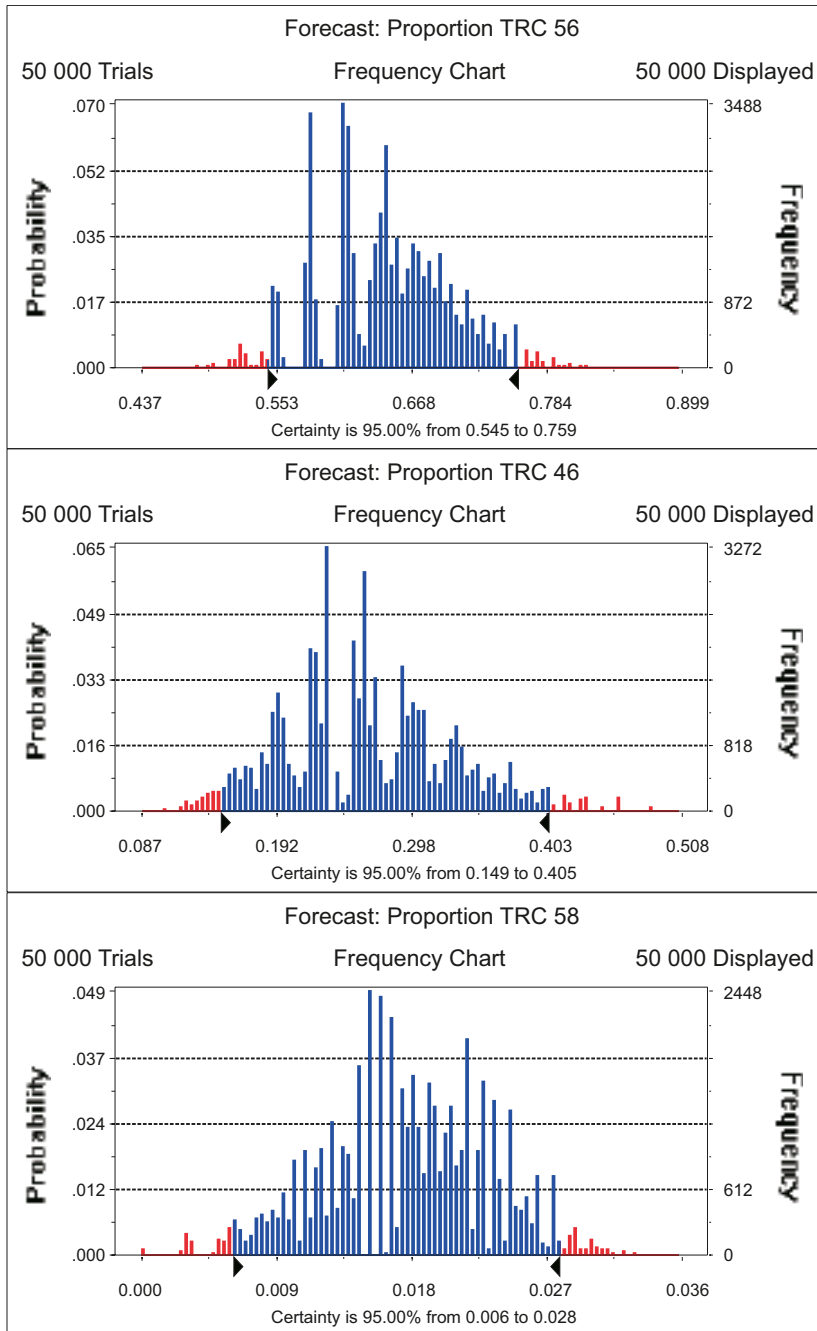
Table L-10. Proportions, transition probabilities and typical lengths for subdomain M5 for 8 m data. Se also text in Table L-1.

TRC	Proportion	Isotropic transition probabilities to TRCs (embedded) and typical lengths (m). (Lengths shown in bold)			
		<i>TRC 33</i>	<i>TRC 56</i>	<i>TRC 46</i>	<i>TRC 58</i>
<i>TRC 33</i>	0.01	8.11	0.77	0.13	0.10
<i>TRC 56</i>	0.68	0.05	30.42	0.49	0.47
<i>TRC 46</i>	0.13	0.01	0.75	9.25	0.24
<i>TRC 58</i>	0.18	0.01	0.81	0.18	12.86

TRC proportions and confidence intervals

Each graph below shows the distribution of mean proportions for a particular TRC in a domain generated by the bootstrap method. For each TRC, the 95% two-sided confidence limits for the mean volume proportions of TRCs are indicated.

Domain A



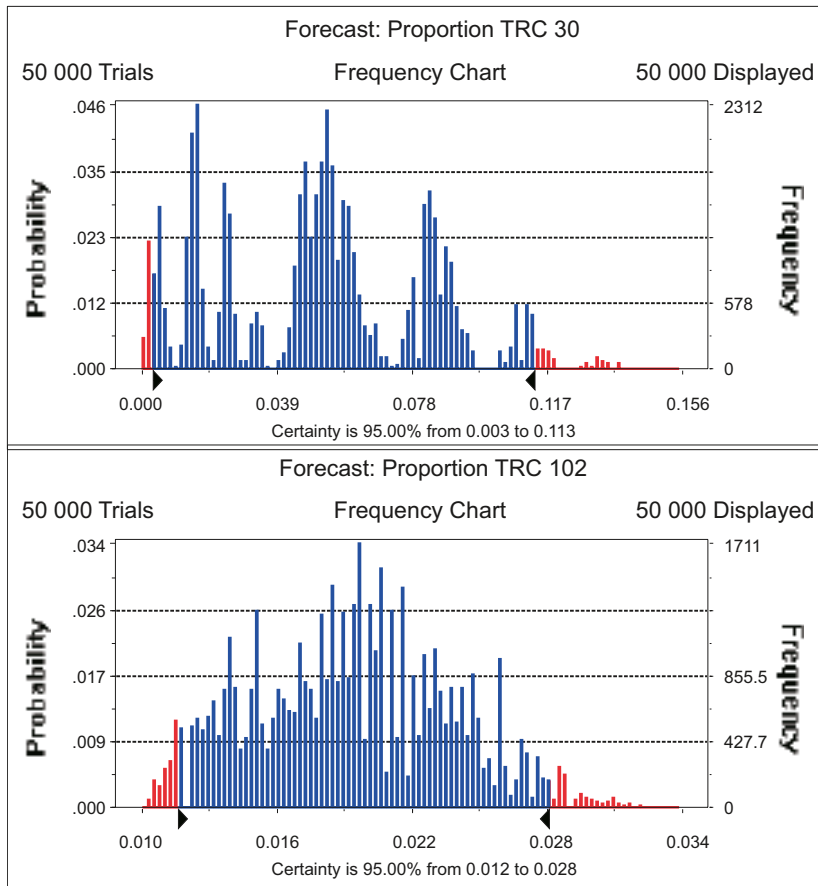
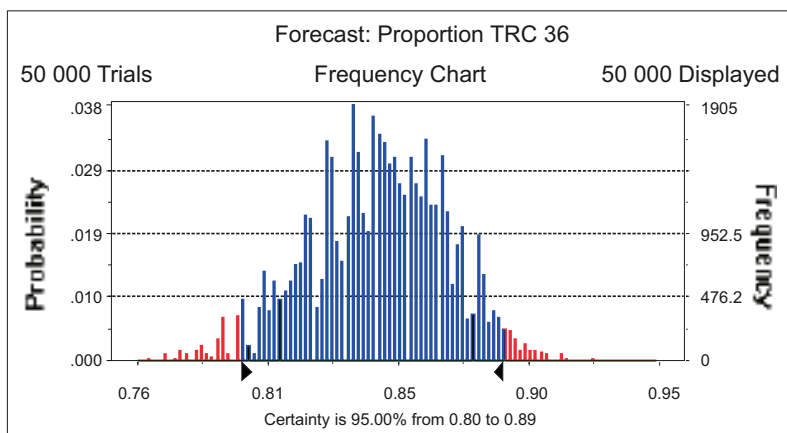


Figure M-1. Distributions of mean proportions of TRCs generated by the bootstrap method for domain RSMA01 based on 2 m data from the six boreholes used for lithological simulations. 95 % confidence intervals are indicated.

Domain D



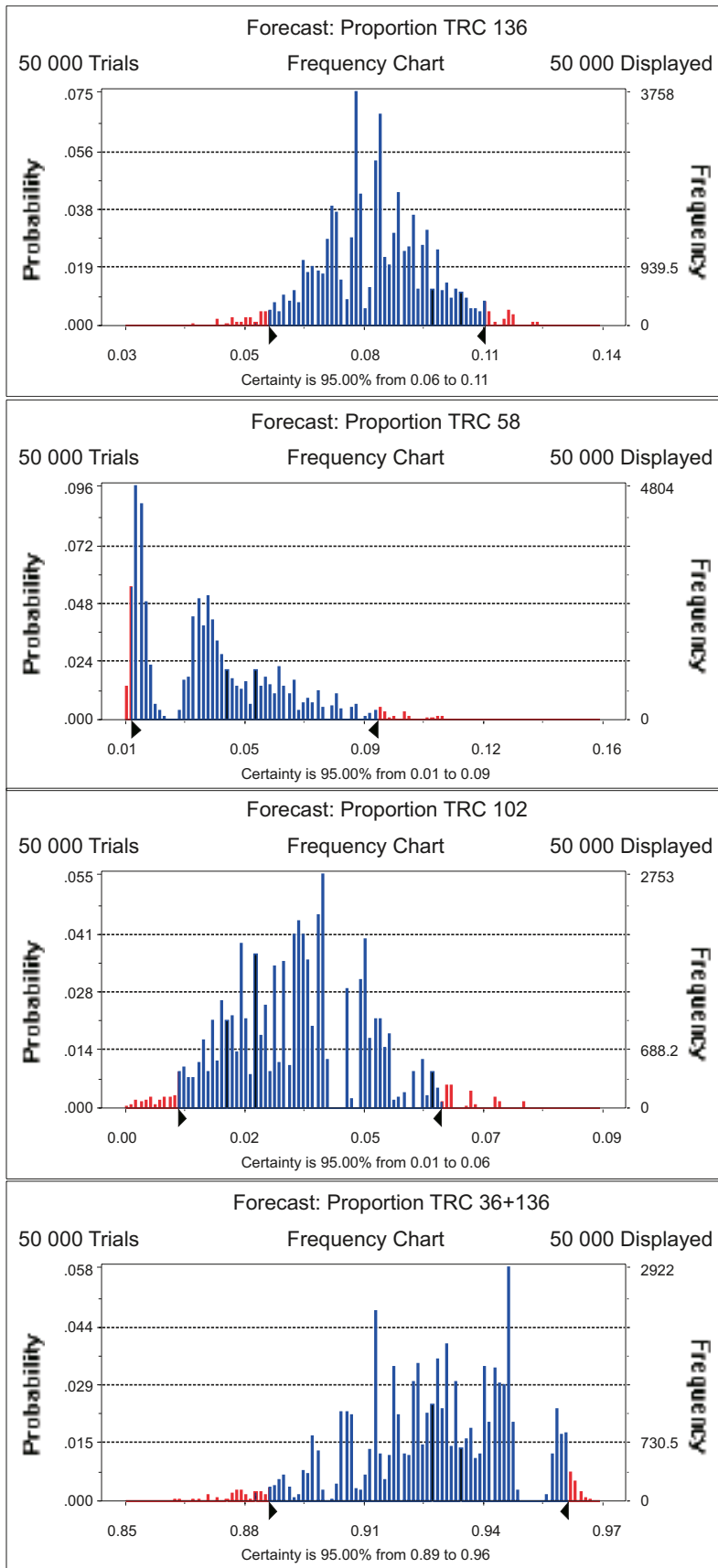


Figure M-2. Distributions of mean proportions of TRCs generated by the bootstrap method for domain RSMD01 based on 2 m data from the six boreholes used for lithological simulations. 95 % confidence intervals are indicated.

Domain M

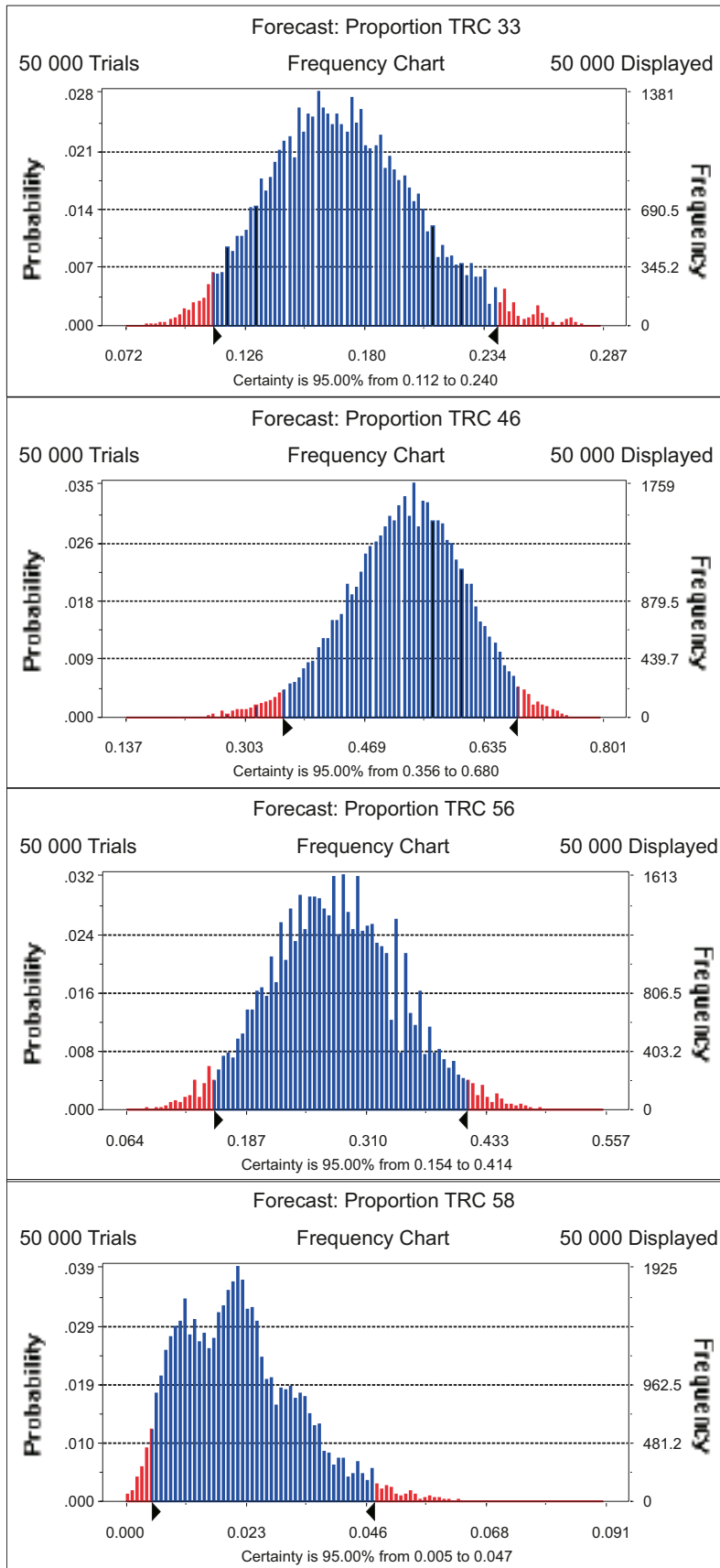


Figure M-3. Distributions of mean proportions of TRCs generated by the bootstrap method for domain RSMM01 based on 2 m data from the eight boreholes used for lithological simulations. 95 % confidence intervals are indicated.

Conditional stochastic simulation of thermal conductivity

Introduction

Conditional simulation was performed for a volume of rock at depth below the Oxhagen area and conditioned on data from borehole KLX05, corresponding to an elevation of between –247 m and –407 m. KLX05 is lithologically heterogenous and was therefore considered particularly suitable for simulation. The dimensions of the simulation volume are 100 m, 100 m, and 160 m in the x, y and z directions respectively, and the resolution is 2 m.

The method for conditional simulation is essentially the same as for unconditional simulation (Section 4.2.2). In a similar way as for unconditional simulations, simulation of the spatial distribution of lithologies (TRCs) and the spatial distribution of thermal conductivity for each TRC produce sets of realisations which are merged to generate realisations of thermal conductivity for the chosen rock volume.

Geological input

The borehole length interval in KLX05 used for conditioning (295 m to 472 m) belongs to thermal subdomain M2 within rock domain RSMM01 (Section 5.3.3). The section is comprised mainly of diorite-gabbro (501033, TRC 33) and Ävrö quartz monzodiorite (501046, TRC 46) with minor amounts of Ävrö granodiorite (501056, TRC 56) and fine-grained granite (511058, TRC 58). Proportions of each TRC are 51%, 40%, 6% and 3% respectively. Subdomain M2 has slightly different TRC proportions (Table 5-18); it is dominated by Ävrö quartz monzodiorite with a high content of diorite-gabbro.

Lithological data used for conditioning has a resolution of 2 m. TRC 58, which is comprised mainly of fine-grained granite, has been modelled as horizontal dyke-like bodies with a horizontal extension in the x and y directions that is 10 times longer than the vertical extension or thickness. The degree of anisotropy is based on expert judgements /Wahlgren 2008/. The choice of orientation is based on the geological interpretations in /Wahlgren et al. 2008/.

Stochastic simulations of TRCs (lithology)

With the exception of TRC 58, which was modelled as anisotropic, the spatial properties of the TRCs used for conditional lithological simulations are similar to those used in the unconditional simulations of subdomain M2 (Table 5-18). An alternative approach would have involved establishing a spatial model based on the data in the borehole section in KLX05 intersecting the simulation volume. However, such a model would have been based on very little data, and therefore associated with large uncertainty.

A detailed description of the spatial models and the results of the conditional simulations of the spatial distribution of TRCs are presented in Appendix O. A total of 100 realisations were produced.

Spatial statistical models of thermal conductivity for TRCs

In order to perform the conditional simulations of thermal conductivity the following input was required:

- Spatial statistical thermal conductivity models at 2 m scale for each TRC.
- Thermal conductivity values at known data locations.

Spatial statistical thermal conductivity models for each TRC comprise both a probability distribution model and a variogram model. There are two alternatives for this step. One is to use the same models as were used in the unconditional simulations for subdomain M2 as described in Section 5.7.2. The other alternative is to consider the simulated volume as a distinct zone with spatial models based on the thermal data from this volume, in this case from borehole KLX05.

The latter approach could be justified if there was reason to believe that the statistics (mean, variance) of a TRC in this volume differed significantly from other parts of the Laxemar area. The distribution of thermal conductivity for TRC 46 and 56 in KLX05 based on calculations from density in the relevant borehole section show different mean values to several other boreholes in Laxemar (Figure N-1, Table 3-21). However, the fact that these data are derived exclusively from one borehole means that it cannot be claimed with a high degree of certainty that the overall histogram and variogram are inappropriate for this volume. Therefore, this alternative has not been pursued.

TRC 33 was previously divided into sub-TRCs due to the recognition of a low-density variety (33A) and a high-density variety (33B) (Section 5.6.2). The diorite-gabbro bodies present in KLX05 are of the high-density type. Therefore, the model for 33B was used in the conditional simulations.

There are two sources of thermal conductivity data at known locations in the relevant borehole section: TPS-measurements on 12 drill core samples of Ävrö quartz monzodiorite (TRC 46) and diorite-gabbro (TRC 33), and thermal conductivity values calculated from density logs along continuous sections of the borehole for Ävrö quartz monzodiorite (TRC 46) and Ävrö granodiorite (TRC 56). Both these types of data roughly represent the 0.1 m scale, whereas simulation was performed at the 2 m scale. Therefore, a change of support was required. This could be achieved by transforming the data using the probability distribution models previously produced for the 2 m scale (Section 5.7.2). However, it was not considered necessary to perform this upscaling step for the TPS data since these data are very few in number and will have only a very minor impact on the overall simulation results. Moreover, an inspection of the data shows that all values fall within the range of the 2 m models.

An alternative approach was applied to the thermal conductivity values calculated from density for TRC 46 and TRC 56. Upscaling was achieved by applying the SCA algorithm to the 0.1 m borehole values; an upscaled value was calculated from all 0.1 m values within each 2 m borehole section. Each 2 m value was assigned coordinates corresponding to the central point of the 2 m borehole section. TPS data for Ävrö quartz monzodiorite (TRC 46) was not used as conditioning data since calculated values from density are available at the same locations. For TRC 58, no conditioning data was available. The coordinates of the data locations were transformed into the local coordinate system used for the simulation volume

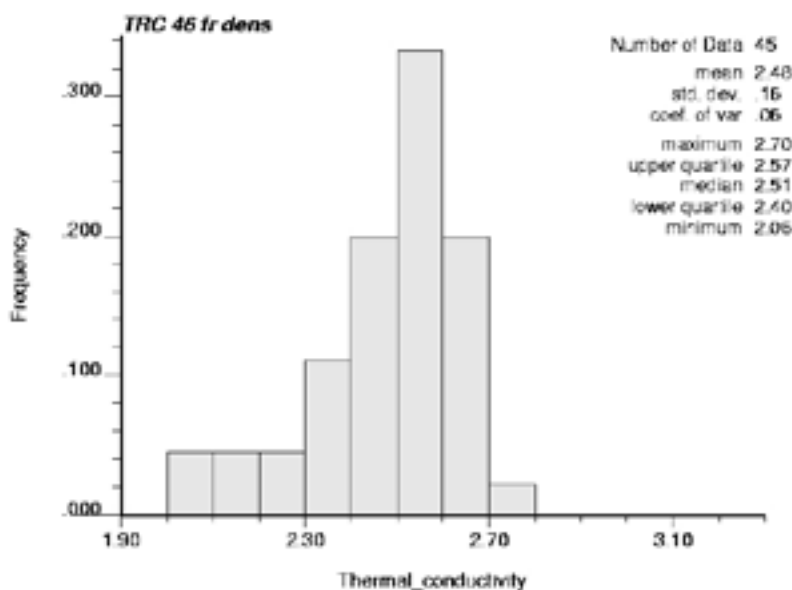


Figure N-1. Histogram of thermal conductivity values calculated from density for Ävrö quartz monzodiorite (501046) occurring between 295 m and 466 m borehole length in KLX05.

Stochastic simulation of thermal conductivity for TRCs

Stochastic simulations of thermal conductivity at the 2 m scale were performed for the four TRCs present within the simulated volume. Each TRC was simulated using the statistical distribution and variogram models defined in Sections 5.7.2 and 5.7.3 and the conditioning data referred in above. Again, 100 realisations were created for each TRC. The algorithm used for the simulation was Sequential Gaussian Simulation (SGS) /Deutsch and Journel 1998/. The software GSLIB was used to perform the simulations.

With the SGS algorithm either simple kriging (SK) or ordinary kriging (OK) can be used /Deutsch and Journel 1998/. The decision of statistical stationarity requires that SK is adopted. However, if the local mean data value is observed to vary significantly with location (non-stationary mean) and there is abundance of conditioning data then OK may be used /Deutsch and Journel 1998/. Using OK, the model mean is locally replaced by a mean re-estimated from the neighbourhood data. The impact of this is usually a poorer reproduction of the histogram and variogram model.

A comparison of thermal conductivity values calculated from density for Ävrö quartz monzodiorite (501046) and Ävrö granodiorite (501056) in borehole KLX05 with other boreholes in Laxemar, eg. KLX12 and KLX13, indicates that the mean changes with location (Table 3-21 and Appendix A). Therefore, it was decided to perform simulations of TRC 46 and TRC 56 using ordinary kriging and TRC 33 and TRC 58 using simple kriging.

For each TRC, histograms of simulated thermal conductivity values from 100 realisations were plotted (Figure N-2).

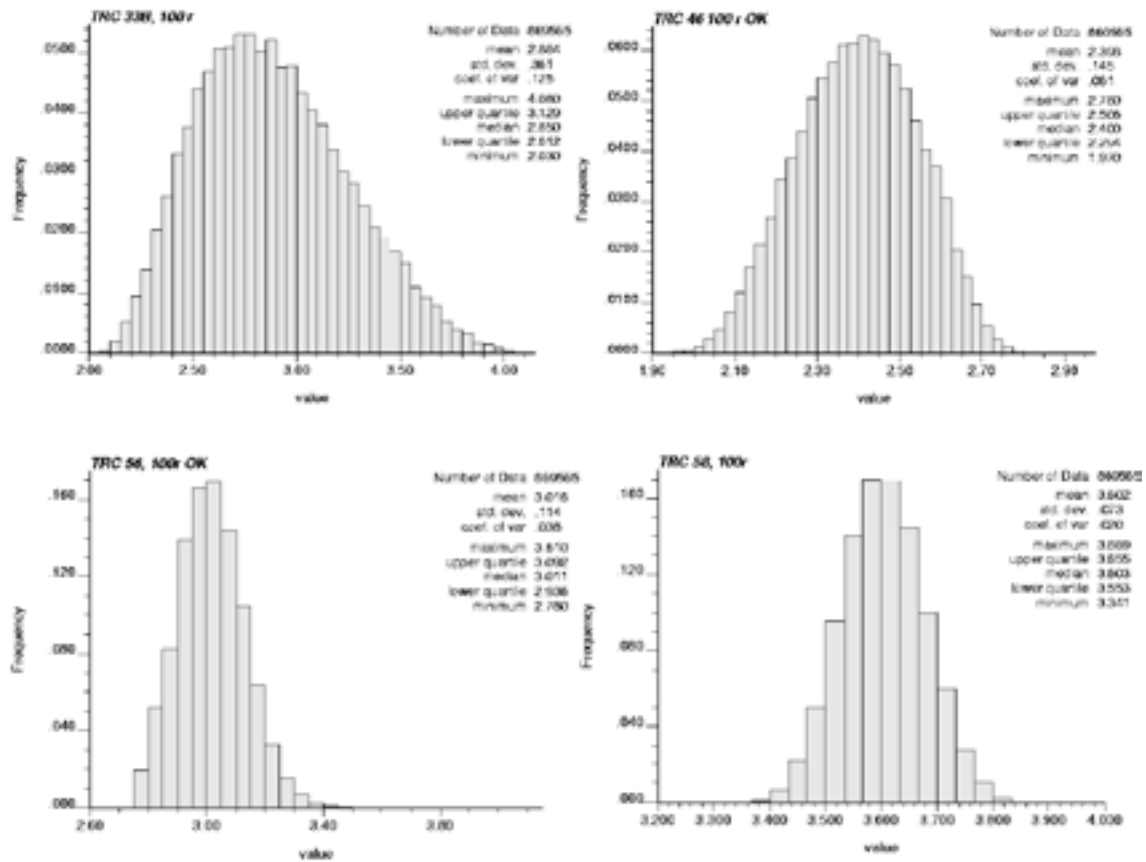


Figure N-2. Histograms of simulated thermal conductivity values at 2 m scale for the individual TRCs in the investigated volume based on 100 realisations. Ordinary kriging was used in the simulation of TRC 46 and TRC 56. Simple kriging was used in the simulation of TRC 33 and TRC 58.

For TRC 33 and TRC 58, the histogram including the mean and standard deviation are similar to the input distribution models, whereas for TRC 46 and 56, the histograms differ slightly from the model histograms (see Appendix F). The mean of the realisations for TRC 46 is similar to the model mean despite the higher mean of the conditioning data and the use of ordinary kriging instead of simple kriging. The standard deviation on the other hand is somewhat higher in the realisations. For TRC 56, the mean and standard deviation of the simulated histogram differ from the model because of the impact of the conditioning data, the kriging method used and the large correlation lengths.

Locations at distances further than the correlation length from known data points are beyond the influence of the conditioning data and are therefore simulated using the model histogram and variogram in the same way as for unconditional simulation. To illustrate how much of the simulation volume is influenced by the conditioning data for TRC 46, a number of simulations were generated with the condition that an unknown location, i.e. a grid node with no conditioning data, must use at least one known data value in the surroundings. An example of such a realisation is shown in Figure N-3. This visualisation shows that many positions (grid nodes) within the simulation volume are not assigned any values because there are no conditioning data within the search radii of the grid nodes. The resulting histogram for TRC 46 based on five realisations is shown in Figure N-4. Note that this more restricted volume yields a higher mean than that given by the entire simulated volume (c.f. Figure N-2). For comparison, a realisation simulated without this condition is also shown in Figure N-3.

Verification of simulations was performed by analysing the extent to which the realisations can reproduce the known data values at specific locations. For a selected number of known data values a comparison was made with simulated values at the same locations (Table N-1). A close correspondence is observed. Because the measured data are not located exactly at the grid nodes, the simulated values deviate somewhat from the measured values.

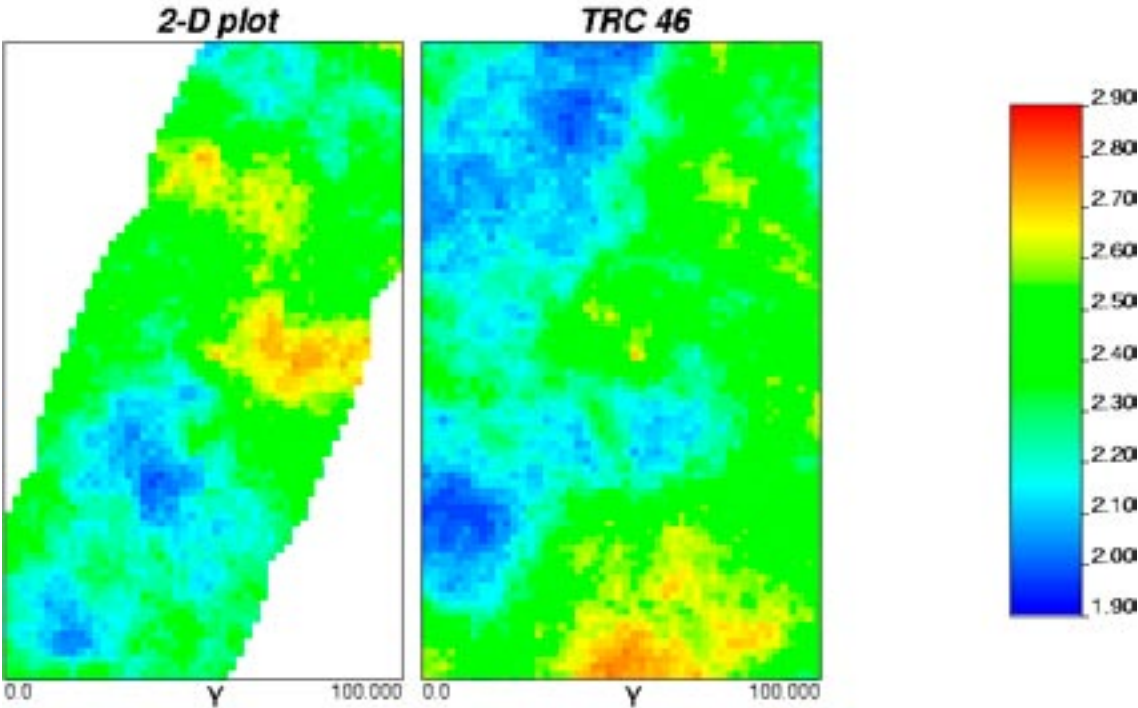


Figure N-3. 2D visualisations of two realisations of TRC 46, one simulated with the condition that an unknown location or grid node must be conditioned by at least one known data value (left), the other simulated without this condition (right). The white areas in the example on the left represent areas that have not been assigned a thermal conductivity value.

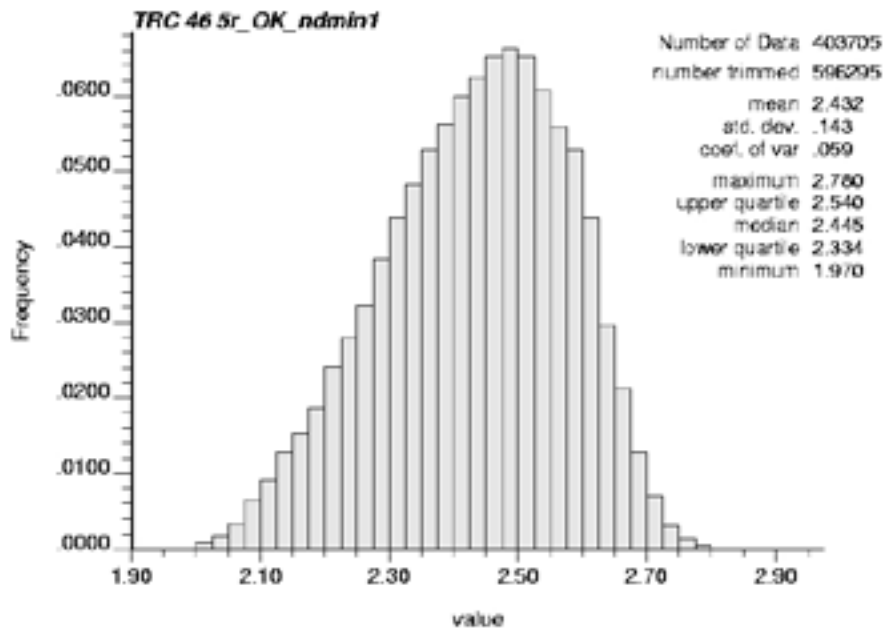


Figure N-4. Histogram of simulated thermal conductivity values for TRC 46 based on simulations (5 realisations) of a volume influenced by the conditioning data.

Table N-1. Comparison of some known data points and simulated values. The conditioning data for TRC 46 are provided by calculations from density logging data. The corresponding values for TRC 33 are derived from TPS measurements.

Borehole length, m	Rock type	TRC	Conditioning data Thermal conductivity, W/(m·K)	Simulated thermal conductivity, mean of 100 realisations, W/(m·K)
302	501046	46	2.39	2.43
444	501046	46	2.55	2.53
349.50	501033	33	2.58	2.61
361.25	501033	33	3.65	3.62

Conditional stochastic simulation of geology

Introduction

This appendix describes conditional stochastic simulations of geological configurations in Laxemar. Previous stochastic simulations of rock domains RSMA01, RSMD01 and RSMM01 in Laxemar were made without conditioning on specific borehole information in the rock volumes. The purpose of the conditional simulations was to evaluate how the simulation method (Markov Chain Monte Carlo simulations, using the T-PROGS software) can reproduce thermal rock unit classes (TRCs) in specific known positions. The simulations were performed in thermal subdomain M2 and were conditioned on borehole KLX05, borehole length 295–472 metres (elevation: –247 m to –407 m).

Simulation

Borehole information

Stochastic simulation was made for subdomain M2 at the 2-metre scale and conditioned on borehole KLX05, borehole length section 295–472 metres. The simulation comprised 100 realisations. The location of the borehole in the simulated rock volume is shown in Figure O-1. The model dimensions were 50 x 50 x 80 cells (100x100x160 metres) in the x,y,z-directions respectively, i.e. a total of 200,000 cells.

The spatial properties of subdomain M2 were estimated based on information from three boreholes: KLX05, KLX12A and KLX13A. Sections shown in Table O-1 were used for the spatial analysis. A total of 478 observations were used for the estimations of the spatial properties.

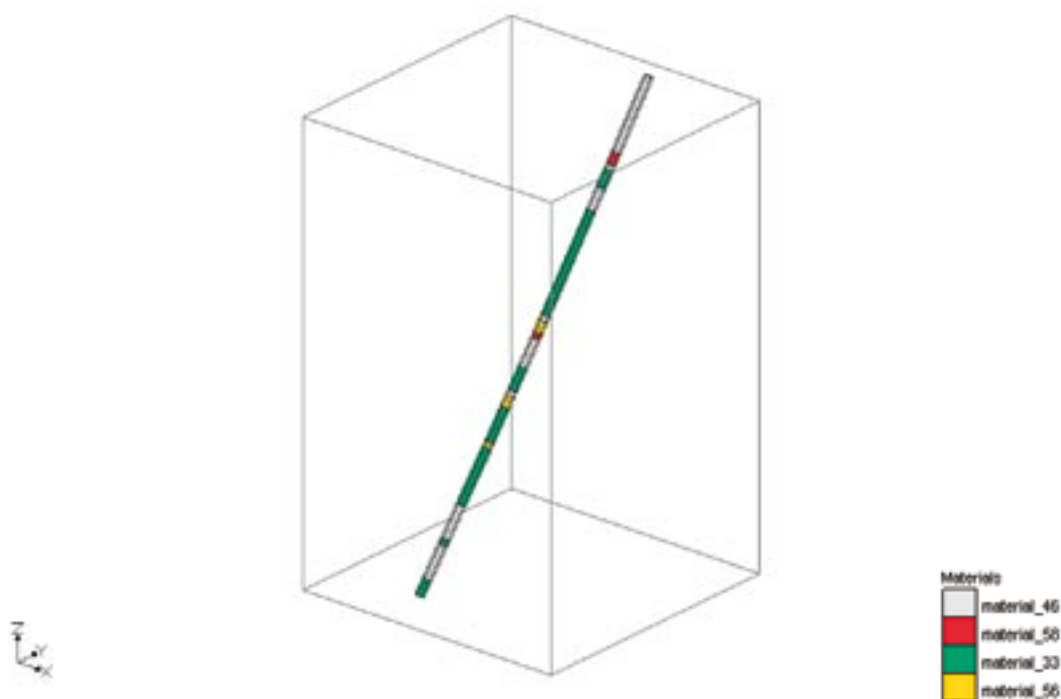


Figure O-1. The location of borehole KLX05, section 292–473 metres in the simulated rock volume. Note that the borehole length illustrated in the figure refers to the data used for spatial analysis and is slightly longer than the length used for conditioning (295–472 m).

Table O-1. Borehole data used for spatial analysis of conditional simulations.

Borehole	Borehole length interval (metres)
KLX05	292–473
KLX12A	102–528
KLX13A	102–456

Spatial properties – results

The spatial properties for subdomain M2 for 2 m data were estimated by transition analysis along the boreholes. The results of the spatial properties analysis are given in Table O-2 and Table O-3. Transition probabilities are presented as embedded probabilities.

The results of the transition analysis for the z direction were adjusted for TRC58 to take into account the geological interpretation of anisotropy. TRC58 was interpreted to occur as thin discs in the x-y plane with length ratio 10:10:1 in the x:y:z directions. Proportions were the same for all directions. Due to the relationship between proportions, typical lengths and transition probabilities, the change in typical length for TRC58 resulted in slightly changed transition probabilities and typical length for TRC46, which was chosen as the “background material” in the simulations. The transition probabilities and typical lengths in the x,y directions after adjusting for the anisotropy of TRC58 are shown in Table O-3. The spatial properties for the z-direction were represented by the information given in Table O-2.

Table O-2. Proportions, transition probabilities and typical lengths in the vertical (z) direction, based on borehole information in thermal subdomain M2. Transition probabilities are shown as embedded probabilities of going from one TRC to other TRCs. Diagonal terms show the typical lengths of TRCs based on all boreholes.

TRC	Proportion	Isotropic transition probabilities to TRCs (embedded) and typical lengths (m). (Lengths shown in bold)			
		TRC 33	TRC 46	TRC 56	TRC 58
TRC 33	0.29	10.77	0.81	0.12	0.08
TRC 46	0.64	0.61	17.04	0.31	0.08
TRC 56	0.05	0.14	0.86	3.07	0.00
TRC 58	0.02	0.40	0.40	0.20	3.00*

* Typical length of TRC58 was estimated to 4.67 m in the transition analysis, but adjusted to 3 m based on geological interpretations.

Table O-3. Proportions, transition probabilities and typical lengths for subdomain M2 in x,y-directions for 2 m data. See also text in Table O-2.

TRC	Proportion	Isotropic transition probabilities to TRCs (embedded) and typical lengths (m). (Lengths shown in bold)			
		TRC 36	TRC 46	TRC 56	TRC 58
TRC 33	0.29	10.77	0.81	0.12	0.08
TRC 46	0.64	0.69	17.91	0.31	0.00
TRC 56	0.05	0.14	0.86	3.07	0.00
TRC 58	0.02	0.40	0.40	0.20	30.00

* Based on geological interpretations, the typical length of TRC58 was estimated to be 10 times the lengths calculated from the transition analysis of borehole data.

Simulation results

The simulation is comprised of 100 realisations. The realisations can be visualised by the 3D-plots in T-PROGS. Figure O-2 gives two examples of visualisations of the realisations.

The visualisation module of T-PROGS can be used to restrict the number of categorical classes to be displayed. This option facilitates views into the simulated volume close to the borehole. Figure O-3 displays two realisations where only TRC58 is displayed.

Figure O-4 displays two realisations where only TRC56 is displayed.

Verification

Methodology

From the previously performed unconditional simulations in Laxemar it has been shown that T-PROGS is capable of accurately reproducing proportions and typical lengths of TRCs. The purpose of this study was to investigate the capability of the model to reproduce TRC information at specific positions in a rock volume.

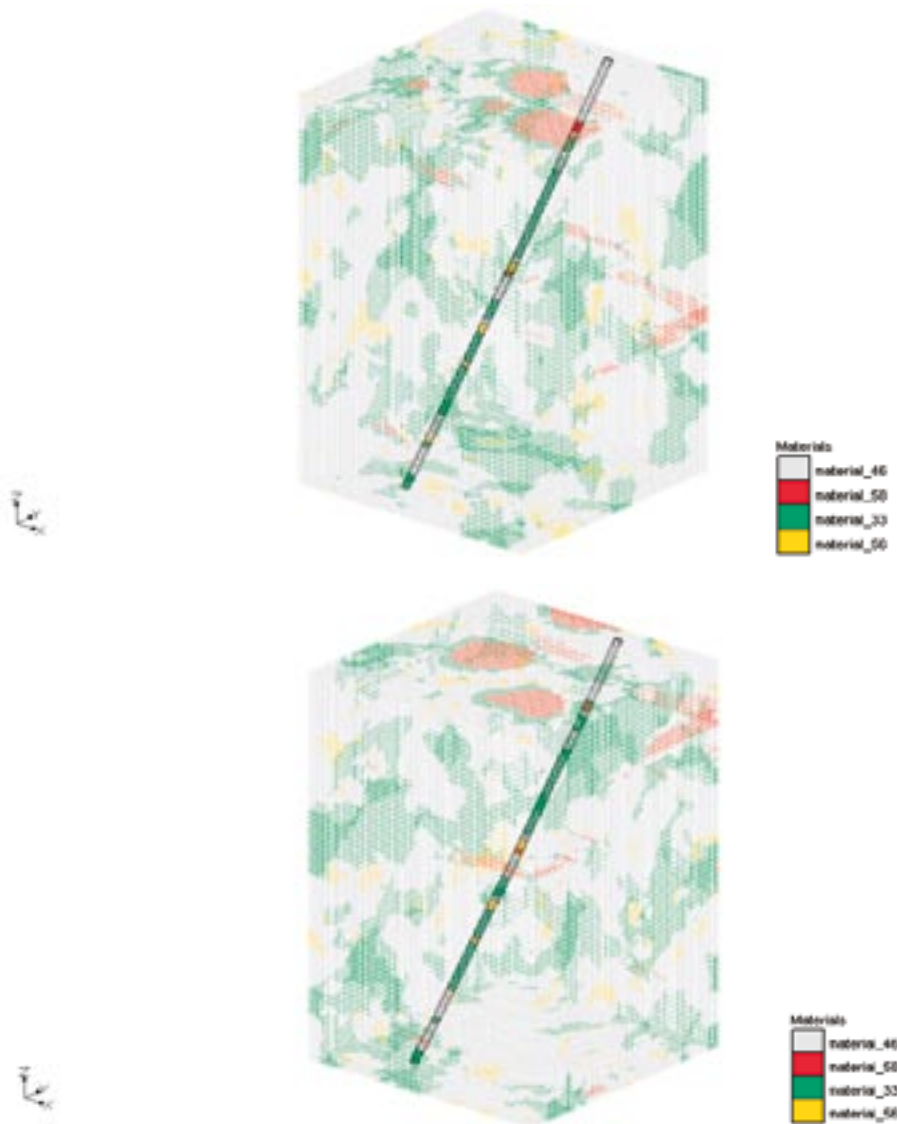


Figure O-2. Two visualisations of realisations of subdomain M2, with 2 m resolution (cell size) and conditioned on borehole KLX05. The simulated rock volume has dimensions 100x100x160 metres.

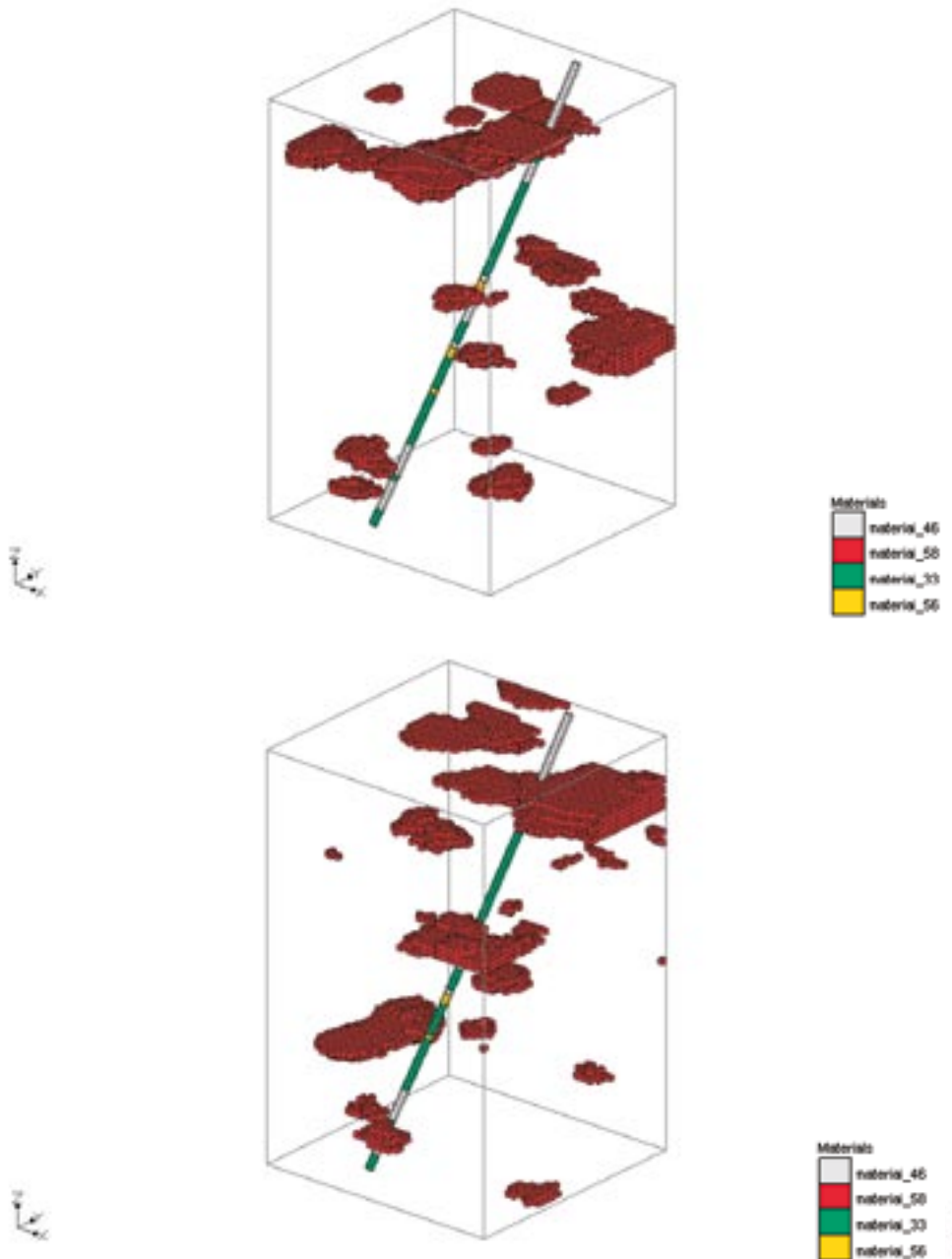


Figure O-3. Two realisations displaying the spatial distribution of TRC58, conditioned on borehole KLX05.

To verify the model a cross-validation approach was used. Information along the borehole KLX05 was left out during simulations and the capability of the model to reproduce missing information was investigated.

Three additional simulations were performed for the validation. Each simulation consisted of 10 realisations and for each simulation the spatial properties estimated from all available borehole information (Table O-2, Table O-3) were used. The thinning of the borehole information was performed according to Table O-4.

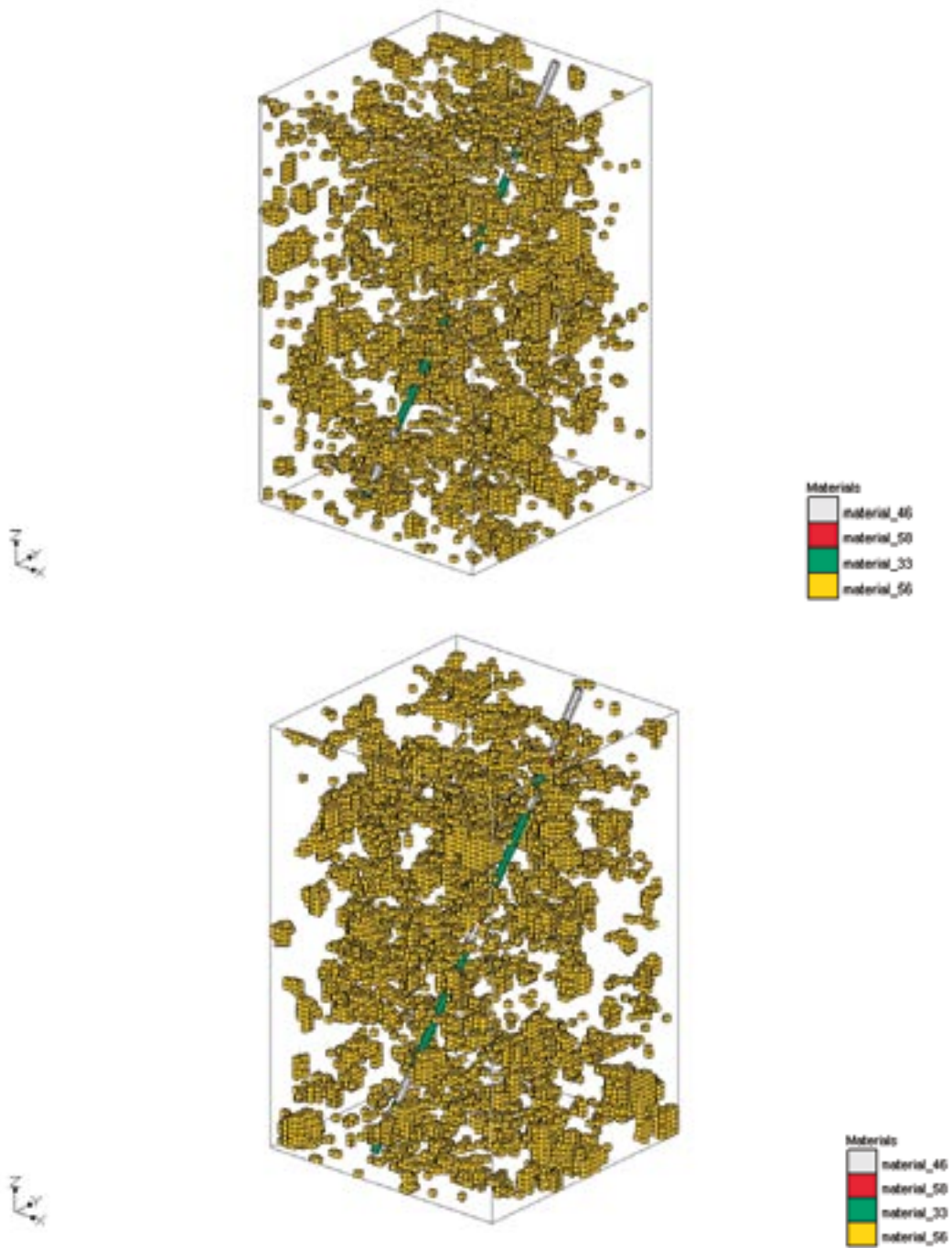


Figure O-4. Two realisations displaying the spatial distribution of TRC56, conditioned on borehole KLX05.

Table O-4. The thinning of information in borehole KLX05 in the simulations.

	Proportion missing data in KLX05	Proportion kept data in KLX05	Number of missing values in KLX05	Lengths of strings of missing data (pixels/ metres)
Simulation 1	23%	77%	20	4/8
Simulation 2	40%	60%	35	7/14
Simulation 3	80%	20%	70	14/28

The thinning was made by randomly selecting 5 starting positions in the borehole and excluding information in 8, 14 and 28 metre strings respectively for the three simulations. The purpose of using specified lengths of the strings of missing information was that the reproducibility of the model was assumed to be dependent on both the number of conditioning points and the spaces between these points.

The results of the simulations along the borehole positions were obtained using a Matlab code. Another Matlab code was used to perform statistical analyses of the results. For each simulation, histograms of the error distribution from the 10 realisations were prepared. The mean and the mode of errors were calculated for each simulation.

Results

The results of the simulations with missing information are compiled in Table O-5. The proportions of “correct predictions of boreholes positions with missing information” are shown graphically in Figure O-5 and Figure O-6.

Histograms of the error distributions of the simulations are shown in Figure O-7.

Conclusions

When evaluating the capability of the model to predict missing information, it must be emphasised that the results are always site specific and that general conclusions are difficult to make. However, for the specific situation in subdomain M2 the results show that the T-PROGS model is capable of correctly reproducing a high percentage of missing borehole data (approximately 80 %) when the proportion of the missing information is relatively low (23 %) and when conditioning points are relatively close (8 m). When the proportion of missing information increases and when conditioning points are further separated, the error rates increase. With 80% missing information and with a separation distance of 28 meters between conditioning points, the model is still able to predict slightly more than 50 % of the missing positions correctly.

It should be noted that the typical correlation lengths are only 10 and 3 metres for TRCs 33 and 56, respectively, and 3 metres for the z-direction for TRC58. This means that with a separation distance of 28 meters between the conditioning points, many positions are far from known information. The predictions of such positions are not strongly conditioned and the variability of the prediction is therefore inevitably high.

Table O-5. Results from the validation simulations.

Simulation No.	Spacing in thinning (px/m)	Proportion kept data in KLX05	No of errors (mode)	No of errors (mean)	Prop. correct predictions (mode)	Prop. correct predictions (mean)
1	4/8	77%	3	4.60	85%	77%
2	7/14	60%	12	13.65	66%	61%
3	14/28	20%	24	34.40	66%	51%

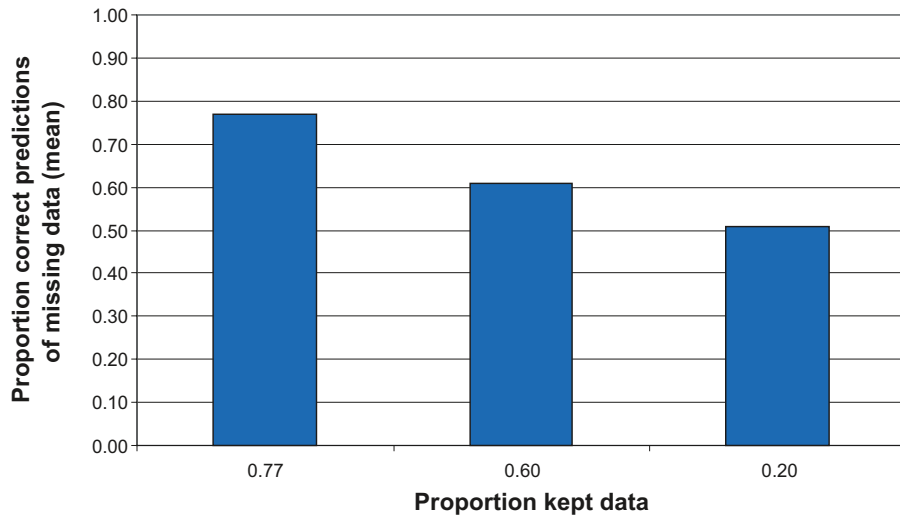


Figure O-5. Proportion (mean) of correct predictions of borehole positions with missing data.

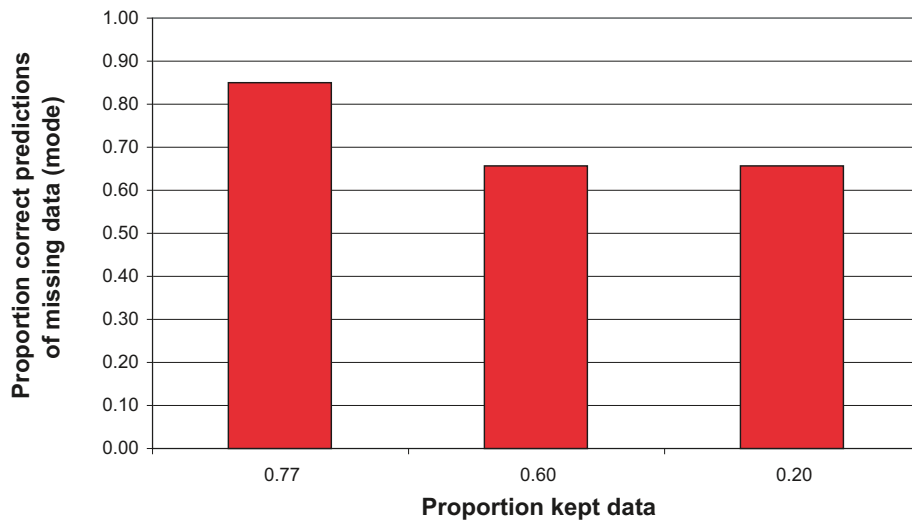


Figure O-6. Proportion (mode) of correct predictions of borehole positions with missing data.

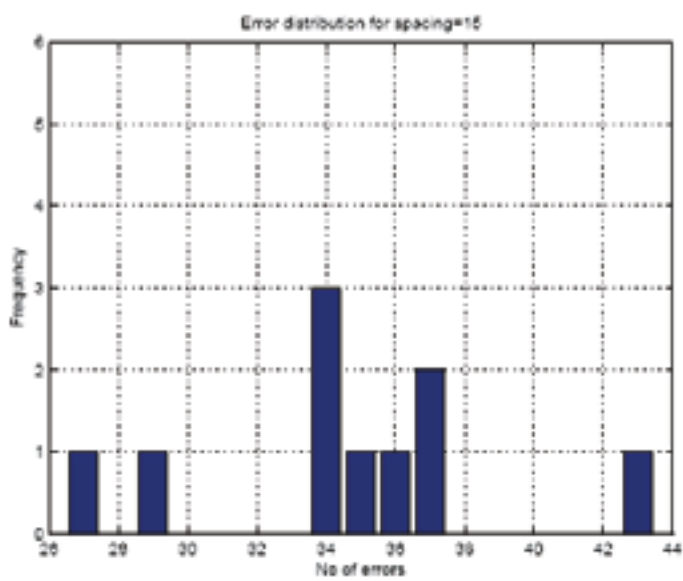
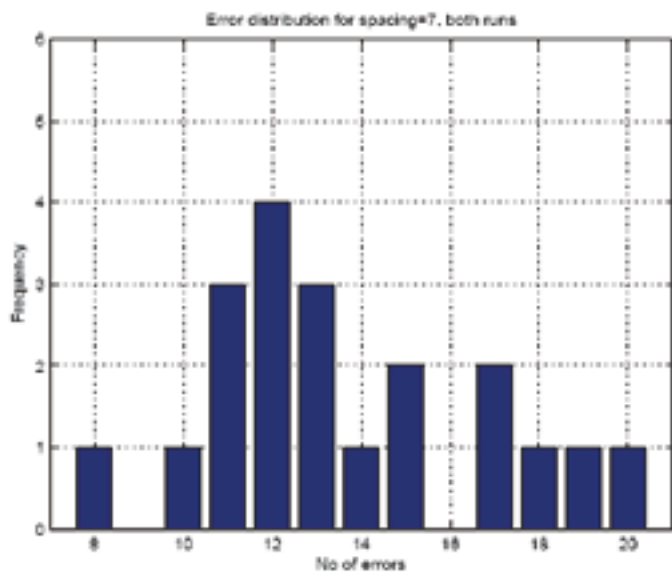
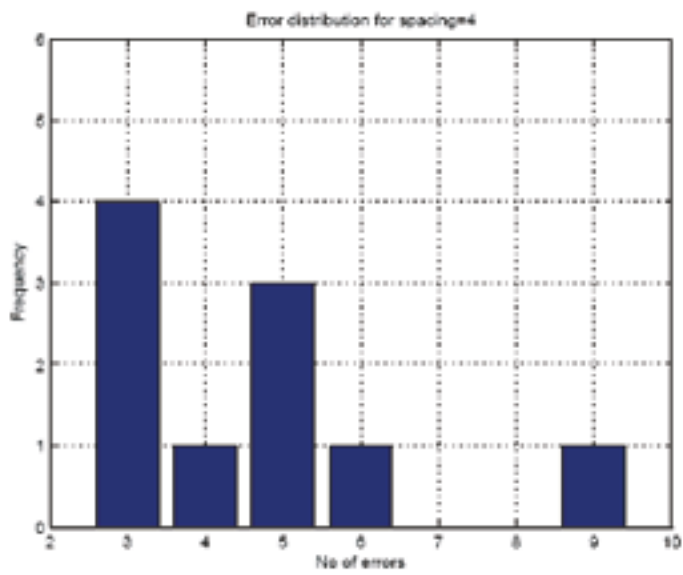

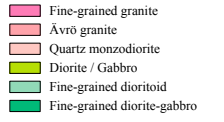
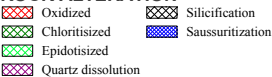
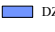
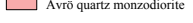

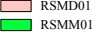
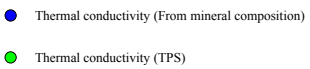
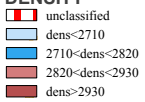

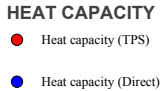


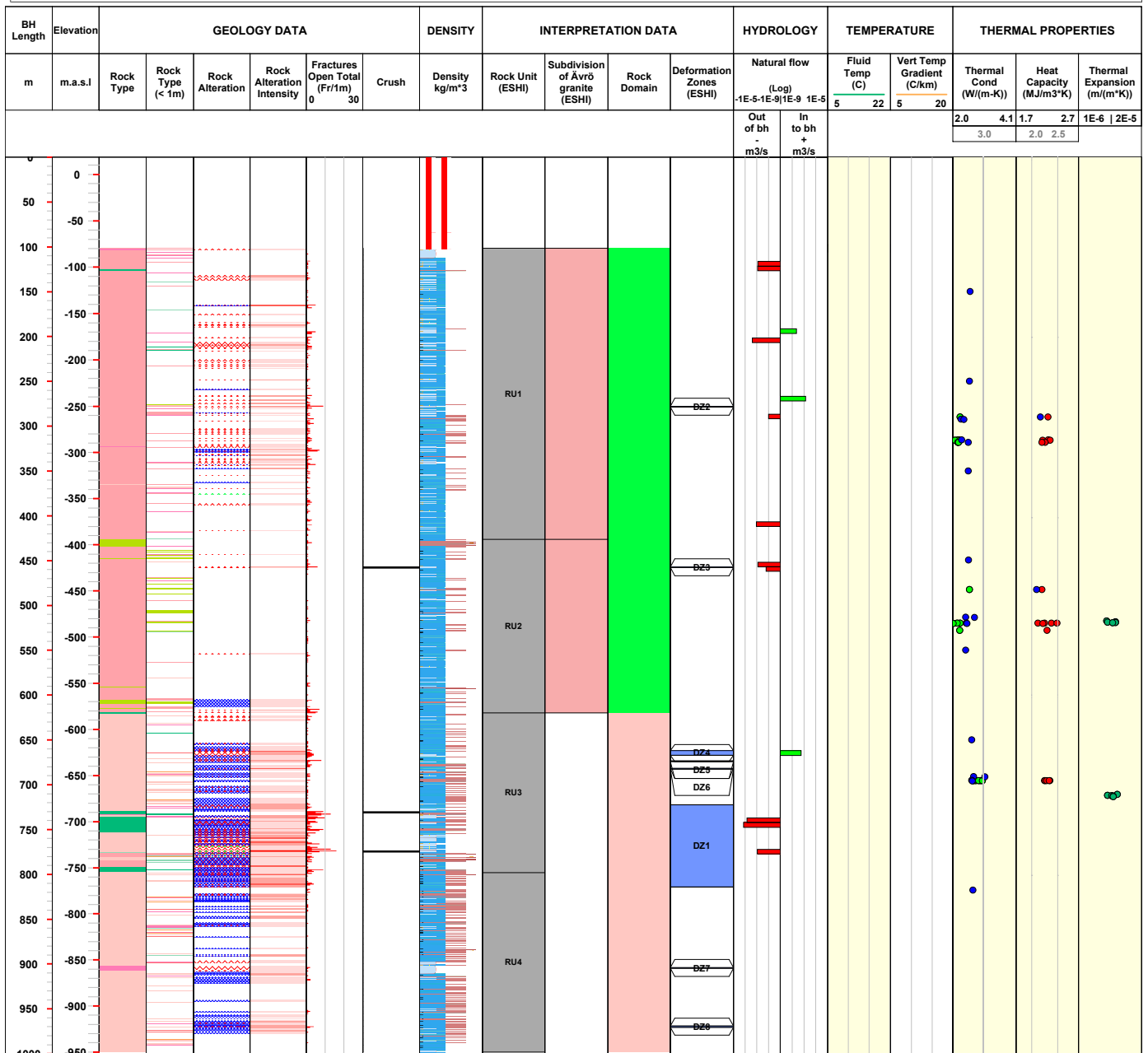
Figure O-7. Error distributions for different amounts of missing data.


WellCad borehole plots

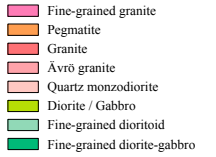


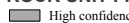

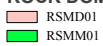
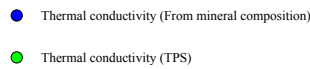
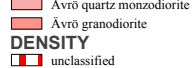
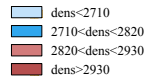
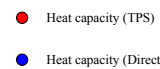
WellCad plots for 14 cored boreholes, showing thermal property and temperature data, together with geological, geophysical (rock density) and hydrogeological data relevant to the interpretation of the thermal data, are presented on the following pages. “Density” refers to the RE_DENSITY_CORR table in Sicada as described in Section 3.7. The Rock Units, Subdivision of Ävrö granite and Deformation zones are based on the extended single-hole interpretations (ESHI) /Wahlgren et al. 2008/. Temperature and temperature gradients are shown only for boreholes for which the temperature loggings are judged to be reliable, as described in Section 3.14.

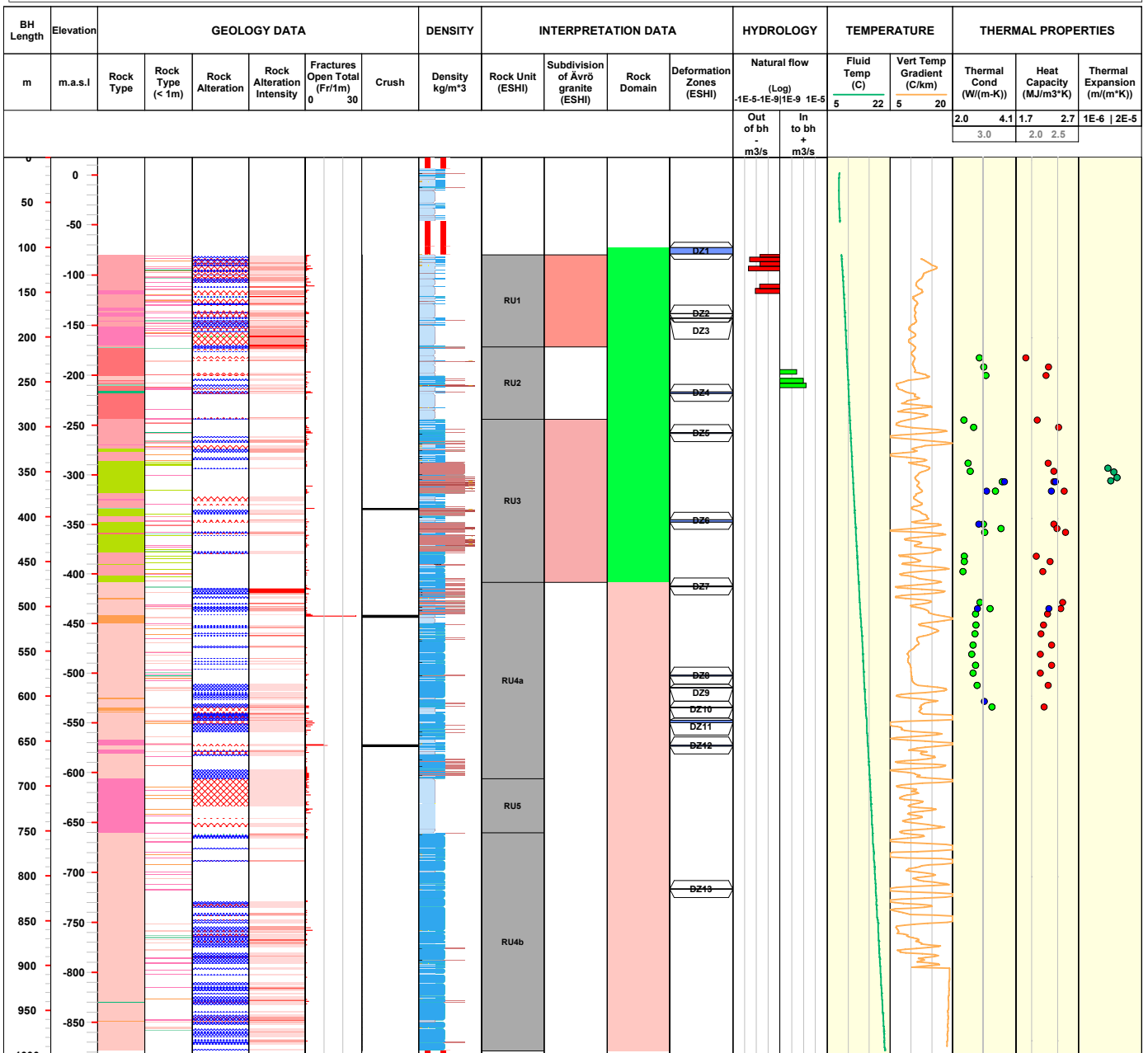
Title KLX03		Site LAXEMAR	Coordinate System RT90-RHB70	Elevation [m.a.s.l.] 18.42
	Borehole KLX03	Northing [m] 6366111.77	Drilling Start Date 2004-05-28 18:00:00	
	Diameter [mm] 76	Easting [m] 1547718.97	Drilling Stop Date 2004-09-07 09:00:00	
	Length [m] 1000.420	Inclination (at borehole collar) [°] -74.92	Surveying Date 2004-05-03 18:37:00	
	Bearing [°] 199.04	Date of mapping	Plot Date 2009-01-11 23:03:55	


ROCK TYPE LAXEMAR 	ROCK ALTERATION 	DEFORMATION ZONE FROM ESHI 	SUBDIVISION OF ÅVRÖ GRANITE 
ROCK ALTERATION INTENSITY 	ROCK DOMAIN 	THERMAL CONDUCTIVITY 	DENSITY 
ROCK UNIT FROM ESHI 			HEAT CAPACITY 

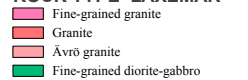


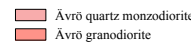
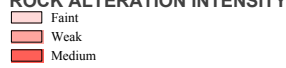

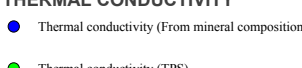
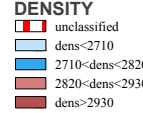

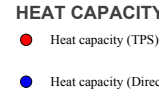


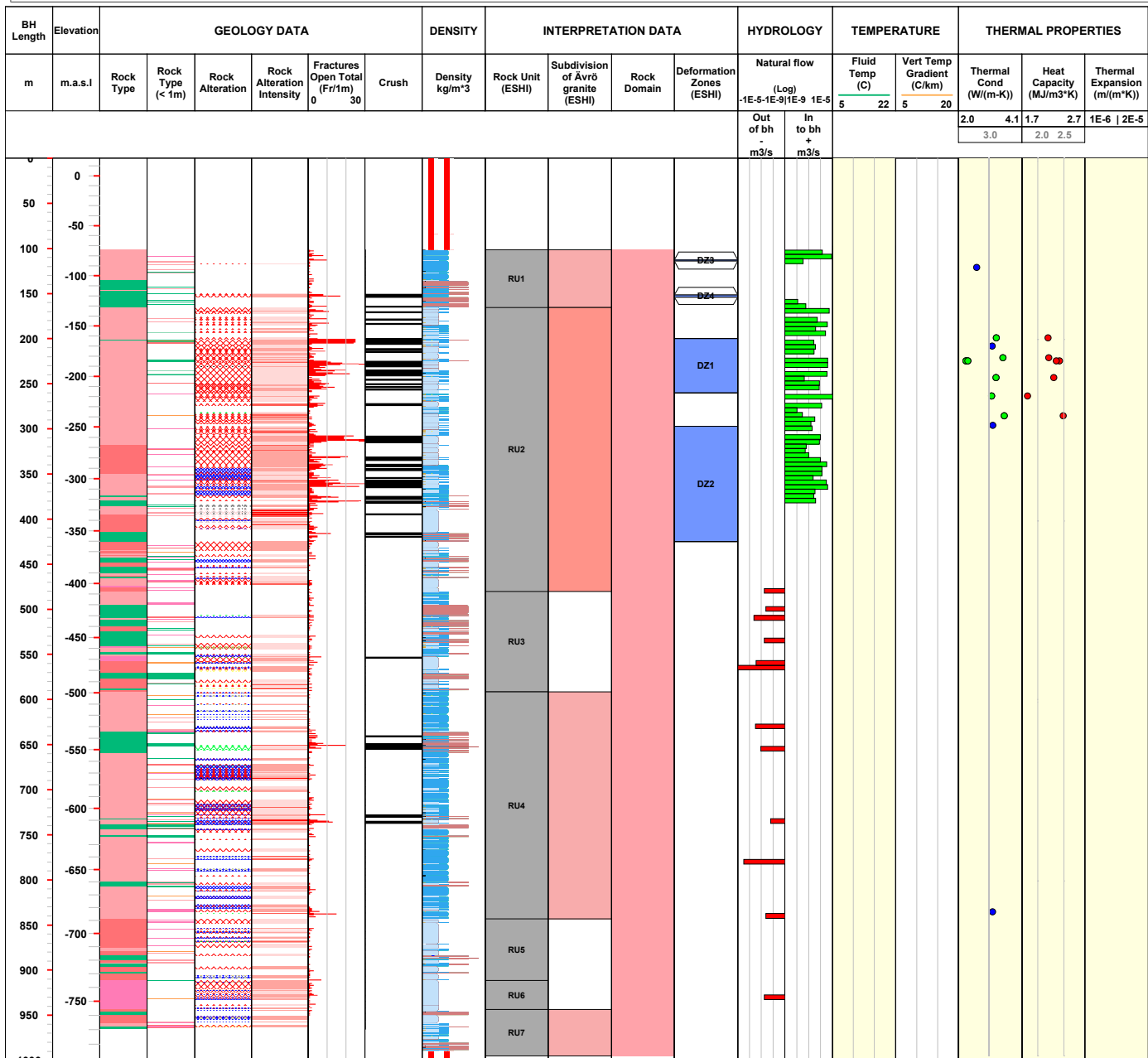
Title KLX05						
	Site	LAXEMAR	Coordinate System	RT90-RHB70	Elevation [m.a.s.l.]	17.56
	Borehole	KLX05	Northing [m]	6365632.52	Drilling Start Date	2004-10-01 14:00:00
	Diameter [mm]	76	Easting [m]	1548909.46	Drilling Stop Date	2005-01-22 13:45:00
	Length [m]	1000.160	Inclination (at borehole collar) [°]	-65.21	Surveying Date	2004-08-11 09:00:00
	Bearing [°]	190.19	Date of mapping		Plot Date	2009-01-11 23:03:55


ROCK TYPE LAXEMAR 	ROCK ALTERATION  ROCK ALTERATION INTENSITY  ROCK UNIT FROM ESHI 	DEFORMATION ZONE FROM ESHI  ROCK DOMAIN  THERMAL CONDUCTIVITY 	SUBDIVISION OF ÅVRÖ GRANITE  DENSITY  HEAT CAPACITY 
---------------------------------------------------------------------------------------------------------------	---------------------------------------------------------------------------------------------------------------------------------------------------------------------------------------------------------------------------------------------------------------------------------------------------------------------------------------------------------	--------------------------------------------------------------------------------------------------------------------------------------------------------------------------------------------------------------------------------------------------------------------------------------------------------------------------------------------------------	---------------------------------------------------------------------------------------------------------------------------------------------------------------------------------------------------------------------------------------------------------------------------------------------------------------------------------------------------

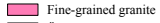
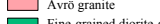
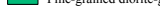
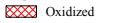
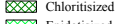
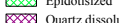

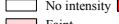
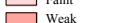


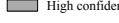

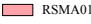


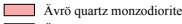
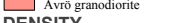
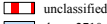
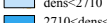
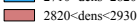





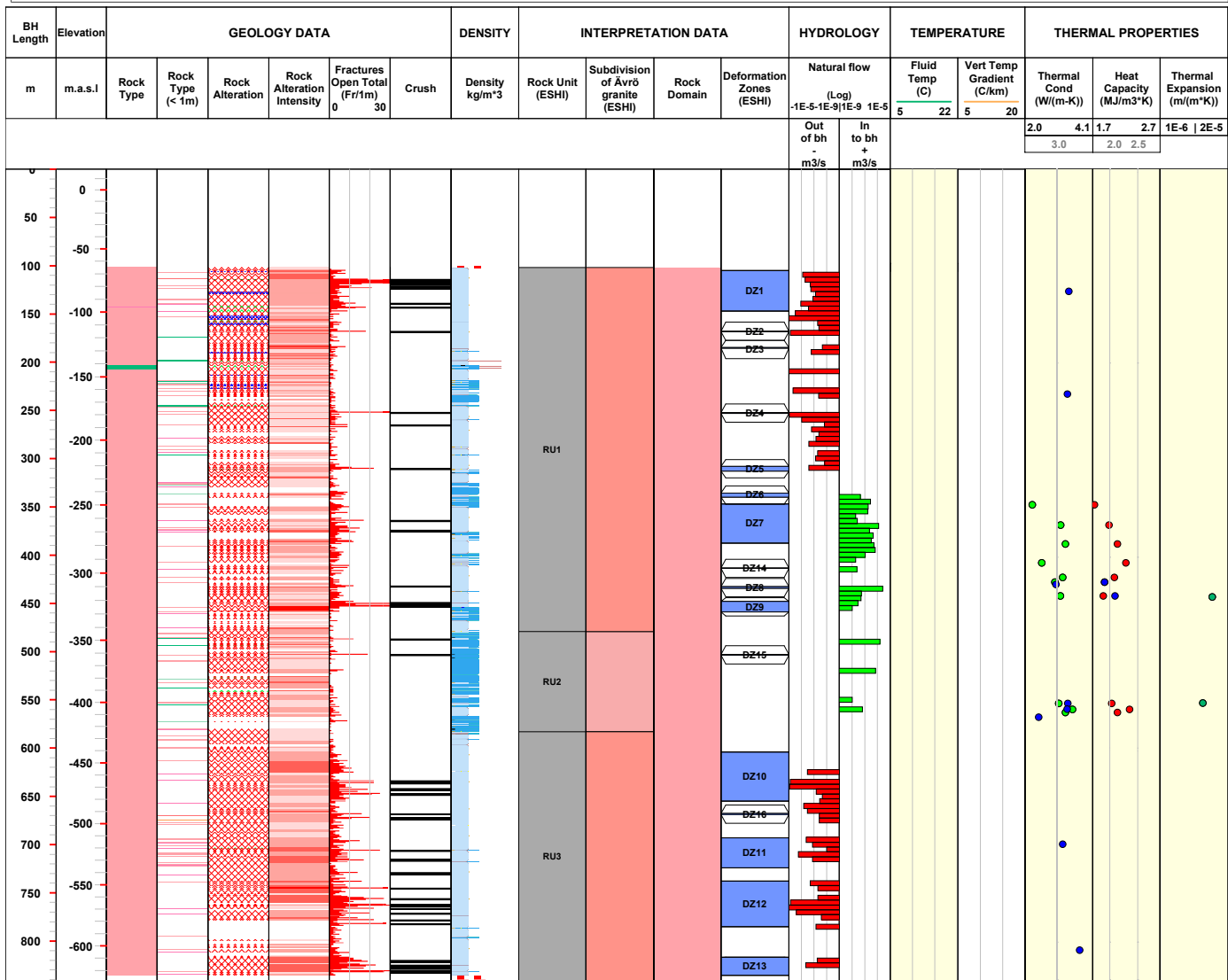
Title		KLX06		Elevation [m.a.s.l.]		17.61	
	Site	LAXEMAR	Coordinate System	RT90-RHB70	Drilling Start Date	2004-08-25 17:00:00	
	Borehole	KLX06	Northing [m]	6367805.82	Drilling Stop Date	2004-11-25 11:30:00	
	Diameter [mm]	76	Easting [m]	1548566.93	Surveying Date	2004-08-03 11:45:00	
	Length [m]	994.940	Inclination (at borehole collar) [°]	-65.19	Plot Date	2009-01-11 23:03:55	
	Bearing [°]	329.65	Date of mapping				


ROCK TYPE LAXEMAR  <ul style="list-style-type: none"> Fine-grained granite Granite Ävrö granite Fine-grained diorite-gabbro 	ROCK ALTERATION  <ul style="list-style-type: none"> Oxidized Epidotized Sericitized Quartz dissolution Silicification Argillization Saussurization Laumontization 	DEFORMATION ZONE FROM ESHI  <ul style="list-style-type: none"> DZ 	SUBDIVISION OF ÄVRÖ GRANITE  <ul style="list-style-type: none"> Ävrö quartz monzodiorite Ävrö granodiorite
ROCK ALTERATION INTENSITY  <ul style="list-style-type: none"> Faint Weak Medium Strong 	ROCK DOMAIN  <ul style="list-style-type: none"> RSMA01 	THERMAL CONDUCTIVITY  <ul style="list-style-type: none"> Thermal conductivity (From mineral composition) Thermal conductivity (TPS) 	DENSITY  <ul style="list-style-type: none"> unclassified dens<2710 2710<dens<2820 2820<dens<2930 dens>2930
ROCK UNIT FROM ESHI  <ul style="list-style-type: none"> High confidence 			HEAT CAPACITY  <ul style="list-style-type: none"> Heat capacity (TPS) Heat capacity (Direct)



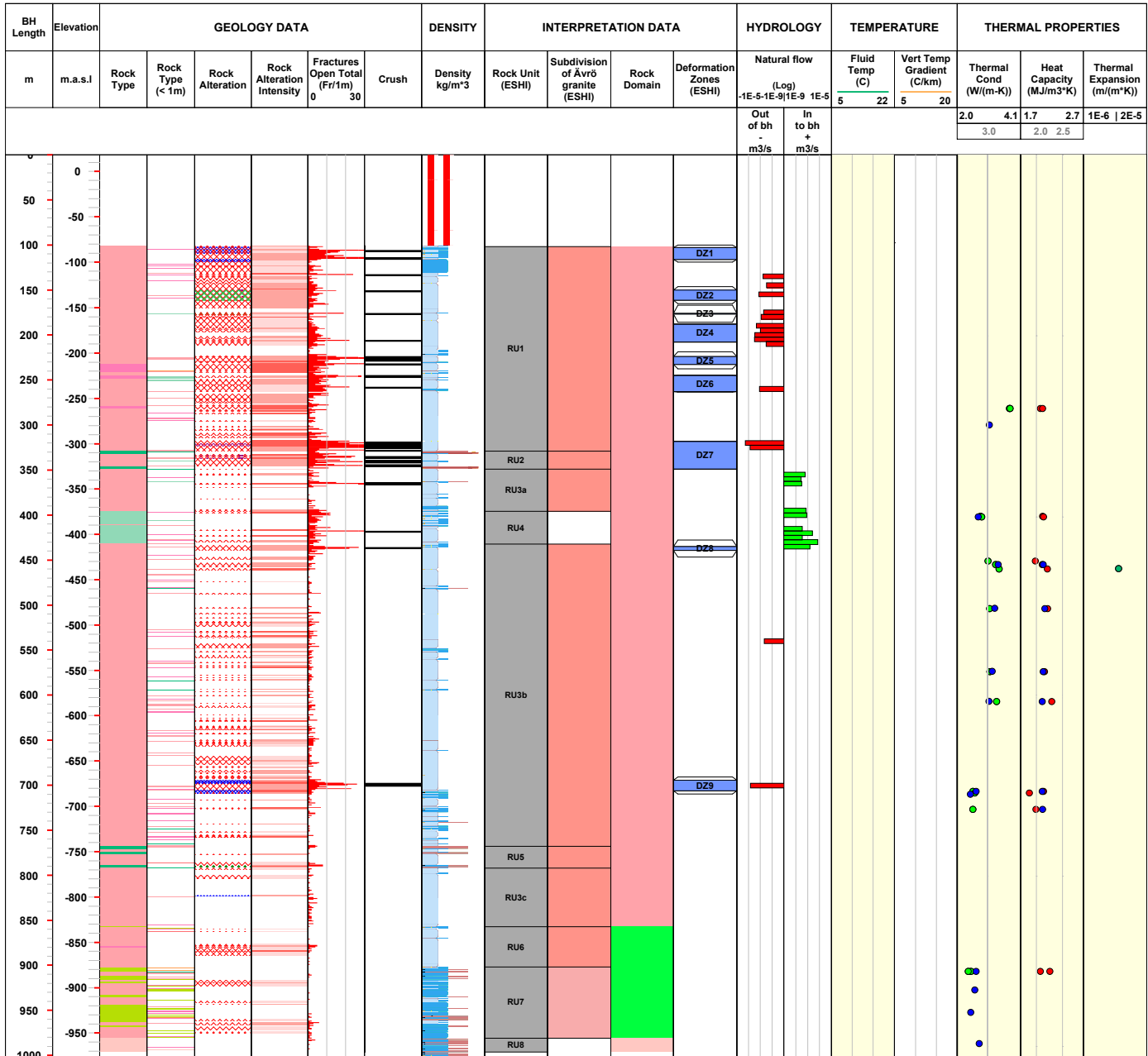
Title KLX07A		Site LAXEMAR	Coordinate System RT90-RHB70	Elevation [m.a.s.l.] 18.40
	Borehole KLX07A	Northing [m] 6366751.28	Drilling Start Date 2005-01-06 14:00:00	
	Diameter [mm] 76	Easting [m] 1549206.90	Drilling Stop Date 2005-05-04 10:00:00	
	Length [m] 844.730	Inclination (at borehole collar) [°] -60.03	Surveying Date 2004-11-23 10:30:00	
	Bearing [°] 174.18	Date of mapping	Plot Date 2009-01-11 23:03:55	


ROCK TYPE LAXEMAR  Fine-grained granite  Ävrö granite  Fine-grained diorite-gabbro	ROCK ALTERATION  Oxidized  Chloritised  Epidotized  Quartz dissolution ROCK ALTERATION INTENSITY  No intensity  Faint  Weak  Medium ROCK UNIT FROM ESHI  High confidence	DEFORMATION ZONE FROM ESHI  DZ ROCK DOMAIN  RSMa01 THERMAL CONDUCTIVITY  Thermal conductivity (From mineral composition)  Thermal conductivity (TPS)	SUBDIVISION OF ÄVRÖ GRANITE  Ävrö quartz monzodiorite  Ävrö granodiorite DENSITY  unclassified  dens<2710  2710<dens<2820  2820<dens<2930 HEAT CAPACITY  Heat capacity (TPS)  Heat capacity (Direct)
-------------------------------------------------------------------------------------------------------------------------------------------------------------------------------------------------------------------------------------------------------------------------------------------------------------------------------------------------------	-----------------------------------------------------------------------------------------------------------------------------------------------------------------------------------------------------------------------------------------------------------------------------------------------------------------------------------------------------------------------------------------------------------------------------------------------------------------------------------------------------------------------------------------------------------------------------------------------------------------------------------------------------------------------------------------------------------------------------------------------------------------------------------------------------------------------------------------------------------------------------------------------------------------------------------------------------------------------------------------	-----------------------------------------------------------------------------------------------------------------------------------------------------------------------------------------------------------------------------------------------------------------------------------------------------------------------------------------------------------------------------------------------------------------------------------------------------------------------------------------------------------------------------------------	-----------------------------------------------------------------------------------------------------------------------------------------------------------------------------------------------------------------------------------------------------------------------------------------------------------------------------------------------------------------------------------------------------------------------------------------------------------------------------------------------------------------------------------------------------------------------------------------------------------------------------------------------------------------------------------------------------------------------------------------------------------------------------------------------------------------------------------------------------------------------------------------------------------------------------------------------------

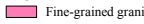
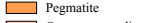
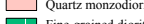
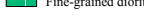
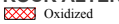
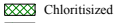
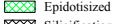

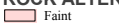
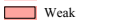
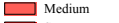
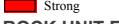

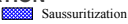












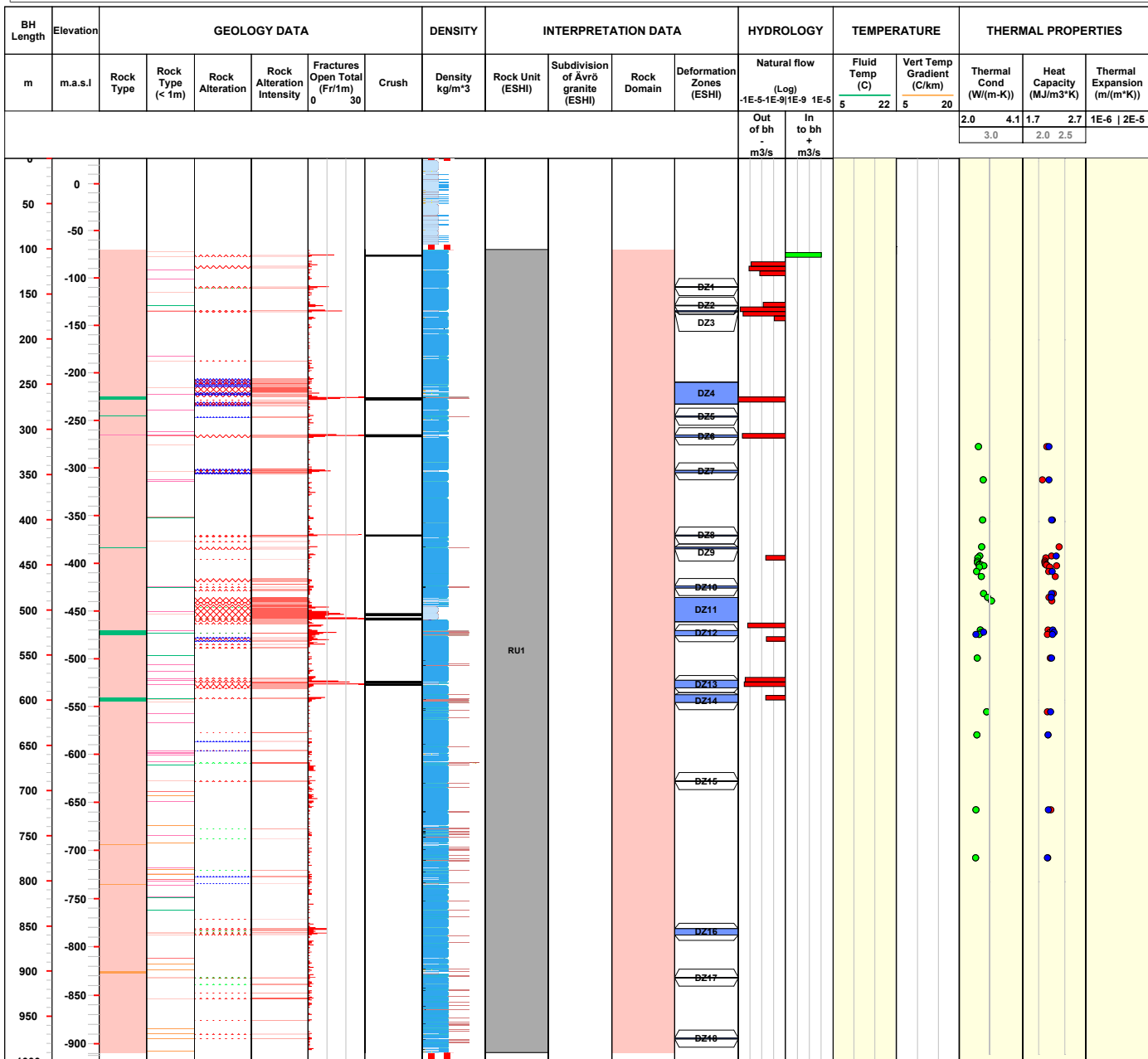
Title KLX10		Site LAXEMAR	Coordinate System RT90-RHB70	Elevation [m.a.s.l.] 18.21
	Borehole KLX10	Northing [m] 6366318.57	Drilling Start Date 2005-06-18 08:00:00	
	Diameter [mm] 76	Easting [m] 1548515.28	Drilling Stop Date 2005-10-15 07:40:00	
	Length [m] 1001.200	Inclination (at borehole collar) [°] -85.18	Surveying Date 2005-05-24 13:40:00	
	Bearing [°] 250.80	Date of mapping	Plot Date 2009-01-11 23:03:55	


ROCK TYPE LAXEMAR Fine-grained granite Ävrö granite Quartz monzodiorite Diorite / Gabbro Fine-grained dioritoid Fine-grained diorite-gabbro	ROCK ALTERATION Oxidized Chloritised Epidotised Sericitised Quartz dissolution Argillization Albitization Saussurization ROCK ALTERATION INTENSITY Faint Weak Medium Strong ROCK UNIT FROM ESHI High confidence	DEFORMATION ZONE FROM ESHI DZ ROCK DOMAIN RSMA01 RSM01 RSM01 THERMAL CONDUCTIVITY Thermal conductivity (From mineral composition) Thermal conductivity (TPS)	SUBDIVISION OF ÄVRÖ GRANITE Ävrö quartz monzodiorite Ävrö granodiorite DENSITY unclassified dens<2710 2710<dens<2820 2820<dens<2930 dens>2930 HEAT CAPACITY Heat capacity (TPS) Heat capacity (Direct)
----------------------------------------------------------------------------------------------------------------------------------------------------------------------	-----------------------------------------------------------------------------------------------------------------------------------------------------------------------------------------------------------------------------------------------------------------------------------	-----------------------------------------------------------------------------------------------------------------------------------------------------------------------------------------------------------	--------------------------------------------------------------------------------------------------------------------------------------------------------------------------------------------------------------------------------------------------------------

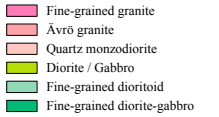
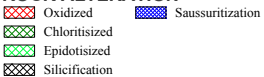
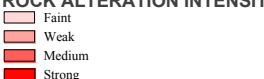

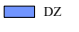
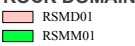
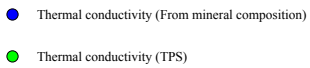
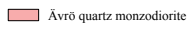
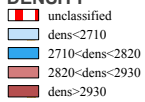
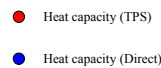


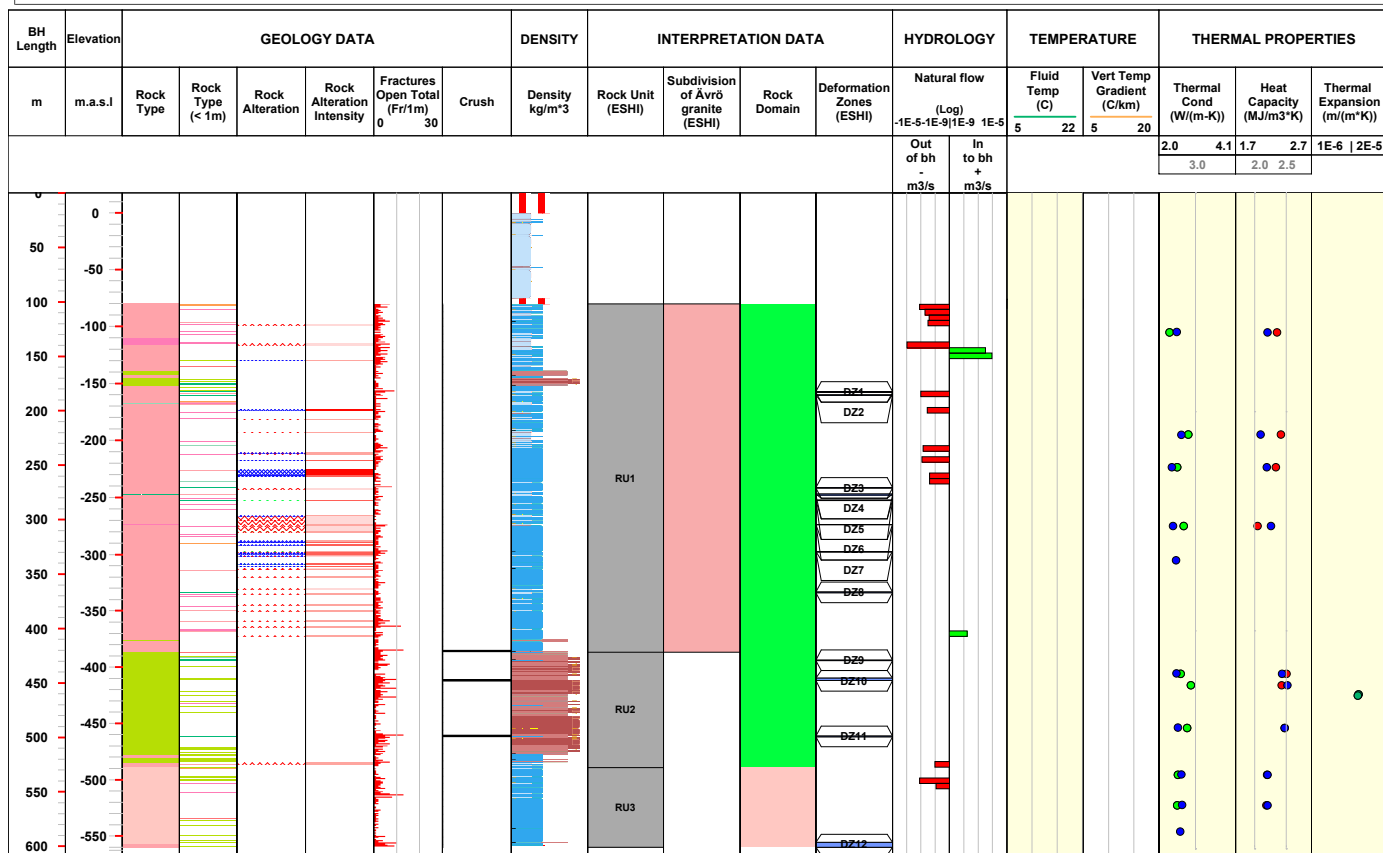
Title KLX11A		Site LAXEMAR		Coordinate System RT90-RHB70		Elevation [m.a.s.l.] 27.12	
	Borehole	KLX11A	Northing [m]	6822.85	Drilling Start Date	2005-11-24 06:00:00	
	Diameter [mm]	76	Easting [m]	-2882.99	Drilling Stop Date	2006-03-02 11:00:00	
	Length [m]	992.290	Inclination (at borehole collar) [°]	-76.76	Surveying Date	2005-10-31 11:25:00	
	Bearing [°]	101.66	Date of mapping		Plot Date	2009-01-11 23:03:55	


ROCK TYPE LAXEMAR  Fine-grained granite  Pegmatite  Quartz monzodiorite  Fine-grained diorite-gabbro	ROCK ALTERATION  Oxidized  Chloritized  Epidotized  Silicification ROCK ALTERATION INTENSITY  Faint  Weak  Medium  Strong ROCK UNIT FROM ESHI  High confidence	DEFORMATION ZONE FROM ESHI  DZ ROCK DOMAIN  RSMD01 THERMAL CONDUCTIVITY  Thermal conductivity (From mineral composition)  Thermal conductivity (TPS)	SUBDIVISION OF ÄVRÖ GRANITE DENSITY  unclassified  dens<2710  2710<dens<2820  2820<dens<2930  dens>2930 HEAT CAPACITY  Heat capacity (TPS)  Heat capacity (Direct)
-------------------------------------------------------------------------------------------------------------------------------------------------------------------------------------------------------------------------------------------------------------------------------------------------------------------------------------------------------------------------------------------------------------------------------------------------------------	-------------------------------------------------------------------------------------------------------------------------------------------------------------------------------------------------------------------------------------------------------------------------------------------------------------------------------------------------------------------------------------------------------------------------------------------------------------------------------------------------------------------------------------------------------------------------------------------------------------------------------------------------------------------------------------------------------------------------------------------------------------------------------------------------------------------------------------------------------------------------------------------------------------------------------------------------------------------------------	---------------------------------------------------------------------------------------------------------------------------------------------------------------------------------------------------------------------------------------------------------------------------------------------------------------------------------------------------------------------------------------------------------------------------------------------------------------------------------------------------------------------------------	-------------------------------------------------------------------------------------------------------------------------------------------------------------------------------------------------------------------------------------------------------------------------------------------------------------------------------------------------------------------------------------------------------------------------------------------------------------------------------------------------------------------------------------------------------------------------------------------------------------------------------------------------------------------------------------------------------------------------------------------------------------------------------------------------------------------------



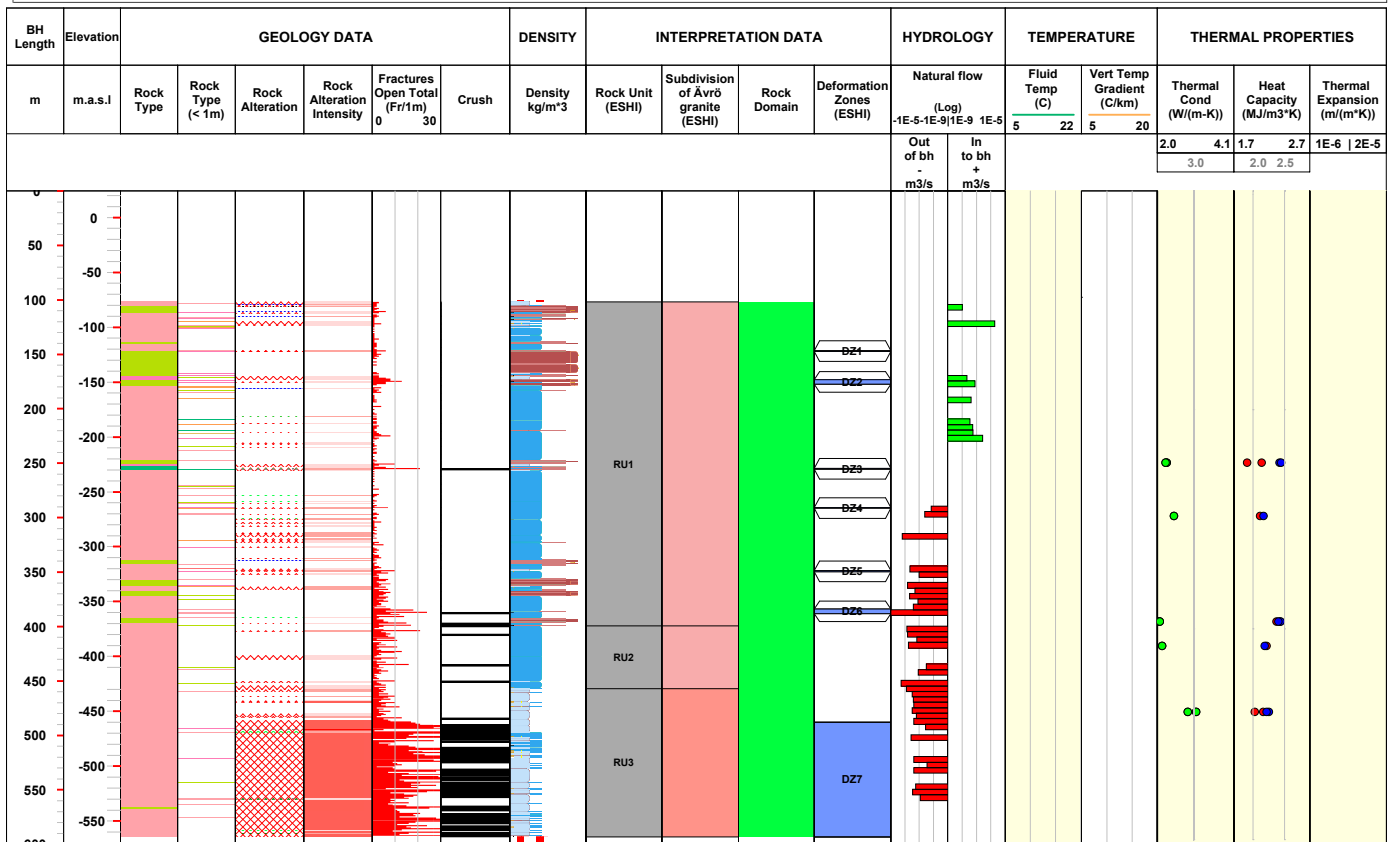
Title KLX12A		Site LAXEMAR	Coordinate System RT90-RHB70	Elevation [m.a.s.l.] 17.67
	Borehole KLX12A	Northing [m] 6365629.96	Drilling Start Date 2005-11-10 09:30:00	
	Diameter [mm] 76	Easting [m] 1548904.49	Drilling Stop Date 2006-03-04 14:48:00	
	Length [m] 602.290	Inclination (at borehole collar) [°] -75.30	Surveying Date 2005-10-19 10:25:00	
	Bearing [°] 315.92	Date of mapping	Plot Date 2009-01-11 23:03:55	


ROCK TYPE LAXEMAR 	ROCK ALTERATION  ROCK ALTERATION INTENSITY  ROCK UNIT FROM ESHI 	DEFORMATION ZONE FROM ESHI  ROCK DOMAIN  THERMAL CONDUCTIVITY 	SUBDIVISION OF ÄVRÖ GRANITE  DENSITY  HEAT CAPACITY 
---------------------------------------------------------------------------------------------------------------	---------------------------------------------------------------------------------------------------------------------------------------------------------------------------------------------------------------------------------------------------------------------------------------------------------------------------------------------------------	--------------------------------------------------------------------------------------------------------------------------------------------------------------------------------------------------------------------------------------------------------------------------------------------------------------------------------------------------------	---------------------------------------------------------------------------------------------------------------------------------------------------------------------------------------------------------------------------------------------------------------------------------------------------------------------------------------------------



Title KLX13A		Site LAXEMAR	Coordinate System RT90-RHB70	Elevation [m.a.s.l.] 24.08
	Borehole KLX13A	Northing [m] 6367546.33	Drilling Start Date 2006-05-19 14:02:00	
	Diameter [mm] 76	Easting [m] 1546787.41	Drilling Stop Date 2006-08-16 09:02:00	
	Length [m] 595.850	Inclination (at borehole collar) [°] -82.23	Surveying Date 2006-03-23 15:45:00	
	Bearing [°] 224.48	Date of mapping	Plot Date 2009-01-11 23:03:55	

ROCK TYPE LAXEMAR Fine-grained granite Ävrö granite Diorite / Gabbro Fine-grained diorite-gabbro	ROCK ALTERATION Oxidized Chloritized Epidotized Silicification Argillization Saussuritization	DEFORMATION ZONE FROM ESHI DZ	SUBDIVISION OF ÄVRÖ GRANITE Ävrö quartz monzodiorite Ävrö granodiorite
ROCK ALTERATION INTENSITY Faint Weak Medium Strong	ROCK DOMAIN RSMM01	THERMAL CONDUCTIVITY Thermal conductivity (From mineral composition) Thermal conductivity (TPS)	DENSITY unclassified dens<2710 2710<dens<2820 2820<dens<2930 dens>2930
ROCK UNIT FROM ESHI High confidence	HEAT CAPACITY Heat capacity (TPS) Heat capacity (Direct)		



Title KLX20A		Site LAXEMAR		Coordinate System RT90-RHB70		Elevation [m.a.s.l.] 27.17	
	Borehole	KLX20A	Northing [m]	6366333.75		Drilling Start Date	2006-03-25 06:00:00
	Diameter [mm]	76	Easting [m]	1546604.94		Drilling Stop Date	2006-04-24 13:20:00
	Length [m]	457.920	Inclination (at borehole collar) [°]	-50.02		Surveying Date	2006-02-22 16:30:00
	Bearing [°]	270.60	Date of mapping			Plot Date	2009-01-11 23:03:55

ROCK TYPE LAXEMAR		ROCK ALTERATION		DEFORMATION ZONE FROM ESHI		SUBDIVISION OF ÄVRÖ GRANITE	
	Dolerite		Oxidized		Albitization		DZ
	Fine-grained granite		Epidotized		Saussuritization		
	Quartz monzodiorite		Quartz dissolution				
	Fine-grained diorite-gabbro		Silicification				
		ROCK ALTERATION INTENSITY		ROCK DOMAIN		DENSITY	
			Faint		RSMD01		unclassified
			Weak				dens<2710
			Medium				2710<dens<2820
ROCK UNIT FROM ESHI				THERMAL CONDUCTIVITY		HEAT CAPACITY	
	High confidence				Thermal conductivity (From mineral composition)		Heat capacity (TPS)
					Thermal conductivity (TPS)		Heat capacity (Direct)

